



HAL
open science

Bispidine-iron (II) complexes as a novel platform for the design of magentogenic probes

Jacek Lukasz Kolanowski

► **To cite this version:**

Jacek Lukasz Kolanowski. Bispidine-iron (II) complexes as a novel platform for the design of magentogenic probes. Other. Ecole normale supérieure de lyon - ENS LYON, 2013. English. NNT : 2013ENSL0849 . tel-01059820

HAL Id: tel-01059820

<https://theses.hal.science/tel-01059820>

Submitted on 2 Sep 2014

HAL is a multi-disciplinary open access archive for the deposit and dissemination of scientific research documents, whether they are published or not. The documents may come from teaching and research institutions in France or abroad, or from public or private research centers.

L'archive ouverte pluridisciplinaire **HAL**, est destinée au dépôt et à la diffusion de documents scientifiques de niveau recherche, publiés ou non, émanant des établissements d'enseignement et de recherche français ou étrangers, des laboratoires publics ou privés.

THÈSE

en vue d'obtenir le grade de

Docteur de l'Université de Lyon, délivré par l'École Normale Supérieure de Lyon

Discipline: Chimie

Laboratoire de Chimie, UMR 5182

École Doctorale de Chimie de Lyon, ED 206

présentée et soutenue publiquement le 30/10/2013

par M. Jacek Lukasz KOLANOWSKI

Bispidine-iron(II) complexes as a novel platform for the design of magnetogenic probes

Directeur de thèse : M. Jens HASSERODT

Après l'avis de : M. Frédéric BANSE

M. Kay SEVERIN

Devant la commission d'examen formée de :

M. Frédéric BANSE, Professeur à Université Paris-Sud XI, **Rapporteur**

M. Peter COMBA, Professeur à Universität Heidelberg, **Examineur**

M. Jean-Pierre DUTASTA, Directeur de Recherches (CNRS) à l'ENS de Lyon, **Président**

M. Jens HASSERODT, Professeur à l'ENS de Lyon, **Directeur de thèse**

M. Kay SEVERIN, Professeur à l'EPFL Lausanne, **Rapporteur**

I would like to dedicate this manuscript to my uncle Antoni who has passed away during the time of its preparation. He will always remain for me a distinct example of a noble, hard work as well as a selfless devotion to relatives and friends.

Chciałbym zadedykować ten manuskrypt mojemu wujowi, Antkowi, który odszedł do wieczności w czasie jego powstawania, a którego życie pozostanie dla mnie na zawsze niedoścignionym przykładem szlachetnej, ciężkiej pracy oraz bezinteresownego i całkowitego poświęcenia dla bliskich.

Acknowledgements

It is my great pleasure to thank Jens Hasserodt for giving me the opportunity to work on this project, which gave me a lot of satisfaction and enabled my scientific development. I am very grateful for the unusual trust, understanding, unique intellectual stimulation and many other things, that I have received in those nearly four years, both on the professional and personal level.

I would like to express my gratitude to Frédéric Banse and Kay Severin for accepting the role of the referees of my manuscript, for their valuable comments and flexibility. I would like also to sincerely thank Jean-Pierre Dutasta and Peter Comba for agreeing on joining the examination committee.

I am very grateful to the collaborators, with whom I had a great pleasure to work. I thank Marc Janier and David Kryza for their interest and fruitful cooperation on the “hot iron” project, to Erwann Jeanneau for the X-ray experiments, Dominique Luneau and Ruben Checa for the measurements of solid state magnetic moment, Olivier Beuf and Laurence Canaple for the MRI experiments and Pauline Bonazza for the biodistribution studies.

My warmest thanks go to the co-workers from the Organic Biochemistry Group, to Jinping, Guillaume and Oliver for the unique atmosphere in our “Bureau International” as well as to the “anciens”: Monica, Anna and Yevgen. Thanks to you coming to work every day (and sometimes during the night) for the last 4 years was for me like coming home. I would like also to thank Fayçal for the inspiring discussions, Maxime for an open-mindedness and translations, Benjamin, Charlene, Corentin, Delphine, Emma, Pauline, Philippe, Sean, Sylvain and those who, despite their short stay, have left unforgettable memories: Cai and Paula as well as Robert and Hanno, who I had a great pleasure to supervise during their internships. Thank you all for providing such an enjoyable work place and turning these years of my French adventure in a truly happy time.

I am very grateful to all colleagues from the whole chemistry department, which made the ordinary working days very pleasant (and efficient!), to Philippe for the care over LC/MS and friendly conversations, Christophe for the “electrochemical” training and good words, Jean-Christophe and Delphine for their smile and good humor, Sandrine for help with the NMR, Menaf, Martin, Julien, Yann, Sébastien, Quentin, Adrien, Thorsten, Yuting, Martine, Alexandre, Laure-Lise, Bastien(s) (les deux ☺), Olivier... Great thanks also to “the biologists”, especially to Gosia, Julia, Monika, Armel, Morgan, Lama and Imtiaz, being always so warm and helpful.

I do not know how to thank those with whom I have spent wonderful moments outside of the laboratory. I am really grateful to Monica, Fabrice and petit Maxence, les Espagnoles (los Polacos ☺) “Anna-Catalana” and Julien, as well as the great group of “foreigners” who shared with me all the good and bad moments of the life of the PhD student - Adi, Cristi, Emel, Michel, Robert, Kaja, Menaf, Guillaume... I will also never forget my team-mates with whom I shared my great passion to football, in particular Remy, Eric, Jocelyn, Sergey, Anghel, Djamel, “Padre” Benjamin and dozens of other colleagues that I met every week to “taper le ballon”.

I would like to thank the „Polish team” from the Paroisse Sainte Trinité, which enriched the last year of my stay in Lyon. I thank Agnieszka, Inga, Kasia, Magda, Grzegorz, Mateusz Z., Mateusz P., Piotr and Agnieszka, Father Tadeusz Śmiech and especially Father Paweł Witkowski, whose attitude and faith have helped me in finalizing my work.

I am also very grateful to those who could not be here in Lyon physically, but remained friends independently on circumstances - to Miłosz, Marta, Łukasz and Michał, Dominika and Łukasz.

There are countless things and no suitable words in which I can thank Gosia, who not only largely contributed to my arrival to France, but who also found, luckily for me, enough strength ☺ to stay next to me during those ”French years”.

I cannot find a simple way to properly express my deep gratitude to my family for their invaluable mental and physical support, which I felt constantly, independently on the circumstances, even from the distance of 1500 km. To my parents, Łucja and Edward for 28 years of their unconditional love and beautiful example; to my sister Ania for her visits and endless speeches on the phone, my brother Tomek for his true fraternal friendship and Agnieszka for having for me always some good words and tolerating my “apartment squatting” at least few times a year.

Nie mogę znaleźć prostego sposobu, żeby właściwie wyrazić wdzięczność mojej rodzinie za jej bezcenne wsparcie psychiczne i fizyczne, które niezależnie od okoliczności czulem nieustannie nawet z odległości 1500 km. Moim rodzicom, Łucji i Edwardowi, za 28 lat ich bezwarunkowej miłości i pięknego przykładu, mojej siostrze Ani za jej wizyty i niekończące się opowieści przez telefon, mojemu bratu Tomkowi za prawdziwą, braterską przyjaźń i Agnieszce za dobre słowo oraz tolerowanie w swoim domu takiego „intruza” jak ja ☺ przynajmniej kilka razy do roku.

Last but not least I would like to thank my school and academic teachers who have developed in me the curiosity towards the surrounding world and “shaped” me as an adult and as a young scientist at the beginning of his adventure. I thank my former teachers: Danuta Jastrzębska and Małgorzata Adamiak, as well as Małgorzata Konarczak-Tymek, Hanna Heimlich and Karol Kacprzak who initially instill in me passion to chemistry. I would like to express my warm gratitude to Henryk Koroniak for his encouragement, kindness and “scientific travel agency” which enabled me to broaden my horizons, as well as Gerd-Voelker Roesenthaler, Sergey Tverdomed, Romana Pajkert and Przemysław Wojtaszek, all of whom played very important role in my “bio-chemical” upbringing

Détails pratiques

Ces travaux de thèse (01/01/2010 – 31/12/2012) se sont déroulés sous la direction du professeur Jens Hasserodt, dans l'équipe de Chimie Bio-Organique, au Laboratoire de Chimie de l'École Normale Supérieure de Lyon, 46 Allée d'Italie, 69007 Lyon, France. Les travaux avec du matériel radioactif ont été réalisés au laboratoire de la Fédération de Médecine Nucléaire – Radiopharmacie dirigé par le professeur Marc Janier, à l'Hôpital Edouard Herriot (Lyon), 5 place d'Arsonval, 69437 Lyon cedex 03, France. Tous les travaux expérimentaux décrits dans ce manuscrit relèvent de mon travail personnel sauf mention explicite du contraire.

Ce travail de thèse a été financé par une bourse doctorale de la Ligue Nationale Contre le Cancer.

TABLE OF CONTENT

Abstract.....	10
Résumé.....	11
Abbreviations	12
STATE OF THE ART.....	17
1. MAGNETIC READOUT AS A DETECTION MODE.....	19
1.1. <i>Detecting a chemical stimulus in solution by responsive probes.....</i>	<i>19</i>
1.2. <i>Molecular and electronic origins of magnetism</i>	<i>20</i>
1.3. <i>Magnetic Resonance Imaging in the detection of paramagnetism</i>	<i>26</i>
2. MAGNETIC RESPONSIVENESS IN METAL COMPLEXES	39
2.1. <i>Introduction to LS-HS equilibria in transition metal complexes</i>	<i>40</i>
2.2. <i>Magnetic responsiveness in solution upon chemical stimulus.....</i>	<i>47</i>
3. TOWARDS MAGNETOGENIC MOLECULAR PROBES IN METAL COMPLEXES	58
3.1. <i>Hallmarks of probe's design – a power of magnetogenesis</i>	<i>58</i>
3.2. <i>(Para)magnetogenesis – magnetic off-ON activation.....</i>	<i>60</i>
3.3. <i>First magnetogenic design for detection of chemical reactivity.....</i>	<i>61</i>
3.4. <i>Bispidines – promising molecular platform for iron(II)</i>	<i>66</i>
RESULTS AND DISCUSSION.....	71
4. OBJECTIVES OF THE PROJECT	73
5. NOVEL SYNTHETIC INTERMEDIATE FOR PREPARATION OF BISPIDINE LIGANDS	75
5.1. <i>Rationale behind the choice of optimal N5 platform</i>	<i>75</i>
5.2. <i>Classic synthetic methodology.....</i>	<i>77</i>
5.3. <i>Alternative synthesis of N7-H platform – protecting group</i>	<i>81</i>
5.4. <i>Deprotection – removal of DMB.....</i>	<i>88</i>
5.5. <i>Perspective - PMB as alternative protecting group.....</i>	<i>92</i>
5.6. <i>Conclusions.....</i>	<i>92</i>
6. BISPIDINE-BASED MAGNETIC OFF-ON DUO.....	93
6.1. <i>Introduction – the concept of overcoming a steric clash</i>	<i>93</i>
6.2. <i>Synthesis of hexadentate bispidine ligands.....</i>	<i>95</i>
6.3. <i>Complexation and solid state structures</i>	<i>98</i>
6.4. <i>Properties in solution</i>	<i>108</i>

6.5.	<i>Summary</i>	116
7.	MAGNETIC EQUILIBRIA IN BISPIDINE-IRON(II) SYSTEM	117
7.1.	<i>Temperature and solvent dependency of magnetic equilibria –ternary vs. binary complex</i>	117
7.2.	<i>Anion sensitivity – towards magnetogenic anion sensors</i>	130
8.	BISPIDINE-IRON(II) SYSTEM IN MRI	144
8.1.	<i>Relaxivities of a pair of off-on model chelates and their MRI characterization</i>	145
8.2.	<i>Off-ON activation in MRI</i>	152
8.3.	<i>Perspectives – towards the response at physiological conditions</i>	159
8.4.	<i>Fine tuning of the physico-chemical properties of bispidines by periphery modification</i> ...	165
8.5.	<i>Summary</i>	172
9.	RADIOLABELING OF IRON(II) COMPLEXES TO STUDY BIODISTRIBUTION <i>IN VIVO</i> ...	173
9.1.	<i>Intro – motivation, objectives and state of the art</i>	174
9.2.	<i>Development of the radiolabeling protocol</i>	175
9.3.	<i>Validation of the protocol - model in vivo study</i>	181
9.4.	<i>Conclusions</i>	185
	CONCLUSIONS AND PERSPECTIVES	187
10.	SUMMARY OF ACHIEVEMENTS	189
11.	GENERAL PERSPECTIVES	191
11.1.	<i>MRI detection of in vivo enzyme activity by 3-component bispidine-iron(II) probes</i>	191
11.2.	<i>Switchable catalysis upon coordination sphere opening</i>	192
11.3.	<i>Magnetogenic probing without opening of coordination sphere</i>	192
	EXPERIMENTAL	195
	SYNTHESIS	197
	<i>General Procedures</i>	197
	<i>Organic synthesis</i>	199
	<i>Complexation</i>	224
	X-RAY STRUCTURES	236
	<i>General procedures</i>	236
	<i>Ligands' structures</i>	237
	<i>Iron(II) complexes</i>	239
	NMR AND MAGNETIC MOMENTS AT VARIED TEMPERATURE	246
	<i>General procedures</i>	246
	<i>Variable-temperature NMR of spin crossover complex [Fe15]</i>	247

<i>Temperature-dependency of magnetic moments of SCO complex</i>	252
<i>Variable-temperature magnetic behavior of other complexes</i>	256
TITRATION EXPERIMENTS – ANIONS’ INFLUENCE ON [Fe15] (IN MEOH)	261
<i>UV-Vis Data</i>	261
<i>Magnetic Moment upon the addition of anions</i>	262
<i>Estimations of binding constants</i>	263
IN VIVO STUDIES	264
<i>MR in vivo images of mice</i>	264
<i>Biodistribution studies with radioactive compound</i>	266
BIBLIOGRAPHY	267
APPENDICES	277
PUBLICATIONS FROM THIS PHD	279
CV – JACEK KOLANOWSKI	305

Abstract

Bispidine-iron(II) complexes as a novel platform for the design of magnetogenic probes

This work concerns the development and characterization of molecular probes that respond to a chemical analyte in a liquid sample by turning from a diamagnetic to a paramagnetic state (off-on mode).

With the aim of designing these tools, we focused on iron(II) chelates of bicyclic bispidines as they promised, among others, sufficient probe stability, even in competitive media like water. This manuscript describes new robust synthetic protocols for their large-scale preparation. Synthesized bispidine-iron(II) complexes were thoroughly characterized in solution (1D/2D NMR, MS, UV-Vis, CV) and in the solid state (X-ray and SQUID). In particular, I report here the first diamagnetic, low spin examples thereof, as well as pairs of structurally related diamagnetic-paramagnetic chelates. It now enables the design of responsive probes for various (bio)-chemical targets (including enzyme biomarkers), accessible by one-step functionalization of a key synthetic intermediate with suitable trigger moieties. The first two such probes are described herein, which respond to the presence of a particular kind of anion or a change in the pH.

In addition, in the course of my work, the unprecedented radioactive iron(II) (Fe-59 isotope) complex of a model water-insoluble ligand was prepared and used in an initial biodistribution study in mice. This original protocol can now be directly adapted to virtually all iron(II)-based probe candidates. Furthermore, the relaxivity data obtained for model MRI-silent and MRI-active chelates, in conjunction with the *in vivo* behavior of the active form in mice, bode well for a creation of an MRI probe functioning in a true off-on mode.

Methodologies and molecular designs described herein enable the development of solution-operating magnetogenic molecular probes, which until now have not been synthesized. The availability of such tools would open up numerous perspectives for technological, environmental and biomedical applications.

Keywords: responsive molecular probes · bispidines · iron(II) · MRI · spin transition · magnetism · imaging agents · water

Résumé

Les complexes de bispidines-fer(II): une nouvelle plateforme pour le design de sondes magnétogéniques.

Cette thèse décrit le développement et de la caractérisation de sondes moléculaires répondant à des analytes chimiques en solution par le passage d'un état diamagnétique à un état paramagnétique (mode off-on).

Dans le but de concevoir de tels outils, nous avons focalisé notre attention sur les chélates de fer(II) avec des ligands de type bispidine bicyclique puisqu'ils présentent, entre autres, une stabilité suffisante même en milieux compétitifs comme l'eau. Ce manuscrit décrit des protocoles synthétiques robustes pour leurs préparations à grande échelle. Les complexes synthétisés ont été entièrement caractérisés en solution (RMN 1D/2D, MS, UV-Vis, CV) et dans l'état solide (rayon X et SQUID). Je suis notamment parvenu à synthétiser le premier exemple de complexe bispidine-fer(II) diamagnétique, bas spin, ainsi qu'à proposer des paires de chélates diamagnétique-paramagnétique aux structures connexes. Nous avons donc à notre disposition un système magnétique off-on valide, qui permet le design de sondes répondant à un stimulus (bio)-chimiques (biomarqueurs enzymatiques par ex.) par fonctionnalisation d'un synthon clé en une seule étape. Les deux premières sondes de ce type sont décrites ici, une répondant à la présence d'anions particuliers et l'autre répondant au pH.

Au cours de ce travail, nous avons également mis au point la préparation du tout premier complexe de fer(II) radioactif avec un ligand insoluble en milieu aqueux et nous l'avons utilisé pour faire une étude préliminaire de biodistribution chez la souris. Ce protocole original pourrait être adapté pour virtuellement toute sonde à base de complexes de fer(II). Les données de relaxivité obtenues pour les modes silencieux et actif en IRM en conjonction avec le comportement *in vivo* de la forme active chez la souris semblent être prometteuses quant à la création d'une sonde IRM fonctionnant sur le principe du mode off-on.

Les méthodologies et designs moléculaires présentés ici ouvrent le champ au développement de sondes moléculaires magnétogéniques opérationnelles en solution, qui n'avait, pour l'heure, jamais été synthétisé. L'avènement de tels outils présente de nombreuses perspectives pour des applications dans les domaines technologiques, environnementales et biomédicales.

Mots-Clés : sondes moléculaires répondeurs · bispidines · fer(II) · IRM · transition de spin · magnétisme · agents d'imagerie · eau

Abbreviations

Textual abbreviations

bistet-tacn	1,4-bis(5-tetrazolyl)methyl-1,4,7-triazacyclononane
bispidine	3,7-diazabicyclononane and its derivatives
BOLD-fMRI	blood-oxygen-level dependent functional magnetic resonance imaging
Bpy	Bipyridine
Bzimpy	bis-benzimidazolepyridine
CA (or CAs)	contrast agent (or contrast agents)
CN	coordination number
COSY	correlation spectroscopy (2D NMR)
CPP	cell penetrating peptide
CS	Curie spin relaxation mechanism
CV	cyclic voltammetry
DCM	Dichloromethane
DD	dipole-dipole interaction (relaxation mechanism)
DDQ	2,3-dichloro-5,6-dicyano-1,4-benzoquinone
Dept	distortionless enhancement by polarization transfer (C-13 NMR experiment)
DIMS (MS)	direct injection mass spectrometry (also abbreviated MS)
DIPEA	(N,N-diisopropyl-N-ethylamine – Hunig base)
DMB	2,4-dimethoxybenzyl moiety
DMF	Dimethylformamide
DMSO	Dimethylsulfoxide
DOTA	1,4,7,10-tetraazacyclododecane-1,4,7,10-tetraacetic acid and all its conjugated bases
dptacn / tptacn	1,4-dipicolyl-1,4,7-triazacyclononane / 1,4,7-tripicolyl-1,4,7-triazacyclononane.
DTPA	diethylene triamine pentaacetic acid (Pentetic acid) and all its conjugated bases
En	Ethylenediamine
[FeX(Y)]Z	complex of iron with polydentate ligand X, monodentate ligand Y both being directly coordinated to the metal centre and Z is the counterion
GBCAs	gadolinium-based contrast agents
HMBC	Heteronuclear multiple-bond correlation spectroscopy (2D NMR)
HOMO / LUMO	lowest unoccupied molecular orbital
HRMS	high resolution mass spectrometry
HS	high spin
HSA	human serum albumin
HSQC	Heteronuclear single-quantum correlation spectroscopy (2D NMR)
IDA	indicator displacement assay
<i>i</i> PrOH	iso-propanol (propan-2-ol)
IR	Infrared spectroscopy
IS / OS / SS	inner (first coordination) sphere, outer sphere and second sphere – water position in the respect to the paramagnetic centre (relaxation theory)

Jmod	j modulation (C-13 NMR experiment)
LS	low spin
MLCT	metal-to-ligand charge transfer band
MR, MRS	Magnetic Resonance, Magnetic Resonance Spectroscopy (imaging modality)
MRI (fr. IRM)	Magnetic Resonance Imaging (Imagerie par Résonance Magnétique)
NMR (1D and 2D)	Nuclear Magnetic Resonance (one- and two-dimensional techniques)
NOESY	Nuclear Overhauser effect spectroscopy (2D NMR)
Oxdz	1,2,4-oxadiazole or oxadiazolyl moiety
Ozd	Oxazolidinone or oxazolidinolyl moiety
paraCEST	paramagnetic Chemical Exchange Saturation Transfer
PB / PBS	phosphate buffer / phosphate buffer saline (1x concentrated)
Pdz	2,3-pyridazine and pyridazinyl moiety
PET	Positron Emission Tomography
phen	Phenantroline or phenantrolinyl moiety
pi = picolyl	(2-pyridyl)methyl moiety
PMB	paramethoxybenzyl moiety
PRE	paramagnetic relaxation enhancement
Py	2-pyridine or 2-pyridyl moiety
RF	radiofrequency impulse
RT	room temperature
SBM	Solomon-Bloembergen-Morgan theory
SC	scalar coupling (relaxation mechanism)
SCO	spin crossover
SNR	signal-to-noise ratio
SPECT	Single Photon Emission Computed Tomography
SPIO	Superparamagnetic iron oxide nanoparticles
SQUID	superconducting quantum interference device
Tacn	1,4,7-triazacyclononane
Tf	trifluoromethanesulfonate (triflate)
TFA	trifluoroacetic acid / trifluoroacetate
THF	tetrahydrofuran
TLC	thin layer chromatography
Tren	tris(2-aminoethyl)amine
Tris	2-hydroxymethyl-2-amino-1,3-propanediol
Ts	para-toluenesulfonyl; thus TsOH: para-toluenesulfonic acid
USPIO	ultrasmall superparamagnetic iron oxide nanoparticles (ultrasmall SPIO)
UV-Vis	ultraviolet-visible light spectroscopy
ZFS	zero-field splitting
β-GAL	<i>beta</i> -galactosidase enzyme

Analytical variables and parameters

A, B, C	Racah parameters
A/\hbar	hyperfine (or scalar) coupling constant (in here: between the proton of water in the first coordination sphere and the electron spin of the paramagnetic center); (theory of relaxation)
B_0 [T]	external magnetic field (in the NMR experiment)
B_1	vector of the magnetic field generated by the radiofrequency excitation impulse in the NMR experiment
β	nephelauxetic effect parameter - ratio between Racah B parameter in the complex (B') to the one of free ion in gaseous state (B)
γ, γ_I [rad s ⁻¹ T ⁻¹]	gyromagnetic ratio, γ_I = nuclear gyromagnetic ratio
DN [kcal mol ⁻¹]	Gutmann's donor number - energy released upon the formation of the 1:1 complex between Lewis base and the standard Lewis acid SbCl ₅
$\delta_d, \delta_p, \delta_H$ [MPa ^{1/2}]	Hansen solubility parameters: energy from dispersion forces (δ_d), dipolar intramolecular force (δ_p) and hydrogen bonds (δ_H) between the molecules
Δ_0 [cm ⁻¹]	d-orbitals' splitting energy (10 Dq)
δ [ppm]	chemical shift of the nucleus (in parts per million) measured from the nuclear reference
$\Delta\delta$ [ppm]	isotropic shift = change in the chemical shift upon the appearance of a paramagnetic quality in an originally diamagnetic sample
ΔH° [kJ mol ⁻¹]	molar standard enthalpy of spin-transition process
ΔS° [J mol ⁻¹]	molar standard entropy of spin-transition process
ε [M ⁻¹ cm ⁻¹]	molar extinction coefficient = molar absorptivity (in UV-Vis spectroscopy)
f, h	dimensionless d-orbitals splitting (f) and d-electrons pairing (k) energy parameters of a ligand in octahedral complexes (Jorgensen equations)
g	electron g-factor (paramagnetic relaxation enhancement equations)
g [cm ⁻¹]	d-orbitals splitting energy parameter of a metal ion in octahedral complexes (Jorgensen equation)
J [Hz]	The internuclear coupling constant (NMR experiments)
k	dimensionless d-electrons pairing energy parameter of a metal ion in octahedral complexes (Jorgensen equation)
K_1	thermodynamic constant of the reaction (of the spin transition LS \leftrightarrow HS)
K_2	thermodynamic binding constant of an anion to the HS form of the complex
L	total orbital angular momentum of the unpaired electrons
M_0	net magnetization vector (for a sample in the external magnetic field)
$\mu: \mu_{eff}, \mu_{HS}, \mu_{LS}, \mu_{HSA}, \mu_e, \mu_p$ [μ_B]	<u>magnetic moment</u> : μ_{eff} = effective (observable) magnetic moment, magnetic moment of the high spin (μ_{HS}), low spin (μ_{LS}) and high spin-anion bound (μ_{HSA}) forms respectively, μ_e = magnetic moment of electron, μ_p = magnetic moment of the proton, μ_B = Bohr magneton = $9.27 \cdot 10^{-24}$ [J T ⁻¹]
μ_0 [T m A ⁻¹]	vacuum permeability = magnetic constant $\approx 1.2566 \cdot 10^{-6}$
P [cm ⁻¹]	effective d-electrons' pairing energy
P^0 [cm ⁻¹]	d-electrons' pairing energy in free metal ion in the gas phase

pKa	negative decimal logarithm from the thermodynamic constant of acid dissociation reaction: $K_a = [A][H]/[AH]$ of the reaction $HA \rightleftharpoons A^- + H^+$
P_m	molar fraction of bound water (in paramagnetic relaxation enhancement theory)
π	“pi” molecular orbital, usually in the context of π -bonding (π -donation or π -accepting) - interaction involving the pi orbitals
q	hydration number (number of coordination sites in the first coordination sphere occupied by water molecules)
$r_{(M-H)}$ [m]	distance between the "relaxing" nucleus (proton) and unpaired electrons - in practice often approximated to the internuclear distance between H from water and paramagnetic metal ion
r : $r_1, r_1^{IS}, r_1^{OS}, r_1^{SS}, r_2$ [mM ⁻¹ s ⁻¹]	<u>relaxivity</u> (relaxation rate per unit concentration of the contrast agent): subscript 1 denotes relaxation rate of longitudinal component of magnetization vector and r_2 refers to the transversal one, superscripts IS, OS and SS refer to the contributions from the relaxation of water protons from the inner sphere (first coordination sphere) outer sphere (bulk) and second sphere (water bound to the periphery of the complex)
R_f	retention factor in the TLC analysis (ratio of a distance covered by the product to the distance covered by the solvent)
S	total spin angular momentum of the unpaired electrons
ΔI	difference between total spin angular momentum of the two compounds (typically of high spin and low spin forms: $S_{HS} - S_{LS}$ where $S_{HS} > S_{LS}$ and S is a spin angular momentum)
σ	“sigma” molecular orbital, usually in the context of σ -bonding - interaction involving σ -orbitals
T [K]	temperature
$T_{1/2}$ [K]	temperature of spin-transition (temperature in which the ratio of low spin \rightleftharpoons high spin isomer is 1)
T_1 : $T_1^{DD}, T_1^{SC}, T_{1,obs}, T_{1,d}, T_{1,paramag}$ [s]	<u>longitudinal (spin-lattice) relaxation time (T_1)</u> and contributions from dipole-dipole (T_1^{DD}) or scalar coupling (T_1^{SC}) relaxation mechanism (theory of relaxation), $T_{1,obs}$ = effective longitudinal relaxation time, in opurely diamagnetic environment ($T_{1,d}$) and contribution from the presence of the paramagnetic quality in the sample ($T_{1,paramagn}$)
T_{1e}, T_{2e} [s]	longitudinal and trasversal electronic relaxation times
T_{1m} [s]	longitudinal relaxation time of the bound water protons
T_2, T_2^* [s]	transversal (spin-spin) relaxation times, T_2^* = transversal relaxation time including field inhomogeneities
τ : $\tau_c, \tau_e, \tau_R, \tau_m$ [s]	<u>correlation times</u> : τ_c and τ_e = specific correlation times of the relaxation process, τ_R = rotational correlation time, τ_m = water residence time; (theory of relaxation).
$1/T, 1/\tau$ [s ⁻¹]	relaxation rates
$\phi, \Delta\phi$ [°]	ϕ = torsional angle measured for the nearest Fe-N bond and respective C-H bond, $\Delta\phi$ = deviation of ϕ from the value of 90 ° at which contact shift is quenched
χ [emu K cm ⁻¹]	magnetic susceptibility
Ω [MPa ^{1/2}]	cavity term in Linear Solvation Energy Relationship for predicting solubility which corresponds to the Hildebrand solubility parameter (square root of cohesive energy density)
ν [cm ⁻¹]	The wavenumber of an excitation in IR spectroscopy in reciprocal centimeters
ν_0 [s ⁻¹]	Larmor frequency (resonance frequency of the non-zero spin nucleus in NMR experiment)
ω : ω_S, ω_I [rad s ⁻¹]	The angular Larmor frequency of electron (ω_S) and proton (ω_I) (theory of relaxation)
Z	The atomic number

PART I

STATE OF THE ART

1. MAGNETIC READOUT AS A DETECTION MODE

1.1. Detecting a chemical stimulus in solution by responsive probes

Small molecules which can generate a distinct physical signal as a consequence of the presence or reactivity of a chemical analyte in liquid samples are powerful tools for studying and monitoring a variety of technological, environmental and biochemical processes. They constitute an important part of a rapidly developing field of Chemical Imaging (are perfectly suited for this purpose)^[1]. The whole range of physical readouts can a priori be envisaged as detectable signals, including electromagnetic waves (absorbance, fluorescence, phosphorescence, interferometry), highly ionizing radiation (radioactivity), acoustics, electric current (conductometry) and magnetism. They are adapted to sensing and imaging purposes to differing degrees and while some are already used in well established techniques, others still await wider recognition.

Responsive probes show distinct advantages over non-reactive ones that always emit a signal: in homogeneous liquid samples, only the use of the former is meaningful; but even in spatially structured, heterogeneous liquid samples (such as biological tissue) those unresponsive probes that have not found their target by simple binding, have to be evacuated to allow for the extraction of information by imaging. The effective removal of this excess proportion is often highly problematic leading to false positive detection, low signal-to-background ratios, and significantly diminish the reliability of the results. Some physical readouts are better suited for the design of agents responding to chemical targets than others. Radioactivity for example is virtually independent of the chemical environment/activity as it is determined by the nature of the nucleus. On the other hand optical properties stem from the electronic system of the molecule and thus are relatively easily modified by chemical interactions. Consequently, the majority of existing responsive probes for chemical stimuli are based on optical detection. (Para)magnetism is yet another property which might be tuned by altering the electronic organization/interactions and thus being available for the design of such tools, but magnetically responsive single-molecule probes for applications in solution are non-existent.

This work describes an original molecular design to address this challenge and hopes to inspire further efforts.

1.2. Molecular and electronic origins of magnetism ^[2] ^[3]

1.2.1. Introduction

Magnetism is a physical property of Matter, which results from its interaction with a magnetic field generated by another magnet. All moving charges a priori generate a local magnetic field which is characterized by the magnetic moment (angular momentum). In addition, an elemental particle has its intrinsic “spin”, so the angular momentum resulting from its precession is characteristic for each type of particle. The magnetic moment of an atom can be divided into three distinct magnetic contributions, differing in strength and derived from different elemental particles of which the atom is composed: a) electronic spin b) orbital angular momentum and c) nuclear spin.

A specific net value of the nuclear spin, characteristic for each isotope, results from the composition of the nucleus and interactions therein. It originates from the intrinsic spins of the nucleons (protons and neutrons), which are ca. three orders of magnitude smaller than the spin of electrons (the spin of a neutron is 960 times and that of a proton 658 times smaller). Consequently, its contribution to the overall magnetic moment is negligible (but it can be of great use when reporting on the electronic structure of the atom and molecules as seen in the case of Nuclear Magnetic Resonance (NMR) – see chapter 1.3.3), and the observed net magnetic moment is principally caused by electronic contributions

1.2.2. Diamagnetic quality

In the atoms (and molecules) the majority of electrons are paired up (Pauli’s exclusion principle), meaning that they attain the spin of the opposite sign when occupying the same orbital, and thus their contribution to the overall magnetic moment is cancelled out. However, the electrons from the same orbital but of opposite spin respond differently to the magnetic field; dependent on the direction of the spin angular momentum (the sign of the spin) they will occupy the space slightly closer or slightly further from the nucleus. This will increase the contribution of the electrons with the spin in the direction opposite to the external magnetic field, and decrease the one parallel to it. In the result it gives rise to the net magnetic moment opposing the magnetic field and thus being repelled by it. The effect, called the diamagnetic contribution, is roughly proportional to the mass of the atom (number of electrons).

1.2.3. Paramagnetism – the consequence of unpaired electrons

When electrons are unpaired, what means that the total electronic spin (sum of the electronic spins) is positive, the paramagnetic behavior is predominant and cancels out the diamagnetic effect. In this case the effective magnetic moment (μ_{eff}) can be given by a formula:

$$\mu_{eff} = [4S(S + 1) + L(L + 1)]^{\frac{1}{2}} \mu_B \quad (1)$$

where S is an overall sum of the electronic spin (spin angular momentum of the electrons), L is the total orbital angular momentum of the electrons (sum of the l quantum numbers of the unpaired electrons) and μ_B is Bohr-magneton.

This formula demonstrates that the electronic spin contribution is directly connected to the number of unpaired electrons which determines the value of (S) and in majority of cases it is dominant. Unlike the movement of the electrons within the particular orbital being at the origin of the diamagnetism, the *orbital paramagnetic contribution* results from the movement of the electron (electronic density) between the electronic orbitals around the nucleus. In order for it to occur, it needs the available vacancies (on the orbitals) of the same energy and symmetry. The initial degeneracy of multiple orbitals may be lost upon the formation of the compounds (approach of the ligand – see discussion below), thus quenching the orbital contribution.

Fig 1 removed

Fig. 1 Shape and annotation of electronic d-orbitals (taken from the web page ^[4]).

Secondly, the symmetry requirement is met only if the orbitals, between which the movement occurs, are related to each other by simple rotation along one of the axes; i.e. if considering the energetically degenerate d-orbitals (model situation of the isolated ions or in theoretical isotropic spherical ligand field – Fig. 1), the electron can “jump” between the d_{xy} , d_{xz} , d_{yz} and $d_{x^2-y^2}$ orbitals thus contributing to overall paramagnetism. Only d_{z^2} is excluded as its symmetry is different (Fig. 1) and thus it cannot take part in generation of the orbital angular momentum. In addition, the orbital to which the electron can be moved, should not yet possess the electrons of the same spin as the moving one, because this would require an extra energy in order to change the orientation of the spin (Pauli’s exclusion principle, see also the discussion on pairing energy below). Thus, the arrangement of the electrons and the energetic positioning of the d -orbitals will have a decisive influence on whether the magnetic moment will be purely a consequence of spin-only contribution or will also have the electronic movement-derived one. As the distance from the nucleus increases, the effects of the movement of the electrons will also be more pronounced, which is often explained by the increased electronic velocity and more pronounced “feeling” of the magnetic field by this charge ^[2]. In the consequence, the orbital contribution will depend to some extent on the Z atomic number. For lighter atoms (lower Z) it will be rather small, but in elements of higher Z , this contribution becomes increasingly important and may even be decisive in determining the magnetic moment. In fact, the existence of the orbital magnetic moment is always associated with the interaction between this and the spin angular momentum, which results in so called spin-orbit

coupling. For heavier elements this effect is strong and thus the determination of the overall magnetic moment requires more complicated calculations (for example j-j coupling model). However, when the interaction is small, as for the lighter elements (like first row transition metals), then the spin and orbital contributions may be treated independently as in the equation above (Russell-Saunders coupling).

1.2.4. Paramagnetism in isolated molecules

If the interaction between the paramagnetic centers occurs (like in the solid state), magnetic moments may spontaneously rearrange causing the appearance of permanent magnetic properties (e.g. ferro- or antiferro-magnetism), which persist also in the absence of the external magnetic field (permanent magnets). Recently, intensive research is pursued in the preparation of the single molecule magnets, where the permanent magnetism can also be stabilized in the isolated molecule. This is possible only when this molecule possesses at least two distinct paramagnetic centers that are still able to interact with each other.

This type of magnetic interaction is not possible in case of mononuclear molecules (one magnetic center per molecule) in solution, where they remain isolated due to the dilution effects (and the surrounding ligands), hence only two basic cases: diamagnetism or paramagnetism, are considered. The former is significantly less pronounced and, even if being an intrinsic property of all materials, it can only be observed in the absence of any paramagnetic contribution. Such materials are by convention often called “non-magnetic”. In the result, the paramagnetic behavior may be selectively detected over the diamagnetic background, what makes it a suitable physical readout for the reporting purposes. Hence, it is in fact the paramagnetic quality which stands behind the term “magnetic signal” and which is the focus of this work.

1.2.5. Features of the paramagnetic signal

In comparison to other physical signals, magnetization offers convincing and attractive benefits:

- (1) High selectivity of the external magnetic field for the non-cancelled spins, which confer the magnetic moment to the sample, promises a **high specificity of the readout** for many environments where no other paramagnetic quality exists.
 - (2) The magnetic signal offers almost **no penetration limits** as the external magnetic field penetrates most obstacles, and thus theoretically no need for local excitation is a priori required (unless resonance detection techniques are used – see below)
 - (3) The unique relative “**inertness**” of the magnetic field towards non-(para)magnetic species, as well as the “transitional” character of the magnetization, which is removed after the removal of the external magnetic field, makes this mode of readout environmentally harmless. This is not the case for many other physical signals, which often damage and permanently alter the molecule or the sample. For example, the highly ionizing radiation (gamma-radiation, electrons, etc) is known to be detrimental to the live organisms, similarly to UV which can
-

alter chemical bonds. In addition, the visible light, or even IR, is diffracted and absorbed by the majority of matrices, leading not only to the distortion or even the loss of the signal but also delivers the energy to the system, heating it up and thus facilitating also a wide range of uncontrollable side effects, including chemical transformations.

- (4) Magnetic signal **does not experience any fatigue**, commonly occurring for fluorescent or radio-active molecules.
- (5) The newly arisen paramagnetic quality is often **accompanied by the change of the other properties** (like optical or conductive – electrical) and thus lead to the opportunity of an orthogonal readout providing the alternative advantages and hence significantly increasing also the applicability of such multimodal tools.

1.2.6. Detection of paramagnetism

Paramagnetic quality can be detected by a variety of different methods and tools (force methods with Gouy's and derived balances ^[5]; induction method-based SQUID device (superconducting quantum interference device) ^[6], Hall-sensors ^[7] and others ^[8]). In particular for solution studies, strategies based on the spin resonance are commonly used and dynamically developing. It is important to point out that they require the excitation of the sample, but the radiofrequencies used for this purpose share the high penetration capacity and environmental harmlessness, and thus do not impair the attractiveness of the magnetic readout as the detection tool (see subchapter 1.3.1, points (2) and (3)).

The direct detection of unpaired electrons within the sample is realized by **Electron Paramagnetic Resonance** (EPR, or ESR - Electron Spin Resonance). The “chemical shift” (resonance frequency) as well as the shape and splitting pattern of the signal may give a lot of information about the surrounding of the unpaired electrons, like other interacting spins (also nuclear spins) and parameters of the media. This method has already been applied in biological models where the so called spin labels (stable organic radicals) are used to tag the biological systems and on the basis of the changes in the signal obtained, the information about the polarity of the media as well as y and z can be drawn. This technique was proven to be useful in monitoring the protein interactions etc.

Indirect detection of paramagnetism by NMR is possible as unpaired electrons can influence both the chemical shifts (Evans' method – see experimental part, Magnetic Resonance Spectroscopy (MRS), paraCEST effect (paramagnetic chemical exchange saturation transfer)) and the relaxation times of the selected nuclei (Magnetic Resonance Imaging (MRI) – see chapter 1.4). The main disadvantage of the NMR is its low sensitivity. The development of the more powerful detectors (bigger magnets – stronger magnetic fields) as well as application of the variable strategies of signal enhancement (for example hyperpolarization) try to address this problem.^[1] On the other hand, large sizes of NMR device and very high costs are often a big problems, but recent

progress in the construction of miniaturized, portable and inexpensive devices promise a further popularization of this powerful technique even in out-of-lab applications.^{[9][10]}

1.2.7. Principles of NMR [11]

Non-zero spin nuclei which precess around their own axis (precession of the angular momentum vector) create weak magnetic dipoles which remain randomly oriented so that the net magnetization is 0. In the external magnetic field B_0 (Fig. 2) those dipoles are forced to align along the magnetic field. For nucleus with a nuclear spin of $\frac{1}{2}$ (like proton) there are only two magnetic states of this alignment available, lower energy parallel and higher energy anti-parallel. The difference between these two states ($\Delta E = \gamma \hbar B_0$ or otherwise $(\gamma h/2\pi)B_0$) which leads to the net magnetization vector parallel to the external magnetic field (M_0 on Fig. 2A), is proportional to the strength of the magnetic field and the nature of the nucleus (γ – gyromagnetic ratio) but it generally remains small (10^{-25} J for a proton in the field of up to 15 T) what corresponds to the radiofrequency wavelengths (RF). In the consequence only a small excess of the nuclei in the lower energy level exists, being responsible for a low sensitivity of the NMR as only a tiny fraction of the whole spin population (at common fields approximately 5 in 1 000 000^[12]) will contribute to the signal (magnetization vector M_0 in Fig. 2 A) in the resonance experiment.

Chemical shift-based detection. The RF energy absorbed by the resonating nucleus, often described as a Larmor frequency $\nu_0 = (\gamma/2\pi)B_0$ (Fig. 2B) depends in fact on the effective magnetic field experienced locally (net result of the B_0 and local magnetic fields). Thus, populations of nuclei in different electronic environment (bonding geometry and character, scalar and spatial coupling, unpaired electrons, etc) will absorb at slightly different frequencies which can be transformed into field-independent characteristic values of chemical shifts. Paramagnetic quality within the sample will significantly modify the local magnetic field and thus may be detected by the observation of the change of chemical shifts, like in the Evans method for determination of the magnetic moment (see experimental part).^[13] This characteristic may be potentially used for detection purposes by the Magnetic Resonance Spectroscopy or in paraCEST contrast agents for MRI.

Relaxation-based detection. Upon the absorption of the energy, the direction of the spin precession (longitudinal component of the M_0 magnetization vector) and its phasing (transversal component) change (Fig. 2 B). The degree of this alteration is dependent on the duration of the excitation impulse (B_1) as well as its direction (90° or 180°). When the RF is stopped, then the system returns to the original ground state (relaxes) (Fig. 2 C). Revival of the longitudinal component characterized by the relaxation time T_1 results from the nuclear spins coming back to the ground state (parallel orientation) by emitting the energy to the environment, and thus it is sometimes described as a *spin-lattice relaxation*. The T_2 transversal relaxation time describes the dephasing process which is much faster than the longitudinal relaxation (T_2 is shorter than T_1) and occurs upon the spin-spin interactions. When the influence of the local inhomogeneities in the

magnetic field caused by the slight differences (chemical shifts) in the Larmor frequency, is taken into account, then the relaxation time of this process is often designated as T_2^* .^[14] Differences in the relaxation dynamics are explored by the MRI technique.

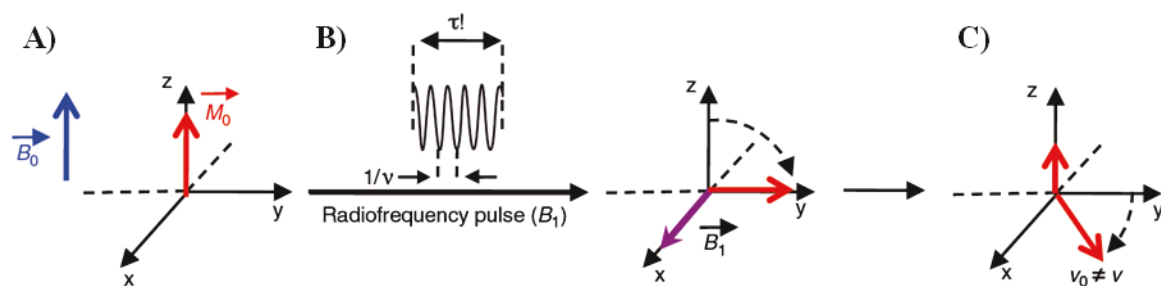


Fig. 2 Schematic behavior of spins in NMR experiment. A) when the sample is placed in the external field, alignment of the spins lead to net magnetization vector M_0 (all spins in phase – no transversal contribution). B) Resonance radiofrequency impulse is applied leading to the loss of longitudinal contribution and gain (phasing) of the transversal one C) recovery of longitudinal vector (T_1 relaxation time) and loss (dephasing of spins) of transversal one (T_2). Taken from Doan et al 2013^[11] – reproduced by permission of WILEY-VCH Verlag GmbH & Co. KGaA, Weinheim (copyright © 2013).

1.3. Magnetic Resonance Imaging in the detection of paramagnetism

1.3.1. General characterization of MRI as an imaging technique

One of the greatest developments in the use of NMR technique for the detection of the paramagnetic quality within the sample is Magnetic Resonance Imaging (MRI). Its importance has been acknowledged with the Noble Prize in Physiology or Medicine to Paul C. Lauterbur and Sir Peter Mansfield in 2003 for their discoveries in the field. MRI is particularly appreciated for its superb spatial resolution of soft tissues (50 μm or even down to 10 μm x 10 μm x 10 μm voxel – the size of the cell – with over 9 T experimental magnets^[15]) and virtually no penetration limits.^[16] As it relies on the magnetic field and radiofrequency wavelengths in order to create an image, it has all the characteristics of the magnetic signal previously described (chapter 1.3.1). In particular, it does not use any harmful, highly ionizing radiation, unlike other competing imaging tools such as Positron Emission Tomography (PET), Computed Tomography (CT), Single Photon Emission Computed Tomography (SPECT) or X-Ray.^[16] and thus it might be used on everyday basis in the clinics (the number of MRI examinations for the patient is not as strictly limited as with other methods mentioned). In consequence, regardless of rather low sensitivity (10^{-9} to 10^{-6} mole of the agent detectable)^[16] MRI is currently one of the main medical imaging modalities widely used in everyday clinical practice. Yet, despite intensive research in the past decade, it furnishes almost exclusively anatomic information, still awaiting a truly functional molecular probe. This development promises a creation of the incomparable tool to precisely study not only a biomedical targets, but thanks to the MRI tunability to virtually any media, also other even the most sophisticated and spatially structured samples.^{[1][16]}

One of the prominent advantages of the MRI, especially when compared to the other techniques for paramagnetism detection, is a multidimensional imaging of even highly complex samples. The information on the precise localization of the signal is encoded by the differences in its frequency and phase from each separate voxel, obtained thanks to the application of the linear field gradient in three distinct directions. On the other hand, contrast in the image is a direct consequence of the spatial difference in the signal intensity of selected nucleus, usually water protons (it is an obvious choice for biomedical applications due to their abundance in the body). It may stem from the difference in the concentration (spin density) as well as from the variation of a T_1 and/or T_2 relaxation times. The image “weighting” which implies the selective measurement of the contribution of only one of these parameters, is possible by a careful choice of the signal acquisition protocol. Spin density-weighted contrast is often too small for diagnostic purposes as many soft tissues have similar water. On the other hand relaxation time-weighting allows for much more pronounced heterogeneity of the signal intensity and thus is preferred in the clinical practice. Despite the fact that the intrinsic differences in the T_1 and/or T_2 of the sample compartments may

sometimes be sufficient, contrast agents (CAs) are commonly used to increase this gap and improve the sensitivity and quality of the image.^{[17] [13] [11]}

1.3.2. Role of contrast agents

MRI CAs catalyze the relaxation process of the neighboring water protons significantly improving the sensitivity of the detection and enabling the distinction between the soft tissues of close intrinsic relaxation properties. In practice, at the end of the last decade around 35 %^[17] to even 40-50 %^[13] of all the MRI exams were performed with a use of CAs. They can target either T_1 , T_2 or both at the same time. Two types of the relaxation catalysts are generally used. Superparamagnetic iron oxide nanoparticles (SPIO or ultrasmall SPIO – USPIO) principally reduce the transversal relaxation time T_2 , what means the loss of the transversal component and thus is associated with darker regions in the T_2 -weighed Magnetic Resonance (MR) image. The diagnostic potential of this ‘negative contrast’ is limited due to the other possible reasons leading to the loss of signal in MRI than the presence of the CA, and as their chemical nature is also not relevant to the subject of this work, they will not be further discussed. Second, and by far more commonly used CAs, which are involved in 90 % of all CAs-assisted MRI examinations in clinics belong to the family of paramagnetic metal complexes and target T_1 , even though their effect on T_2 can also be observed. Reduction of the T_1 is however more attractive because it is significantly longer than T_2 , thus its shortening can be more pronounced and allows for increasing the number of scans in the same time period, leading to the increase in signal intensity (lighter regions on the image). The positive contrast induced by them can then be more unambiguously associated with the contrast agent activity.

From now on I will focus entirely on the T_1 -relaxation, even though some of the considerations below could be valid also for T_2 . In the following chapter I will first discuss the mechanism of longitudinal relaxation and its dependency on the intrinsic parameters of the contrast agent. Then the designs of responsive (“smart”) agents and their suitability for imaging molecular targets will be summarized.

1.3.3. Effectiveness of T_1 -CAs - Paramagnetic Relaxation Enhancement theory

As mentioned above, longitudinal relaxation (described by T_1) happens upon the spin-lattice interactions, the lattice (movement of the spins) being an origin of local fluctuations in the magnetic field. Increasing the field inhomogeneities or the efficiency of their interaction with water protons (or other relaxed nuclei) will shorten the T_1 . In diamagnetic solutions, the relaxation occurs thanks to the magnetic field generated by the neighboring protons and thus is promoted by the increased proton density (concentration of the solvent).

Introduction of the unpaired electrons (paramagnetic quality), which have much higher magnetic moment than protons ($\mu_e = 658 \mu_p$), may catalyze the relaxation much more efficiently. This

fundamental effect lies behind the concept of the use of paramagnetic metal ions as T_1 but also T_2 -CAs in MRI. ^[18]

Theory which describes the efficiency of the relaxation of solvent nuclei in the presence of the paramagnetic compounds is often abbreviated PRE (paramagnetic relaxation enhancement). In general the observed relaxation rate $1/T_{1,obs}$ is a sum of the intrinsic relaxation rate (background relaxation rate, sometimes reduced to a diamagnetic contribution $1/T_{1,d}$) and the relaxation rate stemming from the presence of the paramagnetic substance:

$$\frac{1}{T_{i,obs}} = \frac{1}{T_{i,d}} + \frac{1}{T_{i,paramag}} \quad (2)$$

Paramagnetic relaxation rate is directly proportional to the concentration of the paramagnetic compound [CA] (in mmol/l or mmol/kg of the solvent in higher density samples) by the contrast-agent specific factor of *relaxivity* r_1 ($[mM^{-1}s^{-1}]$), which is a function of its paramagnetism and its interaction with a water protons.

$$\frac{1}{T_{i,obs}} = \frac{1}{T_{i,d}} + \frac{1}{r_1[CA]} \quad (3)$$

Relaxivity can then be decomposed into the inner (r_1^{IS}) and outer sphere (r_1^{OS}) contributions, with a second sphere contribution r_1^{SS} being sometimes separated from the latter.

$$r_1 = r_1^{IS} + (r_1^{SS} + r_1^{OS}) \quad (4)$$

Outer sphere contribution. The r_1^{SS} is generally small (around 10 % of the total relaxivity of classic Gd^{III} complexes) ^[18] and increases only when there exist sites on the periphery of the complex allowing for specific binding of water molecules (and is a sum of relaxation rates of each of these sites). On the other hand, r_1^{OS} which refers to PRE of freely diffusing bulk solvent molecules in the proximity of the complex is not fully understood and thus difficult to be controlled. These contributions can be estimated experimentally on the basis of relaxivity of structurally similar complexes but with closed coordination sphere. Thus, r_1^{OS} was found to amount to the value of at least $1.8 - 2.5 \text{ mM}^{-1}\text{s}^{-1}$ for $Gd(III)$ with $S = 7/2$ and T_{1e} in a range of $0.1 - 1 \text{ ns}$ (half of the $r_1 = 4.1 \text{ mM}^{-1}\text{s}^{-1}$ of $Gd\text{-DOTA}$ at 37°C and 20 MHz), with values for other metals being $1.1 - 1.3 \text{ mM}^{-1}\text{s}^{-1}$ for $Mn(II)$ ($S = 5/2$, T_{1e} of $10 - 100 \text{ ps}$), $0.73 - 0.95 \text{ mM}^{-1}\text{s}^{-1}$ for $Fe(III)$ ($S = 5/2$ and T_{1e} $1 - 100 \text{ ps}$) ^[19] and only $0.05 - 0.1 \text{ mM}^{-1}\text{s}^{-1}$ for $Dy(III)$ ($T_{1e} = 0.1 - 1 \text{ ps}$).^[20] These data suggest a major role of *longer electronic relaxation times* in increasing the outer sphere contribution, with the *magnetic moment being of secondary importance* (for more details see ^[20] and ^[21]).

Inner sphere contribution to the overall relaxation rate of the protons of the bulk solvent stems from the enhanced relaxation rate of the protons of directly coordinated water molecules (denoted as $1/T_{1m}$), which exchange with the bulk solvent at average rate of $1/\tau_m$ (τ_m - residence time), and can be described by the following equation:

$$\frac{1}{T_{1,p}} = \frac{P_m}{T_{1,m} + \tau_m} = \frac{[CA]}{55.55} \frac{q}{T_{1,m} + \tau_m} \quad (5)$$

where P_m is a molar fraction of bound water, equals to number of water molecules in the first coordination sphere (q) multiplied by concentration of the contrast agent [CA] and divided by water concentration, which in diluted solutions is 55.55 M.

In the light of this equation and the discussion above the *number of first coordination sphere water molecules* will have a direct effect on increasing the relaxation rate of the bulk (direct proportionality). Primary significance of shortening *the water residence time* τ_m is the increased number of molecules of bulk solvent which can experience the PRE. However, if paramagnetically-driven relaxation is longer than the time the water molecule spends coordinated to the metal ion, then shortening of τ_m has much lower significance and the process is principally T_{1m} -determined. That is true for most practical examples of gadolinium-based contrast agents (GBCAs), where the T_{1m} is in the range of microseconds, with τ_m being one to few orders of magnitude shorter, and so the understanding of the T_{1m} regulation is of primary importance for interpreting and improving their relaxivity. Nevertheless for other systems of slower average water exchange rate, including for example Fe(III) but even Fe(II), the τ_m control might be dominant.

1.3.4. Relaxation of inner sphere water - Solomon-Bloembergen-Morgan theory

Determination of the relaxation rate of bound water protons ($1/T_{1m}$) is possible from a set of analytical equations (see below) constituting *Solomon-Bloembergen-Morgan theory* (SBM), summarized by Kowalewski et al.^[22] Despite important limitations of this model (see paragraph at the end of this chapter and ^[22] ^[21]) developed principally for Gd(III)-based small complexes, it will be shortly addressed below due to its utility in the interpretation of many experimental results as well as in rational design of new contrast agents with desired properties.

Relaxation of water protons bound to a paramagnetic center happens principally *via* the dipole-dipole interactions (DD) and scalar coupling (SC) (in high field contribution of Curie spin relaxation (CS) might appear ^[23]) which lead to separate but additive contributions $1/T_1^{DD} + 1/T_1^{SC}$. The relevant equations (taken from Toth et al 2013 ^[18]) are presented below but only the DD term will be discussed as the SC (might be important for Mn(II) complexes) is negligible for Gd(III) due to the highly ionic character of its bonds and significant distance between the water proton and the metal center, lowering the hyperfine coupling.

$$\frac{1}{T_1^{DD}} = \frac{2}{15} \frac{\gamma_I^2 g^2 \mu_B^2}{r_{(M-H)}^6} S(S+1) \left(\frac{\mu_0}{4\pi}\right)^2 \left[7 \frac{\tau_{c2}}{1+\omega_S^2 \tau_{c2}^2} + 3 \frac{\tau_{c1}}{1+\omega_I^2 \tau_{c1}^2} \right] \quad (6)$$

where γ_I stands for the nuclear gyromagnetic ratio, g denotes the electron g-factor, r_{GdH} is a distance between the proton and the electron spin (here of Gd ion but generally also any other electron spin), ω_S and ω_I are the Larmor frequencies of electron and proton respectively and τ_c is the correlation time characteristic of the relaxation process, described by the following equation:

$$\frac{1}{\tau_{ci}} = \frac{1}{\tau_R} + \frac{1}{T_{ie}} + \frac{1}{\tau_m}, \quad \text{where } i = 1, 2 \quad (7)$$

where τ_R , T_e and τ_m are rotational, electronic and inner sphere water residence correlation times respectively. Scalar contribution is, in turn, depicted as:

$$\frac{1}{T_1^{SC}} = \frac{2S(S+1)}{3} \left(\frac{A}{\hbar}\right)^2 \frac{\tau_{e2}}{1+\omega_S^2 \tau_{e2}^2} \quad (8)$$

Where A/\hbar is a hyperfine (or scalar) coupling constant between the proton of water in the first coordination sphere and the electron spin of the paramagnetic center and τ_e is the appropriate correlation time, characterized as: ε

$$\frac{1}{\tau_{ei}} = \frac{1}{T_{ie}} + \frac{1}{\tau_m}, \quad \text{where } i = 1, 2 \quad (9)$$

Number of unpaired electrons, which is a crucial determinant of the paramagnetism (magnetic moment) of metal complexes, is also a primary parameter influencing the relaxation rate. According to the SBM theory, relaxation rate $1/T_{1m}$ is proportional to $S(S+1)$ where S is the electronic spin of the metal ion. Indeed, 7 unpaired electrons of gadolinium(III) are principally responsible for the unbeatable relaxivities of Gd(III) based complexes. Nevertheless, transition metals like Fe(III) and Mn(II) (5 unpaired electrons) or even Fe(II) (4 unpaired electrons in the high spin state - HS) could also be potentially considered. For the latter however, the relationship between the number of unpaired electrons and the relaxation rate is more complex, but the general rule that higher number of unpaired electrons mean higher relaxivity, still applies (with rough approximation – for more information please refer to limitations of the SBM theory below and also for example ^[22] ^[18]).

Distance $r_{(M-H)}$ between the unpaired electrons and water protons (often approx. to the distance between the point charges at the nuclei) has significant influence on relaxivity as the dipole-dipole interactions (major contribution to the relaxivity) are highly distance sensitive (factor of $1/r^6$). This parameter can be usually only slightly modified by tilting the plane of coordinated water molecule

(difficult to control) or increasing delocalization of electrons on the ligand (higher covalency of the interaction, explorative for anisotropically distributed d-electrons of transition metals). For most Gd(III) complexes $r_{(M-H)}$ is around 3.1 Å and by SBM theory shortening it by 0.1 Å increases r_I^{IS} by 20 %, lengthening by 0.2 Å, in turn reduces r_I^{IS} by 50 %.^{[18] [20]}

Correlation time τ_c (and τ_e) should be maximized and not exceed the reciprocal of a Larmor frequency (the $\omega^2\tau_c^2$ is then either negligibly small or equal to 1). Water residence time can also influence the relaxivity by influencing this parameter, but its contribution is significant only when τ_m is shorter than both T_e and τ_R (for Gd(III) it may happen at low to medium fields of 0.05 to 3 T what corresponds to 2 to 125 MHz) - for macromolecular complexes in which rotational correlation time is prolonged Fig. 3).

Long **electronic relaxation time T_e** is the second crucial parameter of Gd(III) ion (10^{-6} s) which ensures its high relaxation potential in comparison to other metals, including lanthanides. Complex dependency of T_e on the external magnetic field, symmetry of the complex, rotational motion and degeneration of the valence orbitals, among others, will not be discussed. It suffices to say that according to the SBM, it decreases with the square of the field,^{[20] [24]} what globally reduces r_I^{IS} , provided its crucial contribution to τ_c (equation 7 of SBM) which for classic small-molecule Gd(III) complexes is negligible.^[18] However for other metals it might be a crucial and limiting parameter (Fe(III) or Fe(II) for example, which may have T_e of as low as 1 ps).^[20]

Rotational correlation time τ_R is probably the most extensively used feature to modify the relaxivities of CAs as it promises the highest gains, incomparable with those attainable by realistic changes of any other parameters.^[20] Slowing down the molecular movement is principally achieved by binding to the macromolecule or construction of oligomeric species. Restricted rotation by a creation of the confined cavity is also an option. However, with the increasing magnetic field, this effect is lost (for Gd(III) above 100 MHz – Fig. 3) and thus in the future applications with a much more powerful magnets allowing for higher resolution and increased sensitivity, is of no importance for Gd(III).

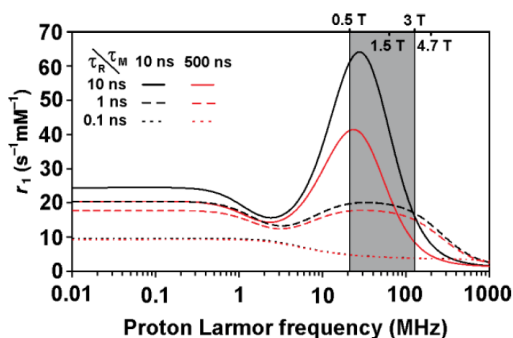


Fig. 3 Field dependency of relaxivity as a function of rotational correlation time, given for two different water residence times – lines are predictions on the basis of SBM theory. Reproduced from Hermann et al 2008^[17] - by permission of The Royal Society of Chemistry (RSC) for the Centre National de la Recherche Scientifique (CNRS) and the RSC (doi: 10.1039/B719704G).

Remark on the limitations of the SBM theory: The SBM theory as previously stated has been developed to explain the behavior of Gd(III)-based small molecule complexes and required several severe approximations. In the consequence, it will apply to some non Gd-metals more (like Fe(III) or Mn(II), provided the inclusion of the scalar coupling mechanism of relaxation) than to the others (Fe(II), Mn(III), Ni(II), etc). The reasons lie in significant differences in the fine electronic configuration, symmetry (asymmetry) and the static zero-field splitting (ZFS - almost inexistent for Gd(III) and very significant for Fe(II), for example) among others, influencing the electronic relaxation times and characteristics of unpaired electrons-induced magnetic field fluctuations. For metals like Fe(II) which is of particular interest for this work, theories describing their relaxivity are complex and of limited analytical application, usually reserved for the specialists,^[18] thus are not covered in this work, but can be found elsewhere.^{[22] [25] [26]} In the consequence for some practical cases including not only different metal ions but sometimes even Gd(III) (if attached to macromolecule especially at low fields), the use of SBM theory might be inadequate and the results of predictions obtained by it have to be treated with the highest caution.

1.3.5. Classic contrast agents

Great majority of all T_1 -CAs are based on Gd(III) due to its superior relaxation properties stemming from the 7 unpaired electrons and long electronic relaxation times.^[18] GBCAs are also the only T_1 -reducing agents, except [Mn(DPDP)]HNa₃ (Teslascan®, DPDP - dipyrroxyl diphosphate, $r_1 = 2.3 \text{ mM}^{-1} \text{ s}^{-1}$ at 1 T in 37 °C),^[27] which are approved for clinical use,^[28] but other metal ions were also proposed in scientific literature, including Fe(III),^{[19] [29]} Cr(III),^[30] and even Fe(II).^{[31] [32]}

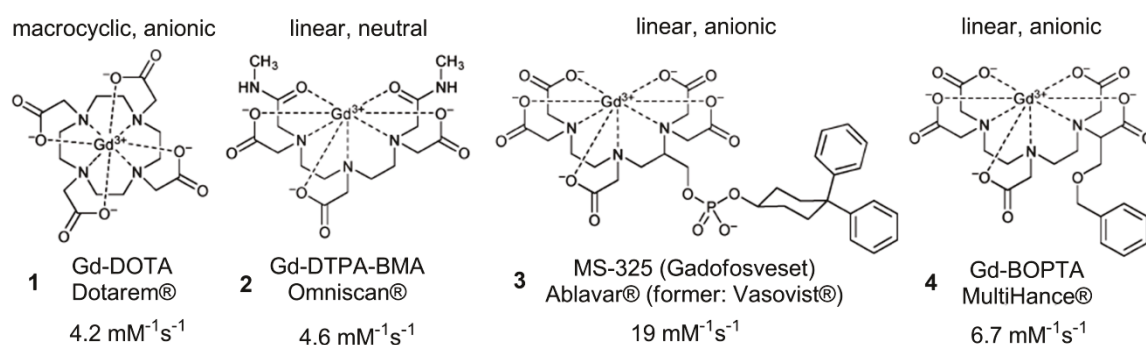


Fig. 4 Selected commercial Gd-based contrast agents. Relaxivities are given for blood at 37 °C and 1 T magnetic field (for Vasovist in 1.5 T). Water molecule is omitted for clarity. Adapted from Hermann et al 2008^[17] - with permission of The Royal Society of Chemistry (RSC) for the Centre National de la Recherche Scientifique (CNRS) and the RSC (doi: 10.1039/B719704G).

In order to minimize the severe toxicity of Gd(III) ion, it is typically encapsulated by octadentate macrocyclic ligands (1,4,7,10-tetraazacyclododecane-1,4,7,10-tetraacetate (DOTA) derivatives, like **1** in Fig. 4) or linear ones (diethylenetriaminepentaacetate (DTPA) derivatives, **2**, **3** and **4** in Fig. 4). In these complexes only one coordination site is left for water molecule to access the paramagnetic metal ion ($q = 1$) in electroneutral (**2** - Gd-DTPA-BMA, Omniscan®, Fig. 4) or

preferably anionic (Gd-DOTA **1**, Dotarem[®], Fig. 4) complex.^[17] Despite these precautions, if a clearance of the agent, which usually is completed within less than 24 h, is hampered, for example due to the renal dysfunction of the patient, then complexes of branched ligands (not so for macrocyclic ones) lead to the development of Nephrogenic Systemic Fibrosis (NFS), associated with the release of Gd(III).^{[33] [34]} Only one water molecule in the first coordination sphere of these complexes, leads to the relaxivities of around $4.5 \text{ mM}^{-1}\text{s}^{-1}$ at 37°C in 1.5 T in blood,^[35] which decrease at higher fields (r_1 of standard complex **1** was $2.4 \text{ mM}^{-1}\text{s}^{-1}$, measured at 7 T)^[31]. The clinically approved contrast agent **3** (Ablavar[®] or formerly Vasovist[®] – Gadovosveset – ligand is an analog of linear DTPA) of improved relaxivity ($r_1 = 19 \text{ mM}^{-1}\text{s}^{-1}$ in 1.5 T at 37°C)^[35] binds to the human serum albumin (HSA), by its hydrophobic tail, what results in a decrease in rotational correlation time. The concept of macromolecule binding, often denoted as RIME (receptor-induced magnetization enhancement), is widely applied in designing new CAs.^{[36] [37]} As I have written above, in accordance to the SBM theory and experimental results, the effect is however lost in the magnetic fields of ($>100 \text{ MHz}$ – see Fig. 3 and discussion above). In addition, branched nature of the ligand used, and increased residence time of the complex due to the protein binding, counteracts the positive influence of the dose-reduction enabled by greater relaxivity, and poses threat of increased toxicity. Apart from these whole body contrast agents, certain specificity of the contrast can be achieved by tissue-specific agents (like hepatobiliary agent Gd-BOPTA (MultiHance[®] – **4** in Fig. 4; BOPTA is the analog of DTPA with one COOH group replaced by $-\text{C}-\text{O}-\text{CH}_2\text{C}_6\text{H}_5$) which show different bio-distribution pattern accumulating in one specific location.^{[17] [28]}

All the agents described above are passive, i.e. their relaxivity is independent on the environment, and resulting contrast stem exclusively from inhomogeneities in their concentration, allowing generally only anatomical imaging.

1.3.6. State of the art in the design of smart contrast agents^{[38] [39]}

Recently, a lot of effort has been made to bring MRI to the league of Molecular Imaging modalities. A step towards this attractive target is a development of “smart” contrast agents which respond to the change in the biochemical condition by changing their relaxation properties and thus modifying a contrast. All parameters discussed in chapter 1.3.3 and 1.3.4 can potentially be envisaged as target for the biochemical stimulus, but in practice for T_1 -responsive agents, most of the strategies are based on the modification of rotational correlation time and hydration number,

Rotational correlation time-mediated change in relaxivity is generally achieved by stimulus-dependent increase of the macromolecule binding or self-assembly. It can be realized by a) metal ions, serving as structural scaffold (Fig. 5A - oligomerization of the contrast agents or Zn(II)-mediated binding to HSA, which increases relaxivity by 40 % in serum)^[40] b) enzymatic catalysis of polymerization^[41]/macromolecule coupling reaction (oxidoreductase, Fig. 5C)^[42] or c) enzymatic cleavage and unmasking the binding moiety (70 % improvement in relaxivity in the presence of 4.5

% HSA was achieved – Fig. 5B).^{[38] [43]} In other example, reduction in “effective” mobility of Gd(III)-based complex bound to protein via prototropically catalyzed formation of additional H-bonds, led to increase of relaxivity from 23 mM⁻¹s⁻¹ at pH 8 to 32 mM⁻¹s⁻¹ at pH 4.^[44]

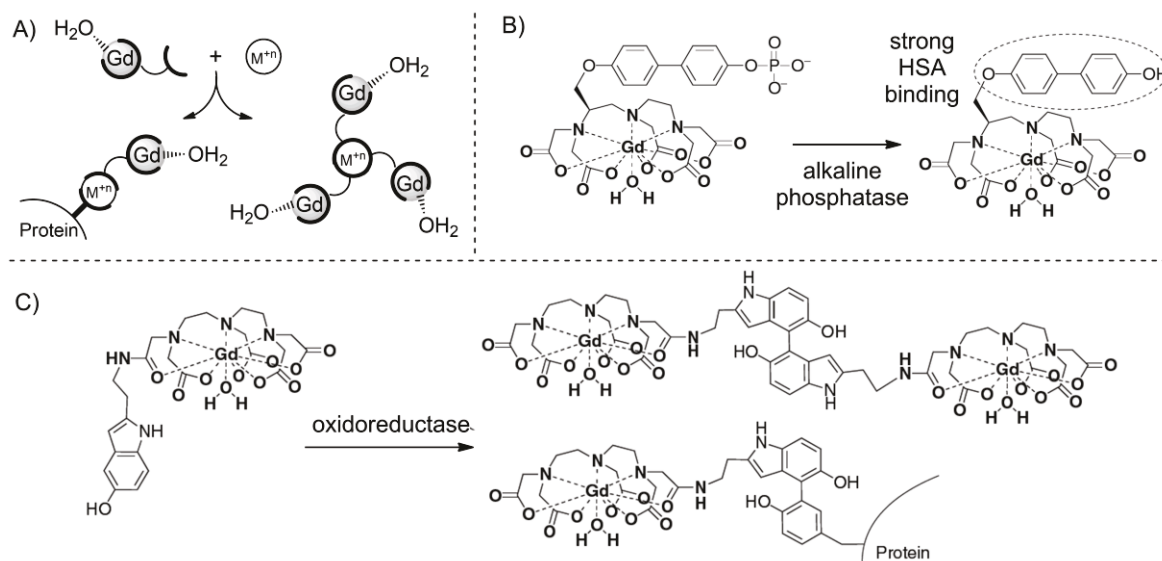


Fig. 5 Examples of responsive strategies aiming at modulation of rotational correlation time. A) Metal-mediated binding to macromolecules or self-assembly B) unmaking binding moiety by enzymatic cleavage C) enzyme-catalyzed protein binding or polymerization. Adapted from Bonnet et al 2013^[38] - with permission of WILEY-VCH Verlag GmbH & Co. KGaA, Weinheim (copyright © 2013).

Unfortunately as mentioned above several times, all the above-mentioned responsive effects are expected to disappear for Gd(III) complexes roughly above 100 MHz (approximately 2.4 T). The overwhelming advantages of *higher sensitivity and greater spatial resolution offered by the stronger magnetic fields*, which more than offsets the intrinsic decrease in r_1 with increasing field, *limits any practical interest of τ_R -based responsiveness*, at least of GBCAs, especially if fine molecular imaging of even cellular distribution of low abundance targets is desired. Even if currently 1.5 T (64 MHz) and 3 T (128 MHz) scanners are the most commonly used in clinics, there exist already the devices for human use which operate at 11.7 T (500 MHz)^[45] and as much as 21.1 T (900 MHz)^[46] magnets can be found in the laboratorial practice for animal use. It is thus easy to imagine the advantages of the ongoing technological progress, if one realizes that even at 3 T only half of the required dose for 1.5 T is sufficient.^[18]

Hydration number q . Responsiveness to the change of hydration number was initially attempted by Meade and co-workers, who designed a Gd(III)-based system, decorated with β -galactose moiety which occupies the space of the ninth coordination site (Fig. 6 A). Upon enzymatic cleavage of the linking bond between the sugar and the complex, β -galactose should be spontaneously replaced by water, increasing hydration number. In practice, 7 days of incubation in unrealistic and highly preferential conditions (1000-fold substrate excess and enormous enzyme quantities) led to only 20 % shortening of the T_1 ^[47]. Introduction of a spacer between the binding unit and the enzymatic substrate improves the enzymatic conversion, but the unmasked self-

immolative arm did not eliminate due to the stabilization from the metal binding (chelate ring formation – see bold in Fig. 6 C).^{[48][49][50]} Only recently a first successful example was reported by Hasserodt et al,^[51] (for discussion see below and chapter 3). Oppositely, unmasking a coordinative moiety upon enzymatic cleavage in another Gd(III)-based $q = 2$ complex (Fig. 6 B) led to 10 % decrease in relaxivity ($q = 1$).^[52]

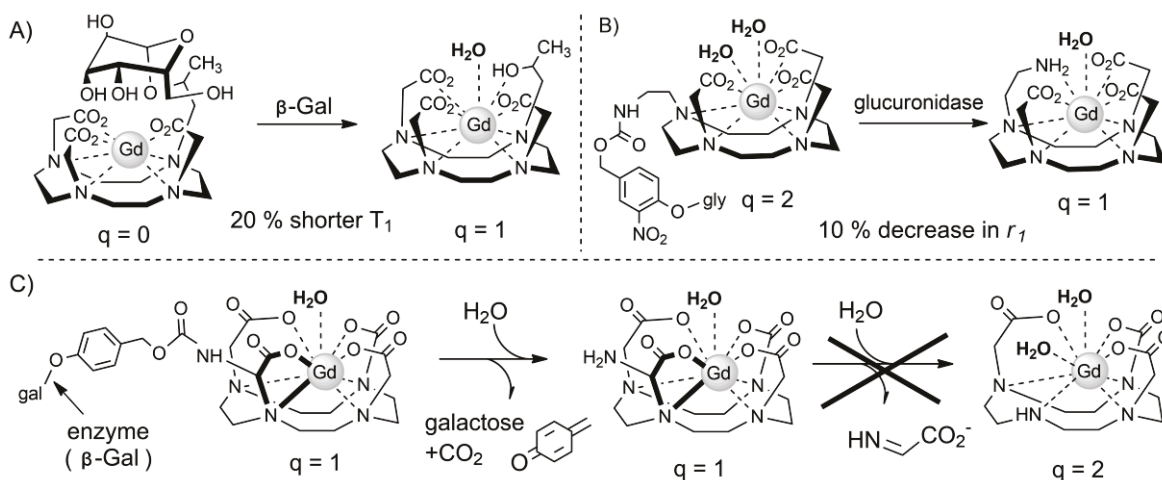


Fig. 6 Enzyme-responsive relaxivity changing strategies based on modification of a hydration number. A) liberation the coordination site – increase in relaxivity upon enzymatic cleavage B) unmasking of binding moiety – decrease in relaxivity C) example of failed attempt – demonstration of the challenge of breaking the chelate ring. Inspired from Bonnet et al (A) ^[38] and Hasserodt et al (B and C) ^[53].

Second approach is based on competition between analyte binding and metal (Gd(III)) coordination (Fig. 7). In one variant of Gd-based complexes, protonation of the bidentate anion HCO_3^- ^[54] or mono-coordinating arm of significant steric clash (one coordination site is sterically masked - Fig. 7 B) ^[55] leads to approximately 300 % increase in relaxivity upon $q = 0$ to $q = 2$ transformation (respectively 1.9 vs. 7.2 $\text{mM}^{-1}\text{s}^{-1}$ and 2.0 vs. 8.0 $\text{mM}^{-1}\text{s}^{-1}$). For initially mono-hydrated chelate, the effect amounts to 70 % increase when adding second water coordination site (4.1 to 7.0 $\text{mM}^{-1}\text{s}^{-1}$).^[56] In another variant a coordinated portion of the Gd(III)-chelate will preferentially bind the targeted metal ion (Fig. 7A), increasing the water accessibility and thus raising r_1 by 70 – 80 % for Ca(II) (10 % *in vivo*) ^[57] up to 103 % ^[58] for Zn(II) (33 % in human blood serum) ^[59] and even 360 % for Cu(I) ^[60] with 2 μM detection threshold for 0.1 mM probe concentration *in vivo* ^[61].

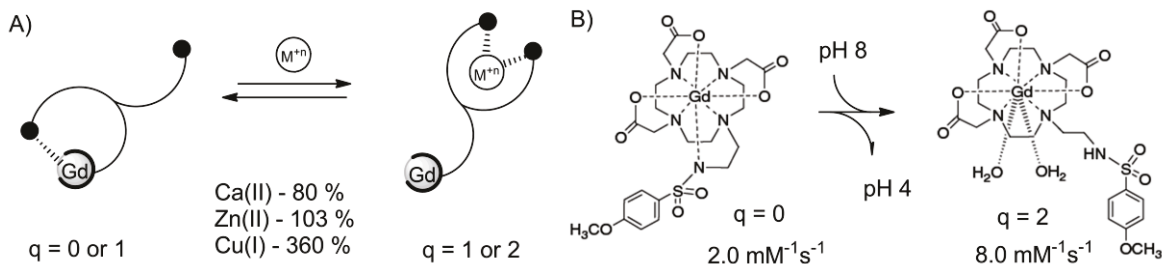


Fig. 7 Changing the hydration number upon analyte's competition for interaction with a coordinated arm A) detection of cations B) pH responsive probe based on the same mechanism. Inspired from Bonnet et al 2013.^[38]

While increasing the hydration number is a direct and efficient way to modify the relaxivity, independently on the external field, it also drastically increases kinetic lability, which directly leads to greater release of highly toxic free Gd(III) cation from its complexes, even despite their unchanged elevated thermodynamic stability.^{[62] [63]} In an *in vivo* molecular imaging, where the common deep tissue penetration (or even cell internalization) to access the molecular target increases residence time of the probe in the body, increasing hydration number to 2 has to be avoided, because it implies even greater (or at the best of cases similar) toxicity, than the one observed upon long residence of the commercial CAs of linear ligands, and leading to the nephrogenic systemic fibrosis (NSF).^{[64] [65]} In consequence, the only biocompatible variation in the hydration number for Gd(III) complexes is between $q = 0$ and $q = 1$ form, what in terms of relaxivity means, at best, not more than doubling the initial value (outer sphere-only contribution is at least $1.8 \text{ mM}^{-1}\text{s}^{-1}$ vs. roughly $4 \text{ mM}^{-1}\text{s}^{-1}$ for standard $q = 1$ complex in 1.5 T – 100 % increase).

Modification of other parameters. Change in chemical parameters of the environment could be transformed into the enhancement of the relaxivity *via* the modification of the water relaxation time and second sphere contribution. The former, valid for τ_m -limited relaxivity condition ($T_{1m} < \tau_m$) can be achieved by the prototropic increase in the rate of proton exchange of the bound water. In consequence 51 % increase in relaxivity when going from higher to lower pH could be achieved, and was further increased by attaching the complex to the macromolecule in medium fields (122 % improvement in relaxivity: $10.8 \text{ mM}^{-1}\text{s}^{-1}$ at pH 9.5 to $24 \text{ mM}^{-1}\text{s}^{-1}$ at pH 6).^[66] Combination of the increased proton exchange rate and facility of H-bonding of the ligand (second sphere contribution) allowed for 85 % enhancement in relaxivity (when going from pH 8.5 to 6).^[67]

Biochemically induced changes modifying the relaxivity of contrast agents include also: increase in their solubility by cleaving off the hydrophobic tails^[68], gradual release of the agents from the nanocapsules changing their τ_R and water accessibility^[69] (almost 50 % at 1.64 T), or internalization of the agents upon the specific redox interaction with the SH groups in the cell membrane^{[70] [71] [72]}. The oxygen partial pressure could be monitored by MRI *via* the Eu(III)/Eu(II) redox pair as while the former is a very poor relaxation catalyst, the latter, isoelectronic with Gd can relaxes water more efficiently.^[73]

1.3.7. Directions of development towards molecular MRI

Implications of always ON probes – quantification issue. In practice, all reported systems which respond by the change in r_1 possess an intrinsic relaxivity, which for Gd(III) cannot be minimized below an outer sphere contribution of $1.8 \text{ mM}^{-1}\text{s}^{-1}$ and stem principally from its long electronic relaxation times and always 7 unpaired electrons.^{[20] [38]} In the result false positives and loss of the weak responses in the increased noise due to the probe-derived contribution have to be feared (see also discussion of magnetogenesis in chapter 3). In order to unambiguously associate the contrast to the activation process of such probes and separate it from the effects of inhomogeneous biodistribution (false positives),^[38] precise concentration of the Gd(III) complex at each location is

required. No successful solution of dealing with this problem has been proposed so far for T_1 -CAs; (a) ratiometric methods where r_2/r_1 ratio is used to assess concentration has not been proven *in vivo* while (b) simultaneous injection of probe and control cannot guarantee the same distribution pattern for both, because it might be very sensitive to even small structural differences. The only idea of quantification of the non-silent responsive contrast agent, which may promise truly reliable results, is to introduce two channels of readout, responsive and environmentally inert (for concentration control). Bimodal agents where responsive MRI is coupled to passive SPECT or PET (or MRS) signal, meet this criteria but the need of satisfying the constraints of both modalities complicates the design and what is even more important, implicates also the loss of the harmless character of the MRI scans, highly appreciated in clinical practice.

Off-ON design. Only recently, Hasserodt's group published a first ever examples of the responsive probes for MRI, which do not emit any signal prior to encounter of their target.^{[74] [51]} While it takes advantage of previously explored idea of 0-to-1 increase in the hydration number upon (bio)chemically induced decoordination of one arm of the complex (see above), its fundamental novelty lies in combining it with a diamagnetic-to-paramagnetic ($S = 0$ to $S = 2$) transformation of the central iron(II) ion in a way that it gives a noticeable contrast ($r_1 = 1.29 \text{ mM}^{-1}\text{s}^{-1}$ in phosphate buffer (PB) at 25°C in 7 T, vs. $2.44 \text{ mM}^{-1}\text{s}^{-1}$ found for Gd(III) in the same experimental conditions^[31]).^[75] In the consequence no contribution from the outer sphere of the silent probe (because no paramagnetism is present!) has to be considered and a true off-on activation is possible. The replacement of highly toxic Gd(III) by a biologically recognized metal ion, decreases also the fear of acute toxicity even upon decomplexation. While the whole concept, being also at the origin of this work, is discussed in details in chapter 3, it is worth to mention here, that the selective chemical activation of the probe, giving a black-to-white type of contrast, led to unprecedented relaxivity increase of 700 % in phosphate buffer saline (PBS) - from $r_1 = 0.08 \text{ mM}^{-1}\text{s}^{-1}$ to $0.64 \text{ mM}^{-1}\text{s}^{-1}$) and 250 % in serum ($0.11 \text{ mM}^{-1}\text{s}^{-1}$ vs. $0.39 \text{ mM}^{-1}\text{s}^{-1}$) at 37°C in a very high field of 11.7 T (500 MHz).

Paramagnetic chemical exchange saturation transfer (paraCEST) is a relatively new concept which is based on the lowering of the intensity of the signal of bulk protons (even though other nuclei can also be envisaged) via the exchange with chemically different pool of protons which were saturated by the resonance impulse. Tuning the proton exchange rate (making it slower or comparable to the difference in the Larmor frequency of two exchangeable pools of protons) and maximizing the chemical shift of exchangeable protons in respect to the bulk water (enabling selective saturation of only one type of proton) are crucial in maximizing the effectiveness decreasing the signal ("negative" contrast is generated). Despite minor relevance of paraCEST to this work, and a negative-type responsiveness, its conceptual compatibility with responsive molecular imaging, which targets the intrinsic limitations of currently existing Gd(III)-based smart agents, is worth mentioning. In particular, it a) allows for simultaneous detection of different biochemical stimuli if several chemically distinctive proton types are used and b) enables straightforward access to the molecular designs of zero-to-nothing type of response, by simple

masking/unmasking of a pool of exchangeable protons. For more information, the reader is referred to other bibliography ^[76] [38].

In summary, most of the strategies applied for increasing the relaxivity of classic contrast agents and thus minimizing the required doses, are ill-suited for the challenges (low target abundance, longer residence times increasing toxicity threats) and requirements (cellular resolution ensured by high fields, low background signal) of the molecular imaging. In particular GBCAs, which are optimal choice for passive contrast enhancement, are biased towards molecular responsive sensing due to the intrinsic background signal (false positives, diminished signal-to-noise ratio (SNR)) and toxicity of the metal ion. Thus, alternative solutions better suited for the new paradigms will probably be required, in order to make the jump from proof-of-concept to real life applications *in vivo*. In this context, transition metal ions with a rich coordination chemistry, sensitivity of the electronic configuration (and thus magnetism) towards chemical environment and certain biocompatibility, may be an attractive system, the potential of which still is largely unexplored.

2. MAGNETIC RESPONSIVENESS IN METAL COMPLEXES

In this chapter I will explain why first row transition metal complexes are the optimal choice for the design of magnetically responsive probes and I will summarize the literature on the reversible magneto-modulation (change of the magnetic properties) in solution upon chemical stimulus. This should provide the reader with an overview over the parameters determining the number of unpaired electrons in metal complexes (and thus their paramagnetism) as well as on how to make the electronic configuration of the metal ion “feel” the presence of the chemical analyte in the environment.

Major part of these considerations are also covered by a minireview “Magnetogenesis in water induced by a chemical stimulus”, which I have co-authored and which has been recently accepted for publication by *Angewandte Chemie International Edition*.

2.1. Introduction to LS-HS equilibria in transition metal complexes

2.1.1. Metal ion complexes as attractive paramagnetic systems

As discussed in more details in chapter 1.2 the total magnetic moment, which generally describes the paramagnetic quality within the sample, is the sum of the magnetic moments of all atoms. However in molecules, where atoms are bound to one another, the valence shell electrons of distinct atoms, interact to create the new molecular orbitals from the atomic ones and thus the electronic configuration is altered, leading usually to “pairing up” of the electrons. The unpaired electrons in organic molecules are called radicals and in the majority of cases they are very reactive and unstable. Metal ions are special in their nature, as they possess stable unpaired electrons and can form coordination compounds, in which the unpaired electrons are still preserved. Thus, the metal complexes constitute the great majority of all single molecule paramagnetic compounds known, but it is only the complexes of few of the 1st row transition metal ions which are capable of adopting at least two magnetically different states depending on the coordinating environment. This is the principal requirement when envisaging the application as responsive probes, what together with the fact that biggest magnetic differences exploitable in single molecules are offered by these metal ions makes them the optimal choice for the design of magnetically responsive probes. Thus, further discussion will focus entirely on these metals and the factors determining the stabilization of low spin (less unpaired electrons) and high spin (more unpaired electrons) configurations, and in the same time the effective magnetic properties.

2.1.2. Sensitivity of d-orbitals' energy on anisotropic ligand field

Provided that the number of the electrons is not altered (no redox – oxidation state unchanged), the modification of the electronic configuration of the metal ions (number of unpaired electrons) which is the essence of the magnetic responsiveness, is possible only thanks to the splitting of the initially degenerate d-orbitals into different energy levels upon the approach of the ligand(s). Unlike s atomic orbitals, the valence d-orbitals of metal ions possess the electron density which is not uniformly spread around the nucleus. Each of five d-orbitals representing the distribution of the electron densities around the nucleus, differ from the others by its precise shape and/or orientation, as presented on Fig. 1. Upon the approach of the ligand, the interactions between the ligand and the metal ion drive the formation of the complex by a creation of the new lower-energy bonding molecular orbitals. However, the energy of the d-orbitals, which in the complex become the anti-bonding ones, increases due to the electronic repulsions between them and the electrons of the ligand. As the ligand approach has its specific direction, the anisotropic “ligand field” is generated, which affects some of the d-orbitals more than the others, splitting their energies and removing the previously existing degeneracy. This new energetic arrangement of the orbitals may then lead to the electronic rearrangement within the d-subshell and hence may alter the number of the unpaired electrons in the molecule, changing its magnetic properties.

2.1.3. Electronic configuration as a function of pairing and splitting energies

In fact, the electronic configuration of the transition metal ions is a consequence of the energetic balance between the two principal parameters: spin pairing energy and the splitting energy (the energetic difference between the d-orbitals). If the pairing energy is higher, then the electrons will occupy the higher energy d-orbitals before pairing up on the lower ones, hence favoring the high spin configuration. With the increase in the splitting energy, the tendency to pair up the electrons, rather than occupying the higher energy orbital, increases, leading to the low spin state.

Different parameters influencing both values are discussed, followed by the short recapitulative and the simple empirical models enabling an estimation the tendency of each metal-ligand compilation to adopt different magnetic states.

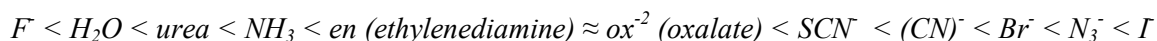
(a) Factors affecting pairing energy

Nature of the metal ion. The endoergic process of pairing up the electrons on the same orbital has two major energetic consequences: 1) overcoming the electrostatic (Coulombic) repulsions between the two negatively charged electrons and 2) loss of the exchange energy derived from the Hund's rule, which is in fact a stabilization energy that is gained upon the increase of the number of unpaired electrons. The former contribution to the pairing energy decreases with an increasing "size" of the orbital, i.e. the further it is from the nucleus the larger the space it occupies and thus the easier it is to fit two electrons in it. Indeed, the 4d and 5d transition metal complexes are almost exclusively low spin, demonstrating that the pairing energy for these ions is minimal, in comparison to 3d ones. The latter effect, which postulates the higher stabilization energy of the systems with increasing number of unpaired electrons, demonstrates well in the high tendency of d^5 configuration (Fe(III) and Mn(II)) to adopt the high spin state over the low spin one.

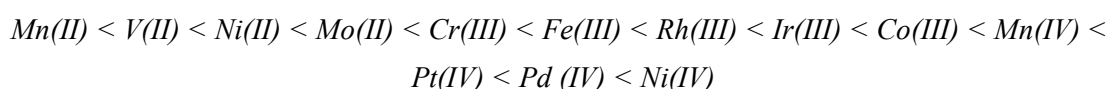
Covalency of ligand-metal interaction - nephelauxetic effect ^{[77] [78] [79]} Metal ion binding to the ligand will generally decrease pairing energy by increasing the size of the electronic cloud. This influence, termed nephelauxetic effect ("cloud expansion"), is the result of the certain covalency (sharing the electrons between both binding partners) of metal-ligand interaction, which can be decomposed into the so called central field covalency of major contribution and minor symmetry restricted covalency. The former refers to the decrease of the effective charge of the metal ion experienced by the valence d-electrons in the consequence of the ligand electron-donation. Similarly to the change in the oxidation state of the metal ion described above, this will weaken the strength of the attraction of the electrons by the nucleus and thus will enable them to occupy the bigger space, lowering the electrostatic repulsions. The latter (symmetry restricted covalency) stems from the delocalization of the electrons on the ligand (with σ being usually more pronounced than π), what is generally more efficient with the e_g -electrons than the t_{2g} ones.^[78]

Formally, the electronic repulsions in metal complexes are described by the Racah parameters A , B and C . While A characterizes the average repulsion energy of electrons (principally does not vary provided the same electronic configuration) the parameter B characterizes the specific electronic

repulsions within the valence d-orbitals (C being less sensitive to outer shell electrons, and usually approximated to $4B$ [77]). In the consequence, nephelauxetic effect can be quantified by the ratio β of the Racah B parameter in the complex (B') to the one for free ion in gaseous state (B). Generally, complexation decreases the pairing energy by roughly 20 %, but as I have mentioned above, the effect is strongly dependent on the nature of the ligand. [78] Thus, the ligands can be organized in the so called nephelauxetic series, according to the influence on the electron-pairing energy, from the weakest (with strongest ionic character of ligand-metal interaction) to the strongest for most covalently bonding ligands, which will also favour the low spin state configuration: [77]



The nephelauxetic effect, as is the covalency of the bonding, is thus also dependent on the metal ion, being increasingly pronounced in the following series: [77] [79]

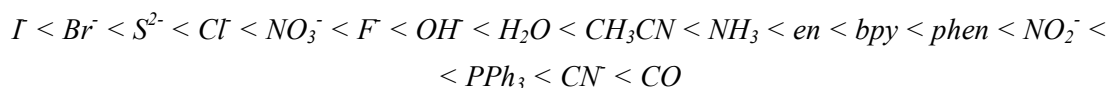


(b) Splitting energy – ligand field effects

Anisotropism (geometry) of the ligand field While pairing energy is principally dependent on the intrinsic nature of metal ion, the splitting energy is in its major part a consequence of the coordination environment (ligand field) and thus its modification is the crucial way, by which the targeted stimuli can be coupled to the magnetic response. The splitting energy depends on the geometry (and symmetry) of ligand's approach: the stronger the overlap of the ligand filled orbitals with the d-orbitals of the metal ion, the greater the effect exerted (the stronger the ligand field) and the energetic difference between d-orbitals increases, favoring the low spin state. This has also its consequences in splitting energy differences between the complexes of different shape. For instance, square planar and tetrahedral complexes are both formed upon the approach of four ligands, but in the square planar geometry the approach is exclusively along the x and y axis, thus strongly destabilizing the $d_{x^2-y^2}$ orbital. The effect on the d_{xy} orbital which lies between the X and Y axis as well as the d_{z^2} orbital which has its part also within the XY plane, is moderate, and there is a high stabilization of the d_{xz} and d_{yz} orbitals which are almost non overlapping with the approaching ligands. Hence, the energy difference between the orbitals is significant. By contrast in the case of tetrahedral complexes, the ligand field is somewhat less anisotropic, hence decreasing the splitting effect. In octahedral complexes, which constitute the majority of all transition metal coordination compounds, six ligands interact with the metal orbitals, with two of them along each axis. In the consequence all the orbitals which lie between the axes are stabilized and those which are positioned along them are significantly destabilized ($d_{x^2-y^2}$ and d_{z^2}). The energy splitting in the octahedral geometry is assigned to be $10 Dq$ and due to the commonness of this geometry, it is often a reference value. It is also worth mentioning that while the splitting energy between the most stabilized and the most disfavored orbital in square planar geometry is bigger than in the octahedral

complexes, in the latter case there are only two energetic levels, the splitting of which is the strongest when the closest orbitals are considered.

Nature of the ligand – σ and π -bonding. The splitting energy also depends on ligand electronics. Strong σ -bonding, as exercised by charged ligands and those of the type NH_3 etc., shorten the metal-ligand distance causing donor electrons to get closer to d electrons and thus inducing the larger energy splitting, which favors the low spin state (LS). The electrons of π -donating ligands destabilize π -bonding and weaken the field splitting. In contrast, π -accepting ligands increase the field splitting because they partially accept the electrons from the d-orbitals of the metal, decreasing the electronic repulsions around it and thus encouraging even more σ donation. In turn, this sigma donation pushes the metal electrons even more towards the empty ligand π^* -orbital increasing the electron density on the ligand and thus also the electronic repulsions, increasing the σ -donation. This synergic interaction strengthens (shortens) the ligand-metal bond, increasing the ligand field. The accuracy of these theoretical considerations is well proven by empirically established spectrochemical series, which order the different types of ligands according to the strength of the ligand field exerted on the metal ion as seen below:

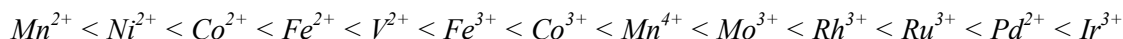


When considering the donor atom, the splitting energies increase in the following order $\text{X} < \text{O} < \text{N} < \text{C}$ which is roughly consistent with decreasing electronegativity of donor atoms and thus the covalent character of the coordination bond. It is in line with the fact that the splitting energy increases when the overlap between the ligand electrons and metal orbitals increase, and the σ -donation from the ligand is the strongest; bonding covalency means that the metal-centered d-orbitals contribution to the coordination bond is higher than in the case of ionic interaction, where the electron density stays rather closer to the ligand and thus exerts less effect on the energies of metal orbitals (less σ -donor character). The decisive effect of the π -acceptance in increasing the effective ligand field is manifested in the class of N-donor ligands, where the stronger σ -donating ligands like NH_3 or ethylenediamine (en) (primary amines) exert lower ligand fields than less basic (less σ -donating) bipyridine (bpy) or phenantroline (phen). This is due to the extension of the pi-conjugated system, which lowers the energy of the π^* orbital and hence encourages the back-donation of the metal d-electrons. Both σ donation and π -accepting are responsible for a very big splitting energy observed in the case of PPh_3 and related ligands.

Nature of the ligand – steric congestion. Despite the important insight into the influence of the ligand electronic character on the splitting energy of metal complexes given by the spectrochemical series, in practice it may sometimes come out to be invalid. One of the reasons of the possible discrepancies are the steric hindrances between the approaching ligands, which may be unable to achieve an optimal overlap of the ligand orbitals with the metal ones and thus limiting the ligand effect – lowering the splitting energy – inducing the HS state. The other common source of deviations from this series is the compatibility of the ligands with metal ions. For those metals with higher number

of electrons in the d-orbital (or lower oxidation states), the pi-accepting character of the ligands may be of crucial importance and thus will determine the effective ligand field, as the back-donation phenomenon is a priori more pronounced in those cases. On the other hand, the higher oxidation state metal ions will favor the ligands with the strongest sigma-donation (so the charged ones for example) as the contribution of the electrostatic interactions to the decrease of the ligand-metal bond and thus the increase of the splitting energy, may in this case be dominant.

Effects of metal ions on splitting energy have also a ligand nature-independent origin and led to the following series based on the relative splitting energies estimated for various metal ions::



The higher oxidation number will not only favor the negatively charged ions, but, from the same reasons, will generally increase any ligand field as the metal-ligand distance will decrease increasing the overlap of the ligand electrons with the metal orbitals, favoring the LS state. Dramatic increase of the size of d orbitals with increasing n quantum number (going from 3d to 4d and further to 5d metal ions) also results in the increased electronic overlap, and thus a drastic rise in the splitting energy. In the consequence practically all complexes of the second-row metal ions are low spin as the intrinsically increased splitting energy will almost always remain higher than relatively low pairing energy for these ions.

(c) Simple estimation of the stability of LS-HS states in typical metal-ligand pairs

Jorgensen^[80] ^[81] has developed very simple models which use the tabulated empirical parameters (Table 1)^[79] for selected ligands and metals to approximate the values of the splitting energy, Δ_0 , (equation (10)) (10 Dq) and pairing energy, P (equation (11')), with the inclusion of the nephelauxetic effect (β – equation (11')). They enable also to assess the tendency of different metal ion-ligand type pairs to adopt either low spin or a high spin state in ideally octahedral complexes. The equations are as follows:

$$\Delta_0 = f * g \tag{10}$$

where f is a ligand parameter and g is the metal ion parameter, and

$$(1 - \beta) = h * k \tag{11'}$$

and

$$P = P^0 * (1 - h * k) \tag{11''}$$

where h is a ligand parameter, k is the metal ion parameter and P^0 is the pairing energy in the free metal ion in the gaseous phase.

The severe approximations of the model does not allow for estimating the effects of the subtleties in the parameters described in chapter 2.2.3 which are at the end vital in determining the effectiveness of the magneto-modulating molecular design. Nevertheless, surprisingly precise

values obtained with this method for simple ligands in octahedral complexes might be a good starting point in judging the potential of magnetically responsive systems.

Config	Cation	g [cm^{-1}]	k	P^0 [cm^{-1}]	Ligand	f	h
$3d^5$	Mn^{2+}	8000	0.07	25500	$(\text{CH}_3)_2\text{NCHO}$		1.20
$3d^8$	Ni^{2+}	8700	0.12		Br^-	0.72	2.30
$3d^7$	Co^{2+}	9000		22500	Cl^-	0.78	2.00
$3d^3$	V^{2+}	12000	0.10		CN^-	1.70	2.10
$3d^5$	Fe^{3+}	14000	0.24	30000	en	1.28	1.50
$3d^3$	Cr^{3+}	17400	0.20		F^-	0.90	0.80
$3d^6$	Co^{3+}	18200	0.33	21000	H_2O	1.00	1.00
$4d^6$	Ru^{2+}	20000			I^-		2.70
$4d^7$	Rh^{3+}	27000	0.28		N_3^-	0.83	2.40
$5d^6$	Ir^{3+}	32000	0.28		NCS^-	1.02	
$5d^6$	Pt^{4+}	36000	0.60		NH_3	1.25	1.40
$3d^4$	Cr^{2+}			23500	ox^{2-}		1.50
$3d^6$	Fe^{2+}			17600	py	1.23	
$3d^4$	Mn^{3+}			28000	SCN^-	0.73	
$3d^3$	Mn^{4+}		0.50				
$4d^3$	Mo^{3+}		0.15				
$3d^7$	Ni^{3+}			27000			
$3d^6$	Ni^{4+}		0.80				
$4d^6$	Pd^{4+}		0.70				

Table 1 Summary of Jorgensen parameters for estimation of splitting and pairing energies of transition metal complexes of common ligands. Data collected from House et al 2013 [79] and George et al 1959 [82].

2.1.4. Practical cases – metal ions with low spin – high spin duos

In experimental practice, the examples of species which may effectively adopt low spin or high spin configuration, depending on the coordination sphere, are principally limited to (pseudo)-octahedral complexes with a d^4 to d^7 configuration and exceptionally also d^8 configuration if the change of geometry from square planar (LS) to tetrahedral (HS) is taken into account.^[83] (Fig. 8). The only diamagnetic configurations within this set is the low spin d^6 (Fe(II) and Co(III)) and the low spin d^8 in a square planar ligand field (Ni(II)). In the high spin configurations, these metals have respectively four ($S = 2$) and two ($S = 1$) unpaired electrons, the former being the highest spin difference per metal ion attainable for the transition metal complexes without a change of the oxidation state. However, in practice, the high splitting energy induced by the Co(III) results in the stabilization of the low spin state in the great majority of its complexes; ligands exercising a particularly weak ligand field (fluoride) are required to turn it into its HS state (see CoF_6^{3-}). The other configuration in which the low spin and the high spin state differ by four unpaired electrons ($7/2 - 1/2 = 2 = S$) is d^5 with Fe(III) and Mn(II) but the latter metal ion suffers from such an elevated pairing energy that it is very difficult to attain its LS state.^[84] In the case of configuration d^4 (Cr(III) and Mn(II)), the low spin state has two unpaired electrons ($S = 1$) and in the high spin

configuration all four are unpaired ($S = 2$). The remaining d^4 metal ions, Ni(III) and Co(II), have the theoretical spins of $S = 1/2$ and $S = 3/2$ for LS and HS respectively.

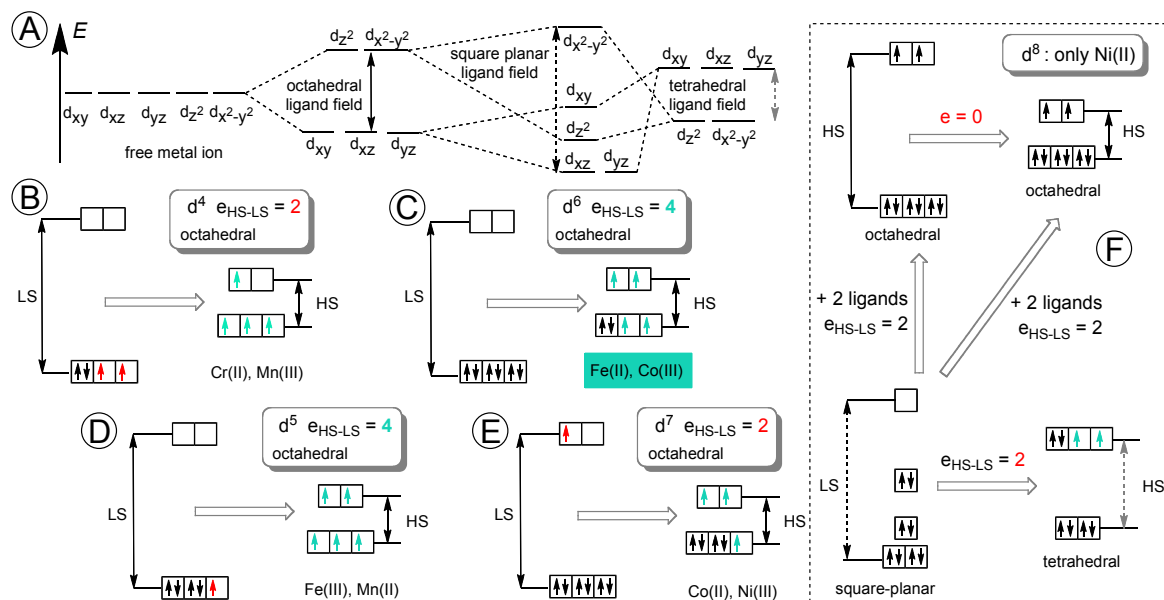


Fig. 8 A) d-orbitals' energy splitting in ligand fields of different geometries B-E) d-electronic configuration in low spin and high spin state of octahedral complexes of first row transition metal ions F) square planar (lower) vs. octahedral (upper) magnetic equilibrium of Ni(II). Reproduced from Hasserodt et al 2013^[53] - by permission of WILEY-VCH Verlag GmbH & Co. KGaA, Weinheim (copyright © 2013).

2.2. Magnetic responsiveness in solution upon chemical stimulus [53]

Change of the magnetic properties upon external stimulus is extensively explored due to its attractiveness for the development of molecular devices, including switches and sensors. The field is however largely focused on the physical stimuli and/or principally on the solid state samples and so they will not be covered in this work. For more information, the reader is referred to multiple reviews including an excellent work of Sato et al (2007) [85] and the two comprehensive compilations edited by Gutlich and Goodwin (2004) [86] [87] [88] and Halcrow (2013) [89].

The following chapter will address only the examples of *single molecules* changing their magnetic properties *in solution* in the response to the *chemical environment*. The majority of the reported cases involve the complexes of the low-denticity ligands what hampers their stability, especially in complex and competitive media like aqueous solutions and biological samples, which are of prime interest for the real-life applications. In the consequence they are not suitable for use as molecular probes, but their analysis may lead to mechanisms of magnetic responsiveness to the analyte-complex interactions which can potentially be explored for sensing if only made specific and introduced to more stable systems.

2.2.1. Introduction to reversible magneto-modulation

In the first part of this chapter I have described the properties of metal ions and ligands which influence the d-electronic configuration and thus the magnetic properties of the compounds. Now the question arises how can these parameters be modified in a controllable way upon chemical stimulus (or more precisely upon different types of complex-analyte interactions) to the extent which implies the change in the number of unpaired electrons and thus in magnetism?

In practice, the only way to chemically modify the intrinsic properties of the selected metal ion is to change its oxidation state, (i.e. the number of the d-electrons), in the process of the inter or intramolecular electron transfer. The former requires a redox-active analyte (in other words a certain redox potential), what might be of particular interest for biomedical applications due to their principal role in controlling the processes of life, including also an evolution of pathologies like cancer.^{[90] [91]} However, the intermolecular redox-based recognition is potentially unselective and requires specific molecular considerations which cannot be directly extended to other chemical activities or analytes and are not fully relevant to the subject of this work, thus it will not be discussed in here despite its attractiveness. On the other hand, the latter does not lead to the overall change in the charge of the complex and so can formally generate the maximum gap in magnetism of only two unpaired electrons, what lags behind some of the classic low spin - high spin equilibria, so its interest for the design of magnetically responsive probes is low. However, the change in the oxidation state of the metal might be coupled to the subsequent change in the spin state as it has a strong influence on the pairing and splitting energies (compare the estimated stability of HS and LS states in Fe(II) and Fe(III) ions). This might theoretically result in the biggest magnetic change

envisaged for mononuclear compound which is from 0 to even 6 unpaired electrons for theoretical d^6 LS-radical precursor – d^5 HS-radical equilibrium. While intermolecular charge transfer required an external redox activation, the intramolecular process can be induced by any chemical interaction which inverses the energetic position of the distinctive HOMO-LUMO orbitals of the donor and acceptor part of the molecule respectively (provided the existence of intramolecular electron transfer mechanism which is relatively easy to achieve). Hence, this process can be controlled by modifying the coordination sphere, which is a much more attractive target for fine tuning the magnetic properties as a function of chemical composition of the environment, and thus is of principal importance for the design of magnetically responsive systems. In the consequence, the magnetism of valence tautomeric compounds (stability of redox isomers) can be controlled in similar ways as complexes exhibiting simple spin-state equilibria and thus examples of both types of systems will be discussed below.

The unique sensitivity of magnetic properties of metal ion complexes to the environment stems principally from the tunability of the coordination sphere i.e. magnetic responsiveness to non-redox analytes is always caused by the changes in the coordination sphere. These changes may be the consequence of the analyte's interaction with a periphery (i.e. coordinated ligand) leading to the modification of the existing coordination bonds, like length (strength) and/or symmetry among others (see chapter 2.2.2.). In other variant, the analyte will directly bind to the metal bringing about more drastic changes to the coordination sphere (coordination bonds' formation and/or breaking) potentially leading to a more drastic magnetic changes (chapter 2.2.3). Certain number of solution phase examples exist and many of them have already been reviewed.^{[92] [93] [94] [95] [96]} With the only exception of the recent work of Hasserodt et al ^{[74] [51]} (see chapter 3 for more details), all the other cases are based on the reversible shift of the chemical equilibrium between the magnetically distinct forms. This reversibility stems from the reversibility of the complex-analyte interactions usually implying a partial change in the ratio between the two coexisting states and subsequent alteration of the degree of paramagnetism. I will thus refer to this process as magneto-modulation, which is more general term than magnetogenesis, discussed in the next chapter and denoting *de novo* generation of the paramagnetism in the sample.

2.2.2. Magneto-modulation via the periphery of the probes

Interactions leading to the change in the magnetic properties of the solution of metal complexes, provided their stability in the media, include principally non-specific electrostatic solvent effects, ion pairing and specific hydrogen bonding, in order of increasing influence.

(a) Non-specific electrostatic interactions

Influence of the increased ability of the solvent to interact with the probe (solvability) on the magnetic properties of metal complexes in spin equilibria ^[97] involving a non-specific electrostatic interactions, can be interpreted in the terms of the “chemical pressure”. By analogy to the physical phenomena which has been observed for solid samples of the spin crossover (SCO) compounds,

the increase in the chemical pressure (stronger solvent-solute interactions – more “polar solvents”) “squeezes” the chelate, stabilizing the less bulky state, which usually means the LS one (low spin complexes have shorter bond lengths than the high spin ones^{[98] [83]}). In addition, this squeezing can be imagined to bring ligands closer to the metal center (shortening of the coordinating bonds) increasing the ligand field and thus further stabilizing the low spin state. In practice these effects are very subtle and thus they could be potentially proposed to explain the solvent-sensitivity only in cases where other mechanisms, including for example H-bonding, were not identified.^[99]

Ion pairing between anions and positively charged metal complexes was also proposed to alter the magnetic equilibria by stabilizing the low spin state,^[100] The effect is usually limited to the apolar media and increases at higher concentration; in polar solvents where solvation enthalpies are significant, the overwhelming excess of solvent molecules removes it. Analysis of magnetic properties of the spin transition $[\text{Fe}(\text{bzimpy})_2](\text{ClO}_4)_2$ complex (bzimpy – dibenzimidazolepyridine) revealed the unusual stabilization of the low spin state in very poor hydrogen-bond acceptors like nitromethane and nitrobenzene, which deviates significantly from the expected trend ($3.29 \mu_B$ and $3.35 \mu_B$ respectively, which is in the range of methanol: $3.0 \mu_B$, and is significantly lower than more polar and much better H-bond acceptors acetonitrile: $3.86 \mu_B$, and acetone: $4.21 \mu_B$).^[101] I suggested that this unexpected behavior may stem from the ion pairing, which in more polar solvents is removed and replaced by H-bonding.

In another case, the stabilization of the low spin state has been associated with the need to increase the cavity within the solvent sheath to adopt to the increased volume of the high spin form.^[102] Energy associated with this process, specific for each solvent, is called “cavity term” Ω which corresponds to the square root of the cohesive energy density, representing directly the van der Waals interactions holding solvent molecules together. It is sometimes introduced to the Linear Solvation Energy Relationship (LSER) for predicting solubility (it is in fact equal to the Hildebrandt solubility parameter),^[103] but seems promising also for the analysis of some magneto-modulation examples in solution. However, the differences in Ω^2 between different solvents do not entirely explain the solvent-dependency in this system. Comparison of the relative strength of H-bonding (Hansen solubility parameter δ_H denoting the energy of H-bonding)^[104] dipolar interactions (δ_p) and dispersion effects (δ_d) in pure solvents reveals the strongest influence of the polar ion-dipole complex-solvent interactions on the position of the spin equilibrium, with the simultaneous (but smaller) importance from the cavity term explained above. In the consequence, acetonitrile ($\delta_p = 18.0 \text{ MPa}^{1/2}$) stabilizes the LS state even more (spin transition temperature $T_{1/2}$ is 345 K) than ethanol ($\delta_p = 8.8 \text{ MPa}^{1/2}$ and $T_{1/2} = 336 \text{ K}$), even though the latter has much bigger cavity term. The inverse relationship between the spin transition temperature (stabilization of the LS state) and the polar parameter is observed for the pair of dichloromethane (DCM) and acetone, what in here indeed is in line with the cavity term differences.

For several valence tautomeric systems,^{[105] [106] [107]} the solvent-dependency of the magnetic (and charge) equilibria can be rationalized on the basis of the difference in the solvation energy between

the higher and lower metal ion oxidation state, as proposed by Benelli et al.^[108] Despite the fact the net charge of both isomers remains the same (because the charge transfer is intramolecular), the variation in the asymmetry of charge distribution (radical is only on one side of the metal ion) and molecular volume (bond length in higher oxidation state is shorter) in these complexes leads to the higher solvation energy (stronger “chemical pressure” in the sense) of the high oxidation state form, and thus its stabilization over the other one in solvents of increasing solvation properties (polarity). The strongest solvent-dependency, which can be explained by this rationale, was observed for the two-electron transfer system $(\text{Mn(IV)})(\text{cat})_2(\text{py})_2$ ($S = 3/2$) vs. $\text{Mn(II)}(\text{SQ})_2(\text{py})_2$ ($S = 7/2$) (where py is pyridine, cat is catecholate and SQ is semiquinoline).^[109] The 100 K difference in the transition temperature between the toluene (250 K) and pyridine (350 K) meant that in the RT the whole population was in the more paramagnetic state in toluene and a change of the solvent to pyridine led to almost complete switch to the ground state. This almost binary response to the change of the solvent is unique for the reversible systems so far reported and thus could be of some attractiveness for the design of magnetically responsive probes, provided its stability. In all the examples presented so far the increased polarity of the solvent stabilized the less paramagnetic state, generally due to its lower molecular radius and thus, higher effective charge density, which decreases its energy due to the more efficient solvation. The opposite case, where the paramagnetic state is stabilized over the diamagnetic one in more polar solvents (DCM over toluene) is a tetrahedral vs. square planar equilibrium in Ni(II) complex of the Schiff base.^[110]

(b) Hydrogen bonding

Few examples exist where the magneto-modulation can be explained by a formation of the hydrogen bonds between the ligand of the metal complex, which usually possesses the H-bond donor sites like NH, and a H-acceptor (solvent or anion). In order for the H-bond formation to induce the magnetic changes, the H-bonding group has to be directly involved into the coordination bond (like the NH coordinating group) or remain in the electronic communication with the coordinating atom (for example via the π -system). In the consequence, the increase in the electron density on heteroatom involved in the H-bond formation with the analyte increases the σ donation (increase its basicity), what shortens the coordination bond and strengthens the ligand field favoring the low spin state.

Indeed, the relationship between the stabilization of the low spin state and the increasing H-bond acceptor character of the solvents (described by the higher Gutmann’s donor number $\text{DN} = \text{energy released upon the formation of 1:1 adduct between the Lewis base and a standard Lewis acid } \text{SbCl}_5$) was confirmed in the Fe(III)-based complexes of hexadentate trien-like ligands.^{[111] [112]} The effect amounted to the $1.5 \mu_B$ difference between the dimethyl sulfoxide (DMSO) and DCM, and was comparable also for the ternary analogs.^{[112] [113]} The H-bonding sites in this system are in fact the coordinating NH-units and thus the effect of the increased electron density of the N atom is directly connected with the increase in σ bonding. For these complexes, the similar but much less pronounced effects could be observed in acetonitrile when varying the counterion; when BPh_4^- has

been replaced by halides, the magnetic moment dropped by $0.2 \mu_B$ ^[111] - $0.3 \mu_B$ ^[112]. Hydrogen-bonding have also been suggested as a main reason for the stabilization of the low spin state of the ternary iron(II) complex in water ($1.2 \mu_B$, $T_{1/2} = 317$ K) over the organic solvents ($3.3 \mu_B$, $T_{1/2} = 244$ K for the least polar nitromethane), but the complex was prone to decomposition especially in high spin state.^[114]

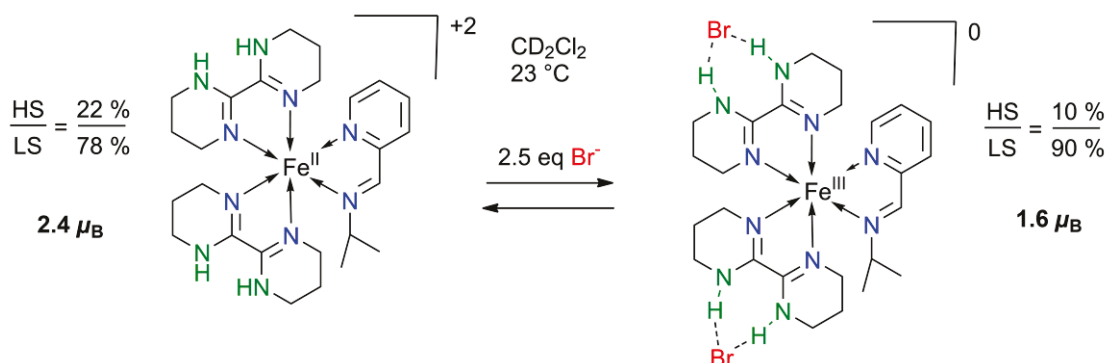


Fig. 9 First concept of magnetically responsive anion chemosensors (here: for Br^- in red) based on H-bonding recognition. Magnetic response is obtained at RT but only in apolar media like DCM. Measured magnetic moment and estimated ratios of high spin-to-low spin state are given in the presence (right) and absence (left) of two equivalents of Br^- anion. In green H-bonding sites. Adapted from Hasserodt et al 2013^[53] - with permission of WILEY-VCH Verlag GmbH & Co. KGaA, Weinheim (copyright © 2013).

The potential of specific H-bonding of the analyte has been also explored by Shores et al. for the design of first magnetically responsive molecular probes for anion sensing.^[115]^[116] The homoleptic quaternary iron(II) complex, possessing three bidentate bis-amidine ligands, each being able to bind the halogen ion with two H-bonds, was shown to respond to the addition of the two eq of Br^- (slightly less for Cl^-) at -40 °C in DCM by a decrease of the magnetic moment from the initial state of $4.7 \mu_B$ to $2.7 \mu_B$.^[115] This change amounts to the decrease of the HS form from 93 % to 30 % and is almost completely absent at RT. The sensitivity to the Br^- anion is somewhat restored at ambient temperature when one of the binding ligands is replaced by a pyridyl-imine type one, which increases the global ligand field and thus stabilizes the LS state, increasing the spin transition temperature (Fig. 9).^[116] In this case, the initial spin equilibrium amounting to the net magnetic moment of $2.4 \mu_B$ (approx. 20 % of HS) was shifted to the low spin side resulting in the value of $1.6 \mu_B$ (10 % HS) in the presence of 2.5 eq of Br^- in DCM (Fig. 9). In order to enable anion detection in more practically relevant polar solvents, where these low-denticity ligand-based complexes are highly unstable, the authors turned to the hexadentate tris(2-aminoethyl)amine (tren)-based ligands.^[117]^[118] In addition, the authors envisaged the alternative design, which theoretically allows for the increase rather than a decrease in the magnetic signal upon anion binding, a significantly more attractive mode of response for the practical applications.^[118] However, despite anion binding in acetonitrile, no change in magnetism could be observed so far and the instability of the probe was not completely suppressed.

(c) Protonation

An extreme case of H-bonding occurs when the proton is completely transferred from the donor to the acceptor. Indeed, in the hexamethylphosphoramide solvent (HMPA), which has a strong Brønsted base character (DN = 30), ternary complex $[\text{Fe}(\text{bzimpy})_2]^{2+}$ was deprotonated.^[101] The negative charge established on the non-coordinating N-atom is delocalized within a heteroaromatic system of benzimidazole, leading to a significant increase of the basicity of the coordinating unit, which is sufficient to render iron(II) purely diamagnetic. In solvents of lower H-bond accepting capacity, the expected gradual relationship between the DN and the amount of the HS state form was reported (acetonitrile: DN = 14.1 (4.21 μ_B , 78 % HS), acetone: DN = 17 (3.86 μ_B) and MeOH: DN = 19 (3.0 μ_B , 56 % HS). Similar magnetic modulation could be obtained by changing the pH of the solution upon the addition of NaOH/HClO₄ in water/EtOH (30:70) but it extends from the completely diamagnetic complex at pH 9 to entirely paramagnetic below pH 3.^[119] In MeOH the addition of 13 eq of Et₃N were required to attain purely diamagnetic state. Sunatsuki et al^[120] have demonstrated that the complete silencing of the paramagnetic compound can be achieved upon the addition of only 3.1 eq of the base which results in deprotonation of three imidazoles on the tripodal hexadentate ligand of the Fe(III) complex in MeOH. The increased pH sensitivity of its magnetic properties in comparison to the previously described example may be partially explained by the increase of the Lewis acid character of Fe(III) in comparison to Fe(II), which in turn increases the acidity of the NH bonds. This improvement in detection is however achieved for a price of permanent residual paramagnetism in the low spin state (for Fe(III) LS $S = 1/2$ instead of $S = 0$ for Fe(II)-LS).

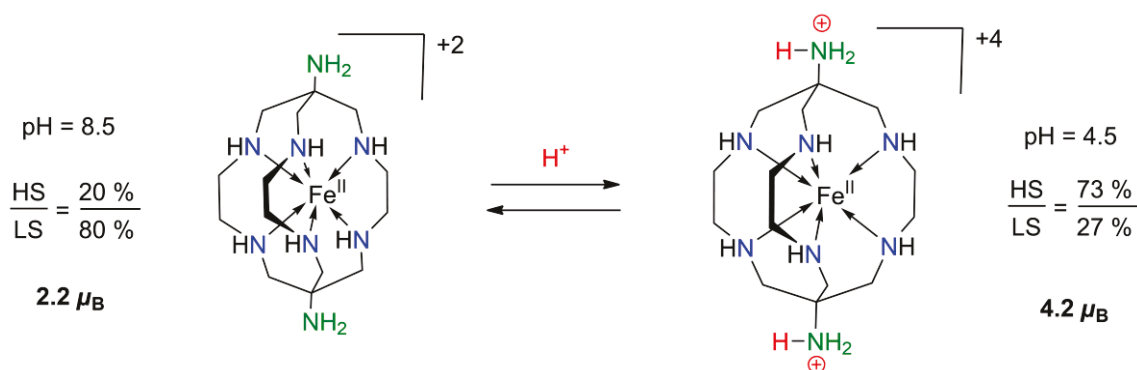


Fig. 10 Magneto-modulation upon protonation of the electronically isolated group (in green) – electrostatic repulsions result in increasing the metal-ligand bond lengths. Measured magnetic moment and estimated ratios of high spin-to-low spin state are given for basic (right) and acidic (left) aqueous solution of the compound at RT. Adapted from Hasserodt et al 2013^[53] - with permission of WILEY-VCH Verlag GmbH & Co. KGaA, Weinheim (copyright © 2013).

Electronic effects are not the only way in which protonation can lead to the change in the magnetic properties of metal complexes. Iron(II) complex of the bicyclic hexadentate aliphatic ligand with six NH-coordinating motifs (sarcophagine), change its magnetic moment from initially intermediate one (2.2 μ_B) to principally HS (4.2 μ_B) upon protonation of the two NH₂ groups attached to the bridging nodes and electronically isolated from the coordination sphere (Fig.

10).^{[121] [122]} The most plausible explanation of this behavior are the electrostatic repulsions between the protonated groups and the metal center which stretch the ligand structure causing the lengthening of the coordination bonds and thus favoring the HS state. The unique feature of this system is its high stability in water, but the sensitivity of the NH coordinated groups to air oxidation and intrinsic incapability of adopting the initially purely diamagnetic state limits its interest for the design of molecular probes.

(d) Lewis acid-base interaction

An original example of the off-on magnetic response induced by the interaction with a periphery was observed in acetonitrile/DCM (5:4) solution of the high-valent manganese oxo-porphyrinoid complex upon the addition of Zn^{2+} , which binds to the oxo-ligand in a Lewis acid-base complex (Fig. 11).^[123] The resulting decrease in electron donor capacity of the oxo-ligand stabilizes the lower oxidation state (IV) of manganese and thus induces the electron transfer from the porphyrinoid part of the ligand to the metal center. This mechanism is similar in its nature to the one discussed for the H bonding, but with opposite effect. In the consequence a highly desired *de novo* induction of the paramagnetism ($4.11 \mu_B$) in initially diamagnetic complex occurs at RT and already after the addition of only one equivalent of the Lewis acid in a solvent of medium polarity. Thus a truly off-on binary response to the presence of the chemical analyte is an undeniable advantage of this system. Nevertheless, while the complex is relatively stable in room temperature despite its high-valent nature, its behavior in more realistic sensing conditions still have to be verified.

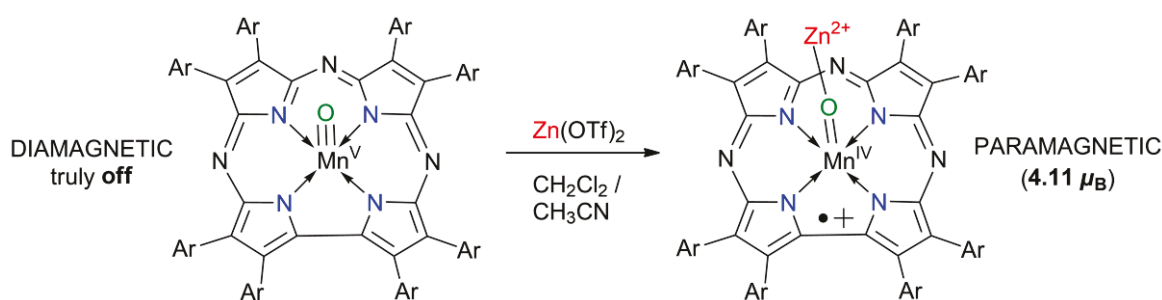


Fig. 11 Magnetic detection of Lewis acid (in red) via charge-transfer induced spin transition. Lewis acid binding leads to a change from an initially diamagnetic state (left) to the paramagnetic analog (right). Adapted from Hasserodt et al 2013^[53] - with permission of WILEY-VCH Verlag GmbH & Co. KGaA, Weinheim (copyright © 2013).

Summary

Non-specific electrostatic interactions, which are usually rather weak and have only a limited influence on the magnetic equilibria (stabilization of the LS state) are not well suited for the design of magnetically responsive molecular probes for more polar media. More specific hydrogen bonding and especially Lewis acid-base interactions, can be potentially made more selective and

theoretically could be envisaged for the design of such probes, but the specificity and high intensity of the response in polar media, and especially in water remain an unmet challenge.

2.2.3. Magneto-modulation via coordinative-bond cleavage/formation

In contrast to the interactions with a periphery, forming and/or breaking of the coordination bonds may generally change the splitting and pairing energy much more drastically, thus leading to a more dramatic changes in magnetism, as desired for sensing purposes. These changes can also be interpreted as the instability of the coordination sphere, which, when controlled, may be envisaged for sensing purposes. In general, two scenarios are possible: 1) replacement of a part of the coordination sphere or 2) a change in the coordination number.

(1) Displacement of ligand(s)

The first in its concept resembles the indicator displacement assays commonly applied in fluorescence-based detection schemes where the replacement of one or more coordination sites on the metal ion scaffold by a molecular target releases the previously quenched fluorophores, giving rise to a reporting signal.^{[124] [125] [126]} In magneto-modulation schemes, the signal generation is not associated with a leaving moiety but with a newly created coordination sphere. Thus in addition to an efficiency of the replacement event, which is the main criterion of selectivity in IDA (indicator displacement assay) strategy, the magnetic response will also depend on the nature of the metal-target bond, which will principally determine the ligand field and thus the splitting energy, providing an additional tool for analytes' distinction.

Replacement of monodentate ligands. In laboratorial practice the systems exhibiting the change in the magnetic properties upon the exchange of three^[127] or two^{[128] [129] [130] [131] [132]} coordination sites in solution are not uncommon. Usually the exchangeable units are acetonitrile molecules (solvent) which initially render the common iron(II) metal ion diamagnetic,^{[129] [131]} but upon the replacement by other analytes (typically anions or substrates in catalysis) the paramagnetism is induced (provided the lower ligand field strength of newly coordinated analytes). The existence of more than one labile sites makes the control of the replacement selectivity very difficult,^[133] and thus, despite some interesting applications of such systems,^[126] their practical use especially in complex media is limited.

On the other hand, systems with only one exchangeable site may a priori be used for the design of responsive magnetogenic probes which would combine the stability in solution with selectivity of the replacement process and still drastic ligand field changes. One of such example can be found in the nature where the paramagnetic quality is created upon deoxygenation of initially diamagnetic heme-triplet oxygen complex,^[134] with antiferromagnetically coupled electronic spins of oxygen and low spin iron(III). This magnetogenesis lies in the basis of a new diagnostic tool, Blood Oxygen-Level Dependent Functional MRI (BOLD-fMRI), for studying principally brain activity and thus being of major importance for neurosciences (Fig. 12).^[135] Several ternary complexes,

principally based on iron(II)-pentadentate ligand units, were found to change their magnetic properties in solution upon the exchange of the monodentate ligand (typically a solvent molecule).^{[136] [137] [138] [139]} Selectivity of sensing in these systems stem from (a) binding affinity and (b) the magnetic effects of coordination. The strength of analyte binding (a), determined by the strength of electrostatic interactions, depends principally on the charge of coordinating unit, favouring anions over electroneutral molecules. If charge is equal, then binding events leading to a more stable (kinetically inert) low spin complexes are favored. In the consequence, addition of even only 1 % of acetonitrile to an aqueous solution of single-site reactive ferrous complex was found to be sufficient to render it fully diamagnetic, proving the low spin complex formation-driven preference for acetonitrile binding over water.^[139] The direction of magnetic switch depends on whether the ligand field exerted by the analyte is weaker (the usual case of the replacement of acetonitrile by majority of anions) or stronger (typically for CN^- , CH_3CN and CO binding) than that of the initial unit. The magnetic response to single-sided variation of the ligand in iron(III)-porphyrinoid complexes, which resulted from the position of the spin equilibria as a function of the stabilization of one of the magnetic states over another by different analytes, constitutes a basis of magnetochemical series - a magnetism-based variation of the classic spectrochemical series discussed in previous chapters.^[140]

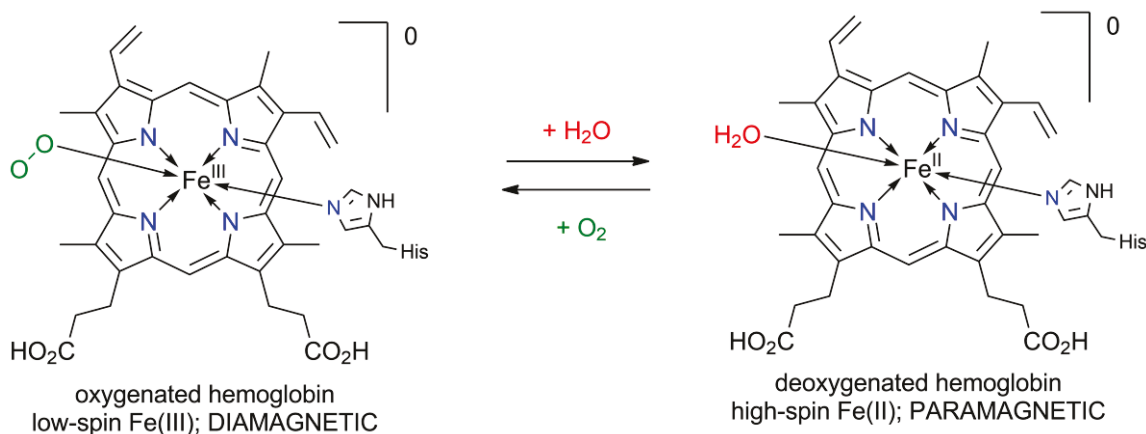


Fig. 12 Natural magnetogenesis in hemoglobine. Bound dioxygen molecule (in green) is in the triplet state. Replacement by water (red) leads to the change in the oxidation state of iron ion and an appearance of paramagnetic quality. Adapted from Hasserodt et al 2013^[53] - with permission of WILEY-VCH Verlag GmbH & Co. KGaA, Weinheim (copyright © 2013).

Decoordination of a tethered arm of the hexadentate ligand, which on the one hand imposes a need of the energetically challenging cleavage of the chelate ring, would in the same way enable a greater analyte selectivity and higher stability of the initial state. Only recently, Hasserodt et al were first to report an example where this process led to a controlled magnetic response.^[74] The initially diamagnetic iron(II) complex of a dipicolyl-triazacyclononane ligand decorated with a pH-sensitive amidine motif was selectively activated upon acidification (pH of transition was 4.5). The primary prerequisite of this concept is the efficient competition of the protons for the electronic density of coordinating unit in aqueous solution, the basicity of which is drastically diminished by

the metal binding (even 7 pH units) and so it requires an initially very basic moiety. Replacement of one of the arms of hexa-dentate ligand by anions (and not pH change) has been successfully attempted for initially high spin complex, but resulting chelate remained high spin and thus in high spin metal complex generally easier due to the higher kinetic lability of the HS over the LS state, but the reported displacement by anion resulted in another high spin complex and thus no magneto-modulation was involved.^[141]

Only after the end of my PhD laboratorial work, a first example has been reported where the replacement (partial) of the tethered arm of a binary low spin complex (diamagnetic iron(II)) upon the addition of an anion (Cl⁻) led to the change of magnetic properties (generation of paramagnetism) in solution (acetonitrile) (Fig. 13). Replacing a labile triazole arm with more basic pyridine removes the effect of anion responsiveness. When triflate (trifluoromethanesulfonate – Tf) was used instead of chloride, triazole arm was not replaced, but the pentadentate analog with one coordination site occupied by the acetonitrile molecule showed magnetic sensitivity towards both anions proving a stabilization effect of the chelate ring. Despite a principal focus of these research on studying catalytic properties, the results are promising for the development of the truly magnetogenic reversible probes for anion sensing, but the assessment of its true potential requires further studies, including anion selectivity and behavior in aqueous media.^[142]

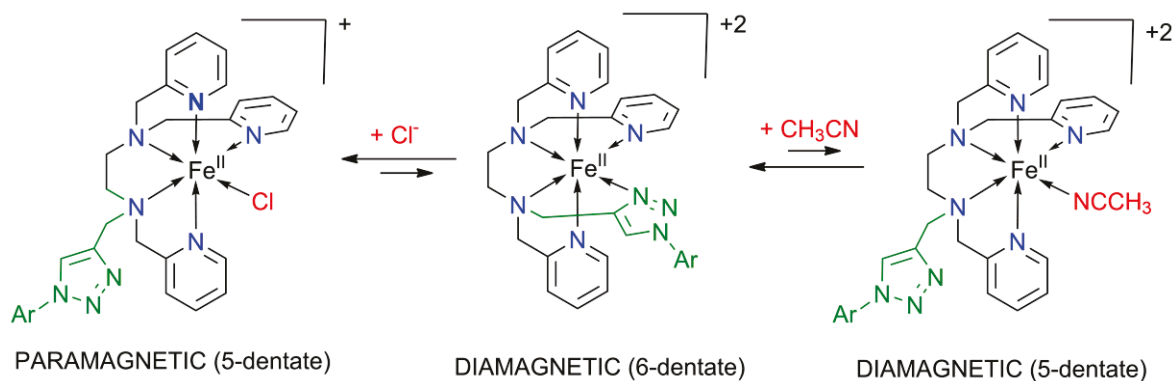


Fig. 13 Recent example of anion-controlled magnetogenesis based on the replacement of the tethered arm (in green) in diamagnetic, binary complex (Segaud et al 2013).^[142]

(2) Change of the coordination number

By far the most common example for magnetic response in solution as a consequence of the change in the coordination number (CN) is the addition of axial ligand(s) to the square planar diamagnetic Ni(II) complexes resulting in paramagnetic octahedral (CN = 6) or tetragonal pyramidal (CN = 5) chelates. Magnetic properties in these systems are determined principally by the geometry of the ligand field and with slight tendency to square-planar stabilization in weaker ligand field^[143]. The square planar geometry favors a low spin diamagnetic configuration of d^8 electrons of Ni(II) and a coordination of principally any ligand in the axial position will always lead to the paramagnetic species, with two unpaired electrons in the octahedral complexes. It is thus the binding tendency which should be modified in order to control magneto-modulation, which depends principally on

the basicity and steric hindrance of the ligand,^{[144] [145] [146]} with some influence of electronic and steric effects of the square planar scaffold.^{[143] [147]} Despite attempts to control these parameters,^{[144] [143] [147] [145] [146]} the stability of the initial square planar diamagnetic state, is challenged by the intrinsic susceptibility to bind strong nucleophiles like water, DMSO and N-donors.^{[92] [148] [149]} Thus, the selectivity especially in the presence of several sterically non-demanding nucleophiles and/or in aqueous solution will always have to be reconciled with the sensitivity of the detection scheme, limiting the practical application of this strategy.

Change in the coordination number can involve also the transition from a LS, CN = 6, octahedral complex to the HS, CN = 7, distorted one. The potentially hexadentate ligand N,N,N-tris(2-pyridylmethyl)- ethylenediamine-N-acetato = tpena) remains pentacoordinated to the Fe(III) in water with one protonated pyridyl group of pKa approx. 5, dangling outside, thus forming a low spin $[\text{Fe(III)(OH)(tpenaH)}]^{2+}$ complex.^[150] Upon the addition of base, deprotonation of the ligand and subsequent coordination of the sixth arm is believed to give rise to the heptacoordinate HS complex. This transition can be reversed by simple addition of an equivalent of the acid. The system seems interesting as a responsive magnetogenic probe, but the confirmation and deeper analysis of the magnetic transition as well as the stability of the complex and tuning of the pH of the dangling group would have to be performed in order to prove its attractiveness.

3. TOWARDS MAGNETOGENIC MOLECULAR PROBES IN METAL COMPLEXES

3.1. Hallmarks of probe's design – a power of magnetogenesis [53]

Successful detection and/or imaging should be *a) specific* (only target-induced signal) *b) sensitive* (maximal SNR) *c) rapid* (fast activation) and *d) not harmful* (non-toxic, non-destructive) for the sample (particularly important for *in vivo* applications). The choice of the physical readout and the particular molecular design will both determine, whether and to what extent these requirements will be fulfilled by the resulting tool. The suitability of paramagnetism for sensing (chapter I) and current strategies in chemical induction of magnetic response in solution (chapter II) were discussed before. Now the question remains, what is the optimal molecular system? Having this in mind we can postulate several most desirable properties which we would like the ideal probe to possess:

- (1) **Maximal signal gap**, which describes the difference between the signal generated by the activated form and the initial state from before target recognition, and is the main component of the SNR. For magnetically responsive probes, it is a difference in the magnetic moment of the two states, and in first row transition metal complexes (optimal for magnetically-responsive probes – see chapter II) it scales up with $S(S+1)$ where S is the spin number. In practice, the greatest paramagnetic difference within one molecule can be attained upon LS-HS transformation of Fe(III) or Fe(II) octahedral complexes (4 unpaired electrons difference, $\Delta I = 2$), or in the result of charge-transfer induced spin transition in the organic radical-iron valence tautomeric complex (maximal theoretical $\Delta I = 3$) (see also chapter 2.1).
- (2) **Binary response**, which means that in the presence of the target, all probe molecules should be transformed by it and thus all should be activated. In order to achieve that, the equilibrium between the initial and activated form should be decided. Reversible probe-analyte binding described in chapter II generally leads to only a partial activation or requires excess of the analyte. On the other hand, if the changes induced by a stimulus would be irreversible, and would lead to activation, the binary response is attained easier. In the consequence, chemical reactivity leading to the cleavage of the covalent bond is an optimal target for designing the 0=>100 % responsive probes.
- (3) **Fast response kinetics**, together with a binary response (2) above, are guarantees of taking the maximal profit from the signal gap described in point 1. Pace of response accelerates the process of getting to the maximal attainable signal, which in the best of cases means a 100 % of the activated probe, allowing also for faster detection. In addition, if spatial imaging is important (precise localization of the signal which is specifically present in only one compartment of the sample), fast activation process decreases the time of attaining maximal

signal, limiting the signal diffusion and minimizing the resolution losses. If a simple detection (no spatial resolution required) of the analyte in a homogenous sample is envisaged, then the diffusion effect is less important, provided that the net total signal of the sample before and after addition of a trigger is collected and measured (only one voxel exists). For reversible binding-type probe-analyte interaction, the recognition is practically instantaneous but it becomes a challenge when the cleavage of the covalent bond is involved, in particular for enzyme detection when enzymatic performance is highly dependent on the recognition of the substrate.

(4) **Robustness** of the probe, especially its inactive state, in the experimental environment (including solvents and other parts of the media but the analyte of the interest), is fundamental for the specificity of detection. It is also the main challenge in solution, in particular for complex and competitive media like aqueous mixtures of multiple chemicals, which are at the same time the most important for practical real life applications. This well recognized difficulty in the use of metal complexes in practically relevant, competitive solvents can be targeted by multidentate ligands, and in particular those which lead to the formation of the binary chelates. For octadentate geometry, which is the most common when considering the first row transition metals capable of magnetic switch (see chapter 2) it means hexadentate systems, but even this may not be sufficient.^{[83] [151]}

(5) **True off state** - no signal generated by the inactive form, which for magnetic signal is achieved by a MAGNETOGENIC system discussed below.

3.2. (Para)magnetogenesis – magnetic off-ON activation

Magnetogenesis is a term that by analogy to fluorogenic probes, was proposed by Prof. Hasserodt to describe a process of *de novo* creation of the paramagnetic quality in a non-magnetic (diamagnetic) sample, which is principally associated with an appearance of the unpaired electrons (see chapter 2). The **off-on** type of response is best suited for the design of activable molecular probes as it offers an unbeatable signal-to-noise ratio, as it means a transition from a “non-magnetic” compound to a “magnetic” one. A simple change in the ‘degree’ of already existing paramagnetism can also be envisaged as a reporting event (either in an on=>off, on=>less-on or on=>more on mode), but this has serious limitations. Agents emitting a residual signal before activation (in the case of magnetism: already paramagnetic), generally offer lower signal-to-noise ratio decreasing the sensitivity of detection. In the consequence, weak signals, which can often be found with non-abundant molecular targets of high interest where the binarity of response is difficult to be achieved, may merge into the background of not entirely silent probe and remain undetected (false negatives). In addition the residual signal makes such systems intrinsically biased towards the ambiguity of the results (see also existing smart contrast agents for MRI as discussed in chapter 1.3). Thus, in the field of Medical Imaging for example, dealing principally with structurally complex samples and where the false-positive diagnosis can have a detrimental effects to the physical but also psychological health of the patient, the clinicians clearly call for **true off=>on designs**, but the advantages of it also in other fields are obvious and appealing, and cannot be overestimated.^[16]

Magnetogenesis in practice - short reminder on magnetic properties of transition metal ions

From the discussion presented in chapter II it is clear that only Ni(II) square planar and Fe(II) octahedral (principally N6 coordination sphere) complexes meet these requirements.^{[83] [151]} Adding to it the requirement of stability of the off state in the aqueous media leaves only Fe(II) low spin octahedral diamagnetic complexes with hexadentate ligands. Minimizing the intrinsic tendency of Ni(II) chelates to coordinate the axial ligands and thus switching to the paramagnetic complex still remains an unmet challenge. By consequence, the practically useful magnetogenic designs can be available only with diamagnetic ferrous complexes of hexadentate ligands, in order to ensure the stability. One such system which was the first ever magnetogenic design for solution detection of chemical analyte, is described in chapter 3.3. with a particular emphasis on the way it addresses all five hallmarks of an optimal responsive molecular probe. Then summary of alternative ligand systems and the emerging attractiveness of bispidines is given in chapter 3.4.

3.3. First magnetogenic design for detection of chemical reactivity

3.3.1. Concept of magnetogenic probe for enzyme activity

The idea of magnetogenic probe proposed originally by Prof. Hasserodt as a first truly off-on operating design for MRI applications,^[75] is based on a transformation of iron(II) low spin diamagnetic state into a paramagnetic high spin one (hallmark (1) and (5)) upon the change from N6 to N5O1 coordination motif, in the consequence of irreversible and specific chemical reaction (see Fig. 14). Probe is composed of a stable metal complex of a hexadentate ligand (hallmark (4)) with conservative N5 backbone, decorated with a 6th coordinating motif, including a “smart” arm bearing a substrate for a molecular target (enzyme), bound to the chelate *via* an auto-immolative spacer. Once the substrate is modified (cleaved) a highly unstable unit is generated which eliminates spontaneously, making a remaining arm prone to decoordination. The replacement of this arm with a solvent water can generally happen in two different ways, but both of them should be spontaneous in the conditions of experiment in order to associate the magnetic signal with a chemical impulse which triggered the cascade. One option, originally envisaged in the design, is a complete removal of this coordinating arm and the other is a spontaneous replacement of a tethered coordinating unit by the water molecules. Similarly to two replacement strategies described in chapter 2.2 and widely used in IDA in fluorescent imaging, the former, while being energetically more demanding (cleavage of chelate ring covalent bond) can be more decisive. Both strategies are discussed below.

Unlike the magneto-modulating systems discussed in chapter 2.2, which interacted with the analyte in a reversible fashion shifting the magnetic equilibrium to one of the sides, the Hasserodt’s design aims at chemical reactivity and thus implies an irreversible transformation of the probe by the stimulus. Drastic alteration of the probe (which breaking of covalent bond truly is) enables effective binary (hallmark (2)) transformation even between largely different forms promising dramatic change of the magnetic properties.

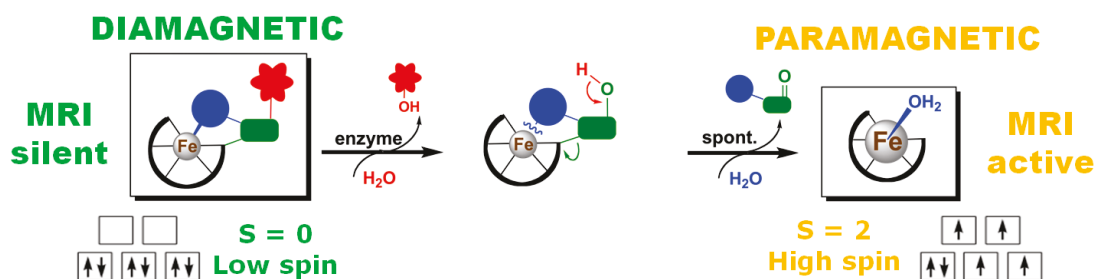


Fig. 14 Magnetogenic concept proposed by Hasserodt. True off=>on irreversible response, modularity of the approach and biocompatibility of the central metal ion are the main advantages.

A decisiveness of interaction which stems from a one-way-activation only, has to compromise the fact of a lack of possibility of real-time monitoring of the temporal fluctuations of chemical stimulus by a single introduction of the probe. On the other hand, visualizing reactivity which

generally has stronger impact on the dynamic variation in the system than simple binding, is a best prognostic of the future changes of the system. This underlies also a great interest of the observation of enzymatic biomarkers in live organisms enabling an early diagnosis, even before the pathology has truly developed.

Except the biological and biochemical importance of the enzymes, which is in fact an ultimate motivation of the project, their catalytic character allows for the amplification of the signal; i.e. many probe molecules can be activated by just one catalytic site, significantly increasing the intensity of the response and thus sensitivity of detection. However, the efficiency of enzymatic catalysis is inseparably connected with the efficiency of substrate recognition which is often a great challenge for synthetic designs and can largely impair the kinetics of transformation (hallmark (3) and thus the detection itself (see for example chapter 1.3 and a discussion of the EgadMe case where 7 days in optimized conditions were required to generate small signal). In the case of the described concept, three-component modular design enables a separation of the stimulus recognition site (enzymatic cleavage) and a signal generating unit by the use of a suitable spacer group, giving more independency in treating each element separately and thus facilitating the design. In addition, it theoretically enables also the adaptation of the molecular design to various enzymatic targets simply by varying the trigger/substrate unit.

Last but not least, use of iron(II) is associated with much lower long-term toxicity risks (hallmark (6)) than for the Gd-based complexes, as it is biologically recognized and recycled.

3.3.2. State of the art in the group's project

First MRI experiments with iron(II) complexes

The relaxivities of initially selected 1,4,7-triazacyclononane (tacn)-based diamagnetic complex **5** ($[\text{Fe}(\text{tptacn})]^{+2}$ tptacn = 1,4,7-tripicolyl-1,4,7-tacn) and two paramagnetic iron(II) chelates **6** and **7** (respectively $[\text{Fe}(\text{dptacn})(\text{H}_2\text{O})]^{+2}$: 1,4-dipicolyl-1,4,7-tacn-iron(II) and $[\text{Fe}(\text{bistet-tacn})(\text{H}_2\text{O})]^0$: 1,4-bis(5-tetrazolyl)methyl-1,4,7-tacn-iron(II)), were reported by the group of Hasserodt et al. (Fig. 15). These measurements for the first time showed that the iron(II) complexes are indeed capable of raising the signal in T_1 -weighted MRI (for **6** $r_1 = 1.29 \text{ mM}^{-1}\text{s}^{-1}$ in PB at 7 T, 300 MHz;^[31] for **7** $r_1 = 0.57 \text{ mM}^{-1}\text{s}^{-1}$ in water at 7 T^[32]). What is maybe even more important, they proved also that tacn-based N6-ligands can efficiently silent iron(II) (T_1 in 4 mM solution of **5** was 1.5 s in comparison to 1.6 s of pure water at 7 T)^{[31] [32]}, what is a primary prerequisite for the design of magnetogenic probes. In vitro studies with complexes **5** and **6** showed a true off-on relationship in the contrast in MRI (Fig. 15B). In addition, electroneutral complex **7** raised contrast also *in vivo* in mice the tibia upon intramuscular injection followed by electroporation to ensure cell internalization (while **5** remained MRI silent under the same conditions Fig. 15 C),^[32] The observed increased biocompatibility of complex **7** is hypothesized to result from a lower osmolarity and a minimized Lewis acid character of iron(II).

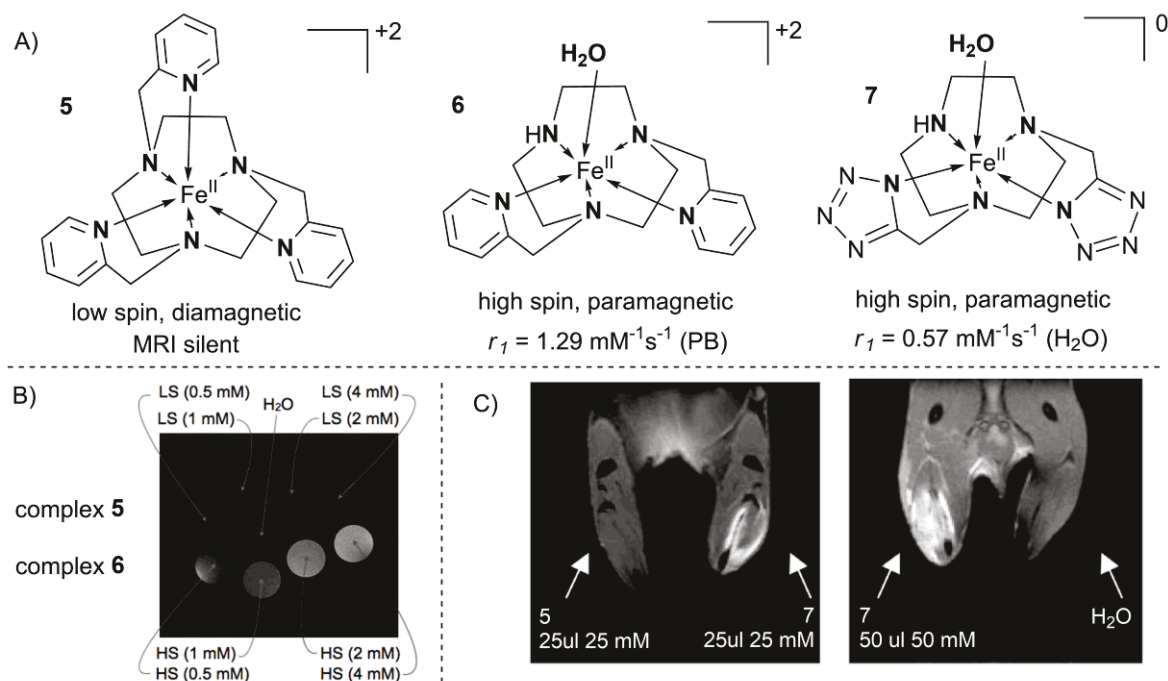


Fig. 15 State of the art in the group in the moment of my arrival – relaxivity of model off and on complexes based on tacn have been tested *in vitro* and *in vivo* but no responsiveness was yet achieved. Panel B) was reproduced from Stavila et al 2008 [31] - by permission of The Royal Society of Chemistry (RSC) for the Centre National de la Recherche Scientifique (CNRS) and the RSC (doi: 10.1039/B719704G). Panel C) - adapted with permission from Touti et al 2011 [32]; copyright 2011 American Chemical Society.

Development of auto-immolative, responsive arms

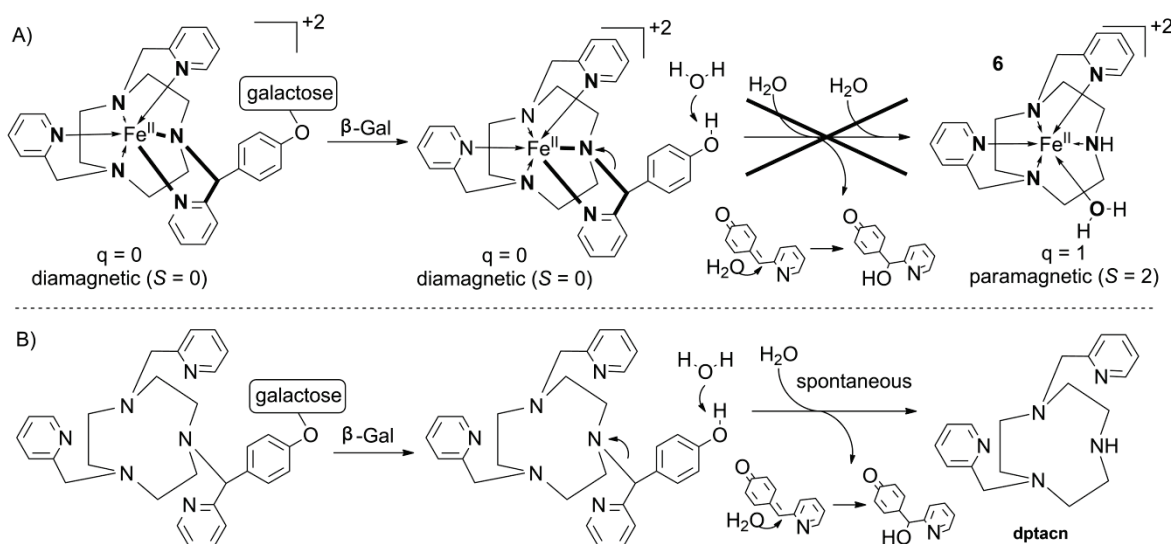


Fig. 16 First (unsuccessful) attempt to obtain the responsive probe based on iron(II)-tacn system. (Stavila et al. 2008 [49]). A) Despite enzymatic cleavage, no breaking of the coordination bond took place. B) in the absence of the metal ion purely organic molecule spontaneously eliminates the 6th coordination arm.

A first attempt of the Hasserodt's group to enzymatically activate the iron(II)-based probe (model β -galactosidase in this case) failed (Fig. 16). Despite the successful cleavage of the enzyme substrate (β -galactose), highly unstable moiety of 6th coordination arm, which in the free ligand

eliminates spontaneously (Fig. 16 B), is stabilized by the coordination to the metal ion and the low spin N6-coordinated iron(II) motif remains untouched even in water (Fig. 16 A). This clearly demonstrates the great challenge of cleaving the chelate ring, especially in macrocyclic binary complex which is even further stabilized by the low-energy low spin state of the central metal ion implicating a much stronger ligand-metal bonding.

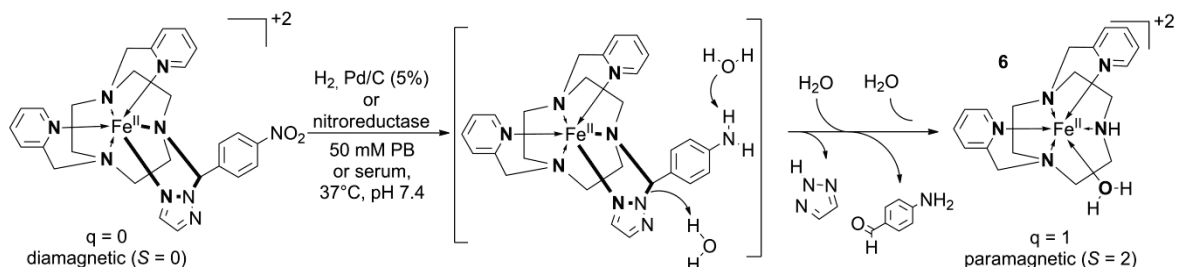


Fig. 17 Improvement of the concept from Fig. 16. This time the immolative moiety came out to be sufficiently unstable after enzymatic cleavage to spontaneously decompose opening an access to the first coordination sphere of the complex for water molecule and thus turning paramagnetic. Adapted from Hasserodt et al 2013^[53] - with permission of WILEY-VCH Verlag GmbH & Co. KGaA, Weinheim (copyright © 2013).

In the consequence, at the beginning of my thesis, other members of the group began to work also on solving this problem. Only recently (April 2013), already after the end of my experimental work, these efforts in fine tuning the stability of this auto-immolative unit led to sufficiently unstable functionality which auto-immolated once unmasked, but in the same time remained intact in the absence of the enzyme (Fig. 17). This probe, based on the originally explored dptacn ligand system, is a first magnetogenic molecular probe for detecting a chemical stimulus in solution, and the first true off-on probe for MRI, which operates in neutral pH.^[51] Its performance *in vivo* is currently being verified.

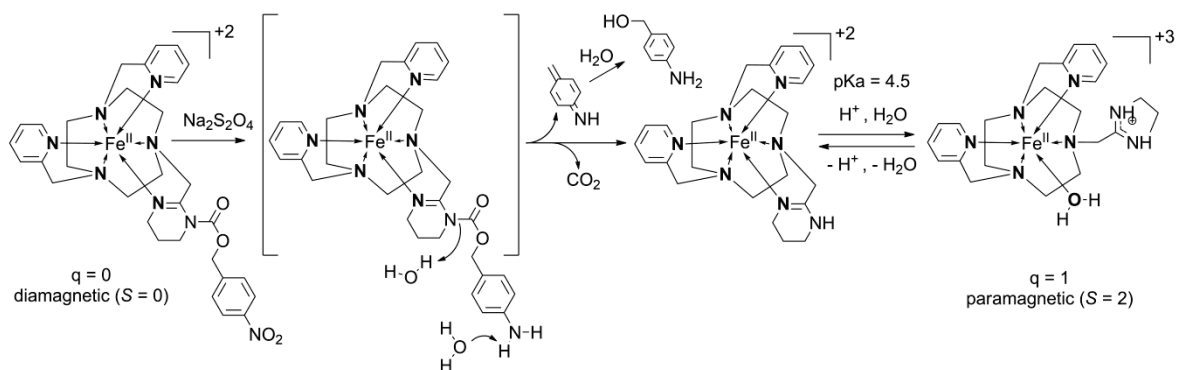


Fig. 18 Alternative responsive strategy based on the pH sensitivity of the substrate-bearing arm. Enzymatic cleavage leads to the unmasking of the pH-sensitive moiety but the Lewis acid character of the iron(II) decreases the pKa by more than 7 units, thus while the enzymatic cleavage happens in the physiological conditions, no magnetic response is obtained unless going to acidic pH. Adapted from Hasserodt et al 2013^[53] - with permission of WILEY-VCH Verlag GmbH & Co. KGaA, Weinheim (copyright © 2013).

At the same time, other strategies have also been pursued by the group. For the moment, only one of them, which is based on the controllable spacer-mediated unmasking the basicity of strongly basic coordinating arm (de-acetylation of amidines), led recently to a selective magnetogenesis

upon the chemical stimulus in aqueous solution (Fig. 18).^[74] However the unexpected stability of the system, stemming from a very strong Lewis-acid effect of iron(II), led to the pH of transition of 7 units below the pKa of free amidine (4.5 vs. approximately 12), despite a successful removal of the masking unit. Current research in the group aim at moving the pH of transition above the neutral pH, in order to ensure spontaneous and complete protonation of unmasked arm coordinated to iron(II) *in vivo*, allowing for a generation of a magnetic signal as a function of the presence of the enzyme.

In the light of the initial success in raising contrast in vivo by a tacn-based model iron(II) complexes, and the difficulties in proving the magnetogenic activation with these systems, my project was proposed in 2009 to turn the bispidine platform into a system suitable for the design of magnetogenic probes and thus expand the palette of future probe candidates with significantly varied properties. In the following, I will briefly discuss different ligand systems in the light of the potential suitability of this project before explaining why our choice has finally fallen on the class of the bispidines.

3.4. Bispidines – promising molecular platform for iron(II)

Diamagnetic ($S = 0$) and paramagnetic ($S = 2$) states of iron(II), as shown in chapter 2, make it perfectly suited for the design of magnetogenic probes. While the majority of ferrous chelates are high spin, the main challenge resides in rendering iron(II) magnetically off (low spin with no unpaired electrons). For the reasons of the stability of the diamagnetic state of iron(II) in competitive media like water, hexadentate ligands^{[152] [93] [95] [96]} with optimal N6-coordination motif and promising strong ligand field, are required.

3.4.1. Available duos with off-on magnetic relationship

In the search for suitable ligands only a limited number of duos of hexadentate LS Fe(II) and structurally related pentadentate HS analogs were identified, all of which, except macrocyclic tacn (1,4,7-triazacyclononane), were branched systems comprising at least four imine-type nitrogens. In particular, single atom branched ligands (atom C of 1,1,1-tris(aminomethyl)ethane, tame, derivatives, and N in tren-derived ligands), required as much as 6 imine-type nitrogens to exert a ligand field strong enough for the stabilization of the LS state, but their robustness in solvents of even medium polarity (like acetonitrile) was not optimal. From tetrasubstituted alkyldiamines bearing pyridine-type pendant arms only trimethylene diamine led to a fully LS state due to the optimal flexibility of the propylene linker (in comparison to an ethylene bridge), and this in spite of the presence of thermodynamically less stable six-membered chelate ring (a butylene-diamine unit would lead to an even less favorable seven-membered chelate ring). Finally, a 1,3,5-triaminocyclohexane-based ligand bearing three pyridinylmethyl arms also led to a binary diamagnetic ferrous complex. However, it was a macrocyclic tacn-based coordinative system which has been identified as optimal for the design and construction of magnetogenic probes, successfully achieved by Hasserodt et al. Its biggest advantage in comparison to the branched examples discussed above is the robustness of the binary complex, thanks to the extra stability contributed by the macrocyclic effect (additional chelate rings), and a ligand field still strong enough (for the version bearing three imine-type pendant arms) to render iron(II) diamagnetic. For more information, the reader is referred to a comprehensive overview of N-based ligands for spin transition in iron(II),^[151] and to our recent work where all existing and some potentially accessible duos are discussed in the light of their suitability for magnetogenic probe design.^[53]

3.4.2. Motivation behind choosing bispidines:

In the light of the doubtful stability of the diamagnetic binary iron(II) complexes of the branched multidentate ligand systems discussed above, in the look for another platform suitable for the construction of robust magnetogenic probes for competitive solutions, Prof. Hasserodt proposed to consider the bicyclic structure of bispidines (3,7-diazabicyclo[1,3,3]-nonane – Fig. 19). The rigidity imposed by adamantane-like structure, and the flexibility of the remaining coordinating arms,

make them suitable for a complexation of a variety of different ions with high stabilities.^[153] Rapid access to the substituted multidentate (only two steps from commercially available substrates) was a great advantage in the light of the multistep routes leading to more sophisticated variants of the existing hexadentate ligands.^[31] In addition, the most commonly accessed and used derivatives of bispidines possess a ketone group and two ester moieties on the periphery of the ligand who are electronically isolated from the coordinating motif. This offers the possibility to fine-tune the physico-chemical properties of the corresponding complexes as well as their bioconjugation without however harming the stability of the probe and its off-state. This is a virtually unique advantage in the range of available multidentate ligands and highly desirable in view of subsequent adaptation to *in vivo* conditions.

Despite these advantages, several issues remained to be solved when the project of this thesis was conceived. First of all, the iron(II) coordination chemistry of bispidines was limited to principally non-binary and exclusively high spin chelates, despite the attractive perspective of a coordination sphere exhibiting 2 aliphatic and 4 imine-type nitrogen atoms. The first three low spin iron(II) complexes in the entire bispidine series, the principal result of the present thesis, remain, for the time being, the only low spin examples. Secondly, coordination motifs used were limited to simple heteroaromatic moieties, which could withstand harsh derivatization conditions used in classic synthetic methodology. The choice of these heterocyclic pendant arms can be considered non-optimal in view of the delicacy of the responsive arms as envisaged by our design considerations.

3.4.3. Synthesis of bispidinones via Mannich-type reaction

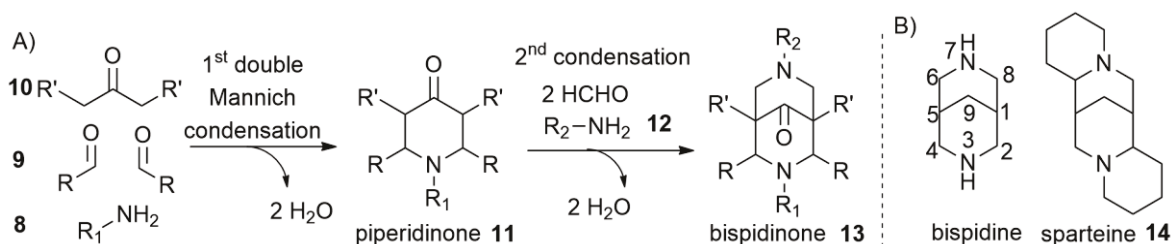


Fig. 19 A) Synthesis of bispidinones by Mannich strategy B) numbering in bispidines and related natural structure.

Bispidines (in fact 3,7-diazabicyclo-[3,3,1]-nonane derivatives – Fig. 19 B) were prepared for the first time by Mannich et al in 1930 who has also coined its name (two condensed piperidine rings – bis-piperidine). In the next years the same structure has been found in sparteine (Fig. 19 B)^[154] (confirmed in 1936^[155]), an alkaloid isolated from natural sources (first isolation^[156]). The original synthetic protocol from 1930 consists of two steps, each of them involving a two one-pot Mannich condensation reactions. In the result, substituted bispidine structure with a with a carbonyl group on bridging C9 atom, called bispidinone (bispidone), can be prepared in only two steps from commercially available ketone backbone (10) and various aldehyde (9) and primary amine precursors (8, 12) (Fig. 19).

Formation of piperidinones (**11**) is relatively easy thanks to the acidity of the C-H protons increased due to the presence of the electron withdrawing R' substituents (Fig. 19) (typically methyl esters). At lower temperatures kinetically more accessible anti isomer is formed in which one R substituent on C-2,4 (Fig. 19) is in the axial position of the chair conformer, and the other is in equatorial one. Upon recrystallization at higher temperature thermodynamically more stable syn isomer is formed with both substituents equatorial, what is also required for effective metal coordination.

Due to the increased steric constraints, the construction of the second piperidinone ring, that leads to the formation of bispidinone **13**, needs boiling alcohol and a totally unsubstituted aldehyde (formaldehyde).^[157] Introduction of additional moieties at position 6 and 8 was reported to be possible only for unsubstituted (or methyl-substituted) N3 and N7 (derived from amine **12**), otherwise a drastic increase in steric congestion disfavors the reaction.^{[158] [159]} Despite other methodologies explored for the preparation of the bispidine-based compounds (including cleavage of the related diazaadamantanes^[160] and intramolecular cyclization of piperidines^[161], the Mannich strategy, or its modifications, remains the most attractive and widely used approach, due principally to **(a) the large scale**, at which it can be conducted, **(b) the ease of product isolation** (recrystallization – no flash chromatography required), **(c) the rapid access** (only two steps), **(d) its convergent quality** starting from **cheap starting material**, and **(e) the possibility to vary the substitution pattern** to a certain extent by simple modification of the starting material

3.4.4. Isomerism in bispidine system and its consequences for complexation

The conformational and configurational complexity of bicyclononanones in solution is subject to the substitution pattern and the chosen synthetic route. It has been thoroughly studied^{[162] [163] [164] [165]} due to its importance for coordination chemistry^[166] and other applications, including receptor binding and control^{[167] [168] [169]}.

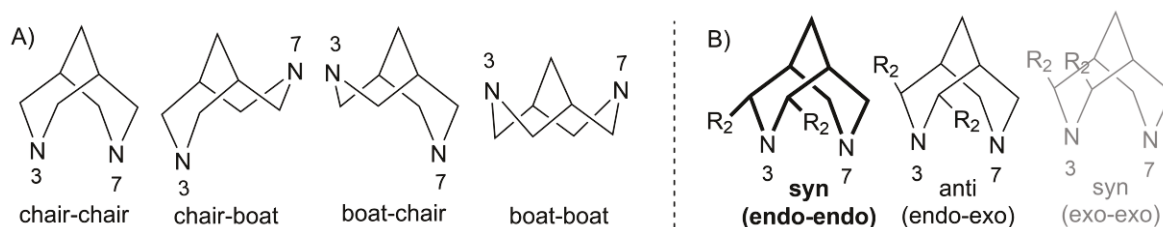


Fig. 20 Main isomerism in bispidines. A) Conformational isomerism of the ring B) Configurational isomerism of the substituents. *In bold* – structure of the bispidine ligands in most of the complexes. *In grey* – improbable configuration R₂ are bulky moieties.

Among four possible conformations of the two piperidine rings (Fig. 20 A), the chair-boat one is favored for more bulky substituents on N-7 and is typically adopted by bispidine ligands in their free form.^{[164] [170]} The tendency to complex metal ions in a multidentate fashion^[171] proves that the conformational switch to the chair-chair isomer is possible. Despite the generally high energy

associated with a boat-boat conformation,^{[172] [170]} this form has recently been observed in the equilibrium with a chair-boat isomer, in di-protonated bispidines symmetrically substituted at nitrogen N3 and N7.^[173]

The mechanism of Mannich condensation of the first piperidinone ring with 2,4 substituents kinetically favors a formation of the anti isomer (one aldehyde-derived moiety in axial-*exo* and the other in equatorial-*endo* position), which can then be switched to the thermodynamically more stable endo-endo syn form (blue in Fig. 20 B), usually at elevated temperatures.^[157] This configurational isomerization, happening principally *via* the retro-Mannich type ring opening reaction,^[172] is important as only equatorial substituents are available for metal complexation.

For more bulky 2/4-substituents (quinolinyl or naphthyl), the restricted rotation may lead to different rotational isomers, which cannot interchange.^[169] Consequently, if a heteroatom from one of the substituents points “up” (*exo* - above the plane of the chair conformer of the ring) – then it will not be able to coordinate to the metal center, but at the same time the substituent proximity may prevent any coordination at this site. In the case where the rotation around the C2-substituent bond is possible, the presence of the metal center will obviously stabilize the “down” (*endo*) orientation of the coordinating heteroatoms.

3.4.5. Coordination chemistry of bispidines

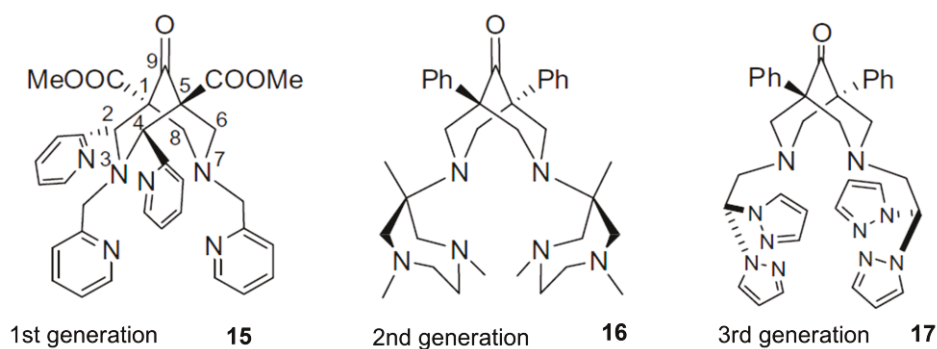


Fig. 21 Different types of bispidine-based hexadentate ligands (Comba et al 2013^[174]).

Bispidines as polydentate ligands for metal complexation. The initial interest in bispidines, which have alkaloid structure, came from their certain biological activity as ligands for the receptors,^{[162] [163] [164] [165]} but in the last 15 - 20 years it is their coordination chemistry which has become a main focus. First metal complexes with a bidentate ligand containing bispidine-like structure (3,7-diazabicyclononane) date back to 1950s.^[160] The first coordination compounds with polydentate bispidinones were reported in 1968^[175] but it is principally the work of Comba et al who have rediscovered them for coordination chemistry in the 1990s. Since then, many different metal ions (Cu(II), Co(II), Ni(II) and Fe(II) among others) have been complexed by tetradentate and higher substituted bispidines of a rather conservative $2Nsp^3$ - $2Nsp^2$ motif, where two alkyl nitrogen donors come from the bispidine backbone and two imine-type ones are a part of

heteroaromatic rings of *syn* 2/4 substituents (so called 1st generation ligands – example is **15** in Fig. 21). The penta- and hexadentate (**15** in Fig. 21) ligands were obtained by introduction of the amines with coordinating motifs in the first (N3 substitution) and/or second (N7 substitution)) step of the Mannich procedure. This polydentate bispidine-based system is well preorganized for metal complexation in pseudo-octahedral geometries. In fact, it is the rigid adamantane-like structure of the aliphatic backbone that confers high stability onto the chelates.^{[176] [177]} Further installation of flexible substituents are responsible for a wide tolerance (low preference) of these ligands for multiple M(II) metal ions.^{[178] [179] [180]} More recently two novel types of bispidine ligands with either an aliphatic (2nd generation, 6 aliphatic Nsp³ - **16** in Fig. 21)^{[181] [174]} or an imine-type coordination sphere (3rd generation, 4 heteroaromatic and two aliphatic – **17** in Fig.21)^[174] were shown to impose, respectively, trigonal prismatic and distorted trigonal prismatic geometries on the resulting transition metal complexes. Among the different metal complexes of bispidine-based ligands, it is those with Cu(II) that have so far been explored the most for technological applications, namely as radioactive tracers for PET imaging^{[182] [183]}, in mechanistic studies of enzyme hydrolase activity^{[184] [185] [186]} and as catalysts of aziridination reactions^{[187] [188] [189]} or sulfoxidation reactions (for Ru(IV) based chelates)^[190].

Iron(II)-bispidine complexes. Most of the existing examples of Fe(II)-bispidine chelates prior to the present thesis were reported in a single work by Borzel et al. dating from 2002.^[191] Only two binary iron(II) complexes of bispidine-based hexadentate ligands were reported (ligand **16**^[192] and **17**^[174] in Fig. 21). While their magnetic properties were not investigated, the light yellow color and the Fe-N bond lengths of ca 2.2 Å suggest their HS state, despite the presence of an N6-coordination motif. This is in agreement with the intrinsically weaker ligand field observed for a trigonal-prismatic ligand approach. The only attempt to obtain a binary octahedral ferrous complex of bispidines resulted in penta-coordination in the solid state, with some evidence of hexa-coordination in solution, but the phenomenon was not confirmed.^[191] Importantly, no diamagnetic iron(II)-bispidine complex was ever reported prior to the results^[193] of this thesis project. chapter 5 and 6 shall describe the challenges associated with the goal of devising the first LS bispidine complexes.

More than a half of all reports on non-sparteine iron(II) chelates are patents (around 40) and only one was published before 2002. This suggests that the practical utility of this system has only been recognized recently. Patented applications of these compounds comprise bleaching agents,^{[194] [195]} peroxide-type accelerators for polymeric resins^[196] and anti-skinning compositions for coatings^[197]. The great majority of reports on iron(II)-bispidine complexes focusses however on their catalytic properties. In the last 10 years several chelates of this system (principally tetra and pentadentate ligand-metal complexes) were prepared and their performance as oxidation catalyst was confirmed in olefins oxidation,^{[198] [199] [200] [201] [202] [203]} CH-hydroxylation,^[204] halogenations,^[205] and sulfoxidation^[206].

PART II

RESULTS AND

DISCUSSION

4. OBJECTIVES OF THE PROJECT

Detection of chemical analytes in solution is very important for biological, technological and environmental applications and is the main focus of chemical sensing. A magnetic readout has the advantages of raising no penetration limits, ensuring signal specificity and being harmless with respect to the sample analyzed which makes it attractive for sensing purposes. MRI is the most sophisticated technique for the detection of paramagnetism, and enables the analysis of highly complex and structurally diverse samples, especially live organisms. However up to date it remains mainly an anatomic imaging modality which uses passive, permanently paramagnetic agents to enhance a contrast between the compartments where they are present and the rest of the sample. All current cases of responsive versions of these agents emit a significant signal even before activation, which limits detection fidelity and sensitivity. By contrast, an off-on type of response would be largely preferable as it offers the highest signal-to-background ratio and minimizes a false positive detection. However only very few examples of a magnetogenic response to a chemical analyte in solution were reported. Iron(II) is the best suited metal for this purpose as it offers a difference of 4 unpaired electrons between the low spin and high spin form, starting from a state with no unpaired electrons at all, and benefits from the best choice of potentially adequate ligands. The main challenge for solution applications is the stability of the complexes, especially in water, which is arguably the most attractive medium for real-world applications. In fact, only binary octahedral complexes can be sufficiently stable under these conditions but they require access to hexadentate ligands that are difficult to synthesize. In the search for suitable systems which may enable a switch between an N₆ and an N_{5O1} coordination motif and thus a change in the magnetic properties, Prof. Hasserodt has originally identified the substituted triazacyclononane. On the basis of this structure, a model diamagnetic and model paramagnetic iron(II) complex were prepared and their off-on nature in MRI experiments was demonstrated. A successful contrast enhancement was also achieved *in vivo* with a paramagnetic electroneutral complex. However, a first-generation strategy to obtain a magnetogenic probe was not successful and thus a variety of other ones began to be investigated in the group at the moment of my arrival.

Aside from a variation of pendent arms that are supposed to enable the metal complex to respond, Prof. Hasserodt looked also for an alternative ligand platform which ensured similar robustness for the high spin and low spin form of the corresponding iron (II) chelate and orthogonal properties to those by a tacn-based system. The class of the bispidines promised to lead to metal complexes of high stability due to their adamantane-like rigid structure. The literature reports on bispidines with simple substitutional patterns, but very few examples of hexadentate ligands exist. The fact that they are prepared in a rapid and large-scale synthetic pathway is highly attractive. However, their further functionalization was generally performed under harsh conditions and was hampered by steric congestion. On top of that, the only existing examples of iron(II)-bispidine complexes were all high spin, even those rare ones comprising a hexadentate ligand. Prof. Hasserodt has

detected the presence of a steric clash in such a reported hexa-coordinate iron(II) complex and postulated that its removal should lead to fully low spin state.

Consequently, the objectives of this PhD project were set to (Fig. 22):

- 1) Prepare a binary diamagnetic iron(II) complex and verify its robustness in aqueous media at room temperature.
- 2) Demonstrate the off-on relationship of N6 vs. N5O1 bispidine-iron(II) complexes in MRI.
- 3) Establish a synthetic pathway to large quantities of a pentadentate platform which would allow for subsequent decoration with the "intelligent" pendent arms developed simultaneously in the group.
- 4) Demonstrate a proof of concept of chemically induced magnetogenic response and its off-on character in MRI.

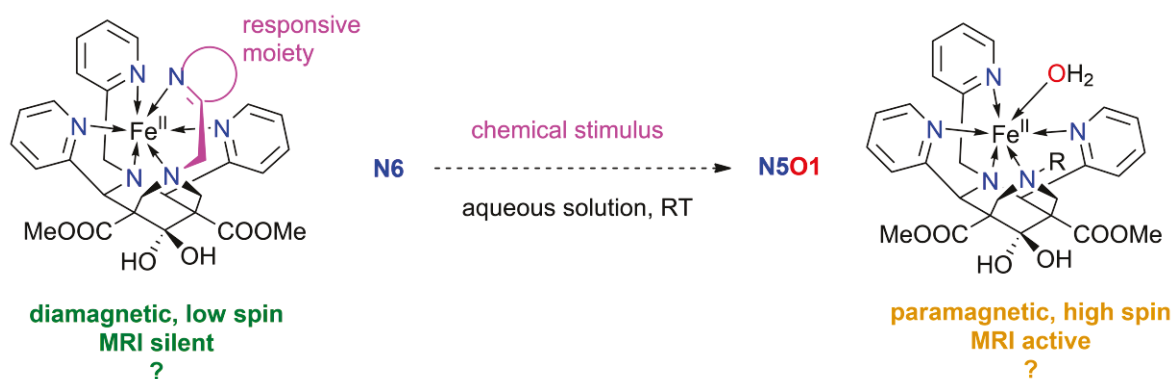


Fig. 22 Magnetogenic concept envisaged for iron(II)-bispidine system.

5. NOVEL SYNTHETIC INTERMEDIATE FOR PREPARATION OF BISPIDINE LIGANDS

5.1. Rationale behind the choice of optimal N5 platform

Our design of off-ON magnetically responsive molecular probes assumes, that the functional compound should possess the conservative N5 coordinating motif of (1) high intrinsic stability and (2) possibly large ligand field, and the control of the magnetic properties of a metal center would be realized by altering the sixth coordination site. To fully explore the potential of our strategy, the sixth coordinating arm should be easily varied (3), with a maximal efficiency (4) and full functional compatibility (5) of synthetic protocol. I would like to recall to the reader that the complexity of the arms, including a variety of functional groups attached and the presence of the meta-stable spring loaded spacer (see also a discussion in chapter 3), often suffers from multistep, tedious and low-yielding preparations so the yield and compatibility of their attachment to the ligand backbone and subsequent complexation cannot be underestimated.

In the view of the above-mentioned requirement, we have identified two pentadentate coordinative platforms based on bispidines, presented on the picture below:

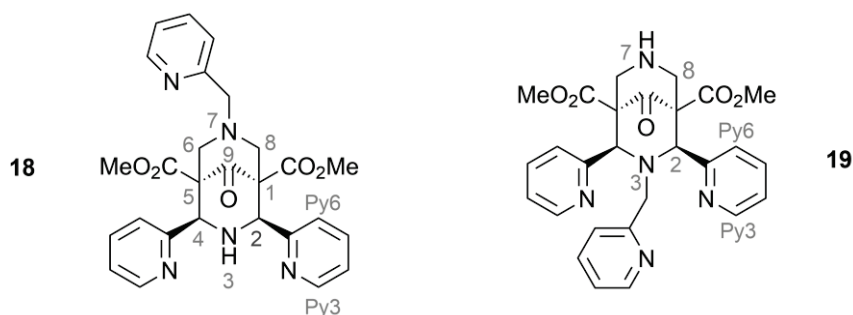


Fig. 23 Selected pentadentate molecular platforms with NH moiety for easy functionalization. Note the numbering of different positions of the bispidine backbone and aromatic substituents (in grey - see also Fig. 19 B, chapter 3.4.3), adopted uniformly throughout this work.

As it has been discussed above bispidines were shown to form highly stable complexes with metal ions, what should ensure also a stability of our complexes in solution applications. In addition, presence of three pyridines, attached to the bicyclic framework should provide a maximal ligand field what increases the chances to achieve the magnetic silencing of iron(II) center upon coordination of the 6th arm. It is also important to notice that the pyridines in position 2 and 4 should be in *syn* configuration in order to enable their coordination to metal center.

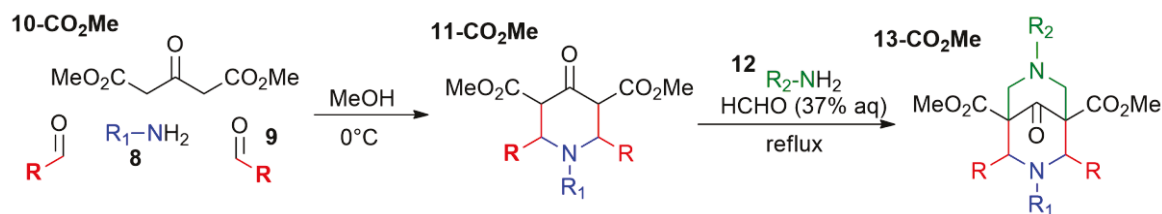


Fig. 24 Classic synthesis of bispidinone ligands in two-step double Mannich reaction. Color code refers to the origins of different parts of the bispidine ligands (13-CO₂Me).

The main novelty of our concept lies in the separation of the arm-introduction and the ring-condensation via a NH-intermediate. Fig. 24 shows how do different coordinative units of bispidine ligands are introduced to the system. While changing the aldehyde (**9**, red in Fig. 24) in the first step leads to the modification of the rigid N4 motif of the bispidines, the substitution of single coordinating arm is realized by varying the amine precursors used in the first (**8**, blue in Fig. 24) or in the second (**12**, green in Fig. 24) ring-condensation step. Thus, independently on which variant would be chosen, the introduced moiety would have to resist harsh conditions of alcohol reflux, which might be incompatible with a variety of functionalities present on the arm and may suffer from poor yields for more bulky substituents.^[164] In addition, it also requires primary amine precursors which might be difficult to access for the elaborate arms. Consequently, a desired N5-platform with a secondary amine ready for simple alkylation by easy to access electrophilic precursors like halogenides, mesylates or tosylates among others, is an attractive alternative.

From the analysis of the previously reported example of near-to-SCO iron(II) bispidine complex (see chapter below) the variation of the N7 substituent was of primary interest and thus the N7-H platform was a first synthetic target. Isomeric platform with a N3-H functionality was found to be an interesting alternative, provided the fact that the binding distance between iron(II) and sixth coordinating unit in a vacant site left by this pentadentate compound differs from that of the N7-H platform. The influence of this variation on the catalytic properties of the derived pair of pentadentate isomeric iron(II) complexes has been demonstrated.^{[198] [201]} Thus, as the metal-ligand bond length has a direct implications on the ligand field strength (see chapter 2) the isomeric chelates with the same coordinating motifs but occupying different coordination sites may offer a distinct magnetic properties.

While N3-platform **18** (Fig. 23) was successfully accessed by applying a standard Mannich protocol, platform **19** required an alternative protocol via the protection-deprotection strategy. The results of these attempts are summarized and discussed below.

5.2. Classic synthetic methodology

5.2.1. Preparation of piperidinone intermediates

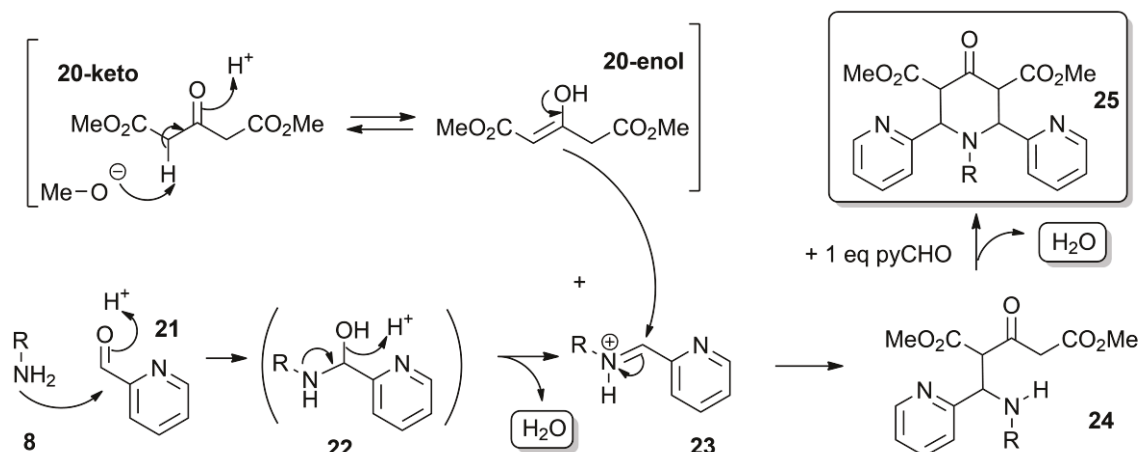


Fig. 25 Mechanism of Mannich reaction on the example of the formation of piperidinone (25).

The preparation of the N-Pi^{[207] [208]} and N-H^[209] piperidinone intermediates (respectively, **29** and **28** in Fig. 26) has been previously reported and the described protocol was applied also in this work. The amine precursor (**8** in Fig. 25) reacts with an aldehyde **21** releasing the water molecule (**22**) and forming an imine intermediate **23**, which in turn experiences the nucleophilic attack from the enolic form of carbonyl precursor **19** yielding the mono-adduct **24** and water. The same reaction sequence is then repeated with an amine and carbonyl being now the same molecule **23**, resulting in the incorporation of the aldehyde residue and subsequent intramolecular cyclization reaction. The fact that the whole process takes place within 5 min at 0 °C indicates a large driving force for the condensation reaction which is probably a release of four molecules of water in the process.

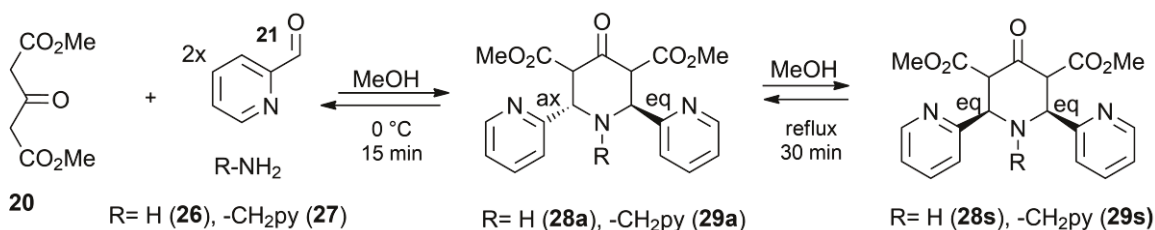


Fig. 26 Synthesis of the piperidinone precursors.

Nevertheless, the presence of the thermodynamically less stable *anti* isomer (**28a** and **29a** in Fig. 26) in the isolated precipitate of both piperidinones, with one pyridine substituent in the *axial* and other in *equatorial* position, suggests partial kinetic control of the reaction. On recrystallization in MeOH, isomerization reaction occurs, leading to a formation of more thermodynamically stable *syn* isomers (**28s** and **29s** on Fig. 26), where the pyridine rings are in equatorial position to

minimize 1,3 diaxial repulsions.^[157] The most probable mechanism of the configurational transformation, performed in refluxing methanolic solution, involves the retro-Mannich ring opening, followed by the rotation of the axial pyridine group and re-condensation.^[172] The desired products were isolated as white crystalline powder and the additional crop could be gained by subsequent repetitive treatment of the filtrate leading to excellent yields of even 96 % for N-Pi (lit. 84 %) ^{[207] [208]} and 85% for N-H piperidinone (lit 67 %) ^[209].

Conclusion: *The simplicity of this reaction and its efficiency allowed for the preparation of more than 100 g of the desired product in one reaction, what demonstrates a great accessibility of this system and potentially enables an easy scale up to even industrial quantities.*

Keto-enol tautomerism in piperidinones. Isolated piperidinones may be expected to exist in a tautomeric keto-enol equilibrium as shown in Fig. 27 due to the acidity of the alfa proton (in bold in Fig. 27) derived from the presence of the electron withdrawing carbonyl functionalities on the adjacent carbon atoms. However, while the N-H piperidinone remains preferentially in the keto form in solution, what results in a relatively simple NMR spectra (due to the symmetry of the keto form), N-Pi compound is in keto-enol equilibrium with a major contribution from the enol form. Detailed NMR analysis involving ¹H and ¹³C NMR, in combination with the 2D experiments (COSY, HSQC and HMBC) allowed for the unambiguous assignment of each individual peak, including those of the aromatic region (note the numbering of different positions in Fig. 27).

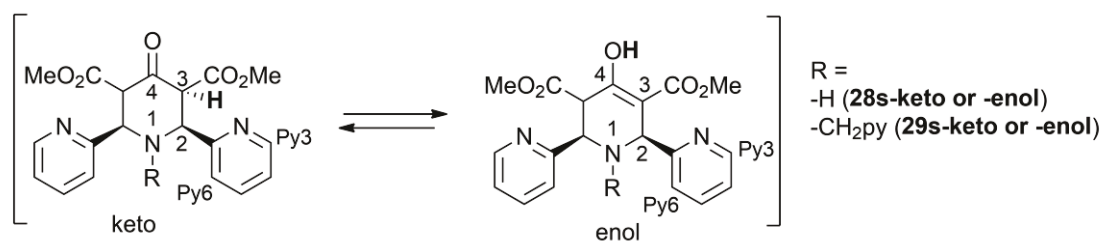


Fig. 27 Keto-enol tautomerization in piperidinone intermediates synthesized in the course of this work. In bold – tautomeric proton. Note the numbering of different positions of the piperidinone ring and of aromatic substituents.

As expected for the *syn* isomer and in agreement with a predicted values, signals from the pyridine substituents are twice of the intensity of those coming from the picolyl substituent and as shown, do not experience the effects of the lowering of the symmetry within the aliphatic ring. In details, aromatic proton in position *ortho* in respect to the heteroatom pyridine ring is the most deshielded and thus most downfield shifted, followed by the one in position *para*. Respectively, the *meta*-position experience the least deshielding from nitrogen atom, and thus its signal appears at higher fields, with a slight relative downfield shift of the proton in position 5 of the pyridyl ring (Py5), next to the quaternary carbon. The loss of symmetry in the enol isomer stemming from the formation of double bond within a piperidine ring is pronounced by a more complex set of signals in aliphatic region, with those from protons H-2 (4.86 ppm, s, 1H), H-5 (4.76 ppm, d, 1H) and H-6 (4.29 ppm, d, 1H) being particularly characteristic and significantly downfield shifted, due to the

presence of the adjacent electron withdrawing groups (esters and enols, but also heteroaromatics). The presence of the signal at 12.55 ppm, attributable to the OH group, further proves the presence of the enol form. Even methoxy groups of the ester moieties become distinguishable upon the dyssymmetrization of the piperidinone ring in the enol form. ^1H NMR spectrum of the keto tautomer exhibits a reduced number of signals due to the presence of the plane of symmetry in the molecule. The position of the tautomeric equilibrium is slightly solvent sensitive with 7 - 10 % of keto form in CDCl_3 solution and 10 - 15 % in DMSO-d_6 .

5.2.2. NH-pentadentate platform by classic Mannich-type approach

Obtained piperidinone precursors were then used in the classic Mannich-type protocol to attempt the preparation of new ligands **18** and **19**. Several examples of substituted bispidines with N3-H unit were previously reported to be accessible by simple variation of the aldehyde precursor in the first step and amine reagent in the second one.^[210] In particular, the reported compounds with pyridyl moieties at positions 2 and 4, possessed methyl^[211] [212] [157] [168] benzyl^[211] [212] and CH_2 -cyclopropyl^[157] substituents at N7. groups. Interestingly a series of tetraarylsubstituted (at positions 2, 4, 6 and 8 of the bicyclic framework - numbering as in Fig. 23) N3-H, N7-H^[158] [213] and N3-H, N7-Me bispidines^[158] has also been successfully prepared. Unlike the majority of 6,8 unsubstituted bispidines, they have preferentially adopted a chair-boat conformation to minimize the steric clash between the aryl substituents. I have thus followed the classic procedure for the formation of bispidinones and by introduction of the picolylamine as the precursor, in the reaction with the N-H piperidinone (**28s** in Fig. 28) and formaldehyde I have obtained a desired compound as large rhombic crystals with a yield of 22 % and I have proved its *syn* configuration by NMR.

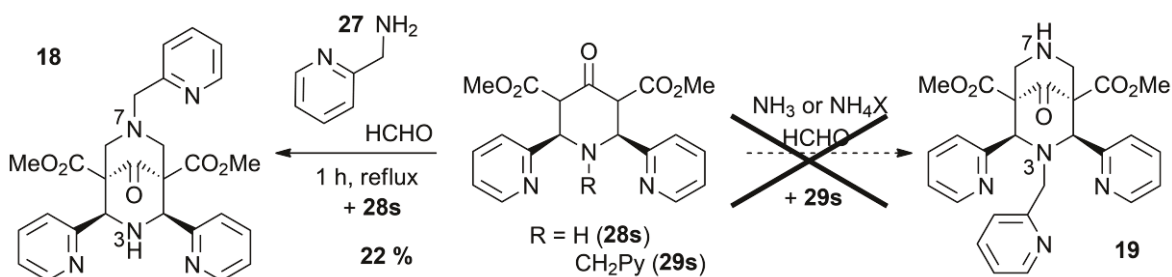


Fig. 28 Direct synthetic attempts towards N-unsubstituted bispidines. Note the numbering in the bispidine backbone and aromatic substituents.

While the synthesis of the N3-H bispidinones was widely reported, the introduction of the NH functionality into the 2,6 substituted bispidine in Mannich reaction was rare. Except the above-mentioned N3-unsubstituted tetraaryl bispidinones^[158] [213] where authors use NH_4Cl with sodium acetate^[158] or NH_4OAc ^[158] as amine precursor, there exist only one other example of N7-H bispidinone-based ligand with N3-C(O)Me, 2,4-py substitution pattern.^[211] However, this early report provided neither NMR nor X-ray analysis of the obtained product and these results were

later on not repeated. The liberation of the N7-H functionality on tetracoordinate bispidinone-like ligand has also been observed in the result of oxidative N-dealkylation of the N7-Me analog coordinated to Co(II) metal ion, in the presence of H_2O_2 and O_2 , but it was not observed for the pentadentate ligands.^[214] Thus from the obvious reasons this type of reaction is not suitable for consideration as the synthetic route towards the desired intermediate.

I was not able to successfully prepare the desired N7-H intermediate bearing the N3-pi substituent by any of the procedures reported for the analogous compound. Despite the variation of the conditions and some indication of the formation of the desired product (molecular mass signal $[\text{M}+\text{H}]^+ = 502$) I have never isolated it, neither unambiguously proven its presence in the reaction mixture. It might be concluded that while unsubstituted ammonia precursors can be successfully used as nucleophiles in Mannich condensation reaction on the level of the formation of piperidinone, the analogous condensation of the second ring with these reagents is problematic. Among the possible reasons for this to take place, which are neither exhaustive, nor experimentally confirmed, it can potentially be the more severe conditions, promoting a side-reactivity of ammonia, and/or instability of the intermediates formed like unsubstituted iminium cations.

5.3. Alternative synthesis of N7-H platform – protecting group

5.3.1. INTRO– the choice of the protecting group:

In the result of unsuccessful attempts to prepare a N7-H precursor directly from the piperidinone, we have proposed the alternative methodology, involving the use of the protecting group. This strategy, even though widely explored by organic chemists, has been rarely used to prepare the ligands for coordination chemistry.

In order to “bypass” the use of the unsubstituted ammonia precursor in the second Mannich condensation step, we have proposed to come back to well documented use of primary amine reagent, but bearing a removable moiety (protecting group), which masks the N7-H functionality.

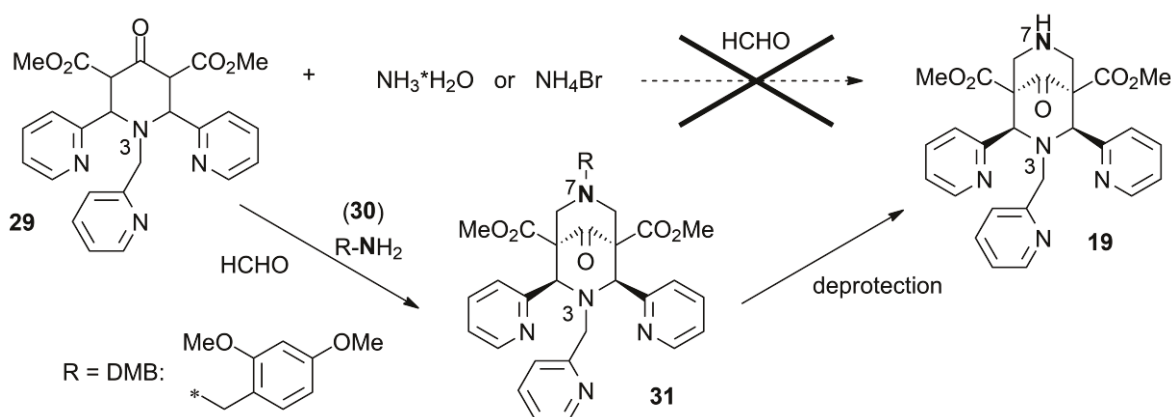


Fig. 29 Direct synthesis from piperidinone (upper line) vs. bypass strategy via DMB protecting group.

A wide range of protecting groups for secondary amines were described,^[215] but the specific requirements of Mannich type synthesis including the need for primary amine precursor and compatibility with water/alcohol reflux, led us to the choice of 3,5-dimethoxybenzyl moiety (DMB). DMB-amine is commercially available, solving the problem of the accessibility of the precursor, and there exist a wide range of deprotecting strategies which could be explored to selectively cleave this moiety from the bispidine backbone. In addition, apolar dimethoxybenzyl group should also facilitate the crystallization.

5.3.2. Mannich-type introduction of DMB-protecting group

Mannich condensation reaction leading to the formation of bispidines, as previously mentioned, is highly sensitive to the steric congestion of the substrates, which also influence its configurational and conformational behavior. 3,5-dimethoxybenzyl group is more bulky than the majority of other moieties previously introduced in the second ring condensation step (like benzyl or picolyl, not mentioning simple methyl etc.) thus its introduction to the already substituted piperidinone N3-Pi is more challenging.

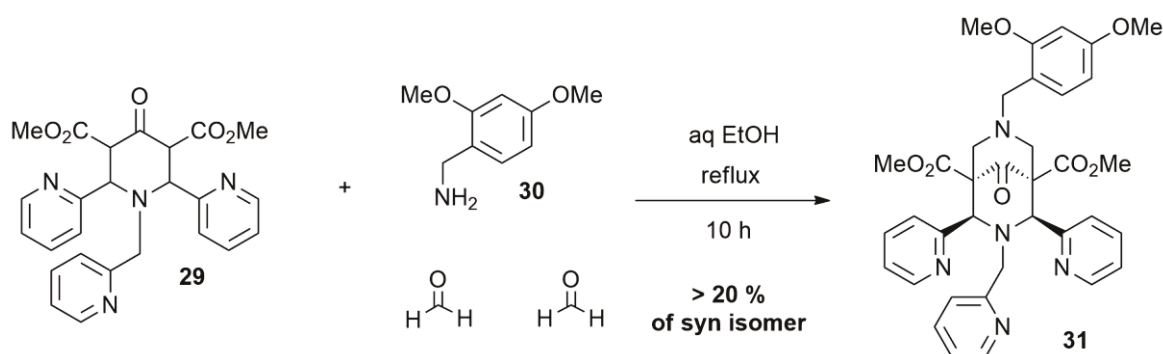


Fig. 30 Introduction of the DMB protecting group to the bispidine skeleton.

Variable conditions were reported in the literature for the synthesis of the bispidinones from piperidinones in Mannich type ring condensation reaction. My slightly adapted protocol involves the gradual addition of 37 % aqueous solution of formaldehyde (2.4 eq), followed by dimethoxybenzyl amine (1.2 eq) to a suspension of the piperidinone in EtOH at 60 °C. The resulting homogenous solution darkened rapidly, first to the orange and then to a dark brown color. Surprisingly, the full conversion of piperidinone could be observed by direct injection mass spectrometry (DIMS) already after 10 min, and stopping the reaction at this point enabled the isolation of the pure *anti* isomer, despite the *syn*-configuration of the piperidinone used. This suggests that at elevated temperatures, which are required for the bispidinone framework formation, the retro-Mannich reaction can take place almost instantaneously in solution, followed by the formation of the kinetically favored *anti exo-endo* isomer. With prolonged heating, the ratio of *syn/anti* isomers increases but it is also associated with the increased product decomposition and/or impurities formation. Switching between the two isomers requires the activation energy and ring opening, which in this form is prone to further decomposition or side reactions, additionally promoted by the high temperature. The isomerization process may thus be quite energetically demanding and in the consequence relatively slow. In addition, the stabilization of the *syn* form over *anti* may not be as significant as in the case of the piperidinone, due to the additional steric strain imposed on the system by the bulky DMB substituent, which is “felt” by the system even more if remaining in *syn-endo* configuration.

5.3.3. NMR analysis of configurational isomerism

In order to effectively follow the reaction and stop it in the most suitable moment, as well as to undoubtedly identify the resulting products I have performed a thorough NMR analysis aiming at assignment of each individual proton and carbon nucleus. Fig. 31 represents the NMR spectrum obtained by me initially from the first attempts to prepare DMB-bispidinone, which allowed me to the identification of two simultaneously occurring configurational *syn-anti* isomers. Only later I was able to prepare pure isomers and confirmed the adequacy of my NMR interpretation.

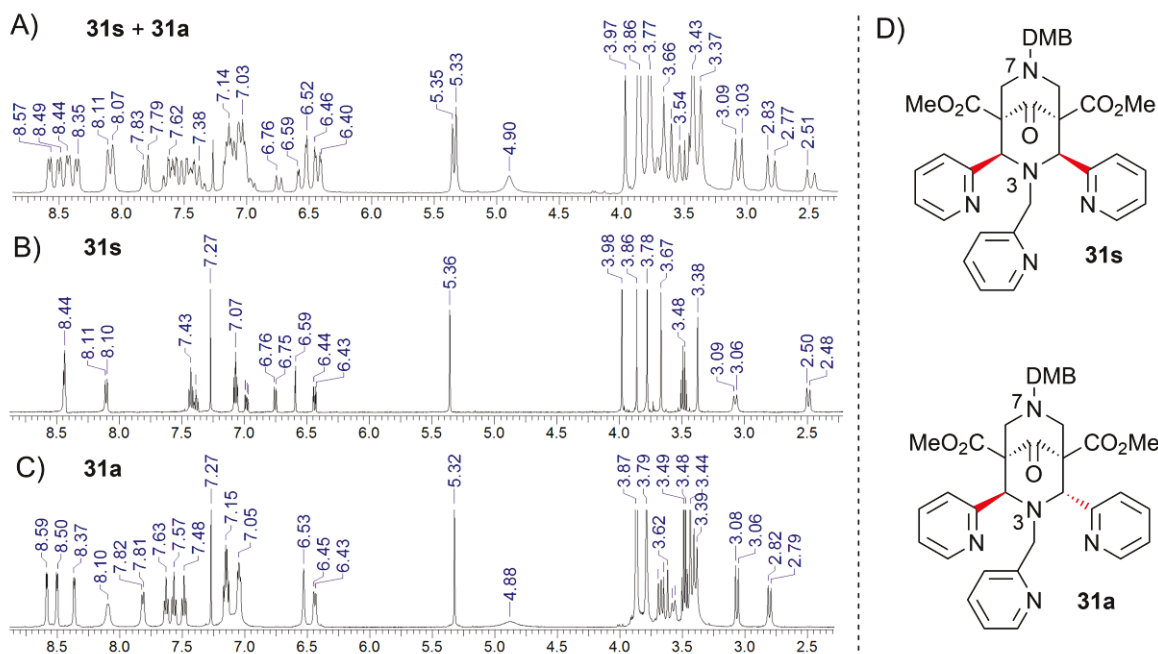


Fig. 31 A) ^1H NMR of the mixture of *syn* and *anti* isomers of DMB-protected bispidine ligand **31** used initially to decipher the nature of the product. For comparison, ^1H NMR spectra of pure *syn* isomer **31s** (B) and pure *anti* isomer **31a** (C)..D) Structures of both isomers (in red – difference in configuration).

The single DIMS signal corresponding to the desired molecular mass of DMB-bispidinone together with a complex NMR spectrum (Fig. 31 A) indicated the presence of several isomers in solution. The complexity of the conformational and configurational behavior of the bispidines has already been discussed. Despite several possible isomers present, the existence of the configurational equilibria in solution during the reaction was the most probable (Fig. 31 D). The restricted rotation isomers were usually observed for more bulky substituents than pyridyl rings in position 2/4 while the bulkiness of the DMB group on position N7 would with the highest probability lead to the favored chair-boat conformation. Analysis of the COSY experiments revealed the existence of five different environments for pyridyl rings four of which having relative integration of 1 H and only one set of signals with the integration 2 H. This is in agreement with a mixture of *syn-anti* isomers, as for the former one two pyridyl rings at position 2 and 4 are symmetric, and thus reducing the number of signals expected by half. N3-pi substituent on the *syn* form as well as all pyridyl groups from the *anti* isomer all should have distinct signals. The main complexity of the spectra came from the fact of the overlap of many signals as well as from the chemical similarity of both compounds despite the differences in isomerism. In the consequence, I have acquired the HSQC and HMBC heterodinuclear (^1H - ^{13}C) as well as j-mod and ^{13}C NMR spectra in chloroform and DMSO and analyzed them in order to identify all the signals in both carbon and proton. NOESY experiment additionally proved the adequacy of my analysis.

As it has already been mentioned, the conformational and configurational behavior of substituted bispidines can be complex. The symmetric spectra (Fig. 31 B) observed for the isolated compound indicated the presence of only one isomeric structure with a plane of symmetry, suggesting the *syn*

configuration of the first piperidinone ring (**31s**). As the *syn exo* configuration on the piperidinone ring of bulky pyridine substituents would impose a high steric clash, the *endo* configuration with aromatic substituents in equatorial position remains the only possible form^[164]. According to the conformational analysis of the 2/4-substituted bispidines, the bulkiness of the N7 substituent may favor the boat conformation of the second piperidinone ring.^[164] This behavior seems to stem from the interaction between the N3 and N7 substituents when both rings remain in chair conformation, but the steric clash between the N7-moiety and 2/4-substituents is not excluded. Our system possess the picolyl group on the N3 and two pyridines at carbons 2 and 4, provoking a certain steric congestion. In the consequence, a bulky dimethoxybenzyl group residing at N7 could be expected to suffer from a significant steric constrains when both aliphatic rings remain in chair configuration and thus the chair-boat conformation seems to be possible. The bulkiness of the DMB group could lead to the energetic barrier of chair-boat conformational flip which is sufficiently high for the two isomers to be observed by NMR.^[164] High sensitivity of C-9, C-1/5 and in particular C-6/8 NMR signals to the conformation of the bispidine backbone, and simultaneous insensitivity to the substitution pattern, was previously reported to concluding on the effective conformation of bispidines in solution.^[168] The analysis of the ¹³C NMR of DMB-compound 31 revealed that the signals of diagnostic carbons C-9 (204.29 ppm) C-1/5 (59.53 ppm) and C-6/8 (62.36 ppm) are within the range proposed for chair-chair conformation, which is respectively 203 - 205 ppm, 58 - 62 ppm and 61 - 63 ppm, in comparison to 202 - 203 ppm, 48 - 52 ppm and 63 - 65 ppm found typically for the chair-boat conformer. It thus demonstrates that the feared bulkiness of the DMB moiety does not hamper the adoption of the chair-chair conformation.

There was also another isomer, which could be isolated from the reaction mixture and the ratio of which to the desired product decreases upon the prolonged heating, suggesting that it rather remains a less thermodynamically stable but kinetically favored form. Similar behavior has been observed for previously reported bispidine ligands.^{[169] [216]} The NMR spectra of this compound (Fig. 31 C) showed a significantly higher complexity than the one of the previously described molecule (**31a**). The presence of only one molecular species has been proven by the 2D HSQC and HMBC experiments which have shown the ³J and ⁴J scalar couplings between the observed signals. In particular, three different pyridine signals were observed, each with the relative intensity 1, indicating the inequality of not only picolyl substituent but also the two pyridine rings at position 2 and 4. Thus, in analogy to the isomerism observable in piperidinone ring, the *exo - endo anti* configuration of the pyridine groups could be deduced. The other possible explanation of this inequality of both heteroaromatics would be a rotational isomerism, but it has only been observed so far for the *ortho* substituted aromatic rings^[158] and thus its occurrence in the analyzed molecules is less probable. The existence of the *anti* configuration is supported by the significant difference between the protons 2 and 4, proving that they are *trans* in respect to each other. The chemical shifts of the carbons C-6 and C-8 (60.50 ppm and 63.99 ppm) remain within the typical region for the chair-chair conformation^[168] of both piperidinone rings.

Conclusion: The NMR analysis of the mixture of the DMB-bearing bispidinone products and their comparison with pure samples of single isomers unambiguously proved the existence of two configurational isomers (*syn* – **31s** - and *anti* – **31a** - in the respect to the pyridyl moieties at positions 2 and 4 of the bispidinone backbone).

5.3.4. Optimization experiments of bispidine formation

Multiple optimization experiments including the variation of the temperature, solvent and reaction time allowed me to repeatedly prepare *syn*-isomer of DMB-bearing bispidinone in up to 21 % yield on over 10 g scale in a single reaction, upon the crystallization of the desired product from MeOH/Et₂O 1:5 solvent mixture. The optimization process was possible thanks to the monitoring of the reaction progress by the ¹H NMR, and more precisely by the observation of the characteristic signals around 5.3 ppm from H-2/4 protons of both forms, which remained distinct even in the presence of the side products, with axial and equatorial H-6/8 proton signals being an additional support. Relative contribution from the impurities could also be roughly estimated by the comparison of the intensities of the diagnostic proton signals of the desired product and the integrated intensity of the aromatic region. These tools enabled me to calculate the changes in the relative quantities of *syn* isomer, *anti* isomer and impurities in the reaction mixture in time, as seen in Fig. 32.

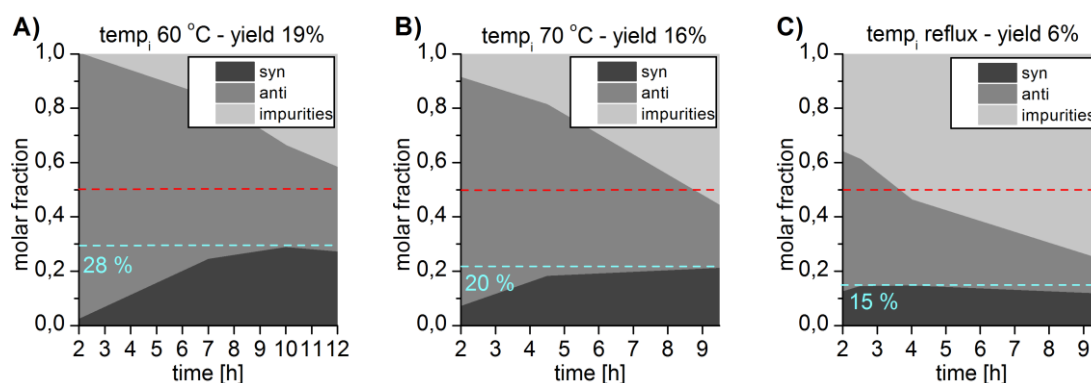


Fig. 32 Changes of the relative quantities of the two isomers (*syn* **31s** – dark grey, *anti* **31a** – grey) and the estimated amount of impurities (on the basis of the integration of the signals of aromatic protons – light grey) in the reaction mixture during the reaction of the formation of the DMB-bispidine ligand **31** as a function of the reaction time and the temperature of the addition of the reactants (A)- initial temperature equal to 60 °C, (B) – 70 °C, (C) – reflux). Light blue dashed line represents the maximal amount of *syn* isomer present in the reaction mixture. Dashed red line represents 50 % value which is a critical relative quantity of the impurities above which a purification is significantly hampered.

By multiple repeats, stopping the reaction each time at different moment and performing the whole procedure for product isolation, I could draw a semi-quantitative conclusions on the relationship between the maximal isolable yield and the relative ratios of different species in reaction mixture. In summary, the biggest quantities of purified *syn* product are achieved for the reaction mixture where the *syn/anti* ratio is between 0.5 - 1 with approximately 30 - 50 % molar of the impurities, as

marked by the red dashed line on Fig. 32, which equals to 25 % global yield of *syn* isomer (see end-time point in Fig. 32 A which gave maximal yields) . In the majority of cases, when the *initiation temperature* was 60 °C, this stage has been achieved after around 6 - 8 hours of reaction and may continue to even 12-14 h of reflux (Fig. 32 A). Addition of the reagents at higher temperature (B in Fig. 32) or even at reflux (C in Fig. 32) shortened this time to around 2 - 4 h and promoted a formation of the side products even more, decreasing the yields (compare maximal attainable amounts of *syn* isomer in light blue in Fig. 32 with the yields isolated). The whole process shall not pass this optimal point, otherwise the amount of impurities, which augments significantly above 60 %, makes the crystallization very difficult if not impossible (Fig. 32 C). On the other hand stopping the reaction at earlier stage results in the mixture with a significant excess of *anti* isomer, requiring a fractional crystallization. This is however more challenging than a separation of the bispidinone from the impurities, due to the high tendency of both isomers to co-crystallize. Thus paradoxically the decomposition of the *anti* isomer, even if the amount of *syn* would not vary, might be beneficial to some extent, until the impurities reach the earlier mentioned level of approx. 50 % which hampers the crystallization.

Fractional recrystallization. Nevertheless, some of the *anti* form can be selectively crystallized, provided its excess in the mixture, from EtOH/Et₂O solution, while the isolation of the *syn* isomer is possible from MeOH/Et₂O solvent mixture, but only when the *anti* isomer is not more than 3-2 times more abundant. The recrystallization of the latter mixed with the residual *syn* form can be performed by refluxing in different alcohols (EtOH, *i*PrOH and MeOH) but independently on the media, the profile of the process remains similar and comparable to the crude reaction (see discussion in previous paragraph and picture above). Methanol seems to be slightly more suitable for the isomerization process as it seems to decrease the amount of impurities formed in comparison to the *i*PrOH. It also allowed to isolate the *syn* product after 8h of reflux of the initial *anti/syn* mixture (1:0.12) in 16 % yield with approximately 10 – 13 % of the product remaining in solution. Thus despite the decrease in the formation of side products, the yield improvement of the isolation-isomerization procedure, even if potentially possible, is not evident. Multiple repetition of the protocol with isolation of the mixture at early stage of the reaction, then fractional crystallization and subsequent isomerization could potentially increase the quantities of isolated products, but the additional workload and materials consumption were considered not to be paid off by a promise of a slight yield improvement. Thus this strategy has been abandoned and replaced by a simple repetition of the whole reaction process which required similar effort and costs, allowing to double the amount of the product. While the isomerization process did not take place in CHCl₃ which was expected as the retro-Mannich reaction require polar protic media, the addition of aqueous solution of acid promoted a formation of the hemiaminal type of product (**31-hemiaminal** in Fig. 33), analogous to the one previously reported to take place in strong acids, like HCl or even HClO₄.^[217] The compound, isolated in 59 % yield as white crystalline solid directly precipitated from a reaction mixture, has been fully characterized by 1D and 2D NMR experiments confirming the hemiaminal structure (Fig. 33). In this place it is noteworthy that acidic catalysis of

isomerization is not an optimal choice as, except the accelerated decomposition (retro-Mannich),^[216] it also poses a threat of the formation of hemiaminal even as a main resulting compound. This effect could possibly be minimized if weaker organic acids like oxalic one, are used, as in the case of bispidine salts formation successfully attempted by Kuhl et al.^[217]

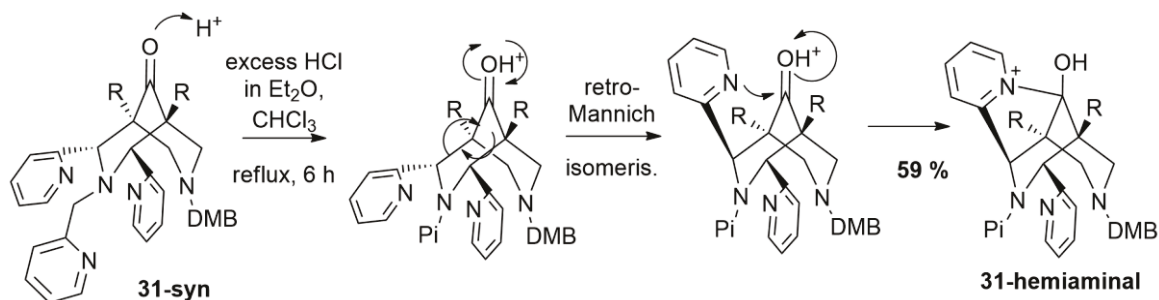


Fig. 33 Proposed mechanism of hemiaminal formation upon acid catalysis. After Kuhl et al 1999.^[217]

Solvent variation. The use of different solvents for the Mannich condensation reaction leading to the formation of the bispidine backbone has been reported. I have thus performed the comparative studies by varying the solvent component, which was either EtOH,^[211] MeOH^[167] or acetone^[164]. The DIMS monitoring after 10 min suggested that the highest conversion of the piperidinone (mass peak $[M+H]^+ = 461$) to bispidinone (mass peak $[M+H]^+ = 652$) occurred in EtOH, with MeOH reaction being slightly inferior and no signs of the desired products were detected in acetone sample, with major contribution of the starting material accompanied by the non-attributable peaks, not present elsewhere. Reactions in alcoholic media were continued at reflux for 40 min and subsequent evaporation of the volatiles. NMR spectra revealed the presence of the desired product in both samples, but the amount of impurities for the methanol-originated product was significantly bigger. On the other hand, 652 mass peak of the DMB-containing bispidinone appeared in acetone solution after 40 min of the reaction, but its relative intensity in comparison to the starting material signal was significantly lower (0.25) than after 10 min in MeOH (ratio = 2) and EtOH (ratio = 4). After two more hours of reflux, the non-volatile residue was analyzed by NMR, indicating a presence of the similar quantities of the *syn* isomer bispidinone as in the case of alcoholic reactions. These results thus suggest that the higher the temperature of the reaction the faster the process, and in the light of no significant improvements in the yield of conversion, or purity, the EtOH remained a solvent of choice.

Conclusion: Upon an optimization of the reaction conditions I am now able to prepare the preorganized endo-endo *syn* isomer of DMB-bearing bispidinone in yields above 20% and on scale exceeding 10 g in one reaction.

5.4. Deprotection – removal of DMB

Once a protecting group has been introduced into the bispidine, deprotection (removal) of this moiety should be performed in order to liberate the N7-H functionality, which is crucial in the preparation of the functionalized bispidine ligands for sensing purposes.

5.4.1. Deprotection by trifluoroacetic acid

The efficient cleavage of the DMB protecting group from the N7 position has been achieved by highly concentrated trifluoroacetic acid (TFA - 20 v/v % in DCM), at slightly elevated temperature, which was a combination of the previously reported procedures.^{[218] [219] [220]} In these conditions, the solution turned dark purple, but the color could not be associated with a reaction progression. Protonation of the tertiary amine provides a good leaving group and replacement of the benzyl functionality. The electron density from the methoxy groups in *ortho* and *para* position may stabilize the positive charge formed on the benzylic carbon upon the liberation of the N7-H functionality and a formation of a *para*-quinone-methide-type molecule **30** that can subsequently regain its aromaticity upon the attack of nucleophile like water molecule (during quenching) to form a 3,5-dimethoxybenzyl alcohol or similar adduct. (Fig. 34).

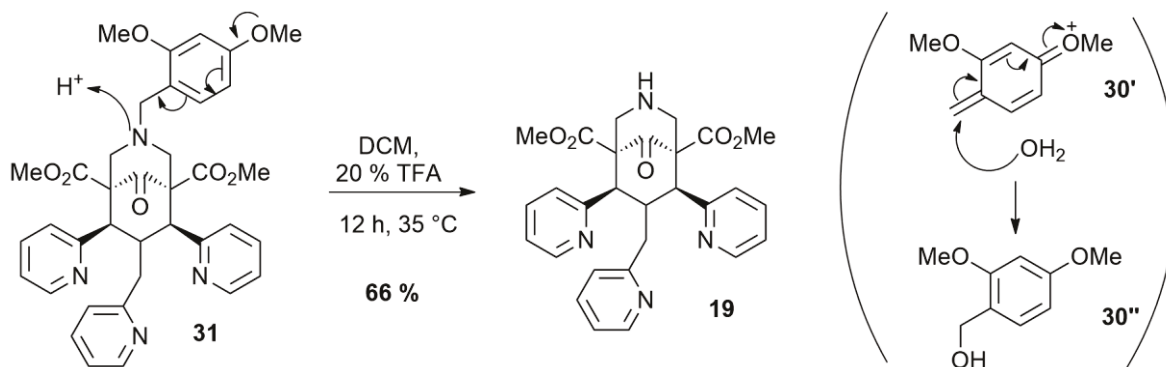


Fig. 34 Removal of a DMB protecting group by trifluoroacetic acid and a suggested mechanism of deprotection.

The recrystallization in a minimal amounts of hot acetonitrile yielded a desired product in the form of fluffy aggregates of very thin rod-like crystalline material with the yield of 66 %. The deprotected ligand molecule contains a free amine which is prone to CO₂ addition and therefore should preferentially be kept under inert atmosphere. The insoluble white precipitate, forming sometimes during the process of crystallization and amounting by mass to even 30 % of the expected product and thus diminishing the yield, was suspected to result from the same CO₂ capture. The precipitate remained insoluble in all tested organic solvents (including hexane, CHCl₃, DCM, alcohols, acetonitrile, acetone and even DMSO) as well as in water, suggesting that it could potentially be the carbamate-like addition product rather than a salt. Treatment of this residue first by a strong acid and then basifying the solution allowed us to recover most of the

desired product trapped in this form (up to approximately 80 %), with some loss due to the undesired side reactions. The reactivity of NH secondary amine towards CO₂ was also suspected to be responsible for drastic lowering of the yield (below 10 %) when using the hydrogen carbonate solution for quenching purposes.

Except the elemental analysis and high resolution mass spectrometry (HRMS) performed on the product isolated in the acid-mediated deprotection reaction, the liberation of the free amine was proven also by the IR stretch at 3311 cm⁻¹ and the broad ¹H-NMR peak at 4.58 ppm. The disappearance of the aliphatic and aromatic signals from a DMB moiety in ¹H and ¹³C NMR spectra prove the removal of the protecting group. The changes in the substitution pattern of the bispidine moiety are also observable by the significant downfield shift of the typical diagnostic signals from protons in the positions-6/8, with the axial protons forming a triplet and the equatorial ones a broad doublet, both resulting from the additional splitting generated by the NH.

5.4.2. Use of other acids

Acid used	Purity	Isolated yield
TFA	> 95 %	66%
BF ₃ *Et ₂ O + H ₂ O	90 - 85 %	50%
HCl (small scale)	90 - 85 %	25%
TsOH*H ₂ O	mixture	not isolable

Table 2 Acid-mediated removal of DMB group from N7 position in bispidines (preparation of the bispidine **19**).

Other acids were also tested as a possible alternative to TFA, but despite the formation of the desired product, in practice they did not give the improvement in the process. Small scale pilot experiments (below 50 mg of the protected bispidine) were performed, with p-toluenesulfonic acid TsOH (10 eq of TsOH hydrate in toluene at reflux), in concentrated 37 % HCl (37% aqueous solution, RT) and 20 % v/v solution of TFA in DCM (RT) for comparison. At high acid concentration the conversion of the starting material was almost complete overnight, with a major mass peak (DIMS) signal from the desired product. 10 eq of TsOH at 100°C led to the appearance of the signal corresponding to a deprotected bispidinone, but the conversion seemed incomplete. The NMR analysis of the residues obtained after reaction treatment (basified by NaOH to pH 9-10 followed by DCM extraction) did not prove the presence of the desired product in TsOH sample, possibly due to the intense signals from unidentified impurities. The deprotected bispidinone (spectrum compared with a pure sample) was formed as a major product (90 % yield by NMR) in TFA-mediated process. The residue obtained from the reaction in concentrated HCl was of comparable and high spectral purity, but unlike in the previous case, it constituted only 25 % of the expected mass of the product, all together summing up to 20 % of overall yield. Due to its simplicity, this method was also tested on the bigger scale but did not lead to the desired

deprotected bispidinone. Instead, the compound with a mass 488 was obtained as a principal product, but the characterization of its precise chemical composition was not attempted as no improvements could be envisaged with further development of this strategy.

The cleavage of the DMB protecting group was also achieved with $\text{BF}_3 \cdot \text{Et}_2\text{O}$, but improved substrate-product conversion in the presence of water or other proton donor in near-equimolar quantities (like ethanedithiol) suggested an involvement of proton formed in situ upon interaction of Lewis acid and protic nucleophile. In particular, no signs of reaction were observed when 1.5 eq of $\text{BF}_3 \cdot \text{Et}_2\text{O}$ was added to the solution of the DMB substrate (approx. 100 - 150 mg) in dry DCM and reacted for 15 h even in 40 °C, independently on the presence of the 1.5 eq of ethanedithiol ($\text{Et}(\text{SH})_2$). However, 15 eq of $\text{BF}_3 \cdot \text{Et}_2\text{O}$ were sufficient to induce the removal of protecting group in both cases. ^1H NMR spectra of the residues obtained upon reactions' treatment after 7 h in RT revealed higher purity and superior product-to-substrate ratio (1:3 over 1:4) of the sample with thiol. Replacement of the $\text{Et}(\text{SH})_2$ by 15 eq of water and the use of 30 eq of $\text{BF}_3 \cdot \text{Et}_2\text{O}$ in dry DCM enabled a deprotection of the DMB with a yield of 45 %, but the purity of the product (90 %) was inferior to the one achieved with TFA procedure.

5.4.3. Alternative deprotection strategies - unsuccessful

Several other strategies were described and thus could be considered for DMB deprotection but they were not suitable in this case. One common methodology involves the use of cerium ammonium nitrate (CAN) but in the presence of strongly chelating moiety like bispidine platform, the metal ion could potentially undergo an undesired complexation. Alternatively a biphasic deprotection with 2,3-dichloro-5,6-dicyano-1,4-benzoquinone (DDQ) has also been reported.^[221] Unfortunately all my attempts to apply these protocols for the deprotection of DMB-bearing bispidinone were unsuccessful as no signs of reaction could be observed even after a week, whether by DIMS from the reaction mixture or NMR analysis of the post-reactional residue.

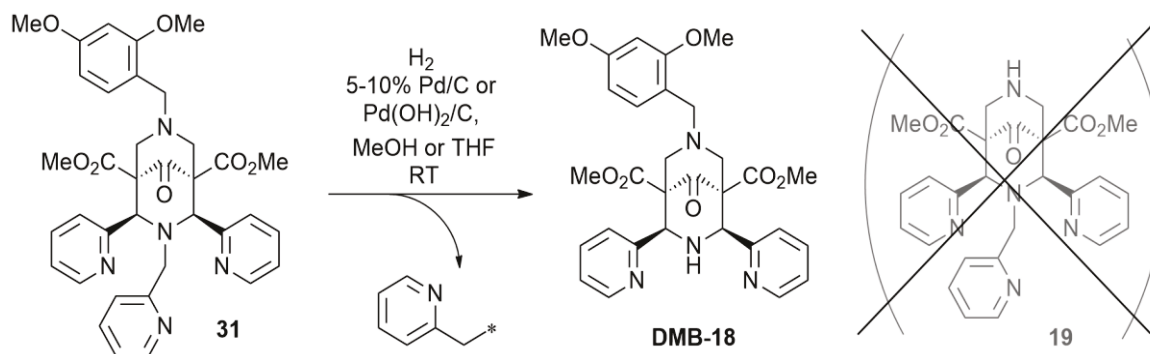


Fig. 35 Favorable removal of picolyl substituent (from position N3) over DMB protecting group (from position N7) by hydrogenation.

Oppositely, the Palladium on charcoal hydrogenation (5% Pd/C^[223], 10% Pd/C^[224] and $\text{Pd}(\text{OH})_2/\text{C}$ ^[225]) showed a conversion by mass spectrometry (MS), but the molecular mass peak

observed did not correspond to the desired product. The NMR analysis further revealed that this reaction has a preference for the cleavage of the electron deficient picolyl substituent from the nitrogen, leaving the electron-rich DMB group intact. The alternative procedure with a use of $K_2S_2O_8$ and K_2HPO_4 in the water/acetonitrile mixture^[226] resulted in the complex mixture of non-identified products, without a signs of the presence of the desired deprotected bispidinone.

Method of deprotection	Result
Acid	successful
DDQ	no reaction
Oxone	mixture
Hydrogenation	cleavage of picolyl

Table 3 Summary of the results of different deprotection methods used to remove the DMB group.

5.5. Perspective - PMB as alternative protecting group

In the perspective, the replacement of the bulky DMB group with a PMB (*para*-methoxybenzyl analog) could be envisaged. The resulting decrease in the steric congestion during the ring condensation reaction could improve the yields of the formation of protected bispidines. In addition, it would also decrease the costs of the process as the prices of DMB-amine are approximately three times those of the PMB amine (35.50 Euros vs. 119 Euros in AlfaAesar online catalogue, 29.08.2013). On the other hand, lower activation of the benzylic carbon could hamper the TFA deprotection reaction. Thus, it remains to be verified whether a) the yields of the bispidinone formation can really be improved by using the PMB amine and b) whether the deprotection is still possible, if not by TFA then maybe by other methods.

5.6. Conclusions

I have established a reliable access to the isomeric pentadentate bispidine-based platforms which should be easily functionalizable and may serve as models for the preparation of the high spin bispidine complexes (the activated, final version (ON) of the bispidine-based magnetogenic probes). In particular, I have developed a unique synthetic protocol to a bispidine with a free N7-H site using a protecting group strategy, a feature not possible via a direct multi-component protocol. The utility of the dimethoxybenzyl moiety was proven by establishing the large scale synthetic protocols for introduction and removal of this protecting group in bispidine systems. In the perspective, the replacement of the DMB with PMB can be envisaged to reduce the costs and possibly improve the yields of the protecting group introduction.

Indispensable knowledge on the control of bispidine synthesis, practical analytical tools developed for their characterization and large scale preparation of versatile intermediates bode well for devising a wide variety of hexadentate ligands.

6. BISPIDINE-BASED MAGNETIC OFF-ON DUO

6.1. Introduction – the concept of overcoming a steric clash

No low spin bispidine iron(II) complex has yet been reported.^{[191] [181] [174]} Even a complexation of the hexadentate N6 bispidine-based ligand possessing 4 pyridyl moieties gave rise to a paramagnetic chelate. In particular, one pendent arm (picolyl substituent on N7) remained uncoordinated in the solid state with SO_4^{2-} counter ion occupying a 6th coordination site (see Fig. 36A). However, coordination of the dangling picolyl arm in solution was suggested on the basis of spectroscopic studies. UV-Vis spectra revealed the presence of the absorption band which, could be attributed to the intense metal-to-ligand charge transfer band (MLCT) characteristic of the LS state. While it suggests that the compound remains “close to the spin crossover” in solution, other interpretations (like charge transfer effects or isomer equilibria) were not excluded or experimentally confirmed.

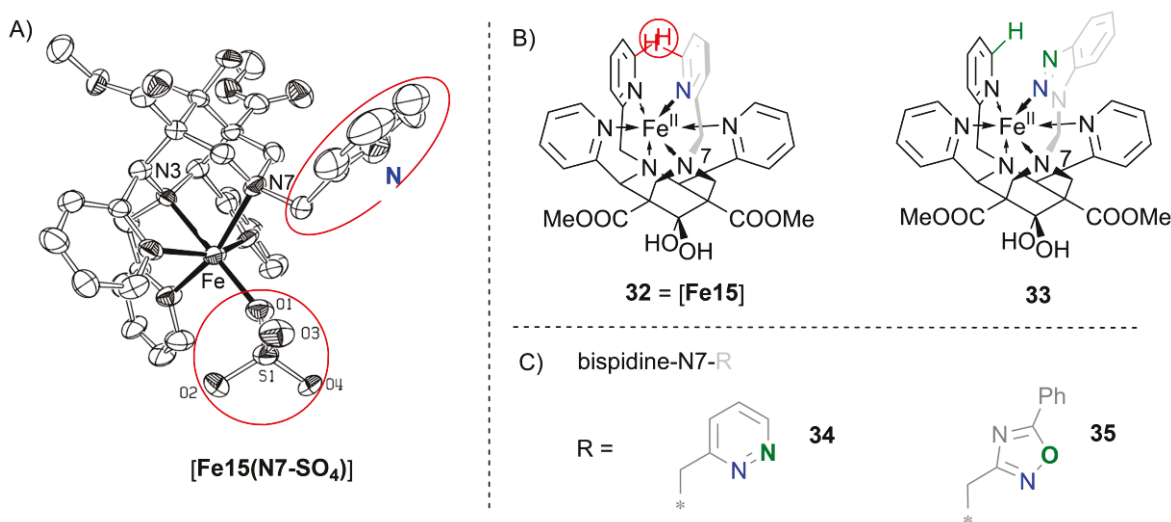


Fig. 36 Steric clash in hexadentate bispidines. A) crystal structure of ferrous complex $[\text{Fe15}(\text{N7-SO}_4)]$ of potentially hexacoordinate bispidine ligand **15** published before^[191] with decordinated picolyl group from position N7 (upper red circle) and SO_4^{2-} counter ion coordinated in its place (lower red circle); structure published in Borzel et al 2002^[191]. B) Modeled structures of low spin complexes (**32** – theoretical 6-coordinate ferrous complex of ligand **15**, corresponding to $[\text{Fe15}]$; **33** – complex of imagined N7-benzotriazole bispidine ligand) and revealed steric clash (red circle). C) Moieties (in grey) without a substituent in *ortho*-position (atom in green) to the coordinating atom (atom in blue) (**34** and **35** – bispidine analogs of ligand **15** with N7-picolyl replaced by methylpyridazine and methyloxadiazole moieties respectively).

6.1.1. Steric clash at the origin of only high spin bispidine ferrous complexes

Prof. Hasserodt has thus looked in more details at the reported ferrous complex of potentially hexadentate but effectively pentadentate bispidine ligand **15** (Fig. 36 A, in red circles

decoordinated picolyl group – upper – replaced by sulfate ion – lower red circle) and performed modeling studies of this structure with MOPAC using the AM1 parameter set, which includes the element iron. When the Fe-N bond lengths in hexacoordinate complex **32** (Fig. 36 B) had been locked at 2.0 Å, typical for the low spin iron(II), the examination of the space-fill scheme of the modeled structure revealed a steric clash involving two *ortho*-hydrogens of the facing pyridine coordinating units grafted on the N3 and N7 atoms of the bispidine backbone (in red)). This steric clash was thus thought of causing a significant deflection of the coordinating surfaces of the pyridines leading to far from optimal coordination geometry and decreasing electronic interactions between the ligand and the central metal ions (the overlap of the ligand electronic orbitals, σ or π^* with d-orbitals of the metal). This in turn was suspected to be a major reason for the destabilization of the low spin state of iron(II) (the detailed mechanism was not important in these considerations but it could be speculated that the destabilization of LS state of Fe(II) could be a consequence of the weaker ligand field (globally) or the loss of symmetry). Indeed, introduction of a steric congestion is widely explored in the design and synthesis of the SCO compounds from the analogous low spin counterparts.^[151] Thus, Prof. Hasserodt hypothesized that the removal of the hydrogen atom from one of the clashing pyridine moieties could restore the optimal coordination geometry and allow the ligand to exert its full potential, generating a strong ligand field, which should reliably stabilize the LS state. Following the above idea, a model experiment with the imaginary complex **33** (imposing Fe-N = 2.0 Å) was carried out showing a perfect fit of the two nitrogen atoms around the iron center with no repulsive interactions, thanks to the replacement of pyridine moiety with the benzotriazole lacking the hydrogen in an *alfa* position to its coordinating nitrogen (Fig. 36 B).

6.1.2. Pyridazine and oxadiazole as coordinating motifs

In order to verify this hypothesis, I have proposed the use of pyridazine and oxadiazole moieties (respectively upper and lower structure in Fig. 36 C, **34** and **35** are the respective bispidine analogs of ligand **15** but with these moieties in position N7) which possess the imine-type N-coordinating site (blue atoms in Fig. 36 C), but without steric clash (hydrogen atom) in *ortho*-position (green atoms in Fig. 36 C). Pyridazine is the closest analog of the pyridine which fulfills the steric requirement and thus was hoped to exert still strong enough ligand field. Indeed, it has been demonstrated^[227] that the di-imine system: 3,3'-bipyridazine (L), unlike the bpy analog, forms low spin complexes with iron(II) ($[\text{FeL}_2(\text{NCS})_2]$ and $[\text{FeL}_3]^{2+}$ salts). It is believed to result in part from the absence of *ortho*-hydrogen atoms in the ligand molecules which cause considerable inter-ligand repulsion in complexes of the related di-imine, 2,2'-bipyridine. Among number of coordinating motifs incorporating pyridazine-like moiety, there exist only one report of metal complexes (Pt^{IV} with ligand (bidentate one) containing the methylpyridazinyl group (picolyl analog)^[228]. Oxadiazole moiety, which should be sterically even less demanding than pyridazine due to the five-membered aromatic ring, coordinate to a variety of metal ions by either of the nitrogen atoms

(some examples of transition metal complexes are given with N4^[229] ^[230] ^[231] and N1 coordination^[232] ^[233], including Fe(II) coordination by N4^[234] and N1^[235] ^[236]). The steric demands of the bulky phenyl substituent in position 3 should however efficiently exclude the possibility of the N4-coordination in the designed complex and increase the pi-accepting character of the ligand which is hoped to pay off for the decrease in basicity and thus weaker sigma donation (decrease of pK_a to approx. -2.6 in comparison to 2.3 for pyridazine and 5.2 of pyridine).^[237] ^[238] In addition, both moieties were easily accessible and thus serving as a good model compounds.

6.2. Synthesis of hexadentate bispidine ligands

Two new hexadentate ligands **34** and **35** (described also in Fig. 36 C) and as a control already reported ligand **15** (Fig. 37) were prepared in order to study the possibility of attaining the diamagnetic low spin state with bispidine systems, which is an essential challenge if the design of truly off-ON magnetogenic probes is considered.

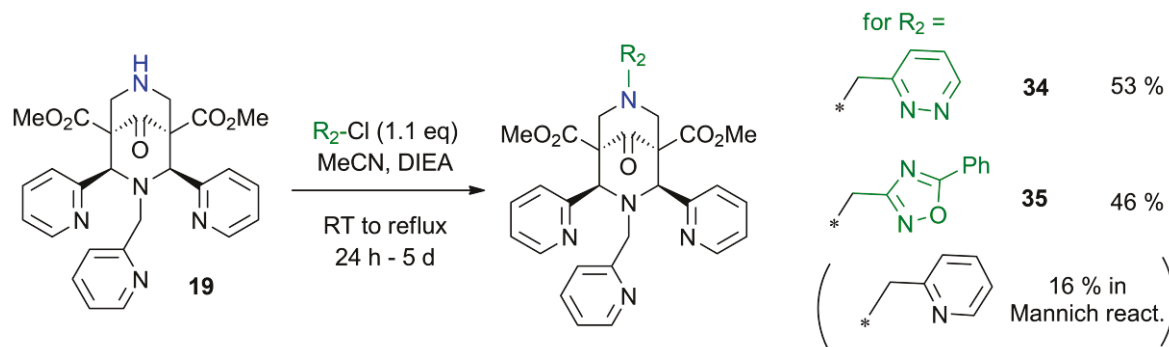


Fig. 37 Preparation of the hexadentate ligands by N7-H functionalization of a key intermediate **19** in S_N2 reaction.

6.2.1. Classic Mannich approach

Synthesis of hexadentate bispidine **15** by Mannich-type reaction was described.^[191] Following the procedure, I was not able to isolate a desired product by recrystallization from EtOH so I have used a combination of *i*PrOH/Et₂O what led to 16 % of isolated yield (lit. 25 %^[191]) and was sufficient for the needs of the project. I have also fully characterized both *syn* and *anti* configurational isomers of this ligand by NMR and studied the reaction progression as in the case of DMB-analog (chapter 5). It confirmed my conclusions that the balance between the isomerization and decomposition/side reactions is principally responsible for the moderate-to-low isolated yields reported for substituted bispidines with more bulky substituents, demonstrating an important limitation of the Mannich-type bispidine synthesis. Preparation of **34** and **35** by this strategy was not attempted due to the limited accessibility of the necessary amine precursors of methylpyridazinyl and methyloxadiazolyl moieties respectively.

6.2.2. Alkylation of N7-H secondary amine of bispidines – S_N2 reaction

In order to study the suitability of alkylation pathway proposed by us for the application with future functional arms, I have successfully prepared oxadiazole and pyridazine ligands with moderate yields (Fig. 37). Phenyloxadiazole methylchloride was commercially available, while pyridazine analog can be prepared in one-step by radical halogenation of a commercial methylpyridazine as described [239]. It is worth mentioning, that the latter decomposes upon prolonged storage at RT or even at 0 °C and thus should be used directly. Alkylation with a crude product of methylpyridazine chlorination, which is a mixture of di-, mono- and non-chlorinated compound, is equally efficient as with a pure mono-chloride and does not lead to any extra side-products because neither methylpyridazine nor dichloromethyl analog can undergo a nucleophilic substitution by secondary amine. In the consequence the use of crude mixture just after quenching and isolation of organic elements is recommended. While for oxadiazole precursor, the reaction was completed after 24 h of reflux in acetonitrile in the presence of DIPEA (N,N-diisopropyl-N-ethylamine – Hunig base) instability of pyridazine chloride at elevated temperatures required longer reaction times, usually several days, at RT. Subsequent purification by flash column chromatography on neutral alumina (**34**) or crystallization (**35**), yielded pure desired ligands, **34** (53 %) and **35** (46 %) all stable at RT and on air and ready to be used in the complexation reaction. The yields could still be significantly improved if bigger scale reaction was performed, as the conversion of the substrate to the product in the reaction mixture is practically complete. Importantly, with this methodology the configuration on the piperidinone (bispidinone) is conserved and thus no impurities from *anti* form or other isomers need to be feared, unlike in the case of Mannich synthesis.

6.2.3. S_N2-type alkylation vs. Mannich condensation – comparison of efficiency

When relative yields of Mannich reaction and alkylation reaction are compared in respect to the piperidinone starting material, then Mannich strategy gives the better overall yield due to the two additional steps connected to introduction and removal of a protecting group required for the alkylation pathway. However, the situation changes when the amount of the arm introduced is the limiting factor (chloride or amine precursor in alkylation and condensation respectively), as it is the case for a design of elaborate molecular tools. Then the superiority of the alkylation approach is reflected by at least two times greater yield of final ligand in respect to the arm precursor (with a reasonable assumption of similar efficiency of Mannich reaction for pyridine and pyridazine precursor).

6.2.4. Attempts to N3-H derivatization

As the steric clash in the modeled system comes from the N3 and N7 substituents, introducing a pyridazine or oxadiazole moiety on N3 atom (platform **18**) instead of N7, is also expected to

eliminate it. However, none of my attempts led to the isolation of the desired product, even if traces of it could be observed by the DIMS. It seems to be evident that the alkylation at position N3 is more challenging than at position N7, which might be a consequence of the steric congestion around this reaction center, hampering the nucleophilicity of N3-H group, particularly important for the S_N2 -type reactions. In the light of initial failures in performing the N3-H alkylation, this strategy was not further developed also due to the success in functionalization of N7-H platform. Grafting the desired moieties on N7-H came out to be swift and neat and led directly to desired ligands, which were sufficient to confirm the possibility of attaining truly diamagnetic state in bispidine-iron(II) system. Nevertheless, at current stage of the development of the project, when the first functional probes are being prepared and the improvements of the MRI signal intensity are searched (see discussions in chapter 7 and 8), a series of N3-derivatized probes may come out to offer significant advantages over, or complimentary to the N7-based systems. Thus, provided that I was able to observe the traces of the alkylation products with N3-platform, further experiments would be highly desired, including a variation of solvents and bases, in order to optimize this process leading to the new analogous ligands and possibly also functionally interesting complexes.

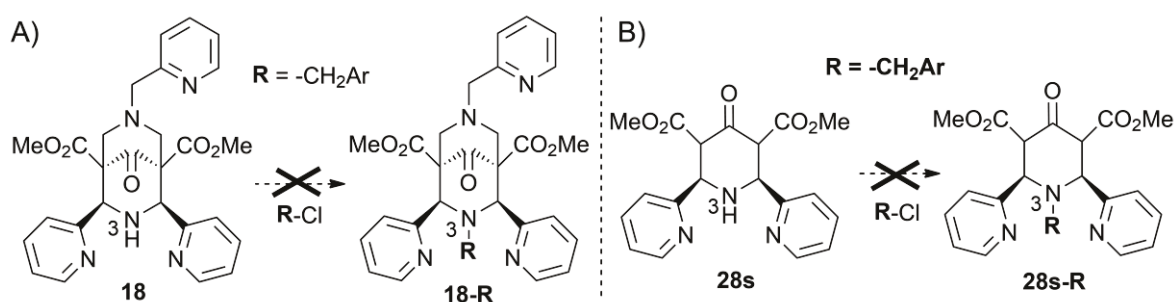


Fig. 38 Unsuccessful alkylation on crowded N3-H position of syn 2/4-substituted bispidinone (A) and piperidinone (B)..

6.2.5. Conclusions

Increased efficiency of ligand preparation with respect to the quantities of the arm-bearing reagent), milder reaction conditions (RT in aprotic solvents) and a use of easily accessible halide precursors are the crucial improvements offered by the alkylation strategy in comparison to the classic synthetic approach. In combination with a relative insensitivity towards the variation of the moiety introduced, unlike in Mannich condensation where the protocol has to be re-optimized for every new substrate, these features of our synthetic approach make it an optimal choice for the preparation of molecular probe and enable us to widen the range of accessible functionalized hexadentate bispidine-ligands.

6.3. Complexation and solid state structures

Three hexadentate (**15**, **34** and **35** in Fig. 39 A) and two pentadentate (**18** and **19** in Fig. 39 B) bispidine-based ligands synthesized in the course of this work were used for a preparation of model off low spin and model on, high spin iron(II) complexes..

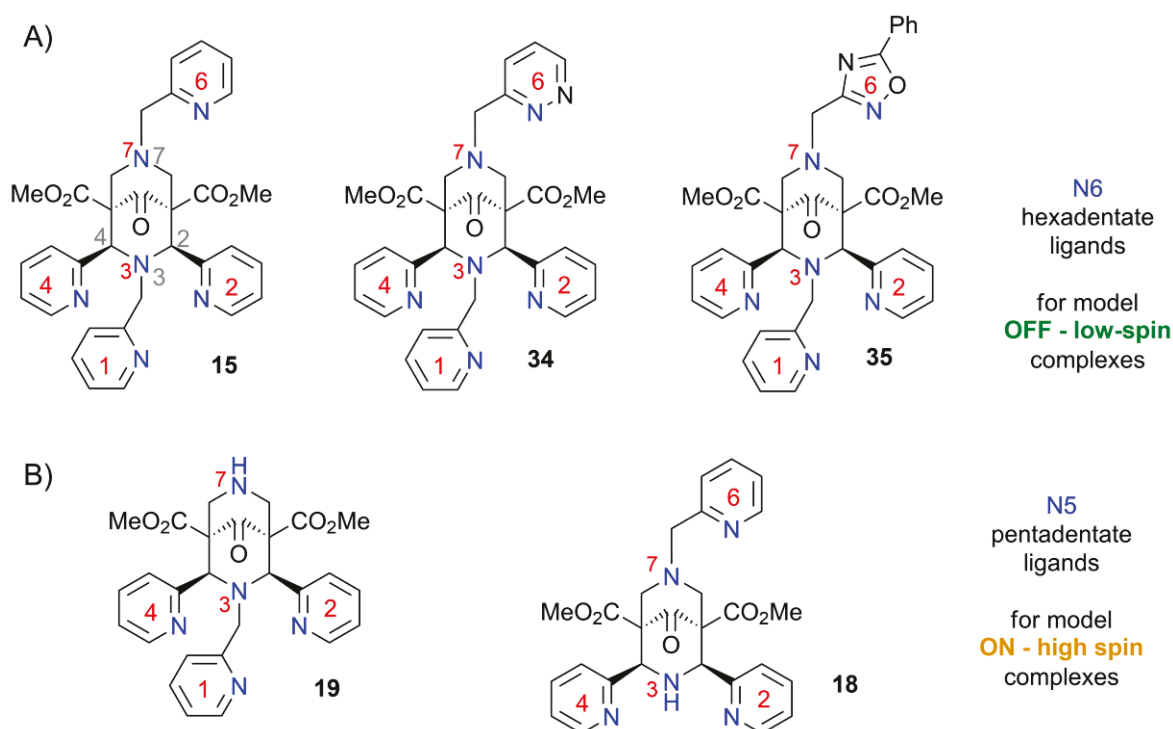


Fig. 39 Structures of model ligands chosen for iron(II) complexation, A) hexadentate and B) pentadentate precursors of model LS and HS complexes respectively. Note the numbering of potentially coordinating units (in red) and their direct relationship to the numbering of the bispidine backbone (in grey – see structure of ligand **15** in panel A and also Fig. 19 B and Fig. 23); moieties **2** and **4** are the substituents at positions **2** and **4** of the bispidine framework, with positions **3** and **7** corresponding to N3 and N7 coordinating atoms.

Iron(II) complexation was typically performed at room temperature in dry, degassed acetonitrile for hexadentate ligands and methanol for pentadentate ones, with usually 5 % molar excess of $\text{Fe}(\text{BF}_4)_2 \cdot 6\text{H}_2\text{O}$ or $\text{Fe}(\text{ClO}_4)_2 \cdot x\text{H}_2\text{O}$ salt, or equimolar quantities of $\text{FeSO}_4 \cdot 7\text{H}_2\text{O}$. The reaction progress was followed by DIMS and stopped upon a complete consumption of the ligand. Purification of the product was performed by its precipitation in the cold solvents and subsequent extensive washing of the precipitate, or directly subjected for crystallization. Variable techniques and solvent combinations were attempted but the best results were generally observed with a gas-liquid or liquid-liquid diffusion of diethyl ether to reaction mixtures with a 5% addition of water. Alternatively, some complexes were also crystallized from wet isopropanol solution and liquid-liquid diffusion of diethyl ether. It is important to notice that obtained low spin complexes were resistant to oxidation or degradation even upon prolonged heating or long term air exposure (over a week), and could be handled freely. High spin ones however were isolated and purified in the atmosphere of the neutral gas, and showed generally an air sensitivity, from degradation/oxidation

occurring within few minutes to several hours upon air exposure. Once in the solid form they were all stable on air. For more information on their stability the reader is referred to the text below when individual examples are discussed in details.

All newly prepared complexes showed a binding of solvent molecule to the keto-functionality in position-9 both in solution and in the solid state, what has been typically observed for other bispidine complexes. Ketalization is a fully reversible process and it is generally a function of the solvent used. Despite the preferable binding of the water molecule, adducts of alcoholic solvents could also be observed in solution by mass spectrometry and methanolate was found in the solid state structure of [Fe18(SO₄)]. For ligands, ketalization was observed in solution by DIMS, but it has not been found in the solid-state structures, suggesting that it is less favorable than in the case of complexes.

6.3.1. Preorganization of bispidine ligands for iron(II) complexation

Monocrystals suitable for X-ray analysis were obtained for the ligand **15**, **18** and **35**, as well as for the *anti* isomer of the ligand **15** (**15a'** and **15a''**) and their comparison demonstrates a high preorganization of the *syn* bispidines for metal complexation (Fig. 40). X-ray experiments were performed by Dr. Erwann Jeanneau from Laboratoire des Multimatériaux et Interfaces (University of Lyon –UCB) (for experimental details please see the Experimental part in this work). All *syn* ligands remain in the chair-chair conformation in the solid state, despite a rather bulky substituents on the N7 atom, indicating that in solution even if chair-boat isomer may exist, it is rapidly and easily flipping to the chair-chair form. For these molecules a simple along-one-bond rotation of the coordinating arms is the only rearrangement required to enable a hexacoordination. For N3-substituted compounds **15** and **35** the two nitrogen atoms of the pyridyl groups in position 2/4 are rotated away from the potential coordination cavity. It is probably due to the electrostatic repulsions between them and the lone pair of the N3, which is blocked in orientation *endo* by the bulkiness of the picolyl moiety. Once metal ion is coordinated, these repulsions disappear and are replaced by a formation of the metal-ligand bonds further stabilizing the chair-chair conformer. While the N7-picolyl is principally already oriented towards the binding cavity, the N3-substituent, due to the greater steric congestion in this part of the molecule, points away from it. Thus the N3-arm, apart from the subtle reorientation of its pyridyl ring, has to rotate also by almost 180 ° along the CH₂-N3 bond. For the pentadentate compound **18** with N3-H functionality, free electron pair of the N3 can occupy the position outside the cavity with H-atom pointing towards it. In the consequence two pyridines on C-2/4 orientate their donor atoms towards the binding site, what is probably additionally favored by the H-bond type of interaction between them and the N3-H. Preorganization of **18** is thus even higher than for **15** and **35**, as the only adaptation for optimal metal binding is an inversion on the nitrogen atom N3, which for H-substituent is rapid at room temperature.

In comparison to the *syn* form, *anti* isomer of dipicolyl ligand (**15a'** and **15a''**, in Fig. 40 D) is much less preorganized for metal complexation and theoretically enables at best only pentacoordination despite the potentially six coordinating moieties present in the molecule. Crystallographic analysis of this product revealed a presence of the two isomeric structures differing by the pyridyl group which attain the axial position. It can be expected as no clear selectivity for a particular side of the molecule exist in terms of the starting point of the retro-Mannich reaction. Boat-chair conformation of these compounds observed in the solid state suggests that it also dominates in solution. If N3 and N atoms from the picolyl substituents are to be available for metal coordination, a flip to chair conformation would have to take place, what implies a rearrangement of the bulky 2/4-substituents, previously axial one becoming equatorial and equatorial one attaining an axial position. Thus the energetic barrier of this process might be elevated hampering the polydentate metal coordination.

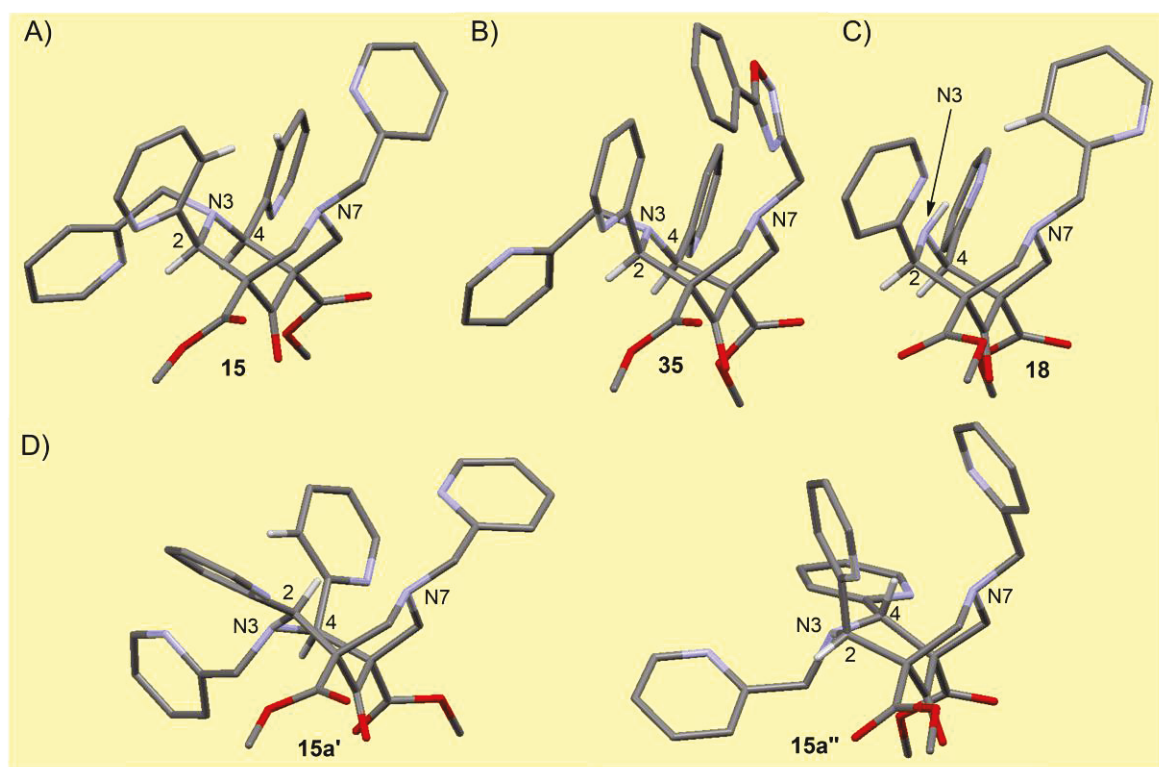


Fig. 40 X-ray structures of the ligands in *syn* (A,B and C) and *anti* (D) configuration. Hydrogen atoms were omitted for clarity except those pointing towards the coordination cavity and H-2/4 to facilitate the distinction of the configuration.

6.3.2. Low-spin bispidine iron(II) complexes – steric clash eliminated

Two binary, ($[\text{Fe}34]^+ \cdot 2\text{BF}_4^-$, $[\text{Fe}35]^+ \cdot 2\text{ClO}_4^-$) and one ternary ($[\text{Fe}19(\text{CH}_3\text{CN})]^+ \cdot 2\text{BF}_4^-$) complexes obtained in the course of this work showed a low spin characteristics in the solid state and are so far (August 2013) the only reported examples of the low spin ferrous chelates.^[193] They were prepared in dry degassed acetonitrile at RT from the corresponding ligands and equimolar quantities of appropriate iron(II) salts. Crystallization by liquid-liquid and gas-liquid diffusion of

diethyl ether to reaction mixtures yielded brown to deep-red colored crystalline material suitable for X-ray analysis in 36 %, 25 % and 17 % yield of the above-mentioned complexes of the ligands **34**, **35** and **19**, respectively. $[\text{Fe19}(\text{CH}_3\text{CN})] \cdot 2\text{BF}_4$ was additionally successfully obtained from reaction in EtOH upon the addition of traces of acetonitrile.

By replacing $\text{Fe}(\text{Tf})_2(\text{CH}_3\text{CN})_2$ in the reported procedure with a $\text{Fe}(\text{BF}_4)_2 \cdot 6\text{H}_2\text{O}$, a binary complex ($[\text{Fe15}] \cdot 2\text{BF}_4$) was isolated by joint efforts with Robert Steinhoff who performed his Master 1 internship in our laboratory under my supervision. I was then able to crystallize it by a standard procedure described above with a 71 % of the total yield and proved its hexacoordinate character, a binding mode not yet reported for this literature-known complex. The X-ray structure of this molecule indeed shows a significant deflection from the optimal geometry of coordination of the N7-substituent (28.38°), proving the modeled steric clash from the *ortho*-hydrogen of N3-picolyl and N7-picolyl substituents facing each other in the chelate (Fig. 41). Replacement of the C-H by N in *ortho* position to the coordinating N6 atom, achieved by the pyridazine-bearing ligand **34**, decreases the degree of deflection by approximately fifty percent (14.74°). Finally, when going from 6-membered aromatic moieties to the 5-membered aromatic ring of oxadiazole with oxygen in *ortho* position (ligand **35**), steric clash is almost entirely eliminated (deflection angle of 3.94°), restoring the optimal coordination geometry found also in sterically unhindered ternary complex of pentadentate bispidine ligand and 6th coordination site occupied by CH_3CN (-6.02°).

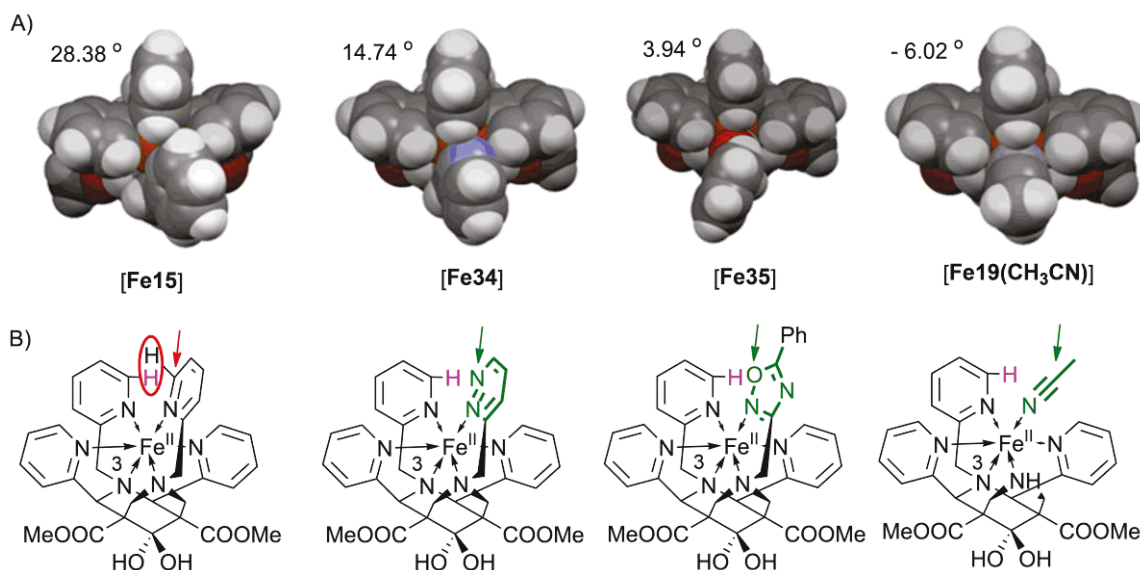


Fig. 41 A) Authentic X-ray structures (space-fill view) of the only existing low spin bispidine-iron(II) complexes demonstrating a steric clash and its variation, including the change of the deflection angle between the two facing coordinating motifs from positions N3 and N7. Adapted from Kolanowski et al 2013 ^[193] - with permission of WILEY-VCH Verlag GmbH & Co. KGaA, Weinheim (copyright © 2013). B) Chemical structures of the complexes from panel A (given for clarity). In green - moieties with reduced steric clash, in violet – ortho-hydrogen from N3-picolyl moiety which is at the origin of the steric clash.

Further analyses of the structures of these complexes reveals general deformation of the octahedral coordination geometry upon the occurrence of the steric clash. One of the parameters which can be discussed is the mean deviation from the optimal 90° angle, which is even 0.5° greater for the

sterically strained complex **[Fe15]** in comparison to two other hexadentate chelates (Table 4). Ternary complex **[Fe19(CH₃CN)]** can be treated as the model for optimal coordination of the 6th arm as acetonitrile does not suffer from any strain and thus can adopt the most favorable position to maximize the ligand field strength and stabilize the low spin state. Indeed, the average difference between the real N-Fe-N angles measured and 90° which is a theoretical angle for the perfectly octahedral structure, is even 1.25° smaller in **[Fe19(CH₃CN)]** than in the most distorted **[Fe15]**, and 0.75° smaller than average deflection in remaining complexes.

In addition, bond distances and deflection angles can also serve to estimate qualitatively the effect of the coordinated moiety on the ligand field. A 30° distortion from the optimal approach of the present in complex **[Fe35]** may significantly impair the orbital overlap, not only in the terms of the less effective sigma donation but also hampered back-bonding. Both parameters will then be reflected in the strength of the bond which in turn is directly associated with the bond length. Despite the fact that for all four complexes Fe-N bonds remain within the usual range of the low spin iron(II) complex (Table 4), the pyridine moiety suffering strain (**[Fe15]**) approaches iron(II) for the distance of more than 0.1 Å greater than oxadiazole substituent or acetonitrile. Fe-N length for pyridazine nitrogen is 1.97 Å what remains almost exactly in the half way between the two others. Thus it could be potentially concluded that the ligand field of oxadiazole binding moiety in **[Fe35]** complex is stronger than the pyridine in **[Fe15]**, even despite a significantly decreased basicity of the oxadiazole nitrogen, and so can be attributed to the geometrical effects. Such a difference in binding one residue seems also to have an effect on other Fe-N bond distances, but it is less pronounced. Nevertheless, the average Fe-N bond distance for **[Fe35]** is 0.04 Å shorter than for complex **[Fe15]**, but the effect is even more subtle for other compounds.

Complex	Fe-N3	Fe-N7	Fe-N2	Fe-N4	Fe-N1	Fe-N6	Mean Fe-N	N3-N7	N2-N4	Defl. angle	Dev from 90°
[Fe15]	1.98	2.08	2.02	1.98	1.99	2.03	2.01	2.81	3.95	28.38	6.02
[Fe34]	1.98	2.08	1.98	1.97	2.00	1.97	2.00	2.83	3.91	14.74	5.49
[Fe35]	1.96	2.09	1.96	1.96	1.95	1.91	1.97	2.84	3.89	3.94	5.45
[Fe19(CH₃CN)]	1.97	2.07	1.98	1.97	1.96	1.92	1.98	2.77	3.92	-6.02	4.77

Table 4 Bond distances and angles in all low spin and near low spin complexes (for the numbering of coordinating N-atoms see Fig. 39).

Differences in the ligand field between the **[Fe15]** and other complexes discussed was confirmed by the SQUID measurements of the temperature-dependent magnetic moment of these compounds, which was performed and largely interpreted by Dr. Ruben Checa and Prof. Dominique Luneau from Laboratoire des Multimatériaux et Interfaces, (University of Lyon – UCB). While the X-ray structure was acquired only at low temperature, the effective spin state of the central metal ion concluded only from the bond length can be misleading. Magnetic measurements confirmed that **[Fe34]** and **[Fe35]** complexes are truly diamagnetic as their magnetic susceptibility remained close to zero and were not changed within a temperature range of 100 K to 300 K. In the contrary,

[Fe15] underwent a gradual spin transition, confirming the predictions from the X-ray structures about a weaker stabilization of the low spin state of iron(II) in this chelate than in the sterically less demanding analogs.

6.3.3. Preparation and solid state structures of high spin complexes

Except a synthesis of the low spin iron(II) chelates of bispidines as the model of the off-state of the future probes, preparation of a high spin counterparts corresponding to the active form was also attempted in order to demonstrate a magnetic duo of related complexes with bispidine-iron(II) system. The initial responsive strategy pursued in our group already before the beginning of my work aimed at enzyme-initiated departure of the whole sixth coordinating arm in tacn system, unmasking a NH functionality in the active form of the probe which would become pentadentate (see chapter 3). As the same approach was originally envisaged for the bispidine system, the active forms of the bispidine-probes would then be ferrous complexes of either N7-H (**19**) or N3-H (**18**) ligands and thus studying of their properties was very important. Up to now compounds prepared by me are the only iron(II) complexes of bispidine-type ligands with a secondary amine moiety – all the reported chelates are high spin but they always involve exclusively tertiary aliphatic amines.

As mentioned above, these compounds were prepared from the FeSO₄ salt in dry degassed methanol under inert atmosphere and their isolation was performed also with the exclusion of air in order to avoid a risk of oxidation, which is common for high spin iron(II) complexes. Low solubility of ferrous sulfate in organic solvents required elevated temperatures, but even if not all inorganic material was initially dissolved, rapid complexation of iron(II) available in solution upon the addition of the ligand interrupted the solubility equilibrium leading to a complete dissolution of the sulfate. Crystallization from the reaction mixtures or from isopropanol upon the ether diffusion enabled an isolation of the desired products as yellow, somewhat transparent crystals, suitable for the X-ray analysis. As previously reported, these complexes, as well as the low spin ones isolated by me, are all in the form of the hydrate on carbon C-9. Nevertheless, addition of other solvent molecules to the ketone on C-9 was also observed by DIMS during the reaction as well as in the crystal structure of [Fe18(SO₄)] where not a hydrate but a methanolate was observed. Solvent addition at this position is fully reversible and is largely a function of the main media component, with a certain preference for water molecules.

Simultaneously, I have also attempted a preparation of the reported high spin complex of hexadentate ligand **15**. Original reported protocol involved a use of Fe(Tf)₂(CH₃CN)₂ salt for the complexation reaction and subsequent crystallization upon the addition of the excess of sulfate, leading to the previously discussed molecule with SO₄²⁻ being coordinated in the place of the N7-picolyl substituent. Instead, I have used directly FeSO₄, as with the pentadentate ligands **18** and **19**, and after only several minutes the reaction seemed to be completed and I could isolate X-ray quality light yellow crystalline material upon ether diffusion to methanolic solution. Structural

analysis in the solid state confirmed the expected pentacoordination of the potentially hexacoordinate ligand **15**, with one coordination site occupied by SO_4 as in the case of reported structure^[191]. However, interestingly, it was the opposite pendent arm (residing on the N3 – [**Fe15(N3-SO₄)**] in Fig. 42) which has been decoordinated suggesting a kinetic control of the coordination process. In the literature example the ligand was left to coordinate to the metal center in the most optimal variant, which according to my x-ray structure of [**Fe15**] discussed above is a proper coordination of the N3-substituent and significant deflection of the moiety on N7. Only then the addition of strongly coordinating sulfate led probably to the replacement of the more labile N7-substituent and subsequent precipitation. Oppositely in my case, sulfate anions coordinated to the iron(II) were only partially replaced by the pentacoordinate motif of the ligand. As the x-ray structure of the ligand **15** suggests, N7-picolyl is better preorganized for metal coordination, while the N3-picolyl has to rotate by 180°, which might even be sterically disfavored once the sulfate is coordinated to the metal center. This hypothesis was not confirmed by any additional experiments, but the observation of effective sulfate coordination suggests a high stability of this compound even in water, despite its high spin state. Such a behavior was thus envisaged by me to be explored more in depth in the anion sensing applications, as described in chapter 7.

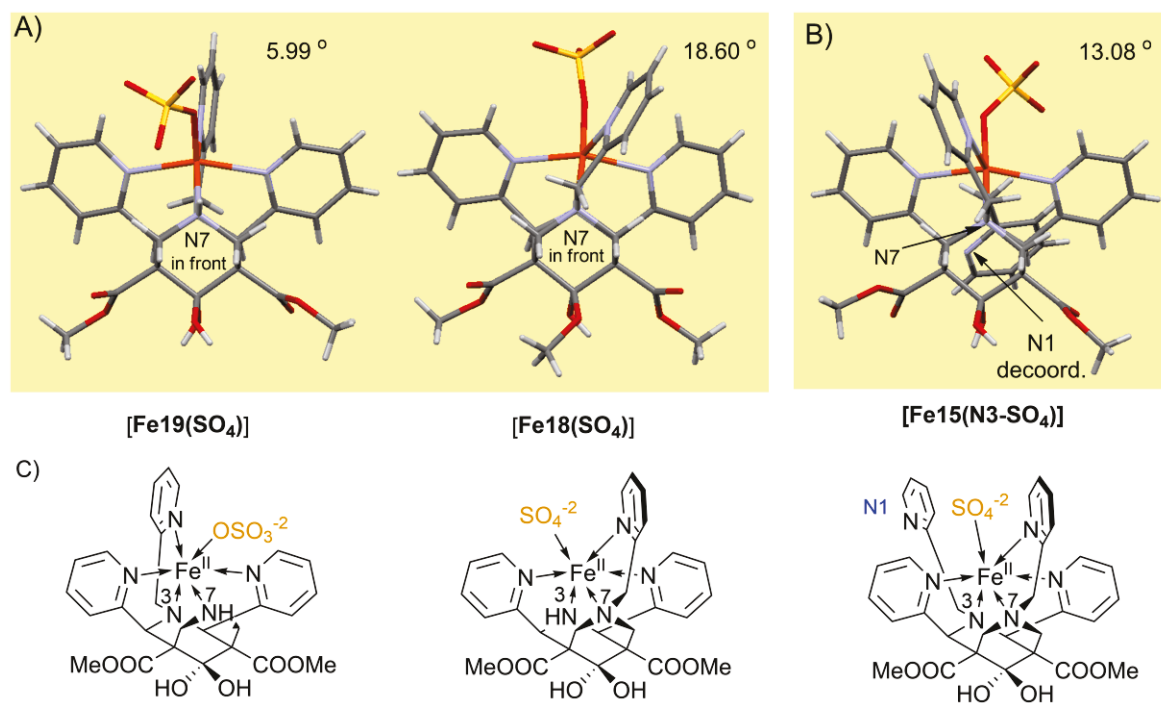


Fig. 42 X-ray structures (view along N7-N3 axis with N7 in the front) of A) two isomeric secondary amine-based iron(II) complexes of bispidines (left and middle) and B) a new coordinational isomer of [**Fe15(SO₄)**] but with N3-picolyl arm dangling away (right structure – [**Fe15(N3-SO₄)**]). Deflection angles between the coordination moieties from positions *trans* to N3 and *trans* to N7 are given. C) Chemical structures corresponding to the X-ray images (in orange – monodentate sulfate anion).

Bond distances in the solid state of three newly prepared high spin iron(II) complexes (X-ray structures in Fig. 42) and three previously reported analogs, one with sulfate coordinated in the

place of N7-arm and two with methyl substituent instead of secondary amine, are given in the Table 5 (newly synthesized complexes - in black, and previously reported - in grey). For all of them, independently on the substitution pattern, the average Fe-N bond lengths are all oscillating within the same range of 2.2 Å characteristic of a high spin state. Individual comparison of the selected Fe-O bond lengths (in bold in Table 5, O from SO₄²⁻ anion) within each isomeric pair confirmed the previous observation that binding is stronger in position trans to N3 than trans to N7, being of particular importance for the design of catalysts.^[191] In particular, bond lengths differed by 0.04 Å for isomeric complexes of ligand **15**, and this difference was slightly lower (0.03 Å, 1.97 Å vs. 2.0 Å) for N-H unsubstituted chelates or slightly higher (0.05 Å – 1.97 Å vs. 2.02 Å) for methyl analogs, do not showing any obvious correlation between the bulkiness of substituent and the bond strength. However, crystal structures of the high spin complexes prepared by me in the course of this work and presented in Fig. 42, show that there is a significant deviation from the optimal coordination geometry of the N7-substituent, similar to the one for low spin chelates, when the sulfate is coordinated *trans* to N7 (13 ° and 19 ° for [Fe15(N3-SO₄)] and [Fe18(SO₄)] respectively). It may thus explain why this binding is weaker than in position trans to N3, like in [Fe19(SO₄)] which does not possess any substituent on N7 and for which the distortion is significantly reduced (only 6 °). These newly observed steric effects, if attained also in solution, may be of particular interest for the optimization of the bispidine-based iron(II) catalysts, by the variation of the N7 substituent and the steric clash it imposes, leading to a modification of the substrate binding.

Complex	Fe-N3	Fe-N7	Fe-N2	Fe-N4	Fe-Y1	Fe-Y6	mean Fe-N	N3-N7	N2-N4
[Fe18(SO ₄)]	2.16	2.34	2.21	2.17	2.00	2.16	2.21	2.82	4.23
[Fe19(SO ₄)]	2.23	2.20	2.23	2.22	2.14	1.97	2.20	2.86	4.29
[Fe15(N3-SO ₄)]	2.20	2.29	2.20	2.24	2.00	2.14	2.21	2.90	4.29
[Fe15(N7-SO ₄)]	2.22	2.27	2.17	2.21	2.20	1.96	2.21	2.88	4.25
[Fe(N3-Me)(SO ₄)]	2.18	2.37	2.19	2.14	2.02	2.13	2.20	2.88	4.24
[Fe(N7-Me)(SO ₄)]	2.23	2.26	2.18	2.22	2.19	1.97	2.22	2.90	4.26

Table 5 Bond lengths and angles of the pairs of HS complexes. In grey - complexes which were already reported.^[191] In bold – bond distances between the Fe(II) and the coordinating atom (Y = N or O) of the monodentate ligand. For the numbering of coordinating moieties (atoms) see Fig. 39.

Structural deformation of the octahedron upon change of iron(II) magnetic properties. Spin state of iron(II) in the complexes of pentadentate bispidine ligands in the solid state (solution behavior will be discussed in chapter 6.4) is a function of the monodentate coordinate substrate. Solid state structures of complexes of [Fe19] systems revealed that a coordination of the sulfate leads to the Fe-N bond lengths of around 2.2 Å, which is a typical value for the high spin iron(II) center and its solid state magnetic properties confirm that (5.35 μ_B at 300 K typical for a high spin iron(II) with *S* = 2). On the contrary a stronger ligand field exerted by acetonitrile is enough to render ferrous ion low spin in [Fe19(CH₃CN)], as proven by less than 2.0 Å Fe-N bond lengths

and diamagnetic behavior in 100 K – 300 K range in the solid state (SQUID measurements). An increased volume of high spin iron(II) ion imposes a “movement” out-of-the-plane of the metal center in the coordinating cavity of bispidine, similarly to the case of the expanding iron center in the heme group upon coordination/decoordination of triplet oxygen which is also associated with a change in the magnetic state. Reasons of such behavior lie in the rigidity of the bispidine ligand, especially in respect to N3-N7 and N2-N4 distances, which can be varied only to limited extent. This variation is thus not sufficient for adapting to the significant increase of the size of iron(II) when moving from a low spin to a high spin state, thus leading to the deformation of the octahedral coordination geometry.

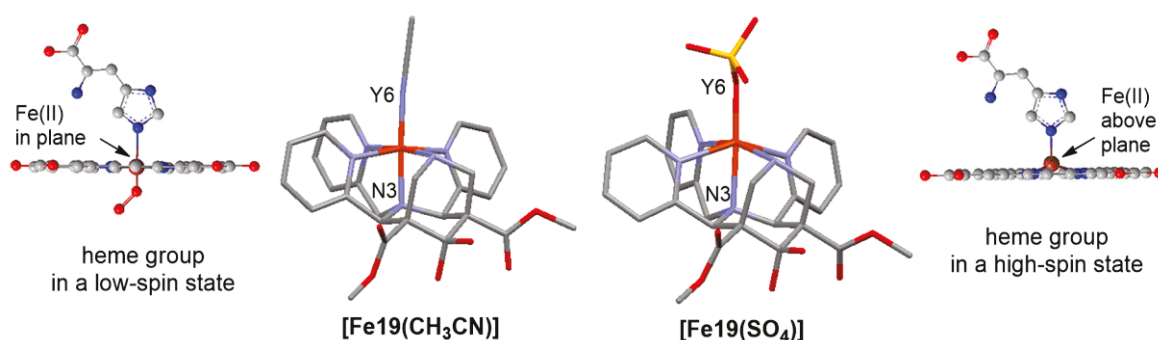


Fig. 43 Iron(II) atomic/radial expansion in high spin complex vs. low spin counterpart and the analogy of this behavior to a similar effect observed for iron center of heme group in hemoglobin.

The observed “movement” by the iron center is well reflected by the differences in the angles between the coordinative bonds (Table 6 on the next page). While the average value calculated for all 12 angles remains 90° for both low spin and high spin compounds, the average deviation from it is twice as big for high spin complexes (approximately 10° vs. 5° per bond angle). Two types of the angles between the coordinative bonds, which are primarily affected and accurately describe the “breathing” type of octahedron’s deformation are (I) Y6-Fe-N_x and related (II) N3-Fe-N_x angles, where N_x are in-plane nitrogen atoms, and Y6 is the coordinating atom of the axial monodentate substituent. Among them, the smallest variation is observed for those involving the Fe-N1 bond, what is in agreement with the highest flexibility of the N1-moiety which can effectively adapt to the structural changes in the complex. N7, N4 and N2 atoms are a part of the rigid bispidine coordination motif and thus their mobility is restricted, imposing the strongest deformations upon the change in the metal ion size, which can be as high as 14° difference in the angles in the low spin and the high spin form, but on average it is above 7° . The angles between the in-plane coordinative bonds (group III in table) are rather weakly affected by the change in the spin state of iron(II) what is consistent with the above-mentioned rigidity of the N7-N3 and N2-N4 structural units.

	<i>Parameter</i>	<i>[Fe19*CH₃CN]</i>	<i>[Fe19*SO₄]</i>	$\Delta_{(LS-HS)}$
group I <i>axial Y6-Fe-Nx in plane</i>	Y6-Fe-N1	99.37	97.69	1.68
	Y6-Fe-N4	94.58	106.28	11.70
	Y6-Fe-N7	86.92	100.92	14.00
	Y6-Fe-N2	98.91	103.67	4.76
	<i>Mean</i>	<i>94.95</i>	<i>102.14</i>	7.20
	<i>st.dev. from 90°</i>	<i>6.49</i>	<i>12.14</i>	5.66
group II <i>axial N3-Fe-Nx in plane</i>	N3-Fe-N1	86.92	81.09	5.83
	N3-Fe-N4	83.08	75.54	7.54
	N3-Fe-N7	86.90	80.44	6.46
	N3-Fe-N2	84.02	74.33	9.69
	<i>Mean</i>	<i>85.23</i>	<i>77.85</i>	7.38
	<i>st.dev. from 90°</i>	<i>4.77</i>	<i>12.15</i>	7.38
group III <i>in plane angles</i>	N1-Fe-N4	87.42	83.20	4.22
	N1-Fe-N2	85.73	84.70	1.03
	N7-Fe-N4	94.25	87.92	6.33
	N7-Fe-N2	91.20	94.55	3.35
	<i>Mean</i>	<i>89.65</i>	<i>87.59</i>	<i>2.06</i>
	<i>st.dev. from 90°</i>	<i>3.08</i>	<i>4.68</i>	<i>1.61</i>
overall summary	<i>Mean</i>	<i>89.94</i>	<i>89.19</i>	<i>0.75</i>
	<i>st.dev. from 90°</i>	<i>4.78</i>	<i>9.66</i>	<i>4.88</i>

Table 6 Bond angles in low spin and high spin [Fe19] metal complexes. For the numbering of coordinating N-atoms see Fig. 39.

6.4. Properties in solution

Despite the successful silencing of the iron(II) magnetism by bispidine-based ligands in the solid state, it is the properties of the synthesized chelates in solution which are of crucial importance for this work. In addition, the results from the solid state, as already discussed in the chapter I, cannot be always extrapolated to the liquid phase, principally due to the loss of cooperative effects and a newly arising but vital issue of the stability of the compounds, especially in polar media. Nevertheless, bispidine-ferrous chelates, especially those of a binary quality, prepared as model off and on versions of the future probes were in most of the cases found not to suffer from these limitations and their solid state magnetic properties were largely reproduced also in solution.

6.4.1. Magnetic moments

The most important parameter for these complexes is their magnetic moment. I have measured it by the NMR method introduced by Evans, which is described in more details in the experimental section. Generally, it is based on the observation of a chemical shift of an internal standard, which in my case was *tert*-butanol (tBuOH), in the presence of the paramagnetic species, in comparison to the same signal from the standard in identical solution but without a substance investigated. As a consequence of the paramagnetism, the signal of all the species in solution should experience a downfield shift, proportional to the concentration and to the magnetic moment, which can thus be retrieved from the chemical shift difference. In practice, the measurement is realized by a system of two co-axial NMR tubes, one containing the reference solution and the other solution of the interest, which are placed in the NMR machine and the ^1H NMR spectrum is recorded. The typical concentration of the paramagnetic substance which I have used for a majority of the experiments was 5 mM with approximately 2 % of tBuOH as a reference.

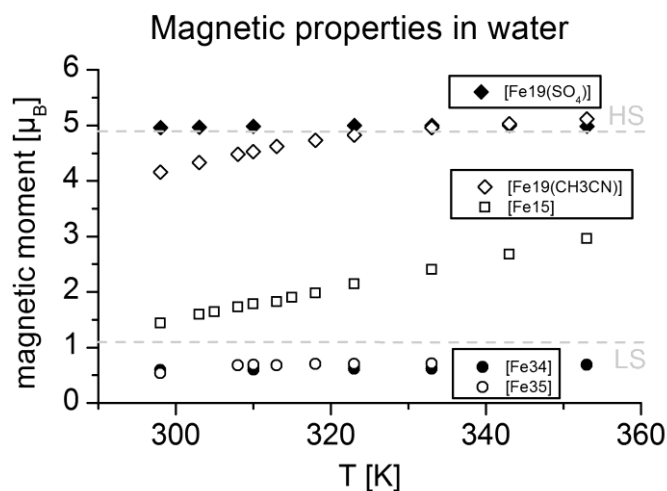


Fig. 44 Temperature dependency of the magnetic moments of selected bispidine complexes synthesized in this work, measured in aqueous solution by Evans' method.

In order to prove the magnetic duality in bispidine iron(II) system, I measured the magnetic moment of representative complexes in aqueous solution at different temperatures, and the results of these measurements are presented in Fig. 44. The NMR shift of the *t*BuOH signal found for fully high spin [**Fe19(SO₄)**] and fully low spin [**Fe35**] complexes, registered at 500 MHz (11.7 T) is shown in Fig. 45, where the smaller peak comes from a *t*BuOH in reference solution and the more intense one is from the solution of the complex.

For the model high spin compound of pentadentate bispidine ligand [**Fe19(SO₄)**] a 103 Hz shift induced by the 5 mM concentration of the complex at room temperature corresponds to magnetic moment of 4.96 μ_B , which does not change with rising temperature (4.98 μ_B at 353 K – the difference of 0.02 μ_B remains within an experimental error). It indicates a fully high spin state of iron(II) possessing 4 unpaired electrons as the spin-only value of $S = 2$ system is 4.9 μ_B . If kept under exclusion of air, magnetic moment of [**Fe19(SO₄)**] remains 5.0 μ_B even over 12 h and/or at elevated temperature, however, when opened to the atmosphere, a degradation of the sample becomes increasingly evident within first hours.

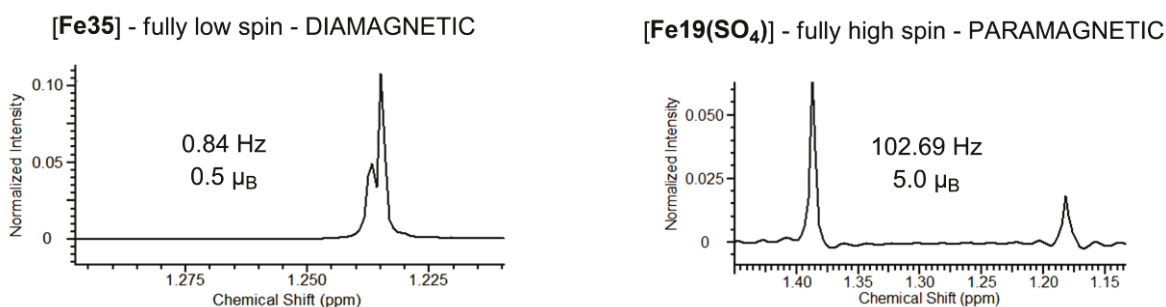


Fig. 45 Spectra of *t*BuOH signal in Evans experiment for model OFF and model ON complex.

Two binary complexes with minimized steric clash were found to be distinctly diamagnetic in aqueous solution, with a subtle shift of the reference signal up-field (diamagnetic shift). The magnetic moment of 0.5 μ_B , found for [**Fe35**] at room temperature, (Fig. 45) was measured at a concentration of 3.3 mM and in 2:1 D₂O/MeOH-d₄ solution due to solubility issues, probably stemming from the apolar phenyl group present at the periphery of the coordinating arm. A tiny increase in the shift has been observed when heating up, corresponding to 0.71 μ_B at 308 K and remaining at this level until 333 K. These subtle variations are not gradual and thus they stem most probably from the resolution limitation of the NMR spectra acquired, but even though, they still remain within a range found typically for a diamagnetic iron(II) complexes. Solubility issues were not encountered for [**Fe34**], the magnetic moment of which hardly varied with temperature (0.59 to 0.69 μ_B between 25 °C and 80 °C) proving its diamagnetic state. For those low spin chelates, magnetic moments did not change even after a week exposure of their aqueous solutions to air, proving the unchallenged stability of the OFF state of the bispidine-iron(II), so important for the construction of solution-phase directed magnetogenic probes (see discussion in chapter 3).

Contrary to the binary complexes, dissolution of ternary $[\text{Fe19}(\text{CH}_3\text{CN})]$ (diamagnetic in the solid state) led to largely high spin properties in water at room temperature, and the magnetic moment of $4.11 \mu_{\text{B}}$ increased to $5.12 \mu_{\text{B}}$ at 353 K. The magnetic moments of even $0.5 \mu_{\text{B}}$ or more above theoretical spin only value of $4.9 \mu_{\text{B}}$ are typically found for iron(II) complexes due to the temperature-independent paramagnetism stemming from the orbital contribution and not from the electronic spin. A detailed analysis of the behavior of this compound, as well as the explanation of intermediate magnetic moments found for a binary $[\text{Fe15}]$ complex are given in chapter 7, and originate from either exchange of the coordinating units (former case) and/or primarily due to a SCO (the latter).

6.4.2. NMR analysis

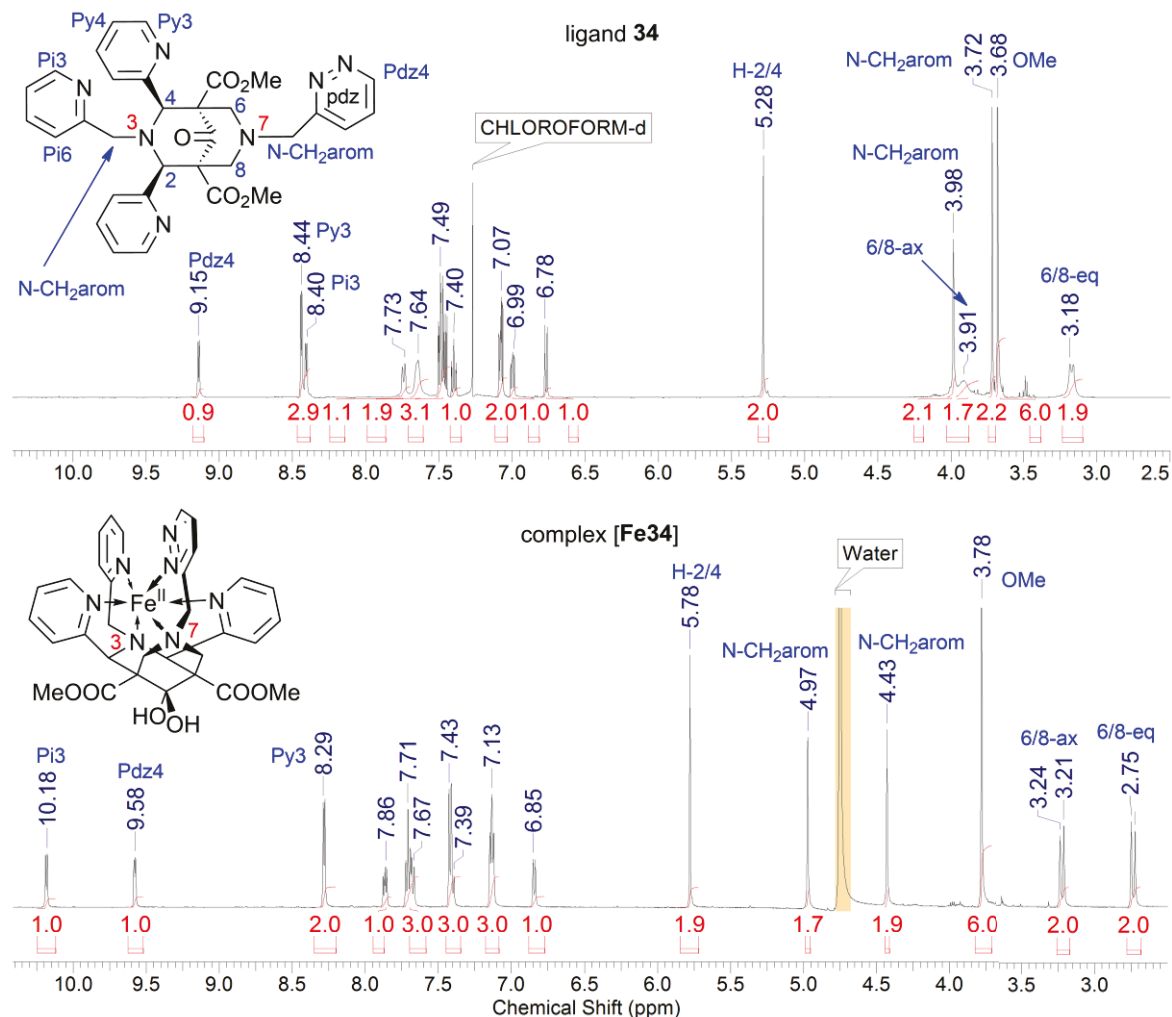


Fig. 46 Change of the NMR spectra of a ligand upon metal complexation (500 MHz, deuterated chloroform for organic ligand **34** (upper panel) and D_2O for corresponding complex **[Fe34]** (lower panel).

Diamagnetic model OFF complexes. The magnetic properties of bispidine complexes described above also directly influenced their NMR spectra. Spectra of **[Fe34]** and **[Fe35]** remained within a

diamagnetic window of 2.5 - 10.5 ppm and were fully assigned. Direct comparison of the chemical shifts in the spectrum of the complex and those for the pure ligand presented in Fig. 46 cannot be made due to the solubility difference between the two, which implicated a use of different solvents for NMR analysis. Certain differences observed upon metal binding are purely associated with the electric field generated by the cationic metal and/or its Lewis-acid character, as proposed before for other diamagnetic coordination compounds,^[240] rather than magnetic properties of iron(II). For example, the lowest-field chemical shifts in the ligands' spectra are those of the aromatic protons adjacent to the nitrogen atom, due to its electron withdrawing character. In turn, due to the resonance effects, those in position 3 and 5 of the heteroaromatic ring (N atom is in position 2) should theoretically be the next most deshielded ones with the one in *para* being the most shielded from all aromatic environments. Metal binding, which is a Lewis acid-base interaction, deprives the coordinating atom of its electron density. In the result, the N bound to the Lewis acid (iron(II)) withdraws electrons even stronger, enhancing the deshielding of all the aromatic signals. The effect is the most pronounced for the closest *ortho*-hydrogens, with other aromatic protons experiencing it less severely. Relatively strong downfield shift of on average 1 - 0.5 ppm, observed for the signals of H-2/4 (5.3 ppm vs. 5.8 ppm), and CH₂ of N-CH₂Ar moieties (4 ppm and 3.7 ppm vs. 5 ppm and 4.4 ppm), is probably also a result of the similar electron-withdrawing mechanism and not a solvent effect. On the other hand, this is not the case for the protons at carbons 6 and 8 of the bispidine backbone, which are not in a direct neighborhood of heteroaromatic ring experiencing the electron deficiency, and so are slightly up-field in comparison to the pure ligands despite the proximity of binding nitrogen.

Except these general trends which are primarily a consequence of the distance of each proton environment from the N-Fe bond, the strength of binding the metal ion by different coordinating atoms and the torsional angles between the C-H and the closest Fe-N bond play an important role and cannot be neglected. In pure ligand, as expected, the protons of the pyridazine ring experience stronger deshielding than those of pyridine due to the presence of two electron-withdrawing heteroatoms. The effect is particularly pronounced for the hydrogen in position *ortho* to the nitrogen atom of pyridazine ring (Pd_z4), which is the most downfield shifted from all the protons of ligand **34** (9.15 ppm, Fig. 46 A), having as much as 0.7 ppm larger chemical shift than corresponding protons of pyridines (8.40 and 8.44 ppm for Pi₃ and Py₃ respectively). However, upon metal coordination, *ortho*-hydrogen from N₃-picolyl moiety ([proton N₃-Pi₃) becomes drastically deshielded and a new chemical shift of 10.18 ppm (Fig. 46 B) is 0.6 ppm and 1.9 ppm more downfield than the respective pyridazine and 2/4-pyridine *ortho*-hydrogens. This dramatic downfield "movement" may potentially be rationalized by the torsional angle of only 1.6 ° between the Fe-H bond and the plane of the N₃-pi heteroaromatic ring, which enables a maximal orbital overlap between the metal and the donor nitrogen, maximizing the electron withdrawing potential of iron(II) binding. The remaining heteroaromatic groups are somewhat distorted in their coordination to the metal center (torsional angle within 5 – 10 ° range) and thus experience weaker effect. This behavior may also be interpreted as torsional-angle dependent difference in contact

shift, provided the presence of residual paramagnetism, as suggested by the non-zero magnetic moment of [Fe34], which is common for iron(II) complexes and stems from the orbital temperature-independent contribution. Despite that, no temperature-dependent paramagnetism was found for this complex, and the NMR spectrum at 353 K was almost identical with the one acquired at RT.

Analogous NMR behavior was found also for the oxadiazole complex [Fe35], what in the light of the discussion above confirms the low spin character of these binary bispidine-iron(II) complexes in aqueous solution, and strongly suggests that their structure found in the solid state is retained in solution.

Paramagnetic, ON state complex. On the other hand, ^1H NMR spectra of [Fe19(SO₄)] which is high spin in the solid state, covered an over 200 ppm range (Fig. 47), as reported for other bispidine-iron(II) complexes ^[191], indicating a significant paramagnetism of this compound in agreement with the high spin ferrous ion.

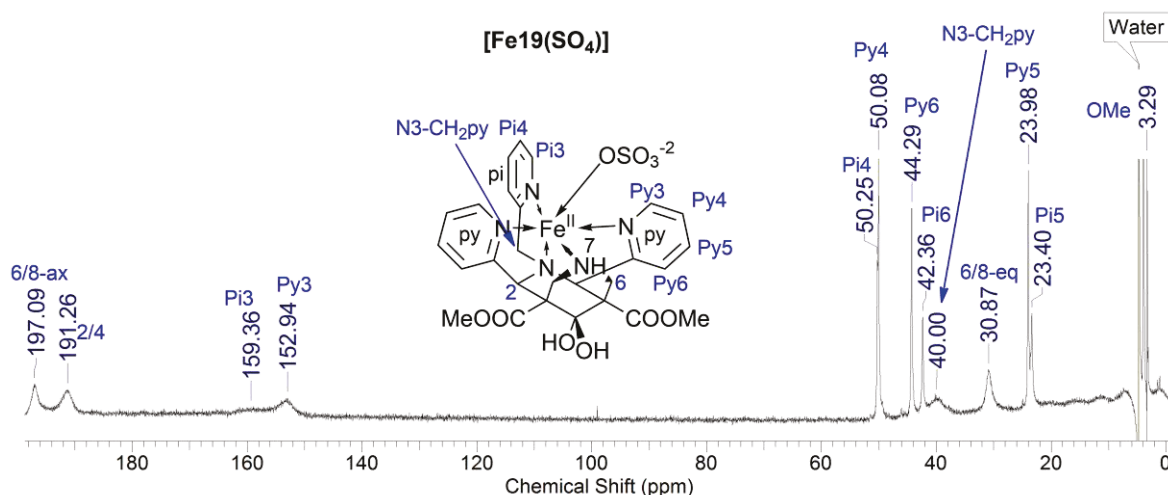


Fig. 47 ^1H NMR spectrum of model high spin bispidine complex in D_2O at 25 °C (500 MHz – 11.7 T). The numbering of the hydrogen atoms (in blue) is in accordance with the one used in this work.

Despite a failure in acquiring proper two-dimensional COSY spectra for this compound, the assignment of the signals can be attempted based on the integrals and the analogy to previously reported complexes, as well as the analysis of the solid state structures. The latter, if assumed that does not change significantly in solution, which is reasonable for the rigid polydentate bispidines, enables the estimation of the paramagnetic influence on each proton environment (isotropic shift) *via* contact (scalar coupling) and pseudo-contact (dipolar interaction) mechanism, as previously reported ^[191] and discussed in chapter 1 (see Paramagnetic Relaxation Enhancement theory for CAs in MRI). In the context of chemical shift, the contact contribution is usually dominant and will depend largely on the torsional angles between the X-H and Fe-N bonds, being quenched for the value of 90 ° and maximal for 180 ° or 0 °. The pseudocontact shift which results from the magnetic field generated by the unpaired electrons, is generally limited and remains proportional to

the reciprocal of the third power of the distance ($1/r^3$) between the spin and the measured nucleus. On the basis of these considerations, the most downfield signals (197.1 ppm and 191.3 ppm) in the spectrum of **[Fe19(SO₄)]** (Fig. 47) should come from the H-6/8ax and H-2/4 protons respectively, as the solid state torsional angles between them and the closest coordinative bond are approximately 170 ° and 165 °. The proximity of the Py3 protons to the coordinating N-atoms from pyridine rings and the torsional angles of approx. 10-15 ° are the reasons for significant low-field shifts of 159.4 ppm for N3-Pi3 and 159.2 ppm for 2/4-Py3 (by integration). As reported before, the remaining aromatic signals should come out around 50 ppm for Py4 and Py6 and approximately at 20 ppm for proton from *meta* position. By this, signals at 50.1 ppm and 50.3 ppm could be attributed to Pi4 and Py4 respectively, with 44.3 ppm and 42.4 ppm for Py6 and Pi6, and finally 24 ppm – Py5 or 23.4 ppm - Pi5. The remaining shifts of 40 ppm and 30.9 ppm may then come from N3-CH₂ and equatorial H-2/4 protons, for which the torsional angles are relatively close to 90 ° (approx. 120 ° and 50 ° respectively) significantly quenching the paramagnetic effect.

6.4.3. Other characterizations

Redox potentials of iron(III)/(II) couples were measured for crystalline samples of near-low spin complexes dissolved in acetonitrile and containing 0.1 M concentration of *n*Bu₄NClO₄. They were approximately 0.65 V for all but the oxadiazole derivative, which gave $E_{1/2} = 0.77$ V (see Table 7).

complex	E_{pa} [V]	E_{pc} [V]	ΔE_p [mV]	$E_{1/2}^{[a]}$ [V]
[Fe15] ·2BF ₄	0.682	0.619	63	0.651
[Fe34] ·2BF ₄	0.677	0.619	58	0.648
[Fe35] ·2ClO ₄	0.800	0.737	63	0.769
[Fe19(CH₃CN)] ·2BF ₄	0.689	0.626	63	0.658

^[a] 1mM solution of complexes in acetonitrile with 0.1M Bu₄NClO₄ as an electrolyte

Table 7 Redox potential of Fe^{3+/2+} couples of the various ligands' complexes. Adapted from Kolanowski et al 2013 ^[193] - with permission of WILEY-VCH Verlag GmbH & Co. KGaA, Weinheim (copyright © 2013).

Importantly, all waves, registered at 5 different scan rates for each compound (50, 100, 150, 200, 250 mV s⁻¹) were fully reversible suggesting no significant changes in the coordination geometry upon oxidation. This is probably a consequence of the high rigidity of bispidine backbone which combines with a flexibility of the other coordinating arms responsible for their tolerance to a wide range for a size of a metal ion.^[178] Redox potentials of below 0.73 V for Fe^{3+/2+} pair were generally attributed to the presence of the N5 coordination sphere with a sixth position occupied by a monodentate ion, like chloride.^[142] This, together with a similarity of $E_{1/2}$ for three distinct bispidine complexes, which is in line with previously reported value of 661 mV for the perchlorate salt of **[Fe15]** in acetonitrile solution in the presence of 0.1 M tetrabutylammoniumtriflate,^[191] may

suggest a ligand displacement in 0.1 M ClO_4^- leading in the consequence to a similar coordination sphere with one anion and conservative N5 binding motif. However, the subsequent UV analysis of these samples reveal that the structure of binary complexes remains unchanged in pure acetonitrile and in the perchlorate solution used for cyclic voltammetry. In the light of this experimental results, low redox potentials of these complexes can be interpreted in terms of the weak ligand field and/or surprising hardness of the bound picolyl and methypyridazine arm, which could in turn result from an equally hampered back-bonding as a consequence of the steric deformation. By contrast, oxadiazole-bearing complex $[\text{Fe35}]\cdot 2\text{ClO}_4^-$ does not suffer any strain and thus can exert its full pi-accepting character additionally increased by the conjugation of the phenyl moiety, leading to 120 mV higher redox potential found for this compound (769 mV). The UV-Vis spectrum of a ternary complex $[\text{Fe19}(\text{CH}_3\text{CN})]$ differed significantly from that in pure solvent, and was compatible with the high spin state of iron (II) confirming the displacement of the acetonitrile monodentate ligand by the anions (perchlorate) what is discussed in more details in chapter 7. In order to measure the true redox potential of this compound with acetonitrile being coordinated to the metal ion, an electrolyte containing a non-coordinating anion like hexafluorophosphate, should be used instead in the future experiments.

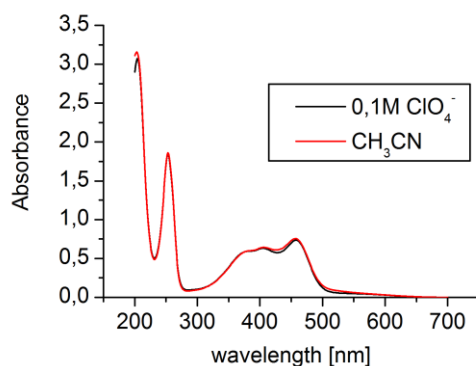


Fig. 48 Superposition of UV-Vis spectrum of 0.1 mM acetonitrile solution of $[\text{Fe15}]\cdot 2\text{BF}_4$ complex in pure solvent and in the presence of 0.1 M of perchlorate salts.

Additional confirmation of the magnetic properties of analyzed complexes is obtained from the analysis of the UV-Vis spectra. For low spin iron(II) complexes the most efficient electronic excitation is a charge transfer between a metal and a ligand, which thus dominates the spectra. The intensity of this band, or more precisely the molar absorptivity for the particular wavelength (molar extinction coefficient ϵ) is a measure of the probability of the transition and for low spin iron(II) complexes it is typically above $10000 \text{ M}^{-1}\text{cm}^{-1}$. High spin complexes on the other hand have a much lower molar absorptivity within this region. Indeed the values calculated for $[\text{Fe34}]$ and $[\text{Fe35}]$ are 10880 and $12580 \text{ M}^{-1}\text{cm}^{-1}$ respectively what is in line with their low spin character. Slightly bigger ϵ for the sterically least strained oxadiazole-derivative may be a consequence of the geometric distortion within the pyridazine-type complex. On the other hand charge transfer band in complex $[\text{Fe19}]$ exhibits only approximately half of the above molar absorptivity ($5580 \text{ M}^{-1}\text{cm}^{-1}$). This is a consequence of the fact that as expected from its intermediate magnetic moment, part of

the population of this chelate in solution will remain in the high spin form, which does not absorb the light as effectively. However, the spin-equilibria does not entirely explain the drop of in the absorptivity of the charge-transfer band observed for [Fe15]. Ternary complex [Fe19(CH₃CN)] which shows an almost high spin magnetic moment in solution (4.11 μ_B) is still effectively excited at the charge transfer frequency, as demonstrated by its absorptivity of 7140 M⁻¹cm⁻¹ at 444 nm. Thus, it can be suspected, that similarly to the [Fe34] complex, the charge-transfer excitation for [Fe15] will suffer from even stronger geometrical deformation caused by the steric clash. On the other pole, entirely paramagnetic complex [Fe19(SO₄)], as expected, does not show as intense absorptivity in the visible spectrum as previously discussed examples, i.e. maximum $\epsilon = 1200$ M⁻¹cm⁻¹ is reached by it for the 407 nm wavelength.

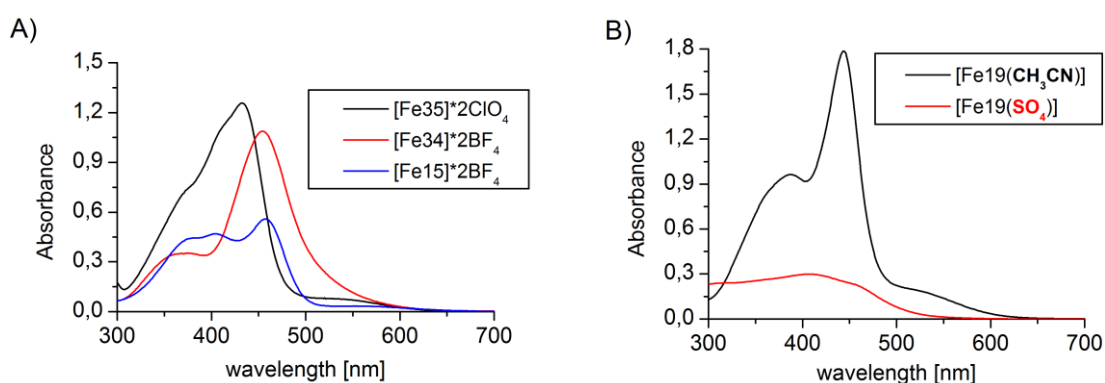


Fig. 49 UV-Vis spectra, measured at room temperature and in aqueous solution, of A) binary complexes (concentration of 0.1 mM) and B) ternary chelates of bispidine ligand **19** (concentration of 0.25 mM).

6.5. Summary

A new synthetic strategy for the preparation of a wide range of single-site substituted bispidine-based hexadentate compounds has been developed. Its efficiency in introducing a coordinating arm representing the 6th coordinating site, as well as its compatibility with many functional groups pave the way to a virtually **unlimited number of highly sophisticated ligands** that cannot be hoped to be accessed by any other, classic methodology.

By removing steric clashes, I have prepared the world's first three low spin hexacoordinate bispidine-iron(II) complexes. In particular, the two binary [Fe34] and [Fe35] complexes were shown to be magnetically and chemically stable in a range of near room temperatures in aqueous media. At the beginning of my thesis, the major hurdle in making future magnetogenic probes based on the bispidine system a serious possibility was the demonstration that a **robust, magnetically silent OFF state** can indeed be reached, and I succeeded doing so.

I have also prepared and characterized new high spin iron(II) complexes in which secondary amine bispidine ligands bind the metal ion in a pentacoordinate fashion with the 6th coordination site occupied by a solvent molecule or an anion. In accordance with the initial design of a magnetogenic probe, these paramagnetic bispidine chelates (especially complex [Fe19]) represent the activated version (the ON form) of a putative magnetogenic probe. Their observed magnetic moment of 5 μ_B **can be regarded as a high-intensity reporter signal.**

Thus, we now possess a new alternative OFF-ON magnetic duo of elevated stability in environmentally relevant conditions. Thanks to my synthetic protocols, we are now in the position to introduce even the most sophisticated responsive moiety into the system, bringing within our reach a class of magnetogenic probes totally independent of the one explored up to now in my group.

Apart from that, **one binary and one ternary complex of intermediate magnetic properties** in aqueous solution were prepared, which are particularly sensitive to different parameters of the environment. The precise discussion of the origin of this behavior as well as the practical relevance of the identified phenomena is discussed in more detail in the following chapter.

7. MAGNETIC EQUILIBRIA IN BISPIDINE-IRON(II) SYSTEM

In the previous chapter I have discussed the preparation of hexadentate bispidine ligands and in particular the magnetic properties of decidedly high spin and low spin complexes in aqueous solution at near room temperatures – conditions which are the most suitable for practical applications. Nevertheless, a new binary complex of previously reported hexadentate bispidine ligand and one chelate of a pentadentate bispidine displaying an acetonitrile in the 6th coordination site show intermediate magnetic properties in solution. The origin of this behavior and the differences between the binary and ternary complex were studied thoroughly and the results are discussed in the following chapter.

7.1. Temperature and solvent dependency of magnetic equilibria – ternary vs. binary complex

7.1.1. Magnetic properties of ternary [Fe19(CH₃CN)] complex in solution

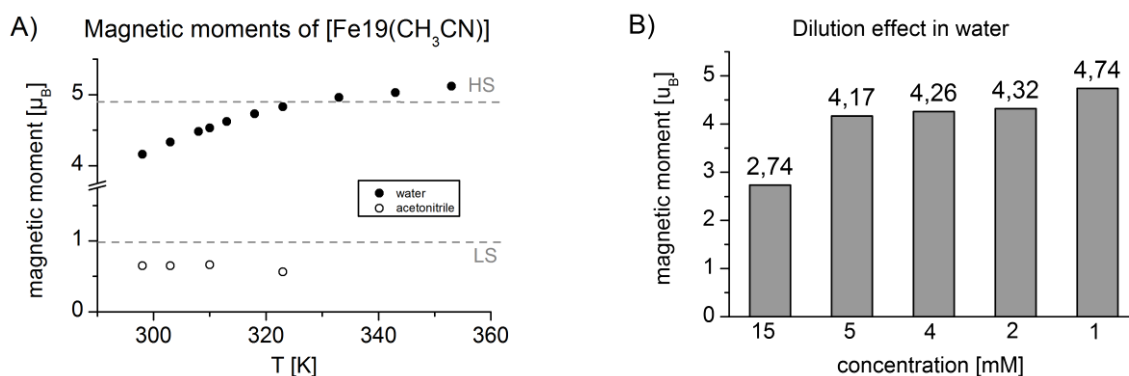


Fig. 50 Solution magnetic properties of [Fe19(CH₃CN)] A) in different solvents B) at different concentrations (for perchlorate salts)

Magnetic moments in solution. In the contrast to examples of binary iron(II) complexes described in chapter 6, ternary complex [Fe19(CH₃CN)] does not maintain its solid state low spin character upon dissolution in water (Fig. 50). In particular, its magnetic moments vary between the intermediate value of 4.16 μ_B for 25 °C (298 K) and 5.12 μ_B at 80 °C which is already within the typical high spin value found for iron(II) complexes (Fig. 50 panel A, black circles). In addition, changing a concentration of this significantly changes the magnetic moment of a sample. In particular for the perchlorate salt of [Fe19(CH₃CN)] was found to be as low as 2.74 μ_B for 15 mM solution and increases to near high spin value of 4.74 μ_B upon 15 x dilution, suggesting a partial exchange of the monodentate ligand for solvent molecules (Fig. 50B). This behavior, found

typically for ternary complexes, is additionally reflected in a significant solvent sensitivity of the magnetic properties of $[\text{Fe19}(\text{CH}_3\text{CN})]$. Namely, dissolution of this compound in CD_3CN leads to $0.65 - 0.56 \mu_{\text{B}}$ value of μ found within a temperature range of $25 - 50^\circ\text{C}$ and above this temperature, coalescence of the signals made calculations impossible (Fig. 50 A, white circles). The diamagnetic properties stem from the fact that a monodentate acetonitrile originally coordinated to iron(II) can only be replaced by its deuterated analog, ensuring that the strong ligand field N6-coordination motif is preserved and the low spin state of iron(II) can be maintained.

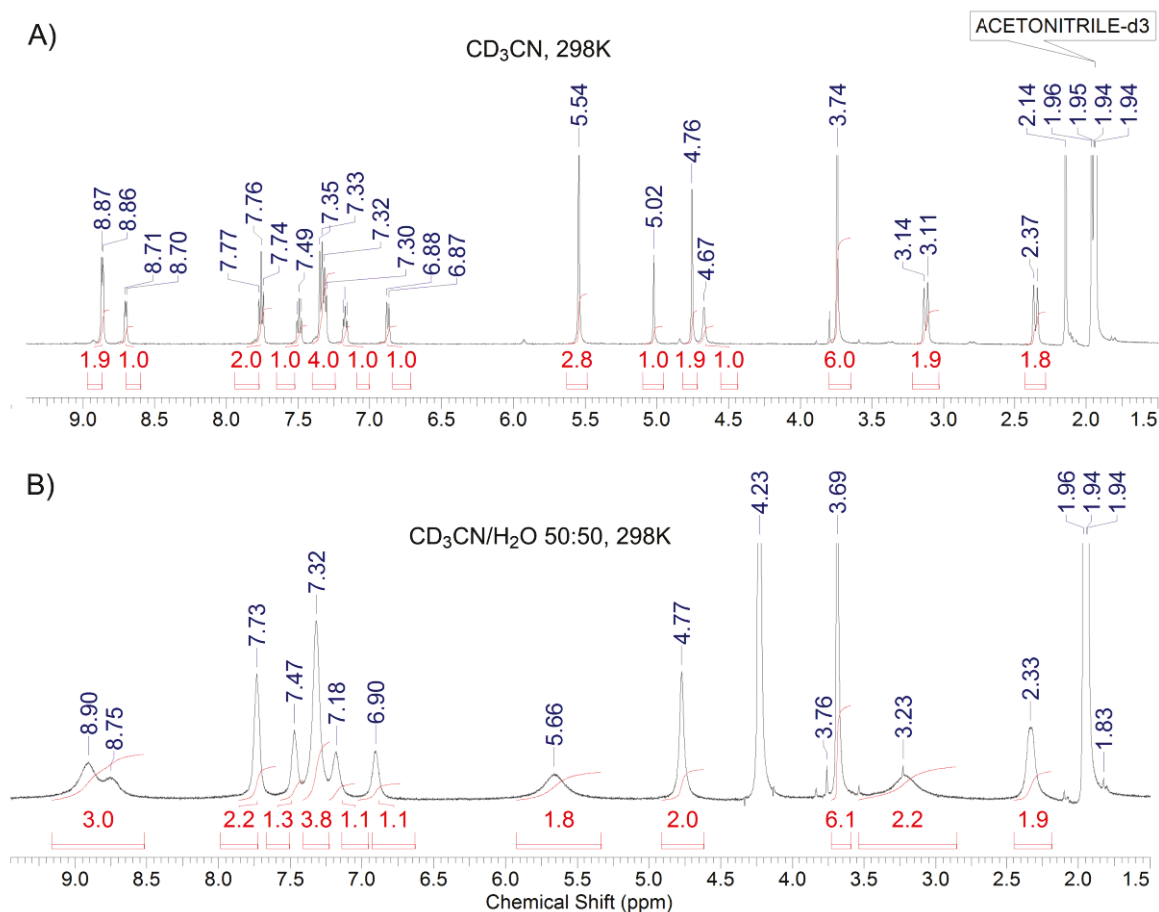


Fig. 51 ^1H NMR spectra of ternary complex $[\text{Fe19}(\text{CH}_3\text{CN})]$ in A) acetonitrile and B) acetonitrile/water 50:50 mixture at 298 K.

NMR spectra. Magnetic properties of $[\text{Fe19}(\text{CH}_3\text{CN})]$ are also reflected by its NMR spectra. In deuterated acetonitrile the chemical shifts of the complex cover the diamagnetic window of 2 - 9.5 ppm at room temperature as well as at 60°C , with a well resolved sharp signals. It is a consequence of the fact that despite the probable dynamic exchange of the monodentate ligand, the coordination motif and thus the ligand field remain unchanged. It also suggests a high structural stability of the N5-bispidine binding motif. The quality of the spectrum obtained in pure D_2O did not allow for the precise analysis of the signals, but a very broad and low intensity peaks seem to extent over a paramagnetic window of 3 - 190 ppm, with similar pattern to the one observed for purely high spin compound $[\text{Fe19}(\text{SO}_4)]$. In 50:50 v/v mixture of D_2O and CD_3CN , the spectrum

remains within the diamagnetic window and is almost identical with the one in pure acetonitrile (Fig. 51). The only differences are significant signals' broadening and the disappearance of the peaks of OH and NH groups due to the replacement of proton by a deuterium from the D₂O co-solvent. It thus proves that while the monodentate ligand is indeed exchangeable in solution, a significant preference for acetonitrile exist, which leads to a stabilization of the diamagnetic form.

7.1.2. Magnetic moments of a binary [Fe15]*2BF₄ complex

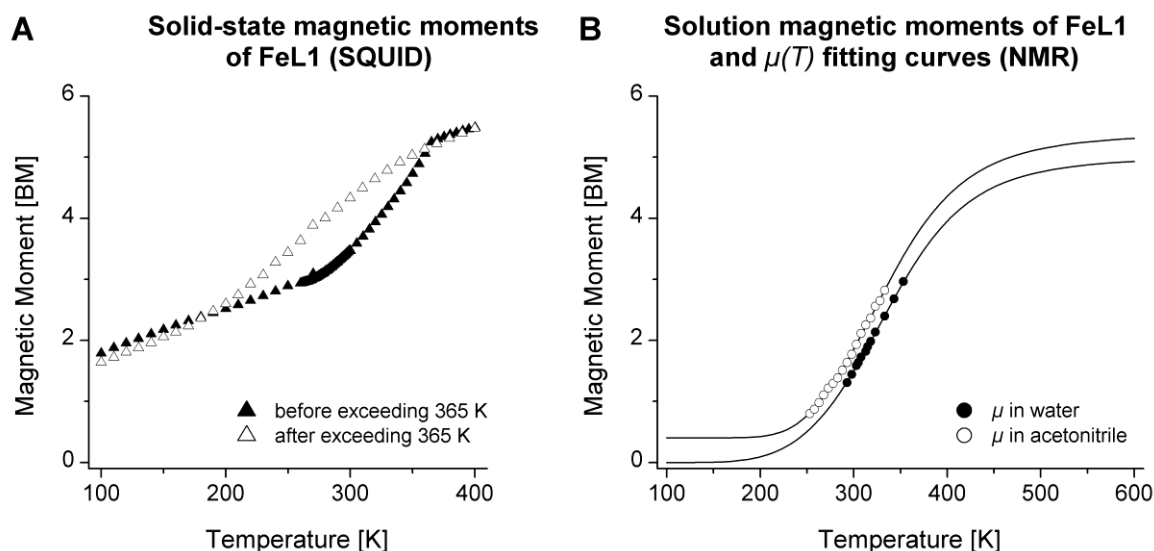


Fig. 52 Temperature dependency of the magnetic moment of [Fe15] complex A) in the solid state, and B) in solution with a curve representing the best thermodynamic fit to the experimental values (solid lines). Taken from Kolanowski et al 2013 [193] - by permission of WILEY-VCH Verlag GmbH & Co. KGaA, Weinheim (copyright © 2013).

Spin crossover (SCO) in the solid state. . As it has already been discussed in the previous chapter, the binary character of complex [Fe15] has been proved in the solid state, but the significant deflection from the optimal coordination of one of the arms, attached to N7, was evident. Solid-state magnetic properties were examined by Dr. Ruben Checa and Prof. Dominique Luneau. The magnetic moment obtained from the SQUID experiment varied with changing temperature indicating a SCO behavior. Multiple attempts to cool down and then heat up a sample within a range 10 K – 350 K gave each time a super-imposable curve with no hysteresis, independent of the direction of the temperature change, as shown by the filled triangles in Fig. 52 panel A. The increase of χT (where χ is the molar magnetic susceptibility and T is temperature) is continuous up until 280 K where it becomes more abrupt. At 350 K χT ($2.64 \text{ emu K mol}^{-1} = 4.60 \mu_B$) is in agreement with a high spin Fe(II). When the heating continued above 350 K, at 365 K ($\chi T = 3.44 \text{ emu K mol}^{-1}$ corresponding to $5.25 \mu_B$) the curve “flattened” and the increase remained gradual up to 400 K ($3.74 \text{ emu K mol}^{-1}$) which was the technical limit of the SQUID instrument. Subsequent cooling decreases χT but, in contrast to cooling done after reaching 350 K, now the

data are not super imposable with the previously obtained ones, as shown by the hollow triangles (Fig. 52A.). This behavior should not be confused with hysteresis. The most plausible explanation is a loss of a solvent molecule from a solid sample which occurs at 365 K and permanently modifies the packing in the solid state thus leading to a slightly modified pattern of the spin transition.

Low solvent –dependency of solution magnetic equilibria. Solution behavior is in good agreement with the one observed for the solid state sample of [Fe15]. Fig. 52 B represents experimental results of magnetic moment measurements in water (filled black circles) and acetonitrile (hollow white circles). For precise numeric values the reader is referred to experimental section. In water, increasing the temperature from 20 °C to 80 °C leads to the change of the magnetic moment from nearly diamagnetic $1.31 \mu_B$ to intermediate value of $2.96 \mu_B$, which indicates that roughly 60 – 70 % of the population of the complex remains in the low spin form. In acetonitrile, unlike in the case of ternary complex [Fe19(CH₃CN)], the magnetism variation upon temperature is quite similar to aqueous solution, but the transition is shifted by approximately 10 K. This subtle solvent sensitivity is most likely a consequence of the difference in the polarity of the media which is then “felt” by the complex only via the non-specific electrostatic interactions, as described in chapter 2. No bond breaking/formation within the first coordination sphere seems to occur during the magnetic transition, because otherwise N6 and N5O1 coordination patterns resulting subsequently from acetonitrile and water coordination should give a significantly different profiles of temperature dependency. Thus it seems that it is the SCO phenomenon, similar to the one found in the solid state and suggested already by Borzel et al, that is responsible for the magnetic changes in solution samples of [Fe15]. However, coordination/decoordination equilibria cannot be entirely excluded, as shown in Fig. 53, and other relevant arguments confirming this hypothesis are discussed below.

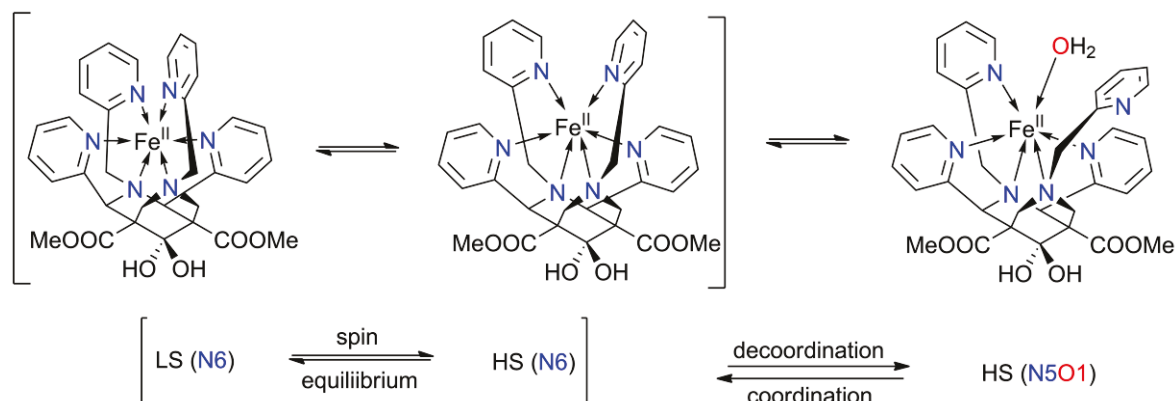


Fig. 53 Proposed spin equilibria of [Fe15] in solution. Adapted from Kolanowski et al. 2013 ^[193] - with permission of WILEY-VCH Verlag GmbH & Co. KGaA, Weinheim (copyright © 2013).

Thermodynamic parameters of spin transition. In order to verify this hypothesis and to better characterize the process, I have extracted thermodynamic parameters associated with it, by fitting

the experimental results to the equation (12), as described also in the paper from 2013 which I have co-authorized ^[193]:

$$\mu_{eff} = \left\{ \mu_{LS}^2 \left[e^{-\Delta H^0/RT} e^{\Delta S^0/R} + 1 \right]^{-1} + \mu_{HS}^2 \left[e^{\Delta H^0/RT} e^{-\Delta S^0/R} + 1 \right]^{-1} \right\}^{1/2} \quad (12)$$

Many variants of calculating the thermodynamic parameters on the basis of experimental results were reported.^{[121] [122] [241] [130]} In general, four parameters can be varied in this equation in order to fit it to the experimentally obtained results, and these are: magnetic moment of the low spin form μ_{LS} , magnetic moment of the high spin isomer μ_{HS} , as well as molar standard enthalpy (ΔH^0) and entropy change (ΔS^0) associated with this process. If the spin-transition is relatively sharp or the temperature range offered by a solvent is large enough, then the magnetic moment of at least high spin or a low spin form can be measured experimentally. Provided this is the case, then only two or three parameters remain to be optimized what significantly facilitates the fitting process and enables a direct extraction of the thermodynamic characteristics.^[242] However in practice, especially for water which can operate only within 100 K range, none of the limiting values of the magnetic moment can be reached. This implies four parameter fit, which is more prone to the significant errors and may generate physically unrealistic values.

The magnetic equilibrium of [Fe15] in acetonitrile and water does not allow for spin transition process to be pushed to the one extremity within the available temperature range. In the consequence, I performed several different fitting experiments for each experimental dataset, which covered the magnetic moments of the compound in the temperature ranges of 253 K to 333 K and 293 K-353 K for acetonitrile and water respectively. Despite the theoretical availability of even lower temperatures for both solvents, the samples and the resulting spectra were abnormally distorted. The overlap of the reference signals and increased viscosity of solutions observed at these experimental conditions led to unreliable readouts and thus they were excluded from the fitting experiment.

The summary of the fitting experiments is given in Table 8 and the representative fitting curves are shown in Fig. 52 B. For more information on the methodology as well as other fitting attempts, the reader is referred to the experimental section. Except the enthalpy and entropy of the spin-transition process, temperature of transition $T_{1/2}$, which corresponds to the situation when exactly half of the population is in the low spin (or a high spin) state ($K = 1$), can also be estimated from the following linear relationship $\ln K = (1/T) * (-\Delta H^0/R) + (\Delta S^0/R)$ derived from the equation 12 (see above).

From the four-parameter fit (Fig. 52 and bold in Table 8) approximate values of thermodynamic parameters were obtained for acetonitrile: $\Delta H^0 = 23.9 - 29.7 \text{ kJ mol}^{-1}$, $\Delta S^0 = 58.3 - 85.8 \text{ J mol}^{-1}\text{K}^{-1}$, $T_{1/2} = 371 \text{ K}$ and for water $\Delta H^0 = 26.8 - 29.5 \text{ kJ mol}^{-1}$, $\Delta S^0 = 68.1 - 80.6 \text{ J mol}^{-1}\text{K}^{-1}$, $T_{1/2} = 278 \text{ K}$. While for water the magnetic moments of the LS and the HS form were close to the spin-only values ($0.00 \pm 0.05 \mu_B$ and $5.02 \pm 0.51 \mu_B$ respectively), in acetonitrile they were somewhat higher

($0.41 \pm 0.13 \mu_B$ and $5.40 \pm 1.22 \mu_B$), but still remained within the typical range of the iron(II) complexes. A deviation from the spin-only values suggest a non-zero temperature-independent paramagnetism originating from an orbital contribution, but it might come from a higher error estimated for these values in acetonitrile than in water. Thus, to verify these results, I have carried out a simplified fits, fixing the HS magnetic moment at spin-only value of $4.9 \mu_B$ ($\mu = 2[S(S+1)]^{1/2}$) or $5.4 \mu_B$ (upper limit of the 5T_2 state) as previously reported.^[122] The obtained values ($\Delta H^\circ = 27.0 - 28.9$ and $26.3 - 28.7 \text{ kJ mol}^{-1}$; $\Delta S^\circ = 69.5 - 77.3$ and $70.6 - 77.2 \text{ J mol}^{-1}\text{K}^{-1}$ for water and acetonitrile, respectively) are consistent with those of the 4-parameter fit, but with much lower error, thus increasing the reliability of the results. $26 - 29 \text{ kJ}\cdot\text{mol}^{-1}$ found for the enthalpy of the spin-transition of [Fe15] are just above the upper limit (the interval is $15 - 25 \text{ kJmol}^{-1}$) of a pure SCO phenomenon^[94], suggesting a trace presence of other magnetic equilibria, like coordination-decoordination.

solvent	μ_{LS} [μ_B]	$\mu_{HS}^{[b]}$ [μ_B]	ΔH° [kJ/mol]	ΔS° [J/(mol·K)]	$T_{1/2}$ [K]
CD₃CN	0.41±0.13	5.40±1.22	26.79±2.93	74.35±13.60	371
Water	0.00±0.05	5.02±0.51	28.11±1.34	74.35±6.28	378
Water	0.06±0.04	4.90 ^[b]	28.47±0.42	75.98±1.28	375
Water	0.00±0.05	5.40 ^[b]	27.23±0.22	70.13±0.68	388
CD ₃ CN	0.46±0.05	4.90 ^[b]	28.18±0.55	75.54±1.67	359
CD ₃ CN	0.41±0.05	5.40 ^[b]	26.80±0.53	72.18±1.59	371

^[b] μ_{HS} fixed at the limiting values for magnetic moments of the high spin iron(II) ion with $S = 2$

Table 8 Estimated values of the spin equilibrium parameters for [Fe15] in solution, obtained from the fit of the temperature-dependent variation of magnetic moments, to the equation (12). Adapted from Kolanowski et al 2013^[193] - with permission of WILEY-VCH Verlag GmbH & Co. KGaA, Weinheim (copyright © 2013).

7.1.3. NMR studies of temperature-driven magnetization process in [Fe15]

Detailed NMR analysis of the [Fe15] liquid samples in different solvents and at various temperatures provides an additional proof for the occurrence of the SCO with a minor contribution from decoordination by one pendent arm.

Note on the reference signal. Before getting into details, it should be pointed out that to facilitate the interpretation of the results, the net chemical shifts are given in reference to the solvent signals which for each spectrum were fixed artificially at the standard values observed at room temperature and in diamagnetic solutions. This procedure does not significantly influence the qualitative or even semi-quantitative interpretation of the results obtained and thus is sufficient for the purpose of

the discussion below. Nevertheless, the limitations of this simplified data treatment, which are not crucial for the system studied but could be important in the future, should be borne in mind.

The possible discrepancies may come from the fact that shift of the bulk solvent, so as of any other internal reference used, including tetramethylsilane, will vary not only with a temperature but also with the changes in the paramagnetism of the sample and the concentration of the paramagnetic compound (like in the case of Evans' method). Thus, even for different batches, the concentration of which was not precisely determined in this work and varied between 5 to 20 mM, the chemical shifts given in the respect to the internal standard will be biased. However, firstly, the paramagnetism of the complex in the whole temperature range investigated does not exceed half of the one observed for entirely high spin compound, which at 5 mM concentration leads to at maximum 250 Hz paramagnetic shift of the reference at RT and in 500 MHz magnetic field (11.7 T). Consequently the approximate variation of the reference signal, coming from the paramagnetic contribution of the measured compound at 20 mM concentration will not exceed 1 ppm (roughly $250 \text{ Hz} * 50 \% * 4$ due to the 4 times higher concentration than the 5 mM discussed above, gives 500 Hz and so 1 ppm). This difference, even if possibly important for the signals which are not strongly shifted, is negligible for the majority of others, for which 1 ppm constitutes less than 5% of the whole shift experienced. In addition, provided that the assumption of diluted solutions holds true (it does even for 20 mM concentration), no concentration dependency exists if the differences between the chemical shifts of protons from the same complex are compared. In the consequence the relative chemical shift can be associated with a change in the paramagnetism with a sufficiently good approximation for concluding on the solution behavior of the complex analyzed.

Solvent effect on NMR spectrum at room temperatures. NMR spectrum of $[\text{Fe15}] * 2\text{BF}_4$ in D_2O clearly shows certain paramagnetism of the sample, as the signals from the complex span the range of 3 – 22 ppm at 298 K. At the same temperature a magnetic moment of the sample was calculated to be $1.47 \mu_{\text{B}}$ which corresponds to approximately 90 % of LS form in solution. At the same temperature the NMR shifts were within the 3 - 28 ppm for acetonitrile and acetone solution and the general pattern of the spectra was almost identical for both solvents. This again suggests that while certain magnetic equilibrium between the HS and LS form truly exist in solution, the first coordination sphere of the complex remains largely unchanged, at least at 298 K. Replacement of one or few coordination arms by a soft N-donor acetonitrile should have a significantly different impact on the magnetism and thus on the range of the NMR signals, than coordination of O-donors like acetone or water because of the difference in the ligand field exerted by these solvents. In addition, complex stability should be higher in acetone than in water or even acetonitrile due to the significantly less competitive character of this solvent, leading to a lower relative concentration of the solvent-binding species. However in the case of $[\text{Fe15}]$ as concluded from Fig. 54, the contribution of the high spin form in aqueous sample, at the same temperature, is lower than the one deduced from the NMR spectrum in acetone. All of that again counteracts the hypothesis of the ligand decoordination in solution.

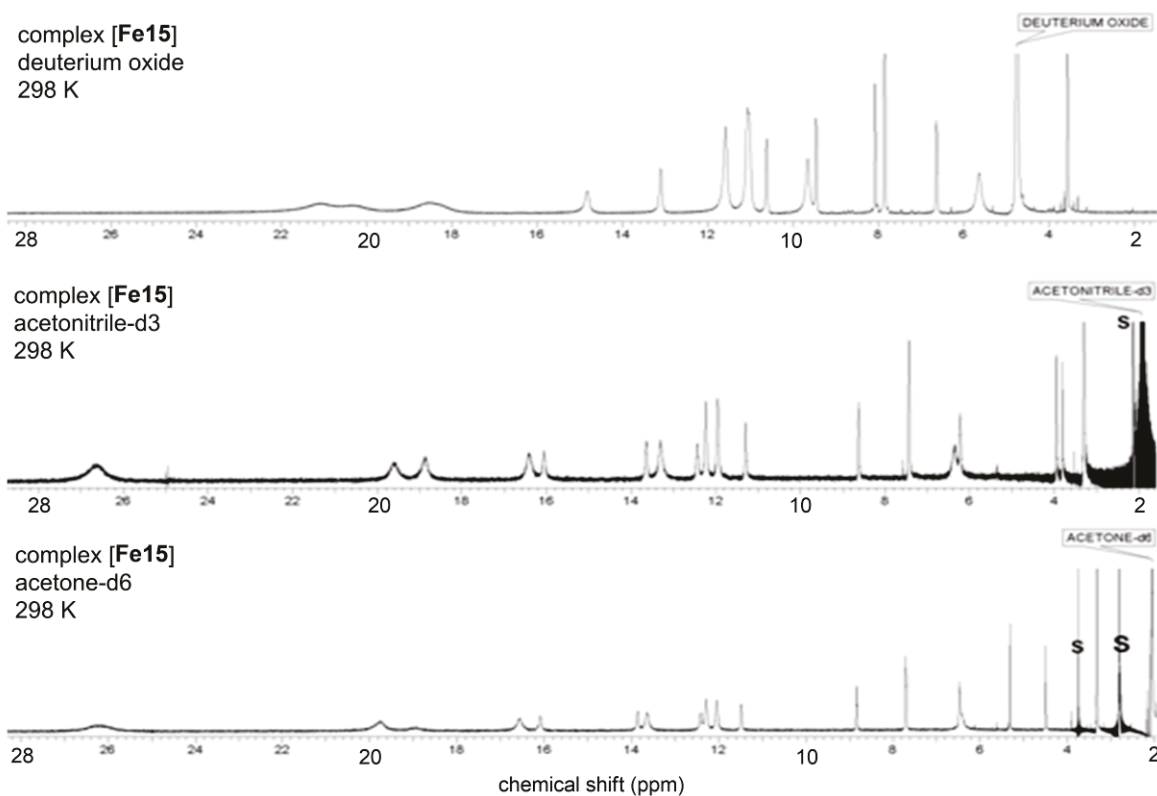


Fig. 54 ^1H NMR spectra of intermediate spin complex **[Fe15]** in different solvents, acquired at 298 K from the 500 MHz NMR device (11.7 T).

Detailed analysis of solution state structure of [Fe15] in a function of temperature. In order to decipher the precise structure of this complex in solution, temperature-dependent “migration” of the ^1H NMR signals was studied in the range of 213 - 323 K, 233 - 333 K and 298 - 353 K for acetone, acetonitrile and water respectively. COSY experiment performed at 213 K in acetone solution, in combination with the comparison with structurally similar complexes **[Fe34]** and **[Fe35]** as well as with a pure ligand 15, allowed for the assignment of all the signals in the proton spectrum (Fig. 55). While OMe signal as well as the one of H-6/8 protons could be assigned directly from the 1H and COSY experiments, 6.27 ppm signal in the spectrum of the complex (panel A in Fig. 55) was attributed to H-2/4 protons from the fact, that it was experiencing a very strong isotropic shift upon heating (in the HS complex it indeed has a chemical shift of 200 ppm). Relevance of the peaks to a particular position of the hydrogen atom within a pyridine ring stems directly from the results of COSY experiment. However, while the signals of 2/4-pyridines could be easily separated by the integral, distinction between the aromatic rings of N3-pi (coordinating moiety N1) and N7-pi (coordinating moiety Y6) was less evident. In the ligand spectrum (Fig. 55 B), the two-dimensional heteronuclear ^1H - ^{13}C experiments (HSQC and HMBC) allowed for assigning the 8.57 ppm signal to the N6-aromatic moiety and 8.37 ppm to the corresponding hydrogen in position ortho-to the N-coordinating unit in the aromatic ring of N3-pi, by a coupling of Pi6 signals with a CH_2 group of a picolyl moiety. These in turn were distinguished by the observation of the proximity of either position 6/8 (for N7-pi – 3.60 ppm) or 2/4 (for N3-pi –

3.66 ppm, overlap with OMe singlet of 6H integral). However, no ^{13}C NMR spectra were successfully registered for the metal complex, excluding the possibility of the HSQC and HMBC-type analysis. In addition, as discussed in chapter 6, there exist no exact analogy between the spectra of the ligand in a free form and in the complex, even if it is diamagnetic.

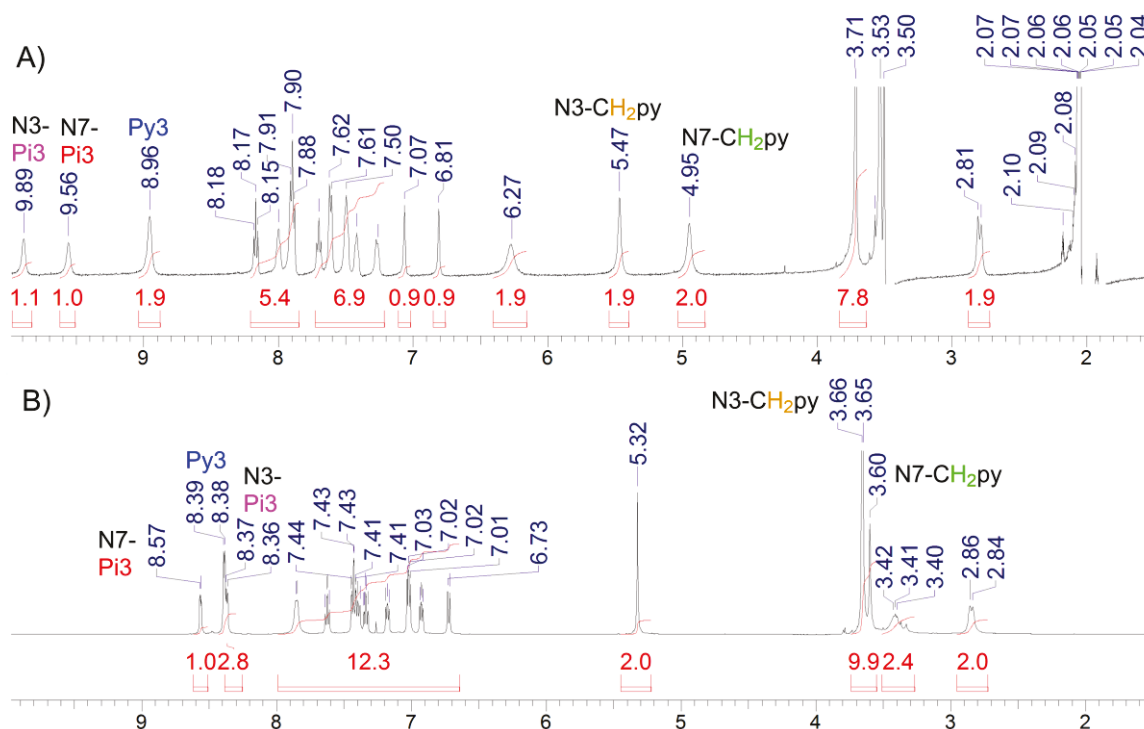


Fig. 55 ^1H NMR spectrum of A) the complex **[Fe15]** in acetone- d_6 at 213 K and B) the pure ligand **15** (*syn* isomer) obtained at room temperature in CDCl_3 . For numbering refer to Fig. 23.

By considering a withdrawal potential of coordinated metal ion and torsional angle dependency of the shifts, similar to the one discussed in details for the complex **[Fe34]** (chapter 6), I proposed to assign the 9.89 ppm and 9.59 ppm chemical shifts respectively to the N3-Pi3 and N7-Pi3 protons. In particular, torsion angles found for the relevant Fe-N and C-H bonds were 4° for the N3-pi, $11.8 - 13.5^\circ$ for 2/4-pyridyls and 16.3° and were associated with shifts of 1.5 ppm, 0.6 ppm and 1 ppm respectively and, as expected, the isotropic shifts were slightly lower than those of sterically less hindered **[Fe35]**. On the other hand, the significant difference of 0.1 \AA in the length of the Fe-N3 (1.98 \AA) and Fe-N7 (2.08 \AA) bonds (Table 5 in chapter 6) should alter the electron-withdrawing potential of N-Fe moiety. In the consequence, it is most probable that the methylene protons close to stronger binding nitrogen will experience stronger relative downfield shift upon complexation. Hence, as in the pure ligand signal corresponding to N3- CH_2py is already slightly downfield the N7- CH_2py , then in the complex 5.47 ppm peak may be assigned to the CH_2 of the N3-pi, with $\delta = 4.95 \text{ ppm}$ coming from N7- CH_2py . Finally, singlets of 1 H intensity at 7.07 ppm and 6.81 ppm, which could not be found in any ligand spectra, and which upon heating shift slightly upfield (or less downfield) in correspondence to the solvent peak, were attributed to OH groups of the

hydrated C=O moiety. The acetalization of C-9 carbon is typically observed for the bispidinone complexes and was also found for all the structures reported in this work. This assignment is supported by the presence of the two singlets also in acetonitrile solution and their disappearance in D₂O, where the proton replacement by deuterium from the bulk occurs.

Proton type	ϕ^c	$\Delta\phi^d$	Bonds to N		Acetone		Acetonitrile			Water	
	[°]	[°]	closest	next	$\Delta\delta-1^e$	rank	$\Delta\delta-1^e$	$\Delta\delta-2^f$	rank	$\Delta\delta-2^f$	rank
6/8-ax	178.46	88.46	2	none	43.3	1	42.45	49.27	1	41.65	1
H-2/4 ^a	164.81	74.81	2	3	39.07	2	37.78	43.47	2	36.54	2
N7-CH ₂ py ^b	-154.6	64.62	2	3	21.75	3	21.18	22.95	3	18.68	5
Py3 ^a	-11.75	78.25	2	none	21.04	4	20	22.66	4	20.29	3
N7-Pi3	16.27	73.73	2	none	20.13	5	18.25	21.57	5	18.43	6
N3-Pi3	-4.03	85.97	2	none	18.47	6	17.93	21.57	6	19.19	4
N3-Pi6	5.87	84.13	3	4	15.38	7	14.93	16.17	8	13.65	8
N3-CH ₂ py ^a	121.33	31.33	2	3	15.32	8	15.25	17.3	7	14.7	7
N7-Pi6	-22.2	67.8	3	4	12.5	9	11.65	13.26	9	11.09	9
Py4 ^a	-23.57	66.43	3	none	9.24	10	8.94	10.13	10	9.18	10
Py6 ^a	14.49	75.51	3	4	8.6	11	8.32	9.54	11	8.57	11
N3-Pi4	-6.74	83.26	3	none	8.42	12	8.22	9.06	12	8.365	12
N7-Pi4	34.54	55.46	3	none	7.85	13	7.42	8.55	13	7.55	13
6/8-eq	-63.18	26.82	2	none	6.89	14	6.75	7.32	14	6.5	14
N7-Pi5	46.64	43.36	4	none	1.88	15	1.97	1.37	15	1.6	15
Py5 ^a	165.17	75.17	4	none	-0.52	16	-0.66	-1.06	16	-0.09	17
OMe					-0.74	17	-0.72	-0.75	17	-0.02	16
OH					-2.76	18	-3.01	-3.8	19		
N3-Pi5	-50.1	39.9	4	none	-3.28	19	-3.21	-3.73	20	-2.36	18
OH					-3.64	20	-2.31	-3.95	18		

a) for these protons two slightly different angles were measured but only the more optimal for contact shift was given. b) significantly different torsional angles for these protons were found. the one of 87.48 ($\Delta\phi = 2.52$) was not included as it will be averaged due to the flexibility of the arm. c) ϕ torsional angle between the C-H and the closest Fe-N bond d) $\Delta\phi$ net difference between the torsional angle and the value 90° e) $\Delta\delta-1$ isotropic shift between 233K and 333K f) $\Delta\delta-2$ isotropic shift between 298 K and 353 K

Table 9. Isotropic shifts and some geometric parameters of different proton environments of [Fe15].

These results could then be directly extrapolated to the CD₃CN solution, in which the ¹H NMR spectrum of [Fe15] was alike. In water, where lowering the temperature was not possible, COSY experiment was performed on the partially paramagnetic sample at room temperature. Most diffused peaks did not give the adequate signal in this experiment. Nevertheless, they could be rather easily described by the analogy to the spectra in acetone and acetonitrile. In addition, by comparing my results with the approximate chemical shifts expected for each proton in the purely high spin bispidine iron(II) complexes described before (chapter 6), I was able to create a dynamic profile of each signal. For the full compilation of the isotropic shifts the reader is referred to the experimental section. Here I would like to discuss only the most representative examples which demonstrate the principle and lead to the most significant conclusions.

In Table 9 proton environments are ordered by decreasing isotropic shift observed upon heating in CD₃CN and acetone-d₆. The relative position of each hydrogen is denoted by the distance (in bonds) from the nearest coordinating atom, what is crucial for the magnitude of the scalar coupling. Second geometric parameter given on the basis of the X-ray structure is a deviation of the torsional angles (ϕ) measured for the nearest Fe-N and respective C-H bond, from the value of 90 ° at which contact shift is quenched; i.e. the highest the $\Delta\phi$ the strongest the theoretical contact shift. From these semi-quantitative data, several interesting conclusions can be drawn. Firstly, the importance of the torsional angle is the best visualized by the difference in the position of the equatorial and axial protons from carbon 6/8. Torsional angle of the proton in axial environment is almost ideal ($\Delta\phi = 88.5^\circ$ in respect to the optimal value of 90 ° for the maximal contact shift) leading also to the highest isotropic shifts observed. On the other hand, $\Delta\phi = 26.8^\circ$ leads to weak isotropic shift, despite a direct proximity of the coordinative bond. Similar considerations may explain the difference in the chemical shift of methylene protons from the picolyl substituents on N3 and N7. The deflection angle found in the crystal structure of this complex imposes a significant twist for the N6-coordinating moiety which in turn implies also a relative change of the position of methylene protons in respect to the Fe-N coordinative bond. In the consequence one of them will be almost exactly perpendicular to the Fe-N bond and the contact shift of it should be significantly quenched, while for another proton it will be increased as the torsional angle increases too. Summarizing, for optimally coordinated picolyl moiety (like N1) $\Delta\phi$ is approximately 30 ° and thus the contact shift for these protons should be limited. On the other hand twist of the binding pyridyl imposes also a twist in the methylene bridge which leads to two inequivalent protons, one with $\Delta\phi$ of 65 ° and thus sensitive to the paramagnetic influence, and another with $\Delta\phi = 2.5^\circ$ with the effect being quenched. Nevertheless, in practice, only one signal for these hydrogens was observed, suggesting that there is a fast equilibrium between the two, which is in line with an expected flexibility of the picolyl arm in solution.

The analysis of a temperature dependency of the signals from aromatic hydrogens in position ortho to the binding nitrogen in organic solvents showed a slightly faster downfield movement of Py3 protons from 2/4-moieties ($\Delta\delta = 21.04$ ppm, 20.13 ppm and 18.47 ppm in acetone-d₆ and 20 ppm, 18.25 ppm and 17.93 ppm in CD₃CN for Py3, N7-Pi3 and N3-Pi3 respectively, in the temperature range of 233 – 323 K). This is probably a consequence of their greater rigidity which in turn ensures an almost optimal torsional angle for the scalar coupling to occur. Despite the biggest $\Delta\phi$ found for N3-Pi3 proton in the solid state, in solution flexibility of the picolyl unit may eliminate this advantage and thus leading to slightly less effective paramagnetic influence. the most effective position of the N3-Pi3 protons to experience paramagnetic influence. Interestingly for aqueous solution one of the Pi3 hydrogen atoms differs more significantly in the isotropic shift observed than it was a case of organic solvents. The signal was originally attributed to the N7-Pi3 and may suggest a small contribution of rapid ligand exchange equilibria. As decoordination in obvious way decreases the contact shift, the averaged signal from bound and displaced forms will thus be upfield in the respect to the ones of permanently bound pyridine moieties. It is also worth to

point out that water stabilizes a low spin state of the compound by approximately 10 K, despite the possible decoordination occurring in this medium, suggesting that 1) decoordinated species is not very abundant and does not contribute significantly to the overall magnetic moment, 2) the non-specific electrostatic interactions stabilizing the less bulky diamagnetic state of the SCO compounds, discussed in chapter 2, are operable also for [Fe15].

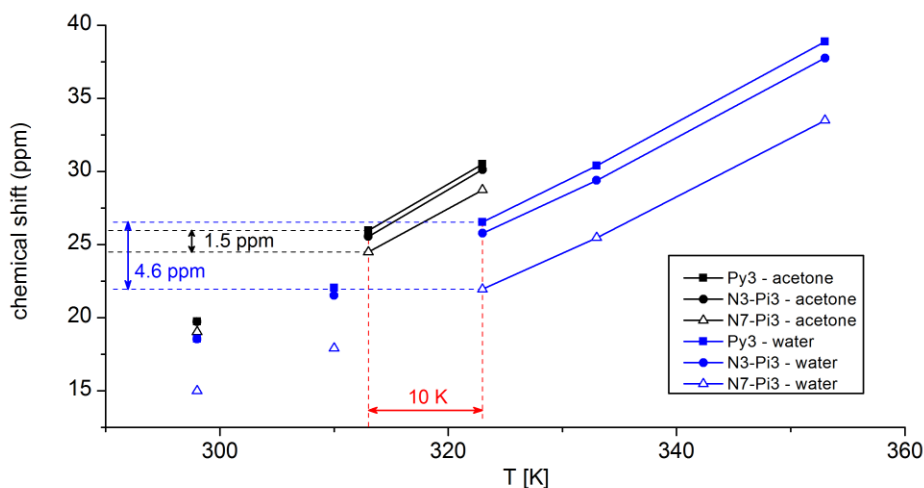


Fig. 56 Difference in the chemical shift of *ortho*-hydrogens of pyridyl moieties of [Fe15] complex measured in deuterated water (blue) and deuterated acetone (black).

Summary. The NMR analysis of this spin-transition system confirmed the relative insensitivity of [Fe15] to the nature of the solvent in a wide range of temperatures. The large temperature dependency of the isotropic shifts of the ligand's protons stems principally from the SCO phenomenon occurring in solution, but a minor decoordination in aqueous media could also be observed. The analysis of the chemical shifts of sterically challenged picolyl moieties revealed that ligand displacement is indeed a consequence of the steric clash, which destabilizes the Fe-N bonds and increases the flexibility of the picolyl arms, making them prone to solvent competition. Nevertheless in pure solvents, its contribution to the overall magnetic moment remains negligible.

Perspective – temperature sensing in aqueous media by Magnetic Resonance Spectroscopy or MRI (paraCEST contrast agents). Isotropic shifts of individual protons are a function of geometric parameters of the structures adopted by the complex in solution. However the rigidity of the bispidine ligands (at least with respect to four coordinating moieties) makes the chemical shifts of most of the signals directly dependent on the magnetic state of iron(II); i.e. the position of the magnetic equilibrium. The latter involves principally the SCO process which is in turn strictly related to the temperature of the environment. By consequence, chemical shifts of well-selected protons may be potentially used as temperature sensors. Probably the best candidates are the axial protons of the bispidine ring (H-2/4 or H-6/8 axial) which are in close proximity to the coordinating atom and adopt an almost optimal angle for contact shift to occur, but at the same time they do not change their relative position to the metal ion as they are part of the rigid adamantane-like

structure. The slope of the chemical shift-temperature dependency for these protons is as high as even 1 ppm per 1 °C for the 343 - 353 K interval. This value compares well with that of the most sensitive temperature sensors currently used for biological applications.^[38]

Complex [Fe15] might potentially be tuned for even better values, provided a slight lowering of the ligand field strength (for example by electron-withdrawing substituents on pyridine rings), which will move the transition temperature $T_{1/2}$ to the value around RT. This will ensure the steepest possible slope of the shift change within the practically most relevant conditions. The principal advantage of such temperature sensors over existing ones is the fact that they allow for the measuring of the signal outside the diamagnetic spectral window avoiding a large background noise. In addition, the bispidine binding ensures also a good stability even in aqueous media. Alternative adaptation of this system to the real-life temperature-sensing applications could include an addition of an amine or amide directly to the aromatic ring of the pyridine ring, which could still experience a paramagnetic shift from the metal center and at the same time would allow for proton exchange with the bulk water. This would then constitute a very attractive moiety for the design of a paraCEST contrast agent for MRI.

7.2. Anion sensitivity – towards magnetogenic anion sensors

For optimal magnetic detection a switch-on of the paramagnetic properties from the initially silent or near silent state upon the presence of the analyte is required. On the other hand a stability of the system has to be large enough to ensure that the activation process is not caused by the media, but only by the compound of the interest in stoichiometric or sub-stoichiometric quantities. The ligand displacement strategy is the most promising one as it offers the biggest gap between the initial and the activated state and thus can lead to more drastic and decisive response than a supramolecular periphery binding. As previously described, the whole concept of this PhD project is based on that fact and proposes switching from the diamagnetic N6-iron(II) to paramagnetic N5O1-iron(II). Original strategy of inducing this switch by generating the coordinatively unstable motif upon the chemical activity is by far the most advantageous for the construction of the magnetogenic probes, as discussed in details in chapter 3. However, the fact of detecting a chemical reactivity makes it unsuitable for the detection of non-reactive analytes. One of the examples of such targets which are not compatible with the cleavage strategy originally pursued in the project of the group are anions. An importance of their detection in biology but also for environmental and industrial applications is well recognized. I have thus proposed that magnetic equilibria described in chapter 7.1 may be used for magnetic anion detection, which up to now, is virtually inexistent. Preliminary results discussed below, which are a subject of the publication being now in preparation, should serve as a motivation for the development of new molecular designs.

7.2.1. Introduction

Currently developed molecular tools for anion sensing are in the great majority of cases fluorescent probes, with some examples of electrochemically responsive ferrocene-type compounds. An intense research in a construction of anion receptors led to the development of the Indicator Displacement Assays which turn the recognition into the signaling event via a formation of so called chemosensing ensemble (CE).^{[125] [126] [124]} It is realized by installing a fluorophore in the receptor cavity, what modifies its optical properties in comparison to the free form (usually quenches it). Anions which are well suited for the recognition site will favorably bind to the receptor, releasing the fluorophore. Great advantage of this approach lies in its simplicity as a wide range of fluorophores and receptors may be envisaged.^[126] In other variant, the replaced dye can be covalently bound to the probe, what for a price of more laborious synthesis and elaborate design, makes the recognition event more difficult but in the same way more selective.^{[126] [243]}

Ions, unlike other analytes, possess a permanent electric charge and thus may get involved in much stronger electrostatic interactions than electroneutral species, what is widely explored for their sensing. However, the main difficulty in detecting anions in comparison to metal cations, especially in practically relevant polar media like water, is their relatively low charge density and structural

diversity. Thus in order to efficiently bind the anion, elaborate recognition systems ensuring multiple electrostatic interactions (including H-bonding) within the properly shaped cavity are required.

Coordinative metal-ligand interactions can be advantageous over purely electrostatic interactions as they offer a stronger anion binding, especially in the polar media like water. Directional character of these interactions, unlike the a-directional electrostatic attractions, offer an additional way for increased selectivity of recognition/detection.^{[133] [126]} Pattern-based recognition between the simple metal ion complexes and suitable mixtures of dyes was successfully applied in a detection of a variety of analytes, including biomolecules and ions. Due to the use of cheap and commercially available substances, these chemosensing ensembles are well suited for the practical application in quality control of technological processes or in food industry, where the chemical complexity of the sample is limited.^[126] Nevertheless, for more complex media selectivity requires that only one coordination site on the metal is free for replacement. Fine tuning of the binding can additionally be realized by the tailoring of the neighboring ligands which will make enough place for only certain shapes of the analytes and will favor one geometric structures over the others. Transition metals would thus be of highest interest due to a variety of structures available and the directionality of the metal-ligand bonds, but unfilled d-orbitals cause the quenching of the dye activity. In the above context, magnetic readout seems to be an excellent solution, as except the different binding affinities, it enables also to differentiate the anions on the basis of the ligand field.

7.2.2. Displacement of free monodentate ligand by anions – chemosensing ensemble for magnetic detection

The acetonitrile binding and subsequent change in the magnetic properties is not unusual and have been reported on several occasions for other pentadentate metal ion complexes, but the strength of this attraction is usually limited. As shown in chapter 7.1, the monodentate ligand (acetonitrile) of the complex $[\text{Fe19}(\text{CH}_3\text{CN})]$ prepared and characterized in the course of this work, is also in a significant extent replaced by the water in aqueous media ($4.11 \mu_{\text{B}}$ when dissolved in water, due to the exchange equilibria). Nevertheless, provided a only 5 mM concentration of the probe, an incomplete replacement is an indication of still high affinity to the bispidine iron(II) complex. In addition, the NMR spectra acquired in the mixture of acetonitrile and water, as discussed in the previous chapter, showed an existence of purely diamagnetic compound but with a fast exchange equilibria leading to the broadening of the signals.

In order to determine the efficiency of acetonitrile binding and thus its magnetic silencing potential, titration experiments were performed on the 5 mM sample of dissolved crystals of $[\text{Fe19}(\text{CH}_3\text{CN})]$ in D_2O in the 200 MHz NMR machine and the results are present in Fig. 57 (in black). First equivalent of acetonitrile added, what in fact means a presence of 2 equivalents in solution together with the one intrinsically present on the complex (10 mM), led to a relative decrease in magnetism

of above $0.4 \mu_B$. Further addition was as expected less and less spectacular in diminishing the magnetic moment of solution. After 10 equivalents of CH_3CN being added ($55 \mu\text{M}$ concentration of acetonitrile) measured magnetic moment was $2.91 \mu_B$ in comparison to $3.88 \mu_B$ of the initial sample. This means that almost half of the complex remains in the low spin state due to the acetonitrile binding, despite the fact that only 1 promile of the solvent is in fact acetonitrile. At 20 eq however the plateau of $2.46 \mu_B$ is reached, and no detectable change in paramagnetism can be found even if the acetonitrile concentration reaches 0.5 M. The use of $[\text{Fe19}(\text{CH}_3\text{CN})]$ for this experiment implicates that we begin with a non-zero amount of the analyte to be tested, thus I have performed the same measurements but with the complex $[\text{Fe19}(\text{SO}_4)]$ which was entirely high spin at RT in aqueous solution ($5 \mu_B$) (Fig. 57 in red). The effect, despite still being observed, was less pronounced than with an acetonitrile-bearing complex, showing the role of the anion in diminishing the effect. In particular, 5 equivalents of acetonitrile were needed in order to achieve approximately the same value of μ_{eff} as after 2 eq added to $[\text{Fe19}(\text{CH}_3\text{CN})]$ what suggests that one sulfate anion would remove an effect of two acetonitrile molecules. However these results, while quite demonstrative, did not take into consideration the concentration effects, which were shown to play a significant role in pure solvents. Another observation of the anion effect on the magnetic properties of acetonitrile-bearing complex was made for BF_4^- and ClO_4^- salts of $[\text{Fe19}(\text{CH}_3\text{CN})]$, which gave rise to $0.2 \mu_B$ higher magnetic moment in the case of perchlorate ($0.1 \mu_B$ per anion equivalent, 10 mM anion concentration) at 5 mM concentration of the probe.

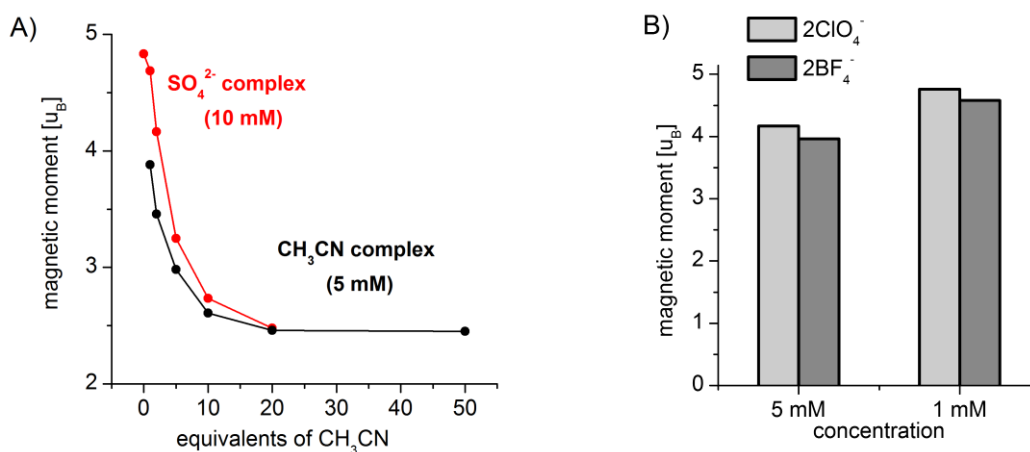


Fig. 57 A) Titration of the Fe19-type complexes by acetonitrile leading to magnetic silencing. Red curve represents titration of the initially purely high spin electroneutral ternary complex $[\text{Fe19}(\text{SO}_4)]$ (10 mM). Black curve joins the experimental points from the titration of the $[\text{Fe19}(\text{CH}_3\text{CN})]$ (5 mM). The experiments were performed at RT in 200 MHz NMR machine. B) magnetic moments of BF_4^- and ClO_4^- salt of $[\text{Fe19}(\text{CH}_3\text{CN})]$ measured in water for 5 mM solutions.

Many different experiments with varying the amount of the probe and acetonitrile in solution were carried away in order to find the optimal conditions. The general conclusion from these experiments is that decreasing the magnetic moment of the sample by adding the acetonitrile increases the relative magnetic response to the presence of the anion, but the effect is modest and might be opposite for those anions which have lower binding affinity to the complex than

acetonitrile. In particular, if the 4 mM solution of the of $[\text{Fe19}(\text{CH}_3\text{CN})] \cdot 2\text{ClO}_4$ is used, then the addition of 2 equivalents of sulfate induces a $0.45 \mu_B$ response from the initial value of $4.26 \mu_B$ to $4.71 \mu_B$. On the other hand if 5 equivalents of acetonitrile are added first and only then 2 eq of sulfate are introduced, the response is $0.55 \mu_B$ from $3.31 \mu_B$ to $3.8 \mu_B$. This amelioration stem probably from the fact that sulfate can bind metal ion preferentially over acetonitrile due to its double negative charge. Thus the more acetonitrile is present in the initial solution the more the magnetically responsive compound (only the low spin compound binding acetonitrile has a potential to generate the magnetic response), i.e. the replacement event is statistically more probable. Acetate sensing was more difficult as this anion showed less of the tendency to bind to the metal center. In the consequence the original response to the addition of acetate, which was $0.09 \mu_B$ ($4.16 - 4.07 \mu_B$ for 5 mM $[\text{Fe19}(\text{CH}_3\text{CN})] \cdot 2\text{BF}_4$) could be slightly ameliorated upon the addition of one equivalent of acetonitrile. In the result of this procedure 5 mM acetate increased the paramagnetism of the sample by $0.18 \mu_B$, which means doubling the initial effect. However further increase of the acetonitrile concentration quenched the responsiveness significantly as the acetonitrile can more effectively compete for complex binding and thus its higher concentration makes the replacement by the weakly binding ion less probable.

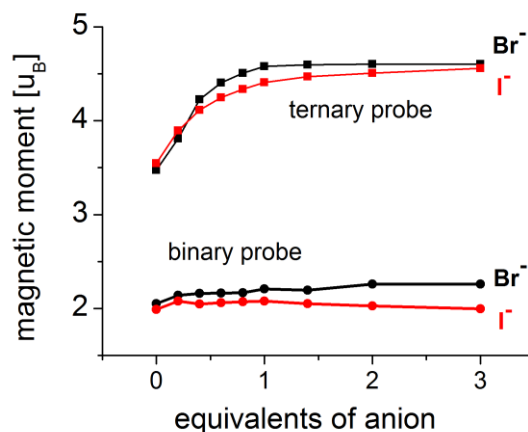


Fig. 58 Comparison of the magnetic responsiveness of binary ($[\text{Fe15}]$) and ternary ($[\text{Fe19}(\text{CH}_3\text{CN})]$) complex in methanolic solution at RT. Change in the magnetic moment of the solution of the complexes upon the addition of the halogenide ions.

The proof of the increased tendency of decoordination found for the monodentate ions in comparison to the replacement of covalently bound arm, which is discussed in the next chapter, is shown in Fig. 58. The titration experiments were performed of the 5 mM solutions of the complexes in deuterated methanol and the NMR spectra for calculation of the magnetic moment were acquired on 500 MHz NMR machine. The inertness of the halogenides binding by the binary $[\text{Fe15}]$ is in clear contrast to the significant magnetic responsiveness of $[\text{Fe19}(\text{CH}_3\text{CN})] \cdot 2\text{BF}_4$. While it can be beneficial if detection of the weakly binding ions is necessary, it is intrinsically associated with decreased selectivity, due to the lower demand for anion coordination.

Understanding of the complicated equilibria in the system could potentially lead to the formulation of the chemical ensembles which will favor binding of one anion over another and will maximize the response. Nevertheless, for the moment the utility of this system due to the lack of selectivity of the response is limited.

7.2.3. Displacement of the tethered arm - towards the binary probe for magnetic anion detection in competitive media

Dynamic exchange equilibria for the ternary complex [**Fe19**], similar to other analogous systems reported before, cannot be easily controlled, especially if several or more analytes are present simultaneously in the sample. The use of a binary probe should improve this situation, as 1) the removal of the one coordination site is more difficult due to the presence of the five membered chelate ring. In addition, 2) the competition from the tethered arm for metal coordination due to its permanently high local concentration, is much bigger than the one of monodentate ligand which will diffuse to the bulk once replaced.

Nevertheless, until the end of my experimental work (end of 2012) no such system was reported, where the replacement of one coordinating arm of the hexadentate ligand, leading to the increased magnetic moment in solution, was a result of the addition of the stoichiometric quantities of the analyte and not the activity of the solvent. The reason lies mainly in the difficulty in overcoming the kinetic inertness of low spin complexes and establishing a strong enough monodentate anion binding to the metal center, which would withstand the competition from the decoordinates arm and the bulk solvent, despite only stoichiometric concentration.

I have identified ferrous complex of ligand **15** as a suitable candidate for such behavior, as it largely remained in its hexacoordinate form in pure solvents, with a small fraction (approx. 10 – 15 %) of the compound being in the N6-coordinated HS state. In the consequence, magnetic moment of the sample was still low (approximately 1.5 - 2.0 μ_B , compare with roughly 1.7 μ_B for $S = 1/2$ systems like low spin iron(III)) but in the same time a small fraction of molecules should remain kinetically labile (HS). The lower kinetic inertness should in addition be a consequence of there was a fraction of the molecules (HS form) which were kinetically labile remaining within a range of the low spin iron(III) but in the same time remained at the beginning of the SCO transition at room temperature.

Even three orders of magnitude higher kinetic lability of the HS Fe(II) complexes in comparison to the LS ones allows to assume that in the experimental conditions (solution in RT of $\mu_{\text{eff}} = \text{approx. } 1.8 \mu_B$ measured in methanol) it is the HS isomer of [**Fe15**] that binds the anions. It is confirmed by almost instantaneous change in the magnetic moment and the UV spectrum observed upon the addition of the anion to methanolic solution of the complex. In the optimal experiment, aqueous solutions would be used, however as it will be discussed later on, the magnetic responsiveness to anion presence in water is significantly diminished, probably due to a large hydration energy,

which in turn stems from the polarity of water and the ability to form hydrogen bonds. Nevertheless, having in mind the need of the development of probes for competitive media, methanol was chosen, as it somewhat resembles water in its tendency of hydrogen bonding and is one of the most polar organic solvents available. In the consequence, in order to ensure the solubility of the anions, their tetra-alkylammonium salts were used for a preparation of a titration solutions.

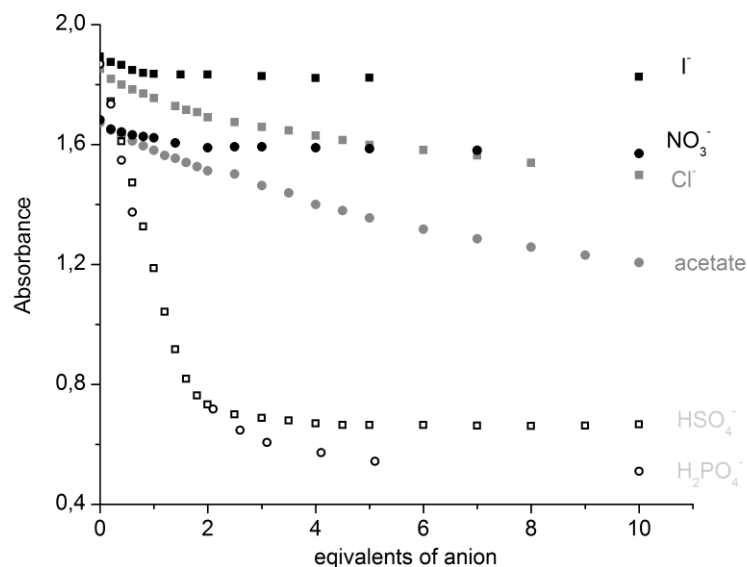


Fig. 59 Evolution of the absorbance intensity at 458 nm measured for 0.2 mM concentration of the probe [Fe15], which is a consequence of the addition of anions..

UV-Vis monitoring of anion binding in MeOH. Titration experiments with several common anions were performed in MeOH solution of the complex. Following the addition of each portion of anion solution to the sample of [Fe15], measurements were performed directly after several seconds of mixing. The effect of anion addition on the magnetic equilibria could often be observed by a naked eye due to the significant lightening of originally light/dark orange solutions upon anion binding, which is consistent with a disappearance of the most intense MLCT band, of the low spin form, principally responsible for the dark color of the samples. For the UV-Vis measurements), 0.2 mM solutions of the complex were used and typically anions were added in 0.2 eq portions until their concentration reached 2 equivalents (0.4 mM). After that point, the addition was performed in 0.5 eq steps until 5 equivalents were added and subsequently 1 eq steps until the final concentration of the anion being 2 mM. Fig. 59 represents the evolution of the absorption at 458 nm which was the most intense peak found for pure [Fe15] in visible range of the spectrum, and was assigned to the (MLCT) of the low spin form. Two (three) other maxima could be found in the proximity of this peak at slightly higher energies (430, 407 and 385 nm) which could be other MLCT bands, present in the spectrum due to the asymmetry of the metal binding in solution being a consequence of the steric clash. Evolution of these signals was parallel to the one of 458 nm. The results of the addition of 100 equivalents are not shown, but for iodide, nitrate as

well as hydrogensulfate and dihydrogenphosphate the absorption intensity at 458 nm did not change significantly, showing that for these cases a plateau was attained. On the other hand, for acetate and chloride the absorbance decreased between 10 and 100 eq of the anion concentration suggesting intermediate binding constants for these ions. A rapid disappearance of the 458 nm absorption band upon the addition of phosphate and sulfate clearly shows that the binding of anion occurs in this case and shifts the magnetic equilibria completely to the side of high spin complex-anion ensemble. For acetate and chloride the effect is even less than half of the one observed with hydrogensulfate or dihydrogenphosphate suggesting that the efficiency of the ligand replacement is significantly lower with these ions. On the other hand, for nitrate and iodide, negligibly small decrease in the absorbance is observed, showing that these ions cannot form stable enough bonds with the metal and/or are efficiently solvated by methanol.

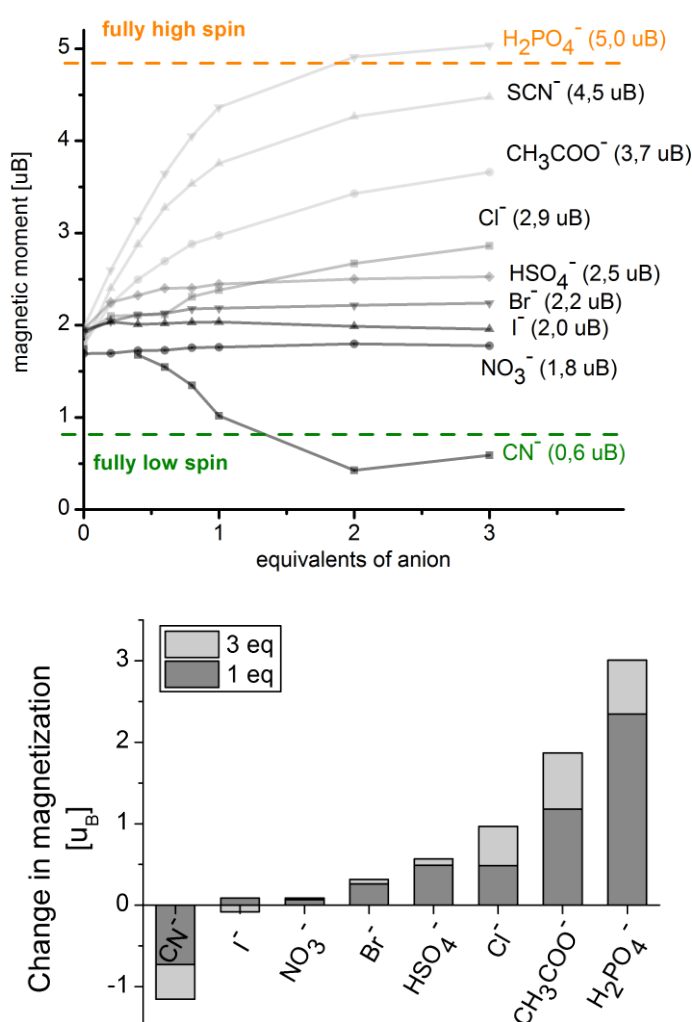
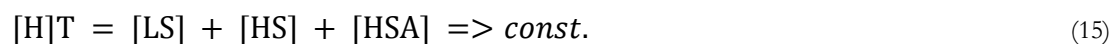
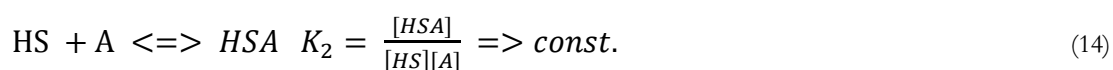


Fig. 60 Magnetic responsiveness of the binary probe **[Fe15]** in methanolic solution at RT for 5 mM solutions, in 500 MHz (11.7 T) NMR device. A) magnetic moments upon anion addition (solid lines joining the experimental points are only for easier orientation) B) relative change of the magnetic moment upon the anion addition in comparison to the solution without an anion presence.

Magnetic effects of anion binding in MeOH. In the majority of examples, the results of Evans' experiment in which the magnetic moment is measured for the 5 mM concentration of the probe at RT in deuterated methanol and in 11.7 T NMR device, are consistent with the effect of anion binding. Again, the addition of phosphate leads to the most decisive response, which amounts to as much as $2.5 \mu_B$ difference between the pure complex and the sample in the presence of 1 eq of phosphate. Addition of two more equivalents of anion completely saturates the probe and the magnetic moment of $5.04 \mu_B$ found for 3 eq solution of the anion with a probe, indicates a full conversion to the high spin state. Increase in paramagnetism is also observed for other anions, with thiocyanate acetate and chloride being the second third and fourth the most efficient binding analytes, For iodide nitrate and bromide, the magnetic effect observed for 15 mM solution of the anions is practically undetectable. The only example which does not fit the pattern observed in the UV-Vis experiment is hydrogensulfate, which despite a significant reduction of the absorption band of the low spin form does not lead to any significant increase in the paramagnetism, despite the fact that its concentration in the NMR experiment is 30 times bigger than in the UV-Vis measurements. This unexpected behavior could not be convincingly explained. Importantly, the additional selectivity of the magnetic response in comparison to the dye displacement assays, which stems from the sensitivity to the pi and sigma donating and accepting character of the anion (ligand field) was demonstrated in experiment with cyanide. As expected already 1 eq of the anion silenced the complex magnetically, which is in agreement with its high ligand field. A very strong affinity to iron(II) found for this ion is not surprising, as the low spin complex resulting from its coordination would show a much shorter iron-analyte bonds and thus would increase its kinetic inertness, as expected.

Estimation of binding constants in MeOH. The results of the magnetic measurements upon titration of the binary complex with anions were also used to estimate the approximate binding constants of the system. Due to the typically found kinetic inertness of the LS form in comparison to the HS isomer,^[244] it can be assumed with a very good approximation that the ligand exchange reaction will happen exclusively with the HS form of the complex. This is in agreement also with the fact that the addition of anion to the solution of the metal could be followed by the UV-Vis spectroscopy and the magnetic moment measurements directly after the addition. So the establishment of the magnetic equilibria was almost instantaneous. This would not be expected if it was the LS form undergoing a reaction with an anion. In the consequence, the following equilibria and the resulting constants can be proposed:



$$CA = [A] + [HSA] \text{ (CA - total conc of anion added)} \quad (16)$$

In combination with the equation which correlates the magnetic moment with a concentration and a magnetic susceptibility

$$\mu = 2.84 \sqrt{\chi_{\mu} T} \quad (17)$$

and thanks to the additiveness of the magnetic susceptibilities:

$$\chi_{\mu} = \chi_{LS} \times x + \chi_{HS} \times (1 - x) \quad (18)$$

I could derive the following analytical expressions which I have used for a calculation of the binding constant:

$$\mu_{obs}^2 = [H]_t * \frac{\mu_{LS}^2 + \mu_{HS}^2 K_1 + \mu_{HSA}^2 K_1 K_2 [A]}{1 + K_1 + K_1 K_2 [A]} \quad (19)$$

And the subsequent quadratic equation with only constants to calculate [A]

$$0 = K_1 K_2 [A]^2 + (1 + K_1 + K_1 K_2 [H]_t - C_A K_1 K_2) [A] + (-C_A (K_1 + 1)) \quad (20)$$

$$a = K_1 K_2; \quad b = 1 + K_1 + K_1 K_2 [H]_t - C_A K_1 K_2; \quad c = -C_A (K_1 + 1)$$

In the least approximate situation, the four parameter fit of the experimental data (magnetic moment observed in the function of the total anion concentration added) should be performed with varying K_2 and the magnetic moments of all three iron(II) containing species in solution. K_i in turn does not have to be fit separately as it can be calculated from the magnetic moments of the low spin and a high spin form and the magnetic moment measured for the sample in pure solvent (when the HS-A adduct is not yet present) according to the equation:

$$K_1 = \frac{\mu^2 - \mu_{LS}^2}{\mu_{HS}^2 - \mu^2} \quad (21)$$

However, the limited amount of the experimental points require that the fit is reduced to at least two parameters or maybe even only K_2 is remained to be varied. Thanks to the previous measurements of the magnetic moments of the high spin and the low spin state of iron(II) described in thermodynamic parameters section in chapter 7.1, I could assume that the magnetic moments of HS and LS in methanol will be somewhere between the values found for water and acetonitrile. Thus for each experimental set I have performed two fitting experiments with μ_{LS} and μ_{HS} values fixed at 0.0 μ_B and 4.9 μ_B , or 0.4 μ_B and 5.4 μ_B respectively. These values are also in agreement with a values typically found for the iron(II) LS and HS complexes (for more argumentation see

chapter 7.1 and the experimental section). For the titration with a phosphate anion, the calculated K_2 was 3713 M^{-1} and 4677 M^{-1} for μ_{LS} and μ_{HS} at $0.0 - 4.9 \mu_{\text{B}}$ and $0.4 - 5.4 \mu_{\text{B}}$ respectively. In both cases the value of μ_{HSA} was $5.44 \mu_{\text{B}}$ which is in agreement with the expectations. For thiosulfate, the values of K_2 were slightly lower (3300 M^{-1} and 4191 M^{-1} for the respective values of μ_{LS} and μ_{HS}) in agreement with the experiment. Nevertheless, the estimated value of μ_{HSA} was 4.8 which is slightly below the high spin limit, but is still acceptable. For the remaining ions, the values of μ_{HSA} calculated by a 2-parameter fit were intermediate between the HS and LS state (μ_{HSA} was $2.5 \mu_{\text{B}}$, $3.5 \mu_{\text{B}}$, $4.3 \mu_{\text{B}}$, and $4.0 \mu_{\text{B}}$ for Br^- , Cl^- , AcO^- and HSO_4^- respectively). These results are physically irrelevant because for none of these ions high enough ligand field can be expected to render iron(II) low spin, even despite the presence of strong ligand field N5 coordination motif. In the consequence I was forced to fix the value of the μ_{HSA} within the range found for the HS complexes ($4.9 \mu_{\text{B}} - 5.4 \mu_{\text{B}}$). The resulting values of the binding constants were within the range of $40 - 65 \text{ M}^{-1}$, $74 - 124 \text{ M}^{-1}$, $102 - 177 \text{ M}^{-1}$ and $446 - 875 \text{ M}^{-1}$ for bromide, sulfate, chloride and acetate respectively. For the latter it means that the affinity of the acetate to the complex is 5 - 10 times lower than that of the phosphate and for the remaining ions K_2 is two orders of magnitude lower. For iodide and nitrate the magnetic effect remains within the experimental error showing that the binding of the coordinative arm is more efficient and thus it will not allow for the sufficiently long residence of these ions to contribute in any way to the paramagnetism of the sample. On the other hand binding of the cyanide seems to be too strong to enable the calculation of the binding constant. Instead, a competition experiments would have to be performed with strong binding anions like phosphate and only the by relative comparison, the effective binding affinity could be estimated.

Lowest detectable limit for phosphate in methanol. These results showed that the phosphate can indeed effectively and quite selectively bind to the complex in methanol, inducing an observable change in the paramagnetism of the sample, which can be used to conclude on the anion presence. In addition, the similar strength of phosphate binding can be found also at lower concentration of the probe and what's more important, also of the anion, as suggested from the UV-Vis experiments. In the consequence, assuming the approximately linear response to the addition of the first equivalent of the hydrogenphosphate and fixing the minimal detectable value of the shift of the reference peak at 1 Hz for the 11.7 T machine (indeed I was able to successfully observe it) as little as 0.1 mM concentration of H_2PO_4^- could theoretically be detected (change of $0.05 \mu_{\text{B}}$) in the described experimental conditions by the probe [Fe15]. While this is not an impressive limit if the fluorescent probes are concerned, it still remains an excellent result for the NMR, what in comparison with all the advantages of the magnetic readout discussed in the chapter 1 of this work, bodes well for the development of this type of probe for real life applications.

These promising results obtained in methanol pushed me to investigate the effect also in water, despite the expected lowering of the sensitivity stemming from the solvating character of aqueous media.

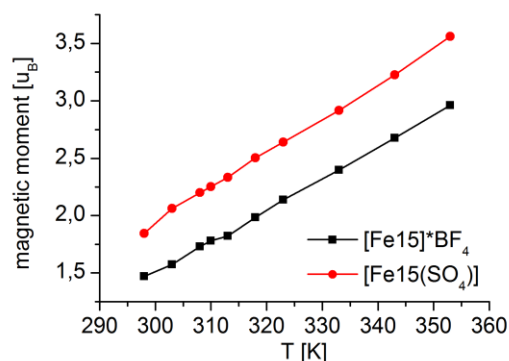


Fig. 61 Temperature-dependent magnetic moments of binary **[Fe15]** and ternary **[Fe15(SO₄)]** complexes of hexadentate ligand **15**, measured in D₂O at 5 mM concentration of the compound. The difference stems from the difference in the coordination capability of the counterions.

Magnetic response to the presence of the phosphate in water. The influence of the counter-ion on the magnetic properties of **[Fe15]·2BF₄** in water was evident from comparison of the magnetic properties of 5 mM liquid samples of crystalline material from binary **[Fe15]** complex and ternary **[Fe15(SO₄)]** with sulfate anion bound in the place of the N3-picoyl arm (Fig. 61). The difference between the two was as much as 0.4 μ_B and interestingly did not change upon heating, suggesting that the binding equilibria were established already at RT (kinetic barrier of the ligand exchange process was not significant for sulfate binding even at RT). This can be translated to 0.7 mM of the sulfate being potentially still detectable by this system, provided its coordination in decreased concentration will not be hampered, which is not evident and need further experiments to be verified.

phosphate	T [K]	μ_{eff} [μ _B]
0 eq	298	1.73
0.2 eq	298	1.79
0.4 eq	298	1.81
0.6 eq	298	1.83
0.8 eq	298	1.82
1 eq	298	1.84
1.5 eq	298	1.85
2 eq	298	1.79
5 eq	298	1.80
5 eq	310	2.11
5 eq	298	2.59

Table 10 Magnetic moments of the aqueous solution of **[Fe15]** upon the addition of the phosphate at neutral pH (buffered solution of 50 mM Tris-HCl pH 7.4).

Detection of phosphate in buffered aqueous solution. On the other hand, upon the addition of the phosphate to 5 mM aqueous solution of **[Fe15]** buffered with 50 mM Tris-HCl at pH 7.4 no

significant changes in magnetic moment could be observed at room temperature (Table 10). However 0.8 μ_B increase of magnetic moment was observed upon heating to 37 °C, which is a biologically relevant temperature, and subsequent cooling to the RT (Table 10). This may be explained by the acceleration of the process of attaining the thermodynamic equilibrium in which a fraction of the complex binds the anion. Even minor increase in the concentration of the less abundant high spin binary complex may have an important influence on the coordination equilibria. As little as 0.21 μ_B increase in the magnetic moment observed upon heating can be translated at this stage of the equilibrium to as much as 50 % increase in the quantity of the high spin isomer. It has been shown in the past that the HS complexes of iron(II) are even 1000 times more labile than the LS counterparts. It is thus the HS binary complex which is a “substrate” in the ligand change reaction and its increased abundance in solution may significantly accelerate the process. In the consequence an accelerated establishment of the thermodynamic equilibrium, induced by increased temperature, but preserved on cooling, leads to the augmentation of the magnetic moment of the sample by 0.8 μ_B in the presence of 5 eq of phosphate ion. This suggests also a high affinity of the metal center for the phosphate anion as otherwise the bulk water molecule would lead to the anion displacement, and then could be further displaced by the coordinating arm which always remains in the proximity.

7.2.4. Future directions in amelioration of the binary probe for anion sensing

Tuning the ligand field for a perfect magnetogenic response. Presence of a steric clash as demonstrated multiple times in this work and by others, promotes the spin transition, thus increasing the kinetic lability due to the increased population of the HS form. However, it could possibly also lead to significantly weaker coordination in the low spin state. In the consequence, anion binding to the HS form, if present, will lead to the establishment of the thermodynamic equilibrium between all three forms, but the ligand displacement may also occur even if 100 % of the complex molecules would be LS, diamagnetic. This hypothesis implies that the increase of the spin-transition temperature in this system (increase of the ligand field for example), provided that compound remains purely diamagnetic at RT, should enable a truly magnetogenic response, i.e. one that starts from a purely diamagnetic probe. One of the options to achieve this would be to modify the aromatic moieties in the pentadentate bispidine platform for increased back-bonding. From the discussion in chapter 2 this could be achieved by lowering the energy of the empty π^* orbital on the ligand or boosting the covalency of the metal-ligand interaction (nephelauxetic effect). Many strategies could possibly be envisaged to achieve this goal, but only two will be mentioned here to show the direction and inspire future design efforts. One practical solution is an extension of the π -delocalization due to the coupling of additional aromatic ring (like in the case of phenyl-bearing oxadiazole moiety of complex [Fe35]). Another is to introduce electron-withdrawing substituents on the aromatic ring which would “empty” the aromatic orbital for

electrons of the metal, but this might have an opposite effect due to significantly decreased sigma-donation (basicity) in the coordinating atoms.

Perspective – tuning the steric congestion to improve selectivity. Fine tuning of the selectivity of this system may be achieved by changing the ligand field, but even more so by modifying the steric clash between the two facing coordinating motifs or the steric demands for the anion coordination site. Possible variation is a decrease of the size of one of the facing aromatic rings (either from N3 or N7-substituent) from six membered pyridine to 5-membered pyrazole. This may lead to a very subtle reduction of deflection, as both substituents possess *ortho*-hydrogens, and thus making the decoordination less favorable (more selective) but still possible. It should be remembered here, that a complete removal of the *ortho*-hydrogen as shown for the example of the pyridazine moiety [Fe34], reduced the deflection angle by half which made N6-coordination permanent. Alternatively, introduction of a substituent on the methylene bridge of the picolyl moiety may hamper the rotation of the moiety and thus the unmasking of the coordination site; even if this still occurs, it will impose an additional steric constraint on anion coordination.

It should be remembered that the steric clash will also have an effect on the ligand field and, vice versa, a ligand field will influence the strength of the coordination of the displaced arm. Thus any future design should take into consideration all parameters together, but the ease of derivatization of bispidines brought within our reach by this work and the resulting perspective of a multitude of coordination motifs maximize our chances of success. In the quest for optimal magnetogenic probes for anion sensing *via* ligand displacement, one recent report is worth mentioning as it describes a chloride example of arm decoordination from a low spin binary iron(II) complex upon addition of an anion, leading to a change in magnetism (see also chapter 2).^[142] The selectivity of the effect, tested exclusively for chloride, and the behavior of the system in more competitive solvents would however be required to conclude on its potential as magnetogenic anion chemosensor.

7.2.5. Conclusions

Near low spin, binary complex [Fe15] in MeOH allows for selective detection of stoichiometric amounts of common anions at ambient temperature and in polar media. An almost quantitative switch to the high spin form was observed upon the addition of 1 equivalent (5 mM) of phosphate, thus enabling a clear-cut detection. Other ions showed weaker response, which is principally a consequence of the less favorable metal binding, but a distinction by the type of magnetic response was also achieved (for CN⁻ ions). Preliminary results in aqueous solution suggest that the magnetic detection of anions by this system can be achieved at even sub-milimolar concentrations. Future studies should provide with a deeper insight into the selectivity of the response in water and physiological media. An improvement in the binding process should also be attempted, possibly by fine-tuning the steric and/or electronic requirements by iterative ligand modification. I have also demonstrated that the use of a proper chemosensing ensemble of ternary bispidine complex and

acetonitrile can lead to a detection of anions in aqueous solution, but the selectivity of this process for only one type of analyte remains still far from optimal.

The above observations demonstrate that the ligand exchange strategy offers a major improvement in the sensitivity in comparison to the only existing magnetically responsive anion chemosensors, which operate via the hydrogen-bonding of the analyte and despite several years of development were successfully applied only in apolar media. Thus, by these results, I hope to inspire new design efforts of magnetically responsive probes for anions or other analytes operating by ligand displacement and to show that the gathered amount of knowledge on the coordination chemistry of iron(II), stemming principally from the interest in spin-transition systems, might be successfully used to benefit the field of anion sensing, largely dominated by fluorescent probes.

8. BISPIDINE-IRON(II) SYSTEM IN MRI

The preceding chapters described the magnetic properties of low spin and high spin bispidine-iron(II) complexes, and promising duos of a diamagnetic/paramagnetic relationship were identified. However, the global focus of the group's project, which my thesis is an element of, rests on the MRI applications of magnetogenic iron(II) complexes. This chapter characterizes the MRI properties of my prepared chelates and proves the relevance of the bispidine-iron(II) system for the design of responsive probes for MRI.

Measurements of the water relaxation times (T_1 and T_2) were performed either by a small-animal machine operating at 7 T or in a 500 MHz (11.7 T) NMR apparatus. The former was done by Prof. Olivier Beuf from the CREATIS Laboratory in Lyon-Villeurbanne (University of Lyon - UCB). The latter was possible thanks to the establishment of a suitable experimental protocol for the NMR software by Prof. Guido Pintacuda from the Center de RMN à Haut Champ de Lyon (University of Lyon - ENS). Dr. Laurence Canaple from the Lyon Institute of Functional Genomics (University of Lyon - ENS), handled all the animal experiments and the images were acquired as before by Prof. Beuf at 7 T.

Unless otherwise stated, standard 4 mM aqueous solutions of the chelates at 25 °C were analyzed. Obtained T_1 values were compared to that of a pure water sample; fortunately his latter value remained reasonably constant between different experiments both at 7 T (1.64 – 1.73 s) and 11.7 T (3.5 s – 3.7 s). In this work, the averaged T_1 reference values of pure water are: 1.645 s and 3.650 s for 7 T and 11.7 T respectively. The T_1 values are all associated with approximately 10 % error, and relaxivities are given with a precision of 0.01 – 0.02 mM⁻¹s⁻¹, implicating that any minor differences cannot be reliably interpreted.

8.1. Relaxivities of a pair of off-on model chelates and their MRI characterization

8.1.1. MRI silent iron(II)-bispidine complexes – model OFF state of the probes

The effect of the bispidine-based chelates on the T_1 longitudinal relaxation time of water protons was studied in order to determine, whether bispidines can lead to the MRI silent iron(II) complexes. This is the main prerequisite for the design of a putative responsive probe that is truly off, the advantage of which was discussed in this work on several occasions. Fig. 62 summarizes the OFF state, MRI silent, model compounds.

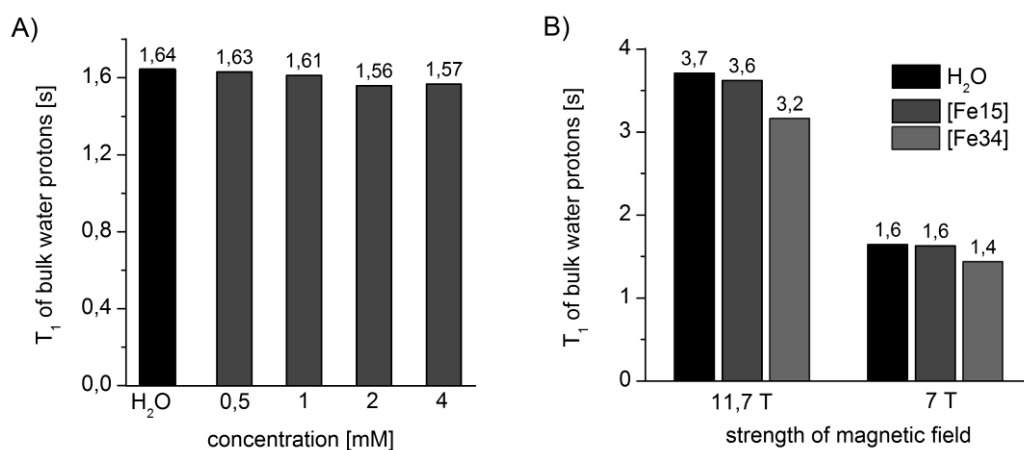


Fig. 62 T_1 relaxation times of bulk water protons A) Measurements taken for powder sample of the complex [Fe15]*2BF₄ in water at RT measured in small-animal MRI device in magnetic field of 7 T at different concentrations B) Field-dependence of the T_1 relaxation times for model off-mode complexes, acquired at 25 °C for 4 mM aqueous samples of crystalline material.

Water T_1 relaxation times of [Fe15], which was the first binary chelate prepared in the course of this work and thus the first tested for its relaxivity, were primarily measured at 7 T in MRI machine at 25 °C at four different dilutions (Fig. 62 panel A). The results obtained show clearly that virtually no effect on the relaxation time occurs for this compound and corresponds to the r_1 relaxivity value of less than 0.01 mM⁻¹s⁻¹ remaining within an experimental error, and is in agreement with the values obtained previously for tptacn-iron(II) complex – model off state of the group.^[31] It is quite surprising in the light of its near low spin but intermediate magnetic moment of 1.47 μ_B found for 5 mM aqueous solutions at the same temperature. This behavior indeed shows that decoordination phenomenon in solution is virtually inexistent and the complex in pure solvent can be treated as a binary chelate with closed coordination sphere with $q = 0$. Otherwise, water molecules excited in the MRI experiment would coordinate to the central metal ion, changing its spin state and benefiting from the relaxation enhancement. In addition, no contribution from the outer sphere can possibly be explained by the short electronic relaxation time, which was reported to have a crucial influence on r_1^{OS} (compare $S = 7/2$ of lanthanide complexes with outer sphere

relaxivity between $2 \text{ mM}^{-1}\text{s}^{-1}$ for gadolinium(III) with T_{1e} of approx. 1 ns, to as little as $0.05 - 0.1 \text{ mM}^{-1}\text{s}^{-1}$ found for analogous terbium(III) and dysprosium(III) – T_{1e} of 0.1 – 1 ps)^[20]. Indeed iron(II) is said to have the electronic relaxation times around 10^{-12} s ^[245] ^[246] ^[31] or 10^{-11} s to 10^{-9} s ^[247] if no cooperativity like (anti)ferromagnetism is found. Despite the fact that no measurements were performed, the compound [Fe15] should be expected to stay rather within a lower limit of this interval (10^{-12} or even less) due to the significant asymmetry and thus probably large ZFS, enhancing the electronic relaxation processes.

As expected, diamagnetic complex [Fe34] did not shorten the T_1 of water protons either (Fig. 62 B). Complex [Fe35] however could not be analyzed due to its low solubility disabling the establishment of a sufficiently high concentration in pure water, as required for T_1 measurements. Crystalline sample used in the experiments should minimize the risk of a free iron contamination. Thus, at 7 T, the 0.2 s shorter T_1 of 4 mM solution [Fe34] in comparison to water may stem from the temperature-independent orbital-derived paramagnetism ($\mu = 0.6 - 0.7 \mu_B$ in water) typically found for iron (II) complexes. In this case, unlike for the [Fe15], significantly reduced steric deflection and a high symmetry of the overall bispidine backbone may both, explain the orbital-contribution to the paramagnetism and in the same time hamper the electronic relaxation process, promote the outer sphere relaxation. In addition, the examination of the solid state structures revealed that tetrafluoroborate may approach the iron center for the distance of approximately 4.6 Å in comparison to 4.9 Å found for the [Fe15]. While it cannot be predicted if the same will really happen in solution for water molecules, the dipolar-dipolar relaxation of outer sphere protons could benefit from this difference, due to its high distance sensitivity (proportional to $1/r^6$). The presence of a non-coordinating nitrogen of pyridazine moiety, may possibly interact with water protons bringing them closer to the metal center and increasing their residence time in the proximity of the moving d-electrons. In the result a second-sphere type of contribution could also be envisaged but it is not evident whether the steric congestion at this site of the molecule will allow for such interaction and to what extent. Other explanations of this effect could potentially be delivered. However, while providing an overview on the complexity of the relaxation phenomena, the discussion remains purely speculative due to the lack of experimental results for other systems enabling comparison, and because the outer sphere relaxation mechanisms are not yet fully understood. *What is even more important, all the above considerations concern a very subtle deviation from the pure water signal (at maximum, $r_1 = 0.02 \text{ mM}^{-1}\text{s}^{-1}$ found for [Fe34] at 7 T) which a) is practically non-detectable as a contrast enhancement and b) remains close to experimental error.*

Field dependency. The net T_1 value of water increased roughly twice when going from the 7 T to 11.7 T, and so did the difference in the T_1 between the reference and the chelates [Fe15] and [Fe34] (Fig. 62 panel B). However, this translates to the “decrease” in the relaxivity (efficiency of T_1 shortening); i.e. 0.2 s difference corresponding to slightly above $0.02 \text{ mM}^{-1}\text{s}^{-1}$ found in 7 T changes into 0.4 - 0.5 s difference in 11.7 T but the calculated relaxivity is below $0.01 \text{ mM}^{-1}\text{s}^{-1}$. This is in line with all the expectations as the increases Larmor frequency reduces the amount of

available sources of spin relaxation in the lattice (see chapter 1). It is thus important to point out, that comparing the differences in the T_1 values at different fields may be misleading if the conclusions on the properties of the contrast agents (relaxivity) are to be drawn.

Reminder on the practical interpretation of T_1 and r_1 . The example of different field measurements discussed above, in which greater ΔT_1 does in fact still mean lower Δr_1 shows the importance of presenting both quantities simultaneously, as their practical interpretation is complimentary. The first can be correlated to the “resolution” of the image available, i.e. the greater the ΔT_1 the more pronounced the difference in the intensity of the signal registered and thus, the difference in the grayscale of the image. The change in relaxivity Δr_1 of the contrast agent is more useful in discussing the influence of the molecular modifications of the probe on the potential to raise the contrast, and indicates how much more of the compound of lower r_1 (initial state of the probe before activation) is required to obtain the same value of T_1 and thus the same signal, at constant experimental conditions. It is thus a good assessment of the background signal coming from the probe and thus a threat of “false positives”. The loss of “resolution” in the relaxation properties at low T_1 values is well demonstrated by the comparison of this parameter for the Gd-DOTA, which was used as positive control in our experiments at 7 T. For 4 mM solutions, the T_1 values ranged between 56 – 51 ms. Despite this tiny net difference, it still equals to as much as 10% change of the T_1 , what is reflected in the calculated relaxivities of 4.2 - 4.7 $\text{mM}^{-1}\text{s}^{-1}$). For 0.5 mM solution of Gd-DOTA in the same experimental conditions, T_1 was around 350 – 370 ms, and thus varied by 20 ms – 5 %. This corresponds to 4.2 – 4.4 $\text{mM}^{-1}\text{s}^{-1}$ which is in agreement with the generally accepted values but is somewhat higher than the values reported by our group before. The significantly improved precision of the estimation of the relaxivity for longer T_1 values demonstrates the “loss of resolution” of the signal enhancement, i.e. even big differences in the relaxivity of the compounds are unnoticeable when the T_1 shortens drastically, meaning that the signal can be easily saturated.

Conclusion: Both analyzed chelates [**Fe15**] and [**Fe34**] are essentially **MRI silent**, proving that a fully OFF state can indeed be achieved for a bispidine ferrous complex (future MRI probes). The two main requirements for that to happen are 1) **a closed coordination sphere** and 2) a generally **diamagnetic** state of iron(II), but a small tolerance for weak paramagnetism is also possible or even with an extra tolerance for weak paramagnetism.

8.1.2. Raising contrast in MR images by paramagnetic bispidine-iron(II) complexes

Reference relaxivity of tacn-based iron(II) complexes. Typical control for the relaxivity of different complexes is usually Gd-DOTA, which in my experiments gave the following values, for the 4 mM aqueous solutions measured at 7 T and at 25 °C: at 4 mM: the $T_1 = 55$ ms and $r_1 = 4.3 \text{ mM}^{-1}\text{s}^{-1}$. However the more reliable comparison of this system could be made with reference

iron(II) complexes, but except the work of our group, no other relaxivity values were ever published for the ferrous chelates and thus the tacn-based iron(II) complexes are the only reference available. The highest reported relaxivity for iron(II) so far was found for the dptacn-iron(II) complex and at 7 T in pure water T_1 is approximately 180 ms, what is consistent with $r_1 = 1.24 \text{ mM}^{-1}\text{s}^{-1}$.^[31] The electroneutral tacn-based complex with two tetrazole arms gave the relaxivity of $0.57 \text{ mM}^{-1}\text{s}^{-1}$.^[32] For the 11.7 T, no value for the dptacn-Fe(II) was published, but my control experiment suggested that it gives the T_1 of around 250 ms at 4 mM concentration, corresponding to approximately $0.95 \text{ mM}^{-1}\text{s}^{-1}$. Relaxivity of only two other compounds raising contrast in MRI and based on iron(II) were studied and they all were prepared in our group.^{[74] [248]} For the chemical identity of the compounds the reader is referred to chapter 3. In here, I would like just to recall the value of 0.35 s ($0.65 \text{ mM}^{-1}\text{s}^{-1}$) in 7 T at 37 °C reported in serum for the dptacn-iron(II) generated in situ upon the chemical stimulus.^[51] Summarizing, the highest values found for iron(II) complexes are $1.25 \text{ mM}^{-1}\text{s}^{-1}$ for 7 T and approximately $1 \text{ mM}^{-1}\text{s}^{-1}$ for 11.7 T, while the relaxivity at the level of $0.5 - 0.6 \text{ mM}^{-1}\text{s}^{-1}$ at 11.7 T could be seen as similar to the one offered by the tacn-system.

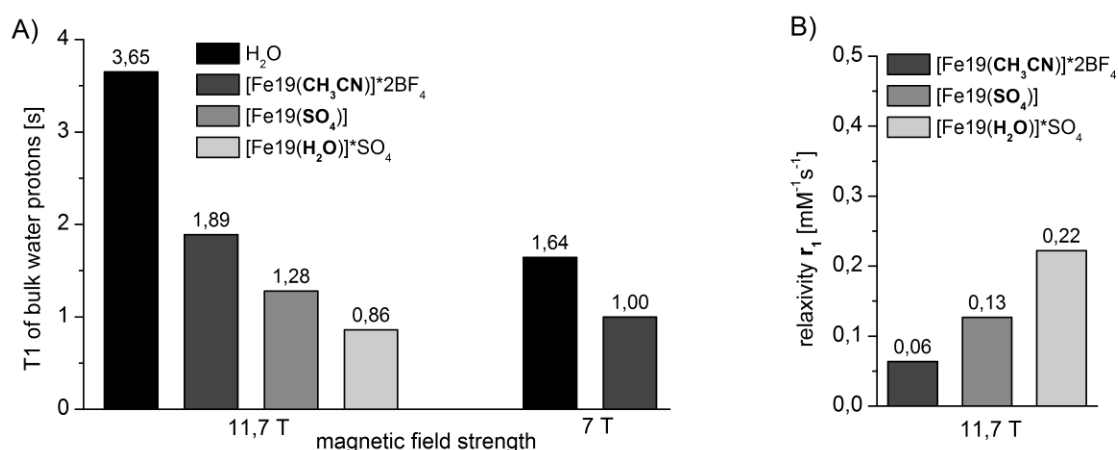


Fig. 63 Relaxation efficiency of bispidine-based iron(II) complexes prepared in the course of this work and measured at 25 °C at two different fields, 11.7 T of NMR machine and 7 T of small animal MRI device. A) T_1 relaxation times of bulk water protons B) calculated relaxivities corresponding to the T_1 values. Please note that the [Fe19(H₂O)] is an assumed form of [Fe19(SO₄)] after heating.

Relaxivity characterization of model [Fe19] molecular platform. Relaxation properties of the paramagnetic bispidine-based iron(II) complexes prepared in the course of this work were studied in above-mentioned standard conditions (4 mM, 25 °C). The results are presented in Fig. 63. Model bispidine high spin compound was prepared from the pentacoordinate platform **19** bearing a secondary amine moiety (N7-H) and was isolated as the sulfate salt, with SO₄²⁻ counter-ion coordinated in the sixth vacant coordination site. The same bispidine-iron(II) pair gave also rise to the alternative complex with CH₃CN coordinated in place of sulfate. [Fe19(CH₃CN)] was diamagnetic in the solid state but upon dissolution in water, it largely lost the acetonitrile molecule which was replaced by water (see detailed discussion in chapter 7). Nevertheless, at the 5 mM concentration, which is very close to the 4 mM of the MRI experiment, its magnetic moment was intermediate, even if close to the purely high spin ($4.11 \mu_B$). This is in agreement with a residual

relaxivity found for this compound, which was $0.10 \text{ mM}^{-1}\text{s}^{-1}$ and $0.06 \text{ mM}^{-1}\text{s}^{-1}$ for 7 T and 11.7 T respectively (dark grey in Fig. 63). On the other hand, purely paramagnetic chelate $[\text{Fe19}(\text{SO}_4)]$ ($\mu = 5.0 \mu_B$) reduced the T_1 more efficiently ($T_1 = 1.28 \text{ s}$ and $r_1 = 0.13 \text{ mM}^{-1}\text{s}^{-1}$ – grey in Fig. 63) but the obtained values were far away from the optimal relaxivity reported for the dptacn-system. Interestingly upon heating to and subsequent cooling of the sample, the improved relaxivity could be observed ($T_1 = 0.86 \text{ s}$, $r_1 = 0.22 \text{ mM}^{-1}\text{s}^{-1}$ – light grey in Fig. 63). This suggests the kinetic inertness of the initial state of the compound after the dissolution in the RT, which in addition is less efficient in the shortening the T_1 than the thermodynamically favorable equilibrium established upon heating. Possible explanation would be that the sulfate anion remains very strongly associated with the metal center limiting the water accessibility and thus disabling the efficient relaxation of water protons. Higher temperatures however, accelerate establishment of the equilibrium of sulfate-water exchange in the first coordination sphere. Nevertheless, the exact position of this equilibrium both under kinetic control (at RT) or in the thermodynamically favored form is difficult to predict. In addition the relaxivity of $0.22 \text{ mM}^{-1}\text{s}^{-1}$ still remains almost 4 times lower than the one reported for dptacn and 2 times lower in comparison to other tacn-based contrast agents reported.

Relaxivity of complexes with undetermined solid-state structure.

Other ferrous complexes of bispidine ligands were prepared, but their structural identity could not be proven due to the impossibility to obtain a crystallized sample. Their purification was thus performed by extensive washing of the obtained reaction residues and confirmed by the DIMS spectra which unfortunately led to high losses of yield. The use of equimolar or sub-equimolar quantities of iron salts (0.95 – 1 eq) should eliminate the iron(II) impurities in the final compounds, provided full conversion of the ligand has been achieved. Unfortunately, this methodology did not allow for the identification of the possible coordination isomers present in the samples and thus the relaxivity results obtained with these complexes cannot be unambiguously interpreted. However, on the basis of the structural diversity of all tested ligands, which was proven by NMR analysis, some potentially useful hypotheses may be formulated to explain the relaxivity of the model high spin bispidine complex. Further experiments would be required in the future to confirm the interpretations proposed.

Replacement of sulfate with less coordinating anion in the iron(II) salt should eliminate, if existing, the negative effects of the high iron(II) affinity which is believed to limit the accessibility of water to the first coordination sphere of the paramagnetic complex. The reaction of the pentadentate ligand **19** with iron(II) tetrafluoroborate salt was performed and the obtained yellow powder was characterized by mass spectrometry indicating the exclusive presence of the compounds of formula $[\text{Fe19}(\text{y})]^{2-y}(\text{BF}_4)_y$. After extensive washing, powder-type material was dissolved in water at 4 mM concentration and its T_1 was measured. Interestingly the results obtained were in agreement with a relaxivity found for the dptacn compounds ($T_1 = 0.23 - 0.24 \text{ s}$ in 7 T corresponding to $r_1 = 0.95 - 0.97 \text{ mM}^{-1}\text{s}^{-1}$) suggesting that indeed bispidines are capable of raising the same signal as the tacn-derived molecules, but they also seem more prone to the influence of the environment.

Some further insight into the origins of the process was expected from the analysis of the iron(II) complex of ligand **15** but in anti configuration (**15a**) in the respect to the pyridine substituents at carbons 2 and 4. By this, one coordination site, but different than in [**Fe19**], remains free for water coordination. In addition, slightly increased steric demands for the coordinative moiety in this case could also destabilize anion coordination and should favor water binding due to its limited bulkiness. The preliminary MRI measurements of the adduct [**Fe15a(Y)**] shown comparable relaxivity to the one found for [**Fe19(SO₄)**], suggesting that the coordination sphere of these molecules in the respect to water contribution is similar ($T_1 = 0.82$ s, $r_1 = 0.23$ mM⁻¹s⁻¹ at 298 K). As no anion interference can be expected in the case of [**Fe15a**] other parameters, like water residence time, may be responsible for 4 times lower relaxivity than the one found for tacn-based chelates. However, the alternative explanation of these results can also be given. The strength of water binding is expected to be higher in [**Fe15a**] than [**Fe19**] due to the typically observed difference in the length of the bonds in these positions and the deformation of the octahedral coordination geometry, as discussed in chapter 6. If that is true, then for both compounds two different parameters seem to play a decisive role – prolonged water residence time for [**Fe15a**] and restricted water access in [**Fe19**] due to the strong ion binding. Solid state structure of the complexes with coordinated water and ¹⁷O NMR studies for estimating the water residence time, as well as simulations on the influence of these parameters on the relaxivity of iron(II) complexes would all be desired to verify the hypothesis.

Pilot *in vivo* experiment. Despite the unexpectedly low relaxivity found for the high spin bispidine complexes *in vitro*, the first trials in mice were quite promising. Mice handling and injections of the samples were performed by Dr. Laurence Canaple while the image acquisition was done by Prof. Olivier Beuf. The previously described injection-electroporation protocol was used, similarly to the experiments performed on tacn-based probes. In order to establish a high concentration of the compound in buffered media, to maximize the chances of signal observation, 10 % DMSO has to be added. Injection of the [**Fe19**] (25 μ l of 50 mM solution) into the muscle, followed by the electroporation to ensure the internalization of the compound, led to the clear lightening of the image at the site of the presence of the compound (Fig. 64). The contrast obtained was comparable with the one of the bistet-tacn-Fe(II) electroneutral complex **7**, injected into the mice according to the same protocol but at 25 mM concentration (only half a dose – see Fig. 64 B). This indeed demonstrates the need for further improvement in the relaxivity of bispidine-iron(II) system to achieve the sensitivity at least of the tacn-based probes. In addition, rather acute reaction of the animal has been observed upon the delivery of the compound and a significant signs of inflammation could be found, which can possibly also be responsible for rising the signal. Future experiments could preferentially be performed with an electroneutral complexes in order to limit the Lewis-acidity of iron(II) which is believed to largely respond for the intolerance of cationic iron(II) complexes with open coordination sphere, as reported before by the group.

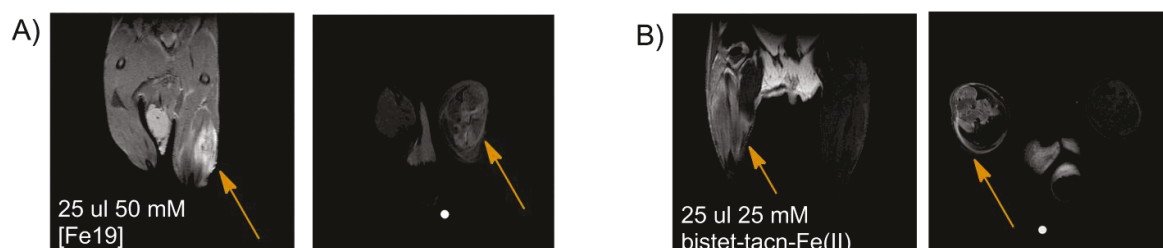


Fig. 64 MRI images of the mouse tibia obtained upon the injection of the A) model high spin bispidine compound [Fe19] in comparison to B) the results of the similar experiment done by other group members with B) electroneutral bistet-tacn iron(II) complex (7) .

Conclusions. I have successfully demonstrated that iron(II)-bispidine complexes can raise contrast in MRI, but so far not to the extent found for the tacn-derivatives. Lower than expected values of r_1 , calculated for model high spin bispidine-iron(II) complex [Fe19(SO₄)] in vitro, seem to be a consequence of the increased affinity of sulfate to the bispidine—encapsulated iron(II). Trial experiments with the analogous complexes of N5-coordination motif but in the absence of the sulfate, suggest that even $1 \text{ mM}^{-1}\text{s}^{-1}$ relaxivity is possible with this system, but the results require confirmation. Despite the limited performance in vitro, the contrast could still be obtained in vivo but with double the dose of the tacn-based probe showing the necessity of the relaxivity improvement. Again, the experiments need to be repeated in order to unambiguously associate the signal with the relaxation properties of bispidine-iron(II) chelates.

8.2. Off-ON activation in MRI

Demonstration of the capability of bispidine-iron(II) systems to raise the contrast in MRI but also to remain MRI silent in the function of the 6th coordinating arm, was a necessary prerequisite which allowed me to explore the true responsiveness of the system and thus delivered an essential proof of the concept of MRI activation of this type of complexes. As it has been described in the introduction (chapter 3) the development of responsive arms is being pursued simultaneously by other members of the group. Thus, the functionalization of the ready bispidine moiety and subsequent construction of the responsive probe was largely dependent on the success of my co-workers. In the consequence the first and so far the only off-ON switchable probe based on bispidines and studied in the MRI are pH-responsive amidine-containing complexes. These are the direct precursors of the enzyme-sensitive probe candidates, which are the analogs of tacn-based complexes reported by the group only in spring 2012. Further strategies are being developed and my high-performance synthetic protocols as well as the accumulated knowledge on the steric and electronic requirements should now allow for their swift adaptation to the bispidine-iron(II) molecular platform.

8.2.1. Synthesis of amidine-bearing bispidine-iron(II) complexes

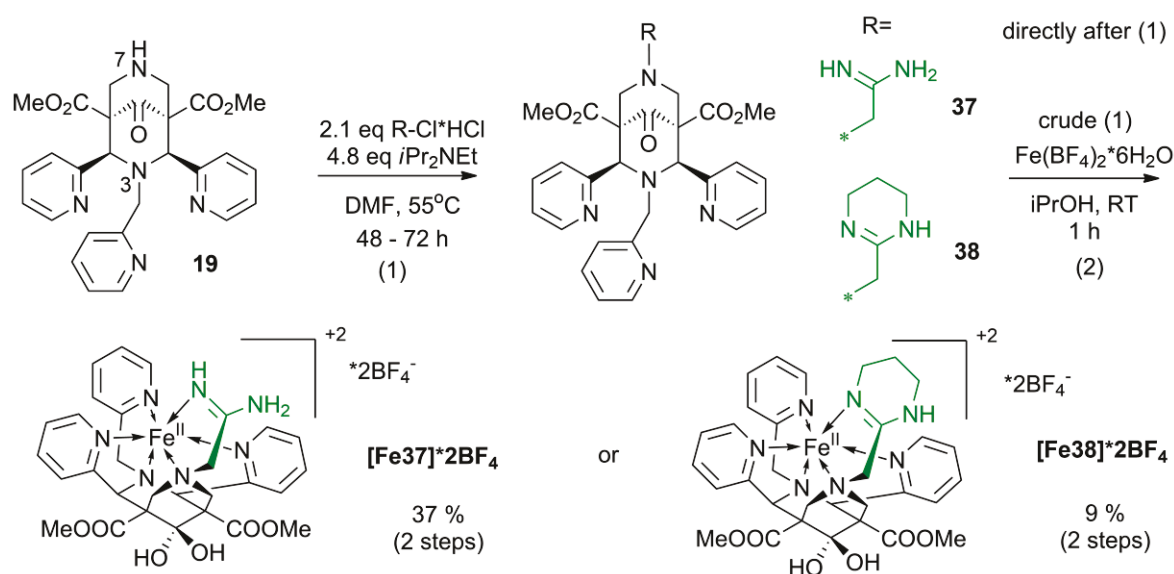


Fig. 65 Synthesis of amidine-containing pH-sensitive bispidine-iron(II) complexes.

Convergent synthetic protocol. Bispidine pentadentate platform **19** (see chapter 5 for its characterization) was functionalized with the simplest open chain and cyclic amidine moieties (Fig. 65), introduced to the reaction in a form of amidine-chloride hydrochloride, as provided by my co-PhD student Faycal Touti who has developed their synthesis. Classic nucleophilic substitution on the N7-H position, as described for a preparation of pyridazine (**34**) and oxadiazole-bearing (**35**)

ligands, was performed in dimethylformamide (DMF) with initially 1.05 eq of the alkylating arm and 2.5 equivalent of the Hunig base. The reaction progress was monitored by the direct injection mass spectrometry (DIMS) and in the presence of the unreacted bispidine platform signal after 24 h, 1.05 eq of hydrochloric salt of respective amidine chloride and 2.3 eq of the Hunig base was added. Full conversion of the bispidine platform **19** was observed after 48 h and 72 h for cyclic and acyclic amidine-bearing ligands (respectively, **38** and **37** in Fig. 65). Their isolation was not attempted due to the previous experience with tacn-analogs, which showed that the highly basic amidine groups instantly capture traces of CO₂ and thus their handling was difficult. In the consequence crude reaction mixtures were placed in degassed *i*propanol (*i*PrOH) and 1.1 eq of Fe(BF₄)₂*6H₂O in *i*PrOH was added drop-wise in inert atmosphere at RT. This led to an instantaneous formation of the light yellowish-greenish precipitates in both cases. DIMS showed a disappearance of the ligand signal already after 5 min post-addition, but the reaction was kept stirring for 1 h after which the precipitate was filtered off. Light color of the solids in combination with a nearly pure DIMS spectra of the desired complexes (*m/z* = 130 signal was attributed to the Hunig base) suggested that a high spin chelate has been formed in the reaction. This could indeed be a kinetically favored product as high pK_a of amidine moieties enable them to effectively compete with the Hunig base for protons coming from the previous step of bispidine alkylation. In the consequence, a very fast reaction and direct precipitation of the complex did not allow for shifting the protonation-metal binding equilibria to the probably more thermodynamically stable iron(II)-amidine bound complex.

Workup of highly basic units. The isolated precipitate was thus re-dissolved in degassed methanol and a 3-fold excess of Hunig base was added. In time solution was darkening (red and deep-red color) indicating a spin switch to the low spin state, which happens upon the deprotonation of amidines and its subsequent metal coordination. After 1 h reaction was stopped, volatiles were evaporated, product re-dissolved in MeOH and solid was precipitated upon the addition of the *i*PrOH. Somewhat light color (but slightly darker in comparison to the first precipitate) suggested, as previously, that the high spin form was dominant in the precipitate. Despite the fact it made the workup more difficult it also boded well for the future pH responsiveness, as it suggested their high tendency to remain in the protonated form, which came out to be insufficient for the tacn-based probes (see chapter 3 for more details on the concept and also discussion below). In the consequence of its inertness to deprotonation, the procedure was repeated several times until deep red crystalline type material could be isolated respectively in 9 % and 37 % 2-step yield for cyclic [Fe**38**]*2BF₄ and acyclic [Fe**37**]*2BF₄ amidines (Fig. 65) (the counter ion was not identified and while in the first approximation BF₄⁻ was assumed, chloride precipitation cannot be excluded). Interestingly, the yield stays in agreement with an increased basicity of the cyclized amidine in comparison to the open chain analog (approximately 1 unit of pK_a difference) and thus a greater inertness of the former to the base reaction. Significant quantities of the possibly high spin forms were isolated (amounting to combined yield of 60 - 70 %) but their analysis was not performed except the mass spectrometry confirming the presence of

the pure desired complexes. In addition, the presence of the products in all filtrates was also spotted suggesting that in the future, if more thorough workup is performed (or stronger bases like DBU are used) the effective yield of a low spin form can be much higher to almost quantitative. The attempts of the crystallization of these products were not successful and so for the preliminary experiments, their powders were used, after the extensive washing with EtOH (solubilizes both complex forms as well as the ligand and the salt of Hunig base). Except DIMS, [Fe37] was also characterized by the ^1H NMR, which showed that all the proton signals remained in the diamagnetic range (0 – 10 ppm) confirming its low spin state. On the other hand only mass spectroscopy signals and the T_1 measurements were obtained for [Fe38]. Thus, in order to unambiguously conclude on the preliminary results of pH titrations, performed with these compounds and discussed below, further characterizations need to be provided and in the best of cases the same experiments should be repeated on the crystalline material. Unfortunately these experiments had to be postponed as the laboratorial work time of my PhD finished with the end of 2012, and now await my successor.

Conclusion: *Direct synthetic access to the functionalized bispidines was achieved from a versatile pentadentate synthetic intermediate 19, developed in this work. Its compatibility with a synthetic protocol for amidine's preparation was confirmed. The desired amidine complexes [Fe37] and [Fe38] were successfully obtained, but at sub-optimal yields. Simple improvement in the workup protocol should boost the efficiency to near-to-theoretical values. Crystallization of these chelates remains to be performed and a full characterization enabling a reliable conclusion on the quality of the samples is required, in particular for the [Fe38].*

8.2.2. First off-on responsive bispidine probe

Reminder on amidine strategy. The whole concept of the responsive probes using this activation strategy was based on a high basicity of the free amidines (pKa of 12 and 13 for acyclic and cyclic form respectively) and approximately 5-order of magnitudes lower pKa's of their carbamylated analogs. In the latter case a coordination to the metal should not be challenged by external factors and thus the diamagnetic state of iron(II) with closed coordination sphere could be envisaged. The situation should change upon the removal of the carbamyl linker, caused, for example, upon chemically (or biochemically) induced auto-immolation cascade and subsequent CO_2 departure (see chapter 3 for the discussion of the concept). In the result, the unmasked basicity of amidines was hoped to lead to the favored protonation of the moiety at neutral pH and subsequent decoordination, opening the first coordination sphere for water. Then the N6-N5O1 change of the coordination motif would stabilize the high spin iron(II) and enhance the relaxivity of water protons. However, for previously reported probes which demonstrated the concept, decoordination of cyclic amidine required a pH of 3 - 4 thus in the neutral pH no magnetogenesis, in spite of the successful departure of the carbamyl moiety, could be observed.

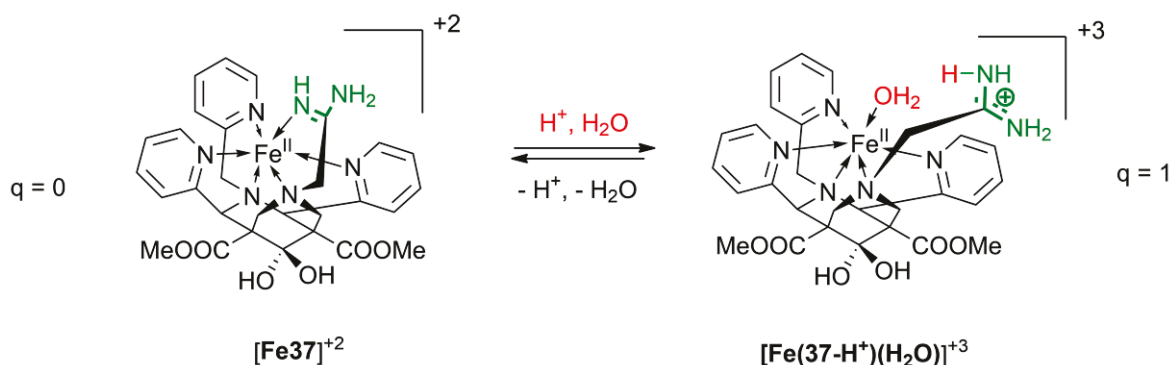


Fig. 66 Scheme of decooordination of the acyclic amidine arm of the bispidine-based ligand **37** upon protonation..

Changes in the relaxivity of [Fe37] upon pH activation. The process of decooordination of amidine arm upon protonation in bispidine system is presented schematically in Fig. 66. The pKa of transition of the bispidine-based complex with acyclic amidine [Fe37] into the complex [Fe(37-H⁺)(H₂O)]⁺³, with an open coordination sphere, was around 4.4 pH (Fig. 67, in black), which is comparable to the one observed for the cyclic amidine on tacn-system.

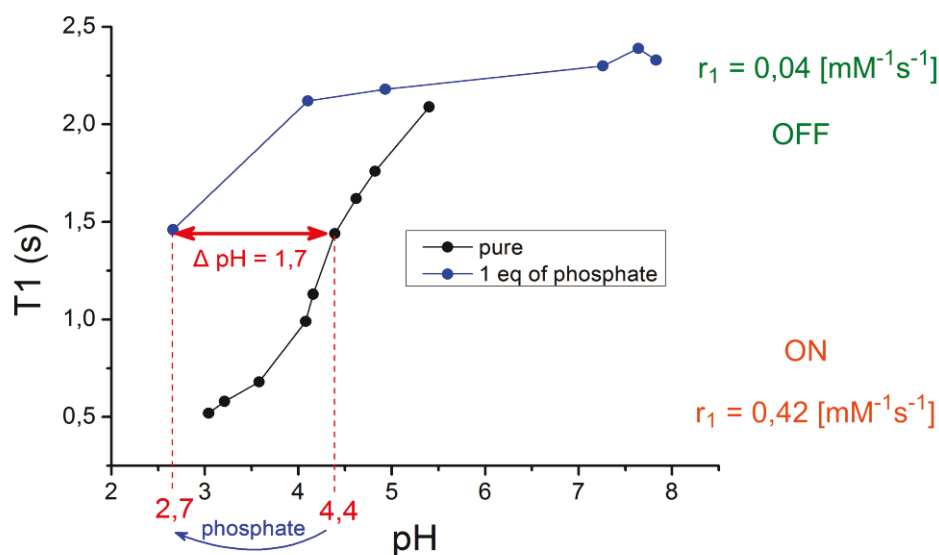


Fig. 67 Titration experiment with bispidine-iron(II) based complex [Fe37] bearing an acyclic amidine moiety (4 mM concentration, 11.7 T, 25 °C). Black points represent the experimental data acquired upon the titration in pure solvent. Blue points correspond to the similar experiment but performed in the presence of 1 eq (4 mM) of phosphate. Lines connecting the point are there for guidance only. Red arrow demonstrates the shift of the pH of decooordination observed upon the addition of the phosphate anion which indicates a phosphate-driven stabilization of the non-protonated form.

To study the pH-induced MRI-activation of the complex [Fe37] the T_1 measurements were performed at room temperature and at 11.7 T for 4 mM solution of the compound (Fig. 66). The pH of the solution was carefully adjusted by stock solutions of hydrochloric acid and sodium hydroxide, followed by the intense mixing. The initial pH after dissolution of the compound [Fe37]

was 5.4 and a respective T_1 was equal to 2.09 s. This is in agreement with the results obtained for the tacn-based probe, and corresponds to the residual relaxivity of $r_1 = 0.04 \text{ mM}^{-1}\text{s}^{-1}$ confirming a largely closed first coordination sphere of this compound. The origin of this tiny deviation from the value found for pure water (3.7 s), despite the diamagnetic type of NMR spectrum of this complex, may suggest minor impurities of free iron. Alternatively, the residual temperature-independent paramagnetism and the second-sphere contribution should also be considered. The latter seems to particularly possible, as this coordinated acyclic amidine moiety, even if largely deprived of its electrons, still possesses hydrogen atoms which increase the residence time of water molecules in the proximity of the metal. Subsequent addition of the acid leads to the reduction of the T_1 and at pH 3 it reaches the value of 0.51 s, indicating a decoordination of the amidine arm as a consequence of its protonation, and a change of $q = 0$ to $q = 1$ (change from $[\text{Fe37}]^{+2}$ to complex $[\text{Fe}(\text{37-H}^+)(\text{H}_2\text{O})]^{+3}$ in Fig. 66). The calculated relaxivity of $0.42 \text{ mM}^{-1}\text{s}^{-1}$ is ten times the one observed for this compound before the addition of acid, and is similar to the one observed before for tacn system as well as the one reported with a new strategy of the group (see chapter 3 for details). In the reference to the bispidine complexes described above, this r_1 is almost a double of the one found for a model high spin $[\text{Fe19}(\text{SO}_4)]$ ($0.2 \text{ mM}^{-1}\text{s}^{-1}$). Possible explanation of this difference is the increased proton exchange rate at lower pH and thus the more effective transmission of the paramagnetic effect to the bulk solvent. Similar mechanism was described for Gd(III) chelates (chapter 1.3 [66]). Nevertheless, the restricted water access to the first coordination sphere and thus decreased effective q hydration number of $[\text{Fe19}(\text{SO}_4)]$, cannot be excluded, as discussed above.

Unprecedented magnitude of r_1 improvement. A 900 % improvement in relaxivity upon the chemical stimulus is by far the highest of all reported examples (see chapter 1.3). [38] It suffices to say that the second and third largest effects lead to 300 % [55] and 360 % [60] change also upon the increase of the hydration number of Gd(III) complexes but the increase of q value was from 0 to 2 and was induced by pH or Cu(I) presence respectively. Obviously, the net relaxivity after activation of our probes cannot be compared to the one found for Gd(III) chelates ($0.42 \text{ mM}^{-1}\text{s}^{-1}$ vs. $8.0 \text{ mM}^{-1}\text{s}^{-1}$ [55] for example) but in the light of the specific requirements of molecular imaging discussed in chapter 1.3, the truly silent initial probe ($r_1 = 0.04 \text{ mM}^{-1}\text{s}^{-1}$ vs. at least $r_1 = 2 \text{ mM}^{-1}\text{s}^{-1}$ for Gd(II) probes) as well as its lower potential toxicity, especially in comparison to the kinetically labile $q = 2$ Gd(III) chelates, are improvements that deserve close attention and further development.

Conclusions: Increase in the r_1 relaxivity upon the pH-induced decoordination of the amidine arm extrapolates the results achieved with the tacn-based analog published recently. Despite the initial problems with achieving satisfactory relaxivities with bispidine chelates, this experiment proves that they are very similar to those of tacn-based probes. $[\text{Fe37}]$ is the first bispidine-based example of a chemically activatable probe for MRI. Straightforward variation of the substituent on amidine moiety should now directly enable targeting of the variety of (bio)chemical stimuli, but still only at low pH. Nevertheless, the 10-fold improvement in relaxivity, unprecedented for any other

responsive probes for MRI, and comparable to that published by our group for tacn systems, encourages further work in shifting the operative pH to physiologically relevant ones.

8.2.3. Different parameters in the determination of the pKa of decooordination

Cyclic amidine derivative. Nevertheless, the real applications of these systems in MRI could only be envisaged if the switch would happen at near to physiological pH, as it is the case for the mentioned Gd(III) probes. In this context it is very promising that for acyclic amidine-bearing probe [Fe37], the pKa is 4.5 and equals to the one observed for the cyclic tacn-variant reported. In the consequence, it can be envisaged with a very high probability that for [Fe38] the pKa of decooordination should be moved to the values of approx. 5.5 pH which starts to approach the limit at which some of the enzymes may already be functional. Indeed, the first rough measurements confirm this hypothesis: at physiological pH the value of T_1 for [Fe38] was 1.61 ($r_l = 0.08 \text{ mM}^{-1}\text{s}^{-1}$) which might be interpreted as the initially diamagnetic probe, but with paramagnetic impurities. Intermediate spin resulting from the steric clash cannot be excluded, but the increased flexibility of the alkyl ring in comparison to aryl one should allow for the adaptation to the optimal coordination geometry. Independently on that, at 4.47 pH, so the approximate pKa of transition in [Fe37], the complex [Fe38] seems already paramagnetic and shortens the T_1 to 0.62 s ($r_l = 0.34 \text{ mM}^{-1}\text{s}^{-1}$) in comparison to T_1 of 1.5 s and $r_l = 0.1 \text{ mM}^{-1}\text{s}^{-1}$ for [Fe37] at the same pH). Thus it suggests a largely completed transition at the investigated pH, meaning that the beginning of the r_l -response can already start roughly at pH of 6 – 6.5 and its pKa should then oscillate within 5.5 in agreement with pKa-based predictions. Nevertheless, as I have mentioned above, these results are not sufficiently reliable and further as well as more detailed experiments are required. Another important observation from these rough measurements is that at pH of 2.44 the T_1 for 4 mM solution of [Fe38] is only 0.181 $\text{mM}^{-1}\text{s}^{-1}$ what corresponds to the $r_l = 1.31 \text{ mM}^{-1}\text{s}^{-1}$. This value is even higher than that observed for dptacn but at 7 T and is unprecedented for iron(II) chelates. The effect could be partially derived from the above-mentioned acceleration of the proton exchange rate (equivalent of water exchange rate) but the largest contribution a decooordination of other pendent arms upon pyridyl's protonation. In the result, the stability of the probe would be significantly challenged and thus it remains to be verified whether the complex still remains present in the sample at the discussed pH.

Decreased electron withdrawing potential of bispidine-complexed iron(II). The fact that the pKa of the amidine transition in bispidine system is higher than in tacn implicates that the electron withdrawing potential of the Fe-N-amidine bond decreases. Two main hypotheses can be forwarded to justify it. One is the effectiveness of the Fe-N bond, in other words, the extent to which amidines on bispidine and on tacn can interact with a metal center. I have shown that bispidines are sterically more demanding and thus the non-optimal coordination could be predicted, leading to the inefficient orbital overlap and thus poor displacement of the electron density to the metal center. However acyclic amidines do not possess any *alfa* substituent, instead only one

hydrogen seems to occupy the space around the coordinating atom. In the consequence, steric reasons are not entirely convincing and have to await confirmation or denial from the X-ray structure. Another reason of slightly higher electron density on amidine unit bound to the iron(II) encapsulated by bispidines might be the diminished Lewis acidity of the metal ion.

Phosphate sensitivity of the pKa of [Fe37]. An interesting observation on the phosphate effect on the pKa of transition was made with [Fe37] system (Fig. 67 – blue points). In the presence of even only 1 equivalent of proton, remarkable stabilization of the low spin, hexacoordinate state occurs, and moves the transition pH to roughly 2.7 which is 1.7 pH units lower than for pure solvent. Phosphate has already been shown to bind preferentially to guanidines via two hydrogen bonds and thus similar binding might be proposed for amidines. Then, via the same mechanism as the one described in chapter 2 for solvent-probe hydrogen bonding, the low spin state would be stabilized as the electron donation to the metal center would increase. Only at significantly lower pH, where the phosphate protonation by the bulk is increased, the subsequent destabilization of this hydrogen bonding and the revival of the amidine decoordination potential could be expected. It would be interesting in the future to attempt the crystallization of the amidines in the presence of phosphate anion and to verify whether this kind of interaction reflects reality. Phosphate stabilizing effect might be worrying in the context of the application of the probe at buffered media, but it also demonstrates to what extent different functional moieties present on the bispidine backbone can transmit the information of the presence of the analyte to the magnetogenic core. Despite the on-off character of this response, the remarkable anion sensitivity in water and the possibility of its spatio-temporal detection in structurally inhomogeneous samples (MRI) cannot be neglected.

Conclusions: Preliminary results of replacing tacn with bispidines seem to bring the pKa values of decoordination one pH unit closer to the physiological conditions. In addition, high relaxivity values ($1.3 \text{ mM}^{-1}\text{s}^{-1}$ at 11.7 T) can be found for the cyclic amidine-derivative [Fe38] in acidic media, but the purity and full chemical characterization of the compound is required before any reliable conclusions can be made. On the other hand high phosphate sensitivity of the [Fe37] complex may hamper the experiments in buffered solutions, but at the same time offers the prospect of the development of anion sensors.

8.3. Perspectives – towards the response at physiological conditions

8.3.1. Increasing a pH of protonation-based magnetogenesis

Current approach – targeting the ligand basicity. The magnetogenic strategy based on pH sensitivity came out to be sufficiently robust for the real life applications led to a significant relaxometric response upon target interaction. However the biggest challenge is to impose a spontaneous decoordination of the pH-sensitive arm already after its activation. For the tacn-based probe, the pKa of transition was found to be at 4.5 for cyclic amidines. Bispidine-iron(II) system seems to offer the possibility of switching already at 5 – 5.5 pH but it still remains insufficient. In order to observe a significant raise in contrast at neutral pH, the pKa of decoordination should be at least one pH unit above 7.4. Current strategies explored in the group aim at the application of even more basic moieties, like guanidines which are expected to move the pKa of decoordination one unit up. To get even greater effect, change of the chelate ring size from 5 to 6 was also envisaged in order to destabilize the coordinative bond by the increased flexibility of the arm. However, for the tacn-system the additional degree of freedom coming from the extra methylene unit in the linker between amidine and the macrocycle does not bode well for reliable metal coordination and the attainment of the low spin state.

Bispidines as attractive alternative. In the context of the above-mentioned difficulties encountered with a tacn system, bispidine-based system may turn out to be a viable alternative.. As discussed earlier on in this chapter, switching between the coordination platforms moves the pKa of decoordination by approximately one unit up. Additionally, for bispidine system, 6-membered chelate rings were already reported for the ligand with two ethypyridyl substituents on the aliphatic nitrogen atoms, but not yet in the context of an iron(II) complex. Nevertheless, combining all the effects with moving to guanidines may already deliver a system deCOORDINATING spontaneously at above 6.5 - 7 pH, depending on the significance of the chelate ring size. This value may already allow for the exploration of magnetogenesis at physiologically relevant conditions, however the binary nature of the response would have to be probably compromised. In any case, the advantages of the bispidine over the tacn system are apparent in this context making the former an attractive choice for the validation of the concept.

Crucial role of Lewis acidity of iron(II). Tuning the ligand, principally by raising its basicity and instability, remains synthetically challenging and poses a significant threat to the attainment of an initially fully silenced chelate. In the result of that, I suggest to move the focus of the future design from the responsive arm to the metal ion. Coordination of the amidines to iron(II) leads to the decrease of their pKa by approximately 7 - 8 units! This mean that the acid-base complex formed between them is highly stable and favorable. Instead of modifying the electron donor potential of the Lewis base, changing the Lewis acidity will equally influence the stability of the adduct. Thus

any attempt to make iron(II) less acidic is a viable solution for the problem of a low pKa of decoordination. Many such modifications can be envisaged, but among them those aiming at decreasing the charge on the metal ion offer the most significant changes. The use of tetrazole coordinating groups which are deprotonated at neutral pH (pKa of approx. 4.5) would significantly increase a sigma donation from the unit compensating largely the positive charge on the metal ion. In the consequence, the electroneutral bistet-tacn complex seem to be much better suited for the pH-based responsive concept than initially proposed dptacn analog.

Charge compensation by tetrazoles. Bispidines decorated with the tetrazole coordinating motifs may also be envisaged. The biggest disadvantage of the replacement of pyridyl with tetrazolyl functionality is a weaker ligand field, which may lead to the intermediate magnetic properties, as reported for the iron(II)-bistet-tacn. However, provided the closed coordination sphere, this residual paramagnetism may have a negligible effect on the relaxivity of water protons, as it was in the case of the SCO complex [Fe15] which remained MRI silent despite the magnetic moment of 1.47 μ_B . Diminished Lewis acidity should destabilize not only the iron-amidine bonds leading to higher pKa of decoordination, but also weaken iron(II)-anion interactions which were responsible for diminished relaxivity of the high spin [Fe19(SO₄)] and reduce a water residence time in the first coordination sphere. In addition, charge compensation makes the catalysis of Fenton type reactions less efficient which together with a reduced osmolarity improves the biocompatibility of the electroneutral iron(II) complexes. In the light of all the above-mentioned improvements envisaged for the tetrazolyl substituted bispidine-iron(II) complex **39** (Fig. 68), there is an undeniable interest in verification of its true performance. Synthetically, an access to the monotetrazolyl analog with this moiety grafted on one of the aliphatic amines of bispidine backbone should not pose any particular problems, provided combination of my synthetic protocols and a methodology of the preparation of the tetrazole-methylchloride synthon, developed earlier in the group.^[249] On the other hand, replacing the 2,4 substituted pyridyl moieties might be more challenging as it requires an aldehyde precursor to be introduced in the first Mannich condensation step. Thus for the first trials, monotetrazole-bearing bispidine ligands should be prepared and tested. Only one tetrazole unit present on the bispidines may in fact be an optimal solution as it may offer a required balance of the reduced Lewis acidity and still strong enough ligand field, which cannot be achieved with a tacn system due to the lack of the synthetic protocol for the efficient desymetrization of the tacn-alkylation pattern.

Charge compensation by carboxylic acids on aromatic substituents. Other strategies aiming at decreasing the effective charge of the complex, leading to the overall better performance and the spontaneous decoordination of activated amidines/guanidines at physiological pH may also be envisaged for bispidines. One straightforward idea, which is already being developed in the group for the tacn system and can be easily transformed to bispidines, is to decorate the pyridine substituent with a carboxylic acid moiety which at physiological pH will become deprotonated. This will then be communicated to the metal center *via* the aromatic pi-conjugation. The effect should then be similar to the one observed for tetrazole-analogs. In bispidine system one, two or

three carboxylates can be introduced leading to a spectrum of differently charged analogous complexes, and in particular also a first anionic iron(II) complex which has never been proposed in the group (40-42 in Fig. 68). This is not possible for the tacn-based systems where only two heteroaromatic rings can be varied and in addition, from synthetic reasons, both generally have to be the same. Whether this substitution will enable a low spin state of iron (II) remains to be verified experimentally.

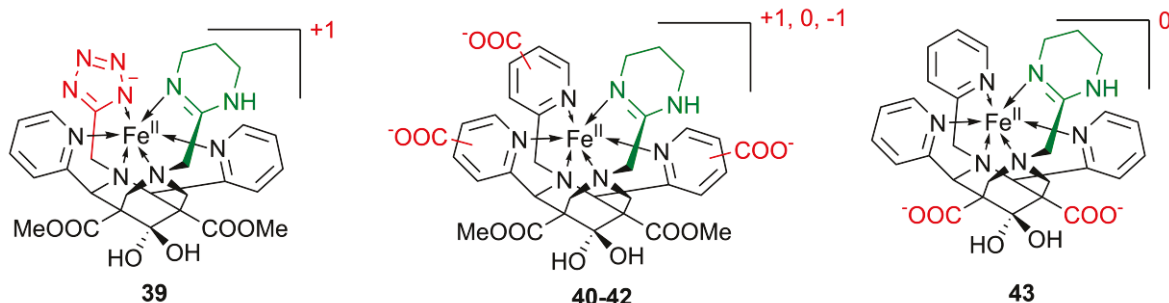


Fig. 68 Proposed selected designs of the bispidine-iron(II) complexes with partially or totally compensated positive charge of iron(II). Please note that the variation in the responsive arm can be achieved independently on the pentadentate platform.

Charge compensation by carboxylic acids on periphery of the ligand. The unique opportunity delivered by the bispidine system in comparison to tacn and most of other polydentate ligands, is to change the charge of the complex, without interfering into the electronic system of the coordination sphere. It is possible by the hydrolysis of the methyl esters on the polar periphery of the bispidinone ligands, which would then upon deprotonation, interact with a metal center purely electrostatically (43 in Fig. 68). The influence is thus the most subtle in the sense that reduced anion and water affinity as well as facilitated establishment of the additional positive charge on the complex upon arm protonation, are achieved without an interference in the spin state of the metal. Thus, while promising similar improvement in relaxivity and smaller but hopefully still sufficient increase of the pKa of decoordination, it is the robustness of the initial diamagnetic state of this probe candidate which may distinct it from the others.

Summary: Replacing the tacn-system by the bispidine platform as the main building block of the pH-operating magnetogenic probes increases the chances of moving the response to the physiological pH. Alternatively to, or in combination with already pursued strategy of the responsive arm's modification, I propose to focus principally on targeting the Lewis acidity of the metal ion, particularly by charge compensation. By this, not only the pKa of decoordination, but also the relaxivity and, as reported previously, also a biocompatibility of the future probes can be increased. Two strategies envisaged already for the tacn system include the use of electronegative tetrazole coordinative arms and the introduction of the carboxylic acid functionalities on the pyridine donors. In addition to those, bispidines may benefit also from the introduction of a negative charge on the electronically isolated periphery upon ester hydrolysis. While being more

subtle, this strategy ensures a preservation of the diamagnetic initial state and a priori does not require an elaboration of new synthetic routes, which are the biggest challenges for the two other approaches.

8.3.2. Alternative responsive arms for bispidine-iron(II) system.

Magnetogenesis upon tautomerization-driven cleavage of the coordinative bond. Alternative strategy for an N6-N5O1 switch involves the use of oxazolone or oxazolidinone-based responsive arms (Fig. 69 – an arm is depicted in green). The concept is similar to the amidine one, but it takes the advantage of the difference in the stability of the two tautomeric forms of the cyclic carbamate. In particular, a much more stable keto functionality is initially masked in the enol-like form upon the alkylation on oxygen (blue circle in Fig. 69), in which the imine-type nitrogen can bind to the metal center hopefully with a strong enough ligand field to render it low spin (**44**). Subsequent activation by the target, leading to the liberation of the oxygen should shift the tautomeric equilibrium from coordinated carbimidole to carbamide, depriving the nitrogen of its sp^2 character and imposing a decooordination upon protonation (**45**).

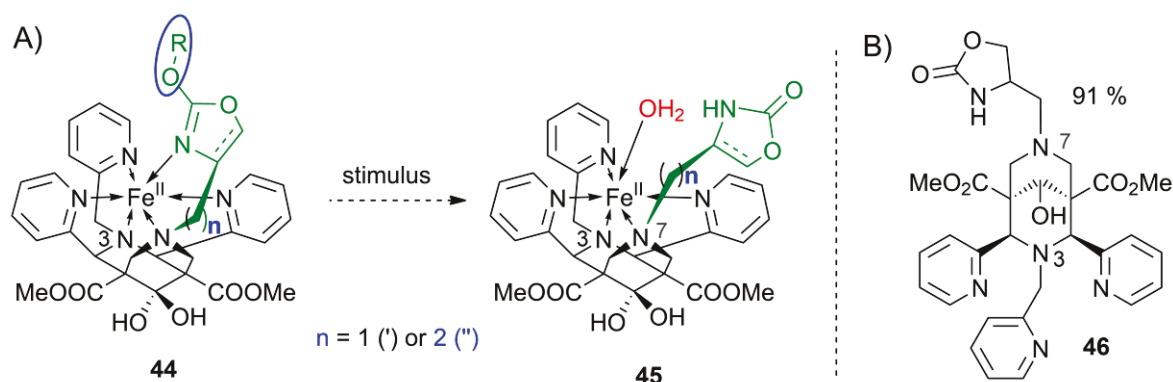


Fig. 69 A) Oxazolone (oxazolidinone) N6-N5O1 activation concept with bispidine-iron(II) system. In blue a substituent in ortho-position which is expected to cause a steric clash, but which is proposed to be alleviated upon the increase of the chelate ring from 5-membered ($n = 1$) to 6-membered one ($n = 2$ – in blue). B) a model oxazolidinone-bearing bispidine-based ligand prepared in this work.

Preparation of the suitable synthons for grafting this moiety on the pentadentate N5-coordination motif is now largely completed by the group and awaits the alkylation to give off the suitable ligands. However at the time of my experimental work, no functional arm of this type was yet available and so I have verified the efficiency of the functionalization of the bispidine N7-H platform with this type of units by performing a model alkylation experiment with chloromethyloxazolidinone, provided by co-PhD student Oliver Thorn-Seshold. The experiment led to the formation of the desired product **46** in the 91 % yield (Fig. 69 B), as confirmed by the NMR. Noteworthy, the bispidine precursor used for this purpose was a classic N7-H platform but with a reduced keto-functionality (for details of this reduction see the following chapter). These results bode well for a preparation of the oxazolone/oxazolidinone-functionalized bispidines and

again confirm the utility of the synthetic protocols developed in the course of this work. The main challenge in applying this strategy lies again in the steric clash imposed by the bulky O-R moiety in position *ortho* to the coordinating nitrogen (in blue circle), which will, with the highest probability, prevent the arm from coordination. In order to address this problem, Prof. Hasserodt proposed to use the ethylene linker between the N7 and oxazolone/oxazolidinone ring, similarly to the one suggested for the amidine strategy. Here however, the main objective is not to weaken the coordinative bond but to enable a coordination thanks to the change in the approach geometry from facial to more bent and in the same time avoiding the steric clash with an *ortho*-hydrogen of the opposing coordinated pyridine ring from substituent on N3. Exchanging the N3-substituent from pyridine to the pyridazine or oxadiazole with no *ortho*-substituent may help in adapting the optimal coordination geometry.

Bispidine-based ligand for a formation of a 6-member chelate ring. As discussed above, both, amidine and oxazolone/oxazolidinone-based strategies can potentially benefit from the increased size of the chelate ring of the responsive arm. For the latter it is even an indispensable condition in order to avoid a steric clash. While 7-membered chelate rings could be considered, they would with the highest probability be unstable. On the other hand, 6-membered rings are thermodynamically more favorable, and thus could be envisaged (for example compound 44'' with $n = 2$ in Fig. 69 A). However, the increased flexibility of the moiety, which for the bispidine and tacn systems is a result of a three single bonds not involved in any rigidifying motif, may result in disfavoring a coordination. The main question thus remains of whether this modification may indeed a) decrease the steric clash and in the same time b) ensure the stability of the initial probes and their diamagnetic state. A formation of the six-member chelate rings involving N7 and N3 substituents with N-donors in bispidine complexes has been reported for pentacoordinate ligands.^[250] For a potentially hexadentate N3,N7-bis-ethylpyridine bispidine (**47** in Fig. 70), the effective binding and a formation of two 6-member chelate rings with N3 and N7 substituents was observed with Co(II) where the M-N bond lengths were all above 2.1 Å. However, in Cu(II) complex in which the average M-N distance was 2.0 Å similarly to the one expected for the LS iron(II), only one of the ethylpyridyl groups remained coordinated.^[216] No studies with iron(II) were performed neither the ligand field strength of this coordinating motif was determined, but the reported data may suggest that two EtPy motifs should not both coordinate in the same time on low spin iron(II). Thus, in order to study the effect, I have prepared a new potentially hexadentate ligand with only one ethylpyridyl in place of picolyl on the nitrogen N7 to mimic the proposed functional probes described above. The synthesis involved the standard Mannich protocol, beginning from the intermediate **29s** and using pyridinethylamine as a 6-member chelate ring precursor (Fig. 70). Unfortunately, even after 5 - 6 h of reflux in THF (tetrahydrofurane), *anti* isomer was by far dominant (**47a**) and was isolated in the yield of 60 % on several gram-scale by flash column chromatography or crystallization from the *i*PrOH/EtOH. Multiple repetition of the crystallization step led finally to the selective separation of the desired *syn* isomer **47s** but only in trace quantities (60 mg, 2 % - Fig. 70). The identity of both compounds was confirmed by a full 1D and 2D NMR

(homo and heteronuclear) characterization. In the future prolonged reaction time and MeOH/Et₂O crystallization mixture solvent could possibly yield higher quantities of the desired isomer. Trial complexation reaction performed on the 50 mg scale led to the formation of the adduct **Fe47** by MS (DIMS m/z: 331 (100) [M]⁺², 707 (88) [M+HCOO]⁺), but no pure product could be successfully isolated. Scaling up is probably the most appropriate improvement which should be attempted with no delay and hopefully lead to the isolation of the complex, to verify the relevance of the increased chelate ring strategies in iron(II)-bispidine system.

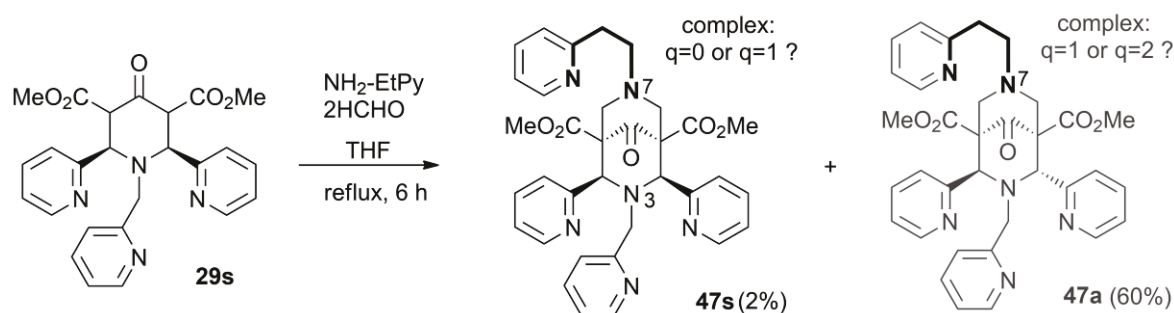


Fig. 70 Preparation of the bispidine-based ligand with a potential to form a six-member chelate ring (in bold) when complexed with iron(II).

Even if the desired formation of the six-membered chelate ring would not take place with a simple ethylene linker, additional precautions can be taken to reinforce the coordination. This includes principally a preorganization of the pendent arm for chelate formation, for example by adding two methyl substituents on the linker or by including it into the aliphatic ring. It remains to be verified if the increased bulkiness of the linker, even if finally leading to the desired removal of the facial steric clash between the coordinating motifs from N3 and N7 substituents, would not in turn create a detrimental steric congestion in the other parts of the molecule.

Magnetogenesis upon breaking of coordinating and covalent bond. Another activation concept, which was the only one developed in the group when I arrived, is based on the complete departure of the coordinating arm upon the unmasking of the unstable moiety, as discussed in details in chapter 3. However, only in spring 2013^[248], after the end of my experimental work, the proof of concept has been delivered by the group and thus I was not able to use it for a construction of bispidine-based magnetogenic probes. In translating the results to the bispidine system, it remains to be verified whether the coordinating unit would pose a steric clash on the facing pyridine and thus lead to a deflection. Five-member aromatic ring of triazole may come out to be sufficiently small to not suffer from this strain, but even if it does, a N3-methylpyridazine unit in place of the picolyl arm on the bispidine backbone should undoubtedly remove the problem. Provided the inexistence of the steric clash, the ligand field imposed by the responsive hetero-aromatic arm should be sufficiently strong, as suggested by the diamagnetic state of compound [**Fe35**] with oxadiazole coordinating motif. Nevertheless the subtle balance between the stability of the intermediate before and after chemical stimulus may be somewhat shifted in the bispidines in comparison to the tacn and thus requires the experimental verification.

8.4. Fine tuning of the physico-chemical properties of bispidines by periphery modification

Great advantage of bispidine system lies in a possibility of the fine tuning of their properties by the periphery modification. One of the examples discussed above would be to hydrolyze the esters and thus introduce an extra negative charge to the complex which would compensate the positive charge of iron(II). However, other variations can be envisaged and may have a beneficial effect on the properties of the future probe candidates.

8.4.1. Altering the C9-keto functionality

Motivation. The main focus of my research in this field was an attempt to alter the keto-functionality of the bispidinones. (1) It has been suggested, that the presence of this moiety may enable a retro-Mannich reaction and thus ligand's decomposition, but it has never been reported for the complex. The advantage of "locking" the molecule by altering the ketone is however more than just a stability of the ligand thanks to the impaired retro-Mannich reaction (**bisp-OH** in Fig. 71). (2) It also decreases the affinity of the molecules to the intramolecular nucleophiles (aminoacid residues of proteins etc). Such a side reactions would not only hamper the biodistribution profile of the probe, but it could also lead to a certain immunogenicity and increase toxicity, as altered proteins would then become recognized as invalid by the immune system. (3) Finally, an alcohol group in the place of ketone could function as molecular anchor and enable a decoration of the future probes with variable units without altering their magnetic properties thanks to the electronic isolation of the periphery. Possible functionalization of C9-OH include an addition of cell penetrating peptide (CPP – poly-arginine chains – **bisp-CPP** in Fig. 71) to enable cell internalization, or a tag sequence for a specific delivery. However many other conjugations could be envisaged including a construction of the dendrimers (**bisp-dendrim** in Fig. 71) for improved response and higher local concentration of the probe, or controlled peptide conjugation. *Summarizing, altering of the ketone moiety on C9 could open up new opportunities for the improved biodistribution, but also should boost the probe's stability and biocompatibility.*

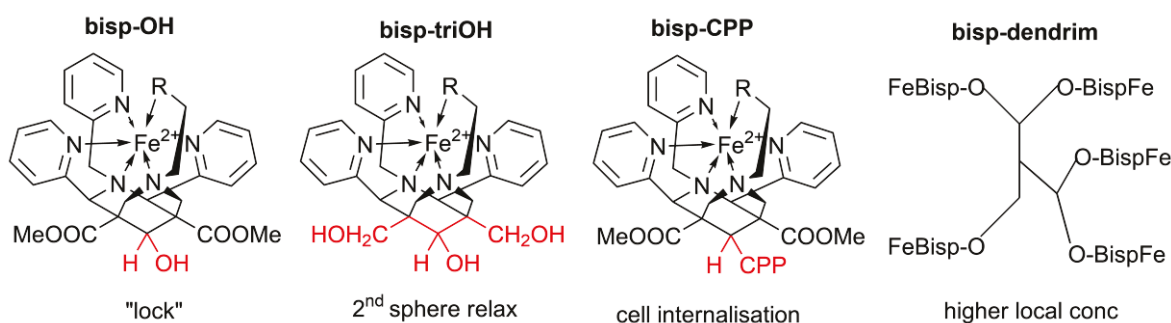


Fig. 71 Examples of possible modifications of the bispidine-periphery and their potential applications.

Failure of the classic protocol for a bispidinol preparation. Reduction of the ketone functionality on bispidines has been reported on several occasions upon the use of sodium borohydride at 0 °C.^{[207] [251]} While in MeOH, two stereoisomers could be formed, only one was observed by previous authors if a reaction was performed in dioxane/water and when the pH of the solution remained slightly basic (within 8-9). Unfortunately, my attempts to repeat the protocol for the DMB protected bispidine were not satisfactory. Neither were they successful for the deprotected version with N7-H bearing moiety. In both cases, even if the reduction was indeed achieved, as shown by DIMS and also the NMR analysis, complex mixtures of products with partial and total hydrolysis of the side ester groups, and possibly even decarboxylation products, were formed each time, despite the variation of temperature, solvent (THF/water, dioxane/water, methanol) quantities of the reducing agent and times of reaction. These mixtures were in addition almost impossible to separate by crystallization or column chromatography even if neutral or basic alumina was used as a separation phase. The former is obviously strongly dependent on the substituents and the irrelevance of the published crystallization protocols to my newly prepared ligands is not unexpected. For flash column chromatography, which surprisingly has never been reported for the bispidine ligands, in the best of cases only a trace quantities of the pure compound could be isolated and this required several subsequent flush column chromatography purification experiments or a preparative TLC (thin layer chromatography) on neutral alumina which has low practical application if larger quantities are to be prepared (only approx. 10 mg by double preparative TLC was obtained).

<i>Reagent</i>	<i>Desired product</i>	<i>Obtained product</i>	<i>Isolated yield of desired product</i>
NaBH ₄	2° alcohol	Mixture	traces
NaB(AcO) ₃ H	2° alcohol	starting material	0
L-Selectride	2° alcohol	starting material	0
NaBH₃CN	2° alcohol	2° alcohol, two isomers	15%
BH₃*THF	2° alcohol	2° alcohol, one main isomer	63%
Grignard reaction	3° alcohol	starting material	0
Wittig Reaction	olefin	undetermined mixture	0
Thiol + BF ₃	thioether	N7-H	0
Hydrazone + NaBH ₃ CN	alkane	2° alcohol	0

Table 11 Summary of pursued synthetic attempts to modify C9-keto functionality in DMB-bispidine ligand **31**.

In the result of the initial failures, I have looked also at other strategies to reduce the ketone functionality on the DMB-bearing intermediate **31**. Firstly, other hydrides but with a lower reducing potential were investigated (Table 11). The reaction with L-selectride at -78 °C in THF did not progress and the starting material remained a main component of the reaction mixture with traces of hydrolyzed product. Sodium triacetoxyborohydride reduction in water/THF mixture at 0 to RT even after 48 hours did not show any reduction product forming (by DIMS). On the other

hand, with sodium cyanoborohydride (NaBH_3CN) in THF/water mixture at $0 - 4^\circ\text{C}$ the reaction occurred but was not complete even after 48 h. It is important to point out that in water solutions, a formation of the hydrate on the ketone moiety could be observed in each case in DIMS experiments, suggesting a significant stability of the hydrate what could hamper the efficiency of the reduction reaction due to the decreased electrophilicity of the C6-carbon bearing two hydroxyl groups. Other strategies for the alteration of the ketone functionality were also envisaged but were not successful (Table 11). In particular, Wittig reaction performed with a methyl-triphenylphosphine reagent generated in situ according to the reported procedure led to the formation of the complex mixtures with no traces of the desired alkyl product. Alkylation with a EtMgBr Grignard reagent did not lead to substrate conversion, even upon heating to RT. Formation of the thioketals in the presence of $\text{BF}_3 \cdot \text{Et}_2\text{O}$ surprisingly led to the deprotection of the DMB group (see chapter 5).

Successful reduction of the C9-funtionality. Interestingly, an attempt to exhaustively reduce ketone moiety via the formation of tosylhydrazones and subsequent reduction with sodium cyanoborohydride NaBH_3CN at reflux in methanolic solution led to the alcohol product **48** in two isomeric forms, with only traces of impurities. This reaction, performed by Hanno Kossen, who was an M1 intern from UCL (London), enabled a selective isolation of only one stereoisomer upon flash column chromatography at 15 % yield (Fig. 73, A). NOESY experiments showed coupling between the C9-H and the axial H-6/8 protons and subsequent interaction between OH proton with the H-2/4, proving the *syn* configuration on the C9 (with OH pointing towards the ring with pyridine substituents) (Fig. 72).

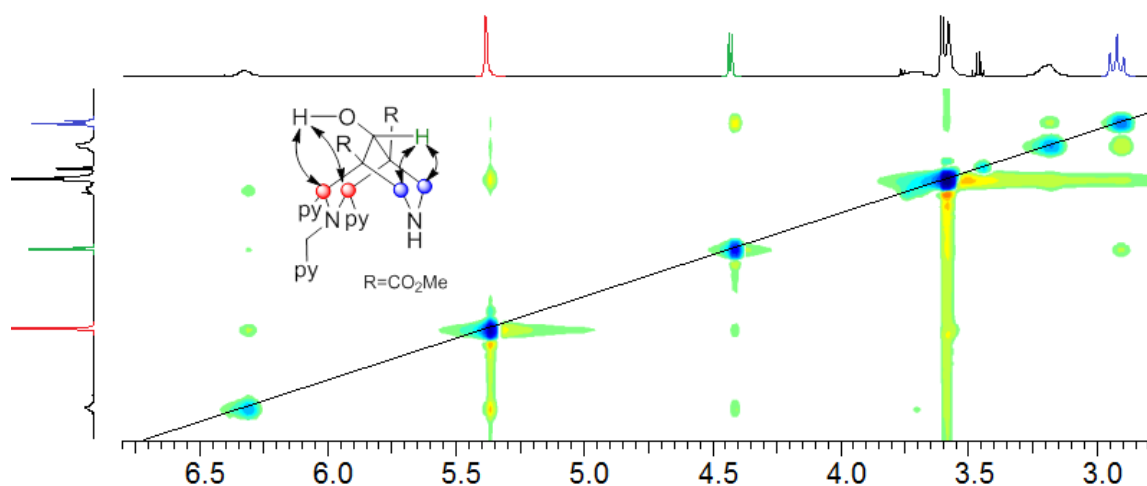


Fig. 72 NOESY experiment of the OH-*syn* DMB-bispidinol – OH group pointing towards the piperidinone ring with 2/4-pyridyl substitution pattern. Color code demonstrates the respective signals: red are the H-2/4, blue are the H-6/8ax and green is the C9-H signal respectively (taken from the laboratorial report of Hanno Kossen).

While another isomer also formed in the reaction, it was not successfully separated. Thus, this method (A – Fig. 73), despite the relatively low yields, enabled a preparation of substantial quantities of DMB bispidinol **48** which could be swiftly deprotected according to the standard TFA

protocol described in chapter 5 (yield: 51 %). The resulting N5-bispidinol platform **49**, remaining in the *syn* configuration in the respect to the OH group, could be obtained with 8 % isolated yield over two steps from the DMB-bispidinone **31s** (method A – see Fig. 73 and experimental section). The compound **49** is suitable for the decoration with the 6th coordination arm. Later on, I have successfully improved the efficiency of a preparation of **49** by using as a reducing agent the BH₃*THF adduct in THF (method B in Fig. 73 and experimental section). After 2 h at 0 to 25 °C and a workup, a DMB-bispidinol could be isolated (54 % yield), or a crude residue (already largely pure) could be used directly in deprotection reaction. It is noteworthy, that deprotection of bispidinol **48** progresses much faster than bispidinone **31s**, and after 3 h the reaction is largely completed with a former one. The overall yield of the two-step 31s => 49 transformation is 37 % by method B and the isolated isomer is identical to the one obtained by method A (*syn* in respect to OH group). Obtained compound **49** is now the initial intermediate of choice in the preparation of any future probes as it offers higher stability of the ligand as well as the possible advantages for the future *in vivo* applications (as discussed above). The high spin complex of this product ([Fe**49**(SO₄)] in Fig. 73) was also successfully isolated and its crystal structure reveals great similarity with the ketalized analogue. It is in agreement with the expectation, that the modification of the periphery, if not changing the charge of the complex, should be innocent in terms of the properties of the coordination sphere. This bodes well for the future functionalization of the probes.

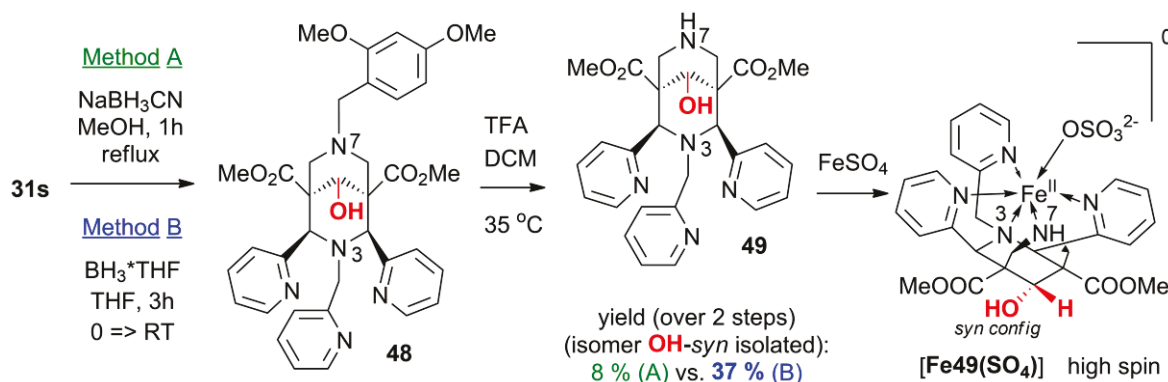


Fig. 73 Successful synthetic protocol for a preparation of the bispidinol N5-intermediate **49** and its complex. Comparison of the effectiveness of two different reduction methods. Note the *syn*-configuration in the respect to the OH group (OH pointing towards the N3-piperidinone ring) of the isolated isomer.

Reduction of the keto moiety in secondary amine 19. The attempts to reduce the ketone moiety already after deprotection were also made, however while the product is formed, its isolation poses extra difficulties due to the need to separate secondary amines. These compounds are generally much less adapted to the purification by flash column chromatography due to their significantly increased affinity to the separating phase, which is already elevated for the tertiary amine analogs. Also, while tertiary amine bispidine ligands were in some cases successfully separated by fractional crystallization, secondary amine analogs all seem to have very similar crystallization properties, principally determined by the secondary character and not substitution pattern. Thus no successful

separation of these compounds by crystallization was achieved. Consequently, this strategy is less convenient than the reduction-deprotection sequence.

8.4.2. Modification of ester groups

Motivation for ester hydrolysis. As it has been discussed in chapter 8.3, saponification of the methyl carboxylates on the bispidine periphery should reduce the Lewis acid character of the iron(II) ion in the complex. This should weaken the bonds between the metal and the pH responsive arm, shifting the magnetogenesis to physiological conditions. In addition, as reported for the electroneutral bistet-tacn-Fe(II) complex (**7**), an improvement in the biocompatibility of the bispidine-iron(II) complexes with a reduced overall charge should also be expected, due to a) a decreased ROS generation by the HS activated form of the probe and b) lower osmolarity.

My synthetic attempts of ester hydrolysis, which was previously reported for the C9-OH derivative.^[182] However, the ligand needed a purification by high-performance liquid chromatography (HPLC) which can lead only to a milligram quantities of the product, which would rule out any real-world application. For sensing purposes of our project, and especially for bispidine-based strategy, access to large quantities of the ligands are the major concern which we pay particular attention to. Thus, several attempts has been made to perform ester hydrolysis and then purify it by classic methods. Unfortunately, up to now, despite evident signs of hydrolysis observed when applying Cs(OH)₂, I was not able to isolate the desired product in a pure form. The main reason lies probably in the increased reactivity of the ketone intermediate towards the nucleophilic OH⁻, which promoted the decarboxylation and could lead to other decomposition reactions. In addition, the formation of the zwitterionic molecule with negatively charged carboxylic acid moieties and positively charged aliphatic amines on the bispidine backbone further complicate the purification, especially as below 100 mg quantities of the starting materials were so far only used in these reactions. Future experiments should thus be performed on the more stable “locked” C9-OH analog, which can now be accessed as described above in this chapter. In addition, scaling up and the use of ion exchange resins are believed to importantly improve the yields and the purification step.

Unexpected formation of monoacid. Interestingly, unusual asymmetric hydrolysis happened when the hexadentate bispidine **15** was left for several months in water/isopropanol. The structure of the precipitating product (**15-COOH**) was determined by the series of 1D and 2D NMR experiments and mass spectrometry and was unambiguously associated with a monoester of carboxylic acid, what may enable in the future to systematically study the effect of the decreased charge of the complex on the relaxation properties (dicationic with classic bispidines, monocationic with asymmetric ligand as described and electroneutral if two esters are cleaved).

Triol. Another compound which has been prepared and which involves the modification of the polar underbelly of the bispidine ligand was a reduction of the DMB-keto derivative to the triol (**31-triOH**), achieved also by Hanno Kossen, upon the use of LiAlH₄. This modification may have

an interesting impact on the relaxivity of the derived complexes (**bisp-triOH** in Fig. 71) as it possibly enables a second sphere contribution thanks to the formation of the hydrogen bonds with water molecules in the bulk. However, the compound has been isolated only with 80 % purity and thus efficient purification method is required in order to envisage its deprotection and subsequent application in a preparation of the bispidine-based probes for MRI.

Varying ester substituent in acetone precursor. Methyl esters present in the bispidine ligands derive from the acetone-1,3-dicarboxylate precursor, which is commercially available at cheap, and their electron withdrawing character facilitates Mannich reaction by increasing the acidity of the alfa-protons. In addition, they are a convenient precursor for the variety of functionalities and thus increase the freedom in fine tuning of the properties of the ligands. However they have been shown to be somewhat unstable in basic conditions. Instead of modifying the esters already in the final probes, choosing differently substituted starting material could be envisaged as a route to a series of different complexes. Thus, for example, simple acetone has been tested in the course of this work (Fig. 74 **50**) but the reaction did not progress as desired, due to the very low acidity of the *alfa* protons and the instability of the terminal enol tautomer, which is the reactive species in Mannich condensation and which for acetone is practically unobserved (does not form). However, diphenyl substituted acetone was reported in the literature to enable a formation of the bispidine structure. Thus for the future modifications, if the increased hydrophobicity of the complexes is desired this strategy can be an attractive alternative to the ester modification of the already formed bispidines. I have already performed a first step towards the synthesis of N3-H type of bispidinones with phenyl moieties instead of ester ones in position 1 and 5, which is a formation of N-H piperidinone **51** (Fig. 74), reported previously in the literature.^[252] However it still remains to be seen if the condensation of the second piperidine ring can also be performed and with what efficiency.

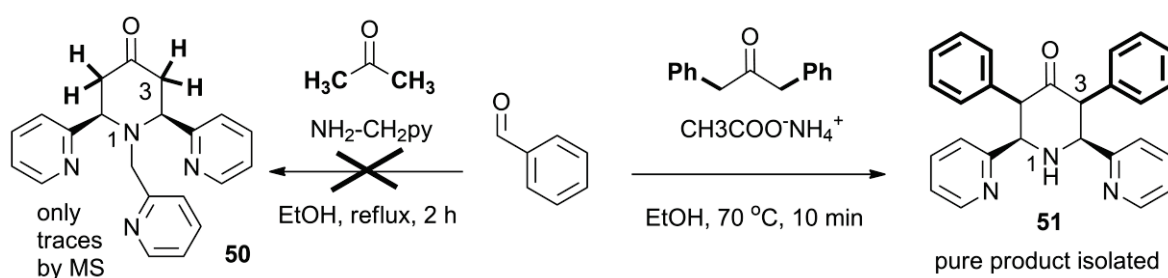


Fig. 74 Piperidinone formation from different acetone precursors. In bold – moieties replacing COOMe groups from the classic backbone of the bispidinone ligands described in this work.

8.4.3. Conclusions

*Periphery modification of the bispidine ligands enables a fine tuning of the physic-chemical properties of the iron(II) chelates without interference with its magnetic properties. Reducing a keto functionality seems particularly important for the biocompatibility and stability of the probes. Previously reported synthetic protocols led to the non-separable mixtures. NaBH_3CN in refluxing methanol or BH_3^*THF in RT were successfully applied to reduce the DMB-keto intermediate **31***

which upon the TFA deprotection leads to the C9-OH analog of the N7-H platform **19** with 2-step yield of up to 40% and at several gram scale. The new platform exhibits an increased stability towards the ligand degradation and forms a high spin complex with iron(II), iso-structural to the one obtained for **19**. This bodes well for the future decoration of the bispdine-based chelates with a variety of groups, opening up new possibilities of the fine tuning of probe's delivery and biocompatibility. Further experiments should answer the question whether the functionalization of the C9-OH is truly possible.

While the possibility of altering the ester functionalities was demonstrated, this did not lead to the isolation of the material of sufficient quality for the complexation reactions. However, insights obtained from these experiments and the proposals of a modification of the existing protocols should enable more efficient and reliable synthesis in the future.

8.5. Summary

The results obtained, both in terms of relaxivity and synthetic feasibility, place us now in a position to explore virtually any strategy of response to a chemical analyte. Several such strategies are currently being explored in our group. Direct attachment of the envisaged functionally responsive arms, equipped with different analyte-sensitive substrates, promises now to lead rather straightforwardly to several molecule candidates that may turn out to fulfill the requirements for an off-ON enzyme-responsive MRI probe. However, such a probe will not be just a mere copy of the tacn-based probes prepared in the team. On the contrary, as shown on the basis of the amidine system, they may offer complementary or superior properties. In addition, the project's global goal still awaits a first *in vivo* demonstration, and bispidine-based candidates now deserve equal consideration for these experiments. In certain respects, they may even outperform tacn-based ones, thanks to the opportunity for fine-tuning of their physic-chemical properties and thus their *in vivo* behavior by modification of their periphery. One such example involved the reduction of the keto moiety from C9 to the corresponding alcohol. The latter is now ready to be used for a construction of a putative magnetogenic probe and its possible conjugation to ligands for targeted delivery.

9. RADIOLABELING OF IRON(II) COMPLEXES TO STUDY BIODISTRIBUTION *IN VIVO*

Current stage of the development of the global project focusing on delivering the magnetogenic molecular probes for MRI place the group in the position to begin the *in vivo* experiments. Thus, the examination of the pharmacokinetics of the probe candidates is desired in order to study the fate of the complexes *in vivo*. However, no practical means to achieve that had been at our disposal. I present herein a new, straightforward method to prepare ^{59}Fe radiolabeled iron(II) chelates for biodistribution studies in mice by scintillation counting. These results were obtained upon the experiments performed in Service of Nuclear Medicine in the Hospital of Edouard Herriot in Lyon, in the collaboration with a team of Prof. Marc Janier. In particular, measurements of the radioactivity *in vitro* and sample dilutions for the final experiment were performed by Dr. David Kryza. Pauline Bonazza performed the experiments on animals which include the probes injection as well as organs separation and subsequent scintillation counting. The results presented in this chapter were summarized in the form of the poster during the “7^{ème} Journée Scientifique CLARA” (2012 – Lyon) and are a subject of the manuscript which is now in preparation.

9.1. Intro – motivation, objectives and state of the art

Ionizing radiation is generally harmful to the subject but has an advantage of unbeatable sensitivity. In the consequence, radiolabeling of the iron(II) complexes with the ^{59}Fe isotope seems very attractive if the detection of even traces of the compound is important. Thanks to the (1) suitably long half-life of 44.5 days, even a time consuming preparations as well as prolonged *in vivo* studies are possible. What is even more important, (2) exchanging the cold iron-56 to the “hot” radioactive iron-59 radioisotope does not change the chemical properties of the probes as it would be the case, if other classically used metal radionuclides would be envisaged. This results in unchanged biodistribution profile upon the labeling, allowing for the direct comparison with the MRI results and reliably informs on the behavior of the original compounds. The main disadvantage of iron-59 is that it cannot be detected in the Computer Tomography type experiments and thus the scintillation counting is required what implicates the (-1) sacrifice of the individual each time the measurement is to be made. On the other hand, this way of measuring the signal (3) enables a very precise quantification and delivers a very detailed pharmacokinetic profiles.

Unfortunately, no methodology have been reported which would enable a reliable preparation of ^{59}Fe radiolabeled iron(II) complexes and no precedence of $^{59}\text{Fe}^{2+}$ -based coordination compound as radioactive tracer exists. The number of scientific publications reporting the use of $^{59}\text{Fe}^{2+}$ radioisotope in the form of ferrous ion is small, and its application is almost exclusively limited to the iron uptake studies. In these experiments, $^{59}\text{Fe}^{2+}$ is typically used in solution with an excess of the ascorbate anion to ensure the stability of the oxidation state (II) ^{[253] [254]}, with only few examples where it is in the form of the divalent salts (succinate, ascorbate, sulfate) ^[255]. Nevertheless none of them are soluble in organic solvents and thus exclude the application in the complexation of the majority of organic ligands. There are very few reports in which the studies with $^{59}\text{Fe}^{2+}$ are performed *in vivo* (in plants ^[256], rats ^[257] and humans ^{[255] [258]}).

Iron-59 radioisotope is typically delivered in the form of iron(III) either as a citrate or as trichloride salt, in acidic aqueous solution to avoid a formation of the undesired oxides and hydroxides. If required, the iron(II) can be prepared upon the addition of the excess of ascorbate (100 – 1000 times). In the past, $^{59}\text{FeSO}_4$ was also commercially available, but any of these forms are suitable for the complexation reactions with organic ligands, as stated previously.

The main objectives of the project were thus to: (1) Exhaustively reduce the commercially available Fe(III)-59 in aqueous 1M HCl, to the ferrous ion in a form of the salts which are soluble in organic solvents; (2) Prepare a model radiolabeled complex in organic media and re-introduce it to the aqueous media suitable for biodistribution studies and (3) Validate the preparation by a successful biodistribution studies in mice. *The new protocol for the versatile derivatization of the metal ferrous complexes with suitable iron(II)-59 precursor is discussed and its utility for biodistribution studies is confirmed.*

9.2. Development of the radiolabeling protocol

First synthetic protocol for a preparation of Fe-59 bearing iron(II) complexes of water-insoluble ligands is presented schematically in Fig. 75. It begins with a quantitative reduction of the commercially available 1M HCl solution of Fe-59 enriched iron(III) chloride by potassium iodide. Subsequent evaporation of the solvent and all the volatiles including I₂ and HCl leads to the off-white inorganic residue from which organic-solvent soluble iron(II) halogenide salts are selectively extracted by suspending it in methanol. Decanted organic solution is then added drop-wise to the methanolic solution of model hexa-dentate ligand and the resulting complex is precipitated upon the addition of the excess perchlorate. All the above-mentioned steps are performed under inert atmosphere to eliminate the iron(II) oxidation, which is no longer feared upon complexation. Thus the obtained solid could be safely filtered and purified by extensive washing with organic solvents. Finally the solid residue is recovered from the substrate upon dissolution in acetonitrile. The evaporation of the solvent leads to the pure radiolabeled complex as brown residue in approximately 50 % isolated yield.

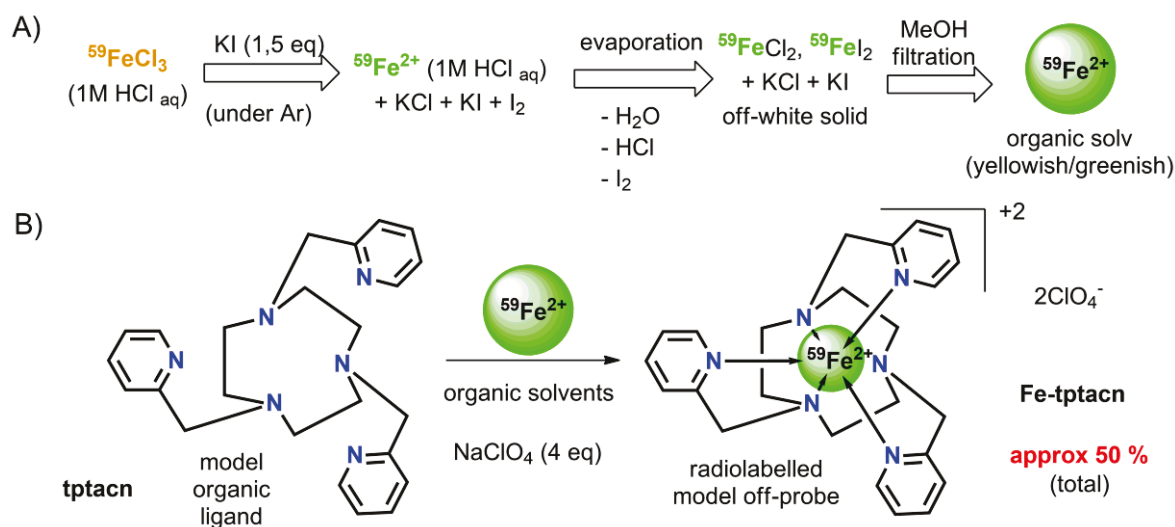


Fig. 75 Protocol for a preparation of the iron(II)-59 complexes of a water-insoluble organic ligand A) reduction of radioactive isotope of iron from ferric to ferrous state B) complexation with the ligand.

9.2.1. Specific restrictions of the project – experimental setup

Work with the hot iron (Fe-59 radioisotope) required special conditions which were provided to me by our collaborators from the Service of Nuclear Medicine from the Hospital Edouard Herriot in Lyon, who possess an adapted lead hood for the radiopharmaceutical manipulations. However, in the nuclear medicine most of the manipulations are typically limited to the simple dilutions of commercially available agents which are then injected to the patients. In the result, the working space available can be limited and no special equipment is necessary to perform it. Thus, one of the crucial challenges of this project was to adapt the methodology of chemical synthesis to the limitations of the available working space (50 cm x 45 cm x 40 cm out of which a volume of

50 cm x 35 cm x 40 cm was practically usable - Fig. 76). To achieve that, the appropriate radiolabeling protocol for derivatization of the future magnetogenic probes had to be possibly simple to limit the necessary equipment and reduce the purification step to simple filtrations or distillation. (both column chromatography and crystallization were not possible due to the safety issues and restricted time of experiment). On the top of that, none of the standard experiments like NMR, Mass Spectrometry, UV-Vis or elemental analysis could be performed with radiolabeled material to prove its purity (no adapted machines of this type for handling radioactive material were available). In the consequence, I had first verified the efficiency and reliability of the protocol by repeating it over 10 times with the “cold” material which could then be thoroughly analyzed and correlated to the desired TLC behavior, used as the indicator of the successful preparation of the radiolabeled derivative. I have also adapted a simple and sensitive chromogenic reaction between the thiocyanate and iron(II) to enable a detection of the traces of the iron in post experimental wastes and on the material used.^{[259] [260]} This was particularly important as a radioactivity of the 59-iron isotope as well as its half-life are both significantly increased in comparison to the common clinically used isotopes (99m-Tc – 6 h, 111-In - 63 h, 166-Ho - 23 h). In the consequence, not only a suitable personal safety precautions are required, but also any eventual contamination with this isotope outside the led hood would implicate serious threat to the functioning of the unit.

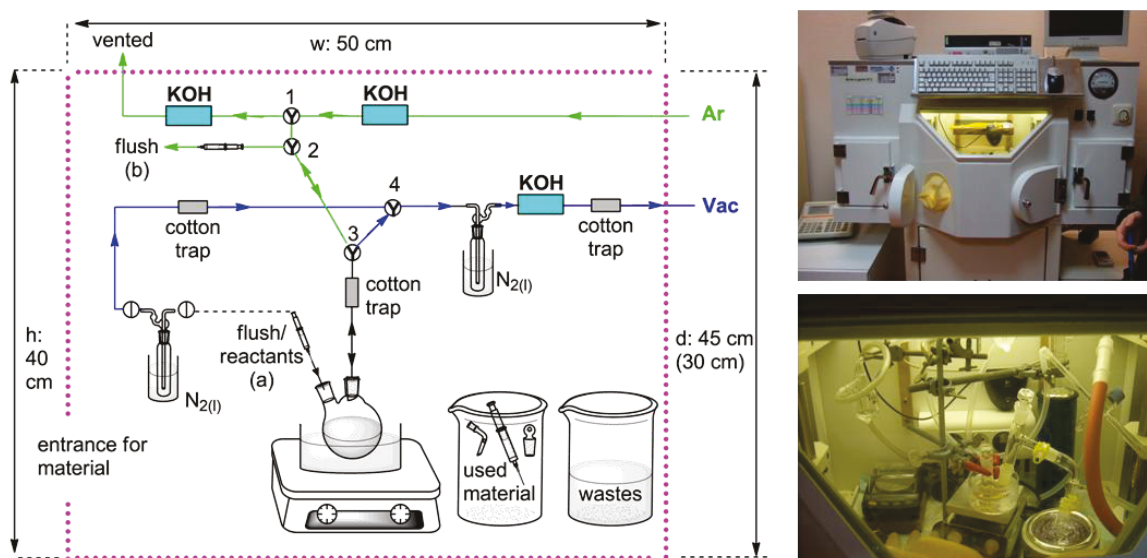


Fig. 76 Scheme of the reaction system and the real photos of the hood in which the experiments were done, from the outside (upper right) and inside during the experiments (lower right).

Considering all these limitations, a specific experimental setup was assembled (Fig. 76). Its uniqueness lies in the fact that while being restricted to the very small space, it allows to perform a variety of chemical transformations nearly as in the typical organic chemistry laboratory. In particular, proper combination of valves and taps plays the role of the small vacuum line enabling to work under inert gas atmosphere. Small distillation set which may be kept under argon or vacuum, replaces the commonly used rotavapors. Second very important feature of this system is

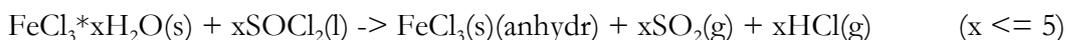
its compatibility with a strict safety requirements. Series KOH and cotton traps between the reactor and the exits of the tubes eliminates the potential risk of room and ventilation system contamination by radioactive solid particles. In addition, KOH traps effectively capture the HCl which could be detrimental to the ventilation mechanism. Finally, a place for the waste containers could also be found, again to prevent any out-of-the-hood contamination.

9.2.2. Reduction of iron(III) chloride

Extraction-dehydration-reduction strategy – failed. As mentioned above, commercially available form of Fe-59 is an iron(III) chloride in 1 HCl solution. Thus the main challenge of the project was to obtain Fe-59 in the form of iron(II) which could be used for the complexation in organic solvents (objective 1 - see chapter 9.1). In the search for the suitable protocol which would enable a quantitative reduction of this material to iron(II) and subsequent isolation of the iron(II) salts soluble in organic media I have explored a chlorination reaction of the chlorobenzene in the presence of the FeCl₃ Lewis acid ^[261] ^[262].



This protocol has been successfully repeated by me in the laboratorial conditions, but starting with the commercially available FeCl₃. In order to ensure that the Lewis acid introduced to this step is in an anhydrous probe, which was the necessary requirement, classic protocol for the dehydration of the chlorides was explored, ^[263] and again with a success, if starting from the commercially available precursor.



However a challenge of isolating the compound in the form of FeCl₃(s) from the acidic aqueous solution, as the one in which the radionuclide is delivered, was not accomplished. The original strategy which was believed to solve the problem was a previously reported extraction of the iron(III) salt from a 7 – 8 M solution of HCl to the iPr₂O. ^[264] Unfortunately, the resulting compound is not indeed the FeCl₃ but a HFeCl₄ ferric acid and thus it is incompatible with the following steps and in particular it does not get reduced in the chlorination of chlorobenzene. In the consequence the strategy had to be abandoned.

Reduction-precipitation strategy – success. I have thus proposed to use the KI as a reducing agent directly in the acidic solution of FeCl₃ and subsequent evaporation of all the volatiles (Fig. 75 panel A). While the exact concentration of iron in the commercially delivered Fe-59 samples was not given, the estimations on the basis of the information from the producer led to the values of below 5 μmol of iron in 5 ml of solution initially corresponding to 36 MBq. However at the day of experiment, 1 ml of this solution had the activity of 3.05 MBq and was not increased as the upper

limit for safety manipulations was set at 4 MBq. In the consequence the net quantity of FeCl_3 involved in the experiment was about 1 μmol (around 0.1 μg). In order to enable reliable manipulations, it has been *combined with a 0.4 ml solution of "cold" FeCl_3 (5.0 mg, 1 eq, 0.031 mmol) in 1.5 M HCl*. Subsequently, reducing agent, KI (7.5 mg, 0.046 mmol, 1.5 eq), was added in the form of 0.25 ml of aqueous solution, what led to the equilibration of the HCl concentration. *The 50 % excess of KI was used to compensate for the possible air oxidation of iron(II) back to iron(III)*. The inert gas atmosphere in which this reaction was performed should however eliminate this possibility and thus the additional KI functioned just as a "redox buffer". The reaction mixture was stirred at 40 °C for 45 min. Already after 5 min the solution turned from initially yellow to dark orange due to the formation of I_2 what indicates the progress of the reaction. After additional 15 min of cooling down at RT, previously dried and Ar-flushed recipient (Fig. 76) was installed at the side neck of the reactor and all the volatiles were evaporated under reduced pressure. Immersing the recipient in the liquid nitrogen was aimed to limit the amount of volatiles which entered the essential nitrogen trap avoiding its blockage. For that reasons, possibly wide connection between the recipient and the reactor was required to ensure that the solidifying water does not block the system also at the level of the recipient-reactor junction. *The initial removal of I_2 could be spotted by the disappearance of the color and then all the remaining water and HCl were evaporated* upon heating to 75 °C within 10 minutes. Subsequently, the system was flushed with Ar and the recipient removed and replaced with a septum to minimize the air access. Further drying of the off-white residue was performed for 15 min under vacuum, after which Ar atmosphere was restored. The intense stirring of the suspension formed upon the addition of the degassed MeOH (0.5 ml) caused a delicate change in the color of the solvent to almost unnoticeably yellowish, greenish suggesting the presence of ferrous ions in solution. This is in agreement with an expectation as the iron(II) salts present in the residue (FeCl_2 and FeI_2 or maybe also mixed $\text{Fe}(\text{Cl})(\text{I})$) are well soluble in polar organic solvents. Subsequent decantation of the solution and washing the residue again with 0.3 ml MeOH should *enable a recovery of all the Fe(II) which are now available for any ligand complexation, while potassium salts remain in the solid form*. However, even if this difference in solubility would not be sufficient to entirely separate iron(II) and potassium salts, their biocompatibility and inertness towards the iron(II) complexation should ensure that the process of the radiotracer preparation is not disturbed in any way.

Summarizing, *the complete reduction of $\text{Fe}(\text{III})\text{Cl}_3$ to Fe(II) by KI and subsequent evaporation of all volatiles leaves off a salt-type residue of products which does not interfere with iron(II) complexation, neither hamper the biocompatibility. In addition, selective solubility of only iron(II) salts in organic media lead to a pure solution of iron(II) which can then be directly used for complexation reaction.*

9.2.3. Isolation of the iron(II)-59 complex.

I have identified the tptacn-iron(II) chelate as a suitable model for the preliminary experiments in order to prove the validity of my experimental protocol. This compound, which is composed of the classic polyamine ligand with a solubility restricted to organic solvents, was already reported by several groups, and was previously used by the team in animal experiments. Despite its lower bio-tolerance than bis-tetrazolyl tacn-iron(II), the swift accessibility of the tptacn ligand and also the superior efficiency of its iron(II) complexation make it more suitable as a model compound and promise high purity of the resulting material. Bispidine complexes were not envisaged for these pilot experiments as their in vivo characterization is almost entirely absent. Thus, methanolic solution of iron(II) from the previous step was then directly added, at 50 °C, to the 1.05 eq of pure the tptacn ligand (Fig. 75 panel B) prepared in advance in the chemistry lab by classic trialkylation of tacn*3HCl, which was kindly provided by Ms. Delphine Pitrat. *A small excess of tptacn should ensure that all iron is encapsulated*, to enable the unambiguity of the scintillation counting. The reaction mixture was subsequently stirred for 30 min at 50 °C, which according to the multiple experiments performed on the “cold” material was largely sufficient to complete the complexation step. Subsequently, 0.5 ml of NaClO₄*H₂O (17 mg, 0.121 mmol, 4 eq) solution in methanol was added to the reaction mixture at 50 °C to enforce a precipitation of the complex. Indeed, after 1 min brown precipitate appeared in solution and the reaction was continued for 5 more minutes after which it was cooled to RT. The suspension was then transferred to the filter and the remaining solid was washed extensively with various solvents (2 times MeOH, 5 times EtOH 5 times iPrOH and once with Et₂O to facilitate drying. Brownish color of the filtrate suggests that some of the compound is lost in this step, as expected, due to the partial solubility of the [Fe(II)tptacn] complex in these solvents. This should maximize the efficiency of the removal of any side products of the reaction, including unreacted ligand, but a priori almost quantitative conversion and subsequent selective precipitation should already lead to the sample of high purity, as confirmed by the “cold” experiments. Subsequently, the recipient has been changed and the solid on the filter was dissolved upon the addition of acetonitrile (all together 5 – 7 ml what in the light of elevated solubility of tptacn-Fe(II) perchlorate in this solvent, enabled a full dissolution of the powder). In turn, acetonitrile solution was set up for evaporation under reduced pressure through a syringe placed in the septum and connected to the vacuum pump. *After 30 min the process was finished and so upon 30 more minutes of drying, the compound was ready to be used for a preparation of the injection solutions for mice experiments.* The activity of the resulting product measured by the scintillation counter gave 1.4 MBq. As the measurements were performed in the flask, the underestimation of the radioactivity was suspected, as previously observed, and thus the probable quantity of the radioactive iron(II) is 1.6 – 1.8 MBq what in comparison to the 3.05 MBq with which we began gives us the yield of slightly above 50 %. The purity of the sample was proven also by the TLC analysis on silica gel in the revealing phase of MeOH/CH₃COO⁻NH₄⁺(aq) 1:1 (R_f = 0.4). Any impurities either from the pure iron or from different ligands should give

significantly different shift in these conditions and thus could be easily detected either under the UV or upon the thiocyanate test used for revelation of the chromatogram. However, *only a single spot on the TLC was found by both means, what together with a high specificity of the protocol involved and the results obtained in a “cold” material experiments gives a strong proof of the purity.*

9.3. Validation of the protocol - model *in vivo* study

9.3.1. Dose estimation

The preliminary toxicity studies with tptacn-iron(II) complex revealed that the highest tolerable dose upon intravenous injection in mice was 100 μ l of 10 mM solution. For scintillation counting the required quantities are significantly lower (0.1 - 0.05 MBq which correspond approximately to sub-microgram quantities but it depend on the degree of the radioactive decay of the sample). However, there are two main reasons why in this work we aimed at maximizing the dose. Firstly, the intrinsic insensitivity of the MRI implicates the use of the milimolar quantities of the probes to observe the contrast in the image. Thus in order to reliably conclude on the pharmacokinetic of the future probe candidates, similar concentrations to the one of the MRI experiment have to be used in the biodistribution studies. Secondly, sub-miligram quantities cannot be handled by the means of typical chemical synthesis which is required for the preparation of the desired complex.

9.3.2. Samples preparation

Comparing the initial radioactivity introduced to the protocol and the one found for the final product I could also estimate the molar quantity of the complex and relate it to the concentration from the toxicity experiments above. We have thus used approximately the same concentration for the “hot iron” experiments. The appropriate samples for mice injections were prepared by Dr. David Kryza, In details, the obtained complex was dissolved in 1.6 ml of 0.15 M Tris-HCl at pH 7.4. In order to ensure the solubility of the sample in the given media, 100 μ l of acetonitrile had to be added. The resulting 10 mM solution was estimated to have an activity ratio of 0.09 MBq per 0.1 ml. Nevertheless, for each syringe prepared for an injection, the precise measurement of the activity has been made in the scintillation counter, and oscillated within 0.09 MBq for each dose (for detailed number for each individual the reader is referred to the experimental part).

9.3.3. Results of biodistribution

The prepared aliquots were then injected in 10 mice, 5 of which were sacrificed after 10 min period and 5 others after one hour. The measurement of the relative quantities of the introduced radioactive Fe-59 tracer followed by the separation of the organs and subsequent scintillation counting. All these experiments were performed by Pauline Bonazza from the team of our collaborators, and the results are summarized in Fig. 77. The biodistribution profile is typical for the iron(II) based compounds. Just at the beginning, the organ where the injection took place (leg) shows the highest concentration of the tracer, while the remaining portion is organ unspecific. After one hour the compound is already significantly cleared from the body as expected due to its inability to penetrate deeper the tissues, and the majority of the tracer can be found on kidneys and bladder + urine, with a significantly diminished quantity in the corpse and in leg. Some of the compound locates also in the liver, as expected for the iron(II)-based species.

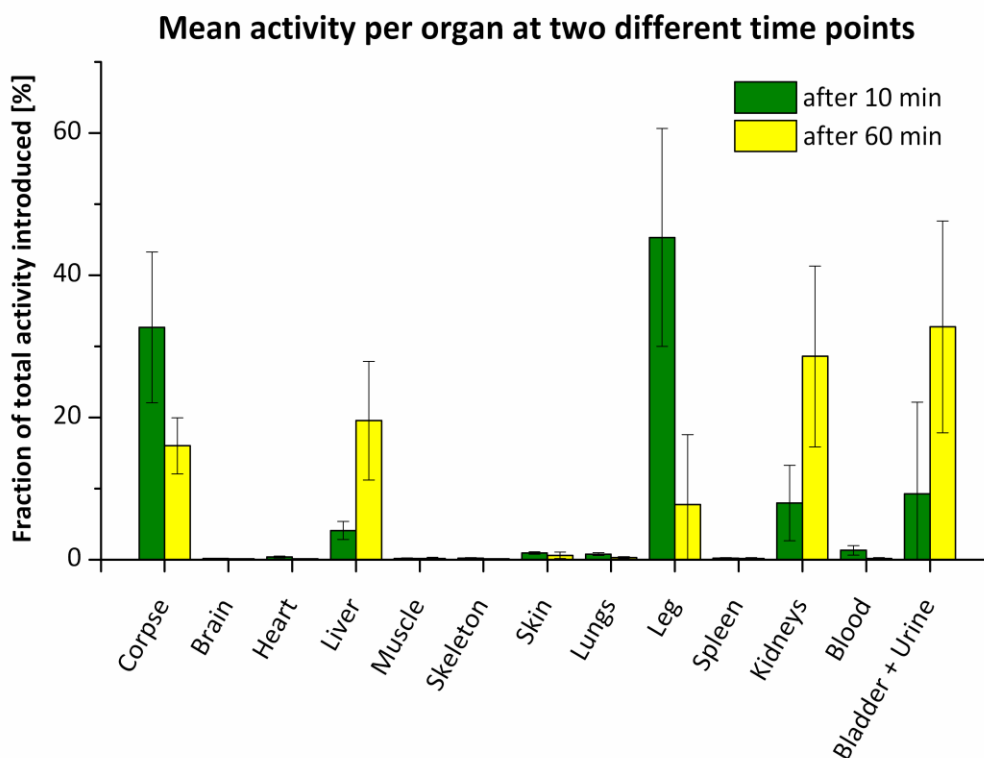


Fig. 77 Biodistribution results in mice obtained with known tptacn-iron(II) complex but in a new form of the Fe-59 radiotracer, by an organ upon the post-mortem scintillation counting.

9.3.4. Perspectives

Co-localization with the MRI signal. The results obtained by scintillation counting are in agreement with an observation made for the biodistribution of dptacn-iron(II) compound injected intravenously in MRI, performed by us in collaboration with . Dr. Laurence Canaple and Prof. Olivier Beuf (50 μ l 10 mM in Tris-HCl 0.2 M pH 7.2 – mouse had to be reanimated proving the higher toxicity of dptacn-iron(II) over tptacn, probably due to the generation of ROS). The contrast has been raised particularly in the bladder (Fig. 78 - green arrows) already after 27 min post injection, similarly to the kidneys (Fig. 78 - yellow arrows), and in both cases it increases in time what indicates, as expected, an increased clearing of the contrast agent from the body. Weak enhancement in the contrast could also be observed for the biliary glad (Fig. 78 - violet arrows) and very weak for the liver (Fig. 78 - blue arrow), in agreement with the scintillation counting of the LS compound. It thus seems possible to co-localize the signal on MRI and unambiguously attribute it to the presence of the injected material. These experiments demonstrate also that the biodistribution profile of the prepared iron(II) complexes is independent on their spin state. An essential difference between the MRI and scintillation counting in this context is that the latter enable the observation of the faith of also the non-activated probes, while the MRI is limited to only active contrast agents. This may lead to a very interesting experiments with an activatable contrast agents; i.e. it may

prove that the lack of the MRI signal in other parts of the body is not only the consequence of the differences in the local concentration of the active probe, but it does really stem from the specific activation in only one body compartment where the target (enzyme) is present.

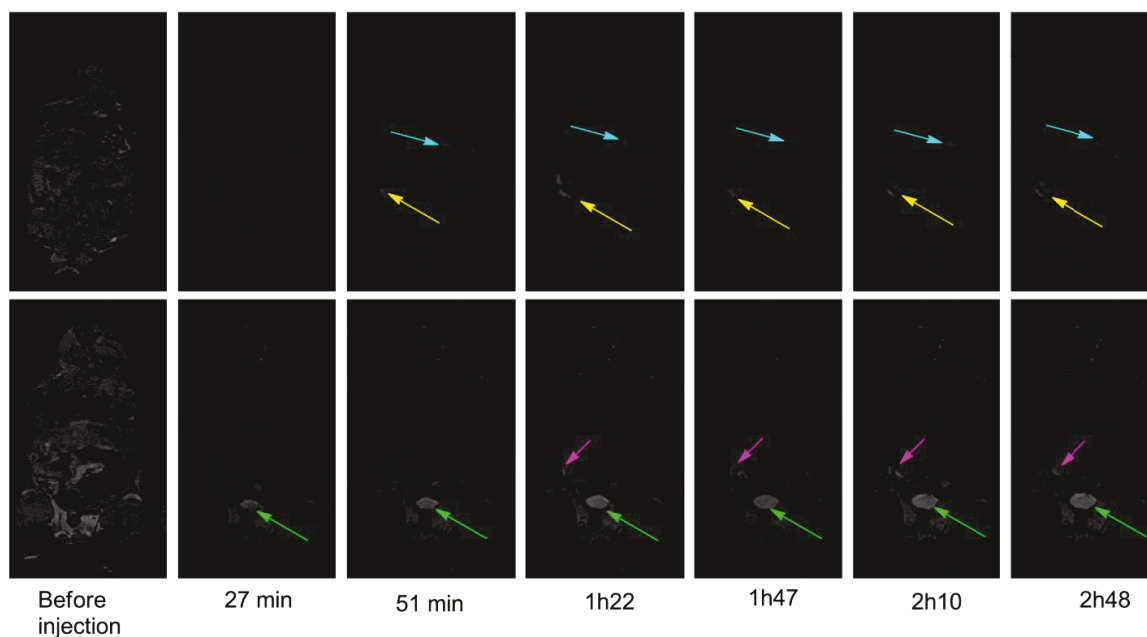


Fig. 78 The MRI results of dynamic biodistribution studies of high spin iron(II)-dptacn complex in mice (intravenous injection of 50 μ l 10 mM in Tris-HCl 0.2 M pH 7.2) performed in a small-animal apparatus at 7 T.

Pharmacokinetic profiles. Despite the non invasiveness of the MRI which is undoubtedly a great advantage, the much higher utility of the scintillation counting in studying biodistribution profile in animals is evident and stems principally from its incomparably higher sensitivity and a possibility of quantification. While for the MRI experiments the mere increase in the signal in bladder and livers could be observed even despite the injection of comparable quantities of the product (Fig. 78 - 50 μ l 10 mM in Tris-HCl 0.2 M of pH 7.2), scintillation counting gives the exact percentage of the injected compound and detects even its minor presence in different parts of the body. The resulting pharmacokinetic profiles, similar to those made for the commercially available Gd-based contrast agents, may facilitate also toxicological studies which in the future could be a very precious experimental proof if the approval for clinical trials of the complexes, is to be requested.

Correlating bispidine's modification with biodistribution. The described protocol can be also used in a much closer perspective. As seen from the experiments, biodistribution profile of our compounds is evidently not satisfactory if any molecular imaging is to be performed. So far the only possibility to localize our probes was to inject them at the site of the interest and perform the electroporation to enable internalization. In this context my work on the modification of the periphery of bispidines, described in chapter 8, is particularly relevant as it may significantly alter the pharmacokinetics, allowing for the targeted delivery even upon intravenous injection. The developed protocol for the derivatization of tptacn can be easily extended to other complexes of

iron(II) and thus it provides us with a tool to assess the efficiency of the tuning of bispidine's biodistribution profile by altering the periphery.

Towards *in vivo* studies with a wide range of iron(II) complexes. The great advantage of this methodology is that it allows to introduce the radioactive Fe-59 radioisotope into the complexes with a ligands which are not water soluble (like for example some porphyrin analogs). It has not been possible before and thus my protocol can be very attractive for a wide range of researchers as it significantly increases the scope of the possible applications, and opens the way to *in vivo* studies for many already existing and future ferrous chelates.

9.4. Conclusions

I have elaborated a rapid access to the ferrous form of radionuclide Fe-59, which now allows for even the most demanding complexations. In particular, various organic solvents are compatible with the protocol, and thanks to an appropriate design, the reactions can be carried out in anhydrous conditions and in the inert atmosphere if necessary. This opens up a way to the Fe-59 introduction into the ferrous complexes of virtually any organic ligand. By using this protocol, I have demonstrated that the renal excretion is a dominant elimination pathway of the model low spin tptacn-complex. In the consequence we possess now a tool to study the *in vivo* behavior of virtually all of the future probe candidates, what can be particularly interesting for following the change in the biodistribution pattern of bispidines upon variation of their periphery and even bioconjugation. Combining the MRI experiments and the scintillation counting is now also possible and may deliver an unambiguous proofs for the selective activation of the responsive probes *in vivo*.

PART III

CONCLUSIONS AND

PERSPECTIVES

10. SUMMARY OF ACHIEVEMENTS

Diazabicyclononanes have been intensively studied for their coordination chemistry in the past 20 years. My PhD thesis has successfully exploited this bicyclic molecular platform for the design of magnetically responsive chemosensors by preparing iron (II) chelates thereof.

In the section on ligand synthesis, a new protocol was elaborated based on the use of a protective group. This allowed for the preparation of a novel pentadentate secondary amine-type intermediate (**19**) on the scale of *dozens of grams*. This intermediate can be swiftly functionalized by alkylation and promises to do so also for fairly complex multi-component moieties. A previously reported strategy was compatible with only simple motifs due to the requirement of large quantities of amine-precursor and the need for relatively harsh reaction conditions during the Mannich-type two-ring-condensation reaction.^{[265] [266]} This work has thus paved the way to a virtually *unlimited number of highly functionalized hexadentate bispidine ligands* that could not have been envisaged before.

The section on chelate synthesis reports on the preparation and characterization of the *first low spin diamagnetic iron(II) complexes of bispidines* in the solid state (**[Fe19(CH₃CN)]**, **[Fe34]**, **[Fe35]**) and in aqueous solution (**[Fe34]**, **[Fe35]**). They were shown to withstand prolonged exposure to competitive aqueous media and open air. The liberation of one coordination site led to the high spin pentadentate analog **[Fe19(SO₄)]**. Thus, bispidines become the second class of ligands that allow for the preparation of a pair of robust ferrous chelates that have a perfect diamagnetic/paramagnetic relationship under environmentally relevant conditions in aqueous media at room temperature.^[53] This bodes well for the design of a responsive probe that operates in a true off-on mode. The *first confirmed example of SCO bispidine-based metal complex* **[Fe15]*2BF₄** was also provided in this work, albeit in the presence of a simultaneous minor component of decoordination-based change in magnetic properties.

The anion-induced controlled exchange of the 6th coordination site in binary bispidine iron(II) complex **[Fe15]*2BF₄** allowed for the *selective detection of anions in polar media by monitoring the “increase” in the paramagnetism* of the sample. To the best of my knowledge only one similar example exists^[142] that dates back to the spring of 2013, so only after the termination of my experimentation for this PhD thesis; here, the increase of the magnetic moment was caused by the exchange of single coordinating arm of the binary complex by the anion and not the solvent. The example presented in my work allowed for the *selective detection of several common anions in MeOH and even in water*, and compares favorably to the above reported case, because that one demonstrated magnetic detection of anions in dichloromethane only^[116].

The MRI silent (off) and MRI active (on) states of the diamagnetic **[Fe34]** and paramagnetic **[Fe19(SO₄)]** model bispidine-iron(II) complexes was proven. The residual paramagnetism present

in the spin-transition compound [Fe15] did not enhance the relaxation rate of water protons, indicating that a closed coordination sphere and a “near-to-low spin” magnetic state of the complex may suffice as requirements for a truly silent proagent. The *in vitro* relaxivity of the model high spin form was approximately 4 – 2 times lower than those found for the tacn-based compounds,^[31]^[32] but was shown to induce a sufficient contrast *in vivo*, albeit at high concentrations. I hypothesize that an improvement in relaxivity may be obtained by reducing the charge of the probe.

The off-on activation of the bispidine-iron(II) chelates in MRI was demonstrated at the example of a pH-responsive analog that made use of an intelligent pendent arm previously reported by the group^[74]. The pH of 4.5 – 5.5 at which the magnetic response could be observed was 1 unit higher than the respective tacn-based counterparts, but still remained below the physiologically relevant range. Nevertheless, this increase in the *pKa*, in comparison to the tacn-based probe, together with the group’s progress in the modification of the pH sensitive arm and the idea of reducing the Lewis-acid character of iron(II) by charge compensation, bode well for the preparation of a bispidine-based probe operating at neutral pH. Other intelligent pendent arms developed in the group were not yet available at the time of the experimental work. However, my successful functionalization of the bispidines with an already activated version of such an intelligent arm and the recent progress of the team^[51] place us now in the position to prepare the first enzyme-responsive bispidine probe. The availability of such a probe can then be hoped to lead to the long-awaited proof of concept of the global project, namely the *in vivo* demonstration.

During this work, I have also elaborated a suitable protocol for a preparation of the first ever *59-Fe(II) radiolabeled complexes of water-insoluble polydentate organic ligands*. This enabled us to perform *biodistribution experiments in mice with a model tptacn-Fe(II) complex* which revealed a classic renal clearance pathway for this compound. Only a limited number of experiments with radioactive *59-Fe(II)* were reported, and all these examples concern its use in the form of simple divalent water soluble salts, usually with a large excess of ascorbate to avoid Fe(III).^[255] ^[253] ^[257] ^[254] ^[256] This new methodology of mine can a priori be extended to any iron(II) complexes of organic ligands. Our group may thus hope to study the biodistribution of any future probe candidates and provide proof of their selective activation in MRI experiments aiming at co-localization.

11. GENERAL PERSPECTIVES

The results of this PhD work form a solid bases for further development of 3-component magnetogenic probes for MRI applications *in vivo*, and the next steps in achieving this goal are briefly described. However, this work demonstrates also how does the powerful concept of solution magneto-genesis (off-on magnetic responsiveness), coined originally by Prof. Hasserodt, can be extended to a variety of detection strategies and other applications. It is thus the aim of the author of this manuscript, to show the way in which the studies on the magnetic properties of the molecules can be adapted to give a new boost to the field of molecular imaging. Some future directions are briefly outlined below, to inspire new molecular designs.

11.1. MRI detection of *in vivo* enzyme activity by 3-component bispidine-iron(II) probes

Proof of magnetogenesis concept *in vivo*. Synthetic protocols established during this work as well as the proof of concept of the magnetogenic activation of bispidine-iron(II) and the subsequent change in the relaxation properties allow now to swiftly functionalize this system with the potentially responsive arms bearing the enzymatic substrate. This should lead in the nearest future to the series of bispidine-based molecular probe candidates for enzymatic activity. After the *in vitro* characterization, which can now be made by the group according to the jointly developed protocols, the attempts to study their *in vivo* properties should be undertaken, in the function of the available biological models. For the time being, we possess an access to the relevant biological models for testing b-galactosidase activity only (mice overexpressing this enzyme constitutively). Recently, a HeLa cell-line with an overexpression of the nitroreductase has been established by my co-PhD student Faycal Touti in collaboration with Dr. Laurence Canaple, and this is believed to enable and induction of a nitroreductase over-expressing tumor upon the injection to the animal. Such a system would enable an *in vivo* examination of all the activation strategies pursued by the group, also for the bispidine system.

Targeting toxicity. The observed toxicity of some of the model compounds still remain to be verified for the future functional probes but as already reported by the team, it could be largely addressed by decreasing the overall charge of the complex. Thus, the development of negatively charged ligands is of major importance at this stage of the project. For the bispidines it could be potentially realized via an introduction of previously reported tetrazole coordinating units, hydrolysis of peripheral esters or ligand functionalization with other negatively charged moieties (see chapter 8 for more details).

Biodistribution profiles and their modification.. If the efficient activatable probe is to be established, or upon the derivatization of the model passive compound with the Fe⁵⁹, studies of the

biodistribution of the bispidine-derived iron(II) complexes upon a variation of the substitutional pattern at the periphery of the probe could be performed (see chapter 8). Alcohol, prepared in this work is a very good starting point for a further functionalization (chapter 8). This is an important issue if enzymatic biomarkers and not a model constitutively expressed enzymes are to be targeted. For maximal local concentration of the agents which is a limiting factor of our strategy, dendrimeric designs or targeted delivery in the nanoparticles could also be potentially envisaged.

11.2. Switchable catalysis upon coordination sphere opening

Another development, which I have already initialized in the laboratory and which takes the advantage of the strategy of opening the first coordination sphere developed by Prof. Hasserodt, is a controlled catalysis. In this sense, a concept of “switchable” catalysts seems to be compatible with the idea of magnetogenic activation presented in this work, even if no evident relationship exist between the spin state of the compound and the catalytic properties it possess. Despite the easy to imagine advantages of such catalysts only a very few successful molecular designs were reported so far which enable a “switching” of the catalytic properties upon external stimulus, and chemically induced switch is particularly rare. Iron(II)-bispidine system is particularly well placed for such design due to its well documented catalytic properties especially in oxidation reactions and its ability to undergo responsive magnetogenesis as documented in this work. I have thus already performed preliminary experiments which suggest that such a chemically driven switch is indeed possible. Further studies including the GC-MS and UV-Vis analysis of the reaction mixtures were envisaged to confirm the results and eventually assess the level of catalytic activation as well as conclude on the true origin of the process. However, due to the lack of time and technical limitations in the availability of the equipment, they had to be suspended and still wait for completion

11.3. Magnetogenic probing without opening of coordination sphere

Despite the main focus on the three component probe’s design proposed by Prof. Hasserodt, the results of my work allow also for envisaging alternative strategies for the detection of the chemical reactivity upon the induction of magnetogenesis. An interesting alternative would be to introduce chemically alterable functionalities on the periphery of the probe (not just binding units) but in electronic communication with a metal center (for example on coordinative pyridine rings). Upon reaction with chemical analyte, they could then communicate its presence by changing the ligand field. If complex is properly tuned (remains on the edge of the spin transition) then such a modification could lead to the significant change in the magnetism.

MRI probes with outer sphere relaxivity response. The detection of this change could be envisaged by MRI if the second sphere outer sphere contribution would be significant. However for

iron(II) its short electronic relaxation time which, in contradiction to the SBM theory developed for Gd(III), does not significantly lengthens even at high magnetic fields, may largely quench the effect. The innovative and promising strategy to improve that would be to introduce an electron spin co-operativity in the system which would slow down the relaxation process (for example by using polynuclear complexes of the single molecular magnet type). Otherwise, analyte-induced spin transition upon the intramolecular charge transfer could also allow for combining the magnetic inertness of LS iron(II) with the high paramagnetism of Fe(III) in the HS state, which in addition has longer relaxation times, which on the top of that increase with increasing magnetic field. For such systems outer sphere mechanism could potentially be superior to the one of Fe(II) chelates.

Magnetogenic probes for MRS. Alternatively, Magnetic Resonance Spectroscopy could be used instead of MRI, as it does not require an open coordination sphere but will detect an isotropic shift which is more directly correlated with a paramagnetism of the sample than the relaxation time of the bulk water protons. In order to improve the sensitivity of the technique and to minimize the background, fluorine atom could be introduced on the magnetogenic complex in a position which experiences significant isotropic shift from the metal ion. Despite the certain inferiority of the MRS technique in comparison to MRI, this could be the easiest way to enable a detection of magnetogenesis in more complex samples than a pure solvent. Many potential molecular designs can be easily imagined if this strategy is to be used and hopefully be developed in the future.

PART IV

EXPERIMENTAL

SYNTHESIS

General Procedures

Solvents and commercially available reagents were purchased from Aldrich, Acros, and Alfa Aesar and used without further purification. Solvents were dried by standing the commercial dry HPLC grade solvents for 24 h on thermally-activated molecular sieves (3 Å for MeOH and EtOH, 4 Å for CH₃CN and Et₂O, sieve activation by 24 h heating at 315 °C) and degassed by a freeze-pump-thaw method (sequence repeated 3-5 times) for complexation reactions. Flash column chromatography was performed using Merck Aluminum oxide 90 active neutral (activity grade I, 0.063-0.200 mm mesh), Merck silica gel Si-60 (40-63 µm) or Sigma-Aldrich Aluminum oxide activated basic (activity grade I, mesh approx 150). Reaction progress was monitored by NMR, MS or thin layer chromatography (TLC) using Merck aluminum oxide neutral aluminum sheets containing F₂₅₄ UV-indicator. They were typically visualized by UV-light (254 nm) or anisaldehyde-based revealing solution in acid (pink and violet spots from keto and hydroxyl groups of bispidine periphery). Melting points were determined on Buchi melting point B-540 apparatus and were uncorrected. Only crystalline batches of bispidine ferrous complexes were used. For all the analyses, crystalline batches of ferrous complexes of bispidines were used, unless otherwise stated. Yields refer to the isolated, spectroscopically pure material unless otherwise stated.

All NMR spectra were acquired on a Bruker AVANCE 500 (500.10 and 125.76 MHz for ¹H and ¹³C respectively) at 298 K (unless otherwise stated). Chemical shifts (δ) are reported in ppm (s = singlet, d = doublet, t = triplet, m = multiplet, br = broad, v. br. = very broad) and referenced to residual solvent peak. NMR coupling constants (*J*) are reported in hertz (Hz). Typically the given ¹³C NMR spectra are in fact the jmod experiments, in which the signals from the CH and CH₃ groups are on the one side of the baseline, with CH₂ and C-q on the other. Assignment of signals in ¹H and ¹³C NMR spectra, when stated, were supported by two-dimensional homo and/or heteronuclear NMR experiments (COSY and/or NOESY/ROESY as well as HSQC and HMBC). NMR of crucial synthetic intermediates and final compounds are also presented in the graphical form. Note the numbering of the NMR signals.

UV-vis spectra were recorded on a V-670 Jasco spectrophotometer at RT.

Low resolution mass spectra, mainly for monitoring the reaction progress, were acquired on an Agilent 1100 Series LC/MSD apparatus in ESI mode upon a direct injection of the sample (DIMS or equivalently MS) with a vaporization temperature of 300 °C. Molecular mass signals (*m/z*) are given with an intensity of the peak in brackets (in %), relative to the highest intensity peak (100 %). Binary solvent mixture acetonitrile-water was used, with aqueous phase containing sodium/ammonium formate. For organic molecules 95:5 and 50:50 acetonitrile-water ratios were

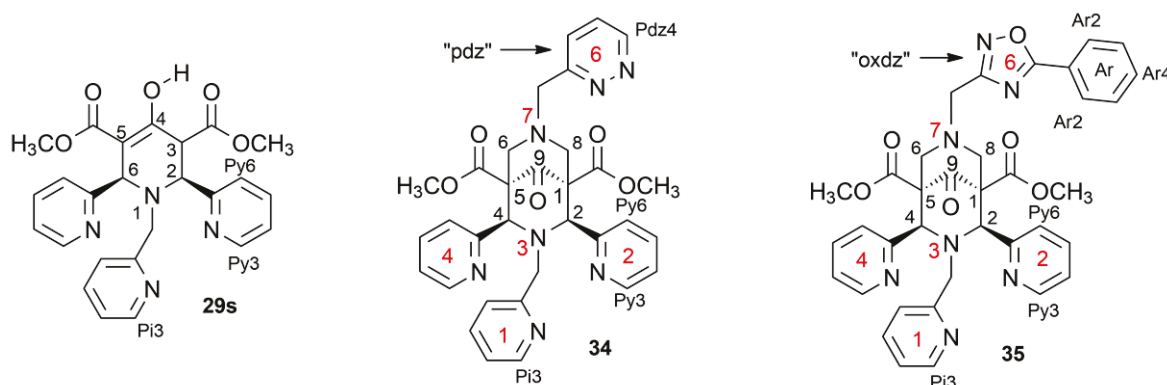
used typically for organic molecules and complexes respectively. It is important for the results comparison and repeatability, especially in the context of the tendency of anion binding of some of the analyzed complexes observed even in MS conditions. Three fragmentation voltages of 70, 120 and 150 eV were used and ion peaks are reported for the positive mode (cationic specie). Whenever given as the final characterization, all the DIMS signals observed are reported. This characteristic was used to confirm the purity and to some extent also identity of the complex formed.

High resolution mass spectrometry measurements and **elemental analyses** were performed at the “Centre Commun de Spectrometrie de Masse” of the University Claude Bernard in Lyon (France) and the Service Central d’Analyse of the CNRS in Solaize (France).

Cyclic voltammetry experiments have been conducted in a standard one-compartment, three-electrode electrochemical cell using a biologic ESP300 potentiostat. Tetra-n-butylammonium perchlorate (TBAP) was used as supporting electrolyte (0.1 M) in acetonitrile. A vitreous carbon working electrode ($\varnothing = 3$ mm, ALS Co) was polished with 1 μm diamond paste before each recording. The counter electrode was a Pt-wire. Electrode potentials are referred to a Ag/AgNO_3 reference electrode (ALS Co, 0.01M AgNO_3 , 0.1 M TBAP in acetonitrile). The concentration of the complexes were established around 1 mM and the measurements were performed at five different scan rates (50, 100, 150, 200, 250 mV/s) all giving similar reversible cyclovoltammograms.

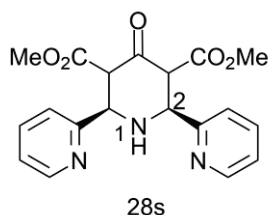
Previously reported compounds are denoted with an asterisk * . All the others which synthesis is described here are to the best of my knowledge, original species.

A reminder on the usual numbering of ligands and precursors for NMR analysis is given in black in figure below. Red numbers on the other hand indicate the specific number of the coordinating moiety (or coordinating atom), used in this work to facilitate the orientation especially in the chelates and when discussing solid state analysis.

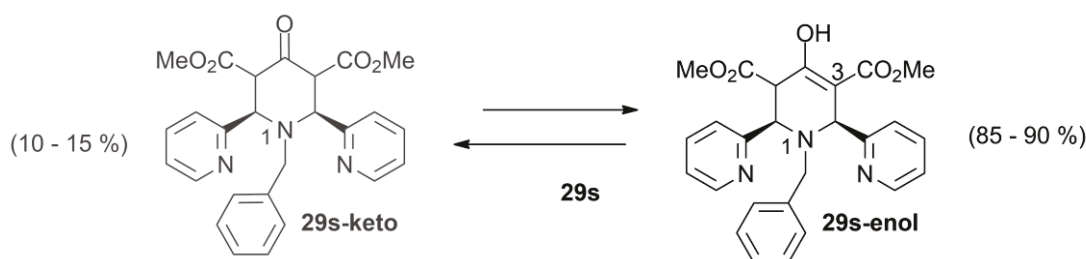


Organic synthesis

PIPERIDINONES

28s* (dimethyl 3,5-dicarboxypiperidinone N-H)

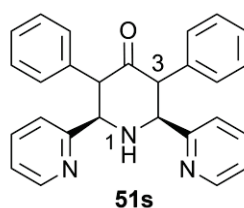
To a solution of pyridine-2-carbaldehyde (8.57 g, 0.08 mol) in 7 ml of MeOH acetone-1,3-dicarboxylate was added (6.97 g, 0.04 mol) and the reaction mixture was placed in an ice bath. Then 10 % aqueous solution of NH_3 (10 ml, 1.5 eq) was added drop-wise over a period of 10 min. The precipitate started to appear at the end of addition, after which the reaction was left stirring at RT for 12 h. The precipitate was filtered and washed with MeOH and dried under vacuum yielding 12.625 g (85 %) of a pure compound (only keto form). ^1H NMR (500 MHz, $\text{DMSO}-d_6$): δ =2.95 (1H, t, J =12.26, NH) 3.53 (6H, s, CO_2CH_3) 4.26 (2H, d, J =10.58, H -3/5) 4.62 (2H, dd, J =12.01, 10.91, H -2/6) 7.32 (2H, ddd, J =7.52, 4.83, 1.10, Py) 7.46 (2H, d, J =7.83, Py) 7.78 (2H, td, J =7.67, 1.77, Py) 8.50 - 8.62 (2H, m, Py 3). ^{13}C NMR (126 MHz, $\text{DMSO}-d_6$): δ = 51.57 (2C, s, CO_2CH_3) 61.59 (2C, s, CH aliph) 63.01 (2C, s, CH aliph) 123.18 (2C, s, Py) 123.26 (2C, s, Py) 136.98 (2C, s, Py) 148.86 (2C, s, Py 3) 158.00 (2C, s, Py 1) 168.60 (2C, s, CO_2Me) 202.18 (1C, s, C-4).

29s* (dimethyl 3,5-dicarboxypiperidinone N-pi) ^{[207] [208]}

To an ice-cold solution of acetone dicarboxylate (60.95 g, 350 mmol) in methanol (150 ml) was added drop-wise picolyl aldehyde (82.54 g, 770 mmol) and picolyl amine (41.74 g, 385 mmol). The reaction was then stirred for 5 minutes on ice and then placed in a freezer ($-20\text{ }^\circ\text{C}$) overnight. The resulting white solid was washed with diethyl ether and recrystallized from ethanol. White, crystalline material formed was filtered off and washed with diethyl ether. The workup of the filtrates gave the additional material which was combined with the first crop yielding 132.30 g (82 %) of a pure product (enol form dominant) as white crystals. M.p. $130\text{-}133\text{ }^\circ\text{C}$; ^1H NMR of the enol form (500 MHz, CDCl_3): δ =3.51 (3H, s, CO_2CH_3), 3.75 (3H, s, CO_2CH_3), 3.77 (2H, s, N-

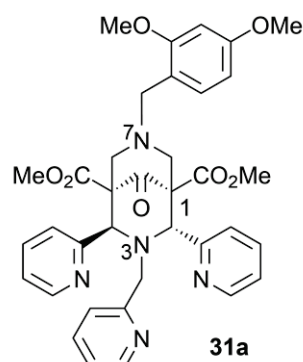
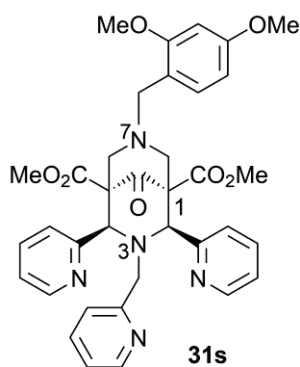
CH_2py), 4.29 (1H, d, $J=8.55$, $H-5$), 4.76 (1H, d, $J=9.40$, $H-6$), 4.87 (1H, s, $H-2$), 7.10 (1H, dd, $J=6.84$, 5.13, $Pi4$), 7.15 (1H, m, $Py4$), 7.36 (2H, d, $J=8.55$, $Py6$), 7.49 (1H, d, $J=7.69$, $Pi6$), 7.55 (1H, td, $J=7.69$, 1.71, $Py4$), 7.68 (3H, m, 2x $Py5$, $Pi5$), 8.45 (2H, t, $J=4.27$, $Py3$), 8.60 (1H, d, $J=3.42$, $Pi3$), 12.56 (1H, s, OH). ^{13}C NMR of the enol form (126 MHz, CDCl_3): $\delta=44.9$ ($C-5$), 51.8 (CO_2CH_3), 52.7 (CO_2CH_3), 53.9 ($\text{N-CH}_2\text{py}$), 59.8 ($C-2$), 61.8 ($C-6$), 98.2 ($C-3$), 122.2, 122.2, 122.6, 122.7, 122.9, 123.3 (2x $Py4$, 2x $Py6$, $Pi4$, $Pi6$), 136.4, 136.5, 136.8 (2x $Py5$, $Pi5$), 148.6, 149.1, 149.2 (2x $Py3$, $Pi3$), 158.3, 159.9, 161.5 (2x $Py1$, $Pi1$), 167.7 ($C-4$), 171.5 (CO_2Me), 172.2 (CO_2Me).

51s* (3,5-diphenylpiperidinone N-H) ^[252]



To a heated solution (60 °C) of ammonium acetate (0.77 g, 10 mmol, 1 eq) in 8 ml of 95 % EtOH, a picolyl aldehyde (2.14 g, 20 mmol, 2 eq) and diphenylacetone (2.10 g, 10 mmol) were subsequently added dropwise. After 10 min at 75 °C, the reaction was cooled down and left stirring for 24 h. The precipitate formed was filtered off and washed with EtOH, Crude product was recrystallized from EtOH/EtOAc 1:2 solvent mixture and upon washing with EtOAc yielded white/yellow crystalline material ^1H NMR (500 MHz, CDCl_3): $\delta=3.85$ - 3.90 (1H, m, NH), 4.20 - 4.22 (2H, m, $H-3/5$), 4.57 - 4.62 (2H, t, $H-2/6$), 6.72 - 6.74 (2H, d, $Py6$), 7.03 - 7.08 (6H, m, 2x $Py4$, 4x Ph), 7.12 - 7.15 (2H, m, Ph), 7.17 - 7.20 (4H, m, Ph), 7.33 - 7.36 (2H, m, $Py5$), 8.64 (d, 2H, $Py3$).

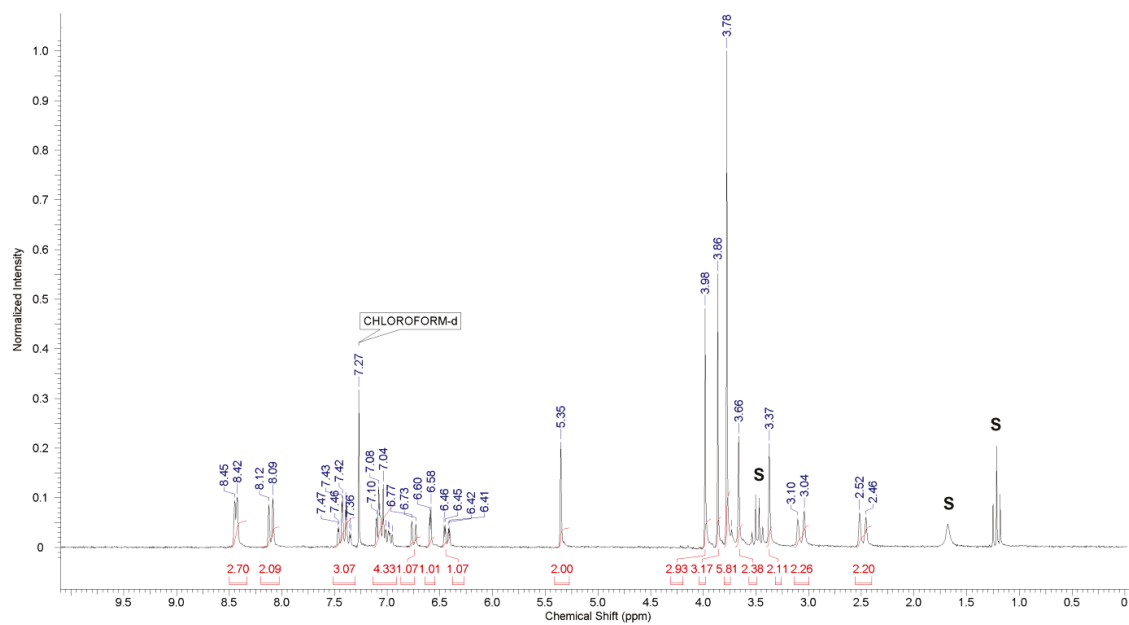
DMB-PROTECTED INTERMEDIATE (N7-DMB)

31 (N3-Pi, N7-DMB bispidinone)

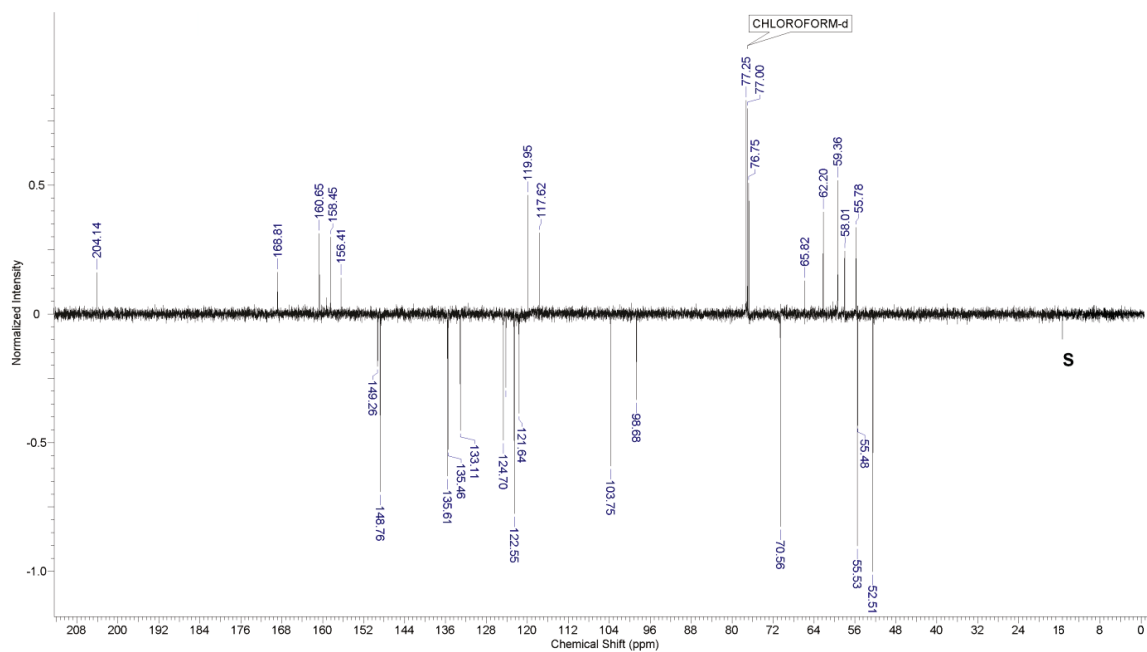
To a solution of piperidinone 1 (43.10 g; 93.6 mmol) in ethanol (600 ml), formaldehyde (37% in H₂O) (17.47 g, 215.3 mmol, 2.3 eq) and dimethoxybenzyl amine (18.00 g; 107,6 mmol; 1.15 eq) were added at 60 °C. Then reaction mixture was stirred under reflux for 8h and all volatiles were removed under reduced pressure. The residue was dissolved on heating in a minimal quantity of methanol (50 ml) and to it diethyl ether was added (150 ml). White crystalline solid, which appeared after several hours at room temperature was filtered off and washed three times with diethyl ether. Working up of the resulting filtrate yields additional material which was combined with the first crop giving in total 12.89 g (21%) of a pure product (31s).

Syn isomer 31s. M.p. 187-190 °C; ¹H NMR (500 MHz, CDCl₃): δ=2.49 (2H, d, *J*=11.6, *H*-6/8 *eq.*), 3.07 (2H, d, *J*=11.9, *H*-6/8 *ax.*), 3.37 (2H, s, N7-CH₂Ar), 3.66 (2H, s, N3-CH₂py), 3.78 (6H, s, CO₂CH₃), 3.86 (3H, s, Ar4-OCH₃), 3.98 (3H, s, Ar2-OCH₃), 5.35 (2H, s, *H*-2/4), 6.43 (1H, dd, *J*=8.12, 2.14, *Ar*5), 6.59 (1H, d, *J*=2.14, *Ar*3), 6.74 (1H, d, *J*=7.69, N3-*Pi*6), 6.97 (1H, ddd, *J*=7.59, 4.81, 0.85, N3-*Pi*4), 7.01 - 7.16 (3H, m, 2x *Py*4, *Ar*6), 7.37 (1H, td, *J*=7.7, 1.7, N3-*Pi*5), 7.42 (2H, td, *J*=7.7, 1.7, *Py*5), 8.10 (2H, d, *J*=8.12, *Py*6) 8.40 - 8.51 (3H, m, 2x N3-*Py*3, N3-*Pi*3). ¹³C-jmod NMR (126 MHz, CDCl₃): δ=52.5 (CO₂CH₃), 55.5 (Ar-OCH₃), 55.5 (Ar-OCH₃), 55.8 (N3-CH₂py), 58.0 (N7-CH₂Ar), 59.4 (*C*-6/8), 62.2 (*C*-2/4), 70.6 (*C*-1/5), 98.7 (*Ar*3), 103.8 (*Ar*5), 117.6 (*Ar*1), 121.6 (N3-*Pi*4), 122.6 (*Py*4), 124.2 (N3-*Pi*6), 124.7 (*Py*6), 133.1 (*Ar*6), 135.5 (N3-*Pi*5), 135.6 (*Py*5), 148.8 (*Py*3), 149.3 (N3-*Pi*3), 156.4 (N3-*Pi*1), 158.5 (*Ar*2), 159.2 (*Ar*4), 160.7 (*Py*1), 168.8 (CO₂Me), 204.1 (*C*-9). IR (solution in DCM) ν_{\max} = 3051-2835 (C-H), 1738 (C=O), 1612 (Ar), 1589 (Ar), 1510 (Ar) cm⁻¹; HRMS (ESI): *m/z* calcd for C₃₆H₃₈N₅O₇: 652.2766 [M+H]⁺; found 652.2768; elemental analysis calcd (%) for C₃₆H₃₈N₅O₇: C 66.35, H 5.72, N 10.75; found: C 65.72, H 6.01, N 10.38.

^1H NMR spectrum of **31s** (500 MHz, CDCl_3 , 298 K):

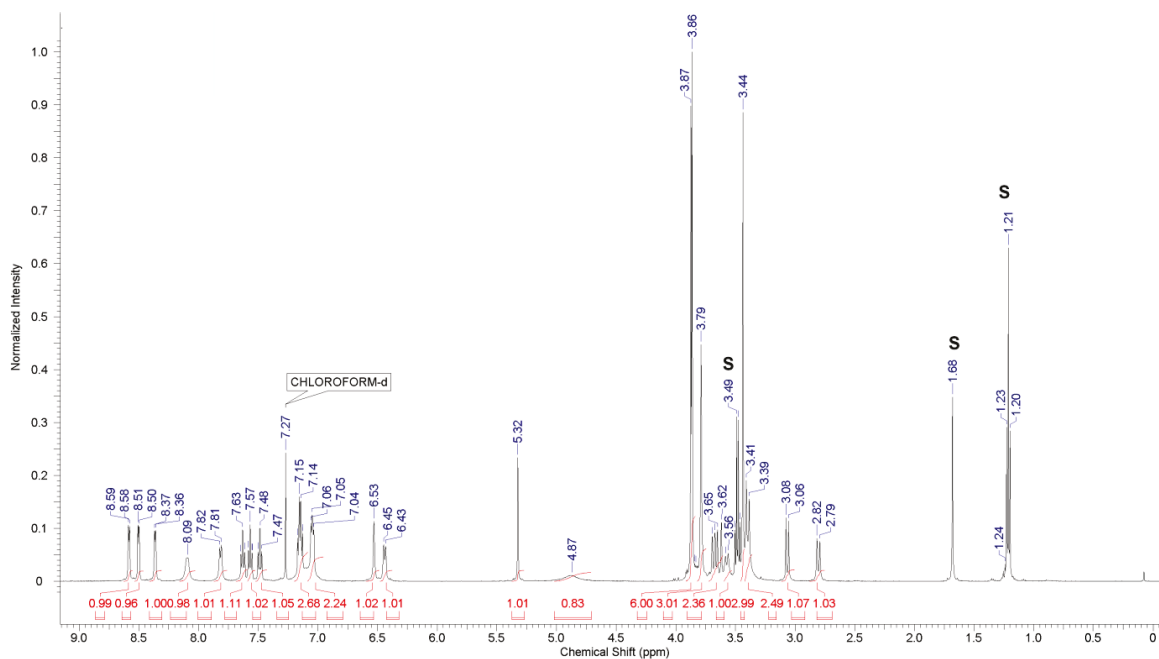


^{13}C -jmod NMR spectrum of **31s** (126 MHz, CDCl_3 , 298 K):

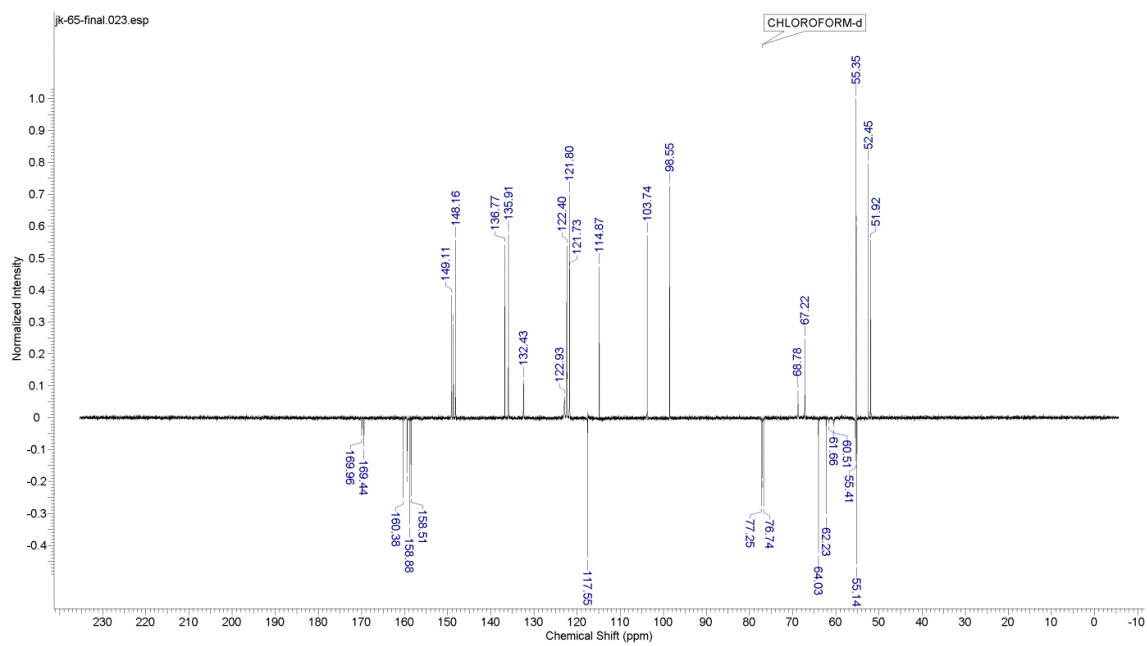


NMR of anti isomer 31a: ^1H NMR (500 MHz, CDCl_3): $\delta=2.81$ (1H, d, $J=11.91$, *H-6 eq*), 3.07 (1H, d, $J=11.00$, *H-8 eq*), 3.40 (3H, d, $J=11.91$, *H-6 ax*, 1H from N7- CH_2Ar , 1H from N3- CH_2py), 3.44 (3H, s, C1- CO_2CH_3), 3.57 (1H, d, $J=11.00$, 1H from N7- CH_2Ar), 3.64 (1H, d, $J=15.58$, 1H from N3- CH_2py), 3.68 (1H, d, $J=11.00$, *H-8 ax*), 3.79 (3H, s, Ar4-OCH₃), 3.86 (3H, s, C5- CO_2CH_3), 3.87 (3H, s, Ar2-OCH₃), 4.87 (1H, br. s., *H-2 eq*), 5.32 (1H, s, *H-4 ax*), 6.44 (1H, d, $J=8.25$, *Ar5*), 6.53 (1H, br. s., *Ar3*), 6.95 - 7.09 (2H, m, C4py(eq)-Py4, *Ar6*), 7.09 - 7.20 (3H, m, C2py(ax)-Py4, C2py(ax)-Py6, N3-Pi4), 7.43 - 7.52 (1H, m, C4py(eq)-Py5), 7.52 - 7.59 (1H, m, N3-Pi5), 7.63 (1H, t, $J=7.79$, C2py(ax)-Py5), 7.82 (1H, d, $J=7.33$, N3-Pi6), 8.09 (1H, br. s., C4py(eq)-Py6), 8.36 (1H, d, $J=4.58$, C4py(eq)-Py3), 8.50 (1H, d, $J=4.58$, N3-Pi3), 8.58 (1H, d, $J=4.58$, C2py(ax)-Py3). ^{13}C -jmod NMR (126 MHz, CDCl_3): $\delta=51.92$ (1C, s, C1- CO_2CH_3), 52.45 (1C, s, C5- CO_2CH_3), 55.14 (1C, s, N3- CH_2py), 55.25 (1C, s, Ar4-OCH₃), 55.35 (1C, s, Ar2-OCH₃), 55.41 (1C, s, N7- CH_2Ar), 60.51 (1C, s, *Ar6*), 61.66 (1C, s, *C-1*), 62.23 (1C, s, *C-5*), 64.03 (1C, s, *C-8*), 67.22 (1C, s, *C-2*), 68.78 (1C, s, *C-4*), 98.55 (1C, s, *Ar3*), 103.74 (1C, s, *Ar5*), 117.55 (1C, s, *Ar1*), 121.73 (1C, s, C2py(ax)-Py4), 121.80 (1C, s, N3-Pi4), 122.36 (1C, s, C4py(eq)-Py4), 122.40 (1C, s, N3-Pi6), 122.93 (1C, s, C2py(ax)-Py6), 132.43 (1C, s, C4py(eq)-Py6), 135.91 (1C, s, C4py(eq)-Py5), 135.94 (1C, s, C2py(ax)-Py5), 136.77 (1C, s, N3-Pi5), 148.16 (1C, s, C2py(ax)-Py3), 148.70 (1C, s, N3-Pi3), 149.11 (1C, s, C4py(eq)-Py3), 156.11-156.17 (1C, br.s., C2py(ax)-Py1), 158.51 (1C, s, C4py(eq)-Py1), 158.88 (1C, s, *Ar2*), 159.44 (1C, s, N3-Pi1), 160.38 (1C, s, *Ar4*), 169.44 (1C, s, CO_2Me), 169.96 (1C, s, CO_2Me).

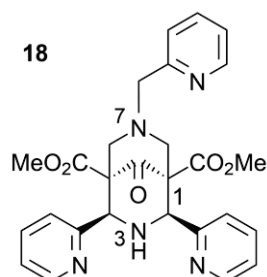
^1H NMR spectrum of **31a** (500 MHz, CDCl_3 , 298 K):



^{13}C -jmod NMR spectrum of **31a** (126 MHz, CDCl_3 , 298 K):

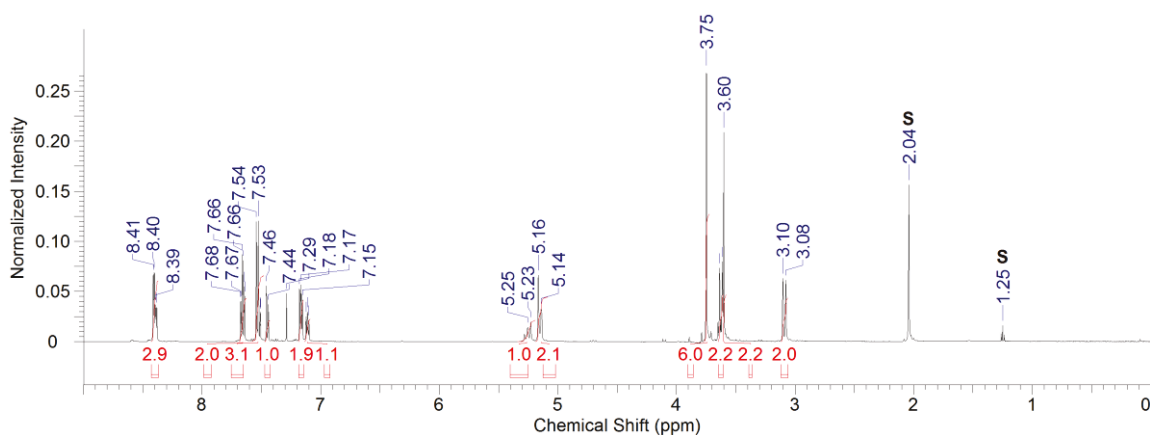


BISPIDINONE SECONDARY AMINES (C9=O, N-H)

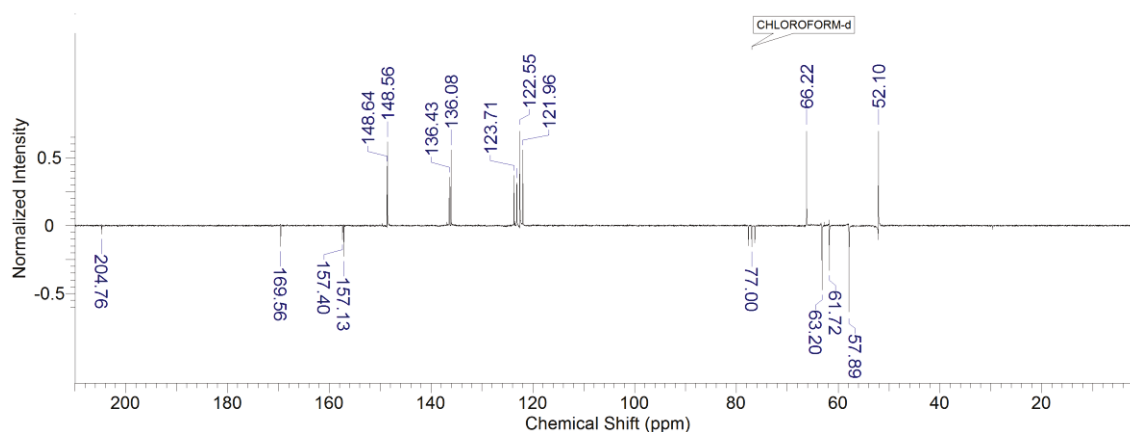
18 (N3-H, N7-pi bispidinone)* [211]

To a solution of NH-piperidinone **28s** (3.695 g, 10 mmol) in hot EtOH (100 ml) a 37 % aqueous solution of formaldehyde (1.962 g, 24 mmol, 2.4 eq) and picolyl amine (1.309 g, 12 mmol, 1.2 eq) were subsequently added. After 12 min of reflux, the reaction mixture was cooled down to RT and continued for 12 h. Then, all the volatiles were removed, residue re-dissolved in 10 ml of EtOH, 10 ml of water were added. After 2 days at 4 °C the resulting crystalline material suitable for x-ray analysis was isolated upon filtration and subsequent washing with - 40 °C EtOH and Et₂O, yielding 1.095 g of desired product (22 %). ¹H NMR (500 MHz, CDCl₃): δ=3.07 (2H, d, ²J=11.74, *H*-6/8 *eq*), 3.58 (2H, s, N7-CH₂py), 3.63 (2H, d, ²J=11.74, *H*-6/8 *ax*), 3.73 (6H, s, CO₂CH₃), 5.07 - 5.18 (2H, m, C, *H*-2/4), 5.21 - 5.27 (1H, m, N3-*H*), 7.10 - 7.12 (1H, m, N7-*Pi*4), 7.15 (2H, dd, *J*=7.34, 5.38, *Py*4), 7.45 (1H, d, *J*=7.83, N7-*Pi*6), 7.48 - 7.56 (3H, m, 2H from *Py*6, 1H from N7-*Pi*5) 7.64 (2H, td, *J*=7.83, 1.96, *Py*5), 8.39 (1H, d, *J*=3.91, N7-*Pi*3), 8.44 (2H, d, *J*=3.91, *Py*3) (3H, m). ¹³C-jmod NMR (50 MHz, CDCl₃): δ=52.10 (2C, s, CO₂CH₃), 57.89 (2C, s, C-6/8), 61.72 (2C, s, C-1/5), 63.20 (1C, N7-CH₂py), 66.22 (2C, s, C-2/4), 121.96 (1C, s, N7-*Pi*4), 122.55(2C, s, *Py*4), 123.14 (2C, s, *Py*6), 123.71 (1C, s, N7-*Pi*6), 136.08 (2C, s, N7-*Pi*5), 136.43 (1C, s, *Py*5), 148.56 (2C, s, *Py*3), 148.64 (1C, s, N7-*Pi*3), 157.13 (2C, s, *Py*1), 157.40 (1C, s, N7-*Pi*1), 169.56 (2C, s, CO₂Me), 204.76 (1C, s, C-9).

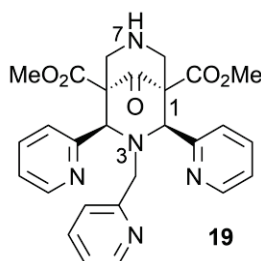
¹H NMR spectrum of **18** (500 MHz, CDCl₃, 298 K):



^{13}C -jmod NMR spectrum of **18** (50 MHz, CDCl_3 , 298 K):



19 (N3-pi, N7-H bispidinone)

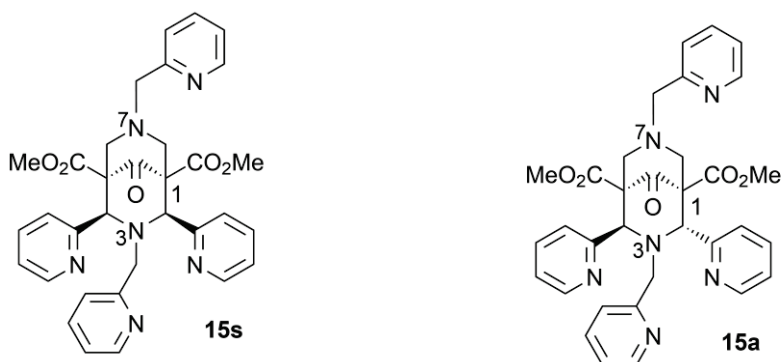


To a solution of **31s** (4.03 g, 6.18 mmol) in dry dichloromethane (100 ml), trifluoroacetic acid was added (20 ml). The reaction was sealed and stirred for 12 h in 35 – 40 °C. Then the reaction was basified on cooling with 2M sodium hydroxide solution and organic phase was separated. Water phase was extracted two times with dichloromethane (2 x 150 ml) and organic fractions were combined. After evaporation of the solvent under reduced pressure the residue was dissolved in a minimal quantity of hot acetonitrile and filtered before precipitating the desired product. After one hour at room temperature the resulting white solid was filtered off and washed with isopropanol and diethyl ether. Working up the filtrate led to the additional material which was combined with a first crop yielding 1.75 g (56 %) of a pure product. M.p. 191-192 °C. ^1H NMR (500 MHz, CDCl_3): δ =3.28 (2H, t, J =13.68, H -6/8 *eq.*), 3.50 (2H, s, N3- CH_2py), 3.64 (6H, s, CO_2CH_3), 4.19 (2H, d, J =12.82, H -6/8 *ax.*), 4.59 (1H, br. s., NH), 5.28 (2H, s, H -2/4), 6.93 (1H, d, J =7.69, N3- $\text{Pi}6$), 6.99 (1H, dd, J =6.63, 4.92, N3- $\text{Pi}4$), 7.15 (2H, m, $\text{Py}4$), 7.33 (2H, d, J =6.84, $\text{Py}6$), 7.42 (1H, td, J =7.69, 1.71, N3- $\text{Pi}5$), 7.60 (2H, td, J =7.69, 1.71, $\text{Py}5$), 8.31 (1H, d, J =4.27, N3- $\text{Pi}3$), 8.60 (2H, d, J =4.70, $\text{Py}3$). ^{13}C -jmod NMR (126 MHz, CDCl_3): δ =52.15 (1C, s, CO_2CH_3), 55.36 (2C, s, C -6/8), 56.80 (1C, s, N3- CH_2py), 64.55 (2C, s, C -2/4), 70.56 (2C, s, C -1/5), 121.44 (1C, s, N3- $\text{Pi}4$), 123.09 (2C, s, $\text{Py}4$), 124.05 (1C, s, N3- $\text{Pi}6$), 125.79 (2C, s, $\text{Py}6$), 135.38 (1C, s, N3- $\text{Pi}5$), 136.13 (2C, s, $\text{Py}5$), 148.46 (1C, s, N3- $\text{Pi}3$), 149.68 (2C, s, $\text{Py}3$), 156.78 (2C, s, $\text{Py}1$), 157.8 (1C, s, N3- $\text{Pi}1$), 168.86 (2C, s, CO_2Me), 203.2 (1C, s, C -9); IR (solution in DCM): ν_{max} = 3311 (NH), 3053-2852 (C-H), 1732 (C=O ester), 1710 (C=O ketone), 1589 (Ar), 1570 (Ar) cm^{-1} ; HRMS (ESI): m/z calcd for

reduced pressure. Drying at high vacuum yielded a yellowish solidifying oil which corresponded to the desired product with 15 % of impurity (as seen by ^1H NMR). The same compound could be obtained upon variation of catalyst (10 % Pd/C or Pd(OH)₂/C) and solvent (MeOH) with similar approximate quantities of by products around 15 – 30 %. ^1H NMR (500 MHz, CDCl₃) – only signals for the product are given: $\delta=2.92$ (2H, d, $J=11.00$, *H-6/8 eq*), 3.29 (2H, s, N7-CH₂Ar), 3.60 - 3.64 (5H, m, 3H from Ar-OCH₃, 2H from *H-6/8 ax*), 3.74 (6H, s, CO₂CH₃), 3.79 (s, 3H, Ar-OCH₃), 5.05 - 5.13 (2H, m, *H-2/4*), 5.20 (1H, t, $J=12.83$, NH), 6.26 (dd, $J=8.25, 2.75$, *Ar5*), 6.30 (d, $J=1.83$, 1H, *Ar-3*), 6.95 (d, $J=8.25$, 1H, *Ar-6*), 7.09 - 7.14 (2H, m, *Py4*), 7.48 - 7.55 (2H, m, *Py6*), 7.57 - 7.63 (2H, m, *Py5*), 8.36 (2H, d, $J=3.67$, *Py3*).

HEXADENTATE BISPIDINONE LIGANDS (C9=O)

15s* and 15a (N3,N7-dipicolyl bispidinone)

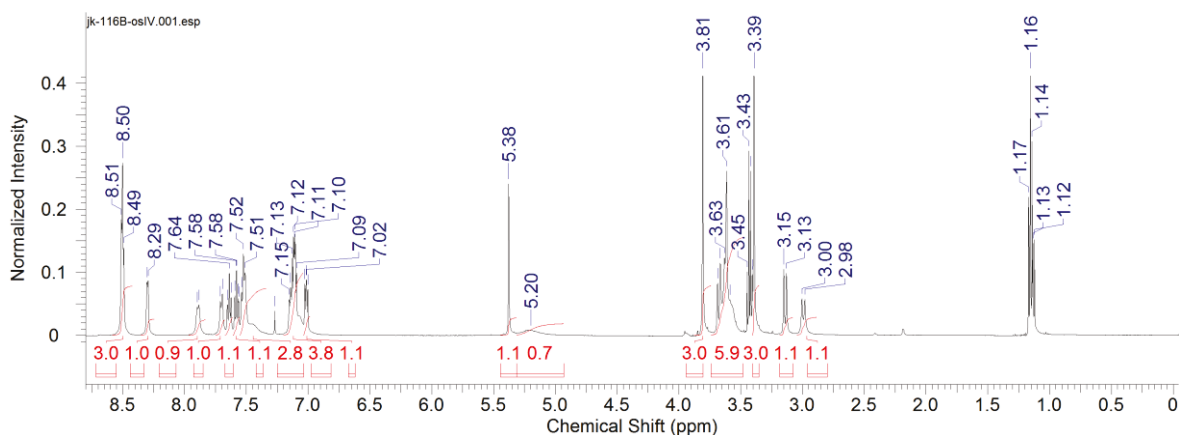


To a refluxed solution of piperidinone **29s** (5.814 g; 12,6 mmol) in THF, formaldehyde (37% solution in H₂O) (2.451 g; 30.2 mmol; 2.4 eq) and 2-(aminomethyl)pyridine amine (1.633 g; 15.1 mmol; 1.2 eq) were added. Then the reaction was stopped after 5h and all volatiles were evaporated under reduced pressure. The residue was dissolved in *i*PrOH and after the addition of diethyl ether the solution was left overnight in room temperature. The resulting white, crystalline solid was filtered off and washed with diethyl ether yielding 0.556 g of a pure anti-isomer. The subsequent workup of the remaining filtrate yielded 3.565 g of a pure trans isomer which was refluxed in 95% ethanol (50 ml) for 4h. Then, the volatiles were removed under reduced pressure and the pure syn isomer was crystallized from *i*PrOH / diethyl ether solution and combined with a first crop yielding together 1.196 g (16 %) of the desired product. For both isomers COSY, NOESY, HSQC and HMBC spectra were also acquired.

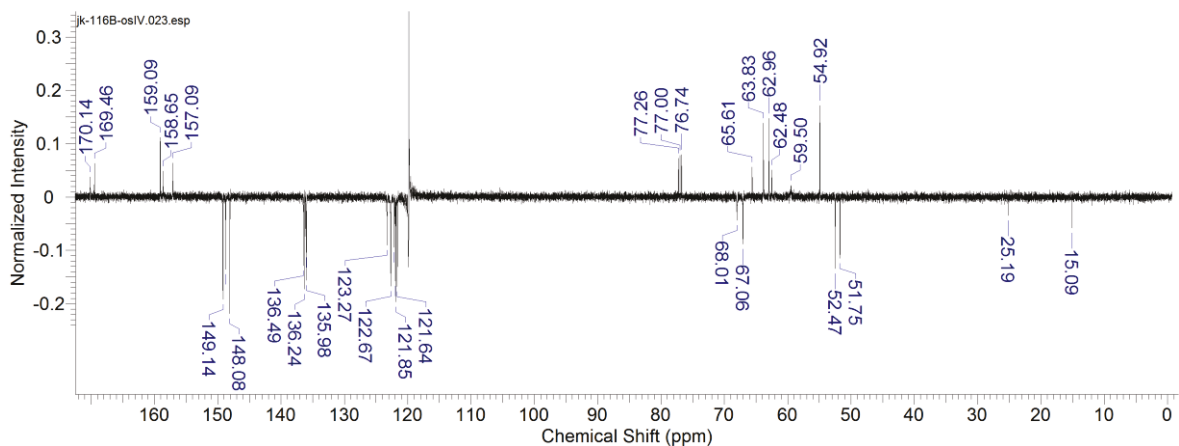
Syn isomer 15s. ¹H NMR (500 MHz, CDCl₃): δ=2.86 (2H, t, *J*=9.78, *H*-6/8 *eq.*), 3.42 (2H, m, *H*-6/8 *ax.*), 3.61 (2H, s, N7-CH₂py), 3.66 (6H, s, CO₂CH₃), 3.67 (2H, s, N3-CH₂py), 5.33 (2H, s, *H*-2/4), 6.73 (1H, d, *J*=6.85, N3-*Pi*6), 6.94 (1H, dd, *J*=6.85, 4.89, N3-*Pi*4), 7.03 (2H, dd, *J*=6.85, 4.89, *Py*4), 7.19 (1H, dd, *J*=6.85, 4.89, N7-*Pi*4), 7.35 (1H, tm, *J*=7.83, N3-*Pi*5), 7.40 (1H, d, *J*=7.82, N7-*Pi*6), 7.44 (2H, td, *J*=7.82, 1,96, *Py*5), 7.63 (1H, tm, *J*=7.83, N7-*Pi*5), 7.85 (2H, d, *J*=4.89, *Py*6), 8.38 (1H, d, *J*=4.89, N3-*Pi*3), 8.40 (2H, d, *J*=3.91, *Py*3), 8.55 (1H, d, *J*=4.89, N7-*Pi*3). ¹³C-jmod NMR (126 MHz, CDCl₃): δ=52.1 (2C, s, CO₂CH₃), 56.6 (1C, s, N3-CH₂py), 58.4 (2C, s, *C*-6/8), 62.83 (2C, s, *C*-1/5), 63.2 (1C, s, N7-CH₂py), 70.4 (2C, s, *C*-2/4), 121.3 (1C, s, N3-*Pi*4), 122.0 (1C, s, N7-*Pi*4), 122.4 (2C, s, *Py*4), 123.5 (1C, s, N3-*Pi*6), 123.9 (1C, s, N7-*Pi*6), 124.7 (2C, s, *Py*6), 135.3 (1C, s, N3-*Pi*5) 135.6 (2C, s, *Py*5), 136.0 (1C, s, N7-*Pi*5), 148.8 (3C, s, N3-*Pi*3, *Py*3), 149.1 (1C, s, N7-*Pi*3), 157.0 (1C, s, N3-*Pi*1) 157.1 (1C, s, N7-*Pi*1), 157.9 (2C, s, *Py*1), 168.7 (2C, s, CO₂Me), 203.1(1C, s, *C*-9). HRMS (ESI): *m/z* calcd for C₃₃H₃₃N₆O₅: 593.2507 [M+H]⁺; found: 593.2492; elemental analysis calcd (%) for C₃₃H₃₂N₆O₅: C 66.88, H 5.44, N 14.18; found: C 66.02, H 5.48, N 14.14.

C4py(eq)-Py6), 8.30 (1H, d, $J=3.91$, C4py(eq)-Py3), 8.46 - 8.54 (3H, m, C2py(ax)-Py3, N3-Pi3, N7-Pi3). ^{13}C -jmod NMR (126 MHz, CDCl_3): $\delta=51.75$ (1C, s, C1-CO₂CH₃), 52.47 (1C, s, C5-CO₂CH₃), 54.92 (1C, s, N3-CH₂py), 59.50 (1C, br. s, C-6), 61.85 (1H, br. s., C-1), 62.48 (1C, s, C-5), 62.96 (1C, s, N7-CH₂py), 63.83 (1C, s, C-8), 67.06 (1C, s, C-2), 68.28 (1C, br. s., C-4), 121.64 (1C, s, C2py(ax)-Py4), 121.85 (1C, s, N3-Pi4), 121.95 (1C, s, N7-Pi4), 122.12 (1C, s, C4py(eq)-Py4), 122.67 (1C, s, N3-Pi6), 122.76 (2C, br. m., C4py(eq)-Py6, C2py(ax)-Py6), 123.27 (1C, s, N7-Pi6), 135.98 (1C, s, C4py(eq)-Py5), 136.05 (1C, s, C2py(ax)-Py5), 136.24 (1C, s, N7-Pi5), 136.49 (1C, s, N3-Pi5), 148.08 (1C, s, C2py(ax)-Py3), 148.74 (1C, s, C4py(eq)-Py3), 149.16 (2C, br. s., N3-Pi3, N7-Pi3), 156.85 (1C, br. s., C2py(ax)-Py1), 157.09 (1C, s, N7-Pi1), 158.65 (1C, s, C4py(eq)-Py1), 159.09 (1C, s, N3-Pi1), 169.46 (1C, s, C1-CO₂Me), 170.14 (1C, s, C5-CO₂Me).

^1H NMR spectrum of **15a** (500 MHz, CDCl_3 , 298 K):



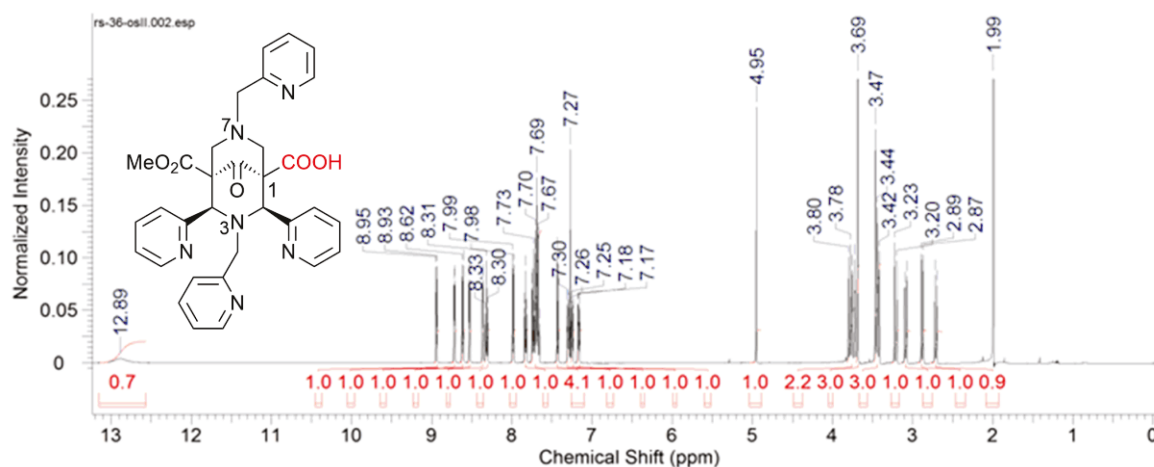
^{13}C -jmod NMR spectrum of **15a** (126 MHz, CDCl_3 , 298 K):



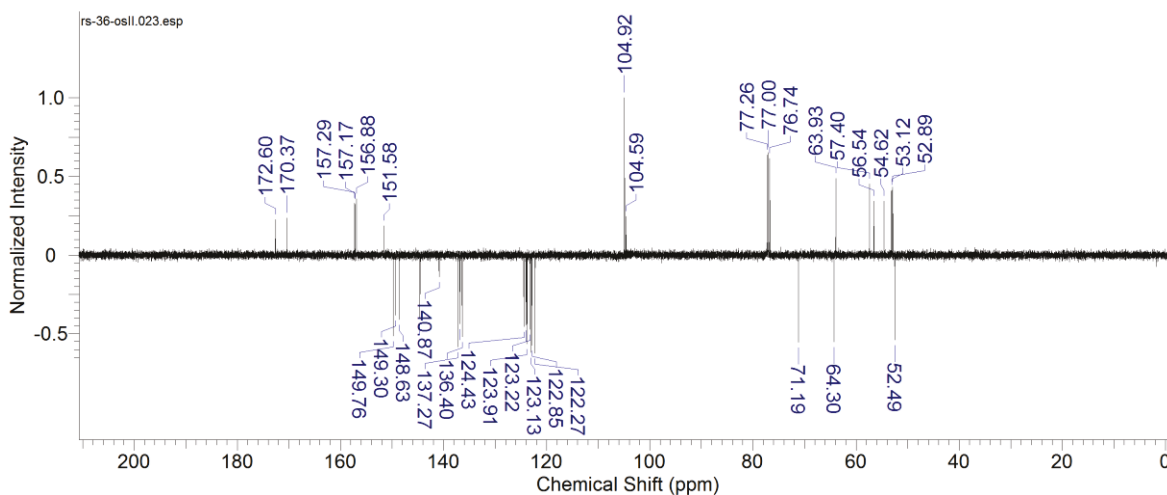
Monoacid 15-COOH. When the reaction mixture after 5 h of reflux was evaporated and re-dissolved in *i*PrOH/H₂O mixture and left for two months standing at RT, then a white precipitate formed on time. After filtration, washing with hot acetonitrile and drying, 1.9 g of pure compound

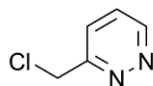
as a white, slightly yellowish solid were obtained (33 % yield). Compound was soluble in chloroform but insoluble in acetonitrile. COSY, HSQC and HMBC spectra were also acquired for this product to confirm the structure. DIMS (ESI): m/z 579 (100 %) $[M+H]^+$. ^1H NMR (500 MHz, CDCl_3): δ =2.71 (1H, d, J =11.97,) 2.88 (1H, d, J =12.82) 3.09 (1H, d, J =11.97) 3.21 (1H, d, J =14.53) 3.39 - 3.49 (3H, m) 3.69 (3H, s) 3.71 - 3.82 (2H, m) 4.95 (1H, s) 7.12 - 7.20 (1H, m) 7.22 - 7.27 (1H, m) 7.30 (1H, dd, J =6.84, 5.13) 7.43 (1H, d, J =7.69) 7.62 - 7.78 (4H, m) 7.80 - 7.86 (1H, m) 7.98 (1H, d, J =7.69) 8.31 (1H, t, J =7.69) 8.36 (1H, d, J =4.27) 8.53 (1H, d, J =4.27) 8.61 (1H, d, J =7.69) 8.72 (1H, d, J =4.27) 8.94 (1H, d, J =5.98) 12.89 (1H, br. s.). ^{13}C -jmod NMR (126 MHz, CDCl_3): δ =52.49, 52.89, 53.12, 54.62, 56.54, 57.40, 63.93, 64.30, 71.19, 104.59, 104.92, 122.27, 122.85, 123.13, 123.22, 123.83, 123.91, 124.04, 124.43, 136.40, 136.88, 137.27, 140.87, 144.59, 148.63, 149.30, 149.76, 151.58, 156.88, 157.17, 157.29, 170.37, 172.60. HRMS $\text{C}_{32}\text{H}_{31}\text{N}_6\text{O}_5$ calc. 579.2350, found 579.2339.

^1H NMR spectrum of **15-COOH** (500 MHz, CDCl_3 , 298 K):

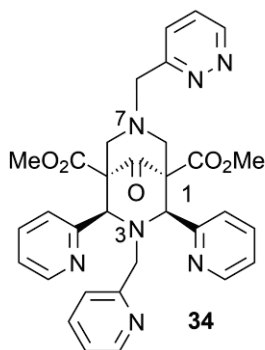


^{13}C -jmod NMR spectrum of **15-COOH** (126 MHz, CDCl_3 , 298 K):

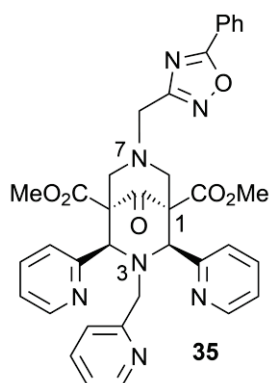


3-(Chloromethyl)pyridazine* [239]

To a refluxed solution of 3-methylpyridazine (1.000 g; 10.6 mmol) in chloroform (25 ml) trichloroisocyanuric acid (0.986 g; 4.2 mmol) was added in portions over 40 min. Then reaction was refluxed for 3 h, cooled down and reaction mixture filtered through a celite pad. The filtrate has been diluted with dichloromethane, washed with 1M NaOH (1 x 40 ml) and brine (1 x 40 ml), dried over Na₂SO₄ and solvent evaporated. The crude product was purified on Silica column (cyclohexane/ethyl acetate 2:1 and then 3:2) yielding pure 3-chloromethylpyridazine (158 mg; 12 %). The product was unstable on storage so it was used directly in the alkylation process (see below). ¹H NMR (200 MHz, CDCl₃): δ=4.81 (2H, s, CH₂Cl), 7.45 – 7.52 (1H, m, *Pdz6*), 7.62 – 7.68 (1H, m, *Pdz5*), 9.05 – 9.08 (1H, m, *Pdz4*).

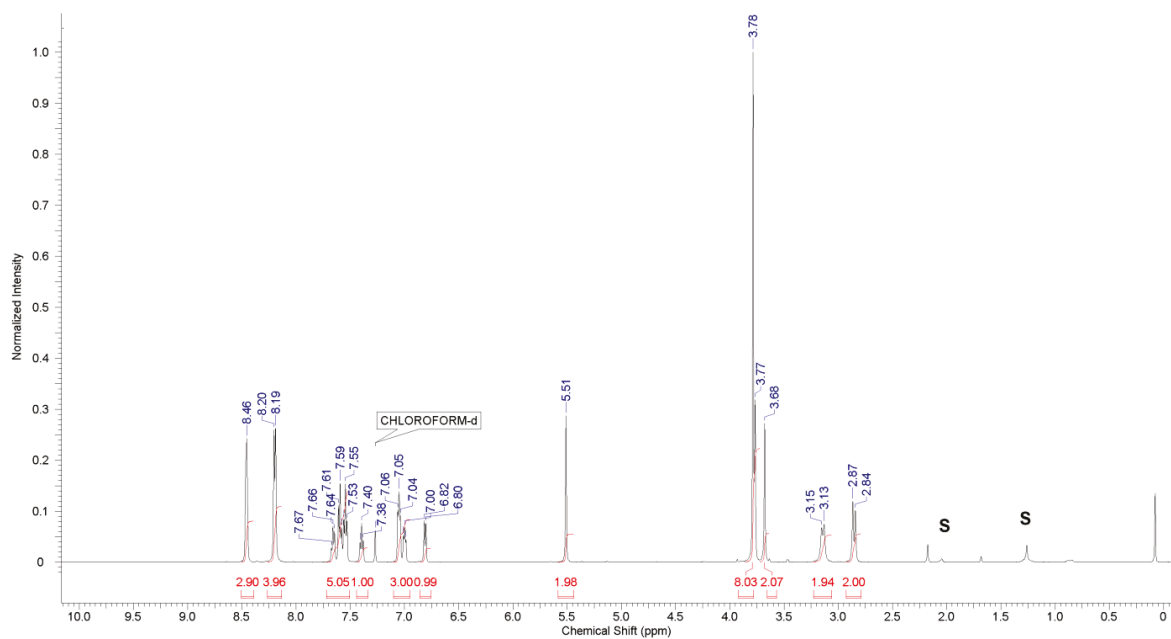
34 (N3-pi, N7-pdz bispidinone) pdz = pyridazine

To a solution of 3-(chloromethyl)pyridazine (129 mg; 1.00 mmol; 1.2 eq) in acetonitrile (15 ml) bispidinone **19** (418 mg; 0.83 mmol; 1 eq) was added followed by the drop-wise addition of DIPEA (190 mg; 1.47 mmol; 1.8 eq). Reaction was continued at room temperature for 72 h until a complete conversion of the main substrate. The solids were filtered and volatiles evaporated under reduced pressure. The residue was dissolved in chloroform and washed with brine and a saturated solution of NaHCO₃. The organic fraction was dried over anhydrous Na₂SO₄ and solvent evaporated. Obtained residue was purified by silica gel flash column chromatography (dichloromethane/*i*PrOH 10:1) yielding 260 mg (53%) of a pure product as a white solid. ¹H NMR (500 MHz, CDCl₃): δ=3.17 (2H, d, *J*=10.76, *H-6/8 eq.*) 3.68 (6H, s, CO₂CH₃) 3.72 (2H, s, N3-CH₂py) 3.91 (2H, br. s., *H-6/8 ax.*) 3.98 (2H, s, N7-CH₂pdz) 5.28 (2H, s, *H-2/4*) 6.77 (1H, d, *J*=7.83, N3-*Pi6*) 7.00 (1H, dd, *J*=6.85, 4.89, N3-*Pi4*) 7.08 (2H, dd, *J*=7.82, 4.89, *Py4*) 7.36 – 7.41 (1H, m, N3-*Pi5*) 7.44 - 7.52 (3H, m, *Pdz5*, 2H from *Py5*) 7.64 (2H, br. s., *Py6*) 7.74 (1H, d, *J*=7.83, *Pdz6*) 8.41 (1H, d, *J*=3.91, N3-*Pi3*) 8.44 (2H, d, *J*=2.93, *Py3*) 9.14 (1H, d, *J*=3.91, *Pdz4*). ¹³C NMR (126 MHz, CDCl₃): δ=52.4 (2C, s, CO₂CH₃), 55.83 (N3-CH₂py), 57.78 (*C-6/8*), 61.12 (N7-CH₂pdz) 63.6 (*C-1/5*), 70.8 (*C-2/4*), 121.4 (N3-*Pi4*), 122.8 (*Py4*), 123.4 (N3-*Pi6*), 125.4 (*Py6*),

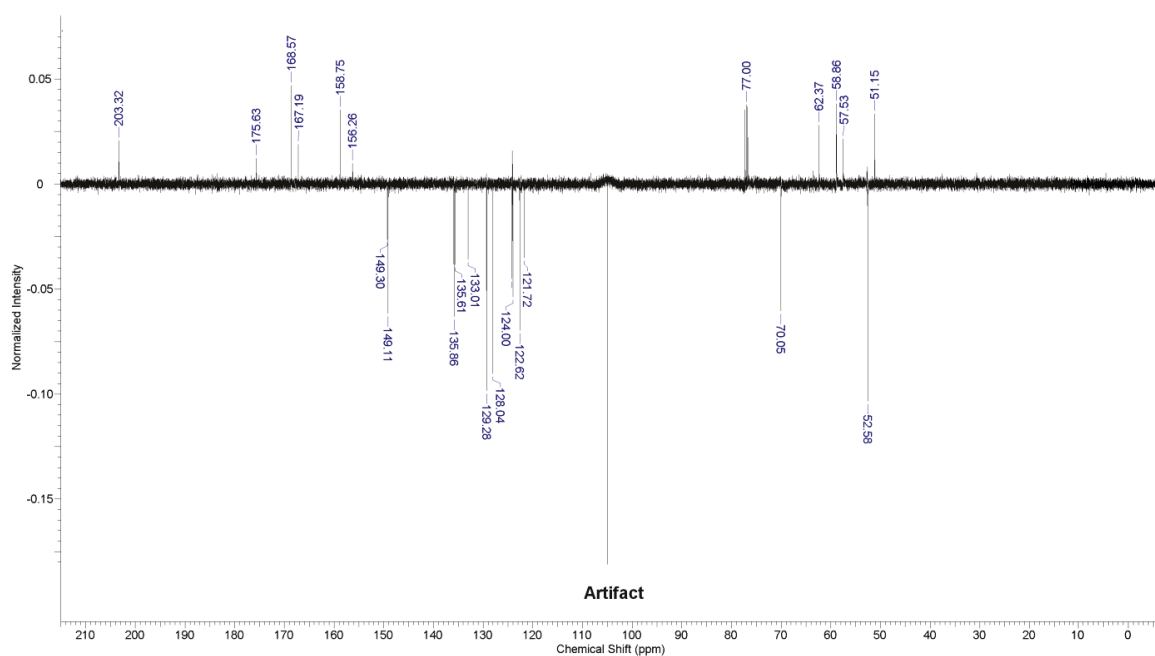
35 (N3-pi, N7-oxdz bispidinone) oxdz = oxadiazole

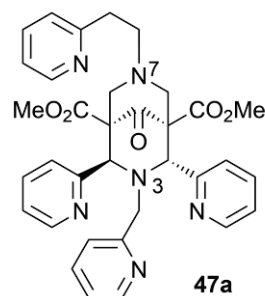
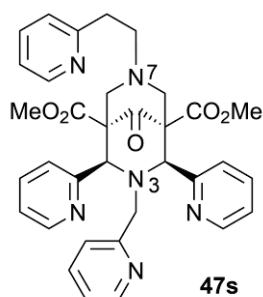
To a solution of bispidinone **19** (300 mg; 0.60 mmol) and 3-(chloromethyl)-5-phenyl-1,2,4-oxadiazole (131 mg; 0.67 mmol; 1.1 eq) in acetonitrile (30 ml) DIPEA (107 mg; 0.83 mmol; 1.4 eq) was added and reaction was refluxed for 24 h. All volatiles were evaporated and the residue was re-dissolved in DCM and washed with brine and saturated solution of NaHCO₃. Organic phase was dried over anhydrous Na₂SO₄ and solvent was evaporated. The white solid crystallized from hot methanol (or methanol / diethyl ether mixture or isopropanol) and was washed with methanol and diethyl ether yielding 136 mg (46%) of a pure product. Workup of the filtrate (crystallization from isopropanol or methanol/diethyl ether mixture) yielded the additional material. ¹H NMR (500 MHz, CDCl₃): δ=2.85 (2H, d, *J*=11.97, *H*-6/8 *eq*), 3.14 (2H, d, *J*=11.11, *H*-6/8 *ax*), 3.68 (2H s, N7-CH₂oxdz), 3.77 (2H, s, N3-CH₂py), 3.78 (6H, s, CO₂CH₃), 5.51 (2H, s, H-2,4), 6.81 (1H, d, *J*=7.69, N3-*Pi*6), 7.00 (1H, t, *J*=5.98, N3-*Pi*4), 7.02 - 7.04 (2H, m, *Py*4), 7.39 (1H, t, *J*=7.27, N3-*Pi*5), 7.54 (2H, t, *J*=7.27, *Py*5), 7.57 - 7.60 (2H, m, *Ar*3), 7.63 - 7.66 (1H, m, *Ar*4), 8.19 (4H, d, *J*=7.69, 2H from *Ar*2, 2H from *Py*6), 8.46 (3H, br. s., 2H from *Py*3, N3-*Pi*3). ¹³C NMR (126 MHz, CDCl₃): δ=51.2 (1C, s, N7-CH₂oxdz), 52.6 (CO₂CH₃), 57.5 (1C, s, N3-CH₂py), 58.9 (2C, s, C-6/8), 62.4 (2C, s, C-1/5), 70.0 (2C, s, C-2/4), 121.7 (1C, s, N3-*Pi*4), 122.6 (2C, s, *Py*4), 124.0 (1C, s, N3-*Pi*6), 124.1 (1C, s, *Ar*1), 124.2 (2C, s, *Py*6), 128.0 (2C, s, *Ar*2), 129.3 (2C, s, *Ar*3), 133.0 (1C, s, *Ar*4), 135.6 (1C, s, N3-*Pi*5), 135.9 (2C, s, *Py*5), 149.1 (2C, s, *Py*3), 149.3 (1C, s, N3-*Pi*3), 156.3 (1C, s, N3-*Pi*1), 158.8 (2C, s, *Py*1), 167.2 (1C, s, *Oxdz*5), 168.6 (2C, s, CO₂Me), 175.6 (1C, s, *Oxdz*3), 203.3 (1C, s, C-9). HRMS (ESI): *m/z* calcd for C₃₆H₃₄N₇O₅: 660.2565 [M+H]⁺; found 660.2529.

^1H NMR spectrum of **35** (500 MHz, CDCl_3 , 298 K):



^{13}C -jmod NMR spectrum of **35** (126 MHz, CDCl_3 , 298 K):



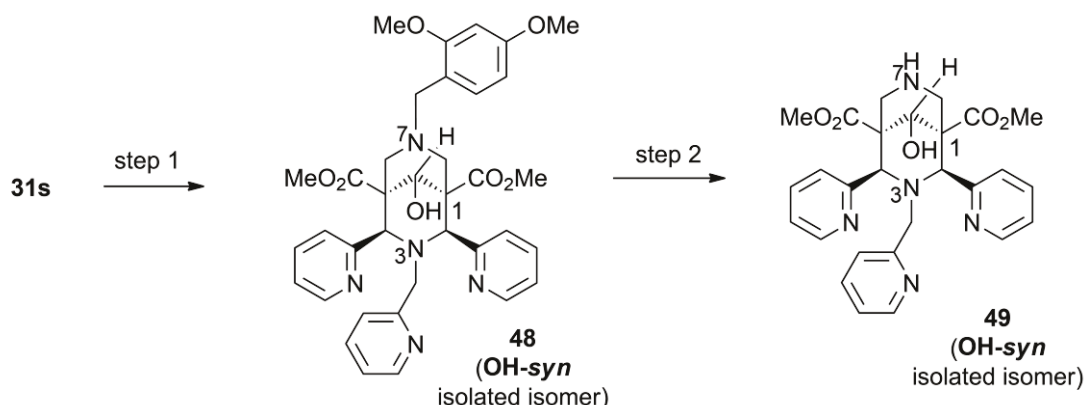
47s and 47a (N3-pi, N7-Etpy bispidinone)

To a refluxed solution of piperidinone **29s** (5.147 g, 11.2 mmol) in tetrahydrofuran, formaldehyde (37% solution in H₂O) (2.451 g, 28.6 mmol, 2.5 eq) and 2-(aminoethyl)pyridine amine (1.660 g; 13.6 mmol; 1.2 eq) were added. Then the reaction was stopped after 4.5 h and all volatiles were evaporated under reduced pressure and residue was resuspended in EtOH and refluxed. After 5 min he precipitate was formed which was then filtered off after 1 h (pure anti isomer) and the volatiles from the filtrate were evaporated under reduced pressure. Subsequent recrystallization from refluxing (1 h) *i*PrOH, led to the isolation of additional material, which was confirmed to be trans isomer. Third recrystallization also from *i*PrOH gave a white solid which was a mixture of the isomers. This was then dissolved in minimal quantities of MeOH and after 7 days in 4 °C pure syn isomer was isolated. Yield: 60 % (anti isomer) and 2 % (syn isomer). Both configurational isomers were characterized additionally by COSY, NOESY, HSQC and HMBC NMR experiments.

Syn isomer 47s. ¹H NMR (500 MHz, CDCl₃): δ=2.70 - 2.84 (4H, m, 2H from N7-CH₂CH₂py, 2H from H-6/8 eq) 2.90 - 2.97 (2H, m, N7-CH₂CH₂py) 3.23 (2H, br. s., H-6/8 ax) 3.76 (2H, s, N3-CH₂py) 3.78 (6H, s, CO₂CH₃) 5.44 (2H, s, H-2/4) 6.80 (1H, d, *J*=7.83, N3-Pi6) 6.95 - 7.08 (1H, m, N3-Pi4) 7.12 - 7.20 (4H, m, 2H from Py4, N7-EtPy4, N7-EtPy6) 7.42 (1H, td, *J*=7.83, 1.96, N3-Pi5) 7.56 - 7.66 (1H, m, N7-EtPy5) 7.70 (2H, td, *J*=7.82, 1.96, Py5) 8.09 (2H, d, *J*=7.83, Py6) 8.45 (1H, d, *J*=3.91, N3-Pi3) 8.51 (2H, d, *J*=4.89, Py3) 8.56 (1H, d, *J*=4.89, N7-EtPy3). ¹³C NMR (126 MHz, CDCl₃): δ=34.95, 52.56, 57.23, 57.64, 58.74, 62.61, 70.43, 121.33, 121.68, 122.74, 123.26, 123.99, 124.63, 135.62, 135.99, 136.40, 149.14, 149.22, 149.29, 158.67, 159.97, 168.96, 203.64.

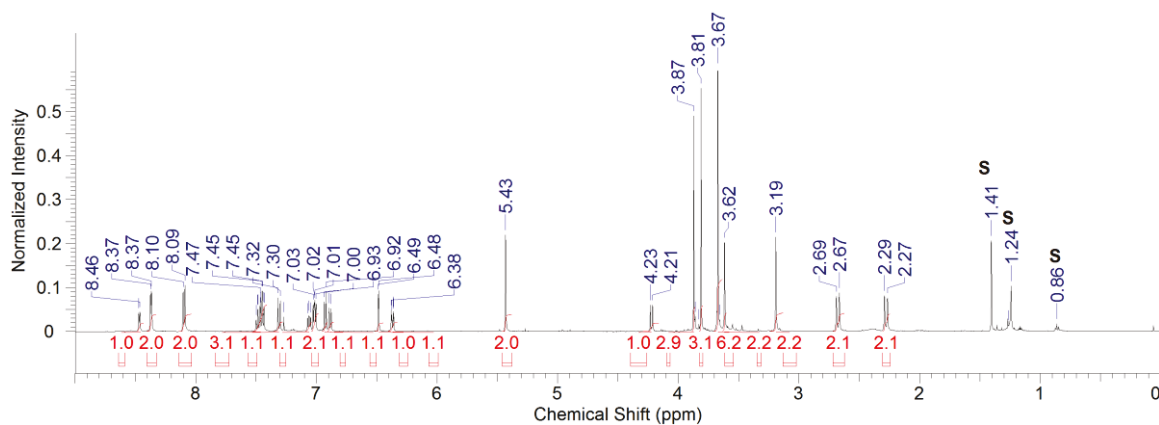
Anti isomer 47a. ¹H NMR (200 MHz, CDCl₃): δ=2.31 - 2.53 (1H, m) 2.55 - 2.77 (3H, m) 2.83 - 2.96 (2H, m) 3.08 (1H, d, *J*=10.56) 3.42 - 3.50 (3H, m) 3.56 - 3.80 (5H, m) 3.86 (3H, s) 3.88 - 4.00 (1H, m) 5.37 (1H, s) 5.59 (1H, br. s.), 6.93 - 7.21 (5H, m), 7.34 - 7.46 (1H, m), 7.50 - 7.77 (6H, m), 8.41 (1H, d, *J*=3.91) 8.48 (1H, d, *J*=4.70) 8.55 (2H, d, *J*=4.70). ¹³C NMR (126 MHz, CDCl₃): δ=35.35 (1C, s, N7-CH₂CH₂py), 51.82 (1C, s, C1-CO₂CH₃) 52.75 (1C, s, C5-CO₂CH₃), 54.91 (1C, s, N3-CH₂py), 55.97 (1C, s, N7-CH₂CH₂py), 58.92 (1C, br. s., C-6), 62.26 (1C, br. s. C-5), 63.73 (1C, s, C-8), 66.91 (1C, s, C-2), 67.69 (1C, br. s. C-4), 119.90 (s) + 121.09 (s) + 121.64 (s) + 121.83-121.95 (m) + 122.33 (s) + 123.05 (s) => (8C, 4x Py4, 4x Py6), 136.11 (1C, s) + 136.35 (1C, s) + 136.49 (1C, s) + 136.60 (1C, s) => (4C, Py5), 148.25 (1C, s) + 148.70 (1C, s) + 149.20 (1C, s) + 149.50 (1C, s) => (4C, Py3), 159.00 (s) + 159.22 (s) + 159.51 (s) => (4C, Py1), 169.90 (1C, s, C1-CO₂Me), 170.78 (1C, s, C5-CO₂Me).

BISPIDINOLS (C9-OH)

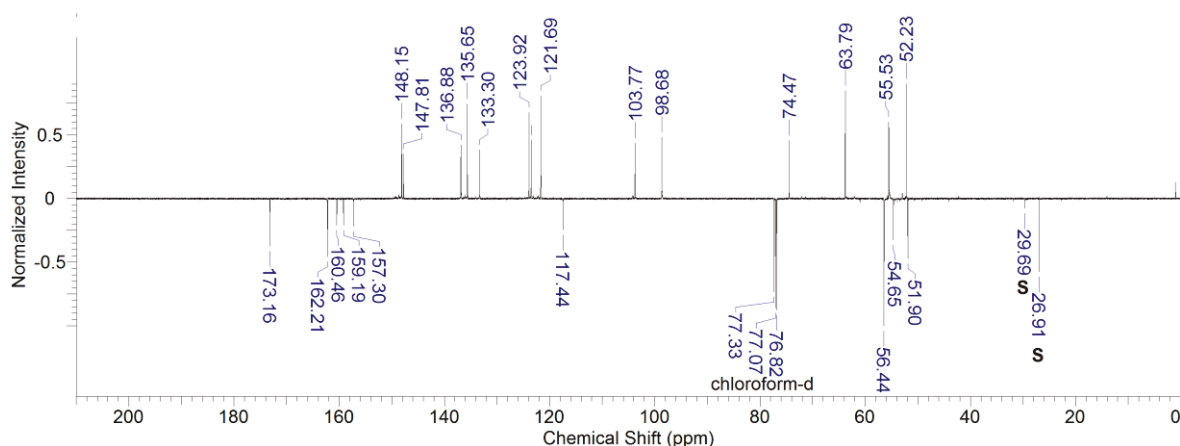
48 and 49 (N3-pi, N7-DMB bispidinol and N3-pi, N7-H bispidinol)

Method A, step one – reduction (48). Methanol (2 mL) was added to a dry flask containing DMB-protected bispidinone **31s** (200 mg, 0.3 mmol). The solution was heated to 100 °C and sodium cyanoborohydride (100 mg, 1.5 mmol), followed by 1 h. of heating at reflux until LCMS showed conversion to a single reduced product. The solvent was then removed on vacuum and the resulting solid dissolved in CHCl₃ (10 mL). This was washed with H₂O (10 mL), NaHCO₃ solution (10 mL) and H₂O (10 mL). The aqueous phase was the back-extracted with CHCl₃ (10 mL). The combined organic fractions were dried (Na₂SO₄), filtered, evaporated and the crude orange oil was purified on Alumina (CHCl₃:cyclohexane:Methanol 75:20:5) to give the white powder of 12 (30 mg, 15%) – **48 OH-syn isomer**. M.p. 162-163 °C; IR ν_{\max} (solution in DCM) 3448 (br, O-H), 3056, 2951, 2839 (C-H), 1745 (C=O ester), 1610, 1589, 1512 (Ar) cm⁻¹. ¹H NMR (500 MHz, CDCl₃): δ =2.28 (2H, d, J =11.97, H -6/8 *ax.*), 2.68 (2H, d, J =11.97, H -6/8 *eq.*), 3.19 (2H, s, N7-CH₂Ar), 3.62 (2H, s, N3-CH₂py), 3.67 (6H, s, CO₂CH₃), 3.81 (3H, s, Ar4-OCH₃), 3.87 (3H, s, Ar2-OCH₃), 4.22 (1H, d, J =8.55, H -9), 5.43 (2H, s, H -2/4), 6.37 (1H, dd, J =8.12, 2.14, Ar 5), 6.47 (1H, s, Ar 3), 6.89 (1H, d, J =7.69, N3- Pi 6), 6.93 (1H, d, J =8.55, Ar 6), 7.02 (2H, t, J =5.98, Py 4), 7.07 (1H, t, J =5.13, N3- Pi 4), 7.31 (1H, d, J =9.40, OH, in COSY interacts with H -9 – 4.22 ppm), 7.45 (2H, t, J =7.69, Py 5), 7.49 (1H, t, J =7.69, N3- Pi 5), 8.10 (2H, d, J =7.69, Py 6), 8.38 (2H, m, Py 6), 8.47 (1H, d, J =3.42, N3- Pi 3). ¹³C-jmod NMR (126 MHz, CDCl₃): δ =51.90 (2C, s, C -1/5), 52.23 (2C, s, CO₂CH₃), 54.65 (1C, s, N3-CH₂py), 55.47 (1C, s, Ar-OCH₃), 55.53 (1C, s, Ar-OCH₃), 56.44 (3C, s, 1C from N7-CH₂Ar, 2C from C -6/8), 63.79 (2C, s, C -2/4), 74.47 (1C, s, C -9), 98.68 (1C, s, Ar 3), 103.77 (1C, s, Ar 5), 117.44 (1C, s, Ar 1), 121.66 (1C, s, N3- Pi 4), 121.69 (2C, s, Py 4), 123.52 (1C, s, N3- Pi 6), 123.92 (2C, s, Py 6), 133.30 (1C, s, Ar 6), 135.65 (2C, s, Py 5), 136.88 (1C, s, N3- Pi 5), 147.81 (1C, s, N3- Pi 3), 148.15 (2C, s, Py 3), 157.29 (1C, s, N3- Pi 1), 159.19 (1C, s, Ar 2), 160.46 (1C, s, Ar 4), 162.21 (2C, s, Py 1), 173.16 (2C, s, CO₂Me); DIMS m/z (ES-API) 654 (100 %) [M+H]⁺; HRMS C₃₆H₄₀N₅O₇ calc. 654.2922, found 654.2914, Anal. calc. for C₃₆H₃₉N₅O₇: C 66.19, H 6.02, N 10.72, found: C 64.77, H 6.10, N 10.40 %.

^1H NMR spectrum of **48** (**OH-syn** isomer) (500 MHz, CDCl_3 , 298 K):



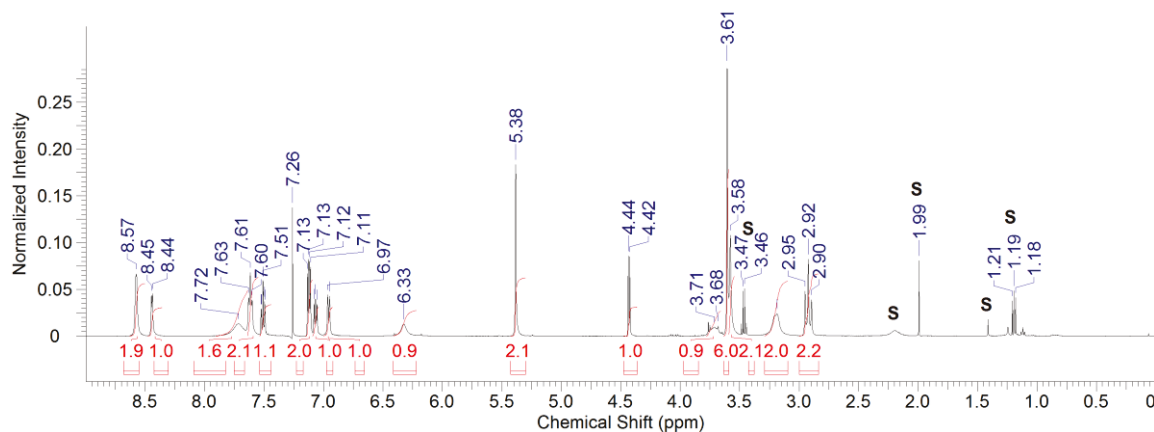
^{13}C -jmod NMR spectrum of **48** (**OH-syn** isomer) (126 MHz, CDCl_3 , 298 K):



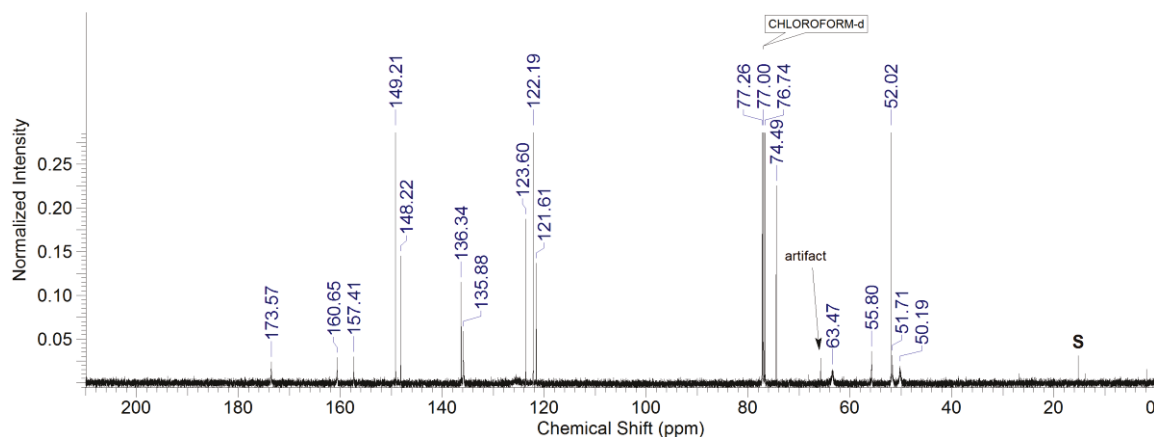
Method A, step 2 – deprotection (49). To the solution of **48** (0.642 g) in dry DCM (15 mL) trifluoroacetic acid (4 mL) was slowly added under inert atmosphere. After 30 min. of heating at 35 °C, a further aliquot (2 mL) of the TFA was added, and repeated after further 15 min (1 mL), until MS showed complete deprotection. The resulting solution was worked up with sodium hydroxide solution (2 M) until pH = 10. The mixture was extracted with DCM (3 x 30 mL), dried (Na_2SO_4), filtered and the solvent removed in vacuum. The resulting crude material was re-crystallized from MeCN (5 mL) after heating at reflux for 10 min followed by filtration of hot reaction mixture. Washing of the solid with Et_2O gave the white crystalline solid => **49** (0.252 g, 51%) – **OH-syn isomer**. M.p. 180-181 °C; IR ν_{max} (solution in DCM) 3455 (br, O-H), 3303 (N-H), 3055, 2949 (C-H), 1734 (C=O ester), 1589, 1570 (Ar) cm^{-1} . ^1H NMR (500 MHz, CDCl_3): δ =2.92 (2H, t, J =13.68, *H*-6/8 *ax.*), 3.19 (2H, br s, *H*-6/8 *eq.*), 3.58 (2H, s, NCH_2pi), 3.61 (6H, s, CO_2CH_3), 3.71 (1H, br s, *NH*), 4.43 (1H, d, J =6.84, *H*-9), 5.38 (2H, s, *H*-2/4), 6.33 (1H, br s, *OH*), 6.96 (1H, d, J =7.69, *Pi*6), 7.07 (1H, m, *Pi*4), 7.12 (2H, m, *Py*4), 7.51 (1H, td, J =7.69, 1.71, *Pi*5), 7.62 (2H, t, J =7.27, *Py*5), 7.72 (2H, br s, *Py*6), 8.44 (1H, d, J =4.27, *Pi*3), 8.57 (2H, s, *Py*3). ^{13}C NMR (126 MHz, CDCl_3): δ =50.19 (2C, br. s, *C*-6/8), 51.71 (2C, s, *C*-1/5), 52.02 (2C, s, CO_2CH_3), 55.80 (1C, s, *N*3- CH_2py),

63.47 (2C, br. s, C-2/4), 74.49 (1C, s, C-9), 121.61 (1C, s, Pi4), 122.19 (2C, s, Py4), 123.60 (2C, s, Py6), 135.88 (2C, s, Py5), 136.34 (1C, s, Pi5), 148.22 (1C, s, Pi3), 149.21 (2C, s, Py3), 157.41 (1C, s, Pi1) 160.65 (2C, s, Py1) 173.57 (2C, br. s, CO₂Me). DIMS (ES-API) m/z 504 (100 %) [M+H]⁺, 526 (5 %) [M+Na]⁺; HRMS C₂₇H₃₀N₅O₅ calc. 504.2241, found 504.2228.; Anal. calc. for C₂₇H₂₉N₅O₅: C 64.44, H 5.81, N 13.92, found: C 63.46, H 5.83, N 13.98 %.

¹H NMR spectrum of **49** (OH-*syn* isomer) (500 MHz, CDCl₃, 298 K):



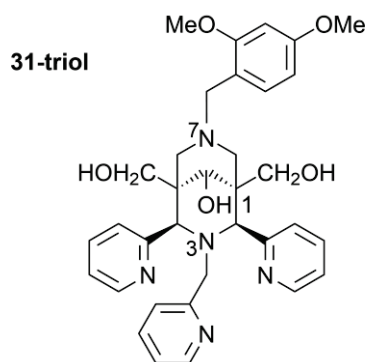
¹³C NMR spectrum of **49** (OH-*syn* isomer) (126 MHz, CDCl₃, 298 K):



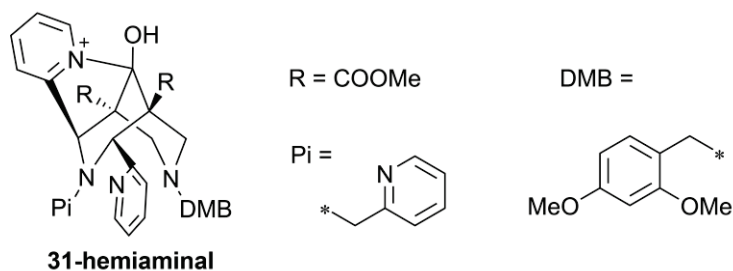
Method B, alternative two-step synthesis of **49.** To a solution of bispidinone 31s (2.426 g, 3.72 mmol) in 130 ml of dry THF a 5 ml of 1M solution of BH₃*THF in THF was added at 0 °C under inert gas atmosphere. After 1 h conversion of the starting material was completed (by DIMS). Subsequently, 20 ml of 1 M solution of HCl in MeOH were added and reaction stirred for 5 h at RT. The resulting solid was filtered off, re-dissolved in MeOH, stirred for 1 h and evaporated to dryness yielding 1.353 g of the solidifying residue of over 90 % purity in the respect to the desired product. DIMS (ESI) m/z = 654 (100) [M+H]⁺, 668. This mixture (1.350 g) has been then used for deprotection reaction, upon the addition of TFA (10 ml) to its solution in dry DCM at 40 °C. After

2.5 h when no starting material could be observed upon DIMS analysis, 100 ml of water and 100 ml of DCM were added and the reaction mixture was basified to the pH of 9 by 2 M aqueous solution of NaOH. Upon intensive stirring for 15 min, the organic phase was separated and the aqueous phase extracted 2 more times with DCM. Organic fractions were combined (500 ml), dried over anhydrous Na₂SO₄ and the volatiles were removed under reduced pressure. Recrystallization of the residue (MS m/z = 504 (100) [M+H]⁺, 654, 624, 626, 596, 476 (all < 10 %) from hot acetonitrile yielded 0.694 mg of the pure desired product **49** as a white needle-like crystalline solid (1.378 mmol, 37 % over two steps). The ¹H and ¹³C NMR are identical with the spectra of **49 OH-syn** isomer obtained by *Method A*. DIMS (ESI) m/z = 504 (100) [M+H]⁺ - pure product.

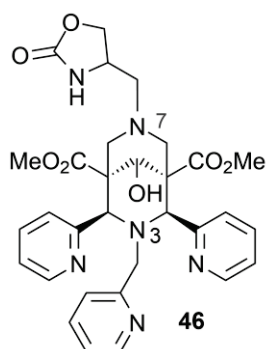
31-triol (N3-pi, N7-DMB bispidine-triol)



To a suspension of lithium aluminum hydride (115 mg, 3.04 mmol) in THF (10 mL), bispidinone **8** (500 mg, 0.76 mmol) was added as a suspension in THF (10 mL) at 0°C. The mixture was then heated at reflux upon which a color change to orange occurred. After 1 h the solution was cooled to 0 °C, the excess LiAlH₄ destroyed with water (1 mL) and the THF evaporated in vacuum. The organic product was then extracted with DCM (2 x 5 mL) and hot DCM (5 mL), dried (Na₂SO₄), filtered and the solvent evaporated to give the crude material of **16** (375 mg, 83 %). The purity of the product was estimated to be 80 % by NMR. ¹H NMR (500 MHz, CDCl₃): δ=1.63 (2H, d, J=11.97, C-6/8 ax.), 2.30 (2H, d, J=11.97, C-6/8 eq.), 3.09 (2H, s, N7-CH₂Ar), 3.49 (6H, m, 4H from CH₂OH, 2H from N3-CH₂py), 3.75 (3H, s, Ar2-OCH₃), 3.89 (3H, s, Ar4-OCH₃), 3.90 (1H, s, H-9), 4.86 (2H, s, H-2/4), 5.20 (2H, s, CH₂OH), 6.29 (1H, dd, J=8.55, 2.56, Ar5), 6.48 (1H, d, J=2.56, Ar3), 6.75 (1H, d, J=7.69, N3-Pi6), 6.85 (1H, d, J=7.69, Ar6), 6.93-7.02 (3H, m, 1H from N3-Pi4, 2H from Py4), 7.35-7.44 (3H, m, 1H from N3-Pi5, 2H from Py5), 8.18 (2H, d, J=7.69, Py6), 8.28 (2H, d, J=5.13, Py3), 8.32 (1H, d, J=4.27, N3-Pi3). ¹³C NMR (126 MHz, CDCl₃): δ=42.6 (C-1/5), 55.2 (1C, s, Ar2-OCH₃), 55.4 (1C, s, Ar4-OCH₃), 55.5 (2C, s, N3-CH₂pi), 56.6 (C-6/8), 56.8 (N7-CH₂Ar), 65.5 (C-2/4), 67.5 (2C, s, CH₂OH), 76.87 (1C, s, C-9), 98.4 (1C, s, Ar3), 103.4 (1C, s, Ar5), 117.8 (1C, s, Ar1), 121.3 (1C, s, N3-Pi4), 121.6 (1C, s, Py4), 123.4 (1C, s, N3-Pi6), 124.4 (2C, s, Py6), 133.0 (1C, s, Ar6), 135.8 (2C, s, Py5), 136.5 (1C, s, N3-Pi5), 147.3 (1C, s, N3-Pi3), 147.3 (2C, s, Py3), 157.4 (1C, s, N3-Pi1), 158.9 (1C, s, Ar4), 160.1 (1C, s, Ar2), 162.7 (2C, s, Py1). DIMS (ES-API) m/z : 598 (100 %) [M+H]⁺.

31-hemiaminal (N3-pi, N7-DMB bispidine-hemiaminal)

Mixture of syn and anti isomer (ratio 0.12 : 1) of bispidinone-DMB (496 mg, 0.761 mmol) in CHCl_3 (5 ml) was treated with 1 ml of 1 M solution of HCl in Et_2O . The reaction was refluxed for 6 h and the appearing white precipitate was filtered yielding 293 mg of a pure product (59 %). Two dimensional COSY, HSQC and HMBC experiments were performed in addition to ^1H and ^{13}C NMR, confirming the structure of the product. ^1H NMR (500 MHz, DMSO-d_6): δ =3.43 (1H, d, J =13.69) 3.54 (3H, s) 3.60 (1H, br. s.,) 3.65 (3H, s) 3.82 (3H, s) 3.86 (3H, s) 3.94 (d, J =12.72, 1H) 4.35 (1H, d, J =10.76) 4.44 (1H, br. s.) 4.66 (2H, br. s.) 4.75 (1H, br. s.) 5.51 (1H, br. s.) 6.68 - 6.87 (2H, m) 6.96 - 7.13 (2H, m) 7.23 (1H, br. s.) 7.60 - 7.82 (3H, m, 3H) (br. s., 1H) 8.35 (2H, s) 8.56 (1H, br. s.) 8.75 (1H, br. s.) 8.94 (1H, br. s.) 9.23 (1H, br. s.) 11.41 (1H, br. s.). ^{13}C NMR (126 MHz, DMSO-d_6): δ =53.73, 53.97, 55.63, 55.66, 56.01, 58.42, 66.43, 98.89, 106.18, 109.37, 124.57, 124.80, 125.54, 134.36, 138.53, 159.65, 162.50, 165.34, 165.74. No signal from the keto C-9 is in agreement with a formation of hemiaminal. HRMS $\text{C}_{36}\text{H}_{38}\text{N}_5\text{O}_7$ calc. 652.2766, found 652.2755.

46 (N3-pi, N7-odz bispidinone) – odz = oxazolidinone

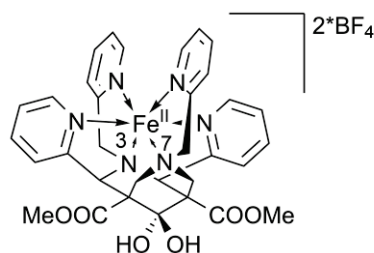
10 ml of dry, degassed acetonitrile were added to a dried flask containing bispidinol 49 (110 mg, 0.218 mmol), 1 equivalent of tosylate of hydroxymethyl oxazolidinone (59 mg, 0.218 mmol) and two equivalents of potassium carbonate (60 mg, 0.435 mmol). After 6 h of reflux no starting material remained so the reaction mixture was cooled down to RT, salts were filtered off and filtrate evaporated. The residue was taken into DCM and the remaining precipitate was filtered off again. After the evaporation of the volatiles, 120 mg of the crude product with almost no NMR-detectable impurities (around 5 %) was obtained (91 % yield). DIMS m/z = 603 (100 %) $[\text{M}+\text{H}]^+$.

The non-equivalence of some of the signals in this NMR spectrum (for example two methyl groups from esters in position 1,5 of the bispidine backbone) may stem from the loss of symmetry of the bispidine ligand upon oxazolidinone grafting. However, more probably it is a consequence of the diastereoisotopic mixture of the oxazolidinone precursor at stereogenic center *odz1*. ¹H NMR (200 MHz, CDCl₃): δ=1.96 – 2.28 (2H, m) + 2.36 (1H, d) + 2.54 (2H, br. s.) + 3.16 (1H, v. br. s.) => (6H, 4H from H-6/8, 2H from N7-CH₂odz), 3.66 (5H, s, 3H from CO₂CH₃, 2H from N3-CH₂py), 3.70 (4H, br. s., 3H from CO₂CH₃ + 1H of *Ozd1*), 3.84 (1H, dd, *J*=8.88, 4.78, 1x *Ozd5 eq*), 4.25 (1H, d, *J*=8.88, *H-9*), 4.37 (1H, t, *J*=8.19, 1 H, 1x *Ozd5 ax*), 5.44 (2H, d, *J*=5.46, *H-2/4*), 6.88 (1H, d, *J*=7.51, N3-*Pi4*), 6.97 - 7.34 (4H, m, 1x N3-*Pi6*, 2x *Py4*), 7.41 - 7.83 (4H, m, 1x N3-*Pi5*, 2x *Py5*), 8.05 (1H, br. s., NH), 8.50 (1H, d, *J*=4.78, *Py3*), 8.65 (1H, d, *J*=3.41, *Py3*), 9.11 (1H, s, N3-*Pi3*). ¹³C NMR (126 MHz, CDCl₃): δ=52.24 (1C, s, CO₂CH₃), 52.37 (2C, s, CO₂CH₃ + *Odz1*), 55.44 (1C, s, N3-CH₂py), 58.22 (1C, N7-CH₂odz), 61.89 (2C, s, C-6/8), 62.59 (2C, s, C-2/4) 67.37 (1C, s, *Odz5*) 74.96 (1C, s, 1 C, C-9), 121.71 (s) 122.22 (s) 122.43 (s) => (3C, *Arom4*), 123.43 (s) 124.86 (s) 128.43 (s) => (3C, *Arom6*), 136.09 (s) 136.36 (s) 136.99 (s) => (3C, *Arom5*), 147.79 (s) 148.92 (s) => (3C, *Arom3*), 157.68 (s) 159.60 (s) => (Cq, *Arom1*).

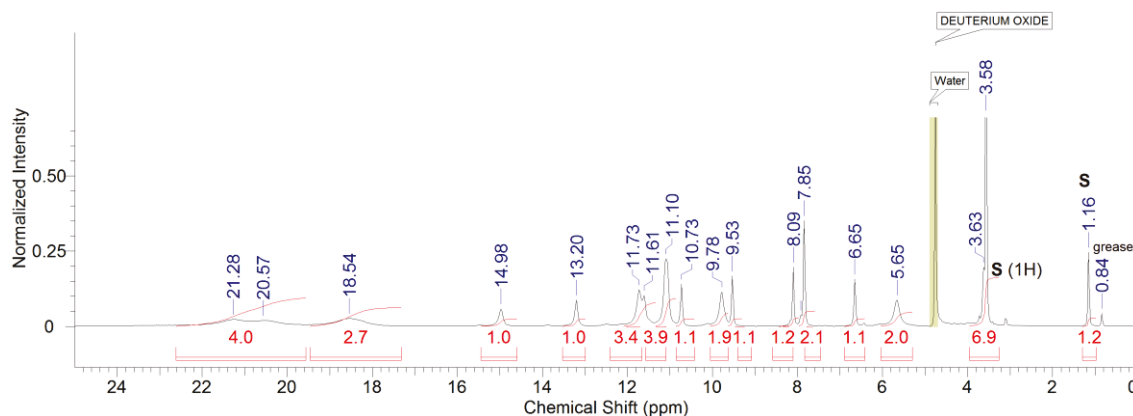
Complexation

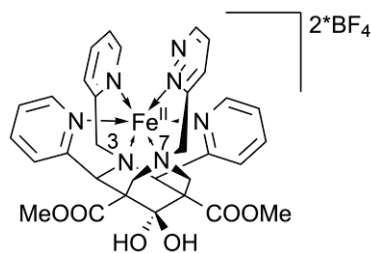
LOW SPIN and SCO COMPLEXES (Structures proven by X-ray)

[Fe15]*2BF₄ (binary/ternary complex of N3-pi, N7-pi bispidinone ligand)

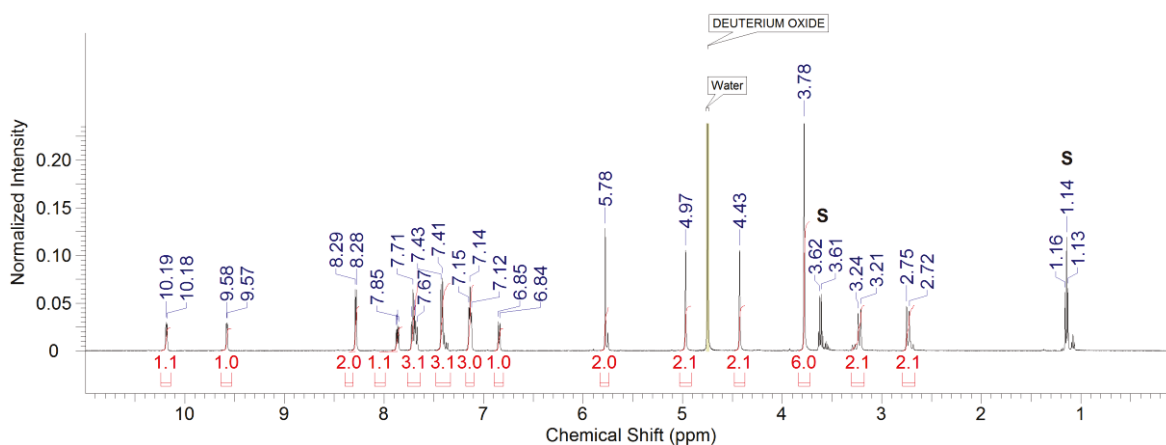


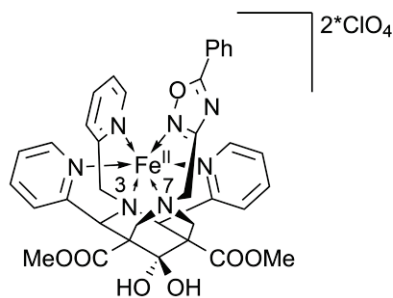
The ligand **15s** (253 mg, 0.427 mmol) was dissolved in degassed, anhydrous acetonitrile (10 ml) and a solution of iron(II) tetrafluoroborate hexahydrate (151 mg; 0.448 mmol) in anhydrous, degassed acetonitrile (5 ml) was added drop-wise on stirring under Argon. Upon addition, the solution immediately turned dark brown. The reaction was continued for 4 h until no more ligand signal was observed by direct injection mass spectrometry. Then, approx. 5 % (v/v) of degassed water was added and the solution was set up for slow gas diffusion of diethyl ether. The resulting dark red (almost black) crystalline material ready for X-ray analysis was collected, washed and dried yielding 278 mg of the desired complex (71 %). ¹H NMR (500 MHz, D₂O – solv. ref δ = 4.75 ppm): δ=3.58 (6H, CO₂CH₃), 5.65 (2H,s, *H*-6/8 *eq*), 6.65 (1H, s, N3-*Pi*5), 7.85 (2H, s, *Py*5), 8.09 (1H, s, N7-*Pi*5), 9.5 (1H, s, N7-*Pi*4), 9.78 (2H, s, N3-*CH*₂py), 10.73 (1H, s, N7-*Pi*6), 11.10 (4H, s, 2H from *Py*4, 2H from *Py*6), 11.61 - 11.73 (3H, m, 1H from N3-*Pi*4, 2H from N7-*CH*₂py), 13.20 (1H, s, N3-*Pi*6), 14.98 (1H, s, N7-*Pi*3), 18.54 (3H, br.s., 1H from N3-*Pi*3, 2H from *Py*3) 20.57 - 21.28 (4H, m, *H*-2/4, *H*-6/8 *eq*). UV-Vis (0.1 mM sol in water): λ_{max} (ε)=554 nm (334 M⁻¹m⁻¹), 458 nm (5560 M⁻¹m⁻¹), 403 nm (4680 M⁻¹m⁻¹), 380 (4390 M⁻¹m⁻¹), 253 (13296 M⁻¹m⁻¹). SQUID suggests SCO, moderately paramagnetic; solution-state μ_{eff} (H₂O, 5 mM, 298 K): 1.44 μ_B, (CH₃CN, 5 mM, 298 K): 1.77 μ_B. CV (E_{1/2}, CH₃CN, 100 mV/s): 651 mV. HRMS (ESI): m/z calcd for C₃₃H₃₄FeN₆O₆: 333.0939 [M+H₂O]²⁺ found: 333.0934 (where M is Fe15); elemental analysis calcd (%) for C₃₃H₃₄B₂F₈FeN₆O₆·2H₂O: C 45.24, H 4.37, N 9.59; found: C 45.53, H 4.24, N 9.66.



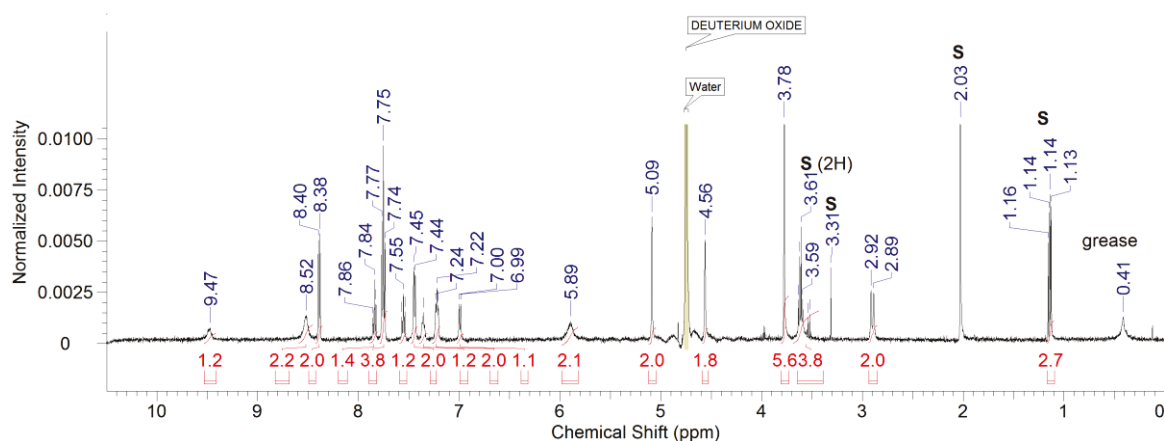
[Fe34]*2BF₄ (binary complex of N3-pi, N7-pdz bispidinone ligand - pdz= pyridazine)

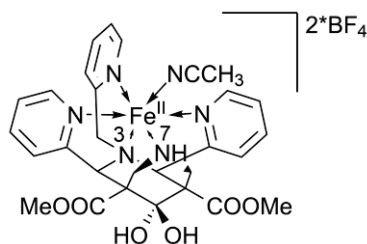
The ligand **34** (100 mg, 0.168 mmol) was dissolved in degassed, anhydrous ethanol (10 ml) and a solution of iron(II) tetrafluoroborate hexahydrate (60 mg; 0.179 mmol) in anhydrous, degassed ethanol (2 ml) was added drop-wise on stirring under Argon. The solution immediately turned dark brown and precipitate appeared at the end of addition. Reaction was continued for 4 hours until the total consumption of the ligand (by MS analysis) and the precipitate was filtered under Argon, washed several times with ethanol and diethyl ether yielding 102 mg of pure product in the form of a dark brown powder. It was then re-crystallized by a liquid/liquid diffusion of diethyl ether into a wet (5% v/v of H₂O) acetonitrile solution of the product. Dark brown crystals, suitable for X-ray analysis were isolated from the mother liquor, washed with ethanol and dried yielding 52 mg (37 %) of a crystalline product used for further analyses. Treating the remaining mother liquor may lead to additional crop. ¹H NMR (500 MHz, D₂O – solv. ref δ = 4.75 ppm): δ=2.74 (2H, d, *J*=13.29, *H*-6/8 *eq*), 3.22 (2H, d, *J*=13, *H*-6/8 *ax*), 3.78 (6H, s, CO₂CH₃), 4.43 (2H, s, N-CH₂arom), 4.97 (2H, s, N-CH₂arom), 5.78 (2H, s, *H*-2/4), 6.84 (1H, d, *J*=7.79, N3-*Pi*6), 7.13 (3H, m, 2H from *Py*4, 1H from N3-*Pi*4), 7.36 – 7.43 (3H, m, *CH*-arom), 7.67 - 7.72 (3H, m, *CH*-arom), 7.86 (1H, dd, *J*=8.25, 5.04, *CH*-arom), 8.28 (2H, d, *J*=5.50, *Py*3), 9.58 (1H, d, *J*=3.67, *Pdz*4) 10.18 (1H, d, *J*=5.96, N3-*Pi*3). UV-Vis (0.1 mM in water): λ_{max} (ε)=455 nm (10870 M⁻¹m⁻¹), 366 nm (3479 M⁻¹m⁻¹), 253 nm (13770 M⁻¹m⁻¹). SQUID indicates low spin, diamagnetic (*g* ≈ 0); solution-state μ_{eff} (H₂O, 5 mM, 298 K): 0.59 μ_B. CV (E_{1/2}, CH₃CN, 100 mV/s): 648 mV. HRMS (ESI) calcd for C₃₂H₃₃FeN₇O₅: 333.5916 [M+H₂O]⁺2 found 333.5910 (where M is Fe34); elemental analysis calcd (%) for C₃₂H₃₃B₂F₈FeN₇O₆·H₂O: C 44.74, H 4.11, N 11.44; found: C 44.31, H 4.16, N 11.83.



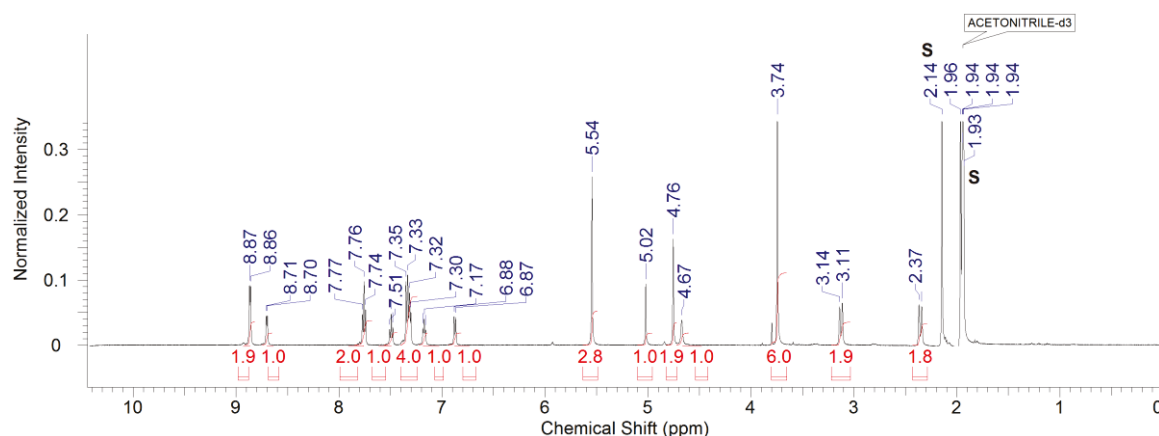
[Fe35]*2ClO₄ (binary complex of N3-pi, N7-oxdz bispidinone ligand – oxdz= oxadiazole)

The ligand **35** (128 mg, 0.193 mmol) was dissolved in degassed, anhydrous CH₃CN (20 ml) and a solution of iron(II) perchlorate hydrate (70 mg; 0.256 mmol) in anhydrous, degassed acetonitrile (2 ml) was added drop-wise on stirring under Argon. The solution immediately turned dark brown and precipitate appeared after 1 h. Then reaction was continued overnight at around 50 °C to ensure the full consumption of the ligand (by DI MS analysis). The resulting precipitate was washed with diethyl ether, re-dissolved in wet acetonitrile (5 % v/v of H₂O) and set up for vapor diffusion of diethyl ether. Volatiles were removed from the filtrate and the residue was set up for crystallization as above. Both batches yielded together 45 mg (25 %) of a crystalline (dark brown) material suitable for X-ray analysis and used for further characterizations. ¹H NMR (500 MHz, D₂O – solv. ref δ = 4.75 ppm): δ=2.90 (2H, d, *J*=13.38, *H*-6/8 *eq*), 3.61 (2H, m, *J*=7.14, *H*-6/8 *ax*), 3.78 (6H, s, CO₂CH₃), 4.56 (2H, s, N-CH₂arom), 5.09 (2H, s, N-CH₂arom), 5.89 (2H, br. s., *H*-2/4), 6.99 (1H, d, *J*=8.03, *CH*-arom), 7.22 (2H, t, *J*=6.69, *CH*-arom), 7.36 (1H, br. s., *CH*-arom), 7.44 (2H, d, *J*=7.36, *CH*-arom), 7.56 (1H, t, *J*=7.70, *CH*-arom), 7.75 (4H, t, *J*=7.70, *CH*-arom), 7.84 (2H, t, *J*=7.36, *CH*-arom), 8.35 - 8.42 (2H, m, *CH*-arom), 8.52 (2H, br. s., *Py*3) 9.47 (1H, br. s., N3-*Pi*3). UV-Vis (0.1 mM in water): λ_{max} (ε)=532 nm (774 M⁻¹m⁻¹), 443 nm (12570 M⁻¹m⁻¹), 254 nm (28704 M⁻¹m⁻¹). SQUID indicating low spin, diamagnetic (*g* ≈ 0); solution-state μ_{eff} (H₂O, 5 mM, 298 K): 0.54 μ_B. CV (E_{1/2}, CH₃CN, 100 mV/s): 769 mV. HRMS (ESI): *m/z* calcd for C₃₆H₃₅FeN₇O₇: 366.5968 [M+H₂O]²⁺ found: 366.5976 (where M is Fe35); elemental analysis calcd (%) for C₃₆H₃₅B₂F₈FeN₇O₇*2H₂O: C 45.84, H 4.17, N 10.40; found: C 45.71, H 3.96, N 10.51.



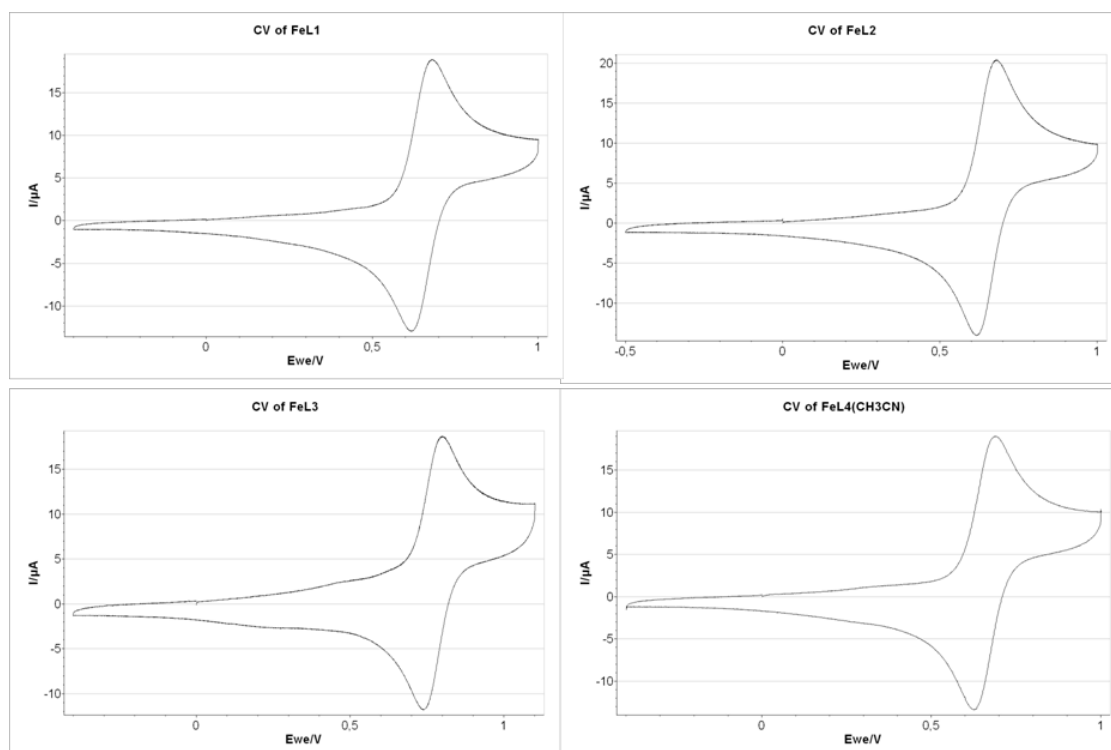
[Fe19(CH₃CN)]*2BF₄ (ternary complex of pentadentate N3-pi, N7-H bispidine ligand)

To the suspension of the ligand **19** (150 mg, 0.300 mmol) in 3.5 ml of dry, degassed acetonitrile in room temperature a solution of iron(II) tetrafluoroborate hexahydrate (105 mg, 0.312 mmol) in 1 ml of dry degassed acetonitrile was added drop-wise under Argon. Upon addition the color of solution turned deep brown and all solids were dissolved. After 1.5 h in room temperature, no more ligand could be spotted on mass spectrum, so the solution was directly set up for vapors' diffusion of diethyl ether. After a week crystals suitable for X-ray analysis appeared so they were filtered off and washed with *i*PrOH and diethyl ether yielding 39 mg (17 %) of the pure product used for further characterizations. ¹H NMR (500 MHz, CD₃CN – solv. ref. δ = 1.96 ppm): δ =2.36 (2H, d, J =13.05, *H*-6/8 *eq*), 3.13 (2H, d, J =13.72, *H*-6/8 *ax*), 3.74 (6H, s, CO₂CH₃), 4.67 (1H, br. s., *NH*), 4.76 (2H, s, N3-CH₂py), 5.02 (1H, s, C9-OH), 5.54 (3H, s, 2H from *H*-2/4, 1H from C9-OH), 6.88 (1H, d, J =8.03, N3-*Pi*6), 7.17 (1H, t, J =6.53, N3-*Pi*4), 7.24 - 7.40 (4H, m, 2H from *Py*4, 2H from *Py*6), 7.49 (1H, t, J =7.70, N3-*Pi*5), 7.76 (2H, t, J =7.53, *Py*5), 8.70 (1H, d, J =5.35, N3-*Pi*3), 8.86 (2H, d, J =5.02, *Py*3). UV-Vis (0.25 mM in acetonitrile): λ_{max} (ϵ)=521 nm (772 M⁻¹m⁻¹), 444 nm (7144 M⁻¹m⁻¹), 380 nm (3828 M⁻¹m⁻¹). Solution-state μ_{eff} (H₂O, 5 mM, 298 K): 4.16 μ_{B} , (CH₃CN, 5 mM, 298 K): 0.57 μ_{B} . CV ($E_{1/2}$, CH₃CN, 100 mV/s): 658 mV. HRMS (ESI): m/z calcd for C₂₇H₂₉FeN₅O₆: 287.5728 [M+H₂O]⁺2 found: 287.5740 (where M is Fe19) elemental analysis calcd (%) for C₂₉H₃₂B₂F₈FeN₆O₆: C 44.09, H 4.08, N 10.64; found: C 44.33, H 4.13, N 10.19.



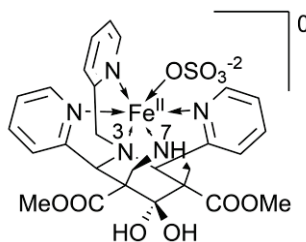
Cyclic Voltammograms of low spin or near low spin complexes

Cyclic voltammograms of [Fe15] (upper left), [Fe34] (upper right), [Fe35] (lower left) and [Fe19(CH₃CN)] (lower right) in acetonitrile. Scan rate used during the experiments presented below was 100 mV/s but we have performed the whole series of experiments with a different scan rates (50, 150, 200 and 250 mV/s) proving the reversibility of the process.



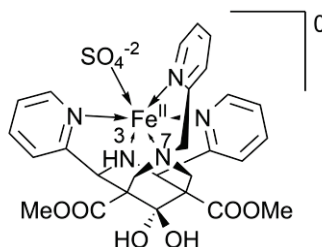
HIGH SPIN COMPLEXES with SO_4^{2-} COUNTER-ION (structures proven by X-ray)

[Fe19(SO₄)] (ternary complex of sulfate and pentadentate N3-pi, N7-H bispidinone ligand)



To the heated (60 °C) solution of the ligand **19** (109 mg, 0.217 mmol) in dry, degassed methanol (8 ml) a hot solution of iron(II) sulfate heptahydrate (60.4 mg, 0.217 mmol) in 4 ml of methanol was added drop-wise. The solution turned yellow and after 30 min in 60 °C, no more ligand was observed by mass spectrometry indicating that the reaction has finished. Hence, it was stopped, ca. 5 % (v/v) of degassed water was added followed by the addition of diethyl ether. After several days pale yellow square-like cubic crystals suitable for X-ray analysis were formed and collected yielding 65 mg (39 %) of the pure product. $R_f=0.37$ (Al neutral, preconditioned in MeOH/CH₃COO⁻NH₄⁺(0.1M in water) 3:1; ran in CHCl₃/MeOH 12.5:1; pure by UV, visible light and after SCN⁻ staining); ¹H NMR (500 MHz, D₂O – solv. ref $\delta = 4.75$ ppm): $\delta=3.97$ (6H, s, CO₂CH₃), 23.40 (1H, s, N3-Pi5), 23.98 (1H, s, Py5), 30.87 (2H, br. s., H-6/8 eq), 40.00 (2H, v. br. s., N3-CH₂py) 42.36 (1H, s, N3-Pi6), 44.29 (2H, s, Py6), 50.08 (2H, s, Py4) 50.25 (1H, s, N3-Pi4), 152.94 (2H, v. br. s. Py3), 159.36 (1H, v. br. s., N3-Pi3) 191.26 (2H, br. s., H-2/4), 197.09 (2H, br. s., H-6/8 ax). UV-Vis (0.25 mM): λ_{max} (ϵ)=414 nm (1188 M⁻¹m⁻¹), 255 nm (10120 M⁻¹m⁻¹). SQUID indicates high spin, paramagnetic ($g = 2.18$); solution-state μ_{eff} (H₂O, 5 mM, 298 K): 4.96 μ_B . HRMS (ESI): m/z calcd for C₂₇H₂₉FeN₅O₆: 287.5728 [M+H₂O]⁺; found: 287.5725 (where M is Fe19); elemental analysis calcd (%) for C₂₇H₂₉FeN₅O₁₀S*2H₂O: C 45.84, H 4.70, N 9.90; found: C 45.93, H 4.63, N 9.58.

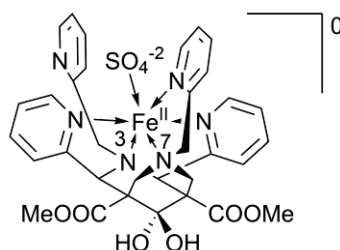
[Fe18(SO₄)] (ternary complex of sulfate and N3-H, N7-pi bispidinone ligand)



To the solution of the ligand (100 mg, 0.200 mmol) in 5 ml of dry degassed MeOH, 3 ml of MeOH solution of FeSO₄*7H₂O (57 mg, 0.205 mmol, 1.025 eq) was added drop-wise on stirring at RT in inert atmosphere. After 4 h of reaction, the solution was set up for crystallization upon vapors diffusion of the Et₂O at 4 °C. After 2 weeks a monocrystalline solid suitable for X-ray analysis was obtained, washed with dry degassed iPrOH and EtOH under argon and dried yielding 10 mg of the

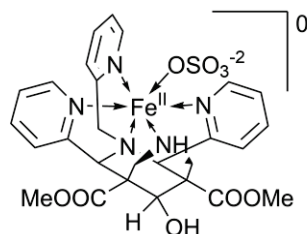
product (7 %) in the form of the yellow crystalline powder. DIMS (ESI) $m/z = 620$ (100) $[M+H_2O+HCOO^-]^+$ 606 (33) $[M+MeOH+OH^-]^+$ 636 (25) 574 (13) $[M+OH^-]^+$ 602 (12) $[M+HCOO^-]^+$ 592 (4) $[M+H_2O+OH^-]^+$ 287.5 (3) $[(M+H_2O)^{+2}]$, 295 $[(M+MeOH)^{+2}]$ $[M+H_2O]^{+2}$ $[M]^{+2}$, $[M+Cl^-]^+$ $[M+H_2O+Cl^-]^+$ $[M+H_2O+HCOO^-]^+$. HRMS (ESI): m/z calcd for $C_{27}H_{29}FeN_5O_6$: 287.5728 $[M+H_2O]^{+2}$; found: 287.5738 ((where M is Fe18).

[Fe15(N3-SO₄)] (ternary/binary complex of sulfate and N3-pi (decoordinated), N7-pi bispidinone ligand)



To a solution of the ligand (200 mg, 0.447 mmol) in dry degassed MeOH (15 ml) a solution of iron(II) sulfate heptahydrate (96 mg, 0.346 mmol, 1.025 eq) in MeOH (7 ml) was added dropwise at RT, turning the solution brown. After 2.5 h no more ligand could be found by MS and so the reaction was stopped and set up for vapours diffusion of Et₂O at RT. Crystalline material suitable for x-ray analysis was obtained after 5 days, which after filtration (decantation) and drying yielded 16 mg of the crystalline product (6 %). DIMS (ESI) $m/z = 711$ (100) $[M+H_2O+HCOO^-]^+$ 701 (10) $[M+H_2O+Cl^-]^+$ 725 (10) $[M+MeOH+HCOO^-]^+$ 333 (6) $[(M+H_2O)^{+2}]$, Solution state $\mu_{\text{eff}} = 1.81 \mu_B$ (D₂O, 5 mM, 298 K). HRMS (ESI): m/z calcd for $C_{33}H_{34}FeN_6O_6$: 333.0939 $[M+H_2O]^{+2}$; found: 333.0930 (where M is Fe15); elemental analysis calcd (%) for $C_{33}H_{34}FeN_5O_{10}S \cdot 2H_2O$: C 49.63, H 4.80, N 10.52; found: C 49.16, H 4.65, N 10.45.

[Fe49(SO₄)] (ternary complex of N3-pi, N7-H bispidinol ligand)

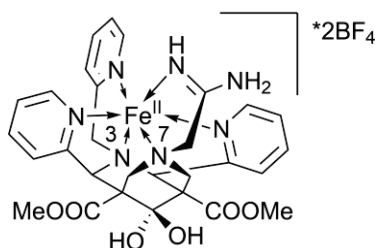


To a solution of the ligand (154 mg, 0.306 mmol) in dry, degassed MeOH (20 ml) a solution of iron(II) sulfate heptahydrate (87 mg, 0.314 mmol, 1.025 eq) in MeOH (7 ml) was added drop-wise at RT. The solution immediately turned yellow and then slightly orange upon further addition, and after 2.5 h at RT no more ligand could be detected by MS. The reaction was stopped and set up for crystallization upon vapors diffusion of Et₂O to the reaction mixture yielding a light yellow crystalline material suitable for X-ray analysis after 2 weeks at 4 °C. After washing the crystal with iPrOH/Et₂O 1:1 solvent mixture and subsequent drying 90 mg of the yellow crystalline product

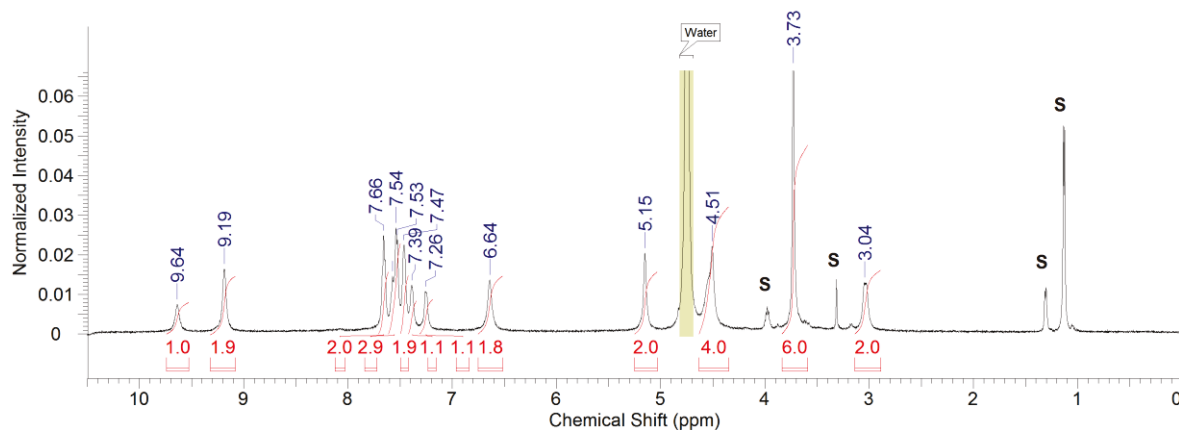
were obtained (45 %). DIMS (ESI) $m/z = 604$ (100) $[M+HCOO^-]^+$ 594 (5) $[M+Cl]^+$. HRMS (ESI): m/z calcd for $C_{27}H_{29}FeN_5O_5$: 279.5754 $[M]^{+2}$; found: 279.5754, elemental analysis calcd (%) for $C_{27}H_{29}FeN_5O_9S \cdot 2H_2O$: C 46.90, H 4.81, N 10.13; found: C 47.15, H 4.65, N 10.10.

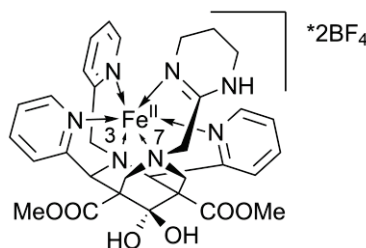
RESPONSIVE COMPLEXES (amidine-based)

[Fe37]*2BF₄ (binary complex of N7-acyclic amidine bispidinone ligand)



To a solution of the N7-H bispidinone **19** (150 mg, 0.30 mmol) and chloromethylamidine hydrochloride precursor (42 mg, 0.325 mmol, 1.08 eq) in dry DMF (5 ml) in Ar atmosphere, a *i*Pr₂NEt (116 mg, 0.9 mmol, 3 eq) was added at 55 °C. After 24 h reaction was not completed (MS showed peak of the ligand [502 m/z] at 80 % intensity of the product peak [558 m/z]) so amidine precursor (40 mg, 0.31 mmol, 1.03 eq) and *i*Pr₂NEt (120 mg, 0.93 mmol, 3.1 eq) were added. After additional 24 h of reaction at 55 °C no more starting material could be detected, all the volatiles were evaporated, residue dissolved in dry degassed *i*PrOH (8 ml) and 2 ml of *i*PrOH solution of iron tetrafluoroborate hexahydrate (112 mg, 0.33 mmol, 1.1 eq) was added drop-wise at RT. Precipitate was formed 5 min after the addition of the iron(II) salt and no ligand signal was present in MS. After 12 h of further reaction in RT, brown precipitate was filtered off, re-dissolved in MeOH with *i*Pr₂NEt (115 mg, 0.89 mmol, 3 eq) and mixture was stirred for 30 min at RT. All the volatiles were evaporated, residue was dissolved in 4 ml of EtOH and upon the addition of 10 ml of *i*PrOH a dark red solid was formed which was filtered off, washed with cold EtOH and *i*PrOH and dried yielding 90 mg of the dark red microcrystalline solid (37 %), which was used for titration experiments. ¹H NMR (500 MHz, D₂O – solv. ref δ = 4.75 ppm) δ=3.04 (2H, br. s., *H*-6/8 eq), 3.73 (6H, s., CO₂CH₃), 4.51 (4H, br. s., 2H from N3-CH₂py, 2H from *H*-6/8 ax), 5.15 (2H, s, *H*-2/4), 6.64 (2H, s, N7-CH₂amidine), 7.26 (1H, s, N3-*Pi*6), 7.39 (1H, s, N3-*Pi*4), 7.47 (2H, s, *Py*4), 7.53 – 7.56 (3H, m, N3-*Pi*5, *Py*6), 7.66 (2H, m, *Py*5), 9.19 (2H, s, *Py*3), 9.64 (1H, s, N3-*Pi*3).

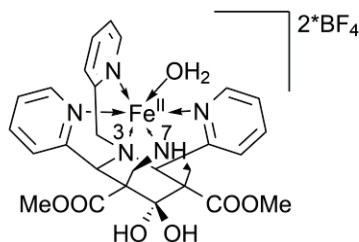


[Fe38]*2BF₄ (binary complex of N7-cyclic amidine bispidinone ligand)

To a solution of the N7-H bispidinone **19** (200 mg, 0.40 mmol) and chloromethylamidine hydrochloride (71 mg, 0.42 mmol, 1.05 eq) in dry DMF (5 ml) in Ar atmosphere, a *i*Pr₂NEt (130 mg, 1.0 mmol, 2.5 eq) was added at 55 °C. After 24 h reaction was not completed (MS showed the peak of the ligand (*m/z* = 502 (35 %)) and the product (*m/z* = 598 (100%)), so amidine reagent (70 mg, 0.42 mmol, 1.05 eq) and *i*Pr₂NEt (120 mg, 0.93 mmol, 2.3 eq) were added. After additional 24 h of reaction at 55 °C no more starting material could be detected, all the volatiles were evaporated, residue dissolved in dry degassed *i*PrOH (10 ml) and 5 ml of isopropanol solution of iron tetrafluoroborate hexahydrate 149 mg, 0.44 mmol, 1.1 eq) was added drop-wise. The reaction mixture turned yellow and formed precipitate was filtered off. The obtained solid (signal of desired complex by MS) was dissolved in MeOH containing *i*Pr₂NEt (180 mg, 1.4 mmol, 3.5 eq) and stirred for 1 h in RT. Volatiles were evaporated, residue was re-dissolved in EtOH (12 ml) and after the addition of *i*PrOH (15 ml) the resulting solution was left at 4 °C. Upon the formation of precipitate, it was filtered off and the residue was again re-dissolved in MeOH/*i*Pr₂NEt (300 mg, 2.3 mmol, 5.8 eq). After 1 h of stirring in RT, volatiles were removed under reduced pressure, residue re-dissolved in EtOH/*i*PrOH mixture and left at 4 °C. Resulting precipitate was filtered off and washed with cold EtOH and *i*PrOH yielding 30 mg of dark red solid (9 %). DIMS (ESI) *m/z* = 335.7 (100) [M+H₂O]²⁺, 326.6 (6) [M]²⁺, 688 (7) [M+Cl]⁺, 706 (9) [M+H₂O+Cl]⁺, 716 (9) [M+H₂O+HCOO]⁺.

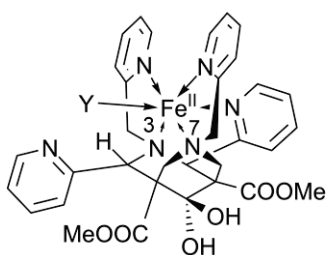
COMPLEXES of HYPOTHETICAL STRUCTURES

[Fe19(H₂O)]*2BF₄ (complex of pentadentate N3-pi, N7-H bispidinone ligand and potentially water).

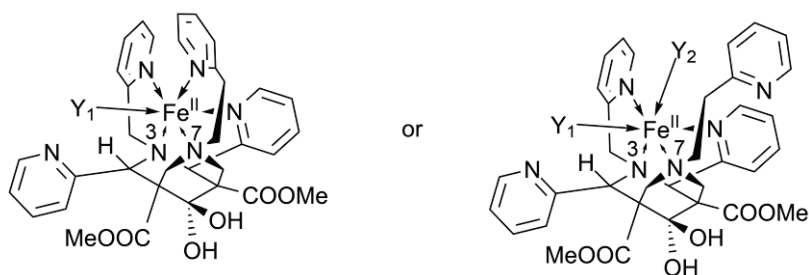


To a solution of the ligand **19** (110 mg, 0.220 mmol) in 4 ml of dry degassed EtOH, a 2 ml of EtOH solution of iron(II) tetrafluoroborate hexahydrate (74 mg, 0.220 mmol, 1 eq) was added at 70 °C. After 5 min the MS showed a full conversion of the substrate so the reaction was cooled down and continued at RT for 12 h. The precipitate which formed in the reaction mixture was filtered off and washed extensively with EtOH (5 times) and *i*PrOH (5 times) and dried yielding 60 mg of the yellow solid which was used for the T₁ measurements. DIMS (ESI) *m/z* = 620 (100) [M+H₂O+HCOO]⁺, 308 (41) [M+H₂O+CH₃CN]²⁺, 602 (13) [M+HCOO]⁺, 287.6 (8) [M+H₂O]²⁺.

[Fe15a(Y)] (complex of pentadentate N3-pi, N7-pi, N2/4-*anti* bispidinone ligand – potentially ternary)



To a solution of the ligand **15a** (138 mg, 0.233 mmol) in 1 ml of dry degassed *i*PrOH, a solution of iron(II) tetrafluoroborate hexahydrate (80 mg, 0.238 mmol, 1.02 eq) was added drop-wise at reflux. After 12 h the reaction was cooled down and the yellow precipitate formed was filtered off and washed extensively with EtOH and MeOH (5 times with each solvent) yielding 125 mg of the product (64 %) in a form of the grayish bluish powder, which was used for T₁ measurements (T₁ = 0.82 s, *r*₁ = 0.23 mM⁻¹s⁻¹ at 298 K and in 11.7 T). DIMS (ESI) *m/z* = 693 (100) [M+HCOO]⁺, 683 (30) [M+Cl]⁺, 324 (7) [M]²⁺.

[Fe47a(Y₁)(Y₂)] (ternary/quaternary complex of N3-pi, N2/N4-anti, N7-EtPy bispidinone ligand)

To a heated solution of the ligand **47a** (137 mg, 0.226 mmol) in the dry degassed mixture of EtOH (1 ml) and CH₃CN (0.4 ml) a solution of Fe(BF₄)₂*6H₂O in dry, degassed EtOH (0.5 ml) was added drop-wise at 60 °C. The solution turned yellow (DIMS m/z: 331 (100) [M]⁺², 707 (88) [M+HCOO]⁺, 681 (35), 354 (16) [M+EtOH]⁺², 607 (9) [L+H]⁺) and then darkened (dark brown color) after 30 min at 60 °C. After 2 h the reaction mixture was cooled down to 4 °C, Et₂O added to precipitate the product and the resulting solid was filtered off and washed three times with MeOH/EtOH mixture (1:1), 5 times with EtOH and 3 times with Et₂O yielding 30 mg of a light grey/blue precipitate (impure product). DIMS: 707 (100) [M+HCOO]⁺, 721 (37), 695(35), 693 (33), 338 (13), 725 (17) [M+H₂O+HCOO]⁺, 620 (16), 681 (5). HRMS C₃₃H₃₂FeN₆O₅ calc. ([M]⁺²) 324.0887, found 324.0920.

X-RAY STRUCTURES

General procedures (adapted from Kolanowski et al 2013 ^[193])

Suitable crystals were selected and mounted on a Gemini kappa-geometry diffractometer (Agilent Technologies UK Ltd) equipped with an Atlas CCD detector and using Mo ($\lambda = 0.7107 \text{ \AA}$) or Cu radiation ($\lambda = 1.5418 \text{ \AA}$).

Intensities were collected at low temperature by means of the CrysAlisPro software (CrysAlisPro, Agilent Technologies, Version 1.171.34.49 (release 20-01-2011) CrysAlis171 .NET) (compiled Jan 20 2011, 15:58:25). Reflection indexing, unit-cell parameters refinement, Lorentz-polarization correction, peak integration and background determination were carried out with the same software. An analytical absorption correction was applied using the modeled faces of the crystal.^[267] The structures were solved by direct methods with SIR97 ^[268] and the least-square refinement on F² was achieved with the CRYSTALS software.^[269]

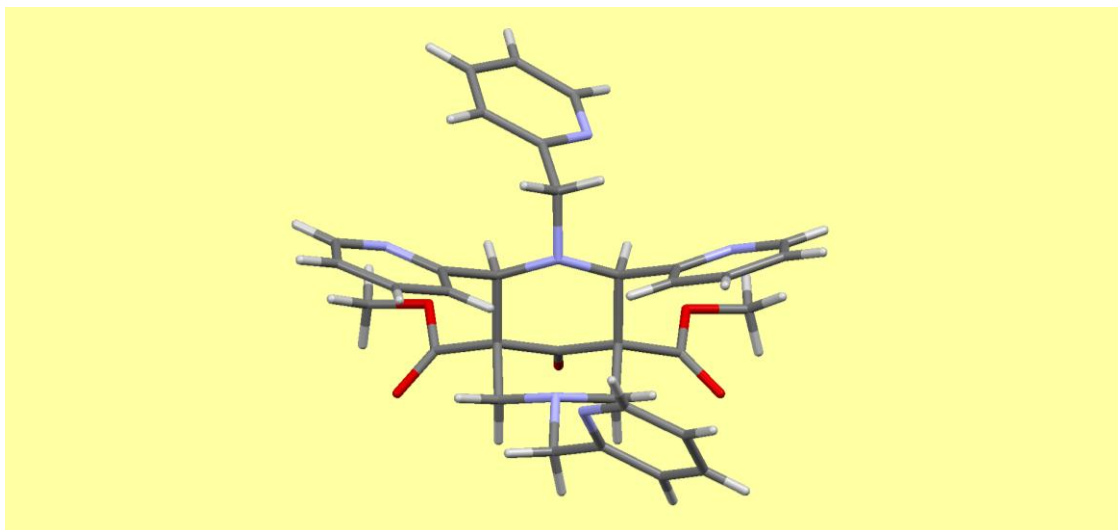
All non-hydrogen atoms were refined anisotropically. The hydrogen atoms were all located in a difference map, but those attached to carbon atoms were repositioned geometrically. The H atoms were initially refined with soft restraints on the bond lengths and angles to regularize their geometry (C---H in the range 0.93--0.98 and N---H in the range 0.86--0.89 \AA) and Uiso(H) (in the range 1.2-1.5 times Ueq of the parent atom), after which the positions were refined with riding constraints.

For compound Fe35, the crystal structure displayed solvent accessible voids of 427 \AA^3 with delocalized electronic density. The contribution of this residual density was removed from the diffraction data with the SQUEEZE routine from the PLATON program ^[270] and led to an estimate of about 1.4 acetonitrile molecules per formula unit.

Appropriate identification numbers of the X-ray structures obtained in the course of this work are given and the original data can be obtained free of charge from The Cambridge Crystallographic Data Centre via www.ccdc.cam.ac.uk/data_request/cif.

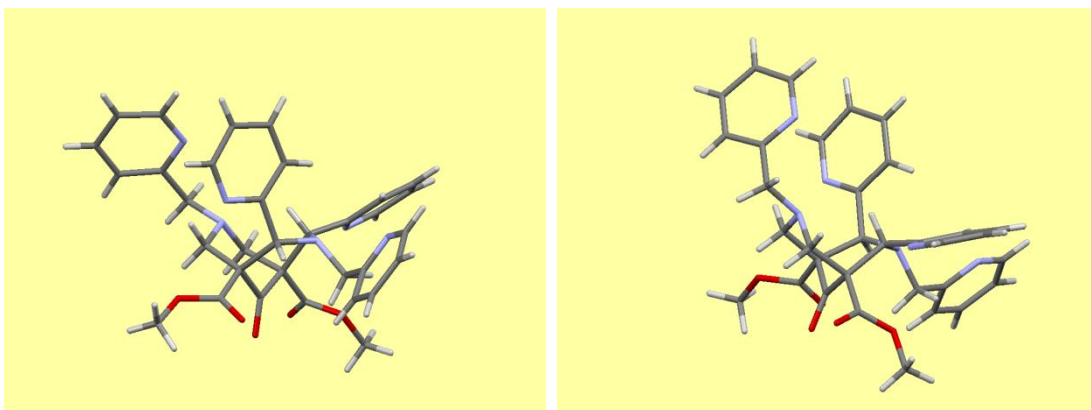
Ligands' structures

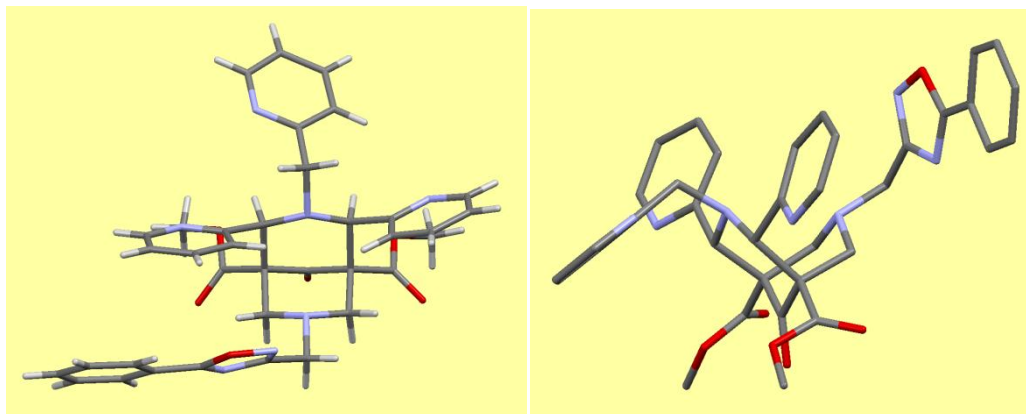
Ligand 15 (CCDC 902550)



Chemical formula : C₃₃H₃₂N₆O₅, Mr = 592.65 g.mol⁻¹, crystal dimensions : 0.46 x 0.59 x 0.71 mm, monoclinic system, space group P21/c, unit-cell dimensions : a = 11.2852 (9) Å, b = 14.3962 (9) Å, c = 18.246 (1) Å, $\alpha = 90^\circ$, $\beta = 104.565 (8)^\circ$ and $\gamma = 90^\circ$, V = 2869.1 (3) Å³, Z = 4, $\rho_{\text{calc}} = 1.372 \text{ mg.m}^{-3}$, $\mu = 0.09 \text{ mm}^{-1}$, Mo K α radiation, $\lambda = 0.7107 \text{ \AA}$, T = 110 K, $\theta_{\text{max}} = 29.5^\circ$, $\theta_{\text{min}} = 3.5^\circ$, no. of measured reflections : 21932, no. of independent reflections : 6995, Rint = 0.038, R[F² > 2 σ (F²)] = 0.053, wR(F²) = 0.125, $\Delta\rho_{\text{max}} = 0.44 \text{ e.\AA}^{-3}$; $\Delta\rho_{\text{min}} = -0.38 \text{ e.\AA}^{-3}$

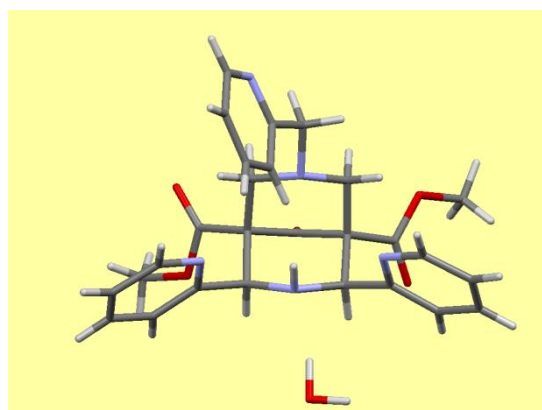
Ligand 15a



Ligand 35 (CCDC 902551)

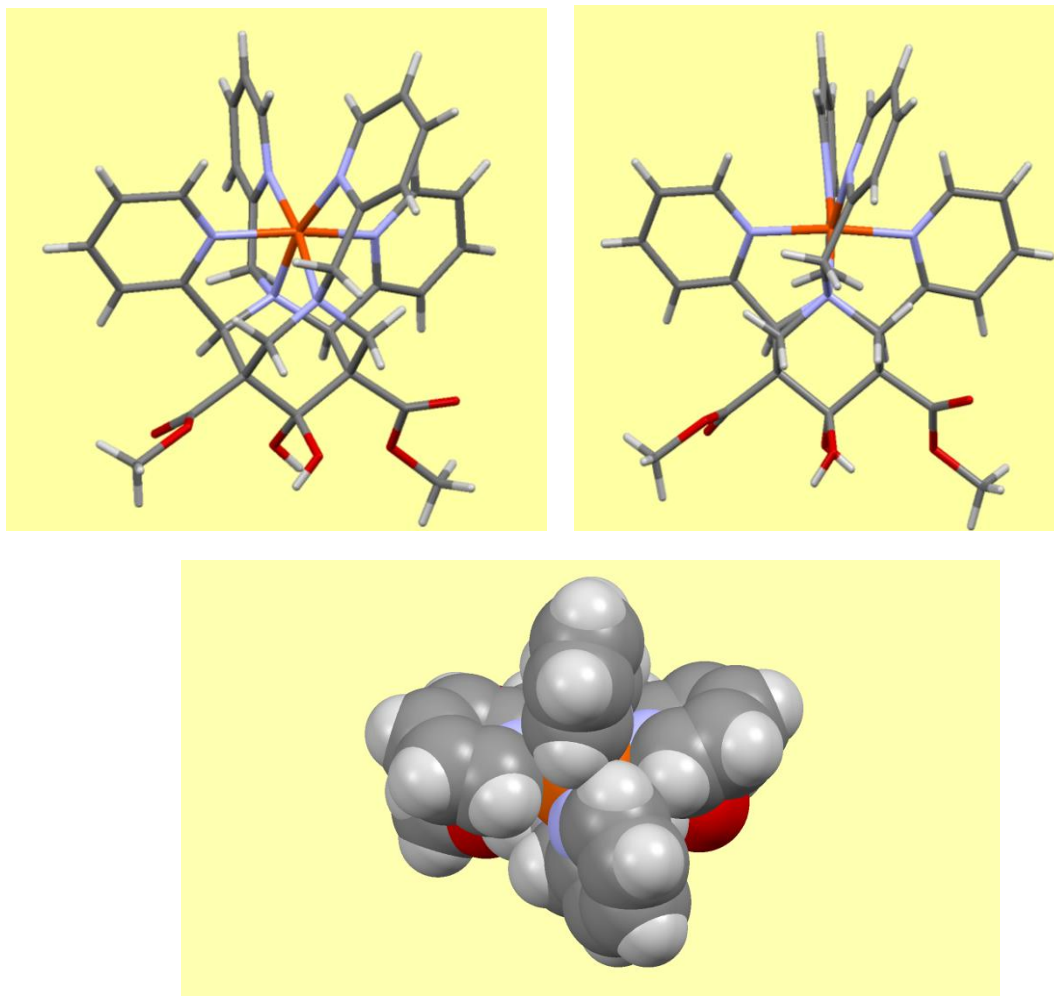
Crystals grown from iPrOH.

Chemical formula : C₃₆H₃₃N₇O₆, Mr = 659.70 g.mol⁻¹, crystal dimensions : 0.182 x 0.222 x 0.533 mm, monoclinic system, space group P21/c, unit-cell dimensions : a = 9.8633 (8) Å, b = 15.327 (1) Å, c = 21.604 (2) Å, $\alpha = 90^\circ$, $\beta = 95.087 (8)^\circ$ and $\gamma = 90^\circ$, V = 3253.1 (5) Å³, Z = 4, $\rho_{\text{calc}} = 1.347 \text{ mg.m}^{-3}$, $\mu = 0.77 \text{ mm}^{-1}$, Cu K α radiation, $\lambda = 1.5418 \text{ \AA}$, T = 110 K, $\theta_{\text{max}} = 66.8^\circ$, $\theta_{\text{min}} = 3.5^\circ$, no. of measured reflections : 22896, no. of independent reflections : 5743, Rint = 0.044, R[F₂ > 2 σ (F₂)] = 0.046, wR(F₂) = 0.129, $\Delta\rho_{\text{max}} = 0.30 \text{ e.\AA}^{-3}$; $\Delta\rho_{\text{min}} = -0.28 \text{ e.\AA}^{-3}$

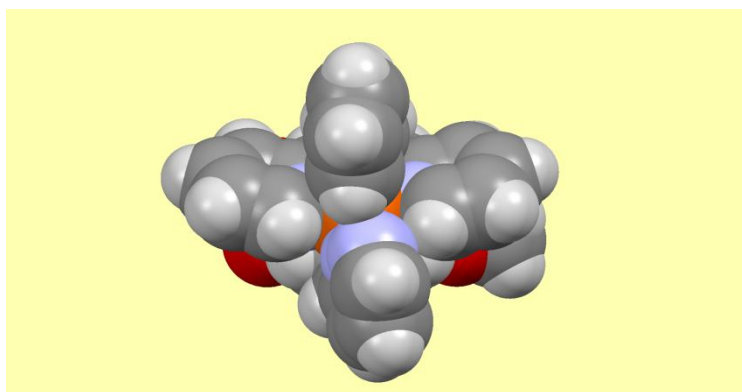
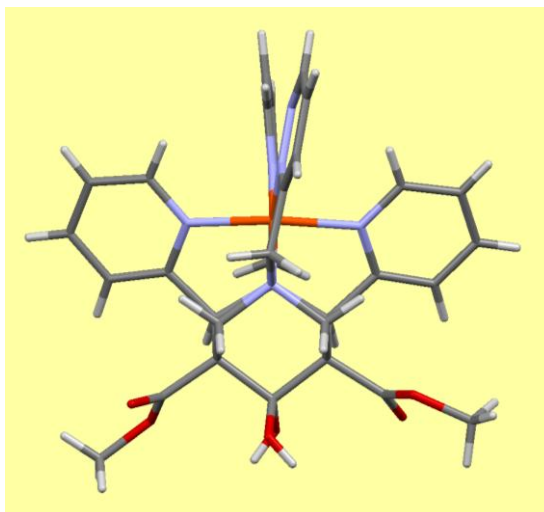
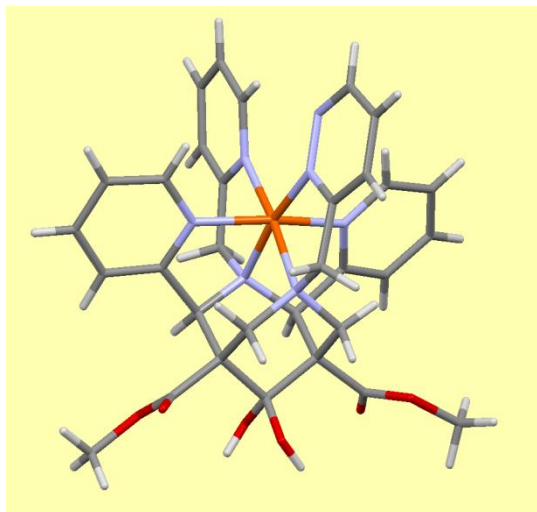
Ligand 18s

Iron(II) complexes

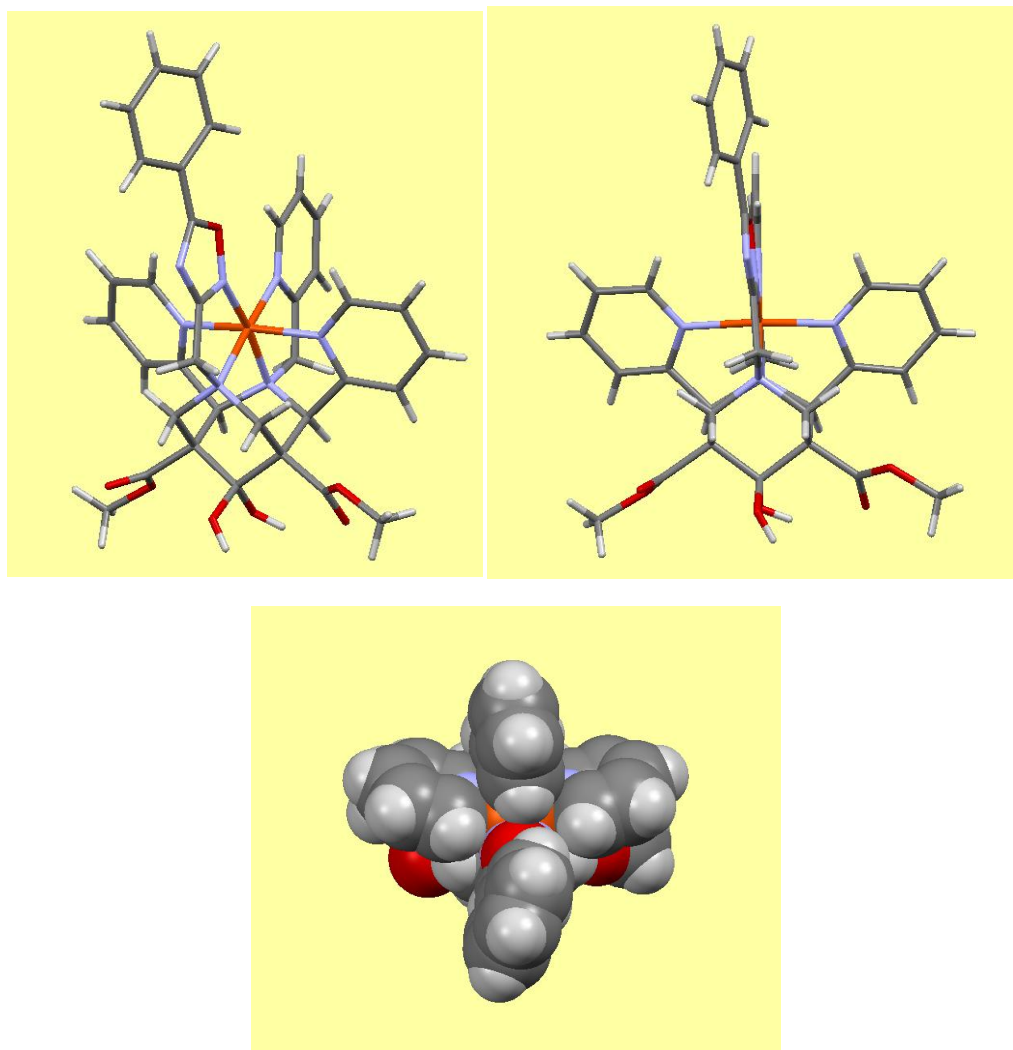
[Fe15]*2BF₄ (CCDC 902554)



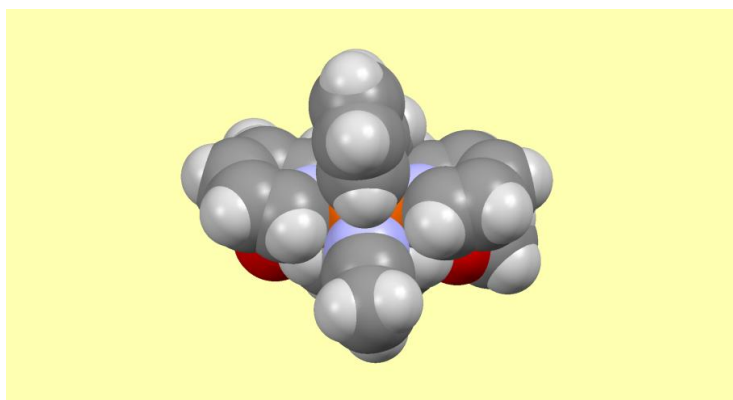
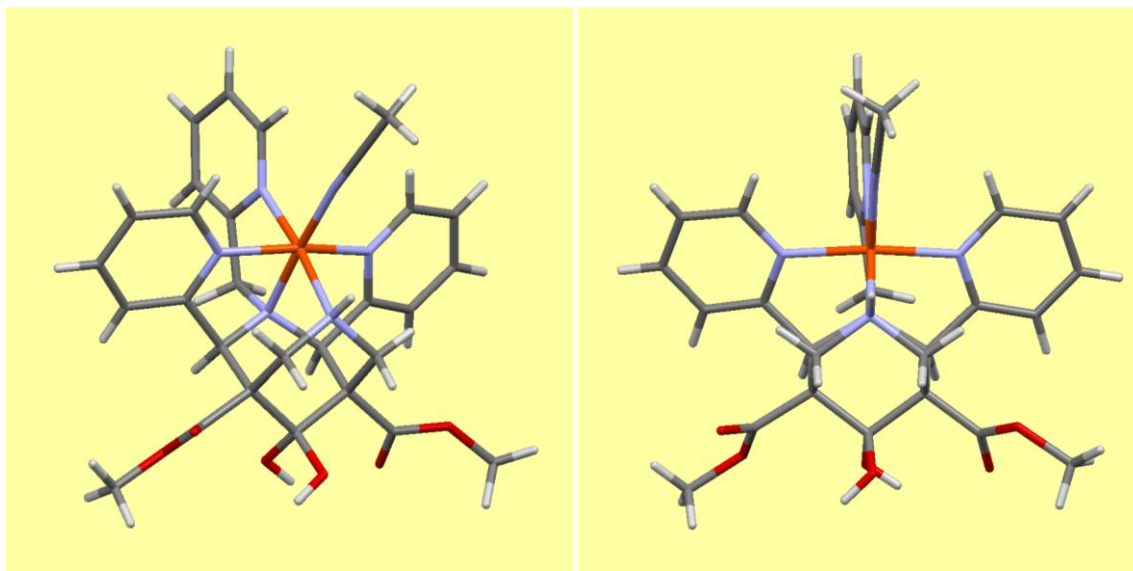
Chemical formula: C₃₃H₃₈B₂F₈FeN₆O₈, Mr = 876.16 g·mol⁻¹, crystal dimensions : 0.105 x 0.179 x 0.473 mm, monoclinic system, space group P21/c, unit-cell dimensions : a = 10.3903 (6) Å, b = 18.170 (1) Å, c = 19.079 (1) Å, α = 90°, β = 101.85 (1)° and γ = 90°, V = 3525.2 (3) Å³, Z = 4, ρ_{calc} = 1.651 mg·m⁻³, μ = 0.53 mm⁻¹, Mo Kα radiation, λ = 0.7107 Å, T = 100 K, θ max = 29.5°, θmin = 3.4°, no. of measured reflections : 74517, no. of independent reflections : 9196, R_{int} = 0.055, R[F₂ > 2σ(F₂)] = 0.039, wR(F₂) = 0.090, Δρ_{max} = 0.58 e·Å⁻³; Δρ_{min} = -0.60 e·Å⁻³

[Fe₃₄]*2BF₄ (CCDC 902552)

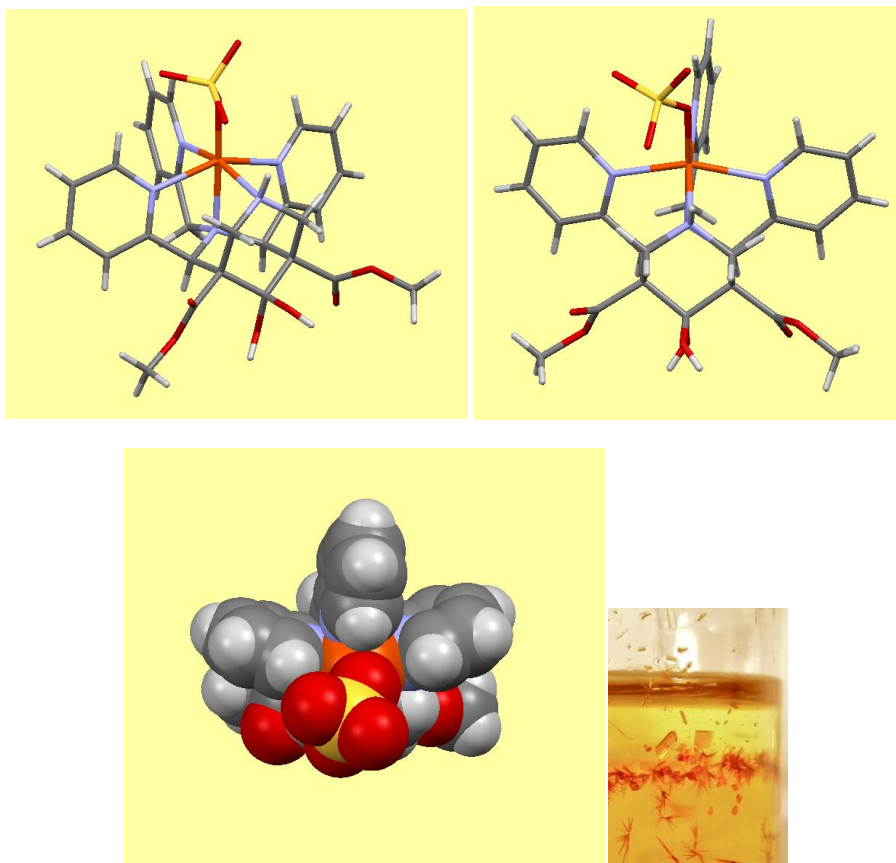
Chemical formula: C₃₄H₃₈B₂F₈Fe₃₄N₈O₇, Mr = 900.18 g·mol⁻¹, crystal dimensions : 0.179 x 0.248 x 0.349 mm, triclinic system, space group P-1, unit-cell dimensions : a = 10.6244 (6) Å, b = 12.3593 (7) Å, c = 15.2033 (9) Å, α = 103.178 (5)°, β = 103.007 (5)° and γ = 98.123 (5)°, V = 1854.5 (2) Å³, Z = 2, ρ_{calc} = 1.612 mg·m⁻³, μ = 0.51 mm⁻¹, Mo Kα radiation, λ = 0.7107 Å, T = 110 K, θ max = 29.5°, θ min = 3.5°, no. of measured reflections : 40829, no. of independent reflections: 9362, R_{int} = 0.042, R[F₂ > 2σ(F₂)] = 0.053, wR(F₂) = 0.124, Δρ_{max} = 1.03 e·Å⁻³; Δρ_{min} = -0.76 e·Å⁻³

[Fe35]*2ClO₄ (CCDC 904020)

Chemical formula: C₃₆H₃₅Cl₂FeN₇O₁₅, Mr = 932.45 g.mol⁻¹, crystal dimensions: 0.096 x 0.195 x 0.289 mm, trigonal system, space group R-3, unit-cell dimensions : a = 23.982 (2) Å, b = 23.982 (2) Å, c = 39.047 (3) Å, $\alpha = 90^\circ$, $\beta = 90^\circ$ and $\gamma = 120^\circ$, V = 19449 (3) Å³, Z = 18, $\rho_{\text{calc}} = 1.433 \text{ mg}\cdot\text{m}^{-3}$, $\mu = 0.54 \text{ mm}^{-1}$, Mo K α radiation, $\lambda = 0.7107 \text{ \AA}$, T = 100 K, $\theta \text{ max} = 29.4^\circ$, $\theta \text{ min} = 3.6^\circ$, no. of measured reflections: 54907, no. of independent reflections : 11013, Rint = 0.099, R[F₂ > 2 σ (F₂)] = 0.120, wR(F₂) = 0.225, $\Delta \rho \text{ max} = 2.33 \text{ e}\cdot\text{\AA}^{-3}$; $\Delta \rho \text{ min} = -1.87 \text{ e}\cdot\text{\AA}^{-3}$

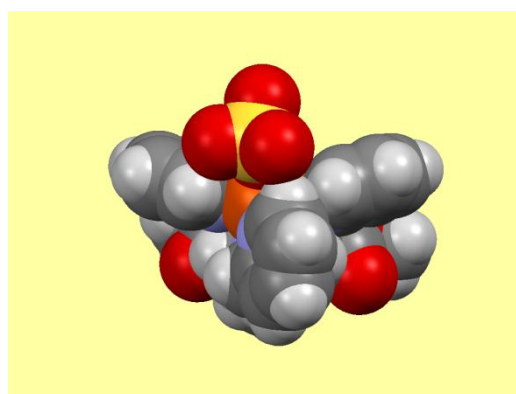
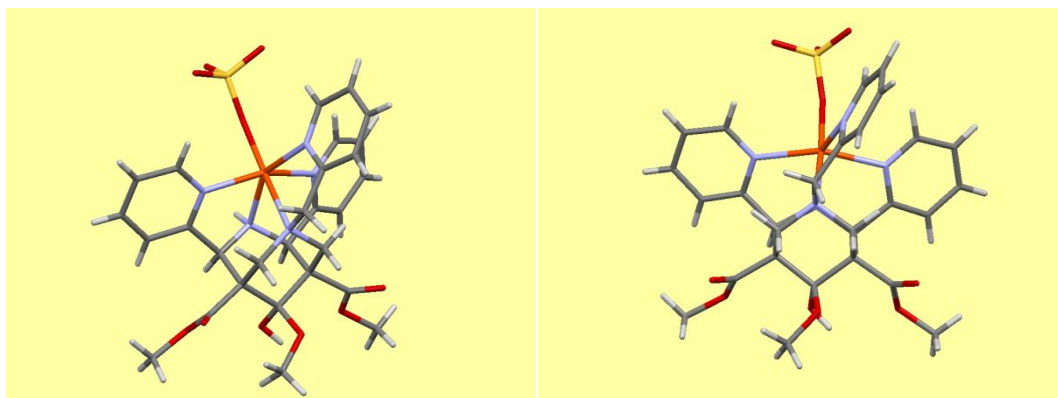
[Fe₁₉(CH₃CN)]*2BF₄ (CCDC 902553)

Chemical formula: C₃₄H₃₈B₂F₈Fe₁₉N₈O₆, Mr = 872.17 g·mol⁻¹, crystal dimensions : 0.123 x 0.287 x 0.362 mm, triclinic system, space group P-1, unit-cell dimensions: a = 11.0566 (8) Å, b = 13.7715 (9) Å, c = 14.718 (1) Å, $\alpha = 66.375 (6)^\circ$, $\beta = 69.925 (6)^\circ$ and $\gamma = 71.325 (6)^\circ$, V = 1884.5 (2) Å³, Z = 2, $\rho_{\text{calc}} = 1.537 \text{ mg}\cdot\text{m}^{-3}$, $\mu = 0.50 \text{ mm}^{-1}$, Mo K α radiation, $\lambda = 0.7107 \text{ \AA}$, T = 100 K, $\theta \text{ max} = 29.5^\circ$, $\theta \text{ min} = 3.5^\circ$, no. of measured reflections : 38176, no. of independent reflections: 9388, Rint = 0.050, R[F₂ > 2 σ (F₂)] = 0.060, wR(F₂) = 0.111, $\Delta\rho_{\text{max}} = 1.79 \text{ e}\cdot\text{\AA}^{-3}$; $\Delta\rho_{\text{min}} = -0.85 \text{ e}\cdot\text{\AA}^{-3}$

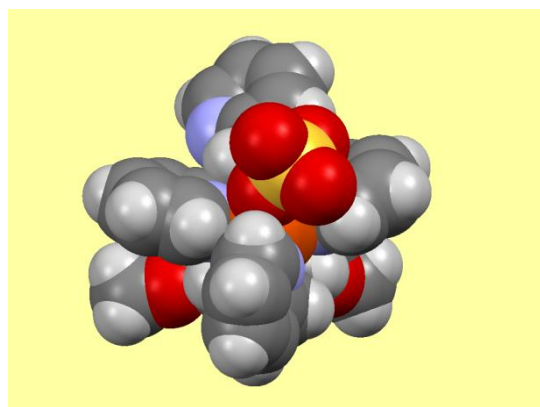
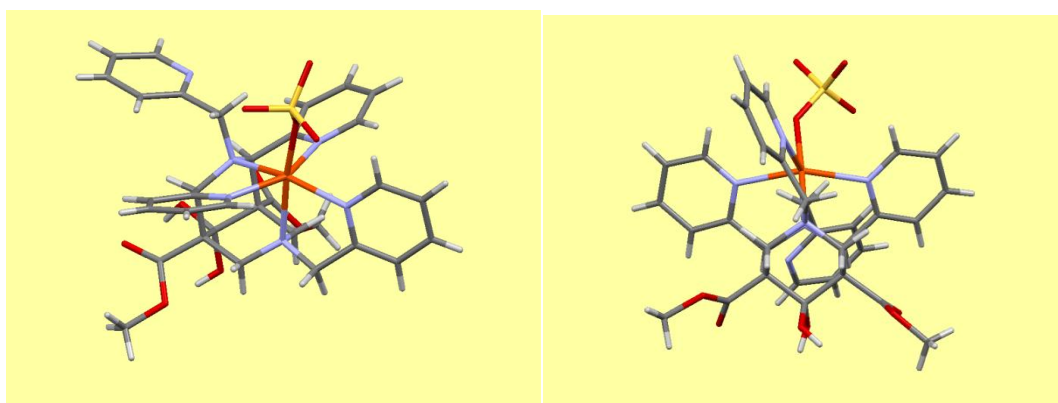
[Fe19(SO4)] (CCDC 902296)

Chemical formula: $C_{57}H_{70}Fe_2N_{10}O_{23}S_2$, $M_r = 1439.07 \text{ g}\cdot\text{mol}^{-1}$, crystal dimensions: $0.030 \times 0.242 \times 0.293 \text{ mm}$, orthorhombic system, space group $Pbca$, unit-cell dimensions : $a = 16.741 (3) \text{ \AA}$, $b = 17.538 (2) \text{ \AA}$, $c = 20.854 (2) \text{ \AA}$, $\alpha = 90^\circ$, $\beta = 90^\circ$ and $\gamma = 90^\circ$, $V = 6123.0 (1) \text{ \AA}^3$, $Z = 4$, $\rho_{\text{calc}} = 1.561 \text{ mg}\cdot\text{m}^{-3}$, $\mu = 5.22 \text{ mm}^{-1}$, Cu $K\alpha$ radiation, $\lambda = 1.5418 \text{ \AA}$, $T = 150 \text{ K}$, $\theta_{\text{max}} = 66.7^\circ$, $\theta_{\text{min}} = 3.4^\circ$, no. of measured reflections : 24753, no. of independent reflections : 5387, $R_{\text{int}} = 0.062$, $R[F_2 > 2\sigma(F_2)] = 0.065$, $wR(F_2) = 0.138$, $\Delta\rho_{\text{max}} = 1.90 \text{ e}\cdot\text{\AA}^{-3}$; $\Delta\rho_{\text{min}} = -0.69 \text{ e}\cdot\text{\AA}^{-3}$

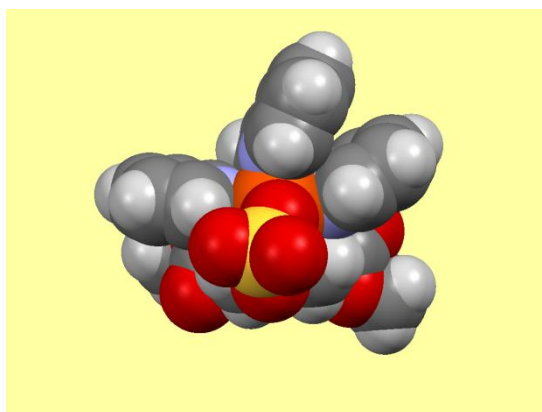
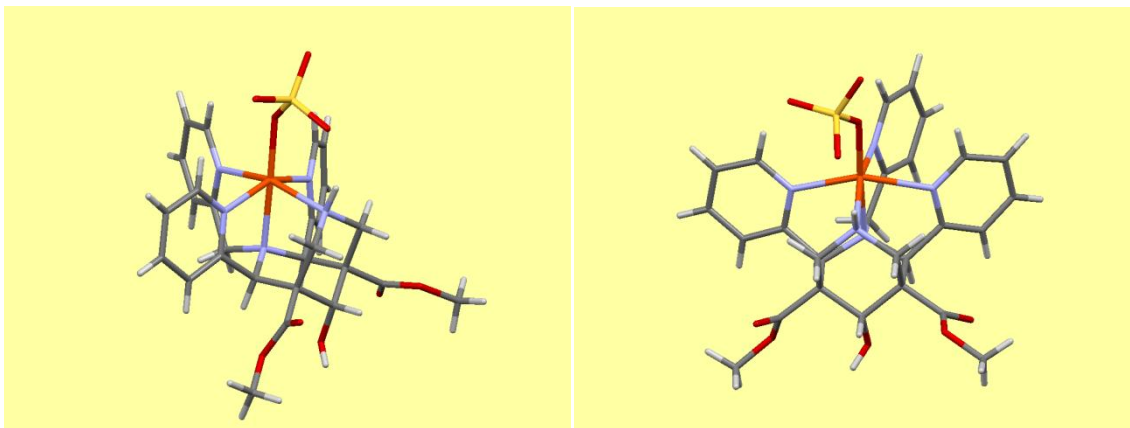
[Fe18(SO₄)]



[Fe15(N3-SO4)]



[Fe49(SO₄)]



NMR AND MAGNETIC MOMENTS AT VARIED TEMPERATURE

General procedures (from Kolanowski et al 2013 ^[193])

Solid state magnetic susceptibility data were collected in the “Laboratoire des Multimatériaux et Interfaces (UMR 5615)” at Université Claude Bernard Lyon 1 (University of Lyon, France) (Prof. Luneau and Dr. Checa), using a SQUID magnetometer from Quantum Design model MPMS-XL instrument in an applied magnetic field of 0.1 Tesla. Compounds **[Fe34]*2BF₄**, **[Fe35]*2ClO₄**, **[Fe19(CH₃CN)]*2BF₄** were measured using a capsule in the temperature range (100-300 K). Compound **[Fe15]*2BF₄** was measured in an aluminum sample holder to allow heating at 400 K and a better heating. All data were corrected for the contribution of the sample holder and diamagnetism of the samples estimated from Pascal’s constants.^{[271] [272]}

NMR spectra were acquired at different temperatures at Bruker 500 MHz apparatus with cooling-heating system. ¹H NMR and if stated, also COSY experiments were performed at different temperatures not less than 10 min after the temperature shown by the detector stabilized at the desired value. Chemical shifts (δ) are reported in ppm and are referred to the solvent peak, which is arbitrary placed at the theoretical value for 298 K.

Magnetic moments in solution were typically determined in water (H₂O/D₂O 85:15) or acetonitrile-d₃ (unless otherwise stated) by the Evans’ method.^{[273] [274]} These experiments were carried out analogously to previously described methods using Bruker 500 MHz and coaxial NMR tube.^[130] All the remarks given above for the Temperature-dependent NMR experiments applied also to the measurements of magnetic moments in solution. A 2 % tBuOH was used as reference in both cases and 5 mM solutions of complexes were used unless otherwise stated. Despite differences in magnetic susceptibilities of various solvents, for diluted solutions (equal or below 15 mM) this parameter can be neglected together with the term including the difference between density of pure solvent and solution.^{[275] [241]} Varied temperature magnetic susceptibilities were corrected in respect to the effect of solvent volume expansion/contraction upon heating/cooling (modified values of solvent densities at different temperatures were applied ^{[276] [277]} to calculate the real concentration of the analyte at different conditions). For deuterated solvents, correction parameters were used, which were calculated by dividing the density of the deuterated solvent by density of non-deuterated analog at the temperature of sample preparation (298 K).^[277] No diamagnetic corrections were used for paramagnetic compounds. However, they can be evaluated either 1) by using this same procedure to also determine the diamagnetic contribution for the corresponding diamagnetic complex with a different metal donor, 2) by use of Pascal’s constants.

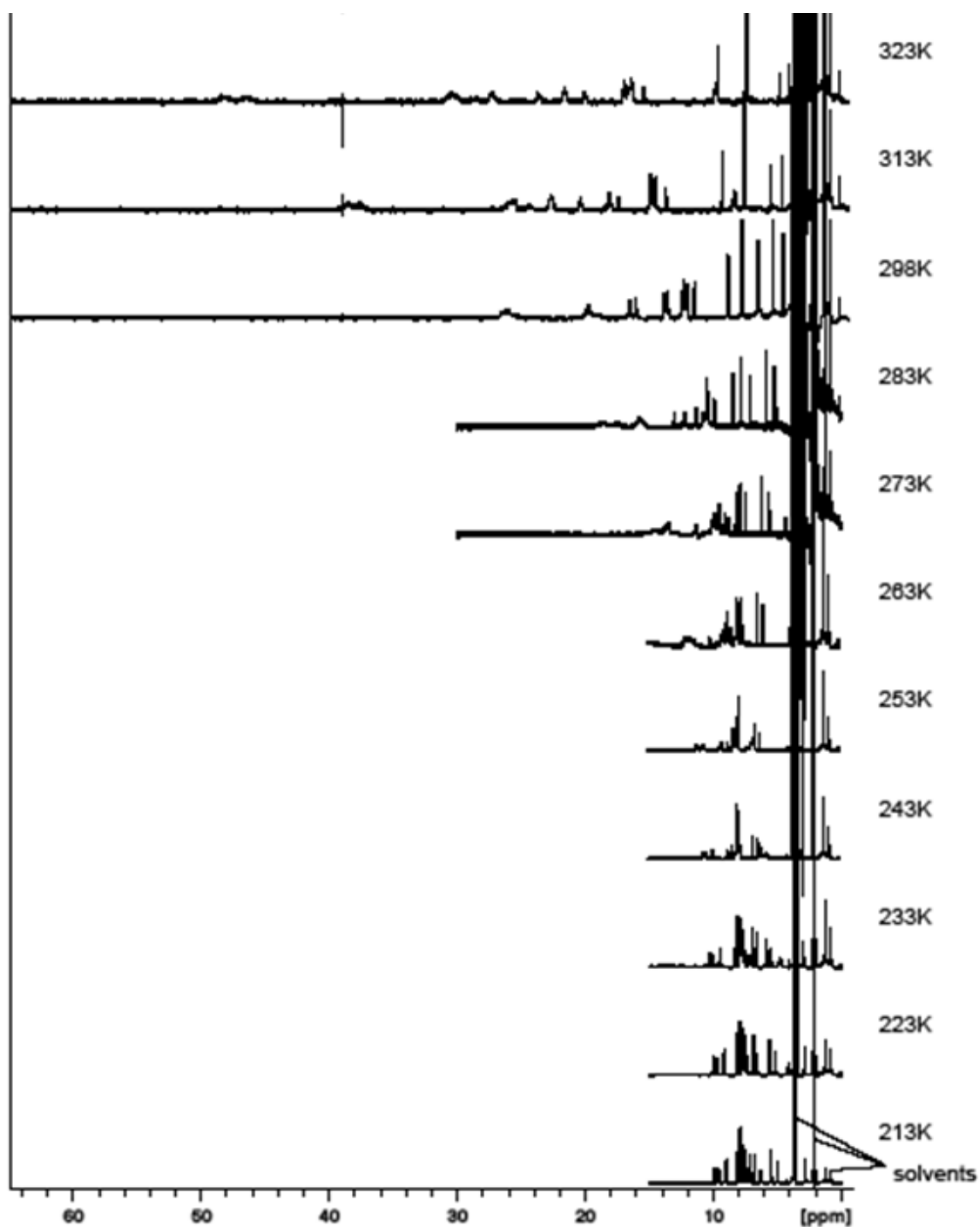
Variable-temperature NMR of spin crossover complex [Fe15]

ACETONE-d6

NMR shifts ([ppm]) of protons of [Fe15] in ACETONE-d6

Temperature [K]		213	223	233	243	253	263	273	283	298	313	323
Proton ID	Integr											
H-6/8 eq	2	2.79	2.86	2.99	3.16	3.41	3.80	4.36	5.10	6.40	8.34	9.88
OMe	6	3.71	3.71	3.71	3.69	3.67	3.63	3.57	3.49	3.34	3.15	2.97
H-6/8 ax	2	3.75	4.10	4.75	5.74	7.16	9.48	12.88	17.40	26.18	38.61	48.05
N7-CH ₂ py	2	4.95	5.15	5.51	6.06	6.84	8.15	10.06-9.49	12.17	16.50	22.66	27.26
N3-CH ₂ py	2	5.46	5.59	5.84	6.19	6.74	7.60	8.81	10.48	13.57	18.17	21.16
H-2/4	2	6.26	6.60	7.18	x	9.23	11.49	14.42	18.47	26.18	37.69	46.25
OH	1	6.87	6.70	6.56	6.41	6.23	5.96	5.64	5.23	4.53	3.59	2.92
OH	1	7.06	6.98	6.88	6.77	6.63	6.44	6.19	5.88	5.35	4.63	4.12
N7-Pi6	1	7.26	7.39	7.60	7.91	8.31	9.18	10.06-9.49	11.36	13.79	17.36	20.10
N7-Pi4	1	7.42	7.48	7.60		8.06	8.48	9.11	9.92	11.45	13.71	15.45
Py4	2	7.49	7.58	7.73		8.25	8.79	10.06-9.49	10.48	12.30	14.92	16.97
Py6	2	7.61	7.70	7.82		8.31	8.79	10.06-9.49	10.39	12.06	14.51	16.42
N7-Pi5	1	7.70	7.72	7.77	7.84	7.91	8.06	8.24	8.45	8.83	9.31	9.65
Py5	2	7.89	7.90	7.90	7.91	7.91	7.91	7.89	7.84	7.74	7.54	7.38
N3-Pi6	1	7.89	8.08	8.32	8.69	9.24	10.14	11.35	13.01	16.01	20.40	23.70
N3-Pi4	1	8.00	8.08	8.21	8.42	8.69	9.05	10.06-9.49	10.76	12.42	14.83	16.63
N3-Pi5	1	8.17	8.14	8.09	8.01	7.91	7.73	7.48	7.14	6.49	5.53	4.81
Py3	2	8.95	9.13	9.45	9.92	10.62	11.77	13.42	15.74	19.73	25.96	30.49
N7-Pi3	1	9.56	9.71	9.99	10.42	11.07	12.12	13.64	15.74	19.73	25.55	30.12
N3-Pi3	1	9.89	10.01	10.26	10.63	11.15	12.12	13.64	15.35	19.01	24.48	28.73

Variable temperature ^1H NMR spectra in Acetone- d_6 (213 K– 323 K)



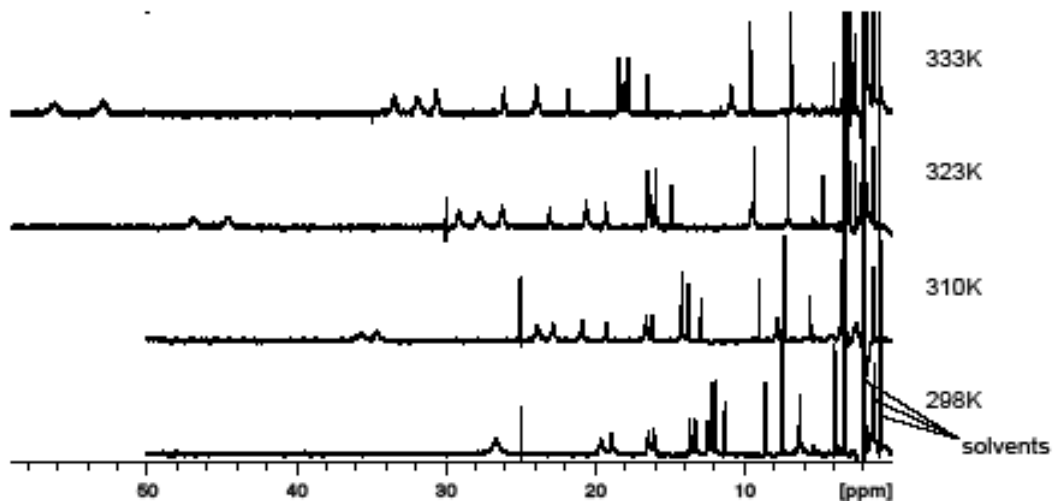
ACETONITRILE-d3

NMR shifts ([ppm]) of protons of [Fe15] in ACETONITRILE-d3

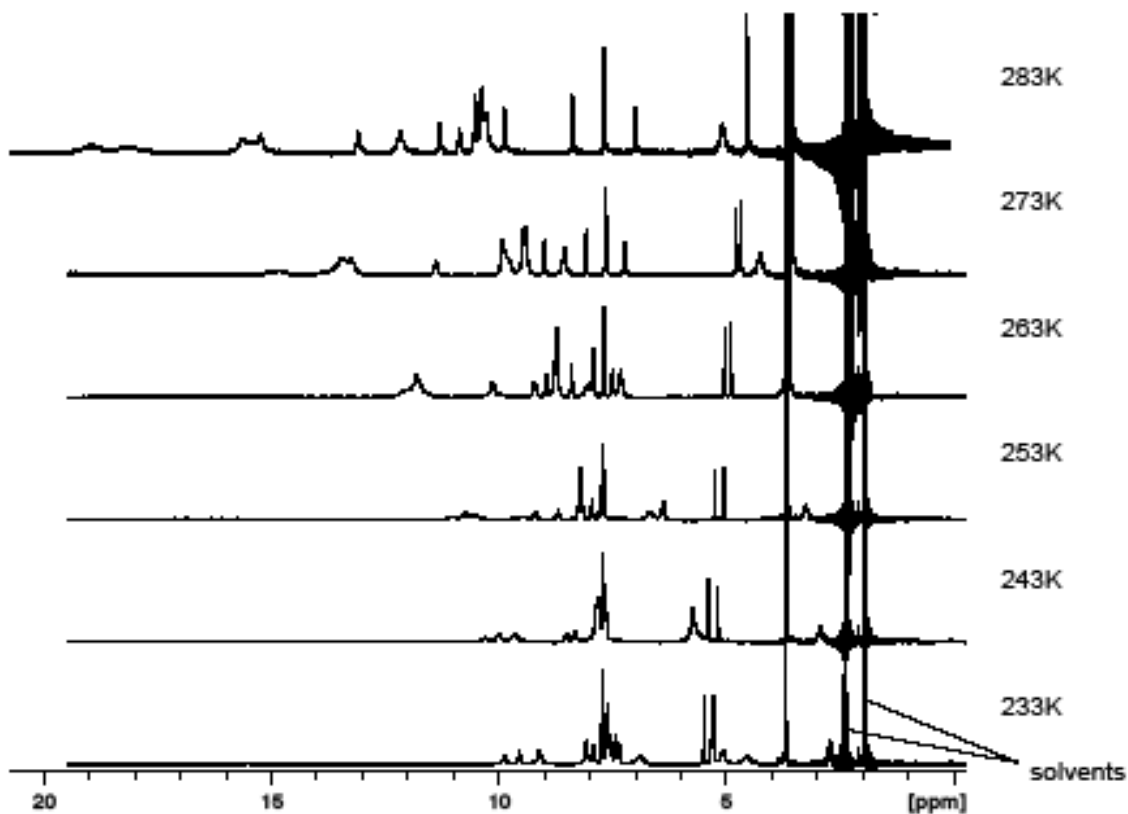
Temp. [K]		233	243	253	263	273	283	298	310	323	333	343	353
TYPE	H												
H-6/8 eq	2	2.72	2.94	3.26	3.70	4.27	4.99	6.34	7.75	9.47	10.80	12.29	13.66
OMe	6	3.69	3.69	3.65	3.60	3.54	3.47	3.30	3.15	2.97	2.83	2.68	2.55
H-6/8 ax	2	4.55	5.73	7.37	10.20	- 13.64 - 6H	18.00	26.26	35.95	47.00	56.32	65.94	75.53
N7- CH ₂ py	2	5.08	5.73	6.69	8.02	9.80- 9.92 - 4H	12.07	16.42	20.82	26.26	30.61	35.09	39.37
OH	1	5.29	5.19	5.06	4.89	4.69	4.44	3.95	3.50	2.98	2.57		
N3- CH ₂ py	2	5.32	5.73	6.39	7.32	8.56	10.10	13.32	16.55	20.57	23.90	27.32	30.62
OH	1	5.50	5.40	5.25	5.04	4.78	4.44	3.80	3.20	2.49			
H-2/4	2	6.90		9.50	11.79	14.91	18.87	26.67	34.76	44.68	53.02	61.70	70.14
N7-Pi5	1	7.36		7.72	7.91	8.08	8.28	8.63	8.95	9.33	9.58	9.82	10.00
N7-Pi4	1	7.44	7.64- 7.74	7.78	8.40	8.99	9.77	11.30	12.87	14.86	16.49	18.19	19.85
Py4	2	7.55	7H and 9.80-	8.21	8.73	9.47	10.41	12.25	14.13	16.49	18.44	20.42	22.38
N7-Pi6	1	7.61	78- 7.9 5H	8.21	8.95	9.92 - 4H	11.19	13.66	16.16	19.26	21.79	24.40	26.92
Py6	2	7.61		8.21	8.73	9.40	10.27	11.97	13.71	15.93	17.75	19.62	21.51
Py5	2	7.72		7.71	7.68	7.65	7.59	7.44	7.27	7.06	6.85	6.83	6.38
N3-Pi5	1	7.91		7.71	7.49	7.24	6.90	6.22	5.54	4.70	3.99	3.26	2.49
N3-Pi4	1	8.08	8.32	8.69	9.21	9.80- 9.92 - 4H	10.76	12.45	14.13	16.30	18.05	19.84	21.51
N3-Pi6	1	8.08	8.50	9.19	10.14	11.38	12.99	16.09	19.18	23.01	26.00	29.20	32.26
Py3	2	9.10	9.63	10.54	11.79		15.51	19.63	23.85	29.10	33.46	37.92	42.29
N7-Pi3	1	9.55	10.00	10.74	11.79	13.23 -	15.12	18.89	22.79	27.80	31.90	36.24	40.46
N3-Pi3	1	9.87	10.29	11.02	11.79	13.64 - 6H	15.31	18.89	22.79	27.80	31.90	36.24	40.46

Variable temperature ^1H NMR spectra of **[Fe15]** in CD_3CN (233 K – 333 K):

333 K – 298 K



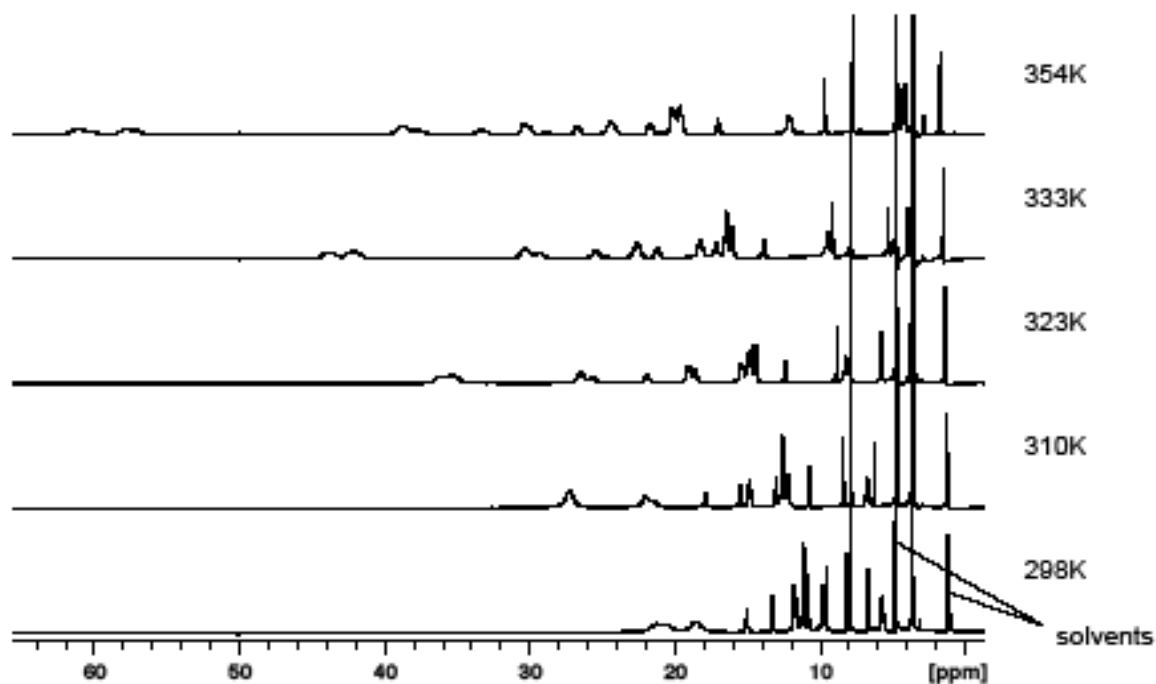
283 K – 233 K



Deuterium oxide

NMR shifts ([ppm]) of protons of [Fe15] in D_2O

Temperature [K]		298	310	323	333	353
Name	Integr					
OMe	6	3.58	3.60	3.59	3.59	3.56
H-6/8 eq	2	5.65	6.78	8.22	9.47	12.15
N3-Pi5	1	6.65	6.29	5.76	5.32	4.29
Py5	2	7.85	7.90	7.91	7.88	7.76
N7-Pi5	1	8.09	8.44	8.83	9.13	9.69
N7-Pi4	1	9.53	10.78	12.45	13.86	17.08
N3-CH ₂ py	2	9.78	12.22	15.45	18.28	24.48
Py4	2	11.10	12.66	14.72	16.47	20.28
Py6	2	11.10	12.51	14.42	16.06	19.67
N7-Pi6	1	10.73	12.63-12.50	14.96	17.21	21.82
N3-Pi4	1	11.61	13.05	14.96	16.47	19.67-20.28
N7-CH ₂ py	2	11.73	14.88	19.04	22.63	30.41
N3-Pi6	1	13.20	15.54	18.65	21.28	26.85
N7-Pi3	1	14.98	17.91	21.94	25.46	33.41
N3-Pi3	1	18.54	21.52	25.75	29.39	37.73
Py3	2	18.54	22.03	26.48	30.39	38.83
H-6/8 ax	2	20.49	27.28	36.07	43.89	62.14
H-2/4	2	21.23	27.28	35.32	42.27	57.77

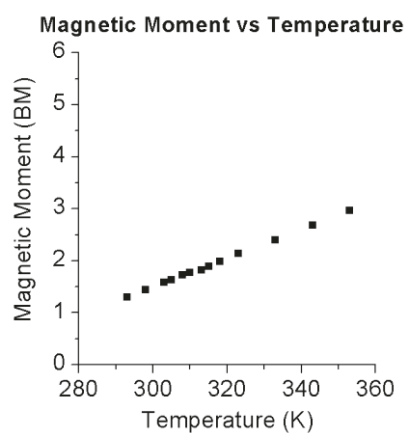
Variable temperature ¹H NMR spectra of [Fe15] in D₂O (298 K – 353 K)

Temperature-dependency of magnetic moments of SCO complex

Magnetic moments of $[\text{Fe15}] \cdot 2\text{BF}_4$ (Evans' method) at different solvents

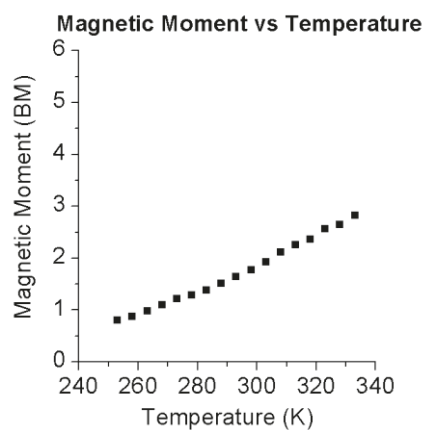
Temp. [K]	Magnetic Moment [BM]
293	1,31
298	1,44
303	1,59
305	1,64
308	1,73
310	1,78
313	1,82
315	1,90
318	1,98
323	2,14
333	2,40
343	2,68
353	2,96

Aqueous solution



Temp. [K]	Magnetic Moment [BM]
253	0,80
258	0,87
263	0,98
268	1,10
273	1,22
278	1,29
283	1,38
288	1,51
293	1,64
298	1,77
303	1,93
308	2,11
313	2,25
318	2,37
323	2,56
328	2,65
333	2,82

Acetonitrile- d_3



Estimation of thermodynamic parameters of magnetic equilibria (fitting of magnetic moments - from Supp Info of Kolanowski et al 2013 [193])

Fitting procedure. The extraction of thermodynamic parameters was performed according to previous reports in many variants. [278] [121] [122] [241] [130] Experimental magnetic moment values can be fit to the following equation (equation (12) from the main text) with four parameters to be optimized (μ_{LS} , μ_{HS} , ΔH° , ΔS°):

$$\mu_{eff} = \left\{ \mu_{LS}^2 [e^{-\Delta H^\circ/RT} e^{\Delta S^\circ/R} + 1]^{-1} + \mu_{HS}^2 [e^{\Delta H^\circ/RT} e^{-\Delta S^\circ/R} + 1]^{-1} \right\}^{1/2}$$

where T is the temperature of the solution. μ_{eff} is the overall magnetic moment of the solution. μ_{LS} and μ_{HS} are the magnetic moments of respectively pure low spin and a pure high spin form of the complex investigated. ΔH° and ΔS° are respectively standard enthalpy and entropy of the spin transition process and R is the gas constant.

In case when the values of μ_{LS} and μ_{HS} are known, the fitting procedure involves only two parameters and hence leads usually straightforward to the solution. [242] When the magnetic moments of the pure low spin and or pure high spin forms were not yet reported and the temperature range available, determined by the solvent, does not allow for pushing the equilibrium to one of the limits (exclusively low spin or high spin form present), the four-parameter fit is required to estimate not only the enthalpy and entropy of the complex but also μ_{LS} and μ_{HS} . This fitting problem leads often to the high uncertainty [241] [130] or even disables the reliable fit completely, especially when the amount of data is limited by the narrow range of available temperatures, being the case particularly for water solutions. Hence, the most obvious strategy is to make the assumptions concerning one of the parameters and fix it, leading to a much simpler and usually significantly less problematic three-parameter fit. One of the options would be to assume the magnetic moment of the low spin or a high spin form on the basis of the experimental data accessible for possibly most similar analogs. However, this requires a particular attention as the temperature-independent-paramagnetism, which is the most common reason for a deviation from the theoretical spin-only values of the magnetic susceptibility of complexes, can vary even among close analogues. Instead, the physically relevant assumptions on the extreme (minimum and maximum) values of μ_{HS} could be made as previously reported [122] to rationalize the results: high spin magnetic moment was fixed to be either 4.9 (minimal value - spin-only value for iron with 4 unpaired electrons where $S = 2$: $\mu = [S(S+2)]^{1/2}$) [279] or 5.4 μ_B (5.5 μ_B is a spin-only value of magnetic moment for species with 5 unpaired electrons and on the top of that great majority of the iron(II) high spin complexes do not exceed this value). [122]

For our purposes, two non-linear fit methods were used in order to find the optimal values of μ_{LS} and μ_{HS} , ΔH° and ΔS° describing the experimental data in the most reliable way, namely Levenberg-Marquardt algorithm and Generalized Reduced Gradient (GRG2) nonlinear

optimization code used by Microsoft Excel 2007 Solver add-in. according to the previously reported method (maximizing the R^2 of the fit and estimating the confidence intervals at 0.01 – Brown 2001^[280] - as well as calculating the error according to the method proposed by Harris et al.^[281]

Fitting results. Parameters obtained from nonlinear fitting curves of the spin transition of [Fe15] are presented in table below.

solvent	method	μ_{LS}	μ_{HS}	ΔH°	ΔS°	$T_{1/2}$
		[μ_B]	[μ_B]	[kJ/mol]	[J/(mol*K)]	[K]
water	Solver (Newton's gradient)	0.00 ± 0.05	5.02 ± 0.51	28.11 ± 1.34	74.35 ± 6.28	378
water	Levenberg-Marquardt	0.00 ± 36612*	4.88 ± 0.90	28.52 ± 6.17	76.24 ± 21.79	374
water	Solver (Newton's gradient)	0.06 ± 0.04	4.90**	28.47 ± 0.42	75.98 ± 1.28	375
water	Levenberg-Marquardt	0.00 ± 37730*		28.34 ± 1.03	75.58 ± 2.86	375
water	Solver (Newton's gradient)	0.00 ± 0.05	5.40**	27.23 ± 0.22	70.13 ± 0.68	388
water	Levenberg-Marquardt	0.00 ± 3488*		27.28 ± 1.03	70.29 ± 2.84	388
acetonitrile	Solver (Newton's gradient)	0.41 ± 0.13	5.40 ± 1.22	26.79 ± 2.93	72.15 ± 13.60	371
acetonitrile	Levenberg-Marquardt	0.40 ± 0.16	5.43 ± 1.21	26.72 ± 3.27	71.85 ± 14.54	372
acetonitrile	Solver (Newton's gradient)	0.46 ± 0.05	4.90**	28.18 ± 0.55	78.54 ± 1.66	359
acetonitrile	Levenberg-Marquardt	0.46 ± 0.06		28.16 ± 0.87	78.48 ± 2.66	359
acetonitrile	Solver (Newton's gradient)	0.41 ± 0.05	5.40**	26.80 ± 0.53	72.18 ± 1.59	371
acetonitrile	Levenberg-Marquardt	0.41 ± 0.08		26.79 ± 0.81	72.14 ± 2.47	371

* abnormally large uncertainty is a sign of over-parameterization (to small part of the curve is covered by the experimental data)

** fixed value of the magnetic moment of the high spin form allows for a 3-parameter fit which leads to lower systematic uncertainties

Short note on the results: In the case of acetonitrile solution of FeL1. data obtained from the measurements within the temperature range of 253 – 333 K were fit by the above-mentioned algorithms (Levenberg-Marquard and Generalized Reduced Gradient nonlinear optimization code used by Microsoft Office Excel's Solver add-in) leading to the comparable values of thermodynamic parameters. As a control. the same methods were applied to fit experimental data into the equation (1) but with μ_{HS} fixed at 4.9 μ_B and 5.4 μ_B .^[11] In the case of aqueous solution of FeL1 the attempts to perform a non-linear fitting by the Levenberg-Marquardt method in all cases

(including those with fixed μ_{HS}) always led to abnormally high errors of the μ_{LS} . suggesting an over-parameterization (* in the table above). It can indicate that the data could suffer from the excessive number of parameters to be fit with covering only a small part of the curve. hence suggesting. that some assumptions considering at least one of the parameters should be made to decrease the number of flexible parameters. On the other hand. Solver supported optimization. performed as described previously[14] furnished reasonable values of the parameters. Three parameter-fits were also performed on experimental data from aqueous solution. All results are included in the table above.

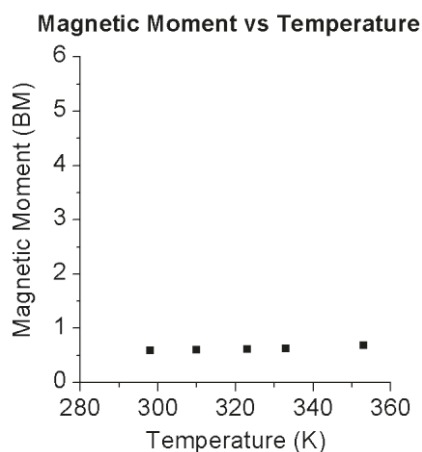
Variable-temperature magnetic behavior of other complexes

[Fe³⁴]*2BF₄

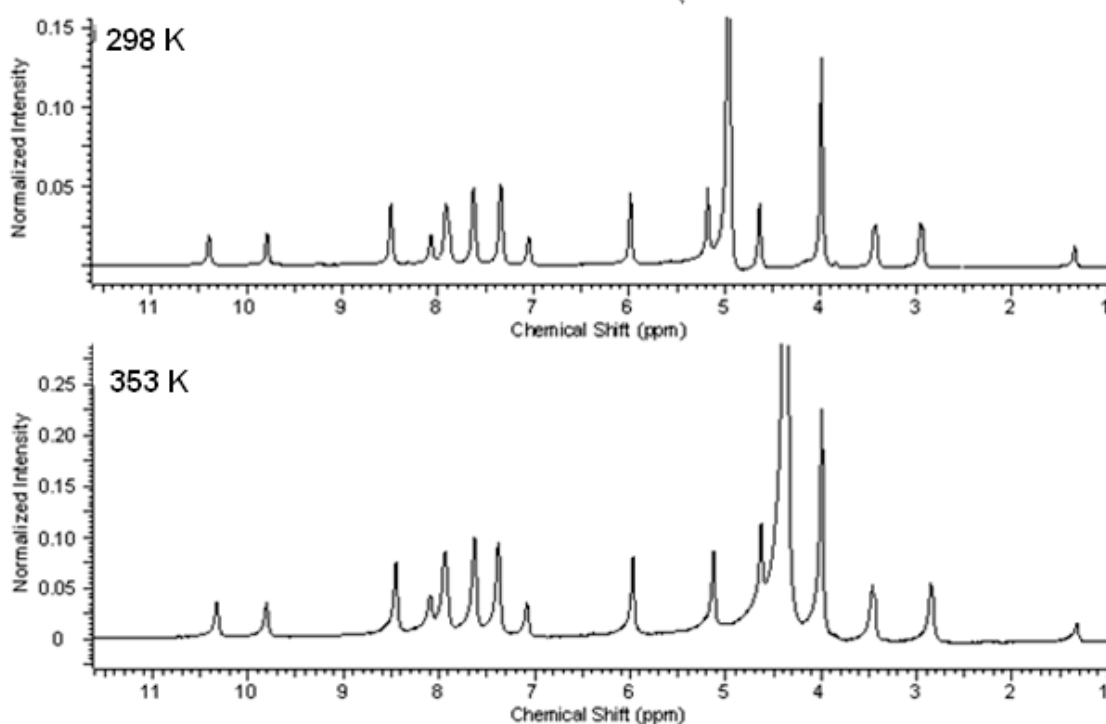
Magnetic moments of [Fe³⁴]*2BF₄ (Evans' method) at different temperatures:

[Fe³⁴] in aqueous solution

Temp. [K]	Magnetic Moment [BM]
298	0,59
310	0,60
323	0,62
333	0,62
353	0,69

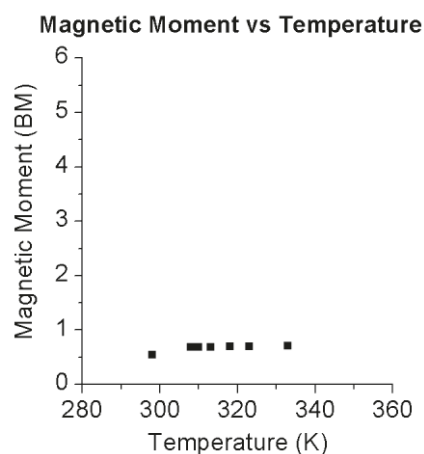
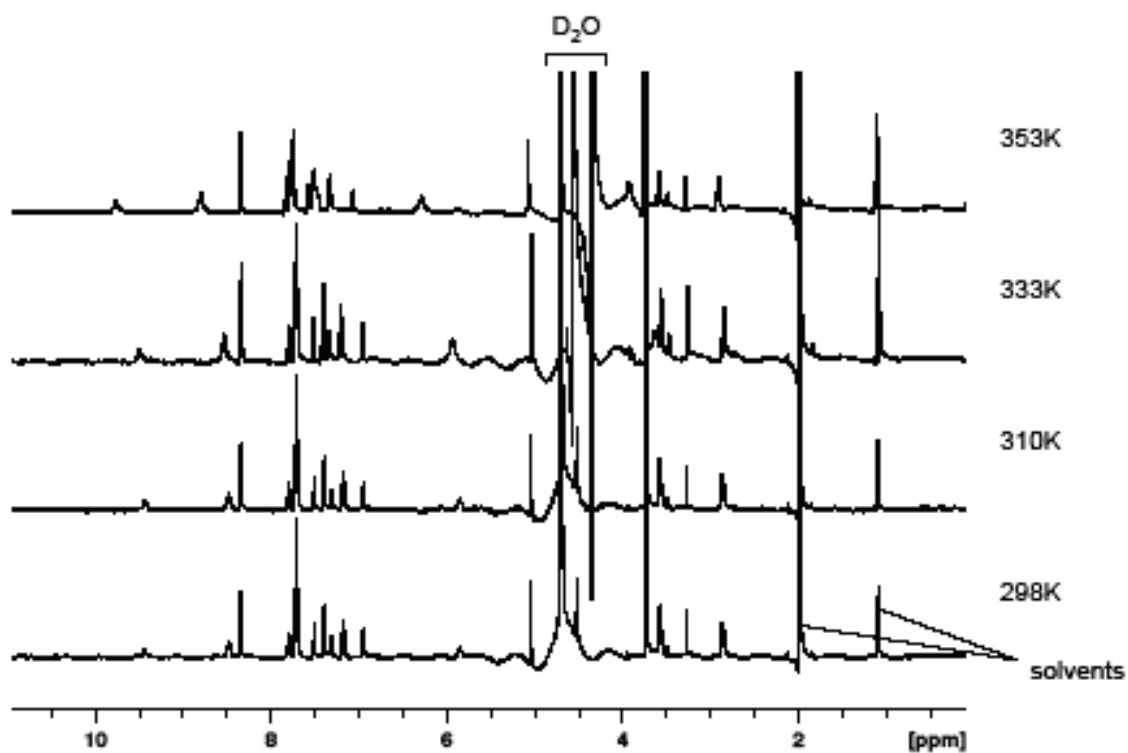


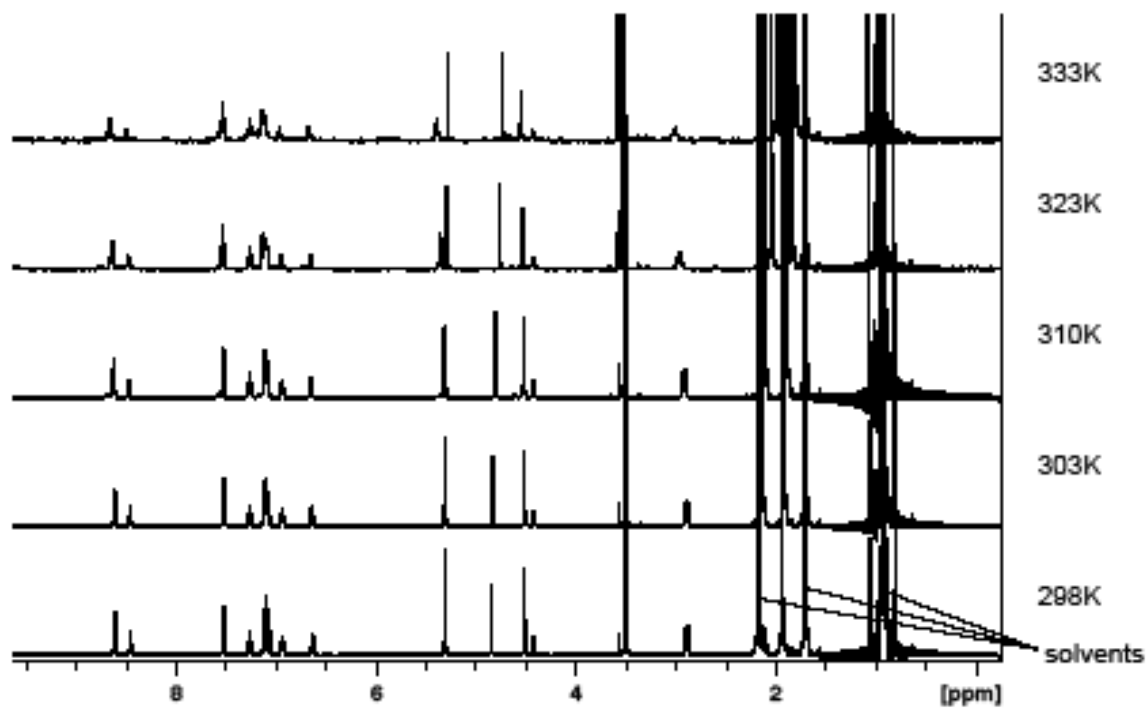
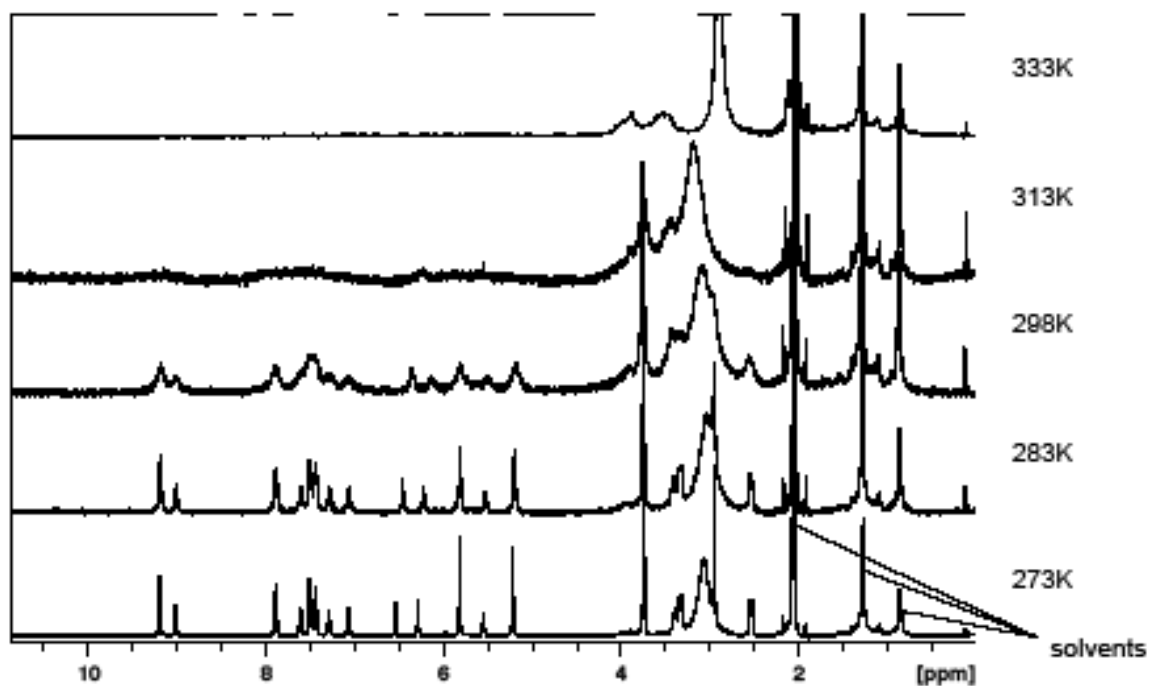
Comparison of ¹H NMR spectra of [Fe³⁴]*2BF₄ at different temperatures (D₂O)



[Fe35]*2ClO₄Magnetic moments of [Fe35]*2ClO₄ (Evans' method) at different temperatures**[Fe35] in aqueous solution**

Temp. [K]	Magnetic Moment [BM]
298	0,54
308	0,68
310	0,69
313	0,68
318	0,70
323	0,70
333	0,71

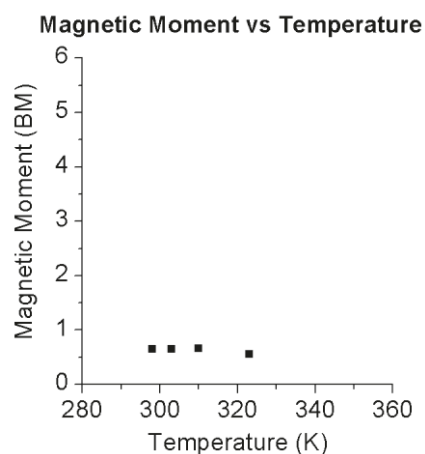
Temperature dependency (298 – 353 K) of ¹H NMR spectra in D₂O

[Fe19(CH₃CN)]*2BF₄Variable temperature ¹H NMR spectra of [Fe19(CH₃CN)]*2BF₄ in CD₃CN (298 - 333 K)Variable temperature ¹H NMR spectra of [Fe19(CH₃CN)]*2BF₄ in Acetone-d₆ (298 - 333 K)

Magnetic moments of $[\text{Fe}_{19}(\text{CH}_3\text{CN})] \cdot 2\text{BF}_4$ (Evans' method) at different temperatures and different solvents

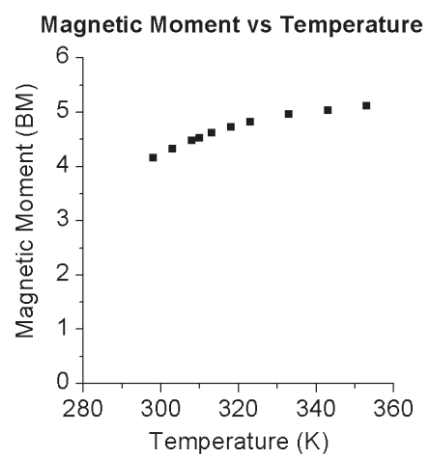
$[\text{Fe}_{19}(\text{CH}_3\text{CN})]$ in acetonitrile- d_3

Temp. [K]	Magnetic Moment [BM]
298	0,65
303	0,65
310	0,66
323	0,56



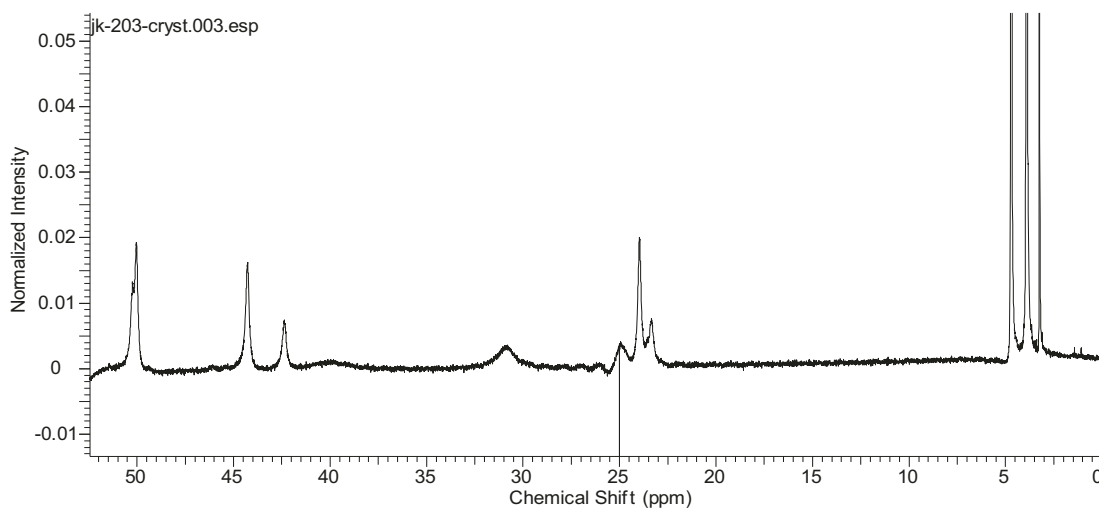
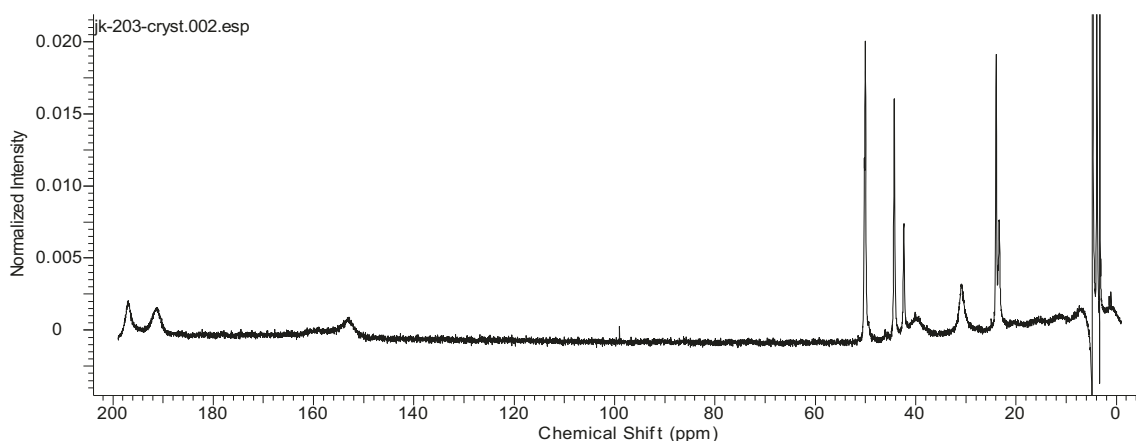
$[\text{Fe}_{19}(\text{CH}_3\text{CN})]$ in aqueous solution

Temp. [K]	Magnetic Moment [BM]
298	4,16
303	4,33
308	4,48
310	4,53
313	4,62
318	4,73
323	4,83
333	4,96
343	5,03
353	5,12

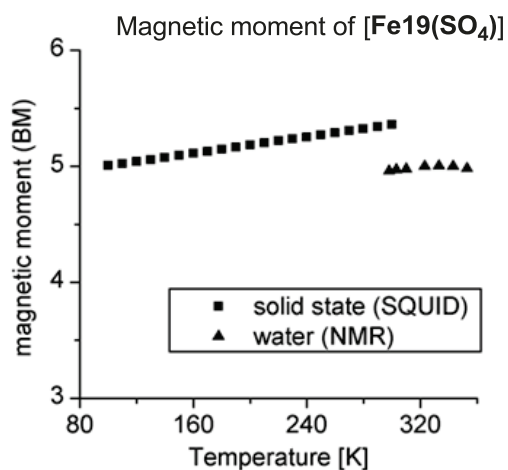


[Fe19(SO₄)]

¹H NMR spectrum of [Fe19(SO₄)]_in D₂O at 298 K (and zoom of 0 - 50 ppm region)



Magnetic moment of [Fe19(SO₄)] in the solid state (SQUID method) and in aqueous solution (Evans' method):



Temp. [K]	Magnetic Moment [BM]
298	4.96
303	4.97
310	4.98
323	5.00
333	5.00
343	5.00
353	4.98

TITRATION EXPERIMENTS – ANIONS' INFLUENCE ON [Fe15] (IN MeOH)

UV-Vis Data

These data recorded on a V-670 Jasco spectrophotometer at RT for 1 cm optical pathway.

Absorbance at 458 nm upon anion addition in MeOH for 0.2 Mm solution of [Fe15]

Anion eq	CH ₃ COO ⁻	Cl ⁻	I ⁻	HSO ₄ ⁻	NO ₃ ⁻	H ₂ PO ₄ ⁻
0	1,672	1,852	1,683	1,883	1,893	1,869
0,2	1,648	1,819	1,652	1,743	1,875	1,734
0,4	1,631	1,800	1,642	1,610	1,865	1,547
0,6	1,612	1,784	1,632	1,472	1,849	1,374
0,8	1,596	1,771	1,627	1,326	1,838	
1	1,580	1,756	1,622	1,187	1,836	
1,2	1,564			1,042		
1,4	1,554	1,728	1,606	0,917		
1,5					1,833	
1,6	1,540	1,716		0,818		
1,8	1,526	1,708		0,762		
2	1,513	1,691	1,590	0,732	1,833	
2,1						0,717
2,5	1,501	1,675	1,593	0,700		
2,6						0,647
3	1,463	1,659	1,593	0,688	1,828	
3,1						0,607
3,5	1,438	1,647		0,679		
4	1,400	1,630	1,590	0,670	1,822	
4,1						0,572
4,5	1,380	1,615		0,665		
5	1,355	1,599	1,586	0,665	1,822	
5,1						0,543
6	1,317	1,582		0,664		
7	1,285	1,563	1,581	0,662		
8	1,258	1,539		0,661		
9	1,231			0,662		
10	1,207	1,499	1,571	0,666	1,826	0,510
20		1,374	1,579		1,825	
30		1,294			1,823	
40			1,578			
100	0,783			0,849	1,815	0,482
110			1,559			
200					1,780	

Magnetic Moment upon the addition of anions

Magnetic moments were collected at 500 MHz standard proton frequency and as previously described. Measurements were done at RT in deuterated methanol for 5 mM concentration of the complex. 2 % tBuOH was used as internal standard. After the anion addition sample was mixed intensely for 30 seconds and then the measurements were performed. Stock solutions of different concentrations of the anions were prepared in deuterated methanol upon dissolution of their tetraalkylammonium salts. Monoanionic species were used in all the cases to enable comparison.

Anion/ equivalents	0,0	0,2	0,4	0,6	0,8	1,0	2,0	3,0
H₂PO₄⁻	1,97	2,60	3,14	3,64	4,05	4,36	4,91	5,04
SCN⁻	1,77	2,40	2,87	3,27	3,53	3,75	4,26	4,47
CH₃COO⁻	1,79	2,23	2,49	2,69	2,88	2,97	3,43	3,66
Cl⁻	1,89	2,10	2,11	2,11	2,31	2,38	2,67	2,86
HSO₄⁻	1,95	2,25	2,32	2,40	2,40	2,45	2,50	2,52
Br⁻	1,92	2,04	2,11	2,13	2,17	2,18	2,21	2,24
I⁻	1,95	2,03	2,01	2,02	2,03	2,03	1,99	1,95
NO₃⁻	1,69	1,69	1,72	1,73	1,76	1,76	1,80	1,78
CN⁻	1,74		1,68	1,55	1,35	1,02	0,42	0,59

Estimations of binding constants

Binding constant were calculated as described in chapter 7 of this work on the basis of the results presented above. Fitting results were obtained upon minimization of the sum of weighted square difference between the observed and calculated values of the magnetic moments but assuming a tolerance for the difference of $0.03 \mu_B$ which was in general the variation between the values obtained for different repeats. Small number of data and limited precision of the Evans method cause that the obtained values cannot be interpreted quantitatively but the relative comparison of the values for different anions can give a general idea of responsiveness. Grey fields in the tables represents the fixed values of the parameters during the fit. Two parameters fits often gave the unreliable values of the magnetic moment for the anion-bound specie. Lower and upper theoretical limit of the stability constant values were obtained from the one parameter fit of K_B for the set of magnetic moments of $0.0 \mu_B$, $4.9 \mu_B$ and $5.4 \mu_B$ (for lower limit) or $0.4 \mu_B$, $5.4 \mu_B$ and $4.9 \mu_B$ (for upper limit) for μ_{LS} , μ_{HS} and μ_{HSA} respectively.

ONE PARAMETER FIT for K_B		
	Fixed parameters	
$\mu_{LS} [\mu_B]$	0.00	0.40
$\mu_{HS} [\mu_B]$	4.90	5.40
$\mu_{HSA} [\mu_B]$	5.40	4.90
Anions	$K_{min} [M^{-1}]$	$K_{max} [M^{-1}]$
Phosphate	3974	20932
Thiocyanate	1473	3728
Acetate	446	875
Chloride	102	177
Sulfate*	74	124
Bromide	40	65

* poor fit

TWO PARAMETER FIT for K_B and μ_{HSA}				
	Fixed parameters			
$\mu_{LS} [\mu_B]$	0.00		0.40	
$\mu_{HS} [\mu_B]$	4.90		5.40	
Anions	$K_{min} [M^{-1}]$	$\mu_{HSA} [\mu_B]$	$K_{max} [M^{-1}]$	$\mu_{HSA} [\mu_B]$
Phosphate	3713	5.44	4677	5.44
Thiocyanate	3300	4.79	4191	4.80
Acetate	1345	4.30	1704	4.31
Chloride	641	3.50	811	3.50
Sulfate*	200	4.00	252	4.00
Bromide	47688	2.25	2008	2.48

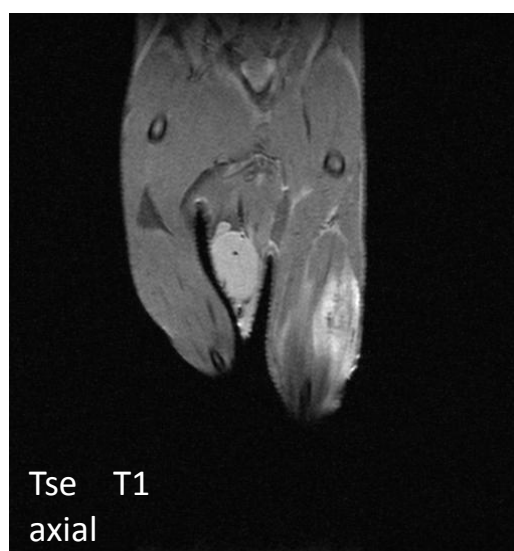
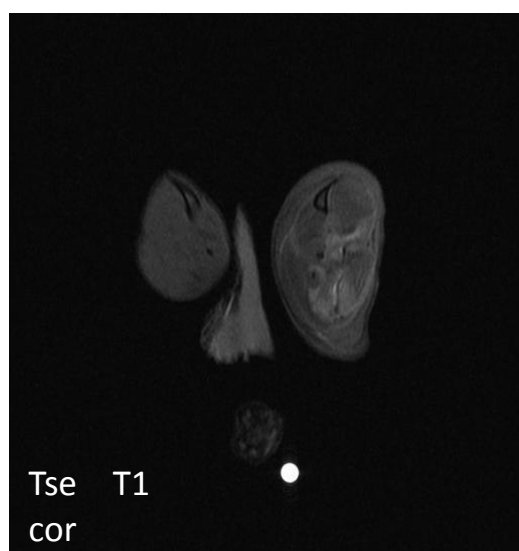
* poor fit

IN VIVO STUDIES

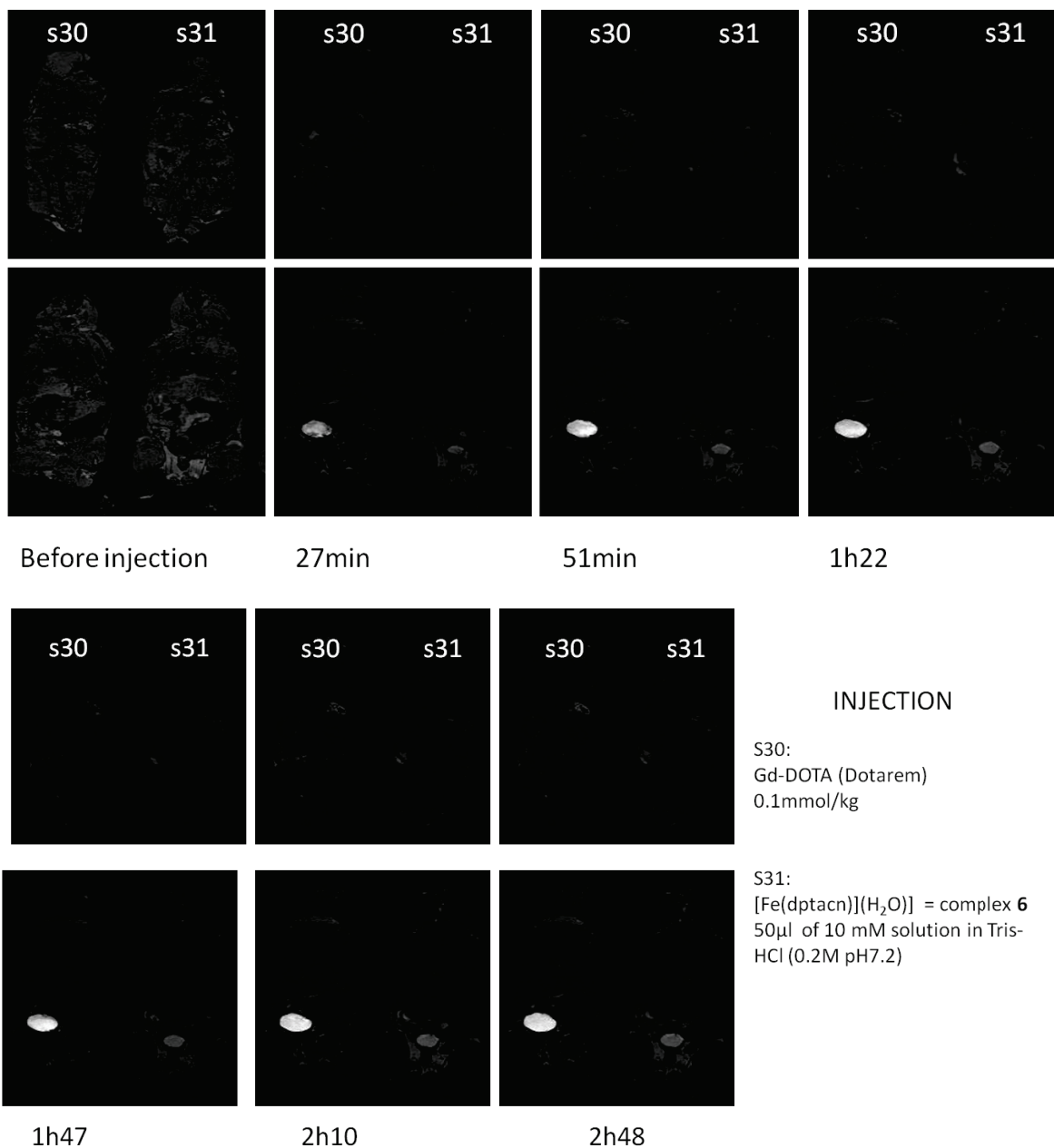
MR *in vivo* images of mice

MRI images were acquired in 7 T small animal MRI apparatus. Wild type mice were used and the injections were performed after anaesthesia with isoflurane. Compounds were injected in buffered solutions (see below).

T₂-weighted (above) and T₁-weighted (below) MRI images upon the injection of [Fe19] high spin bispidine complex. Intramuscular injection of 25 μ l of 50 mM solution of the compound in HEPES buffer at physiological pH was followed by electroporation to ensure probe internalization. Cor denotes coronal slice, axial denotes axial slice.



MRI images acquired after different periods of times after the injection. S30 denotes the individual treated with a standard dose of Gd-DOTA commercial contrast agent (intravenous injection of 0.1 mmol/kg of body weight). S31 is an individual intravenously injected with 50 μ l of 10 mM solution in Tris-HCl 0.2 M pH 7.2 of model dptacn-iron(II) complex **[Fe(dptacn)(Y)]**. This mouse had to be reanimated after the injection due to the toxic effects of the product.



Biodistribution studies with radioactive compound

Model [Fe(tpnacn)] complex (compound 5) derivatized with Fe-59 according to the procedure described in chapter 9 was dissolved in 0.15 M Tris-HCl at pH 7.4 with 5 % of acetonitrile, to obtain final concentration of 10 mM. Approximately 100 µl of this solution were injected intramuscularly (into the leg – see also table below) to each of 10 mice and then upon sacrificing them by decapitation organs were separated and radioactivity for each organ was measured. Precise mass of each individual mouse as well as the dose injected and the obtained results are given in table below.

Radioactivity per organ after 10 min [%]							
Organ	1	2	3	4	5	Mean - 10 min	ST. DEV.
Cadaver	36.04	50.68	31.45	26.05	19.23	32.69	10.60
Brain	0.18	0.26	0.19	0.09	0.17	0.18	0.05
Heart	0.55	0.54	0.35	0.36	0.17	0.39	0.14
Liver	2.98	5.80	3.90	2.56	5.30	4.11	1.26
Muscle	0.24	0.30	0.22	0.07	0.15	0.20	0.08
Bone	0.29	0.33	0.25	0.15	0.14	0.23	0.08
Skin	1.09	0.66	1.02	0.89	1.13	0.96	0.17
Lung	0.95	1.03	0.67	0.80	0.49	0.79	0.19
Leg *	50.20	20.03	56.15	63.34	36.99	45.34	15.33
Spleen	0.21	0.37	0.22	0.17	0.15	0.22	0.08
Kidney	4.83	18.31	4.28	4.83	7.63	7.97	5.30
Blood	2.46	1.69	1.11	0.54	0.94	1.35	0.67

place of the injection which explains the elevated amount of the compound found in this location

Radioactivity per organ after 1 h [%]							
Organ	1	2	3	4	5	Mean - 1 h	ST. DEV.
Cadaver	15.51	12.29	21.49	11.31	19.49	16.02	3.96
Brain	0.19	0.08	0.15	0.06	0.20	0.14	0.06
Heart	0.19	0.08	0.13	0.09	0.20	0.14	0.05
Liver	31.03	12.83	23.78	7.56	22.68	19.58	8.35
Muscle	0.48	0.07	0.11	0.07	0.17	0.18	0.16
Bone	0.20	0.07	0.13	0.04	0.14	0.12	0.06
Skin	0.49	0.25	0.69	0.23	1.49	0.63	0.46
Lung	0.48	0.15	0.42	0.14	0.26	0.29	0.14
Leg*	2.32	1.29	5.51	27.22	2.47	7.76	9.83
Spleen	0.38	0.15	0.15	0.07	0.19	0.19	0.10
Kidney	48.32	20.80	30.31	10.32	33.29	28.61	12.72
Blood	0.39	0.16	17.14	0.09	0.15	0.19	0.12

* place of the injection

BIBLIOGRAPHY

- [1] Nat. Res. Council U. S. A., *Visualizing Chemistry: the Progress and Promise of Advanced Chemical Imaging*, The National Academies Press Washington, D.C., **2006**.
- [2] J. N. Lalena, D. A. Cleary, *Principles of Inorganic Materials Design*, 2nd ed., **2010**.
- [3] <http://wwwchem.uwimona.edu.jm/courses/magnetism.html>, R. J. Lancashire, **2000**, last update: 30/03/2011, accessed: 03/09/2013.
- [4] <http://www.goiit.com/posts/list/community-shelf-the-shapes-of-atomic-orbitals-26409.htm>, V. raghavan, **2007**, last update: 10/09/2007, accessed: 26/09/2013.
- [5] C. J. O'Connor, S. J. Lippard, *Magnetic susceptibility measurements.*, Vol. 29, Progress in Inorganic Chemistry, **1982**.
- [6] J. Clarke, A. I. Braginski, *The SQUID Handbook: Fundamentals and Technology of SQUIDs and SQUID Systems, Vol. 1*, Wiley, **2005**.
- [7] G. Budin, H. J. Chung, H. Lee, R. Weissleder, *Angew Chem Int Ed Engl* **2012**, *51*, 7752-7755.
- [8] P. Marcon, K. Ostanina, *Overview of Methods for Magnetic Susceptibility Measurement*, PIERS, **2012**.
- [9] H. J. Chung, T. Reiner, G. Budin, C. Min, M. Liong, D. Issadore, H. Lee, R. Weissleder, *ACS Nano* **2011**, *5*, 8834-8841.
- [10] M. Liong, M. Fernandez-Suarez, D. Issadore, C. Min, C. Tassa, T. Reiner, S. M. Fortune, M. Toner, H. Lee, R. Weissleder, *Bioconjugate Chem.* **2011**, *22*, 2390-2394.
- [11] B.-T. Doan, S. Meme, J.-C. Beloeil, in *The Chemistry of Contrast Agents in Medical Magnetic Resonance Imaging*, John Wiley & Sons, Ltd, **2013**, 1-23.
- [12] J. C. Gore, H. C. Manning, C. C. Quarles, K. W. Waddell, T. E. Yankeelov, *Magnetic resonance imaging* **2011**, *29*, 587-600.
- [13] C. Tu, E. Osborne, A. Louie, *Ann Biomed Eng* **2011**, *39*, 1335-1348.
- [14] T. J. B. Lambert, E. P. Mazzola, *Nuclear Magnetic Resonance Spectroscopy - An Introduction to Principles, Applications and Experimental Methods*, Pearson Education Inc., New Jersey, **2004**.
- [15] <http://www.diagnosticimaging.com/dimag/legacy/molecularimagingoutlook/2003jun/index.html>, C. Carrington, **2003**, last update: accessed: 02/08/2013.
- [16] M. Baker, *Nature* **2010**, *463*, 977-980.
- [17] P. Hermann, J. Kotek, V. Kubicek, I. Lukes, *Dalton Transactions* **2008**, 3027-3047. <http://dx.doi.org/10.1039/b110420a>
- [18] é. Tóth, L. Helm, A. Merbach, in *The Chemistry of Contrast Agents in Medical Magnetic Resonance Imaging*, John Wiley & Sons, Ltd, **2013**, 25-81.
- [19] N. Richardson, J. A. Davies, B. Radüchel, *Polyhedron* **1999**, *18*, 2457-2482.
- [20] R. B. Lauffer, *Chem. Rev.* **1987**, *87*, 901-927.
- [21] P. H. Fries, E. Belorizky, in *The Chemistry of Contrast Agents in Medical Magnetic Resonance Imaging*, John Wiley & Sons, Ltd, **2013**, 277-309.
- [22] J. Kowalewski, D. Kruk, G. Parigi, in *Adv. Inorg. Chem., Vol. Volume 57*, Academic Press, **2005**, 41-104.
- [23] P. Caravan, C. T. Farrar, L. Frullano, R. Uppal, *Contrast Media & Molecular Imaging* **2009**, *4*, 89-100.
- [24] P. Caravan, J. J. Ellison, T. J. McMurry, R. B. Lauffer, *Chem. Rev.* **1999**, *99*, 2293-2352.
- [25] R. R. Sharp, *Journal of Magnetic Resonance (1969)* **1992**, *100*, 491-516.
- [26] A. Borel, F. Yerly, L. Helm, A. E. Merbach, *J. Am. Chem. Soc.* **2002**, *124*, 2042-2048.
- [27] K. O. Lim, D. D. Stark, P. T. Leese, A. Pfefferbaum, S. M. Rocklage, S. C. Quay, *Radiology* **1991**, *178*, 79-82.
- [28] C. F. G. C. Geraldés, S. Laurent, *Contrast Media & Molecular Imaging* **2009**, *4*, 1-23.
- [29] D. D. Schwert, N. Richardson, G. J. Ji, B. Raduchel, W. Ebert, P. E. Heffner, R. Keck, J. A. Davies, *J. Med. Chem.* **2005**, *48*, 7482-7485.
-

-
- [30] V. M. Runge, M. A. Foster, J. A. Clanton, M. M. Jones, C. M. Lukehart, J. M. S. Hutchison, J. R. Mallard, F. W. Smith, C. L. Partain, A. E. James, *Radiology* **1984**, *152*, 123-126.
- [31] V. Stavila, M. Allali, L. Canaple, Y. Stortz, C. Franc, P. Maurin, O. Beuf, O. Dufay, J. Samarut, M. Janier, J. Hasserodt, *New J. Chem.* **2008**, *32*, 428-435. doi: 10.1039/B715254J
- [32] F. Touti, A. K. Singh, P. Maurin, L. Canaple, O. Beuf, J. Samarut, J. Hasserodt, *J. Med. Chem.* **2011**, *54*, 4274-4278.
- [33] L. Telgmann, C. A. Wehe, J. Kunнемeyer, A. C. Bulter, M. Sperling, U. Karst, *Analytical and Bioanalytical Chemistry* **2012**, *404*, 2133-2141.
- [34] T. Reiter, O. Ritter, M. R. Prince, P. Nordbeck, C. Wanner, E. Nagel, W. R. Bauer, *Journal of Cardiovascular Magnetic Resonance* **2012**, *14*.
- [35] M. Rohrer, H. Bauer, J. Mintorovitch, M. Requardt, H. J. Weinmann, *Investigative Radiology* **2005**, *40*, 715-724.
- [36] R. B. Lauffer, *Magnetic Resonance in Medicine* **1991**, *22*, 339-342.
- [37] P. Caravan, Z. Zhang, in *The Chemistry of Contrast Agents in Medical Magnetic Resonance Imaging*, John Wiley & Sons, Ltd, **2013**, 311-342.
- [38] C. S. Bonnet, L. Tei, M. Botta, é. Tóth, in *The Chemistry of Contrast Agents in Medical Magnetic Resonance Imaging*, John Wiley & Sons, Ltd, **2013**, 343-385.
- [39] J. C. Gore, H. C. Manning, C. C. Quarles, K. W. Waddell, T. E. Yankeelov, *Magn Reson Imaging* **2011**, *29*, 587-600.
- [40] A. C. Esqueda, J. A. Lopez, G. Andreu-De-Riquer, J. C. Alvarado-Monzon, J. Ratnakar, A. J. M. Lubag, A. D. Sherry, L. M. De Leon-Rodriguez, *J. Am. Chem. Soc.* **2009**, *131*, 11387-11391.
- [41] A. Bogdanov, Jr., L. Matuszewski, C. Bremer, A. Petrovsky, R. Weissleder, *Mol Imaging* **2002**, *1*, 16-23.
- [42] E. Rodriguez, M. Nilges, R. Weissleder, J. W. Chen, *J. Am. Chem. Soc.* **2010**, *132*, 168-177.
- [43] R. B. Lauffer, T. J. McMurry, S. O. Dunham, e. al., WO 9736619, **1997**.
- [44] S. Aime, M. Botta, S. G. Crich, G. Giovenzana, G. Palmisano, M. Sisti, *Chem. Commun.* **1999**, 1577-1578.
- [45] J. Henning, O. Speck, *High-Field MR Imaging*, Springer-Verlag, Berlin, **2012**.
- [46] V. Schepkin, M. Elumalai, J. Kitchen, C. Qian, P. Gor'kov, W. Brey, *Magn. Reson. Mater. Phys., Biol. Med.* **2013**, 1-8.
- [47] R. A. Moats, S. E. Fraser, T. J. Meade, *Angewandte Chemie International Edition in English* **1997**, *36*, 726-728.
- [48] T. Chauvin, P. Durand, M. Bernier, H. Meudal, B.-T. Doan, F. Noury, B. Badet, J.-C. Beloeil, É. Tóth, *Angew. Chem. Int. Ed.* **2008**, *47*, 4370-4372.
- [49] V. Stavila, Y. Stortz, C. Franc, D. Pitrat, P. Maurin, J. Hasserodt, *Eur. J. Inorg. Chem.* **2008**, 3943-3947.
- [50] T. Chauvin, S. Torres, R. Rosseto, J. Kotek, B. Badet, P. Durand, É. Tóth, *Chemistry – A European Journal* **2012**, *18*, 1408-1418.
- [51] F. Touti, P. Maurin, J. Hasserodt, *Angew. Chem. Int. Ed.* **2013**, *52*, 4654-4658.
- [52] J. A. Duimstra, F. J. Femia, T. J. Meade, *J. Am. Chem. Soc.* **2005**, *127*, 12847-12855.
- [53] J. Hasserodt, J. L. Kolanowski, F. Touti, *Angewandte Chemie International Edition in English* **2013**, *in press*.
- [54] R. S. Dickins, S. Aime, A. S. Batsanov, A. Beeby, M. Botta, J. Bruce, J. A. K. Howard, C. S. Love, D. Parker, R. D. Peacock, H. Puschmann, *J. Am. Chem. Soc.* **2002**, *124*, 12697-12705.
- [55] M. P. Lowe, D. Parker, O. Reany, S. Aime, M. Botta, G. Castellano, E. Gianolio, R. Pagliarin, *J. Am. Chem. Soc.* **2001**, *123*, 7601-7609.
- [56] M. Woods, G. E. Kiefer, S. Bott, A. Castillo-Muzquiz, C. Eshelbrenner, L. Michaudet, K. McMillan, S. D. K. Mudigunda, D. Grin, G. Tircso, S. R. Zhang, P. Zhao, A. D. Sherry, *J. Am. Chem. Soc.* **2004**, *126*, 9248-9256.
- [57] G. Angelovski, P. Fouskova, I. Mamedov, S. Canals, E. Toth, N. K. Logothetis, *Chembiochem* **2008**, *9*, 1729-1734.
-

- [58] J. L. Major, R. M. Boiteau, T. J. Meade, *Inorg. Chem.* **2008**, *47*, 10788-10795.
- [59] J. L. Major, G. Parigi, C. Luchinat, T. J. Meade, *Proc. Natl. Acad. Sci. U. S. A.* **2007**, *104*, 13881-13886.
- [60] E. L. Que, E. Gianolio, S. L. Baker, A. P. Wong, S. Aime, C. J. Chang, *J. Am. Chem. Soc.* **2009**, *131*, 8527-8536.
- [61] E. L. Que, E. Gianolio, S. L. Baker, S. Aime, C. J. Chang, *Dalton Transactions* **2010**, *39*, 469-476.
- [62] A. D. Sherry, P. Caravan, R. E. Lenkinski, *Journal of Magnetic Resonance Imaging* **2009**, *30*, 1240-1248.
- [63] E. o. Brücher, G. Tircsó, Z. Baranyai, Z. Kovács, A. D. Sherry, in *The Chemistry of Contrast Agents in Medical Magnetic Resonance Imaging*, John Wiley & Sons, Ltd, **2013**, 157-208.
- [64] T. Frenzel, P. Lengsfeld, H. Schirmer, J. Hutter, H. J. Weinmann, *Investigative Radiology* **2008**, *43*, 817-828.
- [65] P. Wedeking, K. Kumar, M. F. Tweedle, *Magnetic Resonance Imaging* **1992**, *10*, 641-648.
- [66] M. M. Ali, M. Woods, P. Caravan, A. C. L. Opina, M. Spiller, J. C. Fettinger, A. D. Sherry, *Chemistry-a European Journal* **2008**, *14*, 7250-7258.
- [67] M. Woods, S. R. Zhang, V. Ebron, A. D. Sherry, *Chemistry-a European Journal* **2003**, *9*, 4634-4640.
- [68] U. Himmelreich, S. Aime, T. Hieronymus, C. Justicia, F. Uggeri, M. Zenke, M. Hoehn, *Neuroimage* **2006**, *32*, 1142-1149.
- [69] J. Martinelli, M. Fekete, L. Tei, M. Botta, *Chem. Commun.* **2011**, *47*, 3144-3146.
- [70] G. Digilio, V. Catanzaro, F. Fedeli, E. Gianolio, V. Menchise, R. Napolitano, C. Gringeria, S. Aime, *Chem. Commun.* **2009**, 893-895.
- [71] G. Digilio, V. Menchise, E. Gianolio, V. Catanzaro, C. Carrera, R. Napolitano, F. Fedeli, S. Aime, *J. Med. Chem.* **2010**, *53*, 4877-4890.
- [72] V. Menchise, G. Digilio, E. Gianolio, E. Cittadino, V. Catanzaro, C. Carrera, S. Aime, *Mol. Pharm.* **2011**, *8*, 1750-1756.
- [73] L. Burai, R. Scopelliti, E. Toth, *Chem. Commun.* **2002**, 2366-2367.
- [74] F. Touti, P. Maurin, L. Canaple, O. Beuf, J. Hasserodt, *Inorg. Chem.* **2012**, *51*, 31-33.
- [75] J. Hasserodt, Contrast Agents for Magnetic Resonance Imaging., WO 2005094903, **2005**.
- [76] E. Terreno, D. D. Castelli, S. Aime, in *The Chemistry of Contrast Agents in Medical Magnetic Resonance Imaging*, John Wiley & Sons, Ltd, **2013**, 387-425.
- [77] C. E. Schäffer, C. Klixbüll Jørgensen, *J. Inorg. Nucl. Chem.* **1958**, *8*, 143-148.
- [78] E. I. Solomon, A. B. P. Lever, *Inorganic Electronic Structure and Spectroscopy, Vol. 1: Methodology*, Wiley-Interscience, **1999**.
- [79] J. E. House, in *Inorganic Chemistry (Second Edition)* (Ed.: H. James), Academic Press, **2013**, 617-642.
- [80] C. K. Jørgensen, in *Oxidation Numbers and Oxidation States*, Springer Berlin Heidelberg, **1969**, 72-119.
- [81] C. K. Jørgensen, *Modern Aspects of Ligand Field Theory*, North-Holland Pub. Co., Amsterdam, **1971**.
- [82] P. George, D. S. McClure, in *Prog. Inorg. Chem., Vol. 1* (Ed.: F. A. Cotton), Interscience Publishers, Inc., **1959**, 381-463.
- [83] P. Gülich, H. A. Goodwin, P. Gülich, H. A. Goodwin, *Vol. 233*, Springer Berlin / Heidelberg, **2004**, 1 - 47.
- [84] B. Trzaskowski, A. Les, L. Adamowicz, *Int. J. Mol. Sci.* **2003**, *4*, 503-511.
- [85] O. Sato, J. Tao, Y.-Z. Zhang, *Angew. Chem. Int. Ed.* **2007**, *46*, 2152-2187.
- [86] P. Gülich, H. A. Goodwin, *Spin Crossover in Transition Metal Compounds I, Vol. 233*, Springer-Verlag, Berlin, **2004**.
- [87] P. Gülich, H. A. Goodwin, *Spin Crossover in Transition Metal Compounds II, Vol. 234*, Springer-Verlag, Berlin, **2004**.
- [88] P. Gülich, H. A. Goodwin, *Spin Crossover in Transition Metal Compounds III, Vol. 235*, Springer-Verlag, Berlin, **2004**.

- [89] M. A. Halcrow, *Spin-Crossover Materials: Properties and Applications*, John Wiley & Sons, Ltd, **2013**.
- [90] L. Marignol, M. Coffey, M. Lawler, D. Hollywood, *Cancer Treat Rev* **2008**, *34*, 313-327.
- [91] L. Chaiswing, W. Zhong, T. D. Oberley, *Cancers (Basel)* **2011**, *3*, 3557-3584.
- [92] J. K. Beattie, *Adv. Inorg. Chem.* **1988**, *32*, 1-53.
- [93] H. Toftlund, *Coord. Chem. Rev.* **1989**, *94*, 67-108.
- [94] H. Toftlund, *Monatshefte für Chemie / Chemical Monthly* **2001**, *132*, 1269-1277.
- [95] H. Toftlund, J. J. McGarvey, P. Gülich, H. A. Goodwin, *Vol. 233*, Springer Berlin / Heidelberg, **2004**, 151-166.
- [96] M. P. Shores, C. M. Klug, S. R. Fiedler, in *Spin-Crossover Materials*, John Wiley & Sons Ltd, **2013**, 281-301.
- [97] N. Hassan, A. B. Koudriavtsev, W. Linert, *Pure Appl. Chem.* **2008**, *80*, 1281-1292.
- [98] R. A. Binstead, J. K. Beattie, T. G. Dewey, D. H. Turner, *J. Am. Chem. Soc.* **1980**, *102*, 6442-6451.
- [99] J. Rall, M. Wanner, M. Albrecht, F. M. Hornung, W. Kaim, *Chemistry – A European Journal* **1999**, *5*, 2802-2809.
- [100] A. J. Conti, C. L. Xie, D. N. Hendrickson, *J. Am. Chem. Soc.* **1989**, *111*, 1171-1180.
- [101] B. Strauß, V. Gutmann, W. Linert, *Monatshefte für Chemie / Chemical Monthly* **1993**, *124*, 515-522.
- [102] E. Evangelio, C. Rodriguez-Blanco, Y. Coppel, D. N. Hendrickson, J. P. Sutter, J. Campo, D. Ruiz-Molina, *Solid State Sciences* **2009**, *11*, 793-800.
- [103] R. Todeschini, V. Consonni, *Handbook of Molecular Descriptors, Vol. 11*, Wiley VCH, **2000**.
- [104] C. M. Hansen, *Industrial & Engineering Chemistry Product Research and Development* **1969**, *8*, 2-&.
- [105] A. Dei, *Inorg. Chem.* **1993**, *32*, 5730-5733.
- [106] O. S. Jung, D. H. Jo, Y. A. Lee, B. J. Conklin, C. G. Pierpont, *Inorg. Chem.* **1997**, *36*, 19-24.
- [107] A. Caneschi, A. Dei, *Angewandte Chemie-International Edition* **1998**, *37*, 3005-3007.
- [108] C. Benelli, A. Dei, D. Gatteschi, L. Pardi, *Inorg. Chim. Acta* **1989**, *163*, 99-104.
- [109] M. W. Lynch, D. N. Hendrickson, B. J. Fitzgerald, C. G. Pierpont, *J. Am. Chem. Soc.* **1984**, *106*, 2041-2049.
- [110] Y. Mori, H. Shirase, Y. Fukuda, *Bull. Chem. Soc. Jpn.* **2008**, *81*, 1108-1115.
- [111] M. F. Tweedle, L. J. Wilson, *J. Am. Chem. Soc.* **1976**, *98 (16)*, 4824-4834.
- [112] E. V. Dose, M. A. Hoselton, N. Sutin, M. F. Tweedle, L. J. Wilson, *J. Am. Chem. Soc.* **1978**, *100*, 1141-1147.
- [113] R. H. Petty, E. V. Dose, M. F. Tweedle, L. J. Wilson, *Inorg. Chem.* **1978**, *17*, 1064-1071.
- [114] S. A. Barrett, C. A. Kilner, M. A. Halcrow, *Dalton Transactions* **2011**, *40*, 12021-12024.
- [115] Z. Ni, M. P. Shores, *J. Am. Chem. Soc.* **2009**, *131*, 32-33.
- [116] Z. Ni, A. M. McDaniel, M. P. Shores, *Chemical Science* **2010**, *1*, 615-621.
- [117] C. M. Klug, A. M. McDaniel, S. R. Fiedler, K. A. Schulte, B. S. Newell, M. P. Shores, *Dalton Transactions* **2012**, *41*, 12577-12585.
- [118] A. M. McDaniel, A. K. Rappe, M. P. Shores, *Inorg. Chem.* **2013**, *51*, 12493-12502.
- [119] M. Enamullah, W. Linert, in *J. Coord. Chem., Vol. 38*, Taylor & Francis, **1996**, 337-346.
- [120] Y. Sunatsuki, H. Ohta, M. Kojima, Y. Ikuta, Y. Goto, N. Matsumoto, S. Iijima, H. Akashi, S. Kaizaki, F. o. Dahan, J.-P. Tuchagues, *Inorg. Chem.* **2004**, *43*, 4154-4171.
- [121] L. L. Martin, K. S. Hagen, A. Hauser, R. L. Martin, A. M. Sargeson, *J. Chem. Soc., Chem. Commun.* **1988**, 1313-1315.
- [122] L. L. Martin, R. L. Martin, A. M. Sargeson, *Polyhedron* **1994**, *13*, 1969-1980.
- [123] P. Leeladee, R. A. Baglia, K. A. Prokop, R. Latifi, S. P. de Visser, D. P. Goldberg, *J. Am. Chem. Soc.*, *134*, 10397-10400.
- [124] L. Fabbrizzi, A. Leone, A. Taglietti, *Angew. Chem. Int. Ed.* **2001**, *40*, 3066-3069.
- [125] B. T. Nguyen, E. V. Anslyn, *Coord. Chem. Rev.* **2006**, *250*, 3118-3127.
- [126] K. Severin, *Curr. Opin. Chem. Biol.* **2010**, *14*, 737-742.
- [127] D. W. Blakesley, S. C. Payne, K. S. Hagen, *Inorg. Chem.* **2000**, *39*, 1979-1989.

- [128] A. Diebold, K. S. Hagen, *Inorg. Chem.* **1998**, *37*, 215-223.
- [129] G. J. P. Britovsek, J. England, A. J. P. White, *Inorg. Chem.* **2005**, *44*, 8125-8134.
- [130] Konstantin P. Bryliakov, Eduard A. Duban, Evgenii P. Talsi, *Eur. J. Inorg. Chem.* **2005**, *2005*, 72-76.
- [131] J. England, G. J. P. Britovsek, N. Rabadia, A. J. P. White, *Inorg. Chem.* **2007**, *46*, 3752-3767.
- [132] Dabrowia.Jc, D. H. Busch, P. H. Merrell, *Inorg. Chem.* **1972**, *11*, 1979-&.
- [133] L. Fabbrizzi, M. Licchelli, G. Rabaioli, A. Taglietti, *Coord. Chem. Rev.* **2000**, *205*, 85-108.
- [134] L. Pauling, C. D. Coryell, *Proc. Natl. Acad. Sci. U. S. A.* **1936**, *22*, 210-216.
- [135] S. Ogawa, T. M. Lee, A. R. Kay, D. W. Tank, *Proc. Natl. Acad. Sci. U. S. A.* **1990**, *87*, 9868-9872.
- [136] J. P. Lopez, F. W. Heinemann, R. Prakash, B. A. Hess, O. Horner, C. Jeandey, J. L. Oddou, J. M. Latour, A. Grohmann, *Chemistry-a European Journal* **2002**, *8*, 5709-5722.
- [137] C. R. Goldsmith, R. T. Jonas, A. P. Cole, T. D. P. Stack, *Inorg. Chem.* **2002**, *41*, 4642-4652.
- [138] N. Ortega-Villar, V. c. M. Ugalde-Saldávar, M. C. Muñoz, L. A. Ortiz-Frade, J. G. Alvarado-Rodríguez, J. A. Real, R. Moreno-Esparza, *Inorg. Chem.* **2007**, *46*, 7285-7293.
- [139] A. Draksharapu, Q. Li, H. Logtenberg, T. A. van den Berg, A. Meetsma, J. S. Killeen, B. L. Feringa, R. Hage, G. Roelfes, W. R. Browne, *Inorg. Chem.* **2012**, *51*, 900-913.
- [140] C. A. Reed, F. d. r. Guiset, *J. Am. Chem. Soc.* **1996**, *118*, 3281-3282.
- [141] M. L. Childers, J. Cho, C. A. S. Regino, M. W. Brechbiel, A. G. DiPasquale, A. L. Rheingold, S. V. Torti, F. M. Torti, R. P. Planalp, *J. Inorg. Biochem.* **2008**, *102*, 150-156.
- [142] N. Segaud, J. N. Rebilly, K. Senechal-David, R. Guillot, L. Billon, J. P. Baltaze, J. Farjon, O. Reinaud, F. Banse, *Inorg. Chem.* **2013**, *52*, 691-700.
- [143] L. Sacconi, P. Nannelli, U. Campigli, *Inorg. Chem.* **1965**, *4*, 818-822.
- [144] L. Sacconi, G. Lombardo, P. Paoletti, *Journal of the Chemical Society (Resumed)* **1958**, *0*, 848-854.
- [145] H. Ohtsu, K. Tanaka, *Inorg. Chem.* **2004**, *43*, 3024-3030.
- [146] S. Thies, C. Bornholdt, F. Köhler, F. D. Sönnichsen, C. Näther, F. Tuczek, R. Herges, *Chemistry – A European Journal* **2010**, *16*, 10074-10083.
- [147] F. A. Walker, E. Hui, J. M. Walker, *J. Am. Chem. Soc.* **1975**, *97*, 2390-2397.
- [148] R. F. Pasternack, E. G. Spiro, M. Teach, *J. Inorg. Nucl. Chem.* **1974**, *36*, 599-606.
- [149] T. La, R. A. Richards, R. S. Lu, R. Bau, G. M. Miskelly, *Inorg. Chem.* **1995**, *34*, 5632-5640.
- [150] M. S. Vad, A. Lennartson, A. Nielsen, J. Harmer, J. E. McGrady, C. Frandsen, S. Morup, C. J. McKenzie, *Chem. Commun.* **2012**, *48*, 10880-10882.
- [151] M. A. Halcrow, *Polyhedron* **2007**, *26*, 3523-3576.
- [152] M. A. Hoselton, L. J. Wilson, R. S. Drago, *J. Am. Chem. Soc.* **1975**, *97*, 1722-1729.
- [153] P. Comba, M. Kerscher, W. Schiek, in *Prog. Inorg. Chem.*, John Wiley & Sons, Inc., **2008**, 613-704.
- [154] G. R. Clemo, R. Raper, *J. Chem. Soc.* **1933**, 644-645.
- [155] G. R. Clemo, W. M. Morgan, R. Raper, *J. Chem. Soc.* **1936**, 1025-1028.
- [156] Stenhouse, *J. Annalen* **1851**.
- [157] A. Samhammer, U. Holzgrabe, R. Haller, *Arch. Pharm.* **1989**, *322*, 551-555.
- [158] L. M. Jackman, T. S. Dunne, B. Muller, H. Quast, *Chem. Ber. Recl.* **1982**, *115*, 2872-2891.
- [159] H. Quast, B. Muller, E. M. Peters, K. Peters, H. G. Vonschnering, *Chemische Berichte-Recueil* **1982**, *115*, 3631-3652.
- [160] H. Stetter, R. Merten, *Chem. Ber.* **1957**, *90*, 868-875.
- [161] G. Dietz, W. Fiedler, G. Faust, *Chem. Ber.* **1969**, *102*, 4147-4151.
- [162] J. E. Douglass, T. B. Ratliff, *J. Org. Chem.* **1968**, *33*, 355-&.
- [163] R. Haller, H. Unholzer, *Archiv Der Pharmazie Und Berichte Der Deutschen Pharmazeutischen Gessellschaft* **1972**, *305*, 855-&.
- [164] R. Caujolle, P. Castera, A. Lattes, *Bulletin De La Societe Chimique De France Partie Ii-Chimie Moleculaire Organique Et Biologique* **1984**, 413-416.

- [165] E. Galvez, M. S. Arias, J. Bellanato, J. V. Garciamoros, F. Florencio, P. Smithverdier, S. Garciblanco, *Journal of Molecular Structure* **1985**, *127*, 185-201.
- [166] P. Comba, M. Kerscher, M. Merz, V. Muller, H. Pritzkow, R. Remenyi, W. Schiek, Y. Xiong, *Chemistry* **2002**, *8*, 5750-5760.
- [167] U. Kuhl, W. Englberger, M. Haurand, U. Holzgrabe, *Arch. Pharm.* **2000**, *333*, 226-230.
- [168] W. Brandt, S. Drosihn, M. Haurand, U. Holzgrabe, C. Nachtsheim, *Arch Pharm (Weinheim)* **1996**, *329*, 311-323.
- [169] T. Siener, U. Holzgrabe, S. Drosihn, W. Brandt, *Journal of the Chemical Society-Perkin Transactions 2* **1999**, 1827-1834.
- [170] R. Caujolle, P. Castera, A. Lattes, *Bulletin de la Société chimique de France* **1984**, *9-10*, 413-416.
- [171] R. Haller, *Arch. Pharm.* **1968**, *301*, 741-&.
- [172] W. Brandt, Siener, T., Holzgrabe, U., Drosihn, S., *J. Chem. Soc.* **1999**, *Perkin Trans. 2*, 1827-1834.
- [173] S. Norrehed, M. Erdelyi, M. E. Light, A. Gogoll, *Organic & Biomolecular Chemistry* **2013**.
- [174] P. Comba, M. Morgen, H. Wadepohl, *Polyhedron* **2013**, *52*, 1239-1245.
- [175] R. Haller, *Archiv Der Pharmazie Und Berichte Der Deutschen Pharmazeutischen Gessellschaft* **1969**, *302*, 113-&.
- [176] G. D. Hosken, R. D. Hancock, *Journal of the Chemical Society-Chemical Communications* **1994**, 1363-1364.
- [177] G. D. Hosken, C. C. Allan, J. C. A. Boeyens, R. D. Hancock, *J. Chem. Soc., Dalton Trans.* **1995**, 3705-3708.
- [178] P. Comba, M. Kerscher, M. Merz, V. Muller, H. Pritzkow, R. Remenyi, W. Schiek, Y. Xiong, *Chem.--Eur. J.* **2002**, *8*, 5750-5760.
- [179] P. Comba, M. Kerscher, *Cryst. Eng.* **2003**, *6*, 197-211.
- [180] P. Comba, W. Schiek, *Coord. Chem. Rev.* **2003**, *238*, 21-29.
- [181] P. Comba, C. Haaf, H. Wadepohl, *Inorg. Chem.* **2009**, *48*, 6604-6614.
- [182] S. Juran, M. Walther, H. Stephan, R. Bergmann, J. Steinbach, W. Kraus, F. Emmerling, P. Comba, *Bioconjugate Chem.* **2009**, *20*, 347-359.
- [183] S. Juran, *Journal of Labelled Compounds & Radiopharmaceuticals* **2009**, *52*, 254-255.
- [184] P. Comba, C. Haaf, S. Helmle, K. D. Karlin, S. Pandian, A. Waleska, *Inorg. Chem.* **2012**, *51*, 2841-2851.
- [185] K. Born, P. Comba, A. Daubinet, A. Fuchs, H. Wadepohl, *JBIC, J. Biol. Inorg. Chem.* **2007**, *12*, 36-48.
- [186] P. Comba, B. Martin, A. Muruganatham, J. Straub, *Inorg. Chem.* **2012**, *51*, 9214-9225.
- [187] P. Comba, C. Lang, d. L. C. Lopez, A. Muruganatham, G. Rajaraman, H. Wadepohl, M. Zajackowski, *Chem.--Eur. J.* **2008**, *14*, 5313-5328.
- [188] P. Comba, C. Haaf, A. Lienke, A. Muruganatham, H. Wadepohl, *Chemistry-a European Journal* **2009**, *15*, 10880-10887.
- [189] C. Busche, P. Comba, A. Mayboroda, H. Wadepohl, *Eur. J. Inorg. Chem.* **2010**, 1295-1302.
- [190] J. Benet-Buchholz, P. Comba, A. Llobet, S. Roeser, P. Vadivelu, S. Wiesner, *Dalton Transactions* **2010**, *39*, 3315-3320.
- [191] H. Borzel, P. Comba, K. S. Hagen, Y. D. Lampeka, A. Lienke, G. Linti, M. Merz, H. Pritzkow, L. V. Tsymbal, *Inorg. Chim. Acta* **2002**, *337*, 407-419.
- [192] P. Comba, C. Haaf, M. Kerscher, A. Lienke, Polydentate amino-substituted 3,7-diazabicyclo[3.3.1]nonan-9-one (Bispidon) ligands and their metal complexes as antitumor and contrast agents and aziridination or bleaching catalysts, WO2009010129A1, **2009**.
- [193] J. L. Kolanowski, E. Jeanneau, R. Steinhoff, J. Hasserodt, *Chemistry – A European Journal* **2013**, *19*, 8839-8849.
- [194] A. J. Adriaanse, D. W. R. Van, R. Hage, M. Ouwendijk, S. M. Veerman, Storage-stable enzymatic liquid bleaching detergent containing boron enzymatic stabilizer, WO2002068574A1, **2002**.

- [195] H. Borzel, P. Comba, R. Hage, M. Kerscher, J. Lienke, M. Merz, Ligand and complex for catalytically bleaching a substrate, WO2002048301A1, **2002**.
- [196] R. Hage, P. V. Wesenhagen, Curing catalysts for air drying inks and coatings with fast curability, WO2008003652A1, **2008**.
- [197] Antiskinning compositions for coatings, EP2474578A1,
- [198] M. R. Bukowski, P. Comba, C. Limberg, M. Merz, L. Que, Jr., T. Wistuba, *Angew. Chem., Int. Ed.* **2004**, *43*, 1283-1287.
- [199] J. Bautz, M. R. Bukowski, M. Kerscher, A. Stubna, P. Comba, A. Lienke, E. Munck, L. Que, Jr., *Angew. Chem., Int. Ed.* **2006**, *45*, 5681-5684.
- [200] P. Comba, S. Fukuzumi, H. Kotani, S. Wunderlich, *Angew. Chem., Int. Ed.* **2010**, *49*, 2622-2625, S2622/2621-S2622/2612.
- [201] M. R. Bukowski, P. Comba, A. Lienke, C. Limberg, d. L. C. Lopez, R. Mas-Balleste, M. Merz, L. Que, Jr., *Angew. Chem., Int. Ed.* **2006**, *45*, 3446-3449.
- [202] J. Bautz, P. Comba, d. L. C. Lopez, M. Menzel, G. Rajaraman, *Angew. Chem., Int. Ed.* **2007**, *46*, 8067-8070.
- [203] J. Benet-Buchholz, P. Comba, A. Llobet, S. Roeser, P. Vadivelu, H. Wadepohl, S. Wiesner, *Dalton Trans.* **2009**, 5910-5923.
- [204] P. Comba, M. Maurer, P. Vadivelu, *Inorg. Chem. (Washington, DC, U. S.)* **2009**, *48*, 10389-10396.
- [205] P. Comba, S. Wunderlich, *Chemistry-a European Journal* **2010**, *16*, 7293-7299.
- [206] M. Jaccob, P. Comba, M. Maurer, P. Vadivelu, P. Venuvanalingam, *Dalton Transactions* **2011**, *40*, 11276-11281.
- [207] R. Haller, U. Ashauer, *Arch. Pharm.* **1985**, *318*, 405-410.
- [208] H. Borzel, P. Comba, K. S. Hagen, C. Katsichtis, H. Pritzkow, *Chem.--Eur. J.* **2000**, *6*, 914-919.
- [209] K. W. Merz, R. Haller, *Pharm Acta Helv* **1963**, *38*, 442-456.
- [210] R. Haller, *Arch. Pharm. (Weinheim)* **1969**, *302*, 113-118.
- [211] R. Haller, *Arzneim.-Forsch.* **1965**, *15*, 1327-1330.
- [212] R. Haller, H. Unholzer, *Archiv Der Pharmazie Und Berichte Der Deutschen Pharmazeutischen Gessellschaft* **1971**, *304*, 866-&.
- [213] A. Komarova, A. Levov, A. Soldatenkov, S. Soldatova, *Chem. Heterocycl. Compd.* **2008**, *44*, 624-625.
- [214] P. Comba, S. Kuwata, G. Linti, H. Pritzkow, M. Tarnai, H. Wadepohl, *Chem. Commun. (Cambridge, U. K.)* **2006**, 2074-2076.
- [215] P. G. M. Wuts, T. W. Greene, *Greene's Protective Groups in Organic Synthesis*, Fourth ed., John Wiley & Sons, Inc, New Jersey, **2007**.
- [216] C. Bleiholder, H. Borzel, P. Comba, R. Ferrari, M. Heydt, M. Kerscher, S. Kuwata, G. Laurency, G. A. Lawrance, A. Lienke, B. Martin, M. Merz, B. Nuber, H. Pritzkow, *Inorg. Chem.* **2005**, *44*, 8145-8155.
- [217] U. Kuhl, A. Cambareri, C. Sauber, F. Sorgel, R. Hartmann, H. Euler, A. Kirfel, U. Holzgrabe, *Journal of the Chemical Society-Perkin Transactions 2* **1999**, 2083-2088.
- [218] M. C. Pirrung, J. Wang, *J Org Chem* **2009**, *74*, 2958-2963.
- [219] C. M. Park, *J. Org. Chem.* **2006**, *71*, 413-415.
- [220] P. Nussbaumer, K. Baumann, T. Dechat, M. Harasek, *Tetrahedron* **1991**, *47*, 4591-4602.
- [221] S. Bernard, D. Defoy, Y. L. Dory, K. Klarskov, *Bioorg. Med. Chem. Lett.* **2009**, *19*, 6127-6130.
- [222] S. G. Davies, A. C. Garner, M. J. C. Long, R. M. Morrison, P. M. Roberts, E. D. Savory, A. D. Smith, M. J. Sweet, J. M. Withey, *Organic & Biomolecular Chemistry* **2005**, *3*, 2762-2775.
- [223] Y. Onozaki, N. Kurono, H. Senboku, M. Tokuda, K. Orito, *J. Org. Chem.* **2009**, *74*, 5486-5495.
- [224] T. Miura, K. Kanemoto, S. Natsume, K. Atsumi, H. Fushimi, T. Yoshida, K. Ajito, *Biorg. Med. Chem.* **2008**, *16*, 10129-10156.
- [225] M. Breuning, M. Steiner, C. Mehler, A. Paasche, D. Hein, *J. Org. Chem.* **2009**, *74*, 1407-1410.

- [226] H. Mastalerz, M. Menard, V. Vinet, J. Desiderio, J. Functomc, R. Kessler, Y. Tsai, *J. Med. Chem.* **1988**, *31*, 1190-1196.
- [227] D. Onggo, A. D. Rae, H. A. Goodwin, *Inorg. Chim. Acta* **1990**, *178*, 151-163.
- [228] M. Nishizeki, Organic electroluminescent substance, organic electroluminescent device, optical imaging device and lighting apparatus, JP2007099962A, **2007**.
- [229] A. Terenzi, G. Barone, P. A. Palumbo, G. Giorgi, A. Guarcello, P. Portanova, G. Calvaruso, S. Buscemi, N. Vivona, A. Pace, *Dalton Trans.*, *39*, 9140-9145.
- [230] M. Massacesi, G. Devoto, G. Gelli, *Spectrochim. Acta, Part A* **1985**, *41A*, 1433-1436.
- [231] O. Y. Ryabukhina, T. A. Yusman, Y. I. Ryabukhin, A. D. Garnovskii, G. N. Dorofeenko, *Koord. Khim.* **1980**, *6*, 1186-1189.
- [232] Y. I. Ryabukhin, N. V. Shibaeva, A. S. Kuzharov, V. G. Korobkova, A. V. Khokhlov, A. D. Garnovskii, *Koord. Khim.* **1987**, *13*, 869-874.
- [233] H. Kim, S. J. Eum, Y. J. Cho, H. J. Kwon, B. O. Kim, S. M. Kim, S. S. Yoon, Novel organic electroluminescent compounds and organic electroluminescent device using the same, EP2062900A1, **2009**.
- [234] B. J. Childs, D. C. Craig, M. L. Scudder, H. A. Goodwin, *Aust. J. Chem.* **1999**, *52*, 673-680.
- [235] J. DiBenedetto, V. Arkle, H. A. Goodwin, P. C. Ford, *Inorg. Chem.* **1985**, *24*, 455-456.
- [236] H. A. Goodwin, F. E. Smith, *Inorg. Nucl. Chem. Lett.* **1974**, *10*, 99-103.
- [237] A. R. Katritzky, C. W. Rees, S. E.F.V., *Comprehensive Heterocyclic Chemistry II*, Pergamon, Oxford, **1996**.
- [238] R. E. Trifonov, A. P. Volovodenko, S. N. Vergizov, N. I. Shirinbekov, V. A. Gindin, A. O. Koren, V. Ostrovskii, *Helv. Chim. Acta* **2005**, *88*, 1790-1797.
- [239] M. G. N. Russell, R. W. Carling, J. R. Atack, F. A. Bromidge, S. M. Cook, P. Hunt, C. Isted, M. Lucas, R. M. McKernan, A. Mitchinson, K. W. Moore, R. Narquizian, A. J. Macaulay, D. Thomas, S.-A. Thompson, K. A. Wafford, J. L. Castro, *J. Med. Chem.* **2005**, *48*, 1367-1383.
- [240] C. Geraldes, M. P. M. Marques, A. D. Sherry, *Inorg. Chim. Acta* **1998**, *273*, 288-298.
- [241] J. W. Turner, F. A. Schultz, *Inorg. Chem.* **2001**, *40*, 5296-5298.
- [242] B. Weber, F. A. Walker, *Inorg. Chem.* **2007**, *46*, 6794-6803.
- [243] R. N. Dsouza, U. Pischel, W. M. Nau, *Chem. Rev.* **2011**, *111*, 7941-7980.
- [244] R. D. Hancock, A. E. Martell, in *Supramol. Chem.*, Vol. 6, Taylor & Francis, **1996**, 401-407.
- [245] Y. Ducommun, K. E. Newman, A. E. Merbach, *Inorg. Chem.* **1980**, *19*, 3696-3703.
- [246] I. Bertini, C. Luchinat, G. Parigi, *Solution NMR of Paramagnetic Molecules*, Amsterdam, **2001**.
- [247] C. Nicolini, J. Chappert, J. P. Mathieu, *Inorg. Chem.* **1977**, *16*, 3112-3115.
- [248] F. Touti, P. Maurin, J. Hasserodt, *Angew. Chem. Int. Ed.* **2013**, n/a-n/a.
- [249] F. Touti, F. Avenier, Q. Lefebvre, P. Maurin, J. Hasserodt, *Eur. J. Org. Chem.* **2010**, *2010*, 1928-1933.
- [250] P. Comba, M. Kerscher, G. A. Lawrence, B. Martin, H. Wadepohl, S. Wunderlich, *Angew. Chem., Int. Ed.* **2008**, *47*, 4740-4743.
- [251] P. Comba, B. Kanellakopulos, C. Katsichtis, A. Lienke, H. Pritzkow, F. Rominger, *J. Chem. Soc., Dalton Trans.* **1998**, 3997-4002.
- [252] T. Ravindran, R. Jeyaraman, R. W. Murray, M. Singh, *The Journal of Organic Chemistry* **1991**, *56*, 4833-4840.
- [253] E. A. Quail, E. H. Morgan, *J. Cell. Physiol.* **1994**, *159*, 238-244.
- [254] M. D. Garrick, R. J. Fletcher, K. G. Dolan, M. A. Romano, J. Walowitz, J. A. Roth, J. N. Umbreit, M. E. Conrad, L. M. Garrick, *Blood* **1999**, *94*, 403A-403A.
- [255] C. Bendergotze, *Fortschritte Der Medizin* **1980**, *98*, 590-594.
- [256] S. Zuchi, S. Cesco, Z. Varanini, R. Pinton, S. Astolfi, *Planta* **2009**, *230*, 85-94.
- [257] R. M. Pascale, M. R. De Miglio, M. R. Muroli, M. M. Simile, L. Daino, M. A. Seddaiu, S. Pusceddu, L. Gaspa, D. Calvisi, G. Manenti, F. Feo, *Hepatology* **1998**, *27*, 452-461.
- [258] C. Bendergotze, C. E. V. Pilar, N. Fischer, *Mon.schr. Kinderheilkd.* **1980**, *128*, 598-601.
- [259] W. C. Butts, Kuehnema.M, Widdowso.Gm, *Clin. Chem.* **1974**, *20*, 1344-1348.

- [260] K. M. Allal, M. Ouchefoun, M. Boumahrez, *J. Chem. Technol. Biotechnol.* **1996**, *66*, 398-404.
- [261] P. Kovacic, N. O. Brace, *Inorg. Synth.* **1960**, *6*, 172-173.
- [262] P. Kovacic, N. O. Brace, *J. Am. Chem. Soc.* **1954**, *76*, 5491-5494.
- [263] A. R. Pray, *Inorg. Synth.* **1990**, *28*, 321-323.
- [264] W. B. Guenther, *J. Chem. Educ.* **1965**, *42*, 277-&.
- [265] C. Mannich, P. Mohs, *Berichte Der Deutschen Chemischen Gesellschaft* **1930**, *63*, 608-612.
- [266] A. Bentz, P. Comba, R. J. Deeth, M. Kerschler, B. Seibold, H. Wadepohl, *Inorg. Chem. (Washington, DC, U. S.)* **2008**, *47*, 9518-9527.
- [267] R. C. Clark, J. S. Reid, *Acta Crystallographica Section A* **1995**, *51*, 887-897.
- [268] A. Altomare, M. C. Burla, M. Camalli, G. L. Casciarano, C. Giacovazzo, A. Guagliardi, A. G. G. Moliterni, G. Polidori, R. Spagna, *J. Appl. Crystallogr.* **1999**, *32*, 115-119.
- [269] P. W. Betteridge, J. R. Carruthers, R. I. Cooper, K. Prout, D. J. Watkin, *J. Appl. Cryst.* **2003**, *36*, 1487.
- [270] A. L. Spek, *Acta Crystallographica* **2009**, 148.
- [271] P. Pascal, *Ann. Chim. Phys.* **1910**, *19*, 5.
- [272] O. Kahn, *Molecular Magnetism*, Weinheim, **1993**.
- [273] D. F. Evans, *Journal of the Chemical Society (Resumed)* **1959**, 2003-2005.
- [274] D. F. Evans, D. A. Jakubovic, *J. Chem. Soc., Dalton Trans.* **1988**, 2927-2933.
- [275] D. H. Grant, *J. Chem. Educ.* **1995**, *72*, 39.
- [276] D. Ostfeld, I. A. Cohen, *J. Chem. Educ.* **1972**, *49*, 829.
- [277] J. England, R. Gondhia, L. Bigorra-Lopez, A. R. Petersen, A. J. P. White, G. J. P. Britovsek, *Dalton Transactions* **2009**, 5319-5334.
- [278] T. H. Crawford, J. Swanson, *J. Chem. Educ.* **1971**, *48*, 382.
- [279] J. L. Deutsch, S. M. Poling, *J. Chem. Educ.* **1969**, *46*, 167.
- [280] A. M. Brown, *Computer methods and programs in biomedicine* **2001**, *65*, 191-200.
- [281] D. C. Harris, *J. Chem. Educ.* **1998**, *75*, 119.

PART V

APPENDICES

PUBLICATIONS FROM THIS PHD

- ***Bispidine Platform Grants Full Control over Magnetic State of Ferrous Chelates in Water***
J. L. Kolanowski, E. Jeanneau, R. Steinhoff, J. Hasserodt; Chemistry – A European Journal 2013, 19, 8839-8849, [full paper](#) – reprinted below with permission of WILEY-VCH Verlag GmbH & Co. KGaA, Weinheim (copyright © 2013).
- ***Magnetogenesis in Water Induced by a Chemical Analyte***
J. Hasserodt, J. L. Kolanowski, F. Touti; Angewandte Chemie International Edition in English 2013, [minireview](#) (in press) – reprinted below with permission of WILEY-VCH Verlag GmbH & Co. KGaA, Weinheim (copyright © 2013).
- ***A robust protocol for radiolabeling of iron(II) metal complexes with Fe-59 isotope for in vivo studies***
J.L. Kolanowski, D. Kryza, P. Bonazza, M. Janier, J. Hasserodt, [communication](#) (in preparation).
- ***A first bispidine-iron(II) magnetogenic probe for a detection of anions in polar media***
J.L. Kolanowski, J. Hasserodt, [communication](#) (in preparation).
- ***Progress in the design of iron (II)-based probes to highlight enzyme activity in magnetic resonance images***
J. Hasserodt, F. Touti, J.L. Kolanowski, A. Singh, R. Steinhoff, P. Maurin, L. Canaple, O. Beuf, J. Samarut, *Bulletin du Cancer* 2011, 98, S71-S72, [conference abstract](#) (6^{èmes} Journées Scientifiques du CLARA, March 2011, Lyon, France).
- ***A simple protocol for introducing the radioactive ⁵⁹Fe²⁺ isotope into a model chelate for MRI that serves to determine biodistribution in mice***
J.L. Kolanowski, D. Kryza, P. Bonazza, P. Maurin, M. Janier, J. Hasserodt, [conference abstract](#) (7^{èmes} Journées Scientifiques du CLARA, March 2012, Lyon, France).
- ***Magnetogenesis with probes that report on (bio-) chemical stimuli***
F. Touti, J.L. Kolanowski, Laurence Canaple, Olivier Beuf, Jacques Samarut, Jens Hasserodt, [conference abstract](#) (48th EUCHEM conference on stereochemistry, May 2013, Burgenstock, Switzerland).

Bispidine Platform Grants Full Control over Magnetic State of Ferrous Chelates in Water

Jacek Lukasz Kolanowski,^[a] Erwann Jeanneau,^[b] Robert Steinhoff,^[a] and Jens Hasserodt^{*[a]}

Abstract: A bicyclic ligand platform for iron(II), which allows total control over the complex's magnetic properties in aqueous solution simply by varying one of the six coordination sites of the bispidine ligand, is reported. To achieve this, an efficient synthetic route to an N5 bispidine framework (ligand L4) that features an unsubstituted N-7 site is established. Then, by choosing appropriate N-7-coordinating substituents, the spin state of choice can be imposed on the corresponding ferrous

complexes under environmentally relevant conditions in water and near-room temperature. Importantly, the first low-spin and diamagnetic iron(II) chelates in the bispidine series, both in the solid state and in aqueous solution, are reported. The eradication of head-on steric clashes between pendent coordi-

nating arms is at the origin of this success. A new pair of constitutionally similar ferrous coordination compounds of a multidentate ligand system is obtained, which exhibits a distinctly binary (off-on) magnetic relationship. The new synthetic intermediate L4 may be substituted in just one step by any desired pendent arm, thus allowing access to complexes with finely tuned magnetic properties.

Keywords: bispidines • chelates • iron • magnetic properties • N ligands

Introduction

Mononuclear coordination compounds of iron(II) most commonly adopt one of two distinct spin states: low spin ($S=0$; diamagnetic) and high spin ($S=2$; paramagnetic), although a borderline case is possible: spin crossover (SCO).^[1] This set of three spin states gives access to a wide range of properties and makes ferrous complexes highly attractive for applications as switches and sensors,^[2–4] as nonheme enzyme models for biomimetic studies,^[5] and as magnetic resonance imaging contrast agents.^[6] There are numerous examples showing different spin states in the solid phase, including both distinct molecules and coordination polymers.^[2,7]

However, solution-phase studies of iron(II) complexes for which the magnetic properties can be finely tuned are scarce, even though they would greatly facilitate the development of the above-mentioned applications that often require compounds to operate in solution. Complexes with multidentate ligands (≥ 4 coordinating atoms), and especially binary complexes, are of prime interest for solution-phase

studies due to their elevated stability.^[8–10] Binary complexes require access to hexadentate ligands, but their syntheses are often far from straightforward and do not allow simple variation of the periphery for tuning of the magnetic properties of the resulting complexes. In view of the difficulties in devising adequate multidentate chelating systems,^[10] only a handful of solution-phase studies of ferrous complexes with tetradentate or higher ligands at different magnetic states have yet been reported.^[8,10–12]

Water is arguably the most intriguing solvent given its omnipresence in biological and environmentally friendly processes. Near-room temperatures are particularly interesting because of their biological relevance and because of the associated simplicity in designing devices that do not require extensive cooling or heating. We have been especially interested^[3,13,14] in obtaining a binary system of constitutionally related ferrous complexes that withstand the hydrolytic/protolytic nature of aqueous media at room temperature, while adopting either a decidedly low-spin^[15] or high-spin state by only slight constitutional variation. Polyaza macrocycles would appear to be the ligands of choice because they not only confer very high stability onto their corresponding ferrous complexes,^[16] but are also known to exercise higher ligand fields than their open-chain counterparts.^[17] Similar benefits may be obtained from the few ligands that are based on a more rigid, multicyclic framework displaying several nitrogen-donor sites.

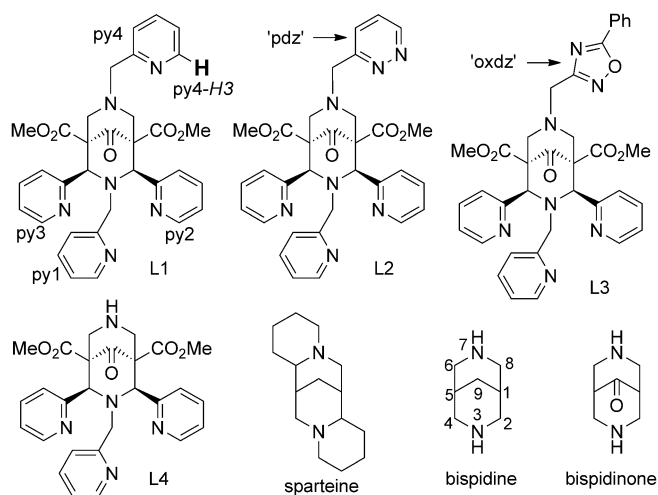
We became interested in the class of bispidines (Scheme 1) for which hexadentate ligands have been reported.^[18,19] This bicyclic system (which is part of the more general class of diazabicyclononanes/sparteines) is of elevated

[a] J. L. Kolanowski, R. Steinhoff,* Prof. Dr. J. Hasserodt
Laboratoire de Chimie, École Normale Supérieure de Lyon
46 allée d'Italie, 69364 Lyon (France)
Fax: (+33)472 72 88 60
E-mail: jens.hasserodt@ens-lyon.fr

[b] Dr. E. Jeanneau
Centre de Diffractométrie Henri Longchambon, Université Lyon 1
5 rue de la Doua, 69100 Villeurbanne (France)

[*] M.Sc. intern on leave from the Technical University of Munich.

Supporting information for this article is available on the WWW under <http://dx.doi.org/10.1002/chem.201300604>.



Scheme 1. The examined ligands and underlying bispidine backbone. pdz = pyridazine, oxdz = oxadiazole.

rigidity with respect to at least four of its N-donor sites. It has been declared particularly suitable for the formation of highly stable complexes and it exercises a high ligand field.^[20] It also offers the unique opportunity to fine-tune the corresponding complexes in regard to total charge, hydrosolubility, and potential affinity to external binding partners by taking advantage only of the periphery of the molecule (the polar “underbelly” consisting of three oxygen-bearing functional groups). Such an opportunity is largely absent for established macrocyclic ligands. Despite the recent progress in the characterization and practical use of bispidine-based ferrous chelates, only their high-spin iron(II) complexes have so far been described.

We now report that bispidines are a suitable platform for creating mononuclear ferrous complexes that adopt the spin state of one’s choice in aqueous solution and at ambient temperature. We elucidate the structural dependence of the spin state, which will enable future workers to fine-tune the magnetic properties of comparable bispidine chelates. Although high-spin bispidine ferrous complexes have been known since 2002, we have now obtained the first ever low-spin bispidine–iron(II) complexes by introducing two rarely used heteroaromatic coordinating moieties (pyridazine or oxadiazole) into the pentadentate bispidine backbone (L4, Scheme 1). The key to the success of our present approach resides in the efficient synthetic access from a single common precursor of bispidines, varying by just one pendent arm, and in the resulting subtle tuning of the ligand field. Thorough analyses in the solid state (five X-ray chelate structures plus two ligand structures, and superconducting quantum interference device (SQUID) measurements) and in solution (magnetic moments, redox potentials, and temperature-dependent proton NMR spectroscopy) form a reliable basis for our conclusions.

Results and Discussion

Bispidines were first reported by Mannich et al. in 1930 who also coined their name.^[21] Bispidinones (Scheme 1) can be readily constructed by two one-pot Mannich condensation reactions from a suitably substituted cyclohexanone. Only 3 years later, the underlying bicyclic structure (3,7-diazabicyclononane) was discovered in the alkaloid sparteine.^[22] Haller et al. reported on the structural diversification of bispidinones in a series of papers from 1965 to 1989;^[23,24] they were also the first to explore their metal coordination chemistry.^[23,25] Further such reports appeared sporadically in the literature,^[26] but it was the group of Comba et al. who put bispidine coordination chemistry on a solid foundation in the past 15 years.^[18,27] Bispidinone Cu^{II} complexes were considered for positron emission tomography imaging because of their elevated stability and the opportunity for facile bio-conjugation.^[28] Bispidinone metal chelates were also explored as catalysts for aziridination,^[29] olefin oxidation,^[30] CH group hydroxylation,^[31] halogenation,^[32] and sulfoxidation,^[33] as well as in nonheme enzymatic models.^[34]

Iron(II) complexes of bispidine-like ligands have attracted particular attention, giving rise to 70 publications in total and 65 in the past 10 years (including 36 patents). Among them, bispidinone chelates are the most important with 47 references. None of these, however, include an example of a truly low-spin complex, either in solution or in the solid state. Only two binary, hexacoordinate bispidine–iron(II) complexes have been reported, but their magnetic properties were not investigated.^[19] However, their color (yellow or light brown) and bond lengths in the solid state (Fe–N bonds of ca. 2.2 Å) suggest a high-spin state. The earliest hexadentate ligand reported by Comba et al. (L1, Scheme 1)^[35] gave a ferrous complex with a solid-state structure revealing its preference for coordinating its counterion (sulfate) rather than the “dangling” pyridylmethyl pendent arm (py4, Scheme 1), and this in spite of the highly favorable five-membered chelate ring that would thus have been formed. The authors claimed, however, that some coordination of this pendent arm can be observed spectroscopically in solution (in all likelihood acetonitrile or methanol).

Based on modeling experiments with a semiempirical dataset covering iron (AM1), we concluded that a severe steric clash between the two coordinating arms facing one another is at the origin of this destabilization of the hexacoordinate state and the resulting preference for a ternary complex. We thus hypothesized that replacement of one of the two pyridylmethyl pendent arms with a spatially less demanding one would eradicate this clash and allow the hexadentate ligand to exercise its full ligand field so as to render the iron center low-spin. We identified the unusual pyridazinylmethyl (L2) and oxadiazolylmethyl (L3) moieties as the candidates most likely to fulfill this requirement because they do not feature any substituent alpha to the coordinating nitrogen atom (in contrast to the pyridylmethyl groups on L1, see Scheme 1).

Solid-state structural analysis: Ferrous complexes of all four ligands presented in Scheme 1 were prepared. All were found to exist as geminal diols (hydrated ketone at position C-9) in the solid state, a phenomenon already observed by Comba et al. The deliberate use of a noncoordinating counterion (BF_4^-) allowed us to obtain monocrystals of $[\text{FeL1}] \cdot 2\text{BF}_4$. Its structural analysis revealed a fully low-spin complex (iron–nitrogen bond lengths of ca. 2.0 Å), albeit severely distorted (Figure 1, see the deflection angle of the pi-

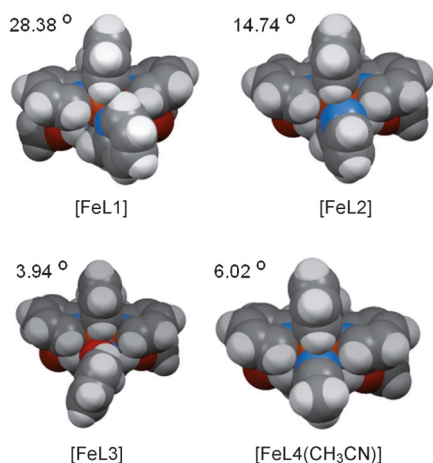


Figure 1. X-ray structural analysis. Illustration by CPK formulae of decreasing steric strain in complexes $[\text{FeL1}]$ (diamagnetic in the solid state/“intermediate spin” in aqueous solution), $[\text{FeL2}]$ (diamagnetic/diamagnetic), $[\text{FeL3}]$ (diamagnetic/diamagnetic), and $[\text{FeL4}(\text{CH}_3\text{CN})]$ (diamagnetic/intermediate spin); torsional angles are given for the two approaching heterocyclic planes grafted onto N-3 and N-7.

colyl planes of py3 and py4), rather than a high-spin complex as previously observed for $[\text{FeL1}(\text{SO}_4)]$.^[35] Inspection of the space-filling model of the diffraction data in Figure 1 immediately confirms our prior assumption that steric clash of the opposing coordinating arms on nitrogen atoms N-3 and N-7 is at the origin of the destabilization of the hexacoordinate isomer in solution, and in the solid state as reported.^[35] When monocrystals of $[\text{FeL2}]$ and $[\text{FeL3}]$ were subjected to X-ray diffraction analysis, the resulting structures revealed a much reduced steric clash for binary complex $[\text{FeL2}]$ and none for $[\text{FeL3}]$ (Figure 1, compare deflection angles between the planes of py3 and pdz and oxdz, respectively). This tendency towards a strainless complex when going from $[\text{FeL2}]$ to $[\text{FeL3}]$ can be explained with the change from a six-membered heterocycle in $[\text{FeL2}]$ (pyridazine) to a five-membered one in $[\text{FeL3}]$ (oxadiazole), which has an even more favorable approach angle. We were delighted to observe that our measure of moving to an azole coordinating arm did not hinder total access to the low-spin state in spite of the lower basicity of azoles. Although 3-methyl-5-phenyloxadiazole sports a $\text{p}K_a$ value of 2.6, those of pyridazine and pyridine are found at 2.3 and 5.2, respectively.^[36] For comparison, ternary complex $[\text{FeL4}(\text{CH}_3\text{CN})]$, also prepared in the context of this work, shows the same

ease of approach of the monodentate ligand acetonitrile, as can be concluded for the oxadiazole moiety in $[\text{FeL3}]$. Accordingly, all three structures also show bond lengths fully compliant with a low-spin state. Thus, the first four low-spin and diamagnetic crystals of bispidine ferrous complexes are reported.

It is instructive to compare these structures with a high-spin bispidine ferrous complex to appreciate the radial expansion that the iron center experiences when switching from low to high spin (Figure 2A). Ternary complex $[\text{FeL4}(\text{SO}_4)]$

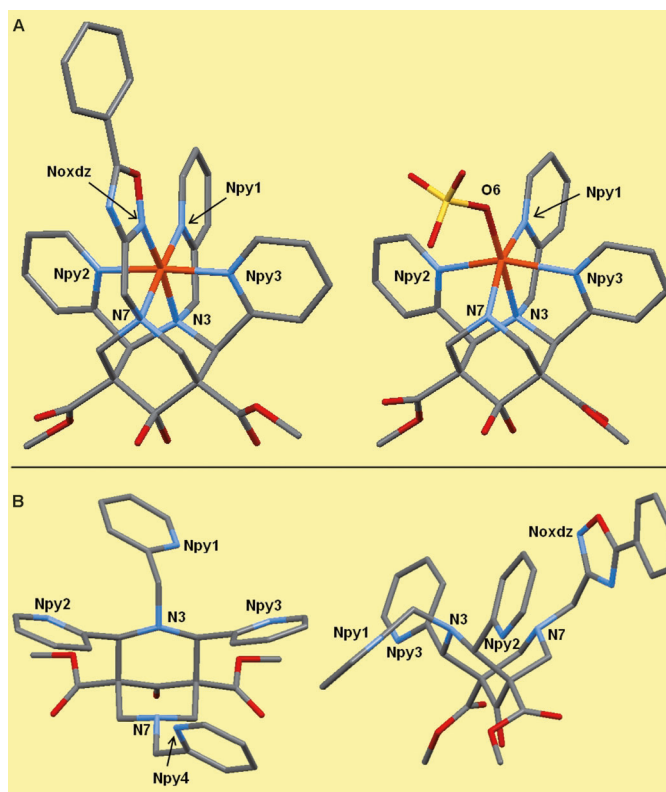


Figure 2. A) Ferrous-center radial expansion in a high-spin complex ($[\text{FeL4}(\text{SO}_4)]$; right) compared with a low-spin complex ($[\text{FeL3}]$; left); hydrogen atoms omitted for clarity. B) X-ray structures of uncomplexed ligands L1 (left) and L3 (right; all hydrogen atoms omitted for clarity) illustrate extensive preorganization for metal chelation.

(SO_4) exhibits an N5O1 coordination motif that exercises a ligand field sufficiently reduced to turn the iron center fully high spin. Capped-stick presentation of the structures of complexes $[\text{FeL3}]$ and $[\text{FeL4}(\text{SO}_4)]$ illustrate the departure from largely collinear coordination bonds for the low-spin state (Npy2-Fe-Npy3 and N7-Fe-Npy1) in favor of a significantly bent orientation in the high-spin state. This is due to all coordination bonds now adopting a length of approximately 2.2 Å.

Finally, examination of the solid-state structures of the uncomplexed ligands L1 and L3 (Figure 2B) reveals the highly preorganized nature of the hexadentate bispidine system. The lone pairs of nitrogen atoms N-3 and N-7 are already locked in the orientation found in their respective metal

chelates. The lone pairs of nitrogen atoms Npy2 and Npy3 from *cis*-pyridyl moieties require only rotation of one single bond to adopt the orientation in the chelate. In the nonchelated form they are found pointing towards the oxygenated underbelly of the ligand, probably for reasons of dipole compensation in the crystal lattice or electrostatic repulsions between them, which disappear once coordinated to the metal ion. This aspect of high preorganization, paired with a hole size more adapted to the oxidation state 2 than 3 of iron,^[37] bodes well for studies on stability in various aqueous media.

Magnetic moments in aqueous solution: All five complexes were studied in aqueous solution by dissolving crystalline samples for maximal measurement accuracy. Their cationic, saline nature made it possible to establish suitable concentrations that facilitated NMR experiments (final concentrations varied slightly around 5 mM). The magnetic moments were determined by the method of Evans^[3,38] using a superconducting NMR spectrometer (500 MHz/11.7 T).^[39] Solvent compositions of either H₂O/D₂O (85:15) or pure CD₃CN and containing an additional 2% *t*BuOH as reference substance were used (Figure 3, see Experimental Section and Supporting Information). Values of magnetic moments in Bohr magnetons (BM) were determined from shifts in the *t*BuOH signal and were corrected for temperature-dependent density changes of the solvent (see also the Experimental Section and Supporting Information).^[40] For the high-spin ternary complex [FeL4(SO₄)], a value of 4.96 BM is found at room temperature, which does not change upon heating (Figure 3); this value is not affected over a period of 12 h under exclusion of air, but exposure to air clearly causes the sample to slowly degrade. On the other hand, binary complexes [FeL2] and [FeL3] give distinctly diamagnetic aqueous samples and show a small diamagnetic (up-field) shift with respect to the reference *t*BuOH signal. The corresponding magnetic moments hardly change with temperature: 0.59–0.69 BM/25–80 °C for [FeL2] and 0.54–0.71 BM/25–60 °C for [FeL3] in D₂O/[D₄]MeOH, 2:1 (the reduced aqueous solubility of [FeL3] required the move to a solvent mixture including methanol; see the Experimental Section). These values correspond well with those for other low-spin ferrous complexes^[13] and do not change over a week of exposure to air.

In contrast to the clear-cut behavior described above, the magnetic moment of an aqueous sample of ternary complex [FeL4(CH₃CN)] exhibits some temperature dependence: 4.16–5.12 BM/25–80 °C. A change in concentration also brings about a significant change in magnetic moment (4.66 BM at 0.5 mM to 2.74 BM at 15 mM, see Figure 3C). These two phenomena indicate the exchange of monodentate acetonitrile with bulk water as seen for other nonbinary iron(II) complexes,^[41,42] which results in a switch from an N6 to the usual N5O1 coordination motif as found also for [FeL4(SO₄)]. As expected, [FeL4(CH₃CN)] samples in acetonitrile solution remain diamagnetic, even upon heating (Figure 3B: 0.65–0.56 BM/25–50 °C (look for ** in Fig-

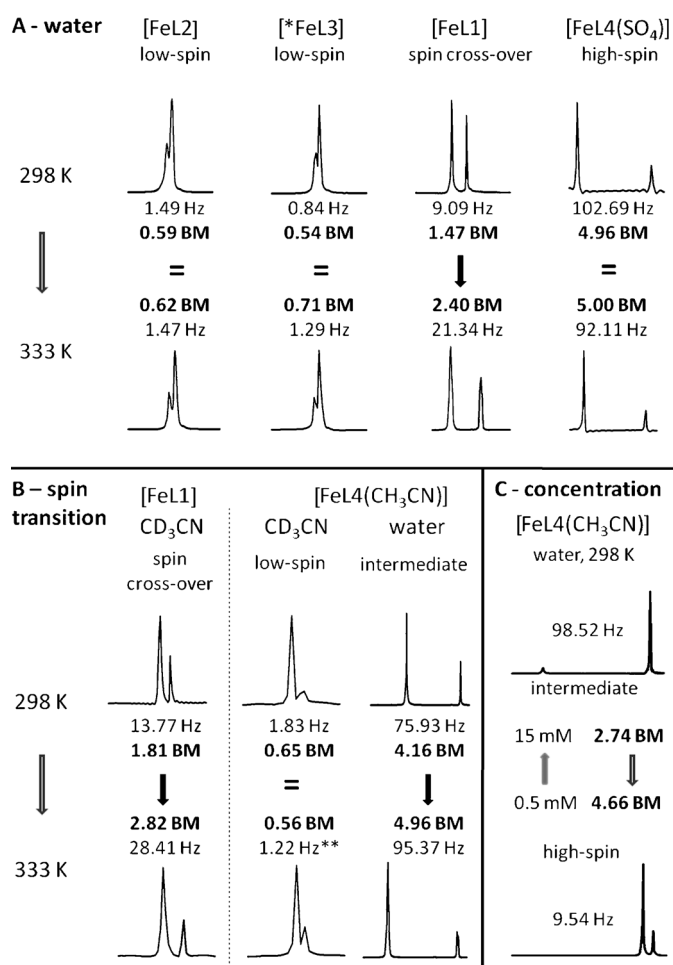


Figure 3. A) Chemical shifts of *t*BuOH and corresponding magnetic moments found for aqueous solutions (ca. 5 mM) with respect to an external reference at two different temperatures (Evans' method); the less intense signal corresponds to *t*BuOH contained in the reference solution. B) Solvent dependence. C) Concentration dependence for [FeL4(CH₃CN)]. Stars refer to deviations from indicated conditions (see the text and Experimental Section for details).

ure 3B); at higher temperature: signal coalescence). For the [FeL1] complex, the influence of rising temperature is much more pronounced: 1.31–2.96 BM at 20–80 °C (Figure 3A, Figure 4A, and the Supporting Information). In other words, dissolution of [FeL1] in water at room temperature already leads to slight paramagnetism. This proves the existence of some type of equilibrium that moves towards paramagnetic species upon heating, without, however, reaching, even at 80 °C, a value that would correspond to the entire population of iron centers being high spin. In contrast to [FeL4(CH₃CN)], the magnetic moment of an [FeL1] sample in CD₃CN does change upon changes in temperature: 0.80–2.82 BM/–20–60 °C (Figure 3A).

Magnetic moments in the solid state: Magnetometric measurements on crystalline, finely grained samples of the low-spin, high-spin, and SCO complexes were carried out with a SQUID instrument. As expected, values for [FeL2] and

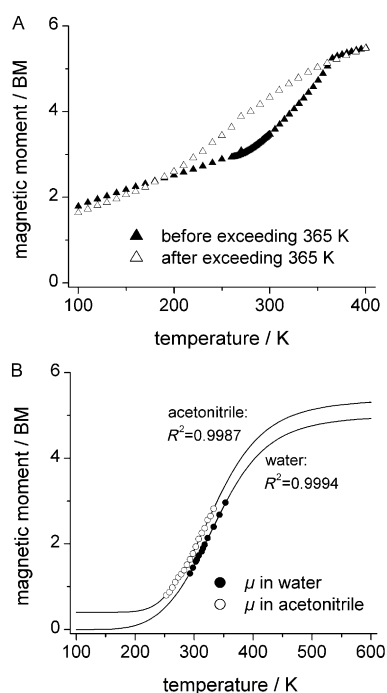


Figure 4. A) Plot of SQUID-derived magnetic moment versus temperature for [FeL1] in the two solid-state forms (the initial one turns into the second one upon heating over 365 K, and refers to the loss of a solvent molecule). B) Plot of NMR-derived magnetic moment versus temperature for [FeL1] in solution; solid lines represent the best theoretical fit of the curves.

[FeL3] were very close to zero and the samples remained diamagnetic within a temperature range between 300 and 100 K, in agreement with the solution data. The high-spin [FeL4(SO₄)] gave a magnetic moment of 5.36 BM at 300 K, consistent with the presence of a high-spin Fe^{II} center and a spin of 2. Upon cooling to 100 K, its magnetic moment decreases subtly, which can be caused by zero-field splitting (ZFS; see also Figure S23 in the Supporting Information). In congruence with the solution behavior, a microcrystalline sample of [FeL1] exhibits a spin transition when cycling between 350 and 100 K (black triangles in Figure 4A). Regardless of the heating/cooling direction, the transition graphs are superimposable, that is, no hysteresis is present. However, when heating above 365 K, the graph corresponding to subsequent cooling adopts an altered profile (white triangles in Figure 4A). This may be explained by the loss of a water molecule from the crystal lattice. Our conclusion that [FeL1] shows true SCO in solution is thus confirmed in the solid state.

Analysis of ¹H NMR spectra: The diverging magnetic susceptibilities are also manifest in the corresponding NMR spectra. Although proton spectra in D₂O for [FeL2] and [FeL3] at room temperature fit into the habitual chemical-shift window for diamagnetic samples (1.0–10.5 ppm for [FeL2] and 1–10 ppm for [FeL3]), that of the fully high-spin ternary complex [FeL4(SO₄)] occupies the expected paramagnetic window of 3–200 ppm (see the Experimental Sec-

tion and Supporting Information). A D₂O sample of [FeL1] gives a spectrum that covers a 1–22 ppm interval at room temperature, and a 1–63 ppm interval at 80 °C (Figure 5 and

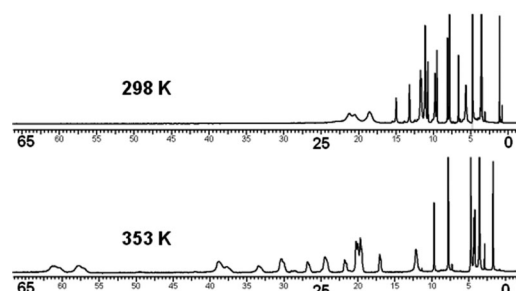


Figure 5. Temperature-dependent evolution of the proton NMR spectrum of [FeL1] in D₂O.

the Supporting Information), with only one set of signals observed at both temperatures. This tendency is maintained in CD₃CN (from 1–10 ppm at –40 °C to 1–60 ppm at 60 °C) and in [D₆]acetone (1–9.5 and 1–50 ppm at –50 and +50 °C, respectively). The spectral profile in both solvents is almost identical despite significant differences in the coordination properties and ligand-field strengths exerted by these solvents. The presence of only a single set of signals in all spectra suggests that the equilibrium present in solution is fast compared to the NMR timescale, even at low temperatures. No signals stemming from a species with a de-coordinated pendent arm were observed; in conjunction with the solvent insensitivity of the [FeL1] spectrum, this strongly suggests the presence of a SCO phenomenon. In contrast to this behavior of [FeL1], a solution of [FeL4(CH₃CN)] in CD₃CN gives a spectrum that occupies the diamagnetic interval of 1–10 ppm, whether at room temperature or at 60 °C because [FeL4(CH₃CN)] and [FeL4(CD₃CN)] are the only species possible. In [D₆]acetone, the coordination of acetonitrile at 0–10 °C is proved by a proton NMR spectrum covering the diamagnetic window of 1–10 ppm. Upon heating, however, severe broadening of the signals is observed (already at 25 °C). This indicates the acceleration of the exchange process of CH₃CN. Subsequently, paramagnetic signals appear and gradually increase at higher temperatures (2–200 ppm at 50 °C), thereby indicating the replacement of the coordinating acetonitrile molecule.

Redox potentials: Cyclic voltammetry (CV) was performed on samples in acetonitrile prepared from crystalline material and containing 0.1 M *n*Bu₄NClO₄. Neither samples in water nor in water/acetonitrile solutions (50:50) could be prepared due to insufficient solubility, probably caused by the high but required salinity of the solution. CV waves of all studied complexes were reversible (see also Figure S28 in the Supporting Information) at all five investigated scan rates (50, 100, 150, 200, 250 mV s^{–1}), thus suggesting no significant variation of the coordination geometry. This can be explained by both the well-described rigidity of the bispidine platform

and its significant tolerance for the size of the metal center.^[43] Interestingly, the binary complexes [FeL1] (SCO) and [FeL2] (low-spin) and the ternary complex [FeL4-(CH₃CN)] (low-spin) all showed comparable $E_{1/2}$ redox potentials of approximately 650 mV (Table 1), similar to the

Table 1. Redox potentials of the low-spin complexes (cyclic voltammetry).

Complex	E_{pa} [V]	E_{pc} [V]	ΔE_p [mV]	$E_{1/2}^{[a]}$ [V]
[FeL1]·2BF ₄	0.682	0.619	63	0.651
[FeL2]·2BF ₄	0.677	0.619	58	0.648
[FeL3]·2ClO ₄	0.800	0.737	63	0.769
[FeL4(CH ₃ CN)]·2BF ₄	0.689	0.626	63	0.658

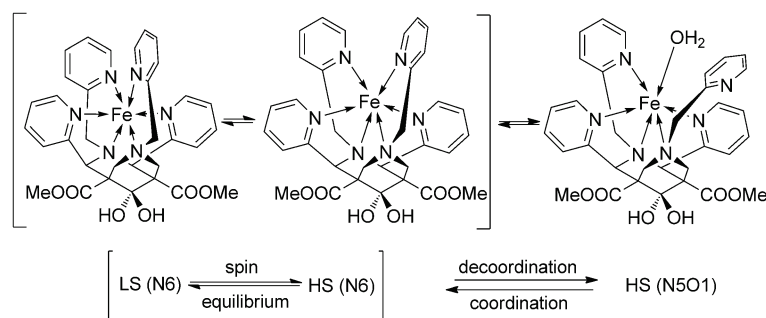
[a] 1 mM in acetonitrile at RT with 0.1 M *n*Bu₄NClO₄ as electrolyte (scan rate: 100 mV s⁻¹). For more details see the Experimental Section and Supporting Information.

previously reported 661 mV for [FeL1]·2ClO₄.^[35] This value for [FeL1] (SCO) could explain the same prolonged stability towards air oxidation as we observed for fully low-spin complex [FeL2]. By contrast, the higher redox potential of [FeL3] (769 mV) indicates the greater inertness conferred by L3 on the iron(II) center relative to the other ligands studied in this work, probably stemming from its significantly softer nature, which may fit the iron(II) state more favorably.

Thermodynamic characterization of [FeL1] spin variation in solution:

Unlike the solvent-dependent high-spin/low-spin character of [FeL4] and that of previously reported bispidine-iron(II) complexes, the intermediate magnetic moments of [FeL1] and their relative insensitivity to the nature of the solvent may be explained by the presence of a SCO phenomenon, as already suggested by Comba et al.^[35] However, a partial contribution by a coordination/decoordination equilibrium cannot be ruled out (Scheme 2).

To gain further insight into the low-spin–high-spin equilibrium in the solution state of [FeL1], we estimated ΔH° and ΔS° of the thermal low-spin–high-spin transition by performing a fit of experimentally determined temperature-dependent solution magnetic moments to the Equation (1).^[44]



Scheme 2. Possible spin equilibria for [FeL1] in solution. LS = low spin, HS = high spin.

$$\mu_{\text{eff}} = \{\mu_{\text{LS}}^2[\exp(-\Delta H^\circ/RT) \exp(\Delta S^\circ/R) + 1]^{-1} + \mu_{\text{HS}}^2[\exp(\Delta H^\circ/RT) \times \exp(-\Delta S^\circ/R) + 1]^{-1}\}^{1/2} \quad (1)$$

In an ideal situation the magnetic moments of the low-spin (μ_{LS}) and/or high-spin (μ_{HS}) form are known or can be obtained by cooling or heating the solution until only one spin state is present. This would allow for a two (or three)-parameter fit of $\mu_{\text{eff}}(T)$ from which the enthalpy and entropy of the spin transition process could be extracted directly.^[45] However, in practice a unique spin state (and the associated magnetic moment) can often not be reached. This then requires a four-parameter fit,^[44] which is more prone to generate significant errors in the estimated values.^[46] This situation is present for [FeL1] in water and in acetonitrile, for which it was not possible to push the spin equilibrium to either extremity of the process. Thus, the four-parameter fit (Figure 4B) to the experimental data (293–353 and 253–333 K in water and acetonitrile, respectively) led to the following approximate values: 1) for water: $\Delta H^\circ = 26.8$ – 29.5 kJ mol⁻¹, $\Delta S^\circ = 68.1$ – 80.6 J mol⁻¹ K⁻¹, and $T_{1/2} = 378$ K; and 2) for acetonitrile: $\Delta H^\circ = 23.9$ – 29.7 kJ mol⁻¹, $\Delta S^\circ = 58.3$ – 85.8 J mol⁻¹ K⁻¹, and $T_{1/2} = 371$ K (Table 2 and Figure S14 in the Supporting Information). In acetonitrile, the values of μ_{LS} (0.41 ± 0.13) BM and μ_{HS} (5.40 ± 1.22) BM suggest a significant contribution of the orbital factor (ZFS) but are still within a typical range for iron(II) complexes, albeit with

Table 2. Estimated values of spin equilibrium parameters for [FeL1] in solution.^[a]

Solvent	μ_{LS} [BM]	$\mu_{\text{HS}}^{[b]}$ [BM]	ΔH° [kJ mol ⁻¹]	ΔS° [J mol ⁻¹ K ⁻¹]	$T_{1/2}$ [K]
CD ₃ CN	0.41 ± 0.13	5.40 ± 1.22	26.79 ± 2.93	72.16 ± 13.60	371
Water	0.00 ± 0.05	5.02 ± 0.51	28.11 ± 1.34	74.35 ± 6.28	378
Water	0.06 ± 0.04	4.90 ^[b]	28.47 ± 0.42	75.98 ± 1.28	375
Water	0.00 ± 0.05	5.40 ^[b]	27.23 ± 0.22	70.13 ± 0.68	388
CD ₃ CN	0.46 ± 0.05	4.90 ^[b]	28.18 ± 0.55	75.54 ± 1.67	359
CD ₃ CN	0.41 ± 0.05	5.40 ^[b]	26.80 ± 0.53	72.18 ± 1.59	371

[a] Fit of experimentally determined magnetic moments at different temperatures to the exponential Equation (1); see the main text and Supporting Information. [b] μ_{HS} fixed at the limiting values for magnetic moments of the high-spin iron(II) ion with $S = 2$ (for more details see the main text and Supporting Information).^[12]

a relatively high error. In water, these parameters are located close to the spin-only values (0 and 4.9 BM) with a lower error than in acetonitrile (μ_{LS} : 0.00 ± 0.05) BM and μ_{HS} : 5.02 ± 0.51) BM). To verify the reliability of these results and to estimate the values with higher precision, we examined the three-parameter best fits as previously proposed by Martin et al.^[12] These are obtained by

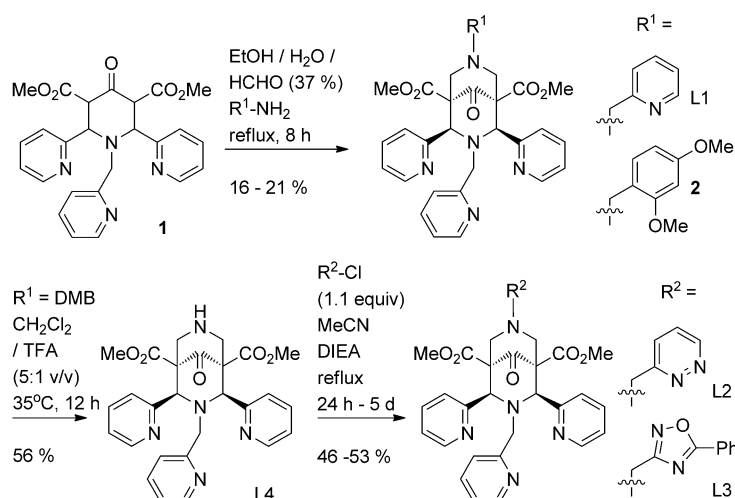
fixing μ_{HS} at 4.90 BM (the lower limit of the spin-only value of high-spin iron(II), estimated on the basis of the spin-only formula $\mu = 2[S(S+1)]^{-1/2}$) and the upper limit of 5.40 (the upper value expected for the 5T_2 state). The values of thermodynamic parameters obtained from this treatment (ΔH° : 27.0–28.9 and 26.3–28.7 kJ mol $^{-1}$; ΔS° : 69.5–77.3 and 70.6–77.2 J mol $^{-1}$ K $^{-1}$ for water and acetonitrile, respectively) are consistent with the results of the four-parameter fit but significantly more precise, thereby increasing its reliability. Our rough estimation of enthalpy and entropy of the spin-transition process in solution places the complex [FeL1] within the typical range cited for iron(II) chelates exhibiting an intermediate magnetic moment in solution ($\Delta H = (30 \pm 15)$ kJ mol $^{-1}$, $\Delta S = (70 \pm 22)$ J mol $^{-1}$ K $^{-1}$).^[9] For a truly “uncontaminated” $^1A_{1g} \leftrightarrow ^5T_{2g}$ SCO in octahedral ferrous complexes, the enthalpy should usually be found between 15 and 25 kJ mol $^{-1}$, a value that increases when another phenomenon such as coordinative isomerism is involved.^[47] In the case of [FeL1], the observed values slightly exceed the upper limit, which suggests that a small contribution from a coordination–decoordination equilibrium is involved.

Ligand and chelate synthesis: Hexadentate bispidine ligands L2 and L3 were prepared via a common intermediate, pentadentate L4 (Scheme 3). A protecting-group strategy, rarely

reach a 20% yield upon continued practice by the experimenter. This modest value can be explained in part by the formation of the kinetically favored configurational isomer (*2'-trans*-dipyridyl; see the Supporting Information), which has already been observed for bispidinones.^[48] On prolonged heating, however, the proportion of the desired *cis* isomer can be maximized as reported for analogous compounds,^[49] albeit to the detriment of yield. In this context it should be stressed that great amounts (40 g and more) of the starting material **1** can be safely introduced into this bicycle-forming step because of the ease of preparation of **1**. The respective multicomponent reaction to form intermediate **1** starts from simple precursors (2-pyridylcarbaldehyde, 2-picolylamine, dimethyl acetone-1,3-dicarboxylate) and is high yielding ($\geq 80\%$). We were thus able to prepare batches of more than 10 g of **2**. Straightforward deprotection of bispidinone **2** by treatment with trifluoroacetic acid (TFA) in dichloromethane then leads to intermediate L4 with a 56% yield of the isolated product.

Finally, introduction of the pyridazinylmethyl and oxadiazolomethyl groups requires access to the respective chlorides. Although the latter chloride is commercially available, the former can be prepared readily by chlorination of commercially available methylpyridazine with trichloroisocyanuric acid.^[50] Alkylation of ligand L4 in position N-7 by these chlorides over 24–72 h furnishes L2 and L3, which can be

purified by flash column chromatography on neutral alumina. Such an alkylation is also an alternative route to L1 by using picolyl chloride. The corresponding chelates were prepared at room temperature in dry, degassed solvents (acetonitrile for [FeL1], [FeL2], [FeL3], and [FeL4(CH₃CN)] and methanol for [FeL4(SO₄)] over 1–12 h by using the following salts: Fe(BF₄)₂·6H₂O for [FeL1], [FeL2], and [FeL4(CH₃CN)]; Fe(ClO₄)₂·xH₂O for [FeL3]; and FeSO₄·7H₂O for [FeL4(SO₄)]. Importantly, completion of the reaction was monitored by mass spectrometry. The fairly pure precipitates thus obtained were then recrystallized by liquid/liquid dif-



Scheme 3. Preparation of the ligands L1–L4. DMB = dimethoxybenzyl, TFA = trifluoroacetic acid, DIEA = diisopropylethylamine.

seen in multidentate ligand synthesis, allowed us to obtain the three ligand variations in just one simple alkylation step so as to carry through as much of the precious precursor (L4) as possible. However, this measure forced us to carefully adapt the synthetic protocol reported for L1^[35] to permit the introduction of a dimethoxybenzyl (DMB) protecting group instead of the picolyl group. The double Mannich reaction from piperidinone **1** to protected bicyclic intermediate **2** is associated with low to modest yields, but can reliably

fusion of diethyl ether into solutions in acetonitrile/methanol to obtain samples suitable for X-ray analysis and for all other characterization.

Conclusion

We have prepared the first known low-spin, diamagnetic, ferrous bispidine complexes, both in solution and in the

solid phase at room temperature. We initially synthesized 1) a binary compound showing evidence of strain induced in parts of the ligand ([FeL1]·2BF₄), and 2) a ternary one that comprises an extra monodentate ligand ([FeL4-(CH₃CN)]·2BF₄). However, in water these complexes adopt a spin equilibrium with partial population of the high-spin version; unsurprisingly, this tendency becomes more pronounced with increasing temperature. For the ternary complex, simple ligand exchange is responsible for this effect, whereas the intermediate spin of binary [FeL1] most likely results from true thermal SCO with potentially some residual contribution from ligand exchange. We then prepared hexadentate bispidine ligands (L2 and L3) that do not suffer induction of strain upon complexation with iron(II), and which therefore give perfectly low-spin iron(II) complexes even in water. We thus show that the electronic spin of iron(II) can be fully or partially muted in solution, as well as in the solid state, by the judicious choice of an appropriate bispidine derivative. The high stability of this suite of constitutionally related chelates bodes well for their future use in the design of responsive off-on probes; only a handful of systems can claim a similar performance. Our bispidine platform should thus find a wide range of solution-phase applications in the biomedical and technological arena.

Experimental Section

General materials and procedures: Reagents and solvents were purchased from Aldrich, Acros, and Alfa Aesar and used without further purification. Solvents were dried by standing the commercial, dry HPLC-grade solvents for 24 h on thermally activated molecular sieves (3 Å for MeOH and EtOH, 4 Å for CH₃CN and Et₂O, sieve activation by 24 h of heating at 315 °C) and degassed by a freeze–pump–thaw method (sequence repeated 3–5 times) for complexation reactions. All NMR spectra were acquired on a Bruker AVANCE 500 instrument (500.10 and 125.76 MHz for ¹H and ¹³C, respectively) at 298 K (unless otherwise stated). Chemical shifts (δ) are reported in ppm (s=singlet, d=doublet, t=triplet, m=multiplet, br=broad, eq.=equatorial, ax.=axial) and referenced to the residual solvent peak. NMR coupling constants (J) are reported in hertz (Hz). UV/Vis spectra were recorded on a V-670 Jasco spectrophotometer. High-resolution mass spectrometry measurements and elemental analyses were performed at the “Centre Commun de Spectrometrie de Masse” of the University Claude Bernard in Lyon (France) and the Service Central d’Analyse of the CNRS in Solaize (France). Cyclic voltammetry (CV) experiments were conducted in a standard one-compartment, three-electrode electrochemical cell with a biologic ESP300 potentiostat. Tetra-*n*-butylammonium perchlorate (TBAP) was used as supporting electrolyte (0.1 M) in acetonitrile. A vitreous carbon working electrode (Ø=3 mm, ALS Co.) was polished with 1 μm diamond paste before each recording. The counter electrode was a Pt wire. Electrode potentials are referred to a Ag/AgNO₃ reference electrode (ALS Co., 0.01 M AgNO₃, 0.1 M TBAP in acetonitrile). The concentrations of the complexes were established around 1 mM and the measurements were performed at five different scan rates (50, 100, 150, 200, 250 mV s⁻¹), all giving similar reversible cyclovoltammograms. Only crystalline batches of bispidine ferrous complexes were used.

Magnetic susceptibilities in solution were determined by the Evans method^[38,51] by using a coaxial NMR tube and *t*BuOH (2%) as reference.^[3,44] Varied-temperature magnetic susceptibilities were corrected with respect to the effect of solvent volume expansion/contraction upon heating/cooling;^[40,41] for more details see the text and Supporting Information. Solid-state magnetic susceptibility data were collected in the

“Laboratoire des Multimateriaux et Interfaces (UMR 5615)” at Université Claude Bernard Lyon 1 (France) by using a SQUID magnetometer (Quantum Design model MPMS-XL) in an applied magnetic field of 0.1 T. Compounds [FeL2], [FeL3], and [FeL4] were measured by using a capsule in the temperature range 100–300 K. Compound [FeL1] was measured in an aluminum sample holder to allow heating at 400 K. All data were corrected for the contribution of the sample holder and diamagnetism of the samples estimated from Pascal’s constants.^[5,52]

Crystallographic data: CCDC-902550 (L1), CCDC-902551 (L3), CCDC-902554 ([FeL1]), CCDC-902552 ([FeL2]), CCDC-904020 ([FeL3]), CCDC-902553 ([FeL4(CH₃CN)]), CCDC-902296 ([FeL4(SO₄))] contain the supplementary crystallographic data for this paper. These data can be obtained free of charge from The Cambridge Crystallographic Data Centre via www.ccdc.cam.ac.uk/data_request/cif.

Compound [FeL1]·2BF₄: Chemical formula: C₃₃H₃₈B₂F₈FeN₆O₈; *M_r* = 876.16 g mol⁻¹; crystal dimensions 0.105 × 0.179 × 0.473 mm; monoclinic; space group *P21/c*; unit cell dimensions *a* = 10.3903(6), *b* = 18.170(1), *c* = 19.079(1) Å; α = 90, β = 101.85(1), γ = 90°; *V* = 3525.2(3) Å³; *Z* = 4; ρ_{calcd} = 1.651 mg m⁻³; μ = 0.53 mm⁻¹; MoK_α radiation, λ = 0.7107 Å; *T* = 100 K; θ_{max} = 29.5°, θ_{min} = 3.4°; no. of measured reflections: 74 517; no. of independent reflections: 9196; *R*_{int} = 0.055; *R*[*F*2 > 2σ(*F*2)] = 0.039; *wR*(*F*2) = 0.090; Δρ_{max} = 0.58 e Å⁻³; Δρ_{min} = -0.60 e Å⁻³.

Compound [FeL2]·2BF₄: Chemical formula: C₃₄H₃₈B₂F₈FeN₈O₇; *M_r* = 900.18 g mol⁻¹; crystal dimensions 0.179 × 0.248 × 0.349 mm; triclinic; space group *P1̄*; unit cell dimensions *a* = 10.6244(6), *b* = 12.3593(7), *c* = 15.2033(9) Å; α = 103.178(5), β = 103.007(5), γ = 98.123(5)°; *V* = 1854.5(2) Å³; *Z* = 2, ρ_{calcd} = 1.612 mg m⁻³; μ = 0.51 mm⁻¹; MoK_α radiation, λ = 0.7107 Å; *T* = 110 K; θ_{max} = 29.5°, θ_{min} = 3.5°; no. of measured reflections: 40 829; no. of independent reflections: 9362; *R*_{int} = 0.042; *R*[*F*2 > 2σ(*F*2)] = 0.053; *wR*(*F*2) = 0.124; Δρ_{max} = 1.03 e Å⁻³; Δρ_{min} = -0.76 e Å⁻³.

Compound [FeL3]·2ClO₄: Chemical formula: C₃₆H₃₅Cl₂FeN₇O₁₅; *M_r* = 932.45 g mol⁻¹; crystal dimensions 0.096 × 0.195 × 0.289 mm; trigonal; space group *R3̄*; unit cell dimensions *a* = 23.982(2), *b* = 23.982(2), *c* = 39.047(3) Å; α = 90, β = 90, γ = 120°; *V* = 19449(3) Å³; *Z* = 18; ρ_{calcd} = 1.433 mg m⁻³; μ = 0.54 mm⁻¹; MoK_α radiation, λ = 0.7107 Å; *T* = 100 K; θ_{max} = 29.4°, θ_{min} = 3.6°; no. of measured reflections: 54 907; no. of independent reflections: 11 013; *R*_{int} = 0.099; *R*[*F*2 > 2σ(*F*2)] = 0.120; *wR*(*F*2) = 0.225; Δρ_{max} = 2.33 e Å⁻³; Δρ_{min} = -1.87 e Å⁻³.

Compound [FeL4(CH₃CN)]·2BF₄: Chemical formula: C₃₄H₃₈B₂F₈FeN₈O₆; *M_r* = 872.17 g mol⁻¹; crystal dimensions 0.123 × 0.287 × 0.362 mm; triclinic; space group *P1̄*; unit cell dimensions *a* = 11.0566(8), *b* = 13.7715(9), *c* = 14.718(1) Å; α = 66.375(6), β = 69.925(6), γ = 71.325(6)°; *V* = 1884.5(2) Å³; *Z* = 2, ρ_{calcd} = 1.537 mg m⁻³; μ = 0.50 mm⁻¹; MoK_α radiation, λ = 0.7107 Å; *T* = 100 K; θ_{max} = 29.5°, θ_{min} = 3.5°; no. of measured reflections: 38 176; no. of independent reflections: 9388; *R*_{int} = 0.050, *R*[*F*2 > 2σ(*F*2)] = 0.060; *wR*(*F*2) = 0.111; Δρ_{max} = 1.79 e Å⁻³; Δρ_{min} = -0.85 e Å⁻³.

Compound [FeL4(SO₄)]: Chemical formula: C₅₇H₇₀Fe₂N₁₀O₂₃S₂; *M_r* = 1439.07 g mol⁻¹; crystal dimensions 0.030 × 0.242 × 0.293 mm; orthorhombic; space group *Pbca*; unit cell dimensions *a* = 16.741(3), *b* = 17.538(2), *c* = 20.854(2) Å; α = 90, β = 90, γ = 90°; *V* = 6123.0(1) Å³; *Z* = 4, ρ_{calcd} = 1.561 mg m⁻³; μ = 5.22 mm⁻¹; CuK_α radiation, λ = 1.5418 Å; *T* = 150 K; θ_{max} = 66.7°, θ_{min} = 3.4°; no. of measured reflections: 24 753; no. of independent reflections: 5387; *R*_{int} = 0.062; *R*[*F*2 > 2σ(*F*2)] = 0.065; *wR*(*F*2) = 0.138; Δρ_{max} = 1.90 e Å⁻³; Δρ_{min} = -0.69 e Å⁻³.

Synthesis: Compound **1** was synthesized according to known procedures.^[53] Preparation of new bispidinone **2** and already reported ligand L1^[53] was performed by modifying the reported methodology. Ligands L2 and L3 were synthesized by alkylation of compound L4 by standard procedures. All complexations were performed under inert argon atmospheres and with dry and degassed HPLC-grade solvents. For more details please see the Supporting Information.

Intermediate 2: Formaldehyde (37% in H₂O; 17.47 g; 215.3 mmol; 2.3 equiv) and dimethoxybenzylamine (18.00 g; 107.6 mmol; 1.15 equiv) were added to a solution of piperidinone **1** (43.10 g; 93.6 mmol) in ethanol (600 mL) at 60 °C. The reaction mixture was stirred under reflux for

8 h and all volatiles were removed under reduced pressure. The residue was dissolved in a minimal quantity of methanol (50 mL) with the help of heating and was then treated with diethyl ether (150 mL). A white crystalline solid appeared after several hours at room temperature, was isolated by filtration, and then washed three times with diethyl ether. A repeat of the procedure on the resulting filtrate yielded additional material, which was combined with the first crop to give a total of 12.89 g (21%) of pure product. M.p. 187–190 °C; $^1\text{H NMR}$ (500 MHz, CDCl_3): δ = 2.49 (2H, d, $^2J(\text{H,H})$ = 11.6 Hz; CH_2 -6/8 eq.), 3.07 (2H, d, $^2J(\text{H,H})$ = 11.9 Hz; CH_2 -6/8 ax.), 3.37 (2H, s; N7- CH_2 Ar), 3.66 (2H, s; N3- CH_2 py), 3.78 (6H, s; CO_2CH_3), 3.86 (3H, s; Ar4- OCH_3), 3.98 (3H, s; Ar2- OCH_3), 5.35 (2H, s; CH -2/4), 6.43 (1H, dd, $^3J(\text{H,H})$ = 8.12, $^4J(\text{H,H})$ = 2.14 Hz; Ar-H5), 6.59 (1H, d, $^4J(\text{H,H})$ = 2.14 Hz; Ar-H3), 6.74 (1H, d, $^3J(\text{H,H})$ = 7.69 Hz; py1-H6), 6.97 (1H, ddd, $^3J(\text{H,H})$ = 7.59, 4.81, $^4J(\text{H,H})$ = 0.85 Hz; py1-H4), 7.01–7.16 (3H, m; py2/3-H4, Ar-H6), 7.37 (1H, td, $^3J(\text{H,H})$ = 7.7, $^4J(\text{H,H})$ = 1.7 Hz; py1-H5), 7.42 (2H, td, $^3J(\text{H,H})$ = 7.7, $^4J(\text{H,H})$ = 1.7 Hz; py2/3-H5), 8.10 (2H, d, $^3J(\text{H,H})$ = 8.12 Hz; py2/3-H6), 8.40–8.51 ppm (3H, m; py2/3-H3, py1-H3); jmod $^{13}\text{C NMR}$ (126 MHz, CDCl_3): δ = 52.5 (CO_2CH_3), 55.5 (Ar3- OCH_3), 55.5 (Ar5- OCH_3), 55.8 (N3- CH_2 py1), 58.0 (N7- CH_2 Ar), 59.4 (C-6/8), 62.2 (C-2/4), 70.6 (C-1/5), 98.7 (Ar-C3), 103.8 (Ar-C5), 117.6 (Ar-C1), 121.6 (py1-C4), 122.6 (py2/3-C4), 124.2 (py1-C6), 124.7 (py2/3-C6), 133.1 (Ar-C6), 135.5 (py1-C5), 135.6 (py2/3-C5), 148.8 (py2/3-C3), 149.3 (py1-C3), 156.4 (py1-C1), 158.5 (Ar-C2), 159.2 (Ar-C4), 160.7 (py2/3-C1), 168.8 (CO_2CH_3), 204.1 ppm (C-9); IR (solution in dichloromethane) ν_{max} = 3051–2835 (C–H), 1738 (C=O), 1612 (Ar), 1589 (Ar), 1510 cm^{-1} (Ar); HRMS (ESI): m/z calcd for $\text{C}_{36}\text{H}_{38}\text{N}_5\text{O}_7$: 652.2766 [$M+H^+$]; found: 652.2768; elemental analysis calcd (%) for $\text{C}_{36}\text{H}_{38}\text{N}_5\text{O}_7$: C 66.35, H 5.72, N 10.75; found: C 65.72, H 6.01, N 10.38.

Ligand L4: Trifluoroacetic acid (20 mL) was added to a solution of **2** (4.03 g; 6.18 mmol) in dry dichloromethane (100 mL). The reaction vessel was sealed and the mixture was stirred for 12 h at 35–40 °C. Then the reaction was basified on cooling with 2M sodium hydroxide solution and the organic phase was separated. The water phase was extracted with dichloromethane (2 × 150 mL) and the organic fractions were combined. After evaporation of the solvent under reduced pressure, the residue was dissolved in a minimal quantity of hot acetonitrile and the solution was filtered before precipitating the desired product. After 1 h at room temperature, the resulting white solid was isolated by filtration and washed with isopropanol and diethyl ether. Working up the filtrate led to additional material, which was combined with the first crop to yield 1.75 g (56%) of pure product. M.p. 191–192 °C; $^1\text{H NMR}$ (500 MHz, CDCl_3): δ = 3.28 (2H, t, J = 13.68 Hz; CH_2 -6/8 eq.), 3.50 (2H, s; N3- CH_2 py1), 3.64 (6H, s; $-\text{CO}_2\text{CH}_3$), 4.19 (2H, d, J = 12.82 Hz; CH_2 -6/8 ax.), 4.59 (1H, brs, 1H; N7-H), 5.28 (s, 2H; CH -2/4), 6.93 (d, J = 7.69 Hz, 1H; py1-H6), 6.99 (dd, J = 6.63, 4.92 Hz, 1H; py1-H4), 7.14–7.16 (m, 2H; py2/3-H4), 7.33 (d, J = 6.84 Hz, 2H; py2/3-H6), 7.42 (td, J = 7.69, 1.71 Hz, 1H; py1-H5), 7.60 (td, J = 7.69, 1.71 Hz, 2H; py2/3-H5), 8.31 (d, J = 4.27 Hz, 1H; py1-H3), 8.60 ppm (d, J = 4.70 Hz, 2H; py2/3-H3); $^{13}\text{C NMR}$ (126 MHz, CDCl_3): δ = 52.1 ($-\text{CO}_2\text{CH}_3$), 55.4 (C-6/8), 56.8 (N3- CH_2 py1), 64.6 (C-2/4), 70.6 (C-1/5), 121.4 (py1-C4), 123.1 (py2-C4, py3-C4), 124.0 (py1-C6), 125.8 (py2-C6, py3-C6), 135.4 (py1-C5), 136.1 (py2-C5, py3-C5), 148.4 (py1-C3), 149.7 (py2-C3, py3-C3), 156.8 (py2-C1, py3-C1), 157.8 (py1-C1), 168.9 ($-\text{CO}_2\text{CH}_3$), 203.2 ppm (C-9); IR (solution in dichloromethane): ν_{max} = 3311 (NH), 3053–2852 (C–H), 1732 (C=O ester), 1710 (C=O ketone), 1589 (Ar), 1570 cm^{-1} (Ar); HRMS (ESI): m/z calcd for $\text{C}_{27}\text{H}_{28}\text{N}_5\text{O}_5$: 502.2085 [$M+H^+$]; found: 502.2069; elemental analysis calcd (%) for $\text{C}_{27}\text{H}_{28}\text{N}_5\text{O}_5$: C 64.66, H 5.43, N 13.96; found: C 64.68, H 5.43, N 13.72.

[FeL1]·2BF₄: The ligand (253 mg, 0.427 mmol) was dissolved in degassed, anhydrous acetonitrile (10 mL) and a solution of iron(II) tetrafluoroborate hexahydrate (151 mg; 0.448 mmol) in anhydrous, degassed acetonitrile (5 mL) was added dropwise with stirring under argon. Upon addition, the solution immediately turned dark brown. The reaction was continued for 4 h until no more ligand signal was observed by direct injection mass spectrometry. Then, approximately 5% v/v of degassed water was added and the solution was set up for slow gas diffusion of diethyl ether. The resulting dark red (almost black) crystalline material ready for X-ray analysis was collected, washed, and dried to yield 278 mg (71%) of

the desired complex. $^1\text{H NMR}$ (500 MHz, D_2O): δ = 3.58 (6H, CO_2CH_3), 5.65 (2H, s; CH_2 -6/8 eq.), 6.65 (1H, s; py1-H5), 7.85 (2H, s; py2/3-H5), 8.09 (1H, s), 9.5 (1H, s), 9.78 (2H, s), 10.73 (1H, s), 11.10 (4H, s), 11.61–11.73 (3H, m), 13.20 (1H, s), 14.98 (1H, s), 18.54 (3H, brs; py1/2/3-H3), 20.57–21.28 ppm (4H, m; CH -2/4, CH_2 -6/8 eq.); UV/Vis (0.1 mm sol in water): λ_{max} (ϵ) = 554 (334), 458 (5560), 403 (4680), 380 (4390), 253 nm ($13296\text{ M}^{-1}\text{ cm}^{-1}$); SQUID suggests SCO, moderately paramagnetic; solution-state μ_{eff} (H_2O , 5 mm, 298 K): 1.47 BM; solution-state μ_{eff} (CH_3CN , 5 mm, 298 K): 1.77 BM; CV ($E_{1/2}$, CH_3CN , 100 mV s^{-1}): 651 mV; HRMS (ESI): m/z calcd for $\text{C}_{33}\text{H}_{34}\text{FeN}_6\text{O}_6$: 333.0939 [M^{2+}]; found: 333.0934; elemental analysis calcd (%) for $\text{C}_{33}\text{H}_{34}\text{B}_2\text{F}_8\text{FeN}_6\text{O}_6\cdot 2\text{H}_2\text{O}$: C 45.24, H 4.37, N 9.59; found: C 45.53, H 4.24, N 9.66.

[FeL2]·2BF₄: The ligand (100 mg; 0.168 mmol) was dissolved in degassed, anhydrous ethanol (10 mL) and a solution of iron(II) tetrafluoroborate hexahydrate (60 mg; 0.140 mmol) in anhydrous, degassed ethanol (2 mL) was added dropwise with stirring under argon. The solution immediately turned dark brown and a precipitate appeared at the end of the addition. The reaction was continued for 4 h until the total consumption of the ligand was observed (by MS analysis), and the precipitate was isolated by filtration under argon, and washed several times with ethanol and diethyl ether to yield pure product (102 mg) in the form of a dark brown powder. It was then recrystallized by a liquid/liquid diffusion of diethyl ether into a wet (5% v/v of H_2O) acetonitrile solution of the product. Dark brown crystals suitable for X-ray analysis were isolated from the mother liquor, washed with ethanol, and dried to yield 52 mg (36%) of a crystalline product used for further analyses. Treating the remaining mother liquor may lead to an additional crop. $^1\text{H NMR}$ (500 MHz, D_2O): δ = 2.74 (2H, d, J = 13.29 Hz; CH_2 -6/8 eq.), 3.22 (2H, d, J = 13 Hz; CH_2 -6/8 ax.), 3.78 (6H, s; $-\text{CO}_2\text{CH}_3$), 4.43 (2H, s; N- CH_2), 4.97 (2H, s; N- CH_2), 5.78 (2H, s; CH -2/4), 6.84 (1H, d, J = 7.79 Hz; CH_{arom}), 7.12–7.15 (3H, m; CH_{arom}), 7.36–7.43 (3H, m; CH_{arom}), 7.67–7.72 (3H, m; CH_{arom}), 7.86 (1H, dd, J = 8.25, 5.04 Hz; CH_{arom}), 8.28 (2H, d, J = 5.50 Hz; py2/3-H3), 9.58 (1H, d, J = 3.67 Hz; py1-H4), 10.18 ppm (1H, d, J = 5.96 Hz; pdz-H4); UV/Vis (0.1 mm in water): λ_{max} (ϵ) = 455 (10870), 366 (3479), 253 nm ($13770\text{ M}^{-1}\text{ cm}^{-1}$); SQUID indicates low-spin, diamagnetic ($g \approx 0$); solution-state μ_{eff} (H_2O , 5 mm, 298 K): 0.59 BM; CV ($E_{1/2}$, CH_3CN , 100 mV s^{-1}): 648 mV; HRMS (ESI) calcd for $\text{C}_{32}\text{H}_{33}\text{FeN}_7\text{O}_5$: 333.5916 [M^{2+}]; found: 333.5910; elemental analysis calcd (%) for $\text{C}_{32}\text{H}_{33}\text{B}_2\text{F}_8\text{FeN}_7\text{O}_5\cdot \text{H}_2\text{O}$: C 44.74, H 4.11, N 11.44; found: C 44.31, H 4.16, N 11.83.

[FeL3]·2ClO₄: The ligand L3 (128 mg; 0.193 mmol) was dissolved in degassed, anhydrous acetonitrile (20 mL) and a solution of iron(II) perchlorate hydrate (70 mg; 0.256 mmol) in anhydrous, degassed acetonitrile (2 mL) was added dropwise with stirring under argon. The solution immediately turned dark brown and a precipitate appeared after 1 h. The reaction was continued with heating to approximately 50 °C overnight to ensure the full consumption of the ligand (by direct injection MS analysis). The resulting precipitate was washed with diethyl ether, redissolved in wet acetonitrile (5% v/v of H_2O), and set up for vapor diffusion of diethyl ether. Volatiles were removed from the filtrate and the residue was set up for crystallization as above. Both batches together yielded 45 mg (25%) of a crystalline (dark brown) material suitable for X-ray analysis, which was used for further characterizations. $^1\text{H NMR}$ (500 MHz, D_2O): δ = 2.90 (2H, d, J = 13.38 Hz; CH_2 -6/8 eq.), 3.61 (2H, q, J = 7.14 Hz; CH_2 -6/8 ax.), 3.78 (6H, s; $-\text{CO}_2\text{CH}_3$), 4.56 (2H, s; N- CH_2), 5.09 (2H, s; N- CH_2), 5.89 (2H, brs; CH -2/4), 6.99 (1H, d, J = 8.03 Hz; CH_{arom}), 7.22 (2H, t, J = 6.69 Hz; CH_{arom}), 7.36 (1H, brs; CH_{arom}), 7.44 (2H, d, J = 7.36 Hz; CH_{arom}), 7.56 (1H, t, J = 7.70 Hz; CH_{arom}), 7.75 (4H, t, J = 7.70 Hz; CH_{arom}), 7.84 (2H, t, J = 7.36 Hz; CH_{arom}), 8.35–8.42 (2H, m; CH_{arom}), 8.52 (2H, brs; py2/3-H3), 9.47 ppm (1H, brs; py1-H3); UV/Vis (0.1 mm in water): λ_{max} (ϵ) = 532 (774), 443 (12570), 254 nm ($28704\text{ M}^{-1}\text{ cm}^{-1}$); SQUID indicated low-spin, diamagnetic ($g \approx 0$); solution-state μ_{eff} (H_2O , 5 mm, 298 K): 0.54 BM; CV ($E_{1/2}$, CH_3CN , 100 mV s^{-1}): 769 mV; HRMS (ESI): m/z calcd for $\text{C}_{36}\text{H}_{33}\text{FeN}_7\text{O}_7$: 366.5968 [M^{2+}]; found: 366.5976; elemental analysis calcd (%) for $\text{C}_{36}\text{H}_{33}\text{B}_2\text{F}_8\text{FeN}_7\text{O}_7\cdot 2\text{H}_2\text{O}$: C 45.84, H 4.17, N 10.40; found: C 45.71, H 3.96, N 10.51.

[FeL4(SO₄)]: A hot solution of iron(II) sulfate heptahydrate (60.4 mg; 0.217 mmol) in methanol (4 mL) was added dropwise to a heated (60 °C) solution of the ligand (109 mg; 0.217 mmol) in dry, degassed methanol (8 mL). The solution turned yellow and after 30 min at 60 °C, no more ligand was observed by mass spectrometry, thus indicating that the reaction had finished. Hence, it was stopped and approximately 5% v/v of degassed water was added, followed by the addition of diethyl ether. After several days pale-yellow square-like cubic crystals suitable for X-ray analysis were formed and collected to yield 65 mg (39%) of the pure product. $R_f = 0.37$ (Al neutral, preconditioned in MeOH/CH₃COO⁻NH₄⁺ (0.1 M in water) 3:1; run in CHCl₃/MeOH 12.5:1; pure by UV/Vis light and after SCN⁻ staining); ¹H NMR (500 MHz, D₂O): δ = 3.97 (s), 22.96 (s), 23.64 (s), 30.65 (v br), 42.14 (s), 44.12 (s), 50.12 (s), 152.62 (v br), 191.16 (v br), 196.29 (v br); UV/Vis (0.25 mm): λ_{max} (ε) = 414 (1188), 255 nm (10120 M⁻¹ cm⁻¹); SQUID indicated high-spin, paramagnetic (g = 2.18); solution-state μ_{eff} (H₂O, 5 mm, 298 K): 4.96 BM; HRMS (ESI): *m/z* calcd for C₂₇H₂₉FeN₅O₆: 287.5728 [M²⁺]; found: 287.5725; elemental analysis calcd (%) for C₂₇H₂₉FeN₅O₁₀S·2H₂O: C 45.84, H 4.70, N 9.90; found: C 45.93, H 4.63, N 9.58.

[FeL4(CH₃CN)]·2BF₄: A solution of iron(II) tetrafluoroborate hexahydrate (105 mg; 0.312 mmol) in dry degassed acetonitrile (1 mL) was added dropwise under argon to a suspension of the ligand (150 mg; 0.300 mmol) in dry, degassed acetonitrile (3.5 mL) at room temperature. Upon addition the color of the solution turned deep brown and all solids were dissolved. After 1.5 h at room temperature, no more ligand was observed on the mass spectrum, so the solution was directly set up for vapor diffusion of diethyl ether. After a week, crystals suitable for X-ray analysis were isolated by filtration and washed with isopropanol and diethyl ether to yield 39 mg (17%) of the pure product, which was used for further characterizations. ¹H NMR (500 MHz, [D₃]acetonitrile): δ = 2.36 (2H, d, *J* = 13.05 Hz; CH₂-6/8 *eq.*), 3.13 (2H, d, *J* = 13.72 Hz; CH₂-6/8 *ax.*), 3.74 (6H, s; CO₂CH₃), 4.67 (1H, brs; NH), 4.76 (2H, s; N₃-CH₂py1), 5.02 (1H, s; C9-OH), 5.54 (3H, s; CH-2/4, C9-OH), 6.88 (1H, d, *J* = 8.03 Hz; py1-H6), 7.17 (1H, t, *J* = 6.53 Hz; py1-H4), 7.24–7.40 (4H, m; py2/3-H4/6), 7.49 (1H, t, *J* = 7.70 Hz; py1-H5), 7.76 (2H, t, *J* = 7.53 Hz; py2/3-H5), 8.70 (1H, d, *J* = 5.35 Hz; py1-H3), 8.86 ppm (2H, d, *J* = 5.02 Hz; py2/3-H3); UV/Vis (0.25 mm in acetonitrile): λ_{max} (ε) = 521 (772), 444 (7144), 380 nm (3828 M⁻¹ cm⁻¹); solution-state μ_{eff} (H₂O, 5 mm, 298 K): 4.16 BM; solution-state μ_{eff} (CH₃CN, 5 mm, 298 K): 0.65 BM; CV (*E*_{1/2}, CH₃CN, 100 mV s⁻¹): 658 mV; HRMS (ESI): *m/z* calcd for C₂₇H₂₉FeN₅O₆: 287.5728 [M²⁺]; found: 287.5740; elemental analysis calcd (%) for C₂₉H₃₂B₂F₈FeN₆O₆: C 44.09, H 4.08, N 10.64; found: C 44.33, H 4.13, N 10.19.

Acknowledgements

A PhD fellowship (2010–2012) for J.L.K. from La Ligue Contre Le Cancer is gratefully acknowledged. We thank Fayçal Touti for technical advice, Oliver Thorn-Seshold for manuscript revision, Sandrine Denis-Quanquin for assistance with NMR experiments, Philippe Maurin for valuable discussions, Christophe Bucher for expert assistance in the cyclic voltammetry experiments, and Dominique Luneau and Ruben Checa for SQUID measurements.

- [1] P. Gütllich, H. A. Goodwin in *Topics in Current Chemistry*, Vol. 233 (Eds.: P. Gütllich, H. A. Goodwin), Springer, Heidelberg, **2004**, pp. 1–47.
- [2] G. J. Halder, C. J. Kepert, B. Moubaraki, K. S. Murray, J. D. Cashion, *Science* **2002**, *298*, 1762–1765.
- [3] a) F. Touti, P. Maurin, J. Hasserodt, *Angew. Chem.* **2013**, *125*, 4752–4756; *Angew. Chem. Int. Ed.* **2013**, *52*, 4654–4658; b) F. Touti, P. Maurin, L. Canaple, O. Beuf, J. Hasserodt, *Inorg. Chem.* **2012**, *51*, 31–33.
- [4] Z. Ni, M. P. Shores, *J. Am. Chem. Soc.* **2009**, *131*, 32–33.

- [5] a) A. L. Feig, S. J. Lippard, *Chem. Rev.* **1994**, *94*, 759–805; b) E. I. Solomon, T. C. Brunold, M. I. Davis, J. N. Kemsley, S.-K. Lee, N. Lehnert, F. Neese, A. J. Skulan, Y.-S. Yang, J. Zhou, *Chem. Rev.* **2000**, *100*, 235–350; c) S. V. Kryatov, E. V. Rybak-Akimova, S. Schindler, *Chem. Rev.* **2005**, *105*, 2175–2226; d) S. Hong, Y.-M. Lee, W. Shin, S. Fukuzumi, W. Nam, *J. Am. Chem. Soc.* **2009**, *131*, 13910–13911.
- [6] a) F. Touti, A. K. Singh, P. Maurin, L. Canaple, O. Beuf, J. Samarut, J. Hasserodt, *J. Med. Chem.* **2011**, *54*, 4274–4278; b) S. J. Dorazio, P. B. Tsitovich, K. E. Sifers, J. A. Sperryak, J. R. Morrow, *J. Am. Chem. Soc.* **2011**, *133*, 14154–14156.
- [7] a) M. A. Halcrow, *Chem. Soc. Rev.* **2011**, *40*, 4119–4142; b) A. B. Gaspar, V. Ksenofontov, M. Serebyuk, P. Gutlich, *Coord. Chem. Rev.* **2005**, *249*, 2661–2676; c) M. A. Halcrow, *Coord. Chem. Rev.* **2009**, *253*, 2493–2514.
- [8] M. A. Hoselton, L. J. Wilson, R. S. Drago, *J. Am. Chem. Soc.* **1975**, *97*, 1722–1729.
- [9] H. Toftlund, *Coord. Chem. Rev.* **1989**, *94*, 67–108.
- [10] H. Toftlund, J. J. McGarvey in *Topics in Current Chemistry*, Vol. 233 (Ed.: P. Gütllich, H. A. Goodwin), Springer, Heidelberg, **2004**, pp. 151–166.
- [11] a) L. L. Martin, K. S. Hagen, A. Hauser, R. L. Martin, A. M. Sargeson, *J. Chem. Soc. Chem. Commun.* **1988**, 1313–1315; b) J. J. McGarvey, I. Lawthers, K. Heremans, H. Toftlund, *Inorg. Chem.* **1990**, *29*, 252–256; c) A. H. R. Al-Obaidi, J. J. McGarvey, K. P. Taylor, S. E. J. Bell, K. B. Jensen, H. Toftlund, *J. Chem. Soc. Chem. Commun.* **1993**, 536–538; d) A. H. R. Al-Obaidi, K. B. Jensen, J. J. McGarvey, H. Toftlund, B. Jensen, S. E. J. Bell, J. G. Carroll, *Inorg. Chem.* **1996**, *35*, 5055–5060; e) H. Börzel, P. Comba, H. Pritzkow, A. F. Sickmüller, *Inorg. Chem.* **1998**, *37*, 3853–3857; f) H. Toftlund, *Monatshfte für Chemie/Chemical Monthly* **2001**, *132*, 1269–1277.
- [12] L. L. Martin, R. L. Martin, A. M. Sargeson, *Polyhedron* **1994**, *13*, 1969–1980.
- [13] V. Stavila, M. Allali, L. Canaple, Y. Stortz, C. Franc, P. Maurin, O. Beuf, O. Dufay, J. Samarut, M. Janier, J. Hasserodt, *New J. Chem.* **2008**, *32*, 428–435.
- [14] J. Hasserodt, *New J. Chem.* **2012**, *36*, 1707–1712.
- [15] S. A. Barrett, C. A. Kilner, M. A. Halcrow, *Dalton Trans.* **2011**, *40*, 12021–12024.
- [16] F. El Hajj, G. Sebki, V. Patinec, M. Marchivie, S. Triki, H. Handel, S. Yefsah, R. Tripiet, C. J. Gomez-Garcia, E. Coronado, *Inorg. Chem.* **2009**, *48*, 10416–10423.
- [17] V. J. Thoen, J. C. A. Boeyens, G. J. McDougall, R. D. Hancock, *J. Am. Chem. Soc.* **1984**, *106*, 3198–3207.
- [18] P. Comba, M. Kerscher, W. Schiek in *Progress in Inorganic Chemistry*, Vol. 55 (Ed.: K. D. Karlin), Wiley-VCH, Weinheim, **2007**, pp. 613–704.
- [19] P. Comba, C. Haaf, H. Wadepohl, *Inorg. Chem.* **2009**, *48*, 6604–6614; P. Comba, M. Morgen, H. Wadepohl, *Polyhedron* **2013**, *52*, 1239–1245.
- [20] a) G. D. Hosken, R. D. Hancock, *J. Chem. Soc. Chem. Comm.* **1994**, 1363; b) G. D. Hosken, C. C. Allan, J. C. A. Boeyens, R. D. Hancock, *J. Chem. Soc. Dalton Trans.* **1995**, 3705.
- [21] C. Mannich, P. Mohs, *Ber. Dtsch. Chem. Ges.* **1930**, *63*, 608–612.
- [22] a) G. R. Clemo, R. Raper, *J. Chem. Soc.* **1933**, 644–645; b) G. R. Clemo, W. M. Morgan, R. Raper, *J. Chem. Soc.* **1936**, 1025–1028.
- [23] R. Haller, *Arzneim.-Forsch.* **1965**, *15*, 1327–1330.
- [24] A. Samhammer, U. Holzgrabe, R. Haller, *Arch. Pharm.* **1989**, *322*, 545–550.
- [25] R. Haller, *Arch. Pharm.* **1969**, *302*, 113–118.
- [26] a) S. Chiavarelli, G. P. Valsecchi, F. Toffler, L. Gramiccioni, *Boll. Chim. Farm.* **1967**, *106*, 301–306; b) O. I. Levina, K. A. Potekhin, E. N. Kurkutova, Y. T. Struchkov, O. N. Zefirova, V. A. Palyulin, N. S. Zefirov, *Dokl. Akad. Nauk SSSR* **1986**, *289*, 876–879; c) D. S. C. Black, G. B. Deacon, M. Rose, *Tetrahedron* **1995**, *51*, 2055–2076; d) S. Z. Vatsadze, N. V. Zyk, R. D. Rakhimov, K. P. Butin, N. S. Zefirov, *Russ. Chem. Bull.* **1995**, *44*, 440–442; e) A. N. Chekhlov, S. Z. Vatsadze, N. V. Zyk, N. S. Zefirov, *Dokl. Akad.*

- Nauk* **1995**, 343, 785–790; f) K.-W. Chi, R. J. Lagow, *Bull. Korean Chem. Soc.* **1996**, 17, 1093–1094.
- [27] a) P. Comba, B. Nuber, A. Ramlow, *J. Chem. Soc. Dalton Trans.* **1997**, 347–352; b) M. Atanasov, P. Comba, S. Helmle, D. Muller, F. Neese, *Inorg. Chem.* **2012**, 51, 12324–12335.
- [28] a) P. Comba, C. Lopez de Laorden, H. Pritzkov, *Helv. Chim. Acta* **2005**, 88, 647–664; b) S. Juran, M. Walther, H. Stephan, R. Bergmann, J. Steinbach, W. Kraus, F. Emmerling, P. Comba, *Bioconjugate Chem.* **2009**, 20, 347–359.
- [29] P. Comba, C. Lang, C. Lopez de Laorden, A. Muruganantham, G. Rajaraman, H. Wadepohl, M. Zajaczkowski, *Chem. Eur. J.* **2008**, 14, 5313–5328.
- [30] a) M. R. Bukowski, P. Comba, A. Lienke, C. Limberg, C. Lopez de Laorden, R. Mas-Balleste, M. Merz, L. Que, Jr., *Angew. Chem.* **2006**, 118, 3524–3528; *Angew. Chem. Int. Ed.* **2006**, 45, 3446–3449; b) J. Bautz, P. Comba, C. Lopez de Laorden, M. Menzel, G. Rajaraman, *Angew. Chem.* **2007**, 119, 8213–8216; *Angew. Chem. Int. Ed.* **2007**, 46, 8067–8070.
- [31] P. Comba, M. Maurer, P. Vadivelu, *Inorg. Chem.* **2009**, 48, 10389–10396.
- [32] P. Comba, S. Wunderlich, *Chem. Eur. J.* **2010**, 16, 7293–7299.
- [33] M. Jaccob, P. Comba, M. Maurer, P. Vadivelu, P. Venuvanalilingam, *Dalton Trans.* **2011**, 40, 11276–11281.
- [34] a) P. C. A. Bruijninx, G. van Koten, R. J. M. Klein Gebbink, *Chem. Soc. Rev.* **2008**, 37, 2716–2744; b) P. Comba, S. Fukuzumi, H. Kotani, S. Wunderlich, *Angew. Chem.* **2010**, 122, 2679–2682; *Angew. Chem. Int. Ed.* **2010**, 49, 2622–2625; c) M. R. Bukowski, P. Comba, C. Limberg, M. Merz, L. Que, Jr., T. Wistuba, *Angew. Chem.* **2004**, 116, 1303–1307; *Angew. Chem. Int. Ed.* **2004**, 43, 1283–1287; d) P. Comba, B. Martin, A. Muruganantham, J. Straub, *Inorg. Chem.* **2012**, 51, 9214–9225.
- [35] H. Börzel, P. Comba, K. S. Hagen, Y. D. Lampeka, A. Lienke, G. Linti, M. Merz, H. Pritzkow, L. V. Tsymbal, *Inorg. Chim. Acta* **2002**, 337, 407–419.
- [36] a) R. E. Trifonov, A. P. Volovodenko, S. N. Vergizov, N. I. Shirinbekov, V. A. Gindin, A. O. Koren, V. A. Ostrovskii, *Helv. Chim. Acta* **2005**, 88, 1790–1797; b) *Comprehensive Heterocyclic Chemistry II* (Eds.: A. R. Katritzky, C. W. Rees, E. F. V. Scriven), Pergamon, Oxford, **1996**.
- [37] P. Comba, W. Schiek, *Coord. Chem. Rev.* **2003**, 238, 21–29.
- [38] D. F. Evans, *J. C. Soc.* **1959**, 2003–2005.
- [39] E. M. Schubert, *J. Chem. Educ.* **1992**, 69, 62–62.
- [40] D. Ostfeld, I. A. Cohen, *J. Chem. Educ.* **1972**, 49, 829.
- [41] J. England, R. Gondhia, L. Bigorra-Lopez, A. R. Petersen, A. J. P. White, G. J. P. Britovsek, *Dalton Trans.* **2009**, 5319–5334.
- [42] A. Draksharapu, Q. Li, H. Logtenberg, T. A. van den Berg, A. Meetsma, J. S. Killeen, B. L. Feringa, R. Hage, G. Roelfes, W. R. Browne, *Inorg. Chem.* **2012**, 51, 900–913.
- [43] P. Comba, M. Kersch, M. Merz, V. Müller, H. Pritzkow, R. Remy, W. Schiek, Y. Xiong, *Chem. Eur. J.* **2002**, 8, 5750–5760.
- [44] J. W. Turner, F. A. Schultz, *Inorg. Chem.* **2001**, 40, 5296–5298.
- [45] B. Weber, F. A. Walker, *Inorg. Chem.* **2007**, 46, 6794–6803.
- [46] K. P. Bryliakov, E. A. Duban, E. P. Talsi, *Eur. J. Inorg. Chem.* **2005**, 72–76.
- [47] M. A. Halcrow, *Polyhedron* **2007**, 26, 3523–3576.
- [48] T. Siener, U. Holzgrabe, S. Drosihn, W. Brandt, *J. Chem. Soc. Perkin Trans. 2* **1999**, 1827–1834.
- [49] C. Bleiholder, H. Boerzel, P. Comba, R. Ferrari, M. Heydt, M. Kersch, S. Kuwata, G. Laurency, G. A. Lawrance, A. Lienke, B. Martin, M. Merz, B. Nuber, H. Pritzkow, *Inorg. Chem.* **2005**, 44, 8145–8155.
- [50] M. G. N. Russell, R. W. Carling, J. R. Atack, F. A. Bromidge, S. M. Cook, P. Hunt, C. Isted, M. Lucas, R. M. McKernan, A. Mitchinson, K. W. Moore, R. Narquizian, A. J. Macaulay, D. Thomas, S.-A. Thompson, K. A. Wafford, J. L. Castro, *J. Med. Chem.* **2005**, 48, 1367–1383.
- [51] D. F. Evans, D. A. Jakubovic, *J. Chem. Soc. Dalton Trans.* **1988**, 2927–2933.
- [52] a) P. Pascal, *Ann. Chim. Phys.* **1910**, 19, 5; b) O. Kahn, *Molecular Magnetism*, Wiley-VCH, Weinheim, **1993**.
- [53] a) R. Haller, U. Ashauer, *Arch. Pharm.* **1985**, 318, 405–410; b) H. Börzel, P. Comba, K. S. Hagen, C. Katsichtis, H. Pritzkow, *Chem. Eur. J.* **2000**, 6, 914–919.

Received: February 16, 2013
Published online: May 13, 2013

Magnetogenesis in Water Induced by a Chemical Analyte

Jens Hasserodt*, Jacek Lukasz Kolanowski, and Faycal Touti

Keywords:

Molecular sensor · magnetization · chemical imaging · iron · water

This minireview aims to shed light on the emergent field of inducing a change in the magnetic properties of a solution-phase sample when exposed to a chemical analyte. While there exists a considerable body of knowledge on materials that alter their magnetic characteristics upon a change in the surrounding physical conditions and even a number of cases of solution-phase samples that do so under these same circumstances, examples of dissolved molecules or particles that react in this fashion at constant conditions and in response to an analyte are limited. While cases in organic solvents are discussed, the emphasis of this article resides on water. Our ambition is to provide the reader with a guideline to the design of new magnetogenic probes for the detection of the chemical analyte of his choice.

1. Introduction

In the field of Chemical Imaging,^[1] magnetic modes of physical detection should be considered an attractive alternative to more established ones like those based on electromagnetic waves (absorbance, fluorescence, phosphorescence, interferometry), radioactivity, or electric currents (conductometry). There are several convincing features arguing in favor of paramagnetic-molecule detection in the solution phase. In contrast to radioactive compounds, the signal is not constantly emitted but only when an external magnetic field is applied (1), a field that interacts very little with other components of the sample (2). The signal and the molecule from which it is originating do not experience any fatigue as is commonplace for fluorescent or radioactive molecules (3). A magnetic detection process is environmentally harmless so that no collateral sample degradation needs to be feared (4). The signal emitted by the magnetic molecule is not depleted during its passage through the sample (5). Finally, highly specific detection is possible for many sample environments since they contain no paramagnetic component (6). A newly established paramagnetic quality may also influence other properties of the sample (optical and relaxatory ones (NMR)) and thus lead to the opportunity of a multimodal readout. As possible weaknesses, (-1) a limited detection sensitivity and (-2)

the need for complex instrumentation should be advanced. Principally, two types of instruments are used to detect paramagnetism in the liquid phase, namely an electron spin resonance (ESR) spectrometer for direct detection or a nuclear magnetic resonance (NMR) spectrometer for indirect detection. The development of small and inexpensive portable NMR devices consisting of a permanent magnet of low field strength is a welcome drive towards instrumentation of significantly reduced complexity.^[2a,b] An opposite trend consists in the development of NMR spectrometers and MRI scanners (Magnetic Resonance Imaging) equipped with super-conducting magnets of ever higher field strength. As this review addresses molecular magnetic properties in solution, tribute has to be paid to the chemists in the field of MRI contrast agents who have devised an extraordinary number of paramagnetic molecules operating in aqueous solution. The magnetic quality of these molecules arises from their permanent electron spin and is detected through its influence on the relaxation time of nuclear spins of neighboring water molecules. This electron spin/nuclear spin interaction is at the origin of the concentration-dependent shortening of the nuclear relaxation times, defined as relaxivity, and can be detected by a variation of the NMR signal. Bloch et al. were the first to suggest in 1946 the use of paramagnetic metal ions for the modification of the NMR signal.^[3] In the decade leading up to the millenium change, it was estimated that more than 30 tons of gadolinium ions were injected into the veins of patients worldwide,^[4] in order to enhance MRI-based clinical diagnostics. The whereabouts of the agent can be depicted in an MR image by translating the variation in the shortening of relaxation times of surrounding water hydrogen nuclei into different grey-scale levels. Importantly, these MRI hypersignals are caused by *recruitment* of permanently paramagnetic agents to a particular location/tissue through passive differential diffusion and distribution processes or by specific delivery strategies. In the past 15 years, new contrast

[*] Prof. J. Hasserodt; J. L. Kolanowski, MSc.; F. Touti, MSc.
Laboratoire de Chimie, UMR CNRS UCBL 5182
Université de Lyon – ENS de Lyon
46 allée d'Italie, 69364 Lyon Cedex 07, France
Fax: +33 (0) 472728860
E-mail: jens.hasserodt@ens-lyon.fr
Homepage: www.ens-lyon.fr/CHIMIE

agents have surfaced that have the added value of responding reversibly or irreversibly to a chemical analyte of interest ($p(O_2)$,^[5] enzymes,^[6a,b] metals,^[7a-c] pH ^[8a,b]) by changing their signaling power. Truly sophisticated concepts have been reported^[7c,9a,b] where the agent's relaxivity is modified under the influence of the analyte. Without any exception, these probes are based on modifying their relaxatory powers; the magnitude of their electronic spin remains untouched. They thus operate by a change in the efficiency of the electron spin/nuclear spin interaction and not a change in magnetization. With this important distinction in mind, we address in this review the *de novo* creation (off-on mode) of an electronic spin in a sample and not simply its increase from a measurable base value, and we call it *magnetogenesis*. This newly created paramagnetic quality may be detected by simple methods not requiring any spatial resolution, or be exploited in advanced chemical and medical imaging that detects the whereabouts of the probe in a complex, heterogeneous and spatially structured sample. The off-on response of magnetogenic probes has attractive advantages for a wide range of applications, including a matchless signal-to-background ratio, the background being the signal in the presence of the molecule (the probe) while the chemical analyte is absent. With the expression *chemical analyte* we imply a chemical or biochemical of interest that interacts with the probe either in a supramolecular fashion or modifies it permanently, and this at constant conditions of the medium (solvent identity, pH, temperature, ionic force, concentration etc.). In the following (chapter 2) we will address the current perception of molecules responding in solution to a change in chemical composition by altering their magnetic properties and furnish selected examples. They do so almost exclusively by an incomplete, gradual and

reversible shift of the spin equilibrium they represent, and we thus refer to it as *magneto-modulation*.

2. State-of-the-art: reversible magneto-modulation

The literature reporting on the modulation of the magnetic properties of a sample by applying an external stimulus is extensive because this field has attractive prospects for the design of molecular devices, switches, sensors, and other applications.^[10] The substantial number of reports on spin equilibria, and in particular magnetically bistable compounds (spin crossover SCO) has been thoroughly reviewed.^[11a,b] Certain subfields were also reviewed elsewhere, including polynuclear metal complexes,^[12] valence tautomeric compounds (VT)^[13] and other charge-transfer systems, such as cyanide-bridged Prussian Blue analogs,^[14a,b] that comprise "molecular squares".^[15] However, the field has principally focussed on *solid-state materials* such as crystalline polymorphs, coordination polymers,^[16] or metal-organic frameworks (MOFs) in order to be able to explore cooperative effects. And it has mostly studied *physical stimuli* to cause a magneto-modulating effect in view of its main ambition to create new memory devices. The influence of non-coordinative chemical components on the magnetic properties of materials has received increased consideration.^[17a,b,c] The fact that the change in magnetization is often associated with a modification of optical^[18a,b] and electrical properties^[19a,b] is explored for multi-signaling applications.^[11a,b]

By contrast, what are the documented cases for *discrete* molecular entities in solution suffering an alteration of their electronic spin state upon interaction with an external stimulus? In fact, only examples of reversible spin equilibria have yet been reported and were reviewed up to the year 2008.^[20a-e] These reactions involve principally mono- or dinuclear coordination compounds of the transition metals. Excess quantities of analyte are required to show a gradual modulation (scheme 1A, B). Apart from the fact that cooperative effects are generally absent for dissolved mononuclear chelates, a wholly new concern arises when moving to the solution phase, namely probe stability, a challenge that has been declared all-important.^[21] A good number of coordination compounds were reported that respond mainly to temperature changes, some to irradiation, while those that react to chemical stimuli are limited and were summarized this year.^[22,21] These are often not explored as responsive, diagnostic probes as they comprise mostly low-denticity ligands resulting in poor stability in competitive solvents. However, the analysis of these cases provides with a welcome overview over the different mechanisms that allow for the control of magnetic properties in solution. Interactions between discrete coordination compounds capable of altering their spin state and other chemicals in solution are either limited to the periphery of the complexes (1) or affect the constitution of the first coordination sphere (2).

Cases for an interaction with the periphery (table 1) are principally based on electrostatic interactions (non-specific interactions, ion pairing or hydrogen bonding). These phenomena are usually limited in their impact (for an exception see ref^[23]). A change in solvent polarity may influence a sample's paramagnetism without any hydrogen-bonding phenomena involved.^[23,24a,b] More polar solvents tend to favor the low-spin state (LS) because of the significantly smaller volume it adopts^[25a,b] (see also central-sphere size difference in schemes). It has been suggested that a switch to the high-spin state (HS) has to compensate for the work required for separating the solvent molecules to provide a suitably sized and



Jens Hasserodt (PhD from Heidelberg Univ) spent 7 years at The Scripps Research Institute with Profs. Lerner and Janda, first as a postdoc, then as a staff scientist, and from jan 1998 as an ass. prof. In sept 2001 he became professor at the ENS Lyon. He dedicated his past 12 years to enzyme inhibition and detection, particularly in the fast growing field of Molecular Imaging.



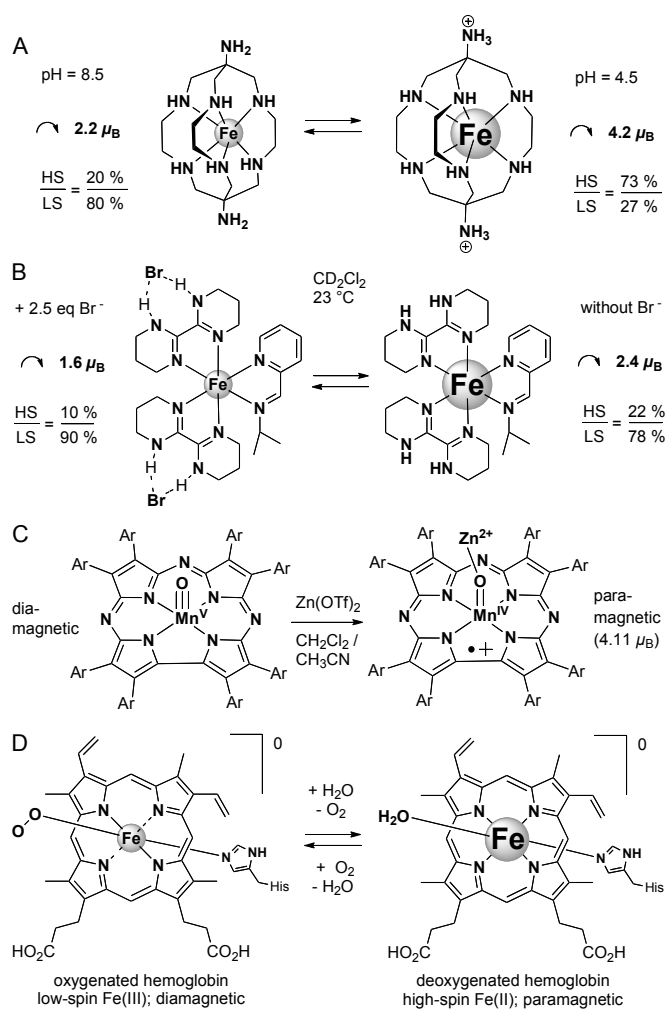
Jacek Kolanowski simultaneously studied biotechnology (BSc in 2007) and chemistry (MSc in 2009 with Prof. Koroniak) at Adam Mickiewicz Univ (Poznan, Poland). He spent one year as research assistant with Prof. Roeschenthaler (Bremen, Germany). Currently he is a PhD student in the group of Prof. Hasserodt. His interests focus on devising chemical tools for solving biological problems.



Faycal Touti was trained both in chemistry (MSc in 2008, ENS Lyon) and pharmacy (MSc 2010, UPS Toulouse). He currently prepares a PharmD and a PhD in the group of Prof. Hasserodt on the development of the first line of magnetogenic probes. His general research interests lie in the field of chemical biology, enabling biotechnologies and chemical probing.

shaped enclosure in which the solute can be accommodated.^[24b] Positively charged complexes may interact with anionic analytes, but the phenomenon is only observed in apolar media and at higher concentrations.^[26] Magneto-modulation caused by hydrogen bonding usually requires electronic communication between the H bond donor or acceptor site and the metal center. Partial proton transfer from an H bond donor site on the periphery increases its electron density which can be transmitted to the coordinating atom. This in return shortens the coordination bond and consequently favors the LS state. Early on it was shown at the example of Fe(III) complexes with tren-like ligands that solvents of higher H-bond acceptor capacity (higher Gutmann donor number DN) promote the LS state.^[27a,b] A similar but much less pronounced effect has been observed for these systems in acetonitrile when exchanging a BPh₄ counterion with a halide ion (stabilization by 0.2 – 0.3 Bohr magnetons μ_B in acetonitrile; μ_B are the units for paramagnetism and the μ_B value is roughly proportional to the spin value).^[27a] In a very recent example, a ternary iron(II) complex exhibiting NH groups in its ligands was shown to be of low intermediate spin at room temp. in water (1.2 μ_B) while being of high intermediate spin in nitromethane (3.3 μ_B).^[28] An extreme case of hydrogen bonding is the total proton transfer from donor to acceptor. In the case of ternary complex [Fe(bzimpy)2]²⁺, deprotonation of its N-H donor site is caused by a solvent of exceptionally high donor number (HMPA, DN = 30) which thus turns the complex diamagnetic. The same compound is already more than 50 % HS in solvents of lower DN (MeOH, DN = 19, 3.0 μ_B , 56 % HS).^[29a,b] For the opposite case, protonation, the example of binary Fe(II) complexes of a class of bicyclic and totally aliphatic hexa-amines, the sarcophagines, is particularly illustrative (scheme 1A).^[30a,b] While no electronic communication between the protonated nitrogen and the metal center can be claimed here, the newly arisen electrostatic repulsion between the metal center and the charged ammonium group likely causes lengthening of the coordination bonds and thus favors adoption of a largely high-spin (HS) state (4.2 μ_B) starting from an initially intermediate spin (2.2 μ_B). Compared to most examples above, these complexes are exceptional in that they are stable in water. However, the already paramagnetic quality of the initial complex (“on”) as well as the susceptibility to oxidation under air limit its interest for further probe development.

Beyond the above, cases of more specific analyte response have also been reported. Shores et al. proposed a quaternary homoleptic ferrous complex comprised of three bidentate bis-amidine ligands as a magneto-responsive anion sensor.^[31] When two equivalents of a bromide salt are added at –40°C in dichloromethane, the magnetic moment of the initial complex (4.7 μ_B , estimated to correspond to 92 % HS) drops to 2.7 μ_B (estimated to be 30 % HS). In order to observe this effect at ambient temperature, one bis-amidine ligand was replaced with a pyridyl-imine ligand, thus obtaining a response to 2.5 eq. of bromide of 1.6 μ_B (approx. 10 % HS) vs. an initial 2.4 μ_B (approx. 20 % HS, scheme 1B, hypothetical structure for bromide effect).^[32] The instability of these complexes, especially in more competitive solvents, the limited magnitude of their response, and their inactivation rather than activation by the analyte has prompted the authors to explore binary complexes comprising tren-based hexa-dentate ligands for the same sensing purpose,^[33] while anion binding in acetonitrile was observed, a magneto-modulating response has not yet been demonstrated. A remarkable case of off-on magnetogenesis via peripheral interaction consists in the Lewis acid-base interaction (Zn²⁺) with a high-valent manganese-oxo porphyrinoid complex (scheme 1C).^[34] The magneto-modulation mechanism in this system is similar to that of H bonding discussed



Scheme 1. Influence of constitutional equilibria on spin equilibria for two Fe(II) complexes (A and B); internal electron transfer caused by peripheral analyte interaction (C); mechanism exploited by BOLD fMRI (D).

earlier but with the opposite effect: the Zinc-oxo interaction withdraws electron-density from the initially diamagnetic metal center thus promoting the adoption of a lower oxidation state and concomitant establishment of a radical cationic character in the ligand. In view of the highly reactive high-valency metal center, it remains to be seen to what extent this strongly magneto-modulating system can be adapted to more realistic sample environments. In conclusion, a pronounced and selective magnetogenic response by weak probe-analyte interactions remains a challenge.

Interactions that affect the constitution of the first coordination sphere (2) promise a much more noticeable change in paramagnetism. Decoordination, if finely controlled, can serve as a mechanism for sensor design but should avoid the replacement of more than one coordinating site on the metal during activation, because this would increase the risk of non-selective probe activation.^[35a-d] Displacement of one coordinating site by another can significantly change the ligand field to give rise to drastic changes in electronic spin. The switch of hemoglobin from a paramagnetic to a diamagnetic state during oxygenation^[36] is an inspiring biological example (scheme 1D). This fortuitously responsive probe has been exploited since the early nineties in Blood Oxygen-Level Dependent Functional MRI (BOLD-fMRI) and has revolutionized the neurosciences.^[37] Several synthetic examples have been reported, too. They may be divided into those where (a) mono-dentate ligands

are displaced on ternary complexes or higher or where (b) a tethered arm of a hexa-dentate ligand is decoordinated, thus amounting to the cleavage of a chelate ring. These strategies are reminiscent of the fluorogenic indicator displacement assays.^[38a,b] While case b) is energetically much more challenging, it offers the prospect of a significantly more stable initial probe and higher analyte selectivity. Examples in category a)^[39a-e] are mostly based on Fe(II) and mainly take advantage of the coulombic attraction between anionic analytes and the cationic metal center which may result in LS to HS activation (or deactivation in the case of CN⁻). Certain neutral interaction partners, e. g. MeCN, displace their mono-dentate competitor by causing an opposite direction of activation (HS to LS) because of the high ligand field they exercise. For category b), it was our group that reported the first controlled example.^[40] The respective ferrous complex (**2/2'**, scheme 6A) showed a large magnetic modulation by pendent-arm de-coordination; it shall be discussed in chapter 4 because it is part of a larger story on a probe that shows irreversible magnetogenesis. Another case of pendent-arm displacement on a HS-Fe(II) complex by an anion did in fact not lead to magneto-modulation.^[41] A very recent example concerns a binary Fe(II) complex the pendent arm of which exhibits a limited ligand field/basicity and is thus partially displaced by chloride in MeCN.^[42] The potential of this system for the design of magneto-responsive probes was however not discussed. A variant of the mechanism of changing the first coordination sphere consists in the additional coordination of a ligand/analyte,^[20a,22] this alters of course the coordination number. The arguably most widely studied examples are diamagnetic square planar Ni(II) complexes that may welcome nucleophilic ligands into their axial position leading to octahedral paramagnetic complexes. Numerous attempts have been made to control this process and the associated magnetogenesis.^[43a-d] However, square planar Ni(II) complexes are intrinsically prone to competitive addition by other nucleophiles such as water or N-donors (see also chapter 3).^[44a-c] Thus the specificity of recognition in complex media and the stability of the square-planar diamagnetic form in aqueous samples are genuinely compromised.

Table 1. Relative performance of reversible magneto-modulation

Nature of probe-analyte interaction	Complex strength vs. solvent competition	Specificity	Effect on magnetic properties	Verdict
Electrostatic ^a	very weak (-)	very low (-)	very weak (-)	3 -
H bonding	weak ()	medium (+)	weak ()	1 +
Coordinative displacement	medium (+)	medium (+)	medium (+)	3 +
Protonation	strong (++)	high (++)	medium (+)	5 +

^a in polar solvents

What all examples from the above have in common is the *reversible* nature of their interaction.^[21] As we shall see at the end of chapter 3 and in chapter 4, a probe that suffers *irreversible* chemical conversion by its target analyte offers the prospect of much higher specificity and higher initial probe stability. In order to target analytes acting as chemical reactants, stoichiometrically or catalytically, the putative probe should comprise a trigger moiety separated from a *magnetogenic core* by an intelligent spacer giving rise to a three-component construct of high modularity.^[45]

3. Five hallmarks of responsive probe design influence the choice of the magnetogenic core

At the beginning of the design of any tool, molecular or other, one needs to set the requirements that it shall satisfy. We advance five (six) principal characteristics that a responsive probe should muster in order to fulfill the promise of effective analyte detection:

- (1) **robustness**
- (2) **fast response kinetics**
- (3) **maximum signal gap**
- (4) **an initially silent probe (off-on)**
- (5) **a decidedly binary response**
- (6) **low toxicity** (if considering in vivo applications)

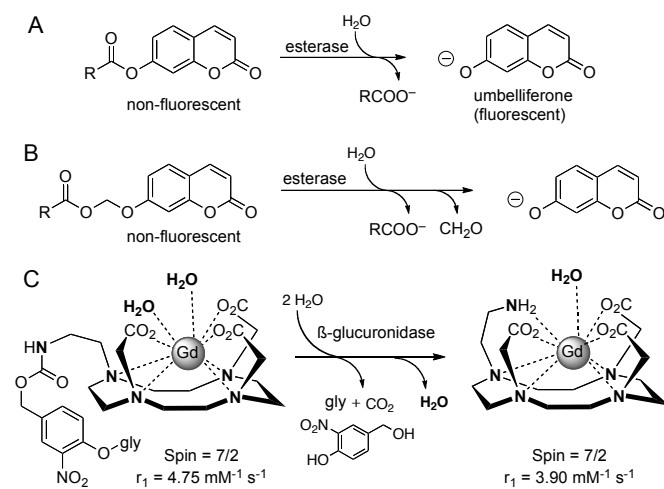
Robustness. A responsive probe must necessarily show an intrinsic reactivity in order to be susceptible to the target analyte. This requirement can become a serious liability in its design in that the molecule may show residual spontaneous degradation in the absence of the analyte. This in turn likely results in the formation of the signaling molecule and thus in a false positive signal, a well-recognized challenge in the design of responsive probes (for two examples see scheme 2A and 2B).^[46a-c] It is often difficult for the reader of scientific reports to assess the robustness of a given probe design at the hands of the furnished response data. If this data is only given for the favorable case of high analyte activity or a large analyte-to-probe ratio, then the active transformation reaction may outrun the spontaneous degradation reaction to such an extent that no increase of a background signal need to be deplored during the monitoring period. In a more realistic setting of a heterogeneous sample with a spatially complex structure, the probe requires time to reach all sites (diffusion), and it may be in this very time span that it starts to generate a false positive signal that seriously puts the active response result into question.

Fast response kinetics is an obvious requirement. A responsive probe may show high, medium or low reactivity toward the target analyte. Its signal may awake via one chemical step or by two or more. The consequences of slow response are dire: higher concentrations of the intact probe and/or the target analyte need to be established on site in order to observe the same signal intensity as for the case of a fast responding probe at the same delay time. The measure of increasing the delay time, by contrast, does not alleviate the situation; the diffusion rate of the activated probe remains roughly the same, and the signal on site does not increase because of loss to other parts. For probes reacting via two steps or more, slow response does not exactly improve this situation: in samples of structural complexity the analyte residing in a particular place may do its duty and chemically modify the probe as planned. However, the slow translation of this modification into a legible signal in the second step, if being the rate-determining one (for an example, see scheme 2B),^[46a] allows the intermediate to diffuse away from the site before “lighting up”. All these considerations can be summarized with the phenomenon of signal dilution and with a decrease in detection sensitivity.

Maximum signal gap. It is plain that no matter the identity of the physical signal that serves to detect the analyte (the detection modality), a maximum emission intensity of the activated probe is always desirable. This ensures highest change between the “before” and “after” state of the responsive probe (for an opposite example, see scheme 1C).^[47] In the particular case of a magnetogenic probe this would imply the generation of a high number of unpaired electrons per nucleus.

Off-on. It is highly desirable to design a probe that is initially silent (scheme 2A and B).^[48] The absence of any signal in the absence of analyte simplifies the interpretation of the image or detection result enormously. It also makes the dream of achieving analyte quantitation much more realistic. For the case of responsive probes for MRI that do already emit a sizeable signal before encounter of the target, it has been repeatedly stressed that unambiguous image interpretation would require knowing the concentration of converted *and* unconverted probe at the site of interest.^[8a,49a-c] Without this knowledge, it cannot be ruled out that the observed signal is simply the result of the accumulation of the untouched probe for physicochemical reasons (biodistribution, diffusion, lipophilicity, charge, etc) without the presence of any analyte at all. For the same reasons outlined above, the opposite scenario of an On→off probe^[31,50] is less attractive (for an example^[47], see scheme 2C).

Binary response. Depending on the nature of the activation reaction (reversible vs. irreversible reaction), the associated chemical equilibrium may be more or less decided in its choice for one side or the other of the equilibrium. In other words, it should be avoided that only part of the population of intact probes is converted by the analyte, or that only part of the population of activated probes does in fact emit a signal (for comparison see scheme 1A and B). The majority of detection schemes covered by table 1 enter into this category. Quite to the contrary: a switch of the entire population from 0 to 100 % should be the goal (true for all examples in scheme 2). Otherwise, the same complications arise that were already mentioned for the previous hallmark of probe design.



Scheme 2. Non-magnetogenic probe examples discussed in the light of hallmark satisfaction (gly = glucuronyl).

Choice of magnetogenic core *Magnetization* is the density of magnetic dipole moments *induced* by the presence of an external magnetic field generated by a permanent magnet surrounding the sample. Such magnetic moments are the result of the spin of electrons and nuclei and of electron orbital movements. One speaks of an electronic and a nuclear angular momentum, and the former is composed of a spin angular momentum and an orbital angular momentum. The nuclear angular momentum can be neglected because it is approximately a 1000 times smaller than the electronic one. A magnetic moment can be detected when a number of *unpaired* electrons is present in the atom. Compounds that possess such unpaired electrons are called *paramagnetic* and are attracted by

the external magnetic field while those that are *diamagnetic* are repelled. The overall spin *S* generated by these electrons is the major contribution to the magnetic moment for elements of lower atomic numbers *Z*. In elements of higher *Z*, the contribution by the electron orbital movement becomes increasingly important. Finally, the electronic spin and the orbital spin can interact (spin-orbit coupling), and this also contributes to the magnetic moment; its level depends on the element and the external magnetic field. Spin-orbit coupling can be quenched to different degrees by influencing the electronic configuration and symmetry by the choice of the surrounding molecular scaffold. While it is very small for 1st row transition metal complexes, it contributes more significantly in heavier d-block metal and lanthanide complexes and can outright exceed the spin-only contribution in actinide complexes.

A probe must possess a portion that is capable of emitting a detectable signal. For a magnetically responsive probe this unit cannot simply possess unpaired electrons and thus a spin and a magnetic moment, but rather it has to be capable of adopting *two different* magnetic states depending on its interaction with the analyte (or stimulus). Three types of structurally analogous pairs may be envisaged where this is possible: (a) a duo where one compound is an organic radical, or (b) an internal redox duo experiencing electron transfer, and (c) one that consists of two spin states (generally a low-spin and a high-spin state).

(a) Radicals While paramagnetic organic radicals may be generated from a diamagnetic precursor and thus fulfill this requirement, they are usually rather unstable. A few exceptions are fairly stable in solution (spin labels among others) and have occasionally been considered for the design of responsive organic compounds becoming paramagnetic radicals or losing this quality.^[51a,b] Examples of organic radicals that change their level of paramagnetism are also common in the design of solid-state paramagnetic-diamagnetic switches that respond to physical stimuli.^[10,52a,b] Upon heating or irradiation, the paramagnetism of the radical becomes quenched because of a change in the relative position in the crystal lattice. These switches are based on a pronounced cooperative effect and their mode of action can thus not be transferred to the solution phase unless some sort of self assembly can be achieved.^[53] On the other hand, a quenching phenomenon of two radicals contained in one isolated molecule has been reported for the solution phase on a number of occasions, but only caused by physical stimuli (summarized in^[10]) or a pH change,^[51a] not so for other chemical ones. Some examples were reported where a photoswitchable moiety caused a change in intramolecular diradical communication, thereby leading to magneto-modulation.^[54a,b]

(b) Intramolecular redox reactions A redox-active analyte may change the magnetic properties of a coordination compound by exchanging electrons directly with the magnetogenic core in an *intermolecular* redox reaction. Such a process makes it rather difficult to confer any detection specificity for a particular analyte onto the probe but should rather serve to characterize a general redox potential as is of great interest for biological research. Any intermolecular electron flow may also cause undesired side reactions. Another way of modifying the magnetic quality of a molecular entity would be an *intramolecular* electron-transfer process, i.e. a redox reaction caused by an external stimulus that is not redox-active. Most transition metal ions that can adopt at least two stable oxidation states are suitable candidates, and even radicals may be considered. An *intramolecular* redox-driven change in magnetism has been *widely* reported both for the solution and the solid state, but almost exclusively as the result of a physical stimulus such as light,

temperature and pressure.^[10,13,14a] Numerous examples for two categories of electron transfer were reported: (i.) ligand-to-metal transfer, also referred to as *valence tautomerism* (VT), including the classic semiquinone-catechol cobalt complexes, where a Co(III) LS center turns into a Co(II) HS one ($\Delta e_{\text{unpaired}} = 3$); and (ii.) metal-to-metal transfer in polynuclear complexes where Fe-Co, Fe-Fe, Fe-Ni couples and others are bridged via ligands such as cyanide, including the classic example of prussian blue $[\text{Fe}_4[\text{Fe}(\text{CN})_6]_3]$. Molecules operating in this fashion must ensure the possibility of electron transfer between the two redox-active portions of the molecule, i.e. between the HOMO of the donor portion and the LUMO of the receptor unit. Here lies the opportunity to make such compounds responding to the presence of a chemical analyte, should they interact in such a fashion so as to invert the HOMO-LUMO relationship leading to electron transfer and the change of the oxidation state of the metal center. If it is coupled with a change of the spin state of a central metal ion, then the change in magnetization can be very high. Only a few examples exist where the intramolecular electron transfer is caused by a purely non-redox active stimulus.^[34,51a,55a-c]

(c) Low-spin / high-spin switching Significant magnetization changes can be obtained from a probe that switches from a low-spin (LS) to a high-spin (HS) state as a response to ligand modification. The ligand field theory stipulates that initially degenerate d orbitals experience a splitting into different energy levels as a result of the approach by the ligand(s) (figure 1A). Some d orbitals are more affected than others because the ligand approach is directional, i.e. metal and ligand orbitals of the same symmetry interact more strongly. By modulating the field these ligands exercise, one may induce the complex to adopt either a LS or HS state. Field splitting depends as much on the sigma-donating as on the pi-accepting capacity of the ligand(s). A good pi-acceptor quality of a given ligand depends on the presence of a low-lying pi-star orbital; the resulting increase of the ligand field is referred to as *back-bonding*. As we shall see below (table 2), imine-type ligands (containing sp²-

configured nitrogen atoms) cause a particularly strong ligand field splitting because of their high sigma-donor and pi-acceptor quality.

The nature of the metal ion also plays a role in field splitting: the higher the oxidation number the higher the energy splitting which favors the LS state. Only octahedral (or pseudo-octahedral) complexes with a d4 to d7 configuration can effectively adopt either a LS or a HS state (figure 1B-E), with the exception of a d8 configuration (figure 1F), should the corresponding complex change its coordination chemistry from square-planar (LS and diamagnetic) to tetrahedral or octahedral (both HS and paramagnetic) in the process.^[11a,22] A tetrahedral geometry normally favors the HS state for 1st-row transition metals because the ligand-induced splitting energy is only 4/9 of that observed for an octahedral coordination geometry, and thus too small to overcome the spin-pairing energy. On the other hand, 2nd- and 3rd-row transition metals are mostly found in the LS state due to strong field splitting. For fundamental reasons, lanthanides are not suitable either as they are always found in only one spin state. Their paramagnetism is also as much dependent on spin-orbit coupling as on their number of unpaired electrons. No matter if the strategy of internal electron transfer (b) or that of LS-HS switching (c) is pursued, the choice of the right metal is of pivotal importance.

Among the properties of metal ions displaying a d4 to d8 configuration, one may identify advantages and drawbacks if viewed in the light of the hallmarks of probe design listed above. In fact, the electronic configuration not only has a critical influence on the maximal signal gap attainable ($e_{\text{HS-LS}}$, difference in unpaired electrons before and after activation), it also determines whether a true off-on activation mode is feasible. In the best of cases, the LS state should show no unpaired electrons at all (diamagnetic, off, Spin = 0) which is only possible for an octahedral d6 and a square-planar d8 configuration. On the other hand, a maximal signal gap is only ensured for d5 and d6 configurations ($e_{\text{HS-LS}} = 4$ e); others give only half this difference (2 e). In theory, the d6 ions Fe(II) and

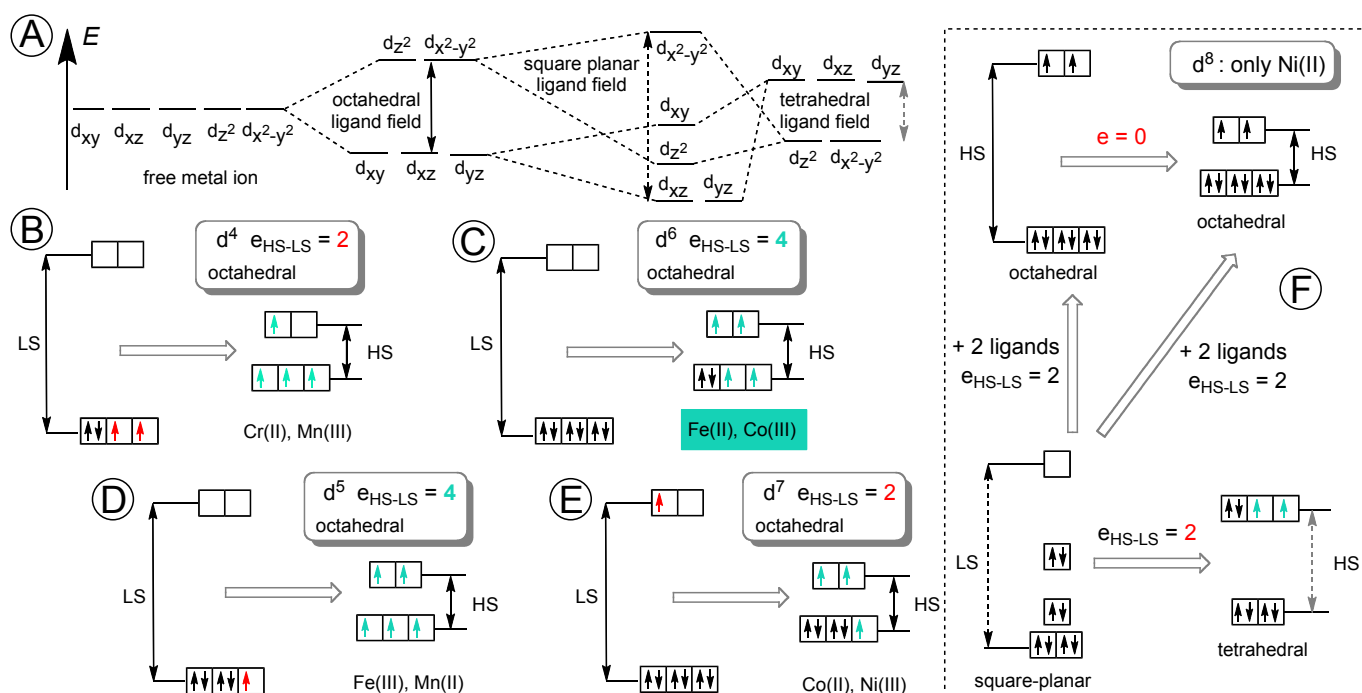


Figure 1. Field splitting (ΔE , length of double arrows) caused by ligands of different strength and resulting d electron configurations for low-spin and high-spin complexes of 1st-row transition metals in light of the presence or absence of an off-on relationship, and the magnitude of the signal gap ($e_{\text{HS-LS}}$); dashed arrow: 1.23 of $\Delta E(\text{octahedral})$; grey dashed arrow: 4/9 of $\Delta E(\text{octahedral})$.

Co(III) can be considered optimal, and the d5 ions Fe(III), Mn(II) and the d8 square-planar Ni(II) as possible alternatives. In practice however, Mn(II) suffers from such an elevated pairing energy that it is very difficult to attain its LS state.^[56] And Co(III) is found in the LS state in the vast majority of cases; ligands exercising a particularly weak ligand field (fluoride) are required to turn it into its HS state (see CoF₆³⁻). Thus no practical ligand system can be found that may cause Co(III) to adopt both of the spin states depending on slight structural modifications

Choice reduced to Fe(II) Another hallmark of probe design is robustness, and the remaining contenders (Fe(III), Fe(II) and Ni(II)) show varying performance in this regard. Ferric complexes (Fe(III)) of both spin states can be quite stable. However, while a good number of ligand systems is known that either leads to LS or HS complexes, this selection is more limited than that known for ferrous complexes (Fe(II)).^[11a] This results in the difficulty to identify a duo of *structurally related* ligands where one causes the corresponding ferric complex to adopt a decidedly LS state while the other leads to a fully HS one. The hope to observe the maximum signal gap (hallmark) theoretically promised by a ferric system is thus diminished. On the other hand, ferrous complexes in the HS state may or may not show a tendency towards oxidation, and the ligand system has thus to be designed so as to minimize it. Importantly, a great range of different ligands is at our disposal causing Fe(II) to adopt either of the two spin states.^[11a,57] This brings within our reach a sharp magnetogenic response caused by ligand modification under the influence of a chemical analyte. Also, LS ferrous complexes are highly stable and show a certain level of kinetic inertness.^[58] Lastly, Ni(II) complexes, while enjoying a true off status for the initial probe and suffering from a mediocre signal gap ($e_{LS-HS} = 2$), adopt a square-planar geometry that is not only unstable in water but also in organic solvents that contain a complex mixture of nucleophiles.^[44a,c] So far, no convincing design has been reported where the LS/off state of Ni(II) chelates was explored for probing/analysis in aqueous or complex samples. Also, only a limited range of ligand systems is available to modulate the spin state of Ni(II) complexes. In the following, we therefore direct our special attention towards Fe(II).

Fe(II) LS / HS duos Well-established methods for tuning the magnetic state of iron(II) in its complexes comprise: (1) variation of the nature of the coordinating atom (mainly, N, O, S), (2) variation of their nucleophilicity / basicity / sigma-donating capacity by for example decoration with electron-withdrawing or -donating groups, (3) variation of the hybridization of N (imine vs. amine = aromatic vs. aliphatic = pi-backbonding or not), (4) impeding optimal orbital

Table 2. Hexa-dentate ligands giving rise to binary Fe(II) complexes

Podand	Base system	N hybridization	Spin state
Branched	Py3tame (C-branched)	6 N-sp2	LS ^[59]
	tptMetame (C-branched)	3 N-sp2, 3 N-sp3	SCO ^[60]
	Py3tren (N-branched)	6 N-sp2	LS ^[61]
	trimethylenediamine	4 N-sp2, 2 N-sp3	LS ^[62]
	2,5,8-triazanon-1-ene	4 N-sp2, 2 N-sp3	LS ^[63]
	cis,cis-1,3,5-cyclohexane	3 N-sp2, 3 N-sp3	LS ^[64,41]
Macrocyclic	triazacyclononane	3 N-sp2, 3 N-sp3	LS ^[65a,b]
Bicyclic	bicyclo[7.5.5]nona-decane	3 N-sp2, 3 N-sp3	LS ^[66a,b]

overlap by introducing steric clash, (5) presence or absence of the macrocyclic effect, and (6) switching between five- and six-membered chelate rings. In applying these criteria, we will not overlook the primordial requirement of solution-phase stability. Indeed, Fe(II) complexes with hexadentate ligands “are known to have stability constants of the order of 10×10^{25} ”^[20b] and “most Fe(II) SCO systems based on multidentate ligands are so stable that ligand dissociation does not interfere with the spin equilibrium even in polar solvents”.^[20d] However, while “ligand dissociation and replacement reactions are more likely to occur for complexes of mono- and bidentate ligands, but even for multidentate ligands replacement of a single chelate arm has been observed.”^[20c] These *thermodynamic* considerations should not hide the fact that for solution-phase applications in complex samples, especially biological ones, *kinetic* ones will almost always override them^[68]: in fact it is the exchange equilibria with other, abundant metal ions and the rates at which they are established that will decide over slow or rapid probe degradation.^[69a,b] What is then expected to work in aqueous media is a ligand system of which a hexa-nitrogen and a penta-nitrogen version are known, because even changing the coordination motif from N6 to N5O1 (scheme 3) will make a switch to a HS system highly likely, provided the oxygen is neither sp²-configured (part of a carbonyl group) nor part of triplet oxygen (see BOLD fMRI). From this it can be concluded that if an octahedral ferrous chelate can be identified that is fully low-spin at room temperature and in aqueous solution, then it is almost guaranteed that a high-spin version thereof can be obtained at the same conditions if one arm becomes de-coordinated or cleaved off.

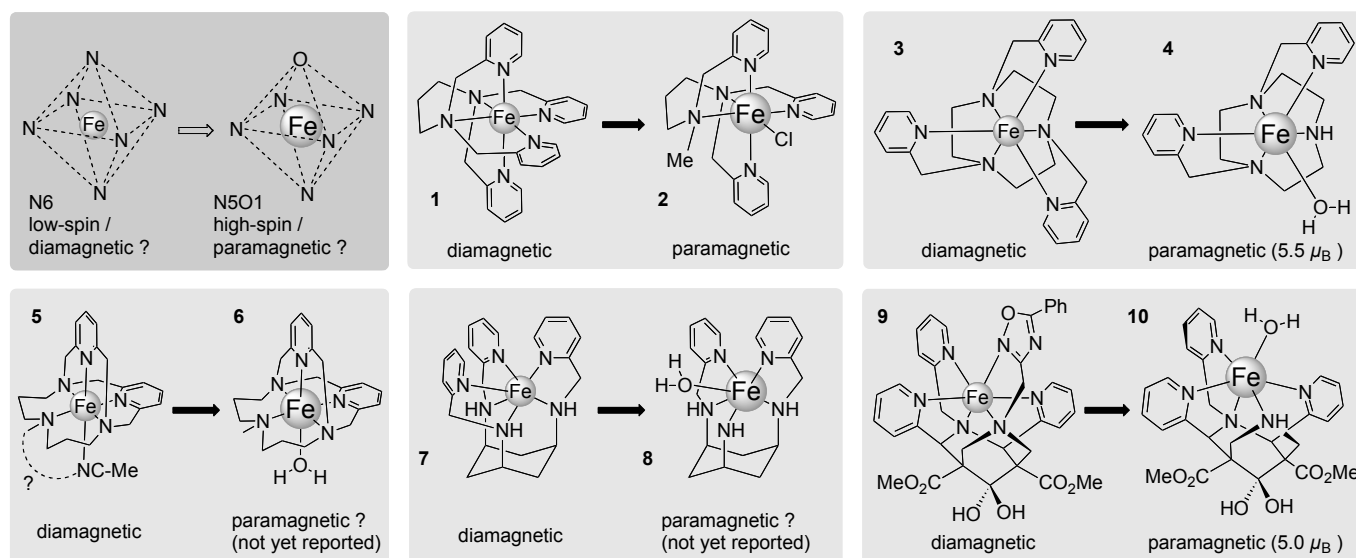
These considerations prompted us to examine the literature for cases of binary ferrous complexes that are fully LS in solution, preferably water (table 2). Among other sources, a broad review article on ferrous complexes with multi-dentate N ligands may serve to identify such LS-HS duos, some of them where both derivatives were already characterized magnetically, others where only one has been done so yet.^[57] However, that review also illustrates that rather few hexa-/penta-dentate systems do in fact ensure a robust low-spin state in order to become attractive for the present task. Multi-dentate ligands giving rise to binary low-spin ferrous complexes comprise (1) branched podands, (2) macrocyclic podands, and (3) multi-cyclic rigid podands (table 2). Branched podand-based N6 Fe(II) chelates can be subdivided by their comprising (a) tripodal ligands branched by a single atom, (b) alkyl-diamine based podands, (c) and two unique cases with special branching units. Examination of examples entering into category 1.a teaches us that a simple branched N6 ligand (tptMetame) cannot force the iron center to adopt the LS state if “only” 3 nitrogens are sp²-configured.^[60] Only ligands displaying fully six imine-type nitrogens have, for the time being, yielded LS complexes: While Py3tame^[59] suffers strain (its LS state can thus be considered weak), Py3tren^[61] exhibits a tendency for pendent-arm decoordination,^[70] and so in spite of the presence of six coordination sites of high ligand field their suitability for the design of a magnetogenic unit remains limited. Alkyl-1,2-diamines (category 1.b) lead to intermediate paramagnetism in Fe(II) complexes despite their generally being equipped with four sp²-configured nitrogens;^[71a,b] they have also been observed to show pendent-arm de-coordination.^[62] Expansion of the ethylene bridge by one further methylene group reliably leads to low-spin complexes (see scheme 3, **1**^[62] and its HS analog **2**^[72]). Three ligands were found entering into category 1.c (unique branched ligands). Only two of them (2,5,8-triazanonene and cis-cis-1,3,5-cyclohexane, **7**) caused the corresponding Fe(II)

complexes to adopt a LS state, but have the advantage to do so not only in the solid state but also in solution, including water.^[63,64,41] They respectively exhibit four and three sp²-configured nitrogens out of six. For category 2 (macrocyclic podands), it should be mentioned that many phthalocyanine Fe(II) complexes were obtained in the LS state, but as complexes comprising tetra-dentate ligands they cannot be of binary quality in octahedral complexes. The rigid planar nature of these N4 macrocyclic ligands precludes the design of N6 derivatives that lead to hexa-coordinate, binary Fe(II) complexes; it has been shown that the required chelate ring sizes are simply too large to form. Accordingly, it is not obvious how this line of ligands may serve for the design of robust magnetogenic probes for the solution phase apart maybe from the synthetically challenging incorporation into a multicyclic system. On the other hand, the tri-pyridylmethyl derivative of the N3 macrocycle tri-azanonane (tacn) has led to the preparation of a fully LS Fe(II) complex (three imines / three amines, scheme 3, **3**) in the solid state.^[65a,b] This LS state is maintained in various aqueous media,^[73] while the corresponding complex lacking one pyridylmethyl arm^[74] is of course HS in nature (**4**).^[73] Both the HS and LS version were shown to be visible and invisible, respectively, in MR images of a live mouse.^[75] As we shall see further on, this system can be effectively transformed into two lines of magnetogenic probes responding to various chemical stimuli. A reported bicyclic N5 ligand may enter into category C. Its dark-red ternary ferrous complex (**5**) was recrystallized from acetonitrile and proved to be LS in the solid state.^[66a,b] The sixth coordination site was occupied by an acetonitrile ligand. No hexa-dentate ligand nor its corresponding complex has yet been reported, but there is no reason why this system may not also serve as a promising target for the design of a robust magnetogenic probe by introduction of another pendant arm (**6**). We recently reported new N6 members for category C, namely two bicyclic, rigid and hexadentate ligands of the unique class of the bispidines (scheme 3).^[67b] Multi-dentate bispidines have previously been declared to form highly stable complexes.^[67a,b] We prepared new bispidine ligands that led to the discovery of the first two binary LS Fe(II) chelates (**9**) for this large class of bicyclic structures. Their LS nature and high stability was confirmed in water and organic solvents at ambient temperature, and their magnetism was explored exhaustively.^[67b] Simple removal of one coordinating arm leads to a fully HS system in water (**10**, 5.0

μ_B).^[67a,b] A new robust off-on duo of ferrous complexes in aqueous media at room temperature has thus become available. While macrocyclic as well as bicyclic ligand platforms (categories 2 and 3) may generally require significantly higher synthetic efforts, it is important to note that the reported hexa-dentate bispidine ligands can be efficiently prepared on the scale of 10 grams.^[67b]

In conclusion, this literature survey reveals that *binary* LS Fe(II) complexes are after all not that numerous. It also teaches us that simple branched N6 ligands do not appear to impose a LS state if they do not exhibit more than 3 imine-type coordination sites. For this reason and for reasons of solution stability, consideration of macrocyclic or bicyclic N6 ligands should be favored. Some of the promising LS-HS duos for the design of a putative magnetogenic probe are presented in scheme 3.

Irreversibility Duos of constitutionally distinct Fe(II) complexes can be interconverted by either a reversible or an irreversible interaction with the analyte. A reversible mode is characterized by a lower energy difference between starting material and product and thus a weak driving force and a less decided thermodynamic equilibrium. This may have seriously unwelcome consequences if aiming at more competitive media (water) or more complex samples containing a variety of nucleophiles^[21] where non-specific interactions cause various degrees of false signal generation (hallmark: robustness). Also, while a reversible mode of action has the advantage of being *likely* instantaneous (hallmark kinetics), total stability for both states may not easily be achieved. So even if the analyte/probe ratio significantly exceeds 1:1, it usually does not manage to switch the probe entirely to the opposite state and one is confronted with the presence of subtle spin equilibria (see hallmark “binary response”, and scheme 1 A and B). On the other hand, an irreversible activation process, where the probe suffers permanent covalent modification by its target analyte, theoretically offers total transformation, a decided shift of the reaction equilibrium, and thus a perfectly binary response (hallmark). This also opens up the opportunity to render the initial probe structure much more stable towards its environment (hallmark, scheme 2C). Yet it is by no means obvious how to achieve this practically. The initial structure would have to store a high energy content that is only unleashed when the two specific reaction partners meet, thus ensuring a sufficient driving force for total transformation. Even if an instantaneous

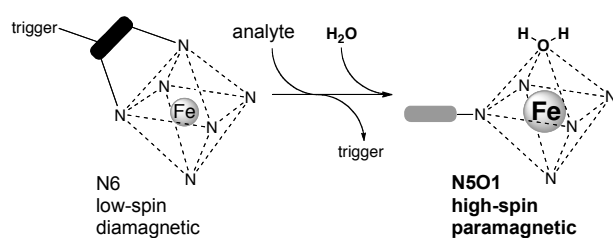


Scheme 3. Reported fully LS ferrous complexes and their structurally related HS counterparts.

response is often impossible to realize in irreversibly responding probes, at least the chemist can work toward conversion kinetics that correspond favorably with the physical detection process and may even achieve some degree of temporal resolution. What also sets the detection of a chemical reactivity apart from that of simple analyte presence is the characterization of *molecular function* in a sample, whether it being a biological one or a technological one. Should this reactivity be of catalytic nature, then the detection process may become highly sensitive in view of the low to very low analyte-probe ratios that may be reached (“catalytic signal amplification”).

Three-Component Design An irreversible response can arguably be achieved only by exploiting the intrinsic *reactivity* of an analyte and not by its mere presence as is the case in the magneto-modulating examples of chapter 2. If the analyte exercises a chemical reactivity, then one needs to identify a moiety (a trigger) to be incorporated into the probe that is susceptible to this reactivity. Once the moiety transformed by the analyte, then this chemical event needs to be transduced to the coordination unit of the probe, i.e. the “signal-emitting device”. Indeed, irreversibly responding probes targeting chemically reactive analytes are widely explored for optical detection (fluorescence). They are often constructed as three-component probes (scheme 2B and 4) where the central unit is an auto-immolative spacer; this ensures (a) maximum adaptability to the chemical reactivity of the target analyte and a generally modular design that aids in adaptation to specific needs (solubility, pharmacokinetics, biocompatibility, bioconjugation) and (b) more freedom in achieving maximum thermodynamic and kinetic stability of the initial chelate. However, this measure of spacer incorporation also increases the complexity of the construct, and its immolation during a response event constitutes an extra chemical reaction associated with its own kinetics; in the best of cases, they should not be slower than those of probe conversion by the analyte.

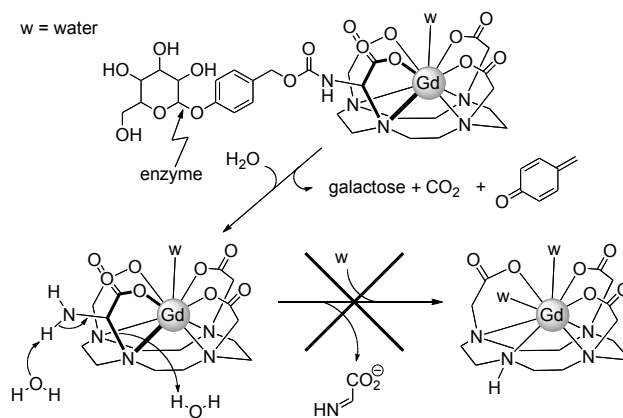
4. Irreversible magnetogenic response



Scheme 4. Irreversible magnetogenic response to an analyte by a 3-component probe.

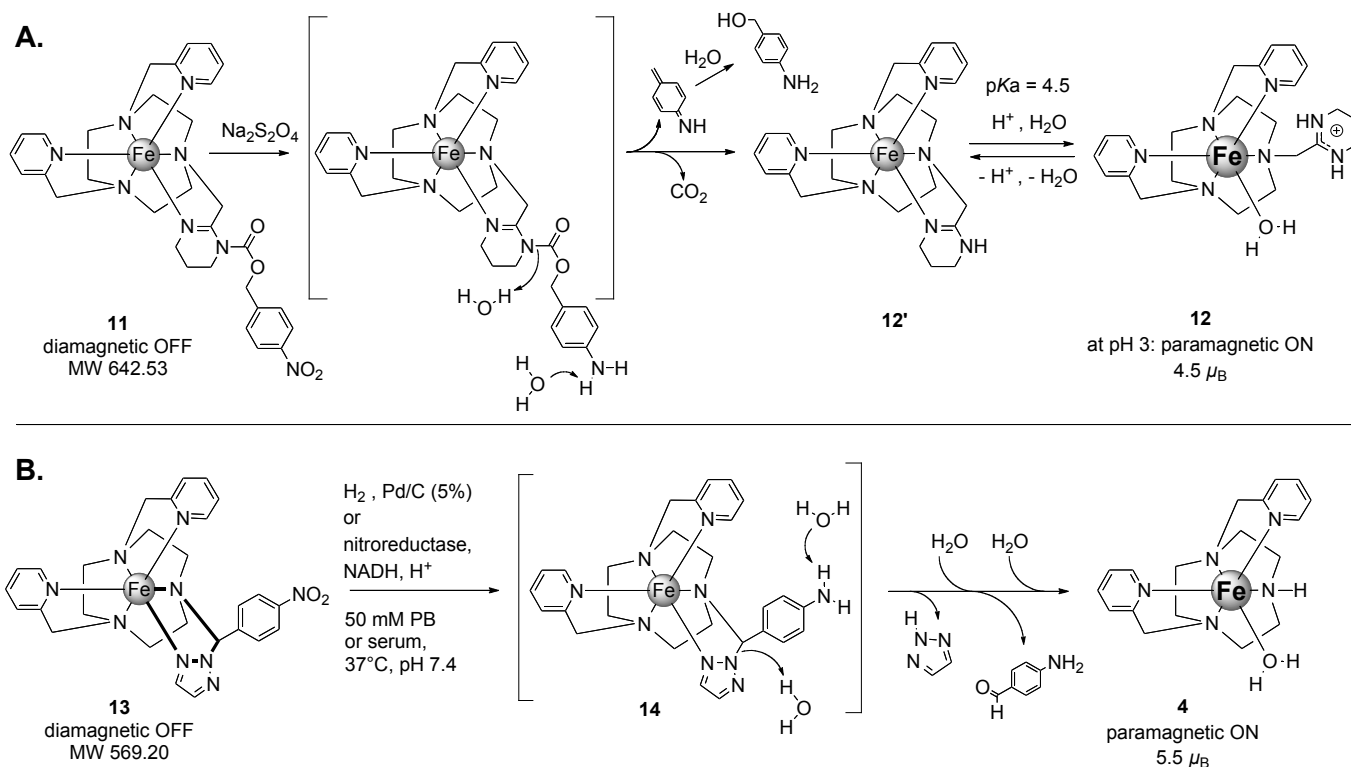
We have now seen the toolbox presently available for the construction of an iron(II)-based magnetogenic core. The remaining task consists in the identification of an irreversible chemical reaction that decisively modifies the first coordination sphere to satisfy the hallmark features from above. Either this may be achieved by the de-coordination of a pendent arm or its entire loss by fragmentation. Triggering de-coordination of a pendent arm requires the unmasking of a property that favors it, for instance competition between pendent-arm coordination and protonation. On the other hand, causing its entire loss by fragmentation calls for the cleavage of a covalent bond within a chelate ring comprising the multi-dentate ligand. Cleaving a ring system of five or six members in general is energetically a highly demanding task. Two unsuccessful cases of auto-immolative schemes involving a coordination compound may

serve as examples: (1) a pendent arm comprising a para-hydroxybenzyl-like spacer did not immolate because it was a constitutive part of a five-membered chelate ring;^[77] however, it was shown to fragment willingly if the same hexa-dentate ligand was not complexed by a central iron atom; (2) an amina (an N/N acetal) did not immolate to result in coordinating arm departure because it was an integral part of a chelate ring involving a gadolinium ion^[50,78] (see bold-face ring in scheme 5) even though it is well known that simple amins with N-H bonds are not stable in aqueous media. These insights served us to produce two new strategies^[40,79] to defeat the imposing strength of the chelate effect (a thermodynamic hurdle) and to observe suitably fast response kinetics in spite of the rigid, multi-cyclic chelate structure (an activation barrier).



Scheme 5. Stabilisation of an amina by incorporation into a chelate ring.

In the first one (Scheme 6A),^[40] the activation cascade comprises three subsequent events: (a) trigger transformation by the analyte, (b) spacer immolation and (c) pendent-arm de-coordination caused by protonation. In fact, analyte action causes the de-acylation (or more precisely: de-carbamoylation) of a coordinated amidine moiety and thus the unmasking of its particularly high basicity. While uncoordinated amidinium ions exhibit a pK_a of 12.6, their amino-acyl counterparts sport a value of only 7.6, in other words a basicity lower by five orders of magnitude. Not surprisingly, these pK_a's become largely perturbed if the amidine is engaged in a coordination bond. The value for the amidine unit in the activated iron complex (12/12') was found at 4.5 and thus eight orders of magnitude lower than for an uncoordinated amidine. Extrapolating this difference to the acylated version should give an even lower pK_a for the initial probe **11**. This would make it largely immune to decoordination caused by protonation and would thus contribute to its robustness. Equally important for probe robustness is the established high stability of the aliphatic carbamyl link towards spontaneous hydrolysis and the decidedly low-spin nature of the coordination motif. As a result, probe **11** is remarkably stable in aqueous media (pH 3.5): it shows no signs of degradation over two days at room temperature or 1.5 hours at 100°C. The chelate effect is defeated here, and the ring opened, thanks to the high basicity of a pendent coordinated arm, but only at a pH lower than 4.5. While this effect has been exploited with other molecular moieties to open chelate rings^[80] its masking in the design of a responsive probe and the use of an amidine to benefit from the presence of an imine of high ligand field are new to this field. The separation of the trigger unit from the coordination motif (modular design) will likely allow



Scheme 6. Two independent concepts for magnetogenic probes.^{[40] [79]} Five-membered chelate ring to be cleaved highlighted in bold-face (B).

for future adaptation to a variety of other chemical analytes. It remains to be seen whether this promising irreversible probe technology can be made operative at neutral pH and in physiological media.

The second strategy (scheme 6B)^[79] gave rise to a magnetogenic probe (**13**) that indeed functions at neutral pH in physiological media including blood serum. Probe activation does not comprise separate spacer immobilization but rather, initial trigger transformation by the chemical analyte results directly in the opening of a chelate ring (bold-face in scheme 6B). This became possible only by screening the structure space for the optimal combination of iron chelation and the right mixed aminal comprising a 1,2,3-triazole unit and a macrocyclic nitrogen atom. This unit is stable, and only stable, if being engaged in a five-membered iron chelate ring and bearing a phenyl substituent. In the absence of iron chelation, it instantaneously hydrolyses if exposed to traces of water. Probe **13** responds when electronic communication between the analyte-susceptible trigger (a nitro group) and the aminal triazole is reversed

by reducing the nitro group to an electron-donating amine. The resulting construct (**14**) may be considered a phenylogous ortho-amide with a free NH unit and a reasonably good leaving group (triazol). Therefore, cleavage of the chelate ring can occur by simple elimination, not nucleophilic attack of any sort; this may explain the good response kinetics with a half-time of roughly 20 minutes in 50 mM phosphate buffer at 37°C (figure 2, left panel). The chemical analyte may be molecular hydrogen in the presence of a catalyst (Palladium on carbon) or even the enzyme nitroreductase that operates with the cofactor NADH. The hexa-dentate ligand underlying probe **13** can be synthesized in a convergent three-component condensation in benzene from the corresponding penta-dentate ligand, para-nitro-benzaldehyde, and 1,2,3-triazole. The general reaction has been introduced and explored in the 90s by Katritzky et al.^[81] It is a condensation reaction that stores considerable energy in the forming aminal. We demonstrated that this highly unstable species can be trapped by titration with an iron salt. Nitro substitution makes it perfectly stable in physiological media. The complex therefore can be regarded as spring-loaded, an all-important aspect in the defeat of the chelate effect once the nitro group reduced. Magnetogenesis in aqueous samples of probe **13** can not only be easily monitored by NMR spectroscopy (determination of the longitudinal relaxation time T_1 of the water hydrogen resonance, figure 2, left panel), these T_1 values can also be measured and translated into grey-scale images (phantom images) by Magnetic Resonance Imaging (figure 2, right panel). Both monitoring modes illustrate also the total stability of the probe in the absence of the analyte (hallmark robustness).

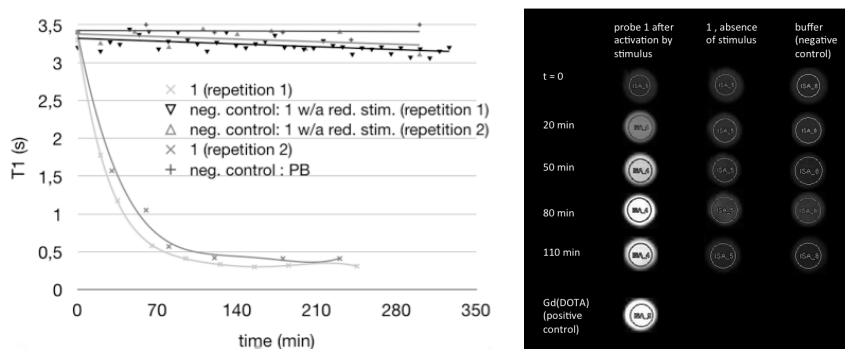


Figure 2. Water- T_1 (NMR) monitoring (left) and T_1 -weighted MRI monitoring (right) of magnetogenic response by probe **13**.

5. Conclusions and Future Directions

New enabling technologies are in urgent need to advance the field of Chemical Imaging.^[1] A magnetic mode may prove a welcome alternative to current optical ones in the detection of responsive molecular probes, whether in samples of technological interest, of biological origin, or *in vivo*. A range of mechanisms have been reported that can modulate the magnetic properties of discrete molecules in solution in response to an analyte. The feebleness of this response, its lack of specificity and the instability of the systems in competitive solvents calls for new design initiatives. In contrast to their reversible mode of response, probes that react irreversibly should offer high specificity, robustness, and a decisive response. In the biomedical arena, the field of the anatomical imaging modality MRI stills seeks probes to render the dream of routine *Molecular MRI* a reality. Strategies have been suggested that give rise to significant signal differences upon activation, but they are not based on magneto-modulation. Activatable probes that give off a non-negligible signal before encounter of their target or that do not show total transition in the presence of it may prove useful if they are detected by an additional, orthogonal detection mode followed by careful analysis. However, those MRI probes that respond to a (bio-)chemical analyte in an off-on mode promise simple and robust detection and thus have been called for on numerous occasions.^[48,49b,82] A magnetogenic concept,^[73,83a-c] as described above, appears to be a viable answer. It is based on iron in its oxidation state II and thus benefits from (a) its environmentally benign nature (green chemistry) but especially (b) the principal possibility to eradicate its spin altogether ($S = 0$, off) and (c) its metabolic recognition and homeostatic management in all live organisms.

Future challenges in its further development depend on the application. For analysis of complex biological samples the activated probe should not be hampered by other sample components to develop its full signal. Response kinetics should approach an instantaneous quality, especially for *in vivo* use. Toxicity issues arising from the high-spin nature of the activated probe should be minimized. Selectivity for a given chemical analyte will require a whole world of adaptation efforts that go beyond the chemical mechanisms covered by this review. Biologists call for reversibly responsive probes that detect the presence of dynamically expressed proteins of interest. In view of their presence in only tiny concentrations, the design of such a probe remains a formidable task. With the contents of this small survey, we hope to have provided the reader with a source of inspiration for his own design endeavors.

J.L.K. and F.T. thank the Ligue Contre le Cancer and the Ministère de la Recherche (both France) for a PhD fellowship, respectively.

Received: ((will be filled in by the editorial staff))

Published online on ((will be filled in by the editorial staff))

- [1] Nat. Res. Council U. S. A., *Visualizing Chemistry: the Progress and Promise of Advanced Chemical Imaging*, National Academies Press, Washington (DC), **2006**.
- [2] a) H. J. Chung, T. Reiner, G. Budin, C. Min, M. Liong, D. Issadore, H. Lee, R. Weissleder, *ACS Nano* **2011**, *5*, 8834–8841; b) M. Liong, M. Fernandez-Suarez, D. Issadore, C. Min, C. Tassa, T. Reiner, S. M. Fortune, M. Toner, H. Lee, R. Weissleder, *Bioconj. Chem.* **2011**, *22*, 2390–2394.
- [3] F. Bloch, W. Hansen, M. Packard, *Phys. Rev.* **1946**, *69*, 127–127.
- [4] P. Caravan, J. J. Ellison, T. J. McMurry, R. B. Lauffer, *Chem. Rev.* **1999**, *99*, 2293–2352.
- [5] S. Aime, M. Botta, E. Gianolio, E. Terreno, *Angew. Chem. Int. Ed.* **2000**, *39*, 747–750.
- [6] a) J. W. Chen, M. Querol Sans, A. Bogdanov, R. Weissleder, *Radiology* **2006**, *240*, 473–481; b) Y. Li, V. R. Sheth, G. Liu, M. D. Pagel, *Contrast Media Mol Imaging* **2010**, 219–228.
- [7] a) A. Jasanoff, *Curr. Op. Neurobiol.* **2007**, *17*, 593–600; b) J. L. Major, G. Parigi, C. Luchinat, T. J. Meade, *Proc. Natl. Acad. Sci. U. S. A.* **2007**, *104*, 13881–13886; c) E. L. Que, C. J. Chang, *Chem. Soc. Rev.* **2010**, *39*, 51–60.
- [8] a) S. Aime, F. Fedeli, A. Sanino, E. Terreno, *J. Am. Chem. Soc.* **2006**, *128*, 11326–11327; b) Y. Wu, T. C. Soesbe, G. E. Kiefer, P. Zhao, A. D. Sherry, *J. Am. Chem. Soc.* **2010**, *132*, 14002–14003.
- [9] a) B. Yoo, M. D. Pagel, *Front. Biosci.* **2008**, *13*, 1733–1752; b) C. Shen, E. J. New, *Curr. Opin. Chem. Biol.* **2013**, *17*, 158–166.
- [10] O. Sato, J. Tao, Y.-Z. Zhang, *Angew. Chem. Int. Ed.* **2007**, *46*, 2152–2187.
- [11] a) *Spin Crossover in Transition Metal Compounds I: Vol 1 (Topics in Current Chemistry)*, P. Gutlich, H. A. Goodwin (Eds.), Springer, **2004**; b) *Spin-Crossover Materials*, M. A. Halcrow (Ed.) Wiley, Oxford, UK, **2013**.
- [12] O. Kahn, *Angew. Chem. Int. Ed.* **1985**, *24*, 834–850.
- [13] C. G. Pierpont, *Coord. Chem. Rev.* **2001**, *216–217*, 99–125.
- [14] a) C. G. Pierpont, *Coord. Chem. Rev.* **2001**, *219*, 415–433; b) N. Shimamoto, S.-I. Ohkoshi, O. Sato, K. Hashimoto, *Inorg. Chem.* **2002**, *41*, 678–684.
- [15] G. N. Newton, M. Nihei, H. Oshio, *Eur. J. Inorg. Chem.* **2011**, *2011*, 3031–3042.
- [16] O. Kahn, C. J. Martinez, *Science* **1998**, *279*, 44–48.
- [17] a) G. J. Halder, C. J. Kepert, B. Moubaraki, K. S. Murray, J. D. Cashion, *Science* **2002**, *298*, 1762–1765; b) O. Cador, A. Dei, C. Sangregorio, *Chem. Commun.* **2004**, 652–653; c) D. Pinkowicz, R. Podgajny, B. Gawel, W. Nitek, W. Lasocha, M. Oszajca, M. Czaplak, M. Makarewicz, M. Balanda, B. Sieklucka, *Angew. Chem. Int. Ed.* **2011**, *50*, 3973–3977.
- [18] a) M. Engeser, L. Fabbrizzi, M. Licchelli, D. Sacchi, *Chem. Commun.* **1999**, 1191–1192; b) C. Edler, C. Piguet, J.-C. G. Bünzli, G. Hopfgartner, *Chem.-Eur. J.* **2001**, *7*, 3014–3024.
- [19] a) M. E. Itkis, X. Chi, A. W. Cordes, R. C. Haddon, *Science* **2002**, *296*, 1443–1445; b) N. Hoshino, F. Iijima, G. N. Newton, N. Yoshida, T. Shiga, H. Nojiri, A. Nakao, R. Kumai, Y. Murakami, H. Oshio, *Nat Chem* **2012**, *4*, 921–926.
- [20] a) J. K. Beattie, *Advances in Inorganic Chemistry* **1988**, *32*, 1–53; b) H. Toftlund, *Coord. Chem. Rev.* **1989**, *94*, 67–108; c) H. Toftlund, *Monatshfte für Chemie/Chemical Monthly* **2001**, *132*, 1269–1277; d) H. Toftlund, J. J. McGarvey, in *Spin Crossover in Transition Metal Compounds I: Vol 1 (Topics in Current Chemistry)*, Springer Berlin / Heidelberg, **2004**, pp. 151–166; e) N. Hassan, A. B. Koudriavtsev, W. Linert, *Pure Appl. Chem.* **2008**, *80*, 1281–1292.
- [21] M. P. Shores, C. M. Klug, S. R. Fiedler, in *Spin-Crossover Materials* (M. A. Halcrow, Ed.) Wiley, Oxford, UK, **2013**, pp. 281–301.
- [22] B. Weber in *Spin-Crossover Materials* (M. A. Halcrow, Ed.) Wiley, Oxford, UK, **2013**, pp. 55–76.
- [23] D. Siretanu, D. Li, L. Buisson, D. M. Bassani, S. M. Holmes, C. Mathonière, R. Clérac, *Chem.-Eur. J.* **2011**, *17*, 11704–11708.
- [24] a) J. Rall, M. Wanner, M. Albrecht, F. M. Hornung, W. Kaim, *Chem.-Eur. J.* **1999**, *5*, 2802–2809; b) E. Evangelio, C. Rodriguez-Blanco, Y. Coppel, D. N. Hendrickson, J. P. Sutter, J. Campo, D. Ruiz-Molina, *Solid State Sciences* **2009**, *11*, 793–800.
- [25] a) R. A. Binstead, J. K. Beattie, T. G. Dewey, D. H. Turner, *J. Am. Chem. Soc.* **1980**, *102*, 6442–6451; b) P. Gutlich, H. A. Goodwin, in *Spin Crossover in Transition Metal Compounds I, Topics in Current Chemistry*, Springer, Berlin, **2004**, pp. 1–47.
- [26] A. J. Conti, C. L. Xie, D. N. Hendrickson, *J. Am. Chem. Soc.* **1989**, *111*, 1171–1180.
- [27] a) M. F. Tweedle, L. J. Wilson, *J. Am. Chem. Soc.* **1976**, *98*, 4824–4834; b) R. H. Petty, E. V. Dose, M. F. Tweedle, L. J. Wilson, *Inorg. Chem.* **1978**, *17*, 1064–1071.
- [28] S. A. Barrett, C. A. Kilner, M. A. Halcrow, *Dalton Trans.* **2011**, *40*, 12021–12024.
- [29] a) W. Linert, M. Enamullah, V. Gutmann, R. Jameson, *Monatshfte für Chemie/Chemical Monthly* **1994**, *125*, 661–670; b) M. Enamullah, W. Linert, *J. Coord. Chem.* **1996**, *38*, 337–346.
- [30] a) L. L. Martin, K. S. Hagen, A. Hauser, R. L. Martin, A. M. Sargeson, *Chem Comm* **1988**, 1313–1315; b) L. L. Martin, R. L. Martin, A. M. Sargeson, *Polyhedron* **1994**, *13*, 1969–1980.
- [31] Z. Ni, M. P. Shores, *J. Am. Chem. Soc.* **2009**, *131*, 32–33.
- [32] Z. Ni, A. M. McDaniel, M. P. Shores, *Chem. Sci.* **2010**, *1*, 615–621.
- [33] A. M. McDaniel, C. M. Klug, M. P. Shores, *Eur. J. Inorg. Chem.*

- 2013, 2013, 943–950.
- [34] P. Leeladee, R. A. Baglia, K. A. Prokop, R. Latifi, S. P. de Visser, D. P. Goldberg, *J. Am. Chem. Soc.* **2012**, *134*, 10397–10400.
- [35] a) L. Fabbrizzi, M. Licchelli, G. Rabaioli, A. Taglietti, *Coord. Chem. Rev.* **2000**, *205*, 85–108; b) D. W. Blakesley, S. C. Payne, K. S. Hagen, *Inorg. Chem.* **2000**, *39*, 1979–1989; c) K. P. Bryliakov, E. A. Duban, E. P. Talsi, *Eur. J. Inorg. Chem.* **2005**, *2005*, 72–76; d) J. England, G. J. P. Britovsek, N. Rabadia, A. J. P. White, *Inorg. Chem.* **2007**, *46*, 3752–3767.
- [36] L. Pauling, C. D. Coryell, *Proc. Natl. Acad. Sci. U. S. A.* **1936**, *22*, 210–216.
- [37] S. Ogawa, T. M. Lee, A. R. Kay, D. W. Tank, *Proc. Natl. Acad. Sci. U. S. A.* **1990**, *87*, 9868–9872.
- [38] a) L. Fabbrizzi, A. Leone, A. Taglietti, *Angew. Chem. Int. Ed.* **2001**, *40*, 3066–3069; b) B. T. Nguyen, E. V. Anslyn, *Coord. Chem. Rev.* **2006**, *250*, 3118–3127.
- [39] a) C. A. Reed, F. Guiset, *J. Am. Chem. Soc.* **1996**, *118*, 3281–3282; b) C. R. Goldsmith, R. T. Jonas, A. P. Cole, T. D. P. Stack, *Inorg. Chem.* **2002**, *41*, 4642–4652; c) J. P. López, F. W. Heinemann, R. Prakash, B. A. Hess, O. Horner, C. Jeandey, J.-L. Oddou, J.-M. Latour, A. Grohmann, *Chem.-Eur. J.* **2002**, *8*, 5709–5722; d) N. Ortega-Villar, V. M. Ugalde-Saldivar, M. C. Muñoz, L. A. Ortiz-Frade, J. G. Alvarado-Rodríguez, J. A. Real, R. Moreno-Esparza, *Inorg. Chem.* **2007**, *46*, 7285–7293; e) A. Draksharapu, Q. Li, H. Logtenberg, T. A. van den Berg, A. Meetsma, J. S. Killeen, B. L. Feringa, R. Hage, G. Roelfes, W. R. Browne, *Inorg. Chem.* **2012**, *51*, 900–913.
- [40] F. Touti, P. Maurin, L. Canaple, O. Beuf, J. Hasserodt, *Inorg. Chem.* **2012**, *51*, 31–33.
- [41] M. L. Childers, J. Cho, C. A. S. Regino, M. W. Brechbiel, A. G. DiPasquale, A. L. Rheingold, S. V. Torti, F. M. Torti, R. P. Planalp, *J. Inorg. Biochem.* **2008**, *102*, 150–156.
- [42] N. Ségaud, J. N. Rebilly, K. Sénéchal-David, R. Guillot, L. Billon, J.-P. Baltaze, J. Farjon, O. Reinaud, F. Banse, *Inorg. Chem.* **2013**, 691–700.
- [43] a) L. Sacconi, P. Nannelli, U. Campigli, *Inorg. Chem.* **1965**, *4*, 818–822; b) M. Boiocchi, L. Fabbrizzi, F. Foti, M. Vazquez, *Dalton Trans.* **2004**, 2616–2620; c) H. Ohtsu, K. Tanaka, *Inorg. Chem.* **2004**, *43*, 3024–3030; d) S. Thies, C. Bornholdt, F. Köhler, F. D. Sönnichsen, C. Näther, F. Tuczek, R. Herges, *Chem.-Eur. J.* **2010**, *16*, 10074–10083.
- [44] a) R. F. Pasternack, E. G. Spiro, M. Teach, *Journal of Inorganic and Nuclear Chemistry* **1974**, *36*, 599–606; b) J. K. Beattie, M. T. Kelso, W. E. Moody, P. A. Tregloan, *Inorg. Chem.* **1985**, *24*, 415–418; c) T. La, R. A. Richards, R. S. Lu, R. Bau, G. M. Miskelly, *Inorg. Chem.* **1995**, *34*, 5632–5640.
- [45] F. Kratz, I. A. Muller, C. Rypa, A. Warnecke, *ChemMedChem* **2008**, *3*, 20–53.
- [46] a) E. Leroy, N. Bense, J. L. Reymond, *Biorg. Med. Chem. Lett.* **2003**, *13*, 2105–2108; b) J. A. Richard, M. Massonneau, P. Y. Renard, A. Romieu, *Org. Lett.* **2008**, *10*, 4175–4178; c) L. D. Lavis, T.-Y. Chao, R. T. Raines, *Chem. Sci.* **2011**, *2*, 521–530.
- [47] J. A. Duimstra, F. J. Femia, T. J. Meade, *J. Am. Chem. Soc.* **2005**, *127*, 12847–12855.
- [48] M. Baker, *Nature* **2010**, *463*, 977–980.
- [49] a) M. L. Garcia-Martin, G. V. Martinez, N. Raghunand, A. D. Sherry, S. Zhang, R. J. Gillies, *Magn. Reson. Med.* **2006**, *55*, 309–315; b) E. Terreno, D. D. Castelli, A. Viale, S. Aime, *Chem. Rev.* **2010**, *110*, 3019–3042; c) V. Catanzaro, C. V. Gringeri, V. Menchise, S. Padovan, C. Boffa, W. Dastrù, L. Chaabane, G. Digilio, S. Aime, *Angew. Chem. Int. Ed.* **2013**, *52*, 3926–3930.
- [50] T. Chauvin, P. Durand, M. Bernier, H. Meudal, B. T. Doan, F. Noury, B. Badet, J. C. Beloeil, E. Toth, *Angew. Chem. Int. Ed.* **2008**, *47*, 4370–4372.
- [51] a) A. Dei, L. Sorace, *Dalton Trans.* **2003**, 3382–3386; b) F. Hyodo, K. I. Matsumoto, A. Matsumoto, J. B. Mitchell, M. C. Krishna, *Cancer Res.* **2006**, *66*, 9921–9928.
- [52] a) J. L. Brusso, O. P. Clements, R. C. Haddon, M. E. Itkis, A. A. Leitch, R. T. Oakley, R. W. Reed, J. F. Richardson, *J. Am. Chem. Soc.* **2004**, *126*, 14692–14693; b) C. S. Clarke, J. Jornet-Somoza, F. Mota, J. J. Novoa, M. Deumal, *J. Am. Chem. Soc.* **2013**, *132*, 17817–17830.
- [53] I. Ratera, D. Ruiz-Molina, J. Vidal Gancedo, K. Wurst, N. Daro, J. F. Létard, C. Rovira, J. Veciana, *Angew. Chem. Int. Ed.* **2001**, *40*, 919–922.
- [54] a) K. Hamachi, K. Matsuda, T. Itoh, H. Iwamura, *Bull. Chem. Soc. Jpn.* **1998**, *71*, 2937–2943; b) K. Matsuda, M. Matsuo, M. Irie, *J. Org. Chem.* **2001**, *66*, 8799–8803.
- [55] a) D. W. Low, J. R. Winkler, H. B. Gray, *J. Am. Chem. Soc.* **1996**, *118*, 117–120; b) T. Kurahashi, A. Kikuchi, T. Toshi, Y. Shiro, T. Kitagawa, H. Fujii, *Inorg. Chem.* **2008**, *47*, 1674–1686; c) M. Nihei, Y. Sekine, N. Suganami, K. Nakazawa, A. Nakao, H. Nakao, Y. Murakami, H. Oshio, *J. Am. Chem. Soc.* **2011**, *133*, 3592–3600.
- [56] M. Trzaskowski, A. Les, L. Adamowicz, *Int. J. Mol. Sci.* **2003**, *4*, 503–511.
- [57] M. A. Halcrow, *Polyhedron* **2007**, *26*, 3523–3576.
- [58] A. E. Martell, R. D. Hancock, *Metal Complexes in Aqueous Solutions*, Plenum Press, New York, **1996**.
- [59] F. L. Urbach, S. O. Wandiga, *J. Chem. Soc. D* **1970**, 1572a–1572a.
- [60] A. H. Al-Obaidi, K. B. Jensen, J. J. McGarvey, H. Toftlund, B. Jensen, S. E. Bell, J. G. Carroll, *Inorg. Chem.* **1996**, *35*, 5055–5060.
- [61] M. A. Hoselton, L. J. Wilson, R. S. Drago, *J. Am. Chem. Soc.* **1975**, *97*, 1722–1729.
- [62] M. Tamura, Y. Urano, K. Kikuchi, T. Higuchi, M. Hirobe, T. Nagano, *J. Organomet. Chem.* **2000**, *611*, 586–592.
- [63] V. M. Ugalde-Saldivar, M. E. Sosa-Torres, L. Ortiz-Frade, S. Bernes, H. Hopfl, *J. Chem. Soc., Dalton Trans.* **2001**, 3099–3107.
- [64] M. L. Childers, F. Su, A. M. Przyborowska, B. Bishwokarma, G. Park, M. W. Brechbiel, S. V. Torti, F. M. Torti, G. Broker, J. S. Alexander, R. D. Rogers, K. Ruhlandt-Senge, R. P. Planalp, *Eur. J. Inorg. Chem.* **2005**, 3971–3982.
- [65] a) L. Christiansen, D. N. Hendrickson, H. Toftlund, S. R. Wilson, C. L. Xie, *Inorg. Chem.* **1986**, *25*, 2813–2818; b) K. Wieghardt, E. Schoffmann, B. Nuber, J. Weiss, *Inorg. Chem.* **1986**, *25*, 4877–4883.
- [66] a) T. J. Hubin, J. M. McCormick, S. R. Collinson, M. Buchalova, C. M. Perkins, N. W. Alcock, P. K. Kahol, A. Raghunathan, D. H. Busch, *J. Am. Chem. Soc.* **2000**, *122*, 2512–2522; b) S. Collinson, N. W. Alcock, A. Raghunathan, P. K. Kahol, D. H. Busch, *Inorg. Chem.* **2000**, *39*, 757–764.
- [67] a) H. Borzel, P. Comba, K. Hagen, Y. Lampeka, A. Lienke, G. Linti, M. Merz, H. Pritzkow, L. Tsymbal, *Inorg. Chim. Acta* **2002**, *337*, 407–419; b) J. L. Kolanowski, E. Jeanneau, R. Steinhoff, J. Hasserodt, *Chem.-Eur. J.* **2013**, *19*, 8839–8849.
- [68] A. D. Sherry, P. Caravan, R. E. Lenkinski, *J. Magn. Reson. Imaging* **2009**, *30*, 1240–1248.
- [69] a) P. Wedeking, K. Kumar, M. F. Tweedle, *Magnetic Resonance Imaging* **1992**, *10*, 641–648; b) M. Port, J.-M. Idee, C. Medina, C. Robic, M. Sabatou, C. Corot, *Biomaterials* **2008**, *21*, 469–490.
- [70] C. M. Klug, A. M. McDaniel, S. R. Fiedler, K. A. Schulte, B. S. Newell, M. P. Shores, *Dalton Trans.* **2012**, *41*, 12577–12585.
- [71] a) J. J. McGarvey, I. Lawthers, K. Heremans, H. Toftlund, *Inorg. Chem.* **1990**, *29*, 252–256; b) J. K. McCusker, H. Toftlund, A. L. Rheingold, D. N. Hendrickson, *J. Am. Chem. Soc.* **1993**, *115*, 1797–1804.
- [72] V. Balland, F. Banse, E. Anxolabehere-Mallart, M. Ghiladi, T. A. Mattioli, C. Philouze, G. Blondin, J. J. Girerd, *Inorg. Chem.* **2003**, *42*, 2470–2477.
- [73] V. Stavila, M. Allali, L. Canaple, Y. Stortz, C. Franc, P. Maurin, O. Beuf, O. Dufay, J. Samarut, M. Janier, J. Hasserodt, *New J. Chem.* **2008**, *32*, 428–435.
- [74] A. H. R. Al-Obaidi, J. J. McGarvey, K. P. Taylor, S. E. J. Bell, K. B. Jensen, H. Toftlund, *J. Chem. Soc. Chem. Comm.* **1993**, 536–538.
- [75] F. Touti, A. K. Singh, P. Maurin, L. Canaple, O. Beuf, J. Samarut, J. Hasserodt, *J. Med. Chem.* **2011**, *54*, 4274–4278.
- [76] a) G. D. Hosken, R. D. Hancock, *J. Chem. Soc. Chem. Comm.* **1994**, 1363–1364; b) G. D. Hosken, C. C. Allan, J. C. A. Boeyens, R. D. Hancock, *J. Chem. Soc., Dalton Trans.* **1995**, 3705–3708.
- [77] V. Stavila, Y. Stortz, C. Franc, D. Pitrat, P. Maurin, J. Hasserodt, *Eur. J. Inorg. Chem.* **2008**, *25*, 3943–3947.
- [78] T. Chauvin, S. Torres, R. Rosseto, J. Kotek, B. Badet, P. Durand, E. Toth, *Chem.-Eur. J.* **2012**, *18*, 1408–1418.
- [79] F. Touti, P. Maurin, J. Hasserodt, *Angew. Chem. Int. Ed.* **2013**, *52*, 4654–4658.
- [80] M. P. Lowe, D. Parker, O. Reany, S. Aime, M. Botta, G. Castellano, E. Gianolio, R. Pagliarin, *J. Am. Chem. Soc.* **2001**, *123*, 7601–7609.
- [81] A. R. Katritzky, X. F. Lan, J. Z. Yang, O. V. Denisko, *Chem. Rev.* **1998**, *98*, 409–548.
- [82] *Molecular Imaging: Principles and Practice*, R. Weissleder, B. D. Ross, A. Rehemtulla, S. S. Gambhir (Eds.) Pmhp USA Ltd, **2010**.
- [83] a) J. Hasserodt, WO2005094903; b) J. Hasserodt, P. Maurin, F. Touti, FR201257413; c) J. Hasserodt, *New J. Chem.* **2012**, 1707–1712.

Entry for the Table of Contents (Please choose one layout)

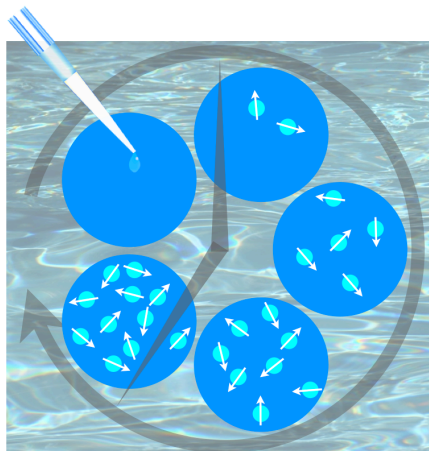
Layout 1:

Magnetogenic probes

Jens Hasserodt*, Jacek Lukasz
Kolanowski, Faycal Touti _____

Page – Page

Magnetogenesis in water induced by a
chemical analyte



This review introduces the limited reports on molecules that change the magnetic properties of a solution-phase sample in response to a chemical stimulus. They all operate by a reversible mechanism. The lessons thus learned enter into thorough considerations for the design of high-performance probes reacting irreversibly as do optically responsive agents. A discussion of the capabilities of two recently reported probes responding irreversibly and in an off-on mode allow the reader to build his own view on this emerging field.

CV – JACEK ŁUKASZ KOLANOWSKI

Address: Laboratoire de Chimie, ENS de Lyon,
46 allée d'Italie, 69364 Lyon, FRANCE
Telephone : +33 (0)472 72 83 96
E-mail : kolanowski.jacek@gmail.com
Nationality: Polish
Date and place of birth: 19.10.1985, Poznań, POLAND



EDUCATION:

- 01.2010 – onwards École Normale Supérieure de Lyon, France – PhD studies: *Bispidine-iron(II) complexes as a novel platform for the design of magnetogenic probes*, supervision: Prof. Jens Hasserodt.
- 10.2005 – 08.2007 Adam Mickiewicz University, Poznań, Poland – BSc degree in Biotechnology: *Potential therapeutic application of resveratrol in processes triggered by sirtuins*, supervision: Prof. Przemysław Wojtaszek.
- 10.2004 – 06.2009 Adam Mickiewicz University, Poznań, Poland – MSc degree in Chemistry: *Novel synthetic method for preparation of ortho-alkylfluorinated arylphosphonates and their reactivity*, supervision: Prof. Henryk Koroniak and Prof. Gerd-Voelker Röschenthaler.
- 09.2002 – 06.2004 High school no. 2, Poznań - International Baccalaureate Program in English.

AWARDS:

- 2010 – 2012 Three-year PhD stipend from Ligue Nationale Contre le Cancer (France).
- 2009 M. Sc. Degree in Fundamental Chemistry awarded with honours (*Maxima Cum Laude*).
- 2009 Distinction in a contest for the best Polish student – *Studencki Nobel 2009*.
- 2005 – 2009 Scientific scholarship – Adam Mickiewicz University, Faculty of Chemistry.

PUBLICATIONS:

- [3] J Hasserodt, JL Kolanowski, F Touti. Magnetogenesis in Water Induced by a Chemical Analyte, *Angewandte Chemie International Edition in English* **2013**, in press – minireview.
- [2] JL Kolanowski, E Jeanneau, R Steinhoff, J Hasserodt. Bispidine Platform Grants Full Control over Magnetic State of Ferrous Chelates in Water, *Chemistry – A European Journal* **2013**, 19, 8839-8849 - full paper.
- [1] SN Tverdomed, J Kolanowski, E Lork, G-V Röschenthaler. An Effective Synthetic Route to Ortho-Difluoromethyl Arylphosphonates: Studies on the Reactivity of Phosphorus- and Fluorine-Containing Functions, *Tetrahedron* **2011**, 67 (21), 3887-3903 - full paper.

CONFERENCES:

- [4] J Kolanowski, D Kryza, P Bonazza, P Maurin, M Janier, J Hasserodt. A simple protocol for introducing the radioactive Fe(II)-59 isotope into a model chelate for MRI that serves to determine biodistribution in mice. *7^{èmes} Journées Scientifiques du CLARA*, 20-21 March **2012**, Lyon – abstract.

- [3] J Hasserodt, F Touti, J Kolanowski, A Singh, R Steinhoff, P Maurin, L Canaple, O Boeuf, J Samarut . Progress in the design of iron(II)-based probes to highlight enzyme activity in magnetic resonance images. *6^{èmes} Journées Scientifiques du CLARA*, 28-29 March **2011**, Lyon – abstract.
- [2] SN Tverdomed, J Kolanowski, E Lork, G-V Rösenthaller. An effective synthetic route to ortho-difluoromethyl arylphosphonates: studies on the reactivity of phosphorus- and fluorine-containing functions. *19th International Symposium on Fluorine Chemistry*, 23-28 August **2009**, Jackson Hole, Wyoming, USA – abstract.
- [1] European Chemistry Thematic Network Annual Conference, 15-18 April **2009**, Poznań, Poland – organizing committee and oral presentation during *European Chemistry Exchange Network – Plenary Workshop*.

ADDITIONAL TRAINING AND WORK EXPERIENCE:

2010 – 2012	ENS Lyon, France - supervision of students Robert Steinhoff (2 nd year of Masters, 2010) and Hanno Kossen (1 st year of Masters, 2011) during their laboratorial internships.
10.2009 – 12.2009	Jacobs University Bremen, Germany – commercial research project in <i>New selective fluorinating agents</i> , supervisor: Prof. Gerd-Voelker Rosenthaller.
08.2009	University of Aarhus, Denmark – summer school <i>Molecular Biosciences International Student Programme (MOBIL)</i> .
07.2009 – 08.2009	Meditech sp. z o. o., Poznan – local supplier of diagnostic equipment for medical use - junior technical troubleshooter.
10.2008 – 02.2009	University of Bremen, Germany – research project in <i>Preparation of fluorinated arylphosphonates</i> , supervisor: Prof. Gerd-Voelker Rosenthaller.
08.2008	GlaxoSmithKline, Stevenage, Great Britain – pharmaceutical company, summer school <i>5th Residential Chemistry Training Experience</i> .
10.2007 – 02.2008	University of Bremen, Germany – LLP Erasmus programme, research project in <i>Phosphorous and Fluoroorganic compounds. Synthesis, reactions and applications</i> , supervisor: Prof. Gerd-Voelker Rosenthaller.

LINGUISTIC COMPETENCES:

English	advanced (level C1 – Cambridge Certificate in Advanced English)
French	intermediate (level B1)
Russian	intermediate (speaking) / basic (reading)
German	basic (level A2)

REFEREES / REFERENCE LETTERS:

Prof. Jens Hasserodt, PhD supervisor, Ecole Normale Supérieure de Lyon, France, *e-mail*: jens.hasserodt@ens-lyon.fr.

Prof. Gerd-Volker Rösenthaller, Master Laboratorial Training supervisor, Jacobs University, Bremen, Germany, *e-mail*: g.roeschenthaler@jacobs-university.de.

Prof. Henryk Koroniak, MSc supervisor, Adam Mickiewicz University, Poznań, Poland, *e-mail*: koroniak@amu.edu.pl.

Prof. Przemysław Wojtaszek, BSc supervisor, Adam Mickiewicz University, Poznań, Poland, *e-mail*: przemow@amu.edu.pl.